INTERNATIONAL DOCTORAL
SCHOOL OF THE USC

Juan José
López Mayán

PhD Thesis

Bioaccumulation and bioavailability studies of silver and titanium dioxide nanoparticles in aquaculture products

Santiago de Compostela, 2023

Doctoral Programme in Chemical Science and Technology

USC
UNIVERSIDADE
DE SANTIAGO
DE COMPOSTELA

TESIS DE DOCTORADO

BIOACCUMULATION AND BIOAVAILABILITY STUDIES OF SILVER AND TITANIUM DIOXIDE NANOPARTICLES IN AQUACULTURE PRODUCTS

Juan José López Mayán

ESCUELA DE DOCTORADO INTERNACIONAL DE LA UNIVERSIDAD DE SANTIAGO DE COMPOSTELA

PROGRAMA DE DOCTORADO EN CIENCIA Y TECNOLOGÍA QUÍMICA

SANTIAGO DE COMPOSTELA

2023

USC
UNIVERSIDADE
DE SANTIAGO
DE COMPOSTELA

UNIVERSIDADE DE SANTIAGO DE COMPOSTELA

DECLARACIÓN DEL AUTOR DE LA TESIS

D./Dña. **Juan José López Mayán**

Título de la tesis: **Bioaccumulation and bioavailability studies of silver and titanium dioxide nanoparticles in aquaculture products**

Presento mi tesis, siguiendo el procedimiento adecuado al Reglamento y declaro que:

1) La tesis abarca los resultados de la elaboración de mi trabajo.
2) De ser el caso, en la tesis se hace referencia a las colaboraciones que tuvo este trabajo.
3) Confirmo que la tesis no incurre en ningún tipo de plagio de otros autores ni de trabajos presentados por mí para la obtención de otros títulos.
4) La tesis es la versión definitiva presentada para su defensa y coincide la versión impresa con la presentada en formato electrónico.

Y me comprometo a presentar el Compromiso Documental de Supervisión en el caso que el original no esté depositado en la Escuela.

En **Santiago de Compostela**, **a 14 de Julio de 2023**.

USC UNIVERSIDADE DE SANTIAGO DE COMPOSTELA

USC
UNIVERSIDADE
DE SANTIAGO
DE COMPOSTELA

AUTORIZACIÓN DEL DIRECTOR / TUTOR DE LA TESIS

Bioaccumulation and bioavailability studies of silver and titanium dioxide nanoparticles in aquaculture products

Dª Elena María Peña Vázquez
Dª. María Carmen Barciela Alonso

INFORMAN:

Que la presente tesis, se corresponde con el trabajo realizado por D. Juan José López Mayán, bajo nuestra dirección/tutorización, y autorizamos su presentación, considerando que reúne los requisitos exigidos en el Reglamento de Estudios de Doctorado de la USC, y que como directora/tutora de esta no incurre en las causas de abstención establecidas en la Ley 40/2015.

De acuerdo con lo indicado en el Reglamento de Estudios de Doctorado, declaran también que la presente tesis doctoral es idónea para ser defendida en base a la modalidad de Monográfica con reproducción de publicaciones, en los que la participación del doctorando fue decisiva para su elaboración y las publicaciones se ajustan al Plan de Investigación.

En Santiago de Compostela, a 14 de Julio de 2023

USC
UNIVERSIDADE
DE SANTIAGO
DE COMPOSTELA

USC
UNIVERSIDADE
DE SANTIAGO
DE COMPOSTELA

ACKNOWLEDGEMENTS

USC
UNIVERSIDADE
DE SANTIAGO
DE COMPOSTELA

ACKNOWLEDGEMENTS

Gracias a mis directoras de tesis **Elena** y **Mari Carmen**, estaré siempre agradecido por haberme dado la oportunidad de poder formarme junto a grandes profesionales como vosotras. Vuestro apoyo y cariño estos años ha sido fundamental para mi desarrollo profesional y personal. **Elena**, gracias por tu gran sonrisa en todo momento. **Mari Carmen**, gracias por tus grandes consejos.

Gracias a mi grupo de investigación **GETEE** por tantos años aprendiendo de la mano de grandes profesionales y personas. **Pilar**, **Antonio**, **Raquel** y **Manolo**, gracias por haberme brindado tanto apoyo, cariño y conocimiento desde el primer momento. **Paloma**, gracias por tu paciencia, tenacidad y ayuda, sin ti gran parte de esta tesis no sería posible.

Gracias a mis vecinos de departamento, el grupo **LIDSA**. No se podría haber tenido mejores compañeros, gracias especialmente a ti, **Marta**, tu calidad humana es excepcional. También a vosotras **Mari** y **Mónica** por toda la ayuda que me habéis proporcionado de forma altruista cuando me surgía algún problema.

Gracias a todos los integrantes del proyecto **NanoCulture**, ha sido un placer contribuir junto todos vosotros a avanzar en el conocimiento en lo referente a nanopartículas en productos acuícolas.

Gracias al grupo **Water Quality**, por darme la oportunidad de realizar la estancia con vosotros, especialmente a **Mónica**, **Laura** y **Begoña**, por recibirme con los brazos abiertos en el **INL** y aportarme una perspectiva diferente del mundo nano.

Gracias a todos mis compañeros de laboratorio, por todos los momentos compartidos y vividos. **Thilini**, **Kolita**, **Ala**, **Vanesa**, **Iván**, **Cristian** y **Max**, compartir con vosotros mi tesis fue una experiencia inolvidable. **Blanca**, mi "TFGanda" favorita, gracias por sacarme tanto trabajo de encima y por las grandes charlas en el ICP-MS.

Gracias por todo **Iria**, **Ana** y **Vanesa**. En vosotras encontré la amistad y espero que por muchos años. **Vanesa**, gracias por todos los aportes calóricos tan necesarios en las largas tardes de ordenador. **Ana**, gracias por hacer que tenga la mente más abierta, por tu compañía en mi etapa final y por ser la mejor compañera de congresos. **Iria** desde el principio hasta el final siempre has estado ahí, **gracias por todo**.

Gracias **Eva** y **Bea**, nos encontramos al principio, pero nuestra amistad continua y tengo la certeza de que lo hará siempre. Especialmente a ti **Bea**, sin tu consejo no me habría embarcado en esta **singladura**.

Gracias a vosotros **amigxs**, los de siempre, por todos los buenos momentos en los que me hicisteis desconectar del mundo nano, especialmente gracias a vosotras **Laura**, **Laury**, **Alba** y **Rebeca**.

USC
UNIVERSIDADE DE SANTIAGO DE COMPOSTELA

Gracias **Emma** y **Pepe** sin vuestro apoyo el comienzo de esta tesis no sería posible. Gracias también por supuesto a todos los compañeros de la **Casa del Mar**.

Gracias a mi gran familia. **Mamá** y **Papá** todo lo que soy hoy es gracias a vosotros, estaré siempre agradecido por los valores que me habéis aportado toda la vida.

Gracias **Ali** y **Ángel** por enseñarme a compartir, hacer de mi infancia una infancia feliz e interesante, hacer que sea mejor persona, y por supuesto a ti **Ali** gracias por darme la mejor familia del mundo, **Noelia** y **Xiana**.

Gracias a mis **abuelos**, ojalá fuerais eternos.

Gracias a ti **Yaky** por ser fundamental en mi vida, darme tantos momentos de alegría, enseñarme a ser paciente y una mejor persona, siempre serás mi mejor amigo.

Gracias a ti **Ana**, por ser mi pilar fundamental durante más de diez años, el apoyo incondicional durante toda esta etapa, y mi compañera de vida.

Esta tesis está dedicada a ti.

USC
UNIVERSIDADE DE SANTIAGO DE COMPOSTELA

“How inappropriate to call this planet Earth, when it's quite clearly Ocean”.

- Arthur C. Clarke

USC
UNIVERSIDADE DE SANTIAGO DE COMPOSTELA

USC
UNIVERSIDADE
DE SANTIAGO
DE COMPOSTELA

FUNDING

-European Union, Interreg Atlantic Area, project NANOCULTURE, (reference EAPA590/2018).

-Development of a Strategic Grouping in Materials–AEMAT, (grant number ED431E2018/08).

- Xunta de Galicia (Grupo de Referencia Competitiva, grant numbers ED431C2018/19, ED431C2012/29).

-Ministerio de Economía Industria y Competitividad (projects INNOVANANO, reference RT2018-099222-B-100).

USC
UNIVERSIDADE
DE SANTIAGO
DE COMPOSTELA

USC
UNIVERSIDADE
DE SANTIAGO
DE COMPOSTELA

USC
UNIVERSIDADE
DE SANTIAGO
DE COMPOSTELA

INDEX

USC
UNIVERSIDADE
DE SANTIAGO
DE COMPOSTELA

INDEX

ABBREVIATIONS ..... **i**

ABSTRACT ..... **vii**

RESUMO ..... **xv**

I. INTRODUCTION **1**

I.1 IMPORTANCE OF AQUACULTURE IN THE WORLD, EUROPE AND SPAIN 3

I.2 SPECIES UNDER STUDY 4

I.2.1 Seaweed 4

I.2.2 Mussels 6

I.2.3 Turbot 8

I.2.4 Other studied fish species 9

I.3 NANOMATERIALS 10

I.3.1 Nanomaterial definition, classification, and properties 10

I.3.2 Nanoparticles under study 14

I.3.2.1 Silver nanoparticles 15

I.3.2.2 Titanium dioxide nanoparticles 16

I. 4 ANALYTICAL TECHNIQUES FOR NANOMATERIAL ANALYSIS 18

I.4.1 Sample preparation 19

I.4.2 Continuous separation techniques 22

I.4.2.1 Field-flow fractionation 22

I.4.2.2 Chromatographic techniques 22

I.4.2.3 Electrophoresis 22

I.4.3 Physicochemical characterization and quantification of nanomaterials 23

I.4.3.1 Electron microscopy 23

I.4.3.2 Surface probe microscopy 24

I.4.3.3 Light scattering techniques 24

I.4.3.4 Electroanalytical techniques 25

I.4.3.5 Spectrometric techniques 25

USC UNIVERSIDADE DE SANTIAGO DE COMPOSTELA

I.4.4 Inductively coupled plasma mass spectrometry 26
I.4.4.1 SP-ICP-MS 26
I.4.4.2 SC-ICP-MS 30
I.5 BIOACCUMULATION, BIOACCESSIBILITY AND BIOAVAILABILITY STUDIES 31
REFERENCES 33

II. OBJECTIVES 47

III. METHODOLOGY 51

IV. RESULTS AND DISCUSSION 57

PART A. DEVELOPMENT OF ANALYTICAL METHODOLOGIES FOR SILVER AND TITANIUM DIOXIDE NANOPARTICLES EXTRACTION 59

CHAPTER 1. ULTRASONICATION FOLLOWED BY ENZYMATIC HYDROLYSIS AS A SAMPLE PRE-TREATMENT FOR THE DETERMINATION OF Ag NANOPARTICLES IN EDIBLE SEAWEED BY SP-ICP-MS 61

1.1 ABSTRACT 63
1.2 INTRODUCTION 63
1.3 MATERIALS AND METHODS 65
1.3.1 Instrumentation 65
1.3.2 Reagents 65
1.3.3 Seaweed samples harvesting and exposure trial 66
1.3.4 Microwave-assisted acid digestion 66
1.3.5 Enzymatic hydrolysis for AgNPs extraction 66
1.3.6 Total Ag determination by ICP-MS 66
1.3.7 AgNPs analysis by SP-ICP-MS 67
1.3.8 Scanning transmission electron microscopy analysis of Macerozyme® R-10 extracts 68
1.4 RESULTS AND DISCUSSION 68
1.4.1 Selection of ultrasound-assisted enzymatic hydrolysis conditions for AgNPs extraction 68
1.4.1.1 Ultrasound amplitude 68
1.4.1.2 Ultrasound sonication time 69
1.4.1.3 Pulsed versus continuous sonication 69

1.4.1.4 Type of sonication (bath versus probe) 69
1.4.1.5 Macerozyme® R-10 concentration 71
1.4.1.6 Incubation (extraction) time 71
1.4.2 Stability of AgNPs size under the selected extraction conditions 72
1.4.3 Efficiency of AgNPs extraction 73
1.4.4 Analytical characteristics of the method 73
1.4.4.1 Matrix effect evaluation 73
1.4.4.2 Sensitivity 74
1.4.4.3 Repeatability and analytical recovery 74
1.4.5 Applications 75
1.5 CONCLUSIONS 79
REFERENCES 80

CHAPTER 2. TITANIUM DIOXIDE NANOPARTICLES ASSESSMENT IN SEAWEEDS BY SINGLE PARTICLE INDUCTIVELY COUPLED PLASMA MASS SPECTROMETRY 83
2.1 ABSTRACT 85
2.2 INTRODUCTION 85
2.3 MATERIALS AND METHODS 87
2.3.1 Instrumentation 87
2.3.2 Reagents 87
2.3.3 Seaweed samples 87
2.3.4. Ultrasound-assisted TiO_2NPs lixiviation with TMAH 87
2.3.5 Microwave-assisted acid digestion for total Ti determination 88
2.3.6 Total Ti assessment by ICP-MS 88
2.3.7 TiO_2NPs assessment by SP-ICP-MS 89
2.3.8 HRTEM-EDX analysis of TMAH extracts 89
2.4 RESULTS AND DISCUSSION 90
2.4.1 Variables affecting the TMAH extraction process 90
2.4.2 Stability of TiO_2NPs 92
2.4.3 Analytical features 93
2.4.4 Applications 94
2.5 CONCLUSIONS 97
SUPPLEMENTARY INFORMATION 98

USC UNIVERSIDADE DE SANTIAGO DE COMPOSTELA

REFERENCES 99

PART B. BIOACCUMULATION OF SILVER AND TITANIUM DIOXIDE NANOPARTICLES IN AQUACULTURE PRODUCTS 103

CHAPTER 3. STUDY OF SILVER NANOPARTICLES BIOACCUMULATION IN CULTURED RED AND GREEN SEAWEED 105

3.1 ABSTRACT 107

3.2 INTRODUCTION 107

3.3 MATERIALS AND METHODS 108

3.3.1 Instrumentation 108

3.3.2 Reagents and materials 109

3.3.3 Seaweed culture and exposure to AgNPs 109

3.3.4 Total Ag determination by ICP-MS after microwave-assisted acid digestion 110

3.3.5 AgNPs analysis by SP-ICP-MS after ultrasound-assisted enzymatic extraction .. 111

3.3.6 Analysis of AgNPs in the enzymatic extracts by electron microscopy 112

3.3.7 Statistical analysis 112

3.4 RESULTS AND DISCUSSION 112

3.4.1 Total Ag determination in seaweed exposed to AgNPs by ICP-MS 112

3.4.1.1 Variation of total Ag content in *Palmaria palmata* 113

3.4.1.2 Variation of total Ag content in *Ulva* sp. 115

3.4.2 AgNPs determination in seaweed exposed to AgNPs by SP-ICP-MS 115

3.4.2.1 AgNPs content and size distribution in *Palmaria palmata* 116

3.4.2.2 AgNPs content and size distribution in *Ulva* sp. 119

3.4.3 Characterization of AgNPs in seaweed enzymatic extracts by electron microscopy 122

3.5 CONCLUSIONS 123

SUPPLEMENTARY INFORMATION 124

REFERENCES 127

CHAPTER 4. BIOACCUMULATION OF TITANIUM DIOXIDE NANOPARTICLES IN GREEN (*Ulva* sp.) AND RED (*Palmaria palmata*) SEAWEED 131

4.1 ABSTRACT 133

4.2 INTRODUCTION 133

4.3 MATERIALS AND METHODS 134

4.3.1 Instrumentation 134

USC UNIVERSIDADE DE SANTIAGO

4.3.2 Reagents 135
4.3.3 Seaweed sample cultivation and exposure to TiO_2NPs 136
4.3.4 Microwave-assisted acid digestion 136
4.3.5 TMAH ultrasound-assisted TiO_2NPs extraction 136
4.3.6 Total Ti determination by ICP-MS and TiO_2NPs analysis by SP-ICP-MS 137
4.3.7 Localization and identification of TiO_2NPs on/in seaweed tissue by electron microscopy techniques. 137
4.4 RESULTS AND DISCUSSION 137
4.4.1 TiO_2NPs characterization 137
4.4.2 Total Ti determination in seaweed samples exposed to TiO_2NPs 138
4.4.2.1 Variation of total Ti content in *Palmaria palmata* (red seaweed) 138
4.4.2.2 Variation of total Ti content in *Ulva* sp. (green seaweed) 140
4.4.3 Analysis of TiO_2NPs in seaweed 142
4.4.3.1 Size distribution and TiO_2NPs content in *Palmaria palmata* 145
4.4.3.2 Size distribution and TiO_2NPs content in *Ulva* sp. 148
4.5 CONCLUSIONS 150
SUPPLEMENTARY INFORMATION 151
REFERENCES 165

CHAPTER 5. BIOACCUMULATION OF SILVER NANOPARTICLES IN MUSSELS AND TURBOT FROM THE ATLANTIC AREA 169
5.1 ABSTRACT 171
5.2 INTRODUCTION 171
5.3 MATERIALS AND METHODS 173
5.3.1 Instrumentation 173
5.3.2 Reagents, standards, and materials 174
5.3.3 Mussel and turbot cultivation 174
5.3.4 Microwave-assisted acid digestion and total Ag determination 175
5.3.5 Enzymatic extraction and AgNPs analysis 175
5.4 RESULTS AND DISCUSSION 176
5.4.1 Mussel bioaccumulation assay 176
5.4.1.1 Total Ag content in mussel samples exposed to PVP-AgNPs 176
5.4.1.2 AgNPs content in mussel samples after exposure 179
5.4.2 Turbot bioaccumulation assay 183

USC UNIVERSIDADE DE SANTIAGO DE COMPOSTELA

5.4.2.1 Total Ag content in turbot samples exposed to PVP-AgNPs 183
5.4.2.2 AgNPs content in turbot samples after exposure 185
5.5 CONCLUSIONS 186
SUPPLEMENTARY INFORMATION 187
REFERENCES 191

CHAPTER 6. BIOACCUMULATION PATTERNS IN AQUACULTURE MUSSELS AND TURBOTS EXPOSED TO DIFFERENT SIZES OF TIO_2NPs 195
6.1 ABSTRACT 197
6.2 INTRODUCTION 197
6.3 MATERIALS AND METHODS 199
6.3.1 Instrumentation 199
6.3.2 Reagents and materials 199
6.3.3 Bioaccumulation study design 200
6.3.4 Microwave-assisted acid digestion and total Ti determination by ICP-MS 201
6.3.5 Enzymatic extractions and determination of TiO_2NPs by SP-ICP-MS 201
6.4 RESULTS AND DISCUSSION 202
6.4.1 Mussel bioaccumulation tests 202
6.4.1.1 Total Ti in mussels 202
6.4.1.2 Total Ti in mussel shells 206
6.4.1.3 TiO_2NPs in mussels 207
6.4.2 Turbot bioaccumulation tests 210
6.4.2.1 Total Ti in turbot 210
6.4.2.2 Total Ti in turbot feces 212
6.4.2.3 TiO_2NPs in turbot 214
6.5 CONCLUSIONS 215
SUPPLEMENTARY INFORMATION 216
REFERENCES 220

CHAPTER 7. PRESENCE OF SILVER AND TITANIUM DIOXIDE NANOPARTICLES IN MARINE SAMPLES FROM THE ATLANTIC AREA 223
7.1 ABSTRACT 225
7.2 INTRODUCTION 225
7.3 MATERIALS AND METHODS 227
7.3.1 Instrumentation 227

7.3.2 Reagents, standards, and materials 227
7.3.3 Sampling and sample pretreatment 228
7.3.4 Total Ag and Ti determination 229
7.3.5. Determination of AgNPs and TiO_2NPs 229
7.4 RESULTS AND DISCUSSION 230
7.4.1 Analytical features of the methodologies 230
7.4.2 Applications 230
7.4.2.1 Total Ag determination 230
7.4.2.2 Total Ti determination 235
7.4.2.3 AgNPs determination 239
7.4.2.4 TiO_2NPs determination 241
7.5 CONCLUSIONS 248
SUPPLEMENTARY INFORMATION 249
REFERENCES 253

PART C. BIOAVAILABILITY OF SILVER AND TITANIUM DIOXIDE NANOPARTICLES IN AQUACULTURE PRODUCTS 257

CHAPTER 8. BIOAVAILABILITY STUDY OF SILVER AND TITANIUM DIOXIDE NANOPARTICLES FROM SEAWEED AND MUSSELS USING CACO-2 CELLS 259
8.1 ABSTRACT 261
8.2 INTRODUCTION 261
8.3 MATERIALS AND METHODS 263
8.3.1 Instrumentation 263
8.3.2 Standards, reagents, and materials 263
8.3.3 Seaweed and mussels samples 264
8.3.4 Sample digestion and extraction procedures 264
8.3.5 *In vitro* digestion procedures 265
8.3.5.1 Bioaccesibility assay 265
8.3.5.2 Cellular transport assay 265
8.3.6 Cell viability 266
8.3.7 Ag and Ti determination by ICP-MS 267
8.3.8 AgNPs and TiO_2NPs nanoparticles determination by SP-ICP-MS and SC-ICP-MS 267
8.4 RESULTS AND DISCUSSION 268

USC UNIVERSIDADE DE SANTIAGO DE COMPOSTELA

8.4.1 Viability assay 268
8.4.2 Total Ag and AgNPs bioaccessibility 268
8.4.3 Total Ti and TiO_2NPs bioaccessibility 271
8.4.4 Total Ag and AgNPs cellular transport 273
8.4.5 Total Ti and TiO_2NPs cellular transport 276
8.4.6 AgNPs and TiO_2NPs in the Caco-2 cell monolayer 278
8.5 CONCLUSIONS 281
SUPPLEMENTARY INFORMATION 282
REFERENCES 286

V. CONCLUSIONS 289

ANNEX I. LIST OF PUBLICATIONS AND CONTRIBUTION 293

ANNEX II. PERMISSIONS 297

USC
UNIVERSIDADE DE SANTIAGO DE COMPOSTELA

ABBREVIATIONS

USC
UNIVERSIDADE
DE SANTIAGO
DE COMPOSTELA

USC
UNIVERSIDADE
DE SANTIAGO
DE COMPOSTELA

ABBREVIATIONS

A

AF4	Asymmetric flow field-flow fractionation
AFM	Atomic force microscopy
AGE	Agarose gel electrophoresis
AgNPs	Silver nanoparticles
ATP	Adenosine triphosphate
ATR-FTIR	Attenuated total reflection-Fourier transform-infrared

B

BCFs	Bioconcentration factors
BSA	Bovine serum albumin

C

CE	Capillary electrophoresis
CB	Conduction band
CPE	Cloud point extraction
CPT	Cloud point temperature

D

DEPs	Differentially expressed proteins
DLS	Dynamic light scattering
DNA	Deoxyribonucleic acid
DRC	Dynamic reaction cell
DSSCs	Dye-sensitive solar cells

E

EC	European Commission
EDI	Estimated daily intake
EDL	Electrical double layer
EDX	Energy dispersive X-rays
EELS	Electron energy loss spectrometry
EFSA	European Food Safety Authority
EM	Electron microscopy
ENMs	Engineered nanomaterials
EPA	Environmental Protection Agency
ESEM	Environmental scanning electron microscopy
ETAAS	Electrothermal atomic absorption spectrometry
EU	European Union
EXAFS	Extended X-ray absorption fine structure

F

FDA	Food and Drug Administration
FFF	Field-flow fractionation

USC UNIVERSIDADE DE SANTIAGO DE COMPOSTELA

FlFFF	Flow field-flow fractionation
FTIR	Fourier transform infrared
G	
GE	Gel electrophoresis
GI	Gastrointestinal
H	
HAADF	High-angle annular dark field
HDC	Hydrodynamic chromatography
HIV	Human immunodeficiency virus
HRSTEM	High-resolution scanning transmission electron microscopy
HRTEM	High-resolution transmission electron microscopy
I	
IARC	International Agency for Research on Cancer
ICP-MS	Inductively coupled plasma mass spectrometry
ICP-OES	Inductively coupled plasma optical emission spectrometry
IR	Infrared
ISO	International Organization for Standardization
K	
KED	Kinetic energy discrimination
L	
LLE	Liquid-liquid extraction
LOD	Limit of detection
LOQ	Limit of quantification
LOD_{number}	Concentration detection limit of nanoparticles
LOD_{size}	Size detection limit of nanoparticles
M	
MALS	Multi-angle light scattering
N	
NMs	Nanomaterials
NOM	Natural organic matter
NPs	Nanoparticles
NSOM	Near-field scanning optical microscopy
NTA	Nanoparticle tracking analysis
O	
OECD	Organization for Economic Co-operation and Development
P	
PAGE	Polyacrylamide gel electrophoresis
PAHs	Polycyclic aromatic hydrocarbons
PCC	Particle collision coulometry

USC UNIVERSIDADE DE SANTIAGO DE COMPOSTELA

PEG	Polyethylene glycol
PVP	Polyvinylpyrrolidone
R	
ROS	Reactive oxygen species
S	
SC-ICP-MS	Single cell inductively coupled plasma mass spectrometry
SD	Standard deviation
SdFFF	Sedimentation field-flow fractionation
SEC	Size exclusion chromatography
SEM	Scanning electron microscopy
SERS	Surface-enhanced Raman spectrometry
SPE	Solid phase extraction
SP-ICP-MS	Single particle inductively coupled plasma mass spectrometry
SPM	Surface probe microscopy
SPR	Surface plasmon resonance
STEM	Scanning transmission electron microscopy
STM	Scanning tunnelling microscopy
T	
TE	Transport efficiency
TEM	Transmission electron microscopy
TiO_2	Titanium dioxide
TiO_2NPs	Titanium dioxide nanoparticles
TMAH	Tetramethylammonium hydroxide
U	
UAE	Ultrasound-assisted extraction
UF	Ultrafiltration
UV	Ultraviolet
V	
VB	Valence band
VIP	Voltammetry of immobilized particles
X	
XANES	X-ray absorption near edge structure spectrometry
XAS	X-Ray absorption spectrometry
XRD	X-Ray diffraction

USC UNIVERSIDADE DE SANTIAGO DE COMPOSTELA

USC
UNIVERSIDADE
DE SANTIAGO
DE COMPOSTELA

USC
UNIVERSIDADE
DE SANTIAGO
DE COMPOSTELA

ABSTRACT

USC
UNIVERSIDADE
DE SANTIAGO
DE COMPOSTELA

ABSTRACT

The constant growth of the world's population demands ever-increasing food production. Pollution and population growth make fishing a non-renewable resource, thus aquaculture is experiencing a very important increase in recent years as a safe source of protein-based food. Aquaculture production has been growing steadily since 1970, surpassing fishing, with 57.3% of world production in 2020. Currently, the main aquaculture-producing country worldwide is China, with Spain in the 25th position.

Although the predominant aquaculture species in the world are fish, algae, mollusks, and crustaceans, in the EU the predominant species are only mollusks and fish. Laminaria (*Saccharina japonica*), European mussels (*Mytilus galloprovincialis* and *Mytilus edulis*), sea bass (*Dicentrachus labrax*), sea bream (*Sparus aurata*), and turbot (*Scophthalmus maximus*) production are very important worldwide. The mainly produced species in the EU are the European mussel, sea bream, sea bass, and Atlantic salmon (*Salmo salar*).

Spain is the main European aquaculture producer in tons followed by France, Italy, and Greece. According to the Spanish Ministry of Agriculture, Fisheries and Food, *Mytilus galloprovincialis* are the most produced mollusks species in Spain, where 98% of production takes place in Galicia (Norwest of Spain). The next species captured in Spain by tons in 2021 were sea bass, rainbow trout (*Oncorhynchus mykiss*), sea bream, and turbot.

Taking into account the global data, due to their high consumption in the Eastern diet, and their recent increase in the Western diet consumption, two types of seaweed (photosynthetic organisms) will be studied in this doctoral thesis. Furthermore, due to the European and Spanish production and their economic importance, the main selected species under study will be mussels (benthic bivalve mollusks), and turbot (benthic fish predators).

The study of the presence of emergent contaminants in aquaculture matrices is very important to ensure food safety and quality. Nanomaterials can be considered emergent contaminants, due to their extensive use in industry and their disposal and persistence in the environment.

The high specific surface area to volume ratio of nanomaterials and nanoparticles changes the physicochemical characteristics from those of bulk substances or larger particles. Due to their novel properties, nanomaterials (NMs) and nanoparticles (NPs) have a wide range of applications in different fields including energy, catalysis, photocatalysis, optics, medicine, industry, electronics and computing, agriculture, environment, and personal and care products, among others. Thus the investigation regarding NMs and NPs has experienced exponential growth in the last few years.

Although there are several kinds of nanoparticles, inorganic nanoparticles like silver nanoparticles (AgNPs) and titanium dioxide nanoparticles (TiO_2NPs) are two of the most employed in the industry due to their exceptional properties.

AgNPs' properties include their biocidal effect, high electrical and thermal conductivity, mechanical, coloration, catalytic, UV-protection properties, and use in surface-enhanced Raman spectrometry (SERS). Thus, AgNPs are commonly applied in biomedical, textiles, health care, electronics, optics, catalysis, environment, food, and even agriculture.

On the other hand, TiO_2NPs' properties include their opacity, photoactivity and photocatalytic properties. Thus, TiO_2NPs are used in several applications including inorganic UV filters, dye-sensitive solar cells (DSSCs), environmental treatment and the decomposition

of harmful chemicals in wastewater, odor removal, and construction of self-cleaning and anti-fogging glasses, and even in printing inks, paper, plastic, condensers, synthetic fibers, ceramics, and electronic components.

The extensive use of AgNPs and TiO_2NPs causes them to be released into the environment where they can be transformed (by agglomeration, aggregation, dissolution phenomena, chemical transformations, or interaction with organic matter, and other contaminants) depending on factors like pH, nanoparticle coating, or even the type of particle.

Thus, the AgNPs and TiO_2NPs can be assimilated and bioaccumulated by marine organisms, and even pass to high links in the food chain. Furthermore, several studies indicate the possible toxicity of these particles in marine organisms, and even in humans. Then, more investigation in this area is necessary. Regarding this, *in vitro* models are commonly employed to study the bioavailability of nanomaterials through cellular transport using cultured cells.

Studying the presence of NMs and NPs in environmental matrices like marine organisms is a challenge due to the complex environmental systems, with low NPs concentrations, in the presence of natural particles of similar or even different natures. The qualitative information about nanomaterials implies their detection and their chemical and physical characterization. Quantitative information about nanomaterials implies the determination of mass and particle number concentration information. Therefore, appropriate separation, pre-concentration, characterization and quantification techniques are necessary for NMs analysis in complex matrices.

Normally the detection, characterization, and quantification of NMs in complex matrices require the combination of various analytical techniques. Sample NPs extractions are commonly needed to isolate NPs from different matrices without nanoparticle alterations. Single particle inductively coupled plasma mass spectrometry (SP-ICP-MS) is one of the most common techniques to study NPs in environmental and biological matrices. SP-ICP-MS is a powerful ICP-MS method for the detection, quantification and characterization of NPs, colloids, and microparticles. It reports qualitative information on the presence of dissolved forms, the quantification of NPs as nanoparticle number as well as mass concentration, and the characterization of the size distribution. SP-ICP-MS together with electron microscopy techniques are the perfect tools combination to obtain NMs information in complex matrices.

Seaweeds are rich in bioactive compounds like polysaccharides, polyphenols, proteins, omega-3, omega-6, fatty acids, selenium, iodine, vitamin B-12, and dietary fibre. They have antiviral, anticancer, and anticoagulant properties. They have applications in the pharmaceutical, cosmetic, textile, and food industries, and recently increased their consumption as food in the Western countries. However, due to the characteristics of their cell wall, seaweeds have the potential to preconcentrate minerals, trace elements and even contaminants from the surrounding water at higher concentrations.

Mussels are very consumed shellfish around the world, especially in the European Union due to their high content of proteins, omega-3, carbohydrates, polyunsaturated fatty acids, and iodine. However, they are also commonly employed in pollution monitoring, due to their presence in all the oceans of the world, their gregarious behaviour, and their capacity to filter high amounts of water, acting as filter feeders.

On the other hand, turbot is a carnivore benthic flatfish highly appreciated around the world due to its high nutritional value and high protein content. However, turbot can accumulate heavy metals throughout the food chain.

Due to their properties and their great consumption, the number of studies about these species has not stopped growing in the last 50 years, being the Agricultural and Biological Sciences, and Environmental Science the main investigation research areas.

USC UNIVERSIDADE DE SANTIAGO DE COMPOSTELA

Therefore, in this doctoral thesis, the bioaccumulation and bioavailability of AgNPs and TiO_2NPs in these important aquaculture products (algae, mussels and turbot) were studied. For that, the development of analytical methodologies for NPs extraction and subsequent determination was necessary. Thus, this doctoral thesis is divided into 3 parts including 8 chapters.

PART A: DEVELOPMENT OF ANALYTICAL METHODOLOGIES FOR SILVER AND TITANIUM DIOXIDE NANOPARTICLES EXTRACTION

CHAPTER 1. Ultrasonication followed by enzymatic hydrolysis as a sample pre-treatment for the determination of Ag nanoparticles in edible seaweed by SP-ICP-MS.

This chapter describes the optimization of the analytical methodology for the separation of AgNPs from seaweed using an ultrasound-assisted enzymatic hydrolysis method and posterior determination by SP-ICP-MS.

Parameters affecting the isolation of AgNPs were optimized using a *Palmaria palmata* (red seaweed) sample previously exposed to AgNPs. The parameters optimized include the type of sonication (bath versus ultrasonic probe), ultrasound amplitude, sonication time, sonication mode (pulsed versus continuous sonication), the concentration of the enzymatic mixture (Macerozyme® R-10), and enzymatic hydrolysis time. The stability of AgNPs during extraction was tested by transmission electron microscopy (TEM) and using a standard of 15 nm of polyvinylpyrrolidone (PVP)-coated AgNPs analyzed by SP-ICP-MS. The extraction efficiency was also checked by comparing the total content in a digested sample with the total content in the same sample extract, with an 80% of extraction percentage. The analytical performance was also evaluated with good results for ICP-MS and SP-ICP-MS. For SP-ICP-MS, the sensitivity of the method was evaluated through the limits of detection. The LOD_{size} were 14 and 12 nm for the 5σ and 3σ criteria, respectively, and the LOD_{number} were 2.40×10^6 part L^{-1} (instrumental limit) and 4.34×10^7 part g^{-1} (referred to wet seaweed sample). Good precision (RSD<10%) and accuracy with recovery percentages of 112±12% were obtained. Finally, the optimized and validated methodology was applied to the analysis of several red (*Palmaria palmata*) and green (*Ulva* sp.) seaweed samples.

CHAPTER 2. Titanium dioxide nanoparticles assessment in seaweeds by single particle inductively coupled plasma mass spectrometry.

This chapter describes the optimization of a method for TiO_2NPs separation from seaweed using an alkaline ultrasound-assisted extraction (UAE) procedure with tetramethylammonium hydroxide (TMAH) and posterior determination by SP-ICP-MS.

The effect of the TMAH percentage in the extracting solution, as well as the volume of extracting solution and sonication (extraction) time, has been fully assessed. Additional experiments also showed that TiO_2NPs were quantitatively released from the seaweed matrix in one UAE step since the analysis of residues gave TiO_2NPs concentrations lower than the limit of quantification (LOQ) of the method. Experiments regarding TiO_2NPs stability showed that the extracted NPs are stable since there were no changes in the number of TiO_2NPs and TiO_2NPs size distributions when exposing TiO_2NPs standards to the optimized extractive conditions. The SP-ICP-MS methodology was properly validated with 50 and 100 nm TiO_2NPs standards. The analytical performance showed good analytical recoveries (115% and 112% for 50 and 100 nm TiO_2NPs standards, respectively), and good reproducibilities (2% for size and

USC DE COMPOSTELA

16% for the number of TiO_2NPs). The sensitivity of the methodology was also assessed by the limits of detection. The LOD_{size} were 37 and 31 nm for the 5σ and 3σ criteria, respectively, and the LOD_{number} were 1.43×10^6 part L^{-1} (instrumental limit) and 5.72×10^4 part g^{-1} (referred to wet seaweed sample). Selected extracts of *Palmaria palmata* and *Ulva* sp. were also subjected to HRTEM-EDX. Finally, the methodology was applied for the analysis of TiO_2NPs in several seaweed samples from the Galician and Irish coasts.

PART B: BIOACCUMULATION OF SILVER AND TITANIUM DIOXIDE NANOPARTICLES IN AQUACULTURE PRODUCTS

CHAPTER 3. Study of silver nanoparticles bioaccumulation in cultured red and green seaweed.

In this chapter, the bioaccumulation of polyvinylpyrrolidone-coated silver nanoparticles (PVP-AgNPs) in red (*Palmaria palmata*) and green (*Ulva* sp.) seaweed was investigated. The bioaccumulation study lasted 28 days in which seaweeds were exposed to different concentrations of PVP-AgNPs (0.1 and 1.0 mg L^{-1}) in marine growing media containing phytoplankton. For the total Ag content determination, the samples were subjected to microwave-assisted acid digestion before analysis by ICP-MS. Ultrasound-assisted enzymatic extraction with Macerozyme® R-10 was used for NPs isolation from the samples, before SP-ICP-MS analysis for the determination of AgNPs content and size distributions.

The maximum concentrations of total Ag measured in the present study were: 0.52±0.04 μg g^{-1} w.w. (wet weight) (at day 21, exposure to 0.1 mg L^{-1} of PVP-AgNPs) and 0.79±0.06 μg g^{-1} w.w. (at day 14, 1.0 mg L^{-1}) in *Palmaria palmata*; and 0.26±0.04 μg g^{-1} w.w. (at day 28, 0.1 mg L^{-1}) and 0.46±0.15 μg g^{-1} (at day 21, 1.0 mg L^{-1}) in *Ulva* sp. The maximum concentrations of AgNPs were achieved at 14 days for *Palmaria palmata* ($1.63\times10^9\pm5.47\times10^8$ part g^{-1} w.w., 1.0 mg L^{-1}) and at 28 days for *Ulva* sp. ($3.23\times10^9\pm2.34\times10^7$ part g^{-1} w.w. , 1.0 mg L^{-1}) with most frequent sizes of approximately 20 nm. Furthermore, these AgNPs most frequent sizes found in the enzymatic extracts measured by SP-ICP-MS agreed with those measured by TEM found in the enzymatic extracts of *Palmaria palmata* and *Ulva* sp.

CHAPTER 4. Bioaccumulation of titanium dioxide nanoparticles in green (*Ulva* sp.) and red (*Palmaria palmata*) seaweed.

In this chapter, red (*Palmaria palmata*) and green (*Ulva* sp.) seaweed have been exposed to two different concentrations (0.1 and 1.0 mg L^{-1}) of citrate-TiO_2NPs of 5 nm and 25 nm for 28 days. For the total Ti determination, the samples were submitted to microwave-assisted acid digestion before the ICP-MS analysis. TiO_2NPs were extracted from the matrix by TMAH alkaline extraction. Then, the number and size of accumulated TiO_2NPs in the alkaline extracts have been assessed by SP-ICP-MS.

Titanium concentrations measured in *Ulva* sp. were higher than those found in *Palmaria palmata* for the same conditions of exposure. The maximum Ti concentration (61.96±15.49 μg g^{-1} w.w.) was measured in *Ulva* sp. after 28 days of exposure to 1.0 mg L^{-1} of 5 nm TiO_2NPs. The concentration and sizes of TiO_2NPs determined by SP-ICP-MS in alkaline seaweed extracts were similar for both seaweeds exposed to 5 and 25 nm TiO_2NPs.

Results indicate that the element is accumulated in *Ulva* sp. mainly as ionic Ti or nanoparticles smaller than the limit of detection in size (27 nm). Furthermore, the

USC UNIVERSIDADE DE SANTIAGO DE COMPOSTELA

internalization of TiO_2NPs in *Ulva* sp. was confirmed by electron microscopy (TEM/STEM) in combination with energy dispersive X-ray analysis (EDX).

CHAPTER 5. Bioaccumulation of silver nanoparticles in mussels and turbot from the Atlantic area.

In this study, mussels (*Mytilus edulis*) and turbots (*Scophthalmus maximus*) were exposed to 15 nm PVP-AgNPs during long exposure times. In the case of mussels, the bioaccumulation assay lasted 28 days. Mussels were exposed to 0.1 and 1.0 mg L^{-1} of PVP-AgNPs, and the entire mussels were homogenized. Turbots exposed to 0, 0.25, 0.75, and 1.5 mg PVP-AgNPs kg^{-1} for 105 days, and the flesh+skin, the liver, and the kidney were studied separately. Total Ag concentration and AgNPs concentration and size distribution in both specimens were determined by ICP-MS and SP-ICP-MS, respectively.

The highest silver concentration in mussels was 1.40±0.25 µg g^{-1} w.w. at the low exposure dose and 28 exposure days. The highest AgNPs concentration in mussels was $2.14\times10^{8}\pm4.49\times10^{7}$ NPs g^{-1} w.w. at the high exposure dose and 28 exposure days. The presence in the tanks of a discharged surface scum containing Ag and AgNPs agrees with the no bioaccumulation at a high exposure dose in comparison to the low exposure dose. On the other hand, in the turbot bioaccumulation assay, the highest Ag concentrations were found in the liver (non-edible part) reaching 6.47±2.46 µg g^{-1} w.w., but no particles were detected in this part. The bioaccumulation study showed the safety of turbot consumption and highlighted the need for a proper depuration process in mussels.

CHAPTER 6. Bioaccumulation patterns in aquaculture mussels and turbots exposed to different sizes of TiO_2NPs.

In this chapter, two predominant aquaculture species in Spain are being examined to determine TiO_2NPs' impact and bioaccumulation. A benthic filtering bivalve (*Mytilus edulis*) and a benthic predator (*Scophthalmus maximus*) were selected for the bioaccumulation assays. The exposure study lasted 28 days in mussels and 90 days in turbot, and specimens were exposed to different concentrations of citrate-TiO_2NPs of 25 and 5 nm. ICP-MS and SP-ICP-MS were used for Ti determination, and TiO_2NPs content and size distribution determination, respectively.

In mussels, Ti and TiO_2NPs concentrations reached 5.19±3.19 µg g^{-1} w.w. and $2.28\times10^{8}\pm5.84\times10^{7}$ NPs g^{-1} w.w. after exposure to 1.0 mg L^{-1} of 25 nm TiO_2NPs for 28 days, and 4.26±0.85 µg g^{-1} w.w. and $4.79\times10^{8}\pm2.36\times10^{8}$ NPs g^{-1} w.w. for 1.0 mg L^{-1} of 5 nm TiO_2NPs for 14 and 21 exposure days, respectively. Mussels exposed to the high dose of 5 nm TiO_2NPs, showed Ti bioaccumulation and more fragile shells. In shells, the highest Ti concentration reached was 12.43±3.45 µg g^{-1} d.w. (dry weight). The highest Ti concentration was found in turbot liver (non-edible part), reaching 1.62±0.44 µg g^{-1} w.w. at 90 exposure days and a dose of 1.5 mg Kg^{-1} fish and day of 5 nm TiO_2NPs. Furthermore, the feces from turbots were also analyzed, and the result showed expelled Ti, reaching a concentration of 40.99±6.62 µg g^{-1} w.w. in the feces of turbot fed with 1.5 mg kg^{-1} of fish and day of 5 nm TiO_2NPs. The results showed the safety of turbot consumption and highlighted the need for a correct depuration process of mussels before commercialization.

USC UNIVERSIDADE DE SANTIAGO DE COMPOSTELA

CHAPTER 7. Presence of silver and titanium dioxide nanoparticles in marine samples from the Atlantic area.

To shed light on the AgNPs and TiO_2NPs presence in several aquatic organisms widely consumed in the Atlantic region, and to preserve food safety, research into these emergent pollutants is required. This chapter reported the presence of AgNPs and TiO_2NPs in photosynthetic organisms such as edible seaweed (*Alaria esculenta*), bivalve mollusks as mussels (*Mytilus edulis*), and fishes as high predators in the food chain (*Salmo*, *Dicentrarchus labrax*, and *Sparus aurata*). To determine the total content of Ag and Ti, seaweed, mussels, and dissected fishes were submitted to microwave-assisted acid digestions before ICP-MS analysis. To determine the AgNPs and TiO_2NPs content and size distribution, enzymatic and alkaline extractions were selected before SP-ICP-MS analysis.

The highest Ag concentrations were found in salmon livers, reaching a value of 0.73±0.07 μg g^{-1} w.w. of Ag, and the AgNPs content reached $2.74\times10^{8}\pm7.78\times10^{7}$ AgNPs g^{-1} w.w. However, the highest Ti concentration was found in seaweed. The total titanium concentration reached 8.48±1.69 μg g^{-1} w.w. and the highest nanoparticle content achieved was $1.35\times10^{8}\pm8.06\times10^{7}$ TiO_2NPs g^{-1} w.w. The results showed the highest accumulation of Ag and Ti in unedible parts of the fishes, but the concentrations detected in the analyzed mussels and especially in seaweed highlight the need for proper depuration before their consumption.

PART C: BIOAVAILABILITY OF SILVER AND TITANIUM DIOXIDE NANOPARTICLES IN AQUACULTURE PRODUCTS

CHAPTER 8. Bioavailability study of silver and titanium dioxide nanoparticles from seaweed and mussels using Caco-2 cells.

This chapter reported the bioaccessibility and the bioavailability of total Ag and Ti, AgNPs and TiO_2NPs in raw and cooked seaweed (*Palmaria palmata* and *Ulva* sp.), and in cooked mussels (*Mytilus edulis*) where all the specimens were exposed to 1.0 mg L^{-1} of 15 nm PVP-AgNPs, to 1.0 mg L^{-1} of 25 nm citrate-TiO_2NPs, and 1.0 mg L^{-1} of 5 nm citrate-TiO_2NPs, in all cases for 28 days. *In vitro* treatments simulating human gastrointestinal digestion were performed to determine the total Ag, total Ti, AgNPs and TiO_2NPs bioaccessibility. Cellular transports for the bioavailability assays were simulated using Caco-2 cell cultures. The gastrointestinal bioaccessible fractions were incubated in six-plate Transwells® for 1 hour, guaranteeing the cell monolayer integrity.

Total Ag and Ti in the digest samples, the bioaccessible fractions, and the apical, and basolateral fractions were determined by ICP-MS. The AgNPs and TiO_2NPs concentrations in the sample extracts, bioaccessible fractions, apical, and basolateral fractions were determined by SP-ICP-MS. Finally, AgNPs and TiO_2NPs content internalized in Caco-2 cells was determined by single-cell-ICP-MS (SC-ICP-MS).

USC UNIVERSIDADE DE SANTIAGO DE COMPOSTELA

RESUMO

USC
UNIVERSIDADE
DE SANTIAGO
DE COMPOSTELA

RESUMO

O constante crecemento da poboación mundial esixe unha produción de alimentos cada vez maior. A contaminación e a multiplicación da poboación fan da pesca un recurso non renovable, polo que a acuicultura está a experimentar un incremento moi importante nos últimos anos como fonte segura de alimentos a base de proteínas.

A produción acuícola crece de forma constante dende 1970, superando á pesca, co 57,3% da produción mundial en 2020. Actualmente, o principal país produtor de acuicultura a nivel mundial é a China, con España no posto 25.

Aínda que as especies acuícolas predominantes no mundo son os peixes, as algas, os moluscos e os crustáceos, na UE as especies predominantes son só os moluscos e os peixes. A produción de laminaria (*Saccharina japonica*), mexillón europeo (*Mytilus galloprovincialis* e *Mytilus edulis*), robaliza (*Dicentrachus labrax*), dourada (*Sparus aurata*) e rodaballo (*Scophthalmus maximus*) son moi importantes a nivel mundial. As especies que se producen principalmente na UE son o mexillón europeo, a dourada, a robaliza, e o salmón Atlántico (*Salmo salar*).

España é o principal produtor acuícola europeo en toneladas, seguido de Francia, Italia e Grecia. Segundo o Ministerio de Agricultura, Pesca e Alimentación de España, *Mytilus galloprovincialis* é a especie de molusco máis producida en España, onde o 98% da produción ten lugar en Galicia (noroeste de España). As seguintes especies capturadas en España por toneladas en 2021 foron a robaliza, a troita arco da vella (*Oncorhynchus mykiss*), a dourada e o rodaballo.

Tendo en conta os datos globais, o seu alto consumo na dieta oriental, e o seu recente incremento no consumo na dieta occidental, nesta tese de doutoramento estudaranse dous tipos de algas (organismos fotosintéticos). Ademais, debido á produción europea e española e á importancia económica, as principais especies seleccionadas para o seu estudo serán os mexillóns (moluscos bivalvos bentónicos) e os rodaballos (peixes depredadores bentónicos).

O estudo dos contaminantes emerxentes na acuicultura é moi importante para garantir a seguridade e calidade dos alimentos. Os nanomateriais poden ser considerados contaminantes emerxentes, debido ao seu uso extensivo na industria, á súa eliminación, e á súa persistencia no medio ambiente.

O aumento da relación entre a superficie específica e o volume dos nanomateriais e das nanopartículas cambia as características fisicoquímicas das substancias a granel ou das partículas máis grandes. Debido ás súas propiedades novidosas, os nanomateriais (NMs) e as nanopartículas (NPs) teñen unha ampla gama de aplicacións en diferentes campos, incluíndo enerxía, catálise, fotocatálise, óptica, medicina, industria electrónica e informática, agricultura, medio ambiente, e productos de coidado persoal, entre outros. Así, a investigación sobre os NMs e as NPs experimentou un crecemento exponencial nos últimos anos.

Aínda que existen varios tipos de nanopartículas, as inorgánicas como as nanopartículas de prata (AgNPs) e as de dióxido de titanio (TiO_2NPs) son dúas das máis empregadas na industria debido as súas propiedades excepcionais.

As propiedades das AgNPs inclúen o seu efecto biocida, a alta condutividade eléctrica e térmica, as propiedades mecánicas, de coloración, catalíticas, de protección UV, e o seu emprego na espectroscometría Raman mellorada en superficie (SERS). Así, as AgNPs

USC UNIVERSIDADE DE SANTIAGO DE COMPOSTELA

aplícanse habitualmente en biomédica, téxtil, coidado da saúde, electrónica, óptica, catálise, medio ambiente, alimentación e mesmo agricultura.

Por outra banda, as propiedades das TiO_2NPs inclúen a súa opacidade, fotoactividade e propiedades fotocatalíticas. Así, as TiO_2NPs utilízanse en varias aplicacións, incluíndo filtros UV inorgánicos, células solares sensibles a colorantes, tratamento ambiental e descomposición de produtos químicos nocivos nas augas residuais, eliminación de cheiros e construción de lentes autolimpadores e antiempañamento, e mesmo en tintas de impresión, papel, plástico, condensadores, fibras sintéticas, cerámica e compoñentes electrónicos.

O uso extensivo das AgNPs e TiO_2NPs fai que sexan liberadas no medio ambiente onde poden transformarse (por fenómenos de aglomeración, agregación e disolución, transformacións químicas ou interacción con materia orgánica e outros contaminantes) dependendo de factores como o pH, o revestimento, ou incluso o tipo de partícula.

Así, as AgNPs e as TiO_2NPs poden ser asimiladas e bioacumuladas por organismos mariños, e mesmo pasar a altos elos da cadea alimentaria. Ademais, varios estudos indican a posible toxicidade deste tipo de partículas en organismos mariños, e mesmo en humanos sendo necesaria a realización de máis estudos nesta área de investigación. Neste sentido, os modelos *in vitro* empréganse habitualmente para estudar a biodispoñibilidade de nanomateriais mediante o transporte celular utilizando células cultivadas.

Estudar a presenza de NMs e NPs en matrices ambientais como organismos mariños é un reto debido aos complexos sistemas ambientais, con concentracións baixas de NPs, en presenza de partículas naturais de natureza semellante ou incluso diferente. A obtención de información cualitativa dos nanomateriais implica a súa detección e a súa caracterización química e física. A información cuantitativa sobre os nanomateriais implica a determinación da concentración de masa e número de nanopartículas. Polo tanto, son necesarias técnicas de separación, preconcentración, caracterización e cuantificación adecuadas para a análise de NMs en matrices complexas.

Normalmente a detección, caracterización e cuantificación de NMs en matrices complexas requiren a combinación de varias técnicas analíticas. As extraccións das NPs da mostra son comúnmente necesarias para illalas das diferentes matrices sen alteracións das mesmas. O plasma de acoplamento inductivo acoplado a espectrometría de masas con detección individualizada de nanopartículas (SP-ICP-MS) é unha das técnicas máis comúns para estudar NPs en matrices ambientais e biolóxicas. SP-ICP-MS é unha potente ferramenta de ICP-MS para a detección, cuantificación e caracterización de NPs, coloides e micropartículas. SP-ICP-MS aporta información cualitativa sobre a presenza de formas disoltas, e información como o número de nanopartículas así como a concentración en masa e a súa distribución de tamaños. SP-ICP-MS xunto coas técnicas de microscopía electrónica son a combinación perfecta de ferramentas para obter a información de NMs en matrices complexas.

As algas son ricas en compostos bioactivos como polisacáridos, polifenois, proteínas, omega-3, omega-6, ácidos graxos, selenio, iodo, vitamina B-12 e fibra dietética. Teñen propiedades antivirais, anticancerosas e anticoagulantes. Así, son moi empregadas na alimentación, en farmacéutica, cosmética, téxtil e animal As algas son moi empregadas na industria alimentaria como aditivo alimentario, e máis recentemente na poboación occidental como alimento. Non obstante, debido ás características da súa parede celular, as algas teñen o potencial de preconcentrar minerais, elementos traza e mesmo contaminantes da auga circundante en concentracións máis altas que na auga do mar.

O mexillón é un marisco moi consumido en todo o mundo, especialmente na Unión Europea polo seu alto contido en proteínas, omega-3, hidratos de carbono, ácidos graxos poliinsaturados e iodo. Non obstante, tamén se empregan habitualmente na vixilancia da

USC DE COMPOSTELA

contaminación, pola súa presenza en todos os océanos do mundo, o seu comportamento gregario e a súa capacidade para filtrar grandes cantidades de auga, actuando como filtradores.

Por outra banda, o rodaballo é un peixe plano bentónico carnívoro moi apreciado en todo o mundo polo seu alto valor nutricional e alto contido proteico. Non obstante, pode acumular metais pesados ao longo da cadea alimentaria.

Polas súas propiedades e o seu gran consumo, a investigación destas especies non deixou de medrar nos últimos 50 anos, sendo as Ciencias Agrarias e Biolóxicas, e as Ciencias do Medio Ambiente as principais áreas de investigación.

Por todo isto, nesta tese de doutoramento estudouse a bioacumulación e biodispoñibilidade de AgNPs e TiO_2NPs nestes importantes produtos acuícolas (algas, mexillóns e rodaballos). Para iso foi necesario o desenvolvemento de metodoloxías analíticas para a extracción de NPs e a súa posterior determinación. Polo tanto esta tese doutoral divídese en 3 partes que constan de 8 capítulos.

PARTE A: DESENVOLVEMENTO DE METODOLOXÍAS ANALÍTICAS PARA A EXTRACCIÓN DE NANOPARTÍCULAS DE PRATA E DE DIÓXIDO DE TITANIO

CAPÍTULO 1. Ultrasonicación seguida de hidrólise encimática como pretratamento da mostra para a determinación de nanopartículas de Ag en algas comestibles mediante SP-ICP-MS.

Este capítulo describe a optimización da metodoloxía analítica para a separación de AgNPs das algas mediante un método de hidrólise encimática asistida por ultrasóns e posterior determinación mediante SP-ICP-MS.

Par a optimización dos parámetros que afectan ao illamento das AgNPs empregouse unha mostra de *Palmaria palmata* (alga vermella) exposta previamente a AgNPs. Os parámetros optimizados inclúen o tipo de sonicación (baño fronte a sonda ultrasónica), a amplitude do ultrasóns, o tempo de sonicación, o modo de sonicación (pulsado fronte á sonicación continua), a concentración da mestura de encimas (Macerozyme® R-10) e o tempo de hidrólise encimática. A estabilidade das AgNPs durante a extracción estudiouse mediante microscopía electrónica de transmisión (TEM) e utilizando un estándar de 15 nm de AgNPs recubertas de polivinilpirrolidona (PVP) analizado por SP-ICP-MS. A eficacia da extracción foi evaluada comparando o contido total de Ag nunha mostra dixerida co contido total no mesmo extracto da mostra, obtendo unha recuperación do 80%. Avaliaronse as características analíticas dos métodos, obtendo bos resultados para ICP-MS e SP-ICP-MS. Para a análise mediente SP-ICP-MS, a sensibilidade do método foi avaliada a través dos límites de detección. O $LOD_{tamaño}$ foi de 14 e 12 nm para os criterios 5σ e 3σ, respectivamente, e o $LOD_{número}$ foi de $2{,}40\times10^{6}$ part L^{-1} (límite instrumental) e $4{,}34\times10^{7}$ part g^{-1} (referido á mostra de algas húmidas). A precisión estudouse mediante a repetibilidade obtendo RSDs inferiores ao 10%, e a exactitude avaliouse mediante a recuperación analítica, resultando nun 112±12%. Finalmente, a metodoloxía desenvolvida foi aplicada á análise de varias mostras de algas vermellas (*Palmaria palmata*) e verdes (*Ulva* sp.).

USC UNIVERSIDADE DE SANTIAGO DE COMPOSTELA

CAPÍTULO 2. Estudo das nanopartículas de dióxido de titanio en algas mariñas mediante espectrometría de masas con plasma de acoplamento inductivo e detección individualizada de nanopartículas.

Este capítulo describe a optimización dun método para a separación de TiO_2NPs en algas mediante o procedemento de extracción asistida por ultrasóns (UAE) baseado no tratamento alcalino con hidróxido de tetrametilamonio (TMAH) e na posterior determinación mediante SP-ICP-MS.

Avaliouse o efecto da porcentaxe de TMAH no proceso de extracción das NPs, así como do volume da disolución de extractante e o tempo de sonicación (tempo de extracción). Experimentos adicionais tamén mostraron que as TiO_2NPs foron exraidas cuantitativamente da matriz das algas nunha sola etapa xa que a análise dos residuos deu concentracións de TiO_2NPs inferiores ao límite de cuantificación (LOQ) do método. Os experimentos relativos á estabilidade das TiO_2NPs mostraron que as NPs extraídas son estables xa que non houbo cambios nin no número nin na distribucións de tamaño das TiO_2NPs ao expoñer os estándares de TiO_2NPs ás condicións extractivas optimizadas. A metodoloxía SP-ICP-MS foi debidamente validada empregando suspensión de TiO_2NPs de 50 e 100 nm. O método mostrou unha boa recuperación analítica (115% e 112% para TiO_2NPs de 50 e 100 nm, respectivamente) e boa reproducibilidade (2% para o tamaño e 16% para o número de TiO_2NPs). A sensibilidade do método foi avaliada empregando os límites de detección. O $LOD_{tamaño}$ foi de 37 e 31 nm para os criterios 5σ e 3σ, respectivamente, e o $LOD_{número}$ foi de $1{,}43\times10^{6}$ part L^{-1} (límite instrumental) e $5{,}72\times10^{4}$ part g^{-1} (referido á mostra de algas húmidas). Extractos seleccionados de *Palmaria palmata* e *Ulva* sp. foron analizados por HRTEM-EDX. Finalmente, a metodoloxía aplicouse á análise de TiO_2NPs en varias mostras de algas da costa galega e irlandesa.

PARTE B: BIOACUMULACIÓN DE NANOPARTÍCULAS DE DIÓXIDO DE TITANIO E PRATA EN PRODUTOS DA ACUICULTURA

CAPÍTULO 3. Estudo da bioacumulación de nanopartículas de prata en algas cultivadas vermellas e verdes.

Neste estudo investigouse a bioacumulación de nanopartículas de Ag recubertas de polivinilpirrolidona (PVP-AgNPs) en algas vermellas (*Palmaria palmata*) e verdes (*Ulva* sp.). O estudo de bioacumulación durou 28 días nos que as algas foron expostas a diferentes concentracións de PVP-AgNPs (0,1 e 1,0 mg L^{-1}) en medios de cultivo mariños contendo fitoplancto. Para a determinación do contido total de Ag, os exemplares foron sometidos a dixestión ácida asistida por microondas antes da determinación mediante ICP-MS. Illáronse as nanopartículas da matriz mediante extracción encimática asistida por ultrasóns empregando Macerozyme® R-10, antes da análise mediante SP-ICP-MS para a determinación do contido e distribucións de tamaño das AgNPs.

As concentracións máximas de Ag total obtidas no presente estudo foron: 0,52±0,04 μg g^{-1} p.h. (peso húmido) (no día 21, exposición a 0,1 mg L^{-1} de PVP-AgNPs) e 0,79±0,06 μg g^{-1} p.h. (no día 14; 1,0 mg L^{-1}) en *Palmaria palmata*; e 0,26±0,04 μg g^{-1} p.h. (no día 28; 0,1 mg L^{-1}) e 0,46±0,15 μg g^{-1} (no día 21; 1,0 mg L^{-1}) en *Ulva* sp. As concentracións máximas de AgNPs alcanzáronse aos 14 días para *Palmaria palmata* ($1{,}63\times10^{9}\pm5{,}47\times10^{8}$ part g^{-1} p.h., 1,0 mg L^{-1}) e aos 28 días para *Ulva* sp. ($3{,}23\times10^{9}\pm2{,}34\times10^{7}$ part g^{-1} p.h.; 1,0 mg L^{-1}) con tamaños máis frecuentes de aproximadamente 20 nm. Ademais, estes tamaños máis frecuentes atopados nos

extractos encimáticos medidos por SP-ICP-MS coincidiron cos tamaños de AgNPs medidos nos extractos encimáticos de *Palmaria palmata* e *Ulva* sp. por TEM.

CAPÍTULO 4. Bioacumulación de nanopartículas de dióxido de titanio en algas verdes (*Ulva* sp.) e vermellas (*Palmaria palmata*).

Neste capítulo, as algas vermellas (*Palmaria palmata*) e verdes (*Ulva* sp.) expuxéronse a dúas concentracións diferentes (0,1 e 1,0 mg L^{-1}) de citrato-TiO_2NPs de 5 nm e 25 nm durante 28 días. Para a determinación do Ti total, as mostras foron sometidas a dixestión ácida asistida por microondas antes da análise por ICP-MS. As TiO_2NPs foron extraídas da matriz mediante extracción alcalina con TMAH. Despois, o número e o tamaño das TiO_2NPs acumuladas nos exemplares foron determinados mediante SP-ICP-MS.

As concentracións de Ti medidas en *Ulva* sp. foron superiores ás atopadas en *Palmaria palmata* para as mesmas condicións de exposición. A concentración máxima de Ti (61,96±15,49 µg g^{-1} p.h.) foi medida en *Ulva* sp. despois de 28 días de exposición a 1,0 mg L^{-1} de TiO_2NPs de 5 nm. A concentración e tamaños de TiO_2NPs determinados por SP-ICP-MS nos extractos alcalinos de algas foron similares para ambas algas expostas a TiO_2NPs de 5 e 25 nm, o que indica que o elemento se acumula en *Ulva* sp. principalmente como Ti iónico ou nanopartículas de tamaño inferior ao límite de detección (27 nm). Ademais, a internalización das TiO_2NPs en *Ulva* sp. foi confirmada por microscopía electrónica (TEM/STEM) en combinación coa análise de espectrometría por dispersión de enerxía de raios X (EDX).

CAPÍTULO 5. Bioacumulación de nanopartículas de prata en mexillóns e rodaballos da zona atlántica.

Neste estudo, mexillóns (*Mytilus edulis*) e rodaballos (*Scophthalmus maximus*), foron expostos a PVP-AgNPs de 15 nm durante longos tempos de exposición. No caso dos mexillóns, o ensaio de bioacumulación durou 28 días, expuxéronse a 0,1 e 1,0 mg L^{-1} de PVP-AgNPs e homoxenizouse a totalidade do mexillón. Para o rodaballo, o ensaio de bioacumulación durou 105 días, expuxéronse a 0; 0,25; 0,75 e 1,5 mg de PVP-AgNP kg^{-1}, e estudáronse por separado a carne+pel, o fígado e o ril. A concentración total de Ag e a concentración de AgNPs e a distribución do tamaño en ambas especies determináronse mediante ICP-MS e SP-ICP-MS, respectivamente.

A maior concentración de Ag nos mexillóns foi de 1,40±0,25 µg g^{-1} p.h. á dose de exposición baixa e 28 días de exposición. A maior concentración de AgNPs nos mexillóns foi de $2{,}14\times10^{8}\pm4{,}49\times10^{7}$ NPs g^{-1} p.h. á dose de exposición alta e 28 días de exposición. A presenza nos tanques de Ag e AgNPs nun residuo excretado polos animais confirma a ausencia de bioacumulación á doce de exposición elevada en comparación coa baixa. Por outra banda, no ensaio de bioacumulación do rodaballo, as concentracións máis altas de Ag atopáronse no fígado (parte non comestible) acadando 6,47±2,46 µg g^{-1} p.h., pero non se atoparon partículas nestas mostras. Os resultados da bioacumulación ratifican a seguridade no consumo de rodaballo e destacan a necesidade dun correcto proceso de depuración do mexillón.

CAPÍTULO 6. Patróns de bioacumulación en mexillóns e rodaballos acuícolas expostos a diferentes tamaños de TiO_2NPs.

USC DE COMPOSTELA

Neste capítulo examináronse dúas especies acuícolas predominantes en España para determinar o impacto e a bioacumulación das TiO_2NPs. Para os ensaios de bioacumulación seleccionáronse

un bivalvo filtrante bentónico (*Mytilus edulis*) e un depredador bentónico (*Scophthalmus maximus*). O estudo de exposición durou 28 días nos mexillóns e 90 días nos rodaballos, e os exemplares foron expostos a diferentes concentracións de citrato-TiO_2NPs de 25 e 5 nm. Utilizáronse ICP-MS e SP-ICP-MS para a determinación de Ti e a determinación do contido e a distribución de tamaños de TiO_2NPs, respectivamente.

Nos mexillóns as concentracións de Ti e TiO_2NPs alcanzaron 5,19±3,19 μg g^{-1} p.h. e $2,28\times10^8\pm5,84\times10^7$ NPs g^{-1} p.h. despois da exposición a 1,0 mg L^{-1} de TiO_2NPs de 25 nm durante 28 días, e 4,26±0,85 μg g^{-1} p.h. e $4,79\times10^8\pm2,36\times10^8$ NPs g^{-1} p.h. para 1,0 mg L^{-1} de TiO_2NPs de 5 nm durante 14 e 21 días de exposición, respectivamente. Os mexillóns expostos á alta dose de TiO_2NPs de 5 nm mostraron bioacumulación de titanio e cunchas máis fráxiles. Nas cunchas, a concentración de Ti máis alta alcanzada foi de 12,43±3,45 μg g^{-1} p.s. (peso seco). A maior concentración de Ti atopouse no fígado de rodaballo (parte non comestible), acadando concentracións de 1,62±0,44 μg g^{-1} p.h. a 90 días de exposición e unha dose de 1,5 mg de 5 nm TiO_2NPs por Kg de peixe e día. Estudouse tamén o contido de Ti nas feces dos rodaballos. Os resultados mostraron que o Ti era expulsado nas feces, acadando unha concentración de 40,99±6,62 μg g^{-1} p.h. nas feces de rodaballo alimentado con 1,5 mg kg^{-1} de peixe e día de TiO_2NPs de 5 nm. Os resultados mostran a seguridade do consumo de rodaballo e destacan a necesidade dun correcto proceso de depuración do mexillón antes da súa comercialización.

CAPÍTULO 7. Presenza de nanopartículas de prata e dióxido de titanio en mostras mariñas da área Atlántica.

Para arroxar luz sobre a presenza de AgNPs e TiO_2NPs en varios organismos acuáticos moi consumidos na rexión atlántica, e para preservar a seguridade alimentaria, é necesaria a investigación destes contaminantes emerxentes. Neste capítulo avaliouse a presenza de AgNPs e TiO_2NP en organismos fotosintéticos como algas comestibles (*Alaria esculenta*), moluscos bivalvos como os mexillóns (*Mytilus edulis*) e peixes como predadores superiores na cadea alimentaria (*Salmo*, *Dicentrarchus labrax* e *Sparus aurata*). Para determinar o contido total de Ag e Ti, as algas, os mexillóns e os peixes disecionados foron sometidos a dixestións ácidas asistidas por microondas antes da análise por ICP-MS. Para determinar o contido de AgNPs e TiO_2NPs así como a distribución do tamaño, seleccionáronse as extraccións encimáticas e alcalinas adecuadas antes da análise por SP-ICP-MS.

As concentracións máis altas de Ag atopáronse nos fígados do salmón, onde a concentración total de Ag alcanzou 0,73±0,07 μg g^{-1} p.h. de Ag, e o contido de AgNPs alcanzou $2,74\times10^8\pm7,78\times10^7$ AgNPs g^{-1} p.h. Non obstante, a maior concentración de Ti atopouse nas algas mariñas. A concentración total de Ti alcanzou 8,48±1,69 μg g^{-1} p.h. e as maiores concentracións de TiO_2NPs acadadas foron $1,35\times10^8\pm8,06\times10^7$ TiO_2NPs g^{-1} p.h. Os resultados mostraron a maior acumulación de Ag e Ti en partes non comestibles dos peixes, pero as concentracións atopadas nos mexillóns analizados e sobre todo nas algas mariñas, poñen de manifesto a necesidade dunha axeitada depuración antes do seu consumo.

USC UNIVERSIDADE DE SANTIAGO DE COMPOSTELA

PARTE C: BIODISPOÑIBILIDADE DAS NANOPARTÍCULAS DE DIÓXIDO DE TITANIO E PRATA NOS PRODUTOS DA ACUICULTURA

CAPÍTULO 8. Estudo de biodispoñibilidade de nanopartículas de prata e dióxido de titanio procedentes de algas e mexillóns mediante células Caco-2.

Neste capítulo inclúese o estudo realizado para avaliar a bioaccesibilidade e a biodispoñibilidade de Ag e Ti total, AgNPs e TiO_2NPs en algas mariñas crudas e cociñadas (*Palmaria palmata* e *Ulva* sp.), e en mexillóns cociñados (*Mytilus edulis*) de exemplares expostos a 1,0 mg L^{-1} de PVP-AgNPs de 15 nm, a 1,0 mg L^{-1} de citrato-TiO_2NPs de 25 nm, e a 1,0 mg L^{-1} de citrato-TiO_2NPs de 5 nm, durante 28 días. Realizouse un proceso de dixestión *in vitro* que simula a dixestión gastrointestinal humana para determinar a bioaccesibilidade total de Ag, Ti total, AgNPs e TiO_2NPs. Simuláronse o proceso de transporte celular para os ensaios de biodispoñibilidade mediante o cultivo de células Caco-2. As fraccións bioaccesibles gastrointestinais incubáronse en Transwells® de seis placas durante 1 hora, garantindo a integridade da monocapa celular.

O contido total de Ag e Ti nas mostras dixeridas, nas fraccións bioaccesibles e nas fraccións apicais e basolaterais determináronse mediante ICP-MS. O contido de AgNPs e TiO_2NPs nos extractos da mostra, nas fraccións bioaccesibles, nas fraccións apicais e basolaterais determináronse mediante SP-ICP-MS. Finalmente, o contido de AgNPs e TiO_2NPs internalizado nas células Caco-2 determinouse mediante ICP-MS operando en modo de detección individualizada de células (SC-ICP-MS).

USC UNIVERSIDADE DE SANTIAGO DE COMPOSTELA

USC
UNIVERSIDADE
DE SANTIAGO
DE COMPOSTELA

I. INTRODUCTION

USC
UNIVERSIDADE
DE SANTIAGO
DE COMPOSTELA

USC
UNIVERSIDADE
DE SANTIAGO
DE COMPOSTELA

I. INTRODUCTION

I.1 IMPORTANCE OF AQUACULTURE IN THE WORLD, EUROPE AND SPAIN

The world's expanding population has an enormous demand for food sources. Although extractive fishing has become increasingly significant in recent years, fishing is now a finite resource due to population growth, the consequences of climate change, and pollution. In fact, world per capita fish consumption increased from 9 kg in 1961 to 20.5 kg in 2019 [1]. Furthermore, 17% of consumed proteins by the world population come from fish [2]. Thus, aquaculture production is necessary to meet the growing global demand for healthy and nutritious aquatic products. Aquaculture and mariculture are the production of animals and plants in water and seawater using techniques designed to make better and more responsible use of natural resources [3]. In these freshwater or saltwater farms, fish, mollusks, algae, crustaceans, and other invertebrates are raised. Furthermore, aquaculture production can take place at sea in hatcheries, like sea bream and sea bass; in rafts and long lines, like bivalve mollusks such as mussels; on land installations near the sea, like turbot; on the beach, like clam plantations, and land installations near a river, like rainbow trout.

Aquaculture is the farming type with less climate impact. World aquatic production (fisheries and aquaculture) in 2020 was 214 million tons. Since the 1970s, production in aquaculture has not stopped growing. Actually, in 2020, aquaculture surpassed fisheries for the seventh consecutive year with 122.6 million tons, with aquaculture accounting for 57.3% of production. The leading aquaculture producer in 2020 was Asia with 91.6% of global aquaculture production, followed by America, Europe, Africa, and Oceania with 3.6, 2.7, 1.9, and 0.2% of production, respectively. Likewise, China was the main country with 57.5% of production, with Spain in 25th place. **Figure I.1.** shows the percentages of saltwater and freshwater aquaculture production in the world (**Figure I.1.(a)**), and in the European Union (EU) (**Figure I.1.(b)**). The outputs of both types of aquaculture (saltwater and freshwater) are almost equal in the world, but in the case of the EU, saltwater aquaculture predominates with more than 70%. **Figure I.1.** also shows the percentages of types of species cultivated in the world (**Figure I.1.(c)**) and in the EU (**Figure I.1.(d)**). While in the world the predominant species are fish, algae, mollusks, and crustaceans, in the EU the predominant species are mollusks and fish [1].

The most cultivated species in tons in the world is the Japanese Laminaria (*Saccharina japonica*) with 12,469,807 t, followed by European mussels (*Mytilus galloprovincialis* and *Mytilus edulis*), sea bass (*Dicentrachus labrax*), sea bream (*Sparus aurata*) and turbot (*Scophthalmus maximus*) with 264,875, 263,781, 259,443, and 77,710 t in 2020, respectively. However, the species that generated the highest value in millions of euros was the white shrimp (*Litopenaeus vannamei*) with 26,929 million euros followed by Atlantic salmon (*Salmo salar*), sea bream, sea bass, turbot, and European mussel with 12,221, 1,164, 1,089, 385, and 285 million euros in 2020, respectively [1,2].

Aquaculture production in the EU contributed 1,094,315 t with a value of 3,777 million euros in 2020, where Spain was the leading producer country in tons, followed by France, Greece, and Italy. However, the country that generated the most millions of euros in 2020 from the sale of its aquaculture goods was France followed by Spain, Grece, and Italy [1].

The most cultivated species in the EU was the European mussel with 409,621 t in 2020, followed by sea bream (93,131 t), sea bass (81,369 t), and Atlantic salmon (14,810 t) in 3rd, 5th,

and 9th place in production, respectively. On the other hand, regarding monetary production European mussels and turbot ranked in 5th and 10th position with 335.08 and 44.90 million euros, respectively [1,2].

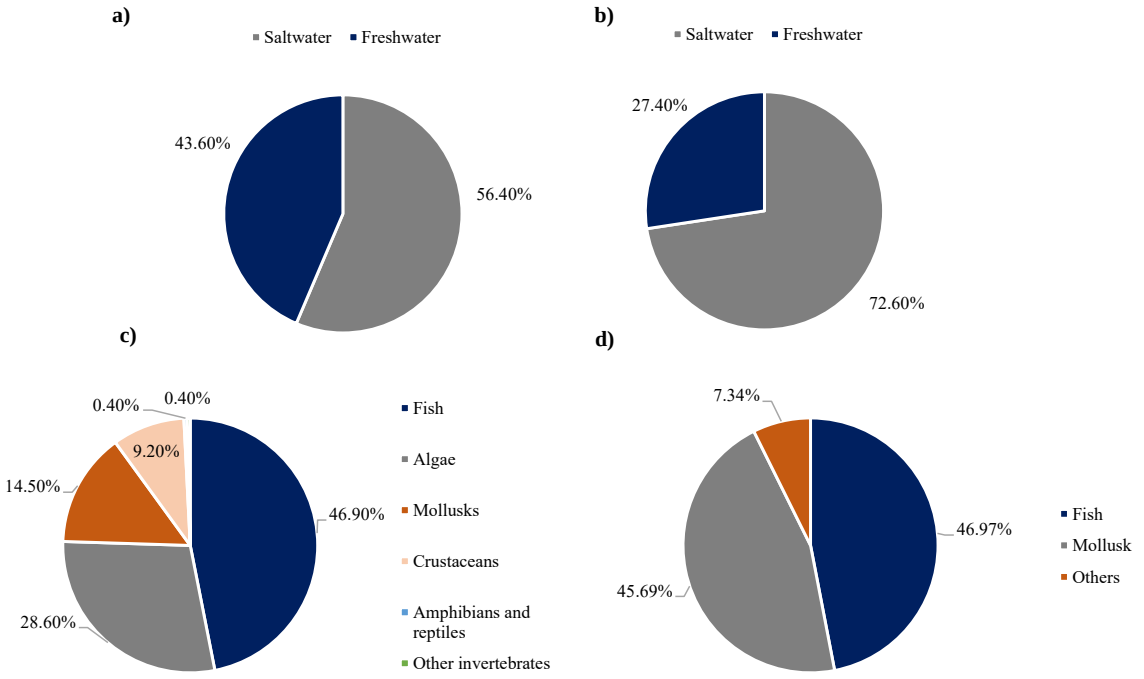

Figure I.1. Percentage of aquaculture production in saltwater and freshwater: (a) in the world, (b) in the European Union; percentage of types of cultured species: (c) in the world, (d) in the European Union.

The world's leading extractive fishing in Spain in the 1960s was diminished by the reduction of fishing possibilities. Aquaculture began in Spain in the 1960s and although it has continued to grow since then, it has not been able to compensate for the volume previously obtained from fishing [1]. According to the Spanish Ministry of Agriculture, Fisheries, and Food, *Mytilus galloprovincialis* is the most produced mollusk species (225,283 t in 2021) in Spain, where 98% of production takes place in Galicia (Northwest of Spain). The next species cultured by tons in 2021 were sea bass (23,933 t), rainbow trout (*Oncorhynchus mykiss*) (15,482 t), sea bream (8,012 t), and turbot (7,630 t), which is 100% produced in Galicia [4].

I.2 SPECIES UNDER STUDY

Taking into account the global data, due to their high consumption in the Eastern diet, and their recent increase in the Western diet, two types of seaweed (photosynthetic organisms) will be studied in this doctoral thesis. Furthermore, considering the previous data on European and Spanish production and their importance, the main selected species under study in this doctoral thesis will be mussels (benthic bivalve mollusks), and turbot (benthic fish predators).

I.2.1 Seaweed

Algae are very simple, unicellular, unicellular grouped in colonies, or pluricellular photosynthetic organisms collaborating as simple organisms. They are found in every part of Earth with enough light to carry out photosynthesis (sea, rivers, lakes, soils, and even in animals

and plants acting as symbiotic organisms). Their size can vary from 3-10 µm in unicellular algae to 70 m in multicellular algae, and they can be classified as microalgae and macroalgae (seaweed). Microalgae can be found as phytoplankton in all ocean waters as well as benthic and littoral habitats, and macroalgae can be found in the littoral zone and include green (Chlorophyta), red (Rhodophyta), and brown (Phaeophyta) seaweed [5].

- Green seaweed:
  The green color of this kind of seaweed is due to chlorophyll a and b in their chloroplasts. They are common in areas with abundant light. The main genera include *Ulva*, *Enteromorpha*, *Chaetomorpha*, *Codium*, and *Cladophora*. The species of *Ulva* are known as sea lettuce due to their delicate and bright green fronds. Although *Ulva lactuca* is the most studied, there are some different *Ulva* species difficult to distinguish. *Ulva* can reach 45 cm, and they live in the intertidal zone of brackish or marine environments, particularly in estuaries over the world [5,6].
- Red seaweed:
  The red color of this kind of seaweed is due to the dominance of phycoerythrin and phycocyanin, which mask the chlorophyll a, β-carotenes, and xanthophylls. Most of the red algae are found from the low tide zone to 100 m in depth. The main genera include *Porphyra*, *Pyropia*, *Chondrus* and *Palmaria*. *Palmaria palmata* grows up to 30-40 cm and has a divided stem in the shape of a fork with smooth leathery fronds. *Palmaria palmata* is rich in proteins and it is harvested for food on shores and areas subjected to tidal currents of the North Atlantic and North Pacific oceans [5,6].
- Brown seaweed:
  The brown color of this kind of seaweed is due to the dominance of xanthophyll pigments and fucoxanthin, which mask other pigments like chlorophyll a and c, β-carotenes, and other xanthophylls. The most common genera include *Ascophyllum*, *Saccharina*, *Laminaria*, *Nereocystis*, *Macrocystis*, and *Sargassum*. Brown seaweed are the largest (up to 30-45 m in length), and they live in shallow waters and shorelines [5,6]. *Alaria esculenta* (*Laminaria* commonly known as dabberlocks or Atlantic wakame) is made up of a central vein from which wavy membranes protrude on either side. This type of algae grows in cold waters on European coasts exposed to waves like Ireland, UK, and Norway. *Alaria esculenta* can grow fast reaching 2-3 m, making it widely used for the production of food and biomass for animal feed. [7,8].

Seaweeds are organisms rich in bioactive compounds that are not present in terrestrial plants, like polysaccharides, polyphenols, and different proteins. Moreover, seaweeds are rich in omega-3, omega-6, fatty acids, vitamin B-12, selenium, and dietary fibre [9]. Furthermore, they are rich in iodine, thus they are commonly employed to treat thyroid goiter [5]. Seaweed consumption has antiviral, anticancer, and anticoagulant properties and the ability to control obesity and diabetes risk factors, as well as gut health [10]. They are used in the food industry and as a food additive; they are also used in pharmaceuticals, nutraceuticals, cosmetics, textiles, animal feed, biofuel, biofertilizers, and even bio-packaging [11].

Already at the beginning of the 21st century, the Japanese per capita seaweed consumption was 5.3 g per day [12]. The 2022 APROMAR report [1] about aquaculture showed that in 2020 the two main aquaculture species produced in tons were two types of algae, the Japanese

Laminaria (*Saccharina japonica*) and Eucheuma (*Eucheuma* and *Kappaphycus*), with Gracilaria (*Gracilaria* sp.) production in 10th place [1]. On the other hand, regarding the Spanish Ministry of Agriculture, Fisheries and Food the production of red and green algae has increased in the last years reaching a production of 0.36 and 1.56 t in 2021, respectively [4]. However, although the western population's diet is changing towards a healthier and more sustainable diet with the introduction of algae for human consumption, most algae production is still destined for the production of agar-agar, alginates and carrageenans used as gelling agents in the food industry [10].

The properties and applications of seaweed are reflected in the research studies with the term seaweed in the Scopus database. **Figure I.2.** shows the increase in the number of publications that include the term seaweed over the years (**Figure I.2.(a)**), and the main research areas (**Figure I.2.(b)**) with Agricultural and Biological Sciences and Environmental Sciences dominating the scene [13].

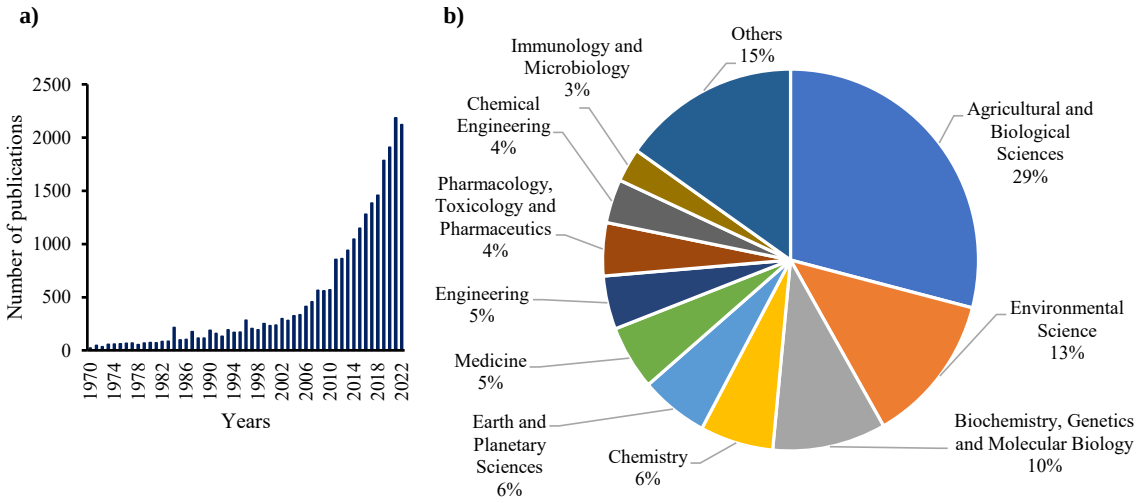

Figure I.2. Evolution of the Scopus database publications with the term seaweed over the years (a); percentages of publications with the term seaweed by research area (b) [13].

Due to the characteristics and structure of the cell wall of seaweed, they have a high potential for concentrating minerals and trace elements present in the surrounding water, and even pollutants, in several orders of magnitude higher than in water [9]. Thus, seaweed can be bioindicators of chemical contaminants like heavy metals [14-16], pesticides [17], polycyclic aromatic hydrocarbons (PAHs) [18], and even emergent contaminants like microplastics [19] and nanoparticles [20].

I.2.2 Mussels

Mussels are bivalve mollusks with two calcified valves (forming the shell), joined together on the dorsal surface, which extends by a flexible joint. The inner surfaces of the valves are covered by a thin mantle. The visceral mass (body) of the bivalve extends from the dorsal insertion to the space (pallial cavity/mantle cavity) between the mantle-lined valves [21]. Mussels in their natural habitat are usually found in the littoral zone forming colonies anchored to the substrate (mainly rocks) through the byssus. Because of their one-link feeding chain, resilient nature, quick rate of growth, and rarity of catastrophic mass mortalities brought on by parasitic microorganisms, they can generate a lot of products at a very reasonable cost [22].

Mussels are popular in the human diet due to their high content of proteins, omega-3, carbohydrates, polyunsaturated fatty acids, and iodine [23]. However, they are also very employed in pollution monitoring, due to their presence in all the oceans of the world, their gregarious behaviour, and their capacity to filter high amounts of water (between 1 and 4 L per hour), acting as filter feeders [24]. As a filterer of phytoplankton and detritus, it is considered the most efficient converter of nutrients and organic matter, produced by marine organisms in the aquatic environment, into nutritious animal protein [22].

The mussel-cultivated species vary according to the country and climate, but the most cultivated mussels are the blue or common mussel (*Mytilus edulis*), and the European mussel (*Mytilus galloprovincialis*) [21]. The exact distribution area of *Mytilus edulis* and *Mytilus galloprovincialis* is unknown due to confusion between *Mytilus* species. *Mytilus edulis* is widespread in the boreal regions, North Carolina, Japan and from the Kara Sea (Russia) to the Mediterranean Sea. On the other hand, *Mytilus galloprovincialis* can be found on the Mediterranean coastline, Galicia, the eastern Atlantic Ocean, Ireland, the United Kingdom and North Africa [25].

Since 95% of the world's mussels come from aquaculture [26], Spain is the largest producer of mussels in the EU, followed by France and Italy. Spanish production takes place in Galicia, with 98% of the total, producing Valencia and Catalonia the other 2%. The mussel cultivation in Galicia takes place in the rías in more than 3,000 rafts grouped and spaced 100 meters apart in raft parks. The rafts are formed by floating structures made of wooden beams and anchored to the seabed. From the base hang a maximum of 600 ropes with a maximum depth of 12 meters, where mussels are cultivated. The culture procedure is divided into five phases including the collection of the seed from rocks, attaching the seed to the ropes, thinning the ropes, growing, and harvesting. Moreover, the season, the localization of the raft, the depth of the mussel in the ropes, and the variation of nutrient water content affect mussel growth until they are available to sell (after 13-16 months) [24,26].

According to the Scopus database [13], the investigation regarding mussels has increased over the past decades, with the evolution of aquaculture in the last few years. **Figure I.3.** shows the increasing evolution of the number of publications in the Scopus database, which includes the term mussel over the years (**Figure I.3.(a)**), and the percentages of publications with the term mussel by research area (**Figure I.3.(b)**).

USC
UNIVERSIDADE DE SANTIAGO DE COMPOSTELA

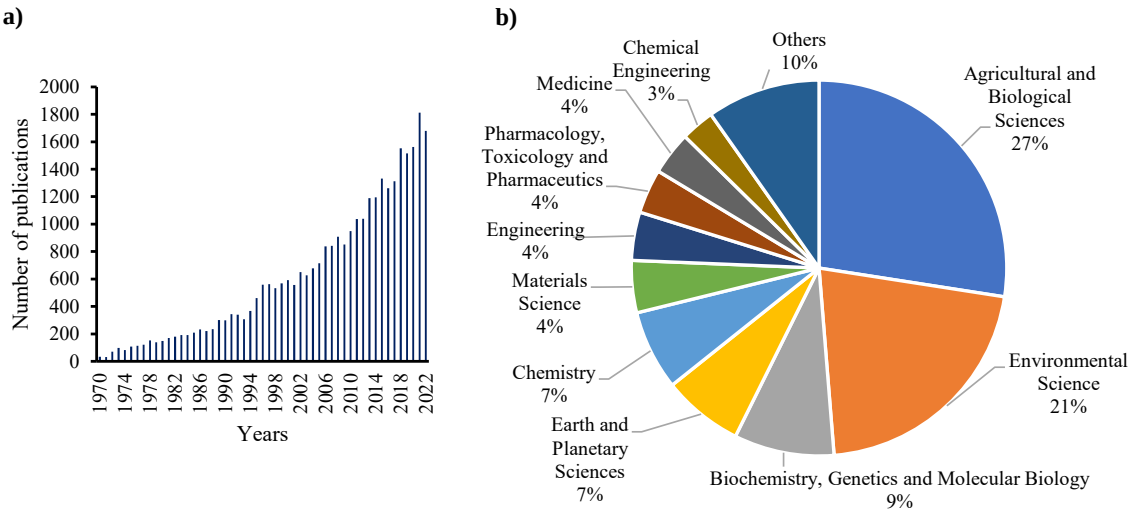

Figure I.3. Evolution of the Scopus database publications with the term mussel over the years (a); percentages of publications with the term mussel by research area (b) [13].

The mussel publications are highlighted in Agricultural and Biological Sciences and Environmental Science with 27 and 21% of publications, respectively. Some of the studies in Environmental Science showed the bioaccumulation of heavy metals and trace elements in mussels from the surrounding filtered water [27-29], and of other emergent contaminants like microplastics, that can absorb other organic compounds in their surfaces and be assimilated by mussels [30]. Furthermore, the toxicity of commonly employed chemical UV filters can affect mussel reproduction [31], and bioaccumulation induces cellular damage and affects the metabolic activity of these animals [32]. Moreover, water contamination with PAHs causes damage to the survival of mussels [33]. Other studies, showed that the extensive use and disposal of nanoparticles in the environment can produce their bioaccumulation, and even affect the byssus stretch [34].

I.2.3 Turbot

Turbot (*Scophthalmus maximus*) is a carnivore benthic flatfish highly appreciated around the world. It has an asymmetrical, almost round body, with the eyes on the left side and without scales but with some bony protuberances [35]. They can live in seawater between 14 and 19 ºC in sandy and muddy bottoms, from shallow waters up to 100 m in depth. Juvenile turbots (until 4-6 months) usually feed on crustaceans and mollusks, and the adults are mainly fed with cephalopods and fish [36,37]. Male turbots mature at two years (around 30 cm length) and females at three years (around 45 cm length). The spawning season occurs between April-August and between May-August in the Mediterranean and Atlantic areas, respectively [38]. Although 92% of turbots are farmed, wild turbots are present in the Northeast Atlantic, the European coast to the Artic Circle, and the Mediterranean and Baltic Sea [39].

The aquaculture of turbot started in Scotland in 1970, but, nowadays, China is the main producing country of turbot aquaculture, and Spain is the main European producer, followed by Portugal [1,39]. The most common turbot aquaculture system consists of onshore exhaustive controlled tanks. The aquaculture juvenile turbot is commonly fed with dry granulated feed and phytoplankton, but hatchery is commonly fed with crustaceans such as Artemia or rotifer [36].

Aquaculture turbot production has grown up in the last few years; thus, the investigation related to this highly appreciated species has increased in the last decades. **Figure I.4.** shows the increase of the term turbot in the Scopus database [13] over the years (**Figure I.4.(a)**) and

the main turbot research areas of study (**Figure I.4.(b)**). Like in seaweed and mussels, Agricultural and Biological Sciences and Environmental Sciences are the main research areas regarding turbot.

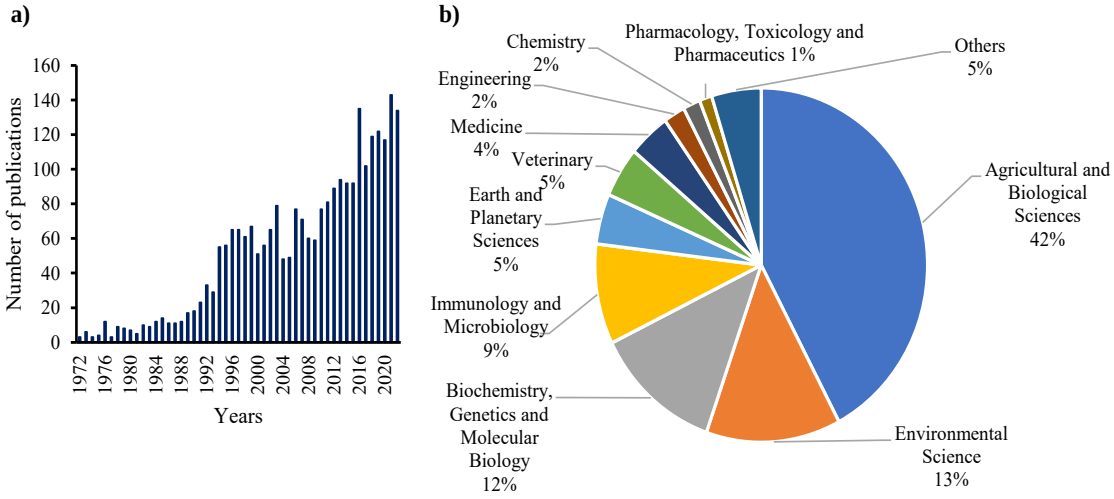

Figure I.4. Evolution of the Scopus database publications with the term turbot over the years (a); percentages of publications with the term turbot by research area (b) [13].

Although most of the studies in the turbot sector are related to disease treatments and focused on biological aspects of the species, and the technological factors of cultivation, environmental studies are also very important to ensure food safety. Turbot can bioaccumulate heavy metals through the food chain [40], suffer oxidative stress from microplastics [41], and experience histological alterations by nanoparticles [42].

I.2.4 Other studied fish species

Sea bream (*Sparus aurata*), sea bass (*Dicentrarchus labrax*) and Atlantic salmon (*Salmo salar*) are fin fish very appreciated by the European population. Indeed, sea bream, sea bass, and salmon were the 3rd, 5th, and 9th most-produced European aquaculture species in tons in 2020 [1]. Atlantic salmon is present on the Atlantic coasts of Europe, from Barents and Baltic Seas to northern Portugal, and around Iceland and south Greenland. Salmon are also present on the coasts of Canada and North America. The juvenile salmon live in freshwater, where they are fed by aquatic larvae and insects. The adult salmon live in seawater where they are fed by small fish and crustaceans until they return to freshwater for spawning. Sea breams are present in the Mediterranean Sea, and in the Atlantic Ocean from the British islands to Cape Verde, and around the Canary Islands. It is a coastal species that lives in rocky and sandy seagrass beds up to 150 m in depth, and it can live in brackish water. It is a mainly carnivorous fish, that feeds on crustaceans, mussels, and fishes. Sea bass is present in the North Atlantic Ocean, from Norway to South Morocco, and in the Mediterranean and the Black Sea. Sea bass lives in shallow coastal areas up to 100 m in depth, can enter brackish waters and is carnivorous, feeding on small fish, invertebrates, crabs, squid and mollusks [25].

USC UNIVERSIDADE DE SANTIAGO DE COMPOSTELA

I.3 NANOMATERIALS

The term "nanoscience" is commonly attributed to the physicist Nobel laureate Dr. Richard P. Feynman, due to his classic science lecture in 1959 entitled "There's Plenty of Room at the Bottom: An Invitation to Enter a New Field of Physics". In this lecture, he talked about the lack of appropriate techniques and equipment to work at atomic and molecular levels, the storage of information at a small scale, and the need for better electronic microscopes to obtain better atom images [43]. The term " nanotechnology" was first defined in 1974 by Norio Taniguchi who described it as "production technology allowing to reach ultrahigh precision and ultrasmall sizes of approximately 1 nm". However, the nanotechnology field did not start its development until the invention of scanning tunnelling microscopy (STM) in 1981 and the atomic force microscope (AFM) in 1986. Both tools allowed taking images of the surfaces with atomic resolutions and moving the individual atoms, as previously predicted by Feynman [44]. Since then, the nanotechnology field has not stopped growing, and several definitions were proposed. The simplest definition of nanotechnology found was "technology of the nanoscale that has application in the real world" where the nanometric scale is considered between 1 and 100 nm (1 nm=one billionth of a meter or 1×10^{-9} m) [45]. Furthermore, nanotechnology is a multidisciplinary field of study that covers the sciences of physics, chemistry, materials, and other engineering sciences [46].

I.3.1 Nanomaterial definition, classification, and properties

Several definitions for nanomaterial (NM) were proposed in the last few years, by different worldwide organizations, including the Food and Drug Administration (FDA), the US Environmental Protection Agency (EPA) [47], and the International Organization for Standardization, (ISO) [48]. Moreover, the European Commission (EC) adopted the nanomaterial definition in their recommendation 2011/696/EU, for the first time [49]. Nevertheless, this recommendation has recently been updated by the European Commission recommendation 2022/C 229/01 [50], where a nanomaterial means "a natural, incidental or manufactured material consisting of solid particles that are present, either on their own or as identifiable constituent particles in aggregates or agglomerates, and where 50 % or more of these particles in the number-based size distribution fulfil at least one of the following conditions:

- One or more external dimensions of the particle are in the size range 1 nm to 100 nm.
- The particle has an elongated shape, such as a rod, fibre or tube, where two external dimensions are smaller than 1 nm and the other dimension is larger than 100 nm.
- The particle has a plate-like shape, where one external dimension is smaller than 1 nm and the other dimensions are larger than 100 nm" [50].

On another note, according to the ISO/TS 27687:2008, a nanoparticle (NP) is a nano-object with three external dimensions at the nanoscale [51].

Different classifications of nanomaterials (NMs) were found and generally, the authors classify the NMs according to their chemical composition, dimensionality, morphology, and even their origin [52,53].

According to their dimensionality, NMs can be classified into 0D NMs with all their dimensions in the nanoscale (this includes spherical nanoparticles, nanorods, hollow spheres, metal NMs, core-shell NMs, and quantum dots), 1D NMs with two dimensions in the nanoscale (this includes metallic, polymeric, ceramic, nanotubes, and nanorod filaments or fibers, nanowires, and nanofibers), 2D NMs with one dimension in the nanoscale (this includes single-layered, multi-layered, thin films, nanocoatings, and nanoplates), and 3D NMs that have various

dimensions in the nanoscale, and they combine nanocrystals in some directions (this include fibers, foams, nanotubes, fullerenes and layer skeletons). The description of the morphology of the NMs includes flatness and sphericity, along with the aspect ratio. Some NMs with different morphologies include nanozigzags, nanohooks, nanorods, nanoplates, nanohelices, nanostars, and nanocubes.

According to their composition, NMs are subclassified into metal oxides like titanium dioxide (TiO_2) or zinc oxide (ZnO), and metals like silver, gold, or copper. Carbon NMs, include carbon in their composition like graphene dots, graphene, or graphene oxides. Organic NMs are formed by non-covalent bonds, and they are made of organic matter but without carbon or inorganic-based nanomaterials. This subclassification includes liposomes, micelles, dendrimers and polymers. Finally, the nanocomposites are made of a combination of different types of NMs. These nanocomposites can combine ceramic, metal, or polymer bulk materials with nanowires or nanofibers made of metal, carbon, or organic elements, to improve properties such as thermal and electrical conductivity, mechanical strength, and toughness.

Other NMs classification takes into account their origin, with subclassification into synthetic or natural NMs. Natural NMs can occur in biological species like microbes or plants as well as a result of human activity. Volcanic eruptions, forest fires and dust storms are the main natural NMs sources and when these phenomena occur the high amount of emitted NMs affects drastically the air quality of the planet. Synthetic NMs are synthesized by humans with chemical, physical, biological, and hybrid methods. A subclassification includes byproduct NMs, which are produced incidentally as a reaction subproduct in combustion processes in motor vehicle engines. Engineered NMs are mostly made of carbon and they are produced due to the combustion of petrol, diesel transportation, coal for power generation, chemical and industrial manufacturing, re-refining, and oil technology [52,53].

Nanomaterials and nanoparticles may differ from identical materials without nanoscale features due to an increase in specific surface area to volume ratio. As a result, nanoparticles' physicochemical characteristics may vary from those of bulk substances or larger particles. The general attributes of NMs can be classified according to their physical and chemical properties [53-55].

Physical properties of NMs

The physical properties include size, shape, surface effects, quantic effects, surface charge and stability, and even mechanical properties.

- Surface effects

  NMs have a higher surface area to volume ratio. Thus, NMs have more proportion of atoms on the surface, and they are more reactive than the well-coordinated and bonded internal atoms. Besides, the high instability of the outer atoms leads to lower melting points. Therefore, small NPs have a higher proportion of atoms on their surface, and they are more reactive than the largest NPs.
- Quantic effects

  The quantic effect usually appears at the nanoscale, and this effect is also responsible for different properties of NMs in comparison to bulk materials. Quantum confinement appears when the low size of the particle is comparable to the wavelength of the electron. Quantum confinement effects describe electrons in terms of energy levels, potential wells, valence bands (VB), conduction bands (CB), and electron energy band gaps. The confinement means restricting the motion of

USC UNIVERSIDADE DE SANTIAGO DE COMPOSTELA

randomly moving electrons to specific energy levels (discreteness). When the particle size is reduced to the nanoscale, the confining dimensions make energy levels discrete and increase the bandgap of the material. The band gap increment can result in different fluorescent colours due to the different sizes of the particles.

- Surface charge and stability

  The surface charge of NMs plays an important role in their aggregation, stability, and affinity. The surface of NMs in an aqueous solution is charged due to the protonation and deprotonation effects, and then an electrical double layer (EDL) is formed to maintain the neutrality. An oppositely charged ion layer in the solution at some distance from the surface balances the surface charges and also creates an electrostatic potential between any point in the mass of the suspending liquid and the surface. The electrostatic potential at the EDL that surrounds a nanoparticle in solution is the zeta potential. The zeta potential indicates the degree of electrostatic repulsion between adjacent and similarly charged particles in a dispersion. The values of zeta potential depend on the particle size, composition and pH of the medium, and higher values indicate higher colloidal stability and lesser aggregation. Values of ±30 mV of zeta potential indicate stable colloidal suspensions.

- Mechanical properties

  NMs have different mechanical properties than bulk materials. The high surface area increases properties like adhesion, hardness, stress and strain, and elastic modulus. Furthermore, inorganic NMs have better mechanical properties than organic NMs, and these usually are dopped with inorganic compounds to obtain better mechanical properties.

Chemical properties of NMs

The chemical properties include the chemical structure and catalytic, optical, electrical, and magnetic properties.

- Chemical structure

  Nanomaterials' surface and internal structures are frequently made up of multiple layers, phases, and/or components, each of which is essential to achieving the required functionality. Depending on external conditions like pressure and temperature, atoms can be arranged in various ways in lattice configurations that give rise to different crystalline structures for some materials with the same proportions of contained elements. Thus, NMs can have different crystal structures with different physicochemical properties, like reactivity and photocatalytic activity.

- Catalytic properties

  NMs usually have catalytical properties due to their high surface area to volume ratio, and it implies a high surface energy which makes them unstable and very reactive materials. A surface with higher energy is more reactive because it will try to reduce its energy by interacting with suitable substances in the surrounding environment. In contrast to bulk materials, which cannot undergo numerous chemical transformations under mild conditions, these distinctive nanoscale features favor chemical transitions in kinetics. In addition, the catalytic properties of these particles, are also caused by a qualitative shift in the electronic structure brought on by quantum confinement and unsaturated atoms on the surface of

USC UNIVERSIDADE DE SANTIAGO DE COMPOSTELA

nanoparticles, which are more reactive than saturated internal atoms due to the higher surface energy derived from their incomplete bonding environments.

- Optical properties

  The different morphologies of the electronic structure of the NMs are responsible for the optical properties such as transmission, absorption, reflection and light emission. The plasmon resonance and the increase in the energy level spacing (quantum effects) contribute to their size-dependent optical properties. The electrons in the NMs do not have as much freedom of movement as in bulk materials, then this quantum confinement causes NMs to have different optical properties. Semiconductor nanomaterials absorb and emit light at specific wavelengths that are highly dependent on the size and shape of the particles.

  These optical properties (emission and absorption) occur when electrons move between the valence band and the conduction band. This band gap increases with the decrease in particle size. Then, a quantum of light (photon) is produced when there is an electron transition from a state of greater to one of lower energy. Their emission wavelengths can be controlled from the ultraviolet through the visible to the near-infrared, altering the size and composition of the nanomaterials.

  The plasmon resonance phenomenon becomes dominant when the particle size is smaller than the wavelength of the input radiation. The coherent excitation of free nanomaterial electrons in the CB and their resonant oscillations in synchronization with the applied light energy cause surface plasmon resonance (SPR). The intensity of this SPR is directly related to the number of excited electrons and the dielectric constant of the medium. Surface plasmon resonance can occur in metals like aluminium, gold, and silver, in which free electrons in the material naturally resonate at a frequency that depends on the composition, size and shape of the particle.

- Electrical properties

  Due to the energy quantization of NMs, when conductive metals are subjected to certain voltages, they can become insulators. The increase in band gap energy with a reduction in particle size of the nanoparticles, particularly for semiconductor nanomaterials, reduces the electrical conductivity of nanomaterials in comparison to bulk materials. The reduction of the material's dimensions will promote crystal perfection or defect reduction, which will result in a reduction in defect scattering and, finally, a decrease in resistivity and conductivity.

- Magnetic properties

  The large surface area to volume ratio of nanostructures makes it more probable that surface atoms will engage in different forms of magnetic interaction with nearby atoms. The NMs can undergo unusual magnetic effects due to interface and surface effects, including electronic environment, charge transfer, symmetry breaking, and magnetic interaction. Thus, a non-magnetic element can become magnetic at the nanoscale level.

With this wide variety of properties, NMs have a wide range of applications in several fields including energy, catalysis, photocatalysis, optics, medicine, industry, electronics and computing, agriculture, environment, and personal and care products, among others [13]. According to the Scopus database [13] the terms “nanomaterial” and “nanoparticle” appeared in publications for the first time in 1973 and 1970, respectively. Since then, the number of publications in which both terms appear has grown exponentially, especially in the last three

decades. **Figure I.5.** highlights the importance of current research on nanomaterials (**Figure I.5.(a)**) and nanoparticles (**Figure I.5.(b)**) over the years, respectively.

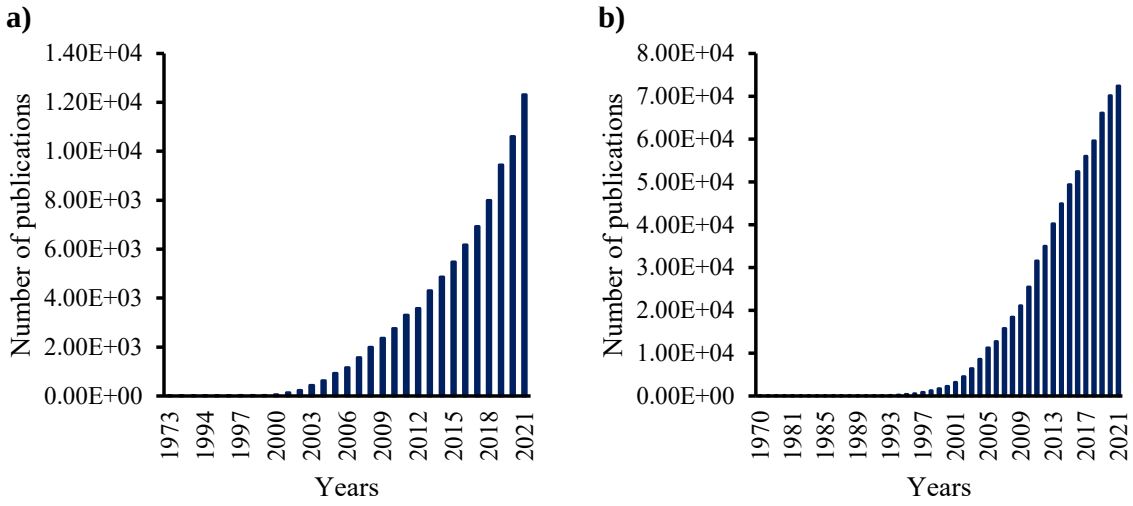

Figure I.5. Evolution of the Scopus database publications with the terms nanomaterial (a) and nanoparticle (b) over the years [13].

I.3.2 Nanoparticles under study

According to the Nanotechnology Product Database (StatNano), silver nanoparticles (AgNPs) and titanium dioxide nanoparticles (TiO_2NPs) are the most widely used along with silicon oxide nanoparticles [56]. **Figure I.6.** shows the numbers of products containing AgNPs and TiO_2NPs in different industrial divisions. In StatNano there are listed 1069 products containing AgNPs, most of them in the medicine, textile, cosmetic, and home appliance sectors. In contrast, 428 products containing TiO_2NPs can be found in cosmetics, construction, textile, and renewable energies [56]. These values highlight the importance of the use of AgNPs and TiO_2NPs.

USC
UNIVERSIDADE DE SANTIAGO DE COMPOSTELA

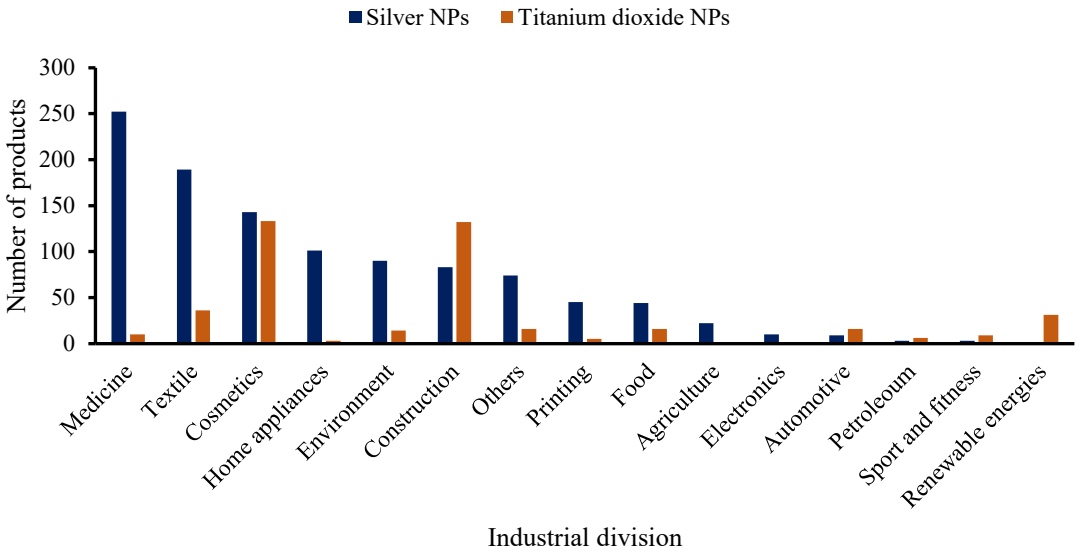

Figure I.6. Nanotechnology Products Database results for the number of products containing AgNPs and TiO_2NPs in the different industrial divisions. Data from [56].

I.3.2.1 Silver nanoparticles

Silver is a noble metal belonging to transition metals and it has high thermal and electrical conductivity. Silver has a white metallic lustre, hardness and little reactivity that make it has been used in jewellery, currency, food serving, and water purification since ancient times, and more recently for electric and industrial applications. Furthermore, Ag^+ has antibacterial properties and it has been used for more than 200 years to treat burn wounds. Silver does not irritate the eyes or skin, it is neither mutagenic nor carcinogenic, and undesirable consequences like argyria are generally the result of incorrect use, typically after oral intake of colloidal Ag solutions [57].

Nowadays, Ag nanoparticles (AgNPs) are gaining significant attention from the scientific community and industries due to their tremendous potential as 0D nanomaterials [58]. Indeed, there are already more than 1,000 consumer products registered that use AgNPs [56], and the production of AgNPs is thought to reach over 800 t per year [59]. AgNPs have novel properties, mainly due to the increase in their surface area to volume ratio. Although the main property of AgNPs is their biocidal effect, other important physicochemical AgNPs properties include their high electrical and thermal conductivity, coloration, catalytic, UV-protection properties, and use in surface-enhanced Raman spectrometry (SERS) [58,60].

AgNPs are applied in several fields including biomedical (drug delivery, cancer therapy, dentistry, cell imaging), textiles (anti-stain textile, UV-blocking textile), health care (cosmetics and UV-protection), electronics (integrated circuit sensors), optics (bio and chemosensors), catalysis (fuel cells), environment (wastewater treatment, air and water purification), food (released from the additive E174) and even agriculture (food quality sensors and food packaging). AgNPs protect against different Gram-positive and Gram-negative bacteria, viruses, and fungi [58,61-66].

Regarding the AgNPs' bactericidal effect, AgNPs are widely employed in the medical industry for disinfecting medical devices, bone cement, surgical instruments, masks, and wound treatment among others. Furthermore, AgNPs are also used in the pharmaceutical and textile industry, and for environmental applications for water and air purification [58,60,67,68].

USC UNIVERSIDADE DE SANTIAGO DE COMPOSTELA

Additionally, AgNPs are increasingly well-known for their ability to prevent various viral infections, including human immunodeficiency virus (HIV-1) and COVID-19 [69-71].

Different capping agents, like sodium citrate, polyvinylpyrrolidone (PVP), and polyethylene glycol (PEG), are commonly used for stabilization and to avoid AgNPs dissolution and agglomeration. Several factors affect the antimicrobial activity of AgNPs, like the size, shape, concentration, surface charge and colloidal state. Besides, there is no scientific consensus as to whether the microbial toxicity of AgNPs is due to the particles themselves or whether it is due to their dissolution and release of ions. Then, the antimicrobial effect of AgNPs could be explained by two steps [63]:

- Physicochemical adhesion of AgNPs on the bacterial membrane, generating membrane destabilization, perforation and holes and cytoplasmic release.
- Damage of microbial subcellular structure by the release of Ag^{+}, generation of reactive oxygen species (ROS) and inactivation of essential molecules such as nucleotides, proteins and enzymes [63].

Humans can be exposed to AgNPs through dermal contact, inhalation, oral administration, and blood circulation [72,73]. Indeed several research groups have investigated the daily dietary, resulting in between 0.4 and 27 µg uptake of Ag [74]. Although bacterial toxicity is a widely employed property of AgNPs, several studies indicate the possible toxicity of AgNPs to animals and even human cells. Indeed, studies demonstrated the AgNPs' toxic effects in albino rat hepatocytes and neuronal cells [75], and human lung epithelial cells [76]. It was also observed that AgNPs affect reproduction and produce morphological deformities in rats [77].

It is believed that smaller AgNPs can pass through the cell wall and the mitochondria where they can affect cellular respiration and adenosine triphosphate (ATP) production through the formation of ROS, and damage the deoxyribonucleic acid (DNA). Moreover, *in vivo* experiments showed the toxicity of AgNPs to mitochondrial functions [78,79].

Although some studies indicate the possible cytotoxicity of AgNPs, this depends on a variety of factors such as the size, shape, capping agent, crystallinity, surface chemistry, ionic strength, pH and even the presence of complexing agents [73]. Then, more investigation is required in this area to clarify the toxicity of the several AgNPs forms.

I.3.2.2 Titanium dioxide nanoparticles

Titanium is a very abundant solid transition metal in the earth's crust, holding the 9th place of abundance in the periodic table. Titanium dioxide (TiO_2), also known as titania, was discovered in 1791. It is the most important Ti compound, and it is commonly used in daily life due to its inertness, non-toxicity, biocompatibility, photoactivity and photocatalytic properties. Their photoactivity and photocatalyst activities were noticed for the first time in 1929 and 1956, respectively [80,81].

TiO_2 is white in color and when it is used in paints is called “titanium white”. Due to its color and photocatalytic properties, TiO_2 is also employed in printing inks, paper, plastic, condensers, synthetic fibers, ceramics, electronic components, and even cosmetics [82]. TiO_2 naturally exists in three different crystalline forms: anatase, rutile, and brookite. Among them, anatase and rutile are more employed due to their properties, and are the most interesting ones for nano applications [54]. Brookite is not commonly found as it is unstable at high temperatures and converts to rutile form; it has orthorhombic symmetry, but rutile and anatase have a tetragonal symmetry (rutile is simple tetragonal and anatase is body-centred tetragonal) [83]. Anatase gained attention as the material selected for applications as gas sensors, solar cells, and

USC UNIVERSIDADE DE SANTIAGO DE COMPOSTELA

photocatalysts. Nevertheless, rutile is more employed in capacitors, filters, power circuits or even temperature condensers [83].

Titanium dioxide nanoparticles (TiO_2NPs) are one of the most widely used metal oxide NPs in the industry according to the Nanotechnology Products Database [56]. In fact, already in 2011, the annual nano TiO_2 production was 10,000 tons per year [84]. The TiO_2NPs' high surface area to volume ratio enhances their light scattering, opacity and photoactivity properties, relative to bulk TiO_2.

The main property of TiO_2NPs is their photocatalytic activity. **Figure I.7.** outlines photocatalysis, which is the combination of catalysis and photochemistry, and that uses light or a catalyst to produce a chemical reaction, in this case, pollutant degradation. The process consists of photoexcitation when TiO_2 absorbs electromagnetic radiation (UV light λ=200-400 nm) and the electrons are excited from the valence band to the conduction band generating electron (e^-)-hole (h^+) pairs. The VB loses electrons and becomes positively charged and the CB gains electrons and becomes negatively charged. Possible recombination of the e^-/h^+ pair occurs due to the low stability of the photogenerated electrons and holes. Then, the e^-/h^+ pairs take part in the oxidation-reduction reactions with species absorbed in the TiO_2 surface, like organic compounds, water, and hydroxide ions (OH^-) generating active species (radicals). The radicals formed in the presence of organic matter, environmental contaminants, and even microorganisms result in their decomposition [82,85]. Anatase presents higher photoactivity than rutile and brookite due to their higher band-gap energy (3.2, 3.02, and 2.96 eV, respectively). Due to their band gaps, anatase always exhibits the type-n conductance, and rutile the unstable type-p conductance. However, due to the anatase-rutile conversion, the TiO_2 is considered a semiconductor with a transition from p-type to n-type at 1,200 K temperature and high oxygen atmosphere [86].

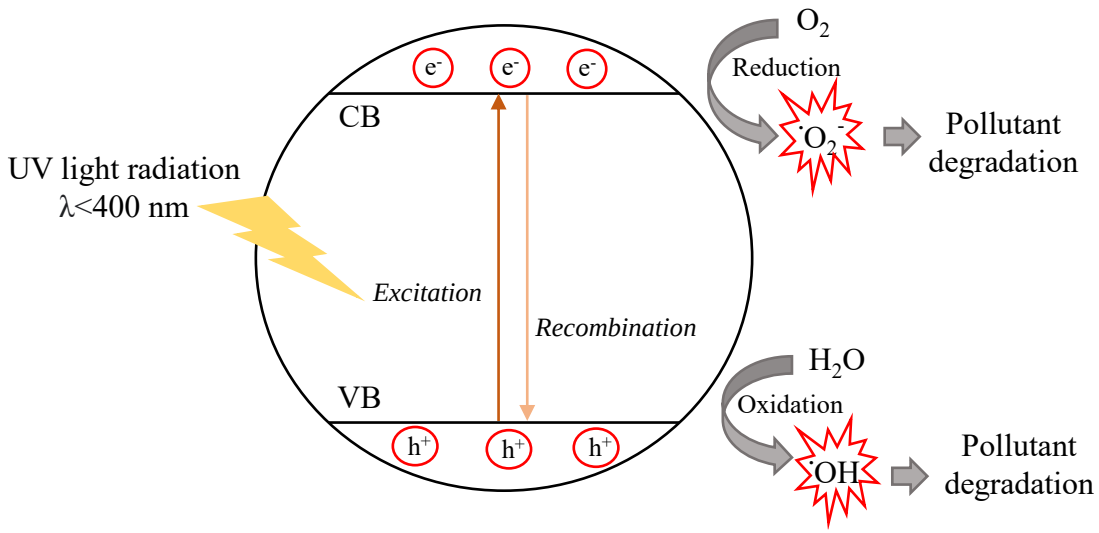

Figure I.7. The phenomenon of photocatalytic degradation. Adapted from [82].

TiO_2NPs photocatalytic property makes them commonly used in applications like environmental treatment and the decomposition of harmful chemicals in wastewater, clean water, odor removal, and construction of self-cleaning and anti-fogging glasses. They can also be used as biocides, and even as catalytic converters in combustion engines. The reactive species formed ($^{\cdot}OH$, $HO_2^{\cdot}$, and H_2O_2) from the photocatalytic process can be used even in

antibacterial, antifungal, and anticancer applications (of carcinoma cells, T24 human bladder cancer cells, HeLa cells, U937 monocytic leukemia cells, and A549 lung cancer cells) [80,86-88].

Due to the high refractive index, strong UV light absorbing capabilities and resistance to discoloration under ultraviolet light of TiO_2NPs, the FDA approves the use of these inorganic filters as UV blockers against UV-A (320–400 nm) and UV-B (290–320 nm) radiation [80,86,89,90].

Furthermore, due to their photovoltaic properties, abundance, low cost, biocompatibility, nontoxic structure, and superior performance than other semiconductor oxides, TiO_2NPs are frequently employed in dye-sensitive solar cells (DSSCs). Indeed, the most effective solar collectors are made of TiO_2NPs, which can capture 3-4% of solar energy [80,86,91].

TiO_2 was popularly used as a food additive (containing TiO_2NPs) for consistency and the white color of some food, and candies. TiO_2 as a food additive is coded E171 in the European Union (EU). However, after their ban in January 2020 by the French government for a year [92] with an extension of another year [93], the European Food Safety Authority (EFSA) [94] concluded that TiO_2 can no longer be considered safe for human consumption, and then, the European Commission (EC) with their Commission Regulation (EU) 2022/63 [95] banned the use of TiO_2 as a food additive beginning in 2022.

On the other hand, the FDA continues to allow the use of TiO_2 as a color additive for food coloring in amounts up to 1% by weight of the food [86]. Further to this, Canada´s Food Health Directorate recently evaluated the security of food-grade TiO_2 as a food additive and concluded that with the existing research, there is insufficient evidence to consider TiO_2 toxic to humans; therefore, they continue to allow its use but they will continue to review future toxicity studies to maintain food safety [96].

The extensive use, mass production, uncontrolled disposal and persistency of TiO_2NPs cause them to be emitted uncontrollably into the environment, where they can be hazardous to organisms [97]. The main exposure routes of TiO_2NPs in humans are dermal contact (mainly through sunscreens), oral administration and gastrointestinal absorption (mainly by E171), and inhalation through the respiratory tract [88].

Therefore, the toxic mechanisms of TiO_2NPs need to be elucidated to understand completely their toxicity. It is believed that the TiO_2NPs toxicity mechanism occurs in three steps, including:

1) ROS production with the induction of electron-hole pairs.

2) Cell wall damage.

3) Lipid peroxidation of cell membrane caused by the attachment of the TiO_2NPs to cells, by electrostatic force enhanced by their high surface area [97].

Several studies were published about the toxicity of TiO_2NPs in algae [98], plants [99], bacteria [100], fish [101] and human cells [102]. However, the toxic effects of TiO_2NPs are also influenced by factors like the physical and chemical properties, sizes, shapes, dispersibility, and precipitation rates of TiO_2NPs in solution [101]. Then, further investigation is needed to ensure TiO_2NPs' safety.

I. 4 ANALYTICAL TECHNIQUES FOR NANOMATERIAL ANALYSIS

The analytical determination of inorganic AgNPs and TiO_2NPs in complex environmental systems, with realistic NPs concentrations, in the presence of natural particles of similar or even different natures, is a challenge. The qualitative information about nanomaterials implies their detection and their chemical (core and coating composition) and physical (size, shape,

USC UNIVERSIDADE DE SANTIAGO DE COMPOSTELA

agglomeration/aggregation) characterization. The quantitative information about NMs implies the knowledge of mass and number concentration information. Therefore, appropriate separation, pre-concentration, characterization and quantification techniques are necessary for NMs analysis in complex matrices [103].

I.4.1 Sample preparation

Sample preparation methods are usually required before NMs analysis by most of the analytical techniques. These methods consist of removing the matrix or separating the NMs from the matrix without altering the NMs' nature. The most common sample preparation methods include digestion/extraction and separation/preconcentration protocols. **Table I.1.** summarizes the information regarding the most common preparation procedures for biological and environmental samples before AgNPs or TiO_2NPs analysis.

Acid-digestion protocols normally employ oxidizing acids to dissolve NMs, degrade the matrix, or both. The use of heat at atmospheric pressure or under pressure with microwave-assisted techniques provides information on the total element content of the NMs present in the sample [104]. Alkaline and enzymatic extractions of NMs are the main separation protocols without size and shape nanoparticle change. Tetramethylammonium hydroxide (TMAH) is commonly employed in NPs extractions for the degradation of organic matter. Sun et al. [105] employed TMAH for the analysis of Ag and Ti-containing NPs from mussel samples. Moreover, Gruszka et al. [106] selected the TMAH methodology as the best way for AgNPs extraction from green microalgae. On the other hand, pectinase and protease enzymes are commonly used to solubilize proteins. Loeschner et al. [107] employed the enzymolysis by proteinase K for AgNPs extraction from chicken meat. Pancreatin/lipase enzymatic mixtures are also employed to isolate AgNPs [104] and TiO_2NPs [108] from seafood. In the case of vegetal tissues, multicomponent enzymatic mixtures such as Maceroenzyme®, are also used to digest plant cell walls and extract the nanoparticles [109,110].

Since the nanoparticle concentration in biological and environmental matrices is small, preconcentration or separation techniques are usually necessary to avoid matrix interferences. Simple particle separation techniques include centrifugation, filtration, ultrafiltration (UF), and dialysis as well as liquid-liquid extractions (LLE) and solid phase extractions (SPE) [103]. Cloud point extraction (CPE) has gained popularity in recent years as a liquid phase extraction technique for the preconcentration of nanoparticles. CPE provides selective separation of nanoparticles from dissolved species, maintaining their size and morphology. CPE commonly uses non-ionic surfactants (such as Triton-X 114) above the critical micellar concentration and the cloud point temperature (CPT). Thus, the nanoparticles are incorporated into the micellar phase from the aqueous one. Some research works reported the use of CPE as a preconcentration and separation step of inorganic nanoparticles, like AgNPs [111] and TiO_2NPs from water samples [112].

Moreover, hexane is also employed as an LLE reagent for TiO_2NPs extraction from sunscreens [113]. Regarding SPE, ionic exchange resins are employed for noble metal nanoparticles extractions including AgNPs [114].

USC UNIVERSIDADE DE SANTIAGO DE COMPOSTELA

Table I.1. Most common preparation protocols of environmental and biological samples for NPs determination.

Analyte	Matrix	Sample pretreatment	Conditions	Ref.
AgNPs	Mussels, cockles, oysters, clams, scallops	Acid digestion (for total Ag)	Microwave-assisted acid digestion HNO_3 + H_2O_2 + H_2O	[104]
	Mussels	Alkaline extraction	5% TMAH + 1300 mg L^{-1} BSA 25º C, 12 h Centrifugation 3000 rpm, 5 min	[105]
	Microalgae	Alkaline extraction	10% TMAH Sonication with ultrasound probe 15 min (100% amplitude, 5 s on/ 3 s off) Room temperature, 24 h	[106]
	Chicken meat	Enzymatic extraction	0.25 mg chicken + 5 mL Proteinase K solution (made by 3 mg mL^{-1} in 50 mM ammonium bicarbonate buffer (pH=7.4) containing 5 mg mL^{-1} SDS and 0.2 mg mL^{-1} sodium azide) 40 min, water bath at 37º C	[107]
	Arabidopsis plants	Enzymatic extraction	Plant sprout (5-8 cm) + 8 mL 2 mM citrate buffer 50 g L^{-1} of Macerozyme® R-10 Shaken 24 h, 37 ºC	[109]
	Mussels, cockles, oysters, clams, scallops	Enzymatic extraction	1.0000 g sample + 7.5 mL of 3 g L^{-1}/ 3 g L^{-1} pancreatin/lipase solution in buffer 0.2/0.2 M NaH_2PO_4/NaOH Incubation 37º C, 150 rpm, 12 h Centrifugation 3900 rpm, 25 min	[104]
	Environmental waters	Cloud Point Extraction	20 mL sample + 500 µL of TX-114 8.6% +750 µL saturated EDTA + 250 µL 1.25/1M HAc/Ac^- buffer (pH=7) Heated 60º C, 20 min Centrifugation 7000 rpm, 20 min and 4 ºC Phase separation	[111]
		SPE with ionic exchange resins	Amberlite IRN-78 with ammonium groups positively charged Adsorbed NPs extracted using 8% (v/v) formic acid in methanol and shaking at room temperature	[114]

USC UNIVERSIDADE DE SANTIAGO DE COMPOSTELA

Table I.1. Continued.

Analyte	Matrix	Sample pretreatment	Conditions	Ref.
TiO_2NPs	Surimi	Enzymatic extraction	1 g sample + 7.5 mL of 8 g L^{-1}/ 8 g L^{-1} pancreatin/lipase solution in buffer 0.2/0.2 M NaH_2PO_4/NaOH 37º C, 200 rpm, 12 h Centrifugation 3900 rpm, 10 min	[108]
	Radish	Enzymatic extraction	0.020 g + 7 mL 2 mM citrate buffer (pH=4.5) + 26.7 g L^{-1}/6.7 g L^{-1} of Macerozyme® R-10 for leaves + stems/roots Shaken 24 h, 37 ºC	[110]
	Pool water	Cloud Point Extraction	10 mL water sample + 300 µL 1% (w/v) TX-114 + 125 µL 0.2 M NaCl Heated 40 ºC, 30 min Centrifugation 3500 rpm, 5 min Phase separation	[112]
	Sunscreens	Hexane extraction	0.1 g sunscreen + 10 mL hexane+ sonication bath for 1 min + to settle for 1 h Centrifugation 3000 rpm, 5 min Separation, and resuspension of Ti residue phase into 20 mL of ultrapure water + sonication bath, 30 min	[113]

I.4.2 Continuous separation techniques

Several techniques showed their ability to separate particles according to their surface, size, density, and charge characteristics. They are usually hybridized with sensitive and selective detectors for the resolution of complex nanoparticulate systems [103].

I.4.2.1 Field-flow fractionation

In field-flow fractionation (FFF), the separation of particles takes place in a flat and elongated channel, without a stationary phase. The separation occurs by applying an external and perpendicular force to the laminar sample flow into the channel. The most employed forces applied for nanomaterial separations are centrifugation in sedimentation FFF (SdFFF), and a perpendicular flow in flow FFF (FlFFF). Asymmetric flow field-flow fractionation (AF4) is the most suitable FlFFF technique to separate nanoparticles, where the cross-flow liquid is affected by all the species in the channel, and separation occurs based on the hydrodynamic size of the particles [103]. NPs are separated according to diffusion coefficients, which are related to their size and density. The position of the particles in the channel determines which streamlines of parabolic velocity flow are applied to them. The smaller particles are more separated from the membrane and elute faster [115]. The offline fractions can be collected and analyzed by ETAAS, ICP-OES or TEM. However, AF4 can be online coupled to several detectors like ICP-MS, UV-Vis, DLS, or NTA. Several authors used AF4 as a separation technique for AgNPs determination in food matrices like chicken meat [107], milk [116], and seafood [115], and in environmental matrices like natural waters [117] and artificial seawater [118]. Furthermore, AF4 was also used for the separation of TiO_2NPs in sunscreens [119] and food matrices containing E171 such as powdered beverages [120] and surimi [121].

I.4.2.2 Chromatographic techniques

Hydrodynamic chromatography (HDC) and size exclusion chromatography (SEC) are chromatographic techniques used for NPs separation. HDC columns are packed with non-porous beads, building up flow channels, where the larger particles elute faster than the small ones that interact with the edges of the capillaries [103]. SEC columns are commonly packed with small, rigid polymeric or silica porous particles. The separation of molecules is according to their size in solution, where the larger particles elute before because they enter fewer pores than the smallest ones [122]. The main difference between both techniques is that in HDC there are no interactions between the nanoparticles and the stationary phase but in SEC this interaction is expected. Chromatographic separation techniques are commonly coupled to different detector systems (ICP-MS, SP-ICP-MS, DLS, UV-Vis, and fluorescence). Although some reports were found about the use of HDC in the separation of AgNPs before their determination in biological samples (like blood plasma of burn patients [123]), and environmental samples (like environmental waters and wastewater [124]), the use of HDC for nanoparticles separation remains underutilized. On the other hand, the main problem for nanoparticles separation is their adsorption in the stationary phases. Thus the stationary phase needs to be selected properly. Amino separation columns in SEC have been proposed for AgNPs separation from ionic Ag in antibacterial products and environmental waters [125].

I.4.2.3 Electrophoresis

The electrophoretic techniques consist of the separation of charged species under the influence of an electric field. Although electrophoretic techniques are not widely used in nanomaterials separation in real samples, some common electrophoretic techniques for

USC DE COMPOSTELA

nanoparticle separation are gel electrophoresis (GE) and capillary electrophoresis (CE). The analytes in GE migrate through a nanoporous gel under an electric field. However, the separations in CE depend on the mobility of charged species under an electrolyte solution in a thin capillary with high voltages applied at both ends [103].

Agarose gel electrophoresis (AGE) was used for polylethylene glycols derivatized AgNPs and AuNPs separations. Moreover, polyacrylamide gel electrophoresis (PAGE) was used to characterize quantum dots. On the other hand, CE can be used for metallic NPs (Au, Pt, and Pd) separation by using sodium dodecylbenzene-sulfonate in the background electrolyte [103].

I.4.3 Physicochemical characterization and quantification of nanomaterials

Several characterization and quantification techniques are available for nanomaterials characterization and/or determination in complex matrices. The most significant techniques are described below.

I.4.3.1 Electron microscopy

Electron microscopy is a powerful tool for nanomaterial analysis due to its ability to visualize particles, their size, shape, aggregation and dispersion state. Although it can not be considered an ideal quantitative technique, it is used as the perfect guide for interpreting the results of other nanoparticle quantification techniques. Scanning electron microscopy (SEM) consists in scanning the surface through a beam of accelerated electrons. The interaction between the beam and the sample generates signals related to its atomic composition and topography, but not the internal composition. In environmental scanning electron microscopy (ESEM), the chamber operates at a low-pressure and high-humidity gaseous environment, and the nanomaterial samples can be visualized in their natural state under humidity conditions up to 100% [126].

On the other hand, transmission electron microscopy (TEM) is the most common technique used for NMs characterization. In TEM, the images come from the transmission of the incident beam through a sample deposited and dried in a TEM grid. Furthermore, SEM and TEM can be coupled with energy dispersive X-rays (EDX) to obtain the elemental composition of the light and heavy elements in the sample. TEM can also be coupled with electron energy loss spectrometry (EELS) to obtain structural and chemical information like the oxidation state of the elements. In scanning transmission electron microscopy (STEM), the determination is performed by transmission in all the sample thicknesses but also allows sweeps [103].

Several studies used electron microscopy, in combination with other techniques, to characterize synthesized AgNPs [127,128] and TiO_2NPs [129,130]. Furthermore, electron microscopy is also reported as a complementary technique for silver and titanium dioxide nanoparticles determination in different kinds of matrices like food and environmental matrices. Verleysen et al. [66] reported the release of AgNPs from the additive E174 used in pastry. Authors characterized AgNPs by TEM and by STEM coupled to EDX to obtain the crystalline structure of particles and mapping [66]. Zhang et al. [131] used TEM and EDX to confirm the presence of AgNPs in oyster tissues exposed to these NPs [131]. Moreover, Farkas et al. [132] characterized AgNPs from the effluent of a washing machine by TEM-EDX [132].

Taboada-López et al. [108] used TEM to characterize the TiO_2NPs present in enzymatic extracts of surimi samples [108]. Windler et al. [133] characterized the TiO_2NPs on the surface of textiles using SEM-EDX, and the TiO_2NPs were released to water in the washed solution by TEM-EDX [133]. Turner et al. [134] characterized TiO_2NPs present on the surface of different plastics by SEM and the presence of Ti by EDX [134].

USC DE COMPOSTELA

I.4.3.2 Surface probe microscopy

Scanning tunnelling microscopy (STM), atomic force microscopy (AFM) and near-field scanning optical microscopy (NSOM) are surface probe microscopy (SPM) techniques suitable for nanostructures investigation. In STM, a tip is brought close to the surface of an object and the interactions between the probe and the surface are measured. The tip is close enough to the sample to be in the tunnelling range. Thus, a voltage applied between the scanning tip and surface and moving through the x-y surface plane, causes tunnelling of the electrons to generate a map of charge density. On the other hand, AFM does not require a conductive surface. The attraction or repulsion between the atoms in the tip and the sample, due to electrostatic van der Waals forces, are transduced into the motion of a micro-machined cantilever (typically made of silicon or silicon nitride).

Although both (STM and AFM) can be used to investigate nanomaterials' size, shape, structure, sorption, dispersion, and aggregation, STM is a popular technique for studying the conductive atomic structures of materials such as carbon nanotubes, fullerenes, and graphene. On the other hand, NSOM combines optical microscopy and SPM. It allows laser light guided in the optical fiber to emit through the tip aperture when it is close to the object. Size and shape nanomaterials information is obtained by NSOM [126,135].

I.4.3.3 Light scattering techniques

Light scattering techniques use the interaction of radiation with a sample to obtain information about the size, shape, structure and aggregation of NMs. Dynamic light scattering (DLS) is the most common scattering technique to measure the hydrodynamic size of nanoparticles in aqueous solutions. Using the time-dependent variations in scattering intensity caused by constructive and destructive interferences, DLS determines the Brownian motion of NPs and correlates this motion to an equivalent hydrodynamic diameter [103]. The main drawback of DLS is that it needs information on the refractive index and the viscosity, which is difficult to know in complex samples [103,136]. Although some reports were found where DLS is employed for AgNPs [117,137] and TiO_2NPs [138,139] characterization, it is commonly combined with other techniques, like SEM and TEM.

Multi-angle light scattering (MALS) provides the ability to measure the physical characteristics generated from the angle dependence of the light dispersed by the particles. Measuring time-averaged scattering intensities of particles at various angles, MALS can provide radius gyration, and in combination with DLS can provide information about particle shape. Since MALS requires cleaner samples than DLS, it is not frequently utilized in the characterization of complex nanomaterial samples.

A light scattering technique called nanoparticle tracking analysis (NTA) uses video microscopy to assess the velocity of particles moving under Brownian motion. A modified Stokes-Einstein equation is used for the determination of the hydrodynamic diameters of the particles. The distance of a particle motion in a time interval is correlated with the hydrodynamic diameter. Thus, the particle number-concentration and hydrodynamic-size distributions are derived by combining and analyzing this data from a large number of particles. NTA is able to measure a huge number of individual NPs in less time than microscopy approaches because it exhibits great sensitivity in terms of particle-number concentration, minimal sample disturbance, and reliable size distributions in the presence of large particles or aggregates [103,137]. The NPs hydrodynamic radius and concentration sometimes are determined using the combination of DLS and NTA. For instance, Gevorgyan et al. [137] used both light scattering techniques for the characterization of green synthesized AgNPs [137].

I.4.3.4 Electroanalytical techniques

The two electroanalytical techniques used specifically for nanomaterial analysis are particle collision coulometry (PCC), and voltammetry of immobilized particles (VIP), which is capable to determine the oxidation state of particles [103]. Therefore, Hernández et al. [140] applied PCC for the quantification and size determination of AgNPs in consumer products. Besides, Vidal et al. [141] reported the use of immobilized nanoparticle voltammetry, for the sorption of AgNPs in suspensions and discrimination of Ag^0 and Ag^+.

I.4.3.5 Spectrometric techniques

Surface-enhanced Raman scattering (SERS) is a spectroscopic technique in which the signals are enhanced by the presence of nanoparticles containing Raman-active species. Differences in the intensity of SERS signals reveal differences in morphologies and sizes of NMs like in the case of Ag nanospheres, nanorods, and nanostars [142].

The absorbance of UV-Vis spectroscopic spectra can be used for NPs composition, size, and shape determination. Nanoparticle size is determined by studying the shape and position of the localized Surface Plasmon Resonance (SPR) peak. The SPR peak for spherical AgNPs (30 nm) and Ag nanorods (40 nm length and 12 nm width) are at 420 nm and 420 and 615 nm, respectively [142,143].

Infrared (IR) spectrometry is used when a molecule has a time-variant dipole moment and its oscillating frequency is the same as the incident IR light frequency. The absorption of IR radiation transfers energy to the molecule and causes the bending, twisting or stretching of the covalent bonds. For nanomaterials applications, the Fourier transform infrared (FTIR) spectroscopy is commonly used to reveal nanomaterial-biomolecule conjugation, like proteins bound to NP surfaces, and to illustrate the conformational states of the bound proteins through the expression of characteristic spectral bands. Furthermore, FTIR can confirm the functional molecules covalently grafted onto carbon nanotubes. Attenuated total reflection-FTIR (ATR-FTIR) spectrometry is a recently developed technique that uses total internal reflection to investigate the structure of adsorbed/deposited species at a solid/air or solid/liquid interface, avoiding the drawbacks of sample preparation complexity and spectral irreproducibility of IR conventional methods. Although ATR-FTIR spectroscopy can be used to investigate the surface features of nanomaterials, it is not a very sensitive surface-analysis method at the nanometer scale [126].

X-ray absorption spectrometry (XAS) provides element-specific qualitative information and quantitative distribution, but not the nature of complex solid and liquid samples. XAS is divided into X-ray absorption near edge structure spectrometry (XANES) which provides information about oxidation state and geometry, and extended X-ray absorption fine structure (EXAFS) which provides element coordination. Some reports about the use of XAS were found to study the accumulation and transformation of NMs in plants exposed to AgNPs [144] and TiO_2NPs [145].

Atomic spectrometry techniques for elemental analysis include electrothermal atomic absorption spectrometry (ETAAS), inductively coupled plasma optical emission spectrometry (ICP-OES) and inductively coupled plasma mass spectrometry (ICP-MS). Although these spectrometric techniques alone can not provide any information about the physicochemical form of the NMs, they can be used for sensitive detection and quantification of the total element content in the sample. The most common technique used for the total element determination in the inorganic NPs is ICP-MS due to the low limits of detection (LOD) achieved (down to ng L^{-1}),

USC UNIVERSIDADE DE SANTIAGO DE COMPOSTELA

while ICP-OES reports LODs of μg L^{-1}. ETAAS can be also used to analyze solid samples as slurries [103].

For NMs determination ETAAS and ICP-OES are commonly coupled with different sample preparation techniques, whereas ICP-MS is commonly online coupled with continuous separation techniques like HDC, SEC, AF4, or working in the new ICP-MS application mode called Single Particle-ICP-MS (SP-ICP-MS) [103,146,147].

Atomic spectrometric techniques were used in several studies for the quantification of Ag and Ti present as AgNPs and TiO_2NPs in different environmental samples [111,112], and even in bioaccumulation and biodistribution studies [146-148].

I.4.4 Inductively coupled plasma mass spectrometry

ICP-MS is one of the most versatile elemental techniques which routinely offers quick multielement analysis and low detection limits for a wide range of materials. Liquid samples are introduced into the ICP-MS through the nebulization system, conformed by a nebulizer and a spray chamber, which nebulize the liquid samples into a polydisperse aerosol. The solvent of the droplets is vaporized into the plasma, and the solid particles are atomized and ionized. Ions are drawn out of the interface and into the mass spectrometer, where they are identified and separated based on their mass/charge (*m/z*) ratio [149].

I.4.4.1 SP-ICP-MS

Single Particle-ICP-MS (SP-ICP-MS) is a powerful ICP-MS method for the detection, quantification and characterization of NPs, colloids, and microparticles. SP-ICP-MS reports qualitative information on the presence of dissolved forms, the quantification of NPs as nanoparticle number as well as mass concentration, and the characterization of the size distribution [150]. SP-ICP-MS works using the principles of the ICP-MS but performs the measurements on a " particle by particle" basis [149].

The methodology under SP-ICP-MS consists in measuring nanoparticles at a very low number of concentrations (10^8 part L^{-1} or lower) and very high data acquisition frequencies (greater than 10^4–10^5 Hz) [103,149]. This allows for distinguishing the transitory signals corresponding to nanoparticles (discrete groups of atoms) from the dissolved analyte (baseline).

The theoretical basis for SP-ICP-MS performance was initially described by Degueldre and Favarger [151] and recently discussed by Laborda et al. [149,150].

Equation I.1., **Equation I.2.**, and **Equation I.3.** summarize the main principles behind SP-ICP-MS.

Taking into account the assumption that one event corresponds to a single particle, the number of events (N_P) in a determined acquisition time (t_i) is directly proportional to the number concentration of particles (C_P).

$$N_P = Q_{sam}\,\eta_{neb}\,t_i\,C_P \quad (\textbf{Equation I.1.})$$

Where Q_{sam} is the sample flow rate and η_{neb} is the nebulization efficiency. Furthermore, the intensity of the event (I_P) is directly proportional to the number of atoms monitored in each detected particle, and then, to the mass of the particle (M_P).

$$I_P = K_{ICPMS}\,K_M\,M_P \quad (\textbf{Equation I.2.})$$

Where K_{ICPMS} is the detection efficiency (ratio of detected ions number versus the introduced ions into the ICP-MS), and K_M is a factor ($K_M=AN_{AV}/M_M$), where A is the atomic

abundance of the selected isotope, N_{AV} is the Avogadro's number, and M_M is the atomic mass of the element.

Moreover, taking into account a homogeneous, solid, and spheric particle **Equation I.2.** can be written as **Equation I.3.**

$$I_P = K_{ICPMS}\, K_M\, \frac{1}{6}\, \pi\, \rho\, F_P\, d^3 \quad (\textbf{Equation I. 3.})$$

Where ρ, F_P, and d are the density, the mass fraction of the element, and the diameter of the nanoparticle, respectively [150].

Thus, when a single particle is nebulized into the plasma, a single pack of ions will be generated. Scans are plotted as the signal intensity versus the signal intensity frequency, with a typical first distribution corresponding to the dissolved analyte and background, and the second one corresponding to the NPs [149]. Each peak in SP-ICP-MS is due to a pack of ions, the particle concentration is directly related to the peak numbers, and the size of the particle is directly related to the intensity of the peak. Finally, the histograms are obtained.

The data acquisition times in SP-ICP-MS can be in the order of milliseconds to microseconds. When the ICP-MS works in millisecond acquisition times, the LODs are independent of dwell times (t_{dwell}) but when the ICP-MS works at microseconds acquisition times the LODs are dependent on t_{dwell} [152].

Thus, Laborda et al. [152] reported a harmonized way to calculate the limits of detection in SP-ICP-MS. LOD_{size} and LOD_{number} are employed to calculate the LODs in SP-ICP-MS. For microsecond t_{dwell} times, the LOD_{size} can be calculated using **Equation I.4.**, where σ_B is the standard deviation of the mean baseline signal, w is the peak width at microsecond times, and t_{dwell} is the dwell time:

$$LOD_{size} = X_D^{size} = \left(\frac{30\, \sigma_B}{\frac{2}{w}\, \pi\, \rho\, F_P\, K_{ICPMS}\, K_M\, t_{dwell}} \right)^{1/3} \quad (\textbf{Equation I. 4.})$$

Furthermore, for the LOD_{size} calculations, a 5σ threshold coefficient was suggested by Laborda et al. [152] to avoid possible false positives (background or dissolved analyte signals) that could occur with a threshold coefficient of 3σ.

The LOD_{number} can be calculated using **Equation I.5.**, where $Y_{N,B}$ is the mean number of particles counted in a blank.

$$LOD_{number} = X_D^{number} = \frac{\sqrt[5]{Y_{N,B}} + 3}{\eta_{neb}\, Q_{sam}\, t_i} \quad (\textbf{Equation I. 5.})$$

Due to their sensitivity, their wide dynamic range, their ability to quantify the NPs' number concentration, characterize their size, and distinguish among the ionic forms, SP-ICP-MS is a perfect tool for NPs study in complex matrices. Indeed, in the last two decades, the investigation related to SP-ICP-MS has increased linearly, mainly in Chemistry and Environmental Science [13]. **Table I.2.** summarizes several reports found in the literature for NPs characterization and quantification in several food and environmental matrices by SP-ICP-MS.

UNIVERSIDADE DE SANTIAGO DE COMPOSTELA

Table I.2. Several nanoparticle studies in different kinds of matrices using SP-ICP-MS as the main analytical technique.

	Matrix	NP type	Sample preparation	Techniques	Analytical information	LOD	Ref
Food	Zebrafish exposed to NPs	TiO_2	Enzymatic extraction Proteinase K	SP-ICP-MS TEM	SP-ICP-MS extracts: $3.1\times10^6\pm0.1\times10^6$ part mL^{-1} Mean sizes:93±3 nm	LOD_{size}: 49±5 nm	[148]
	Zebrafish exposed to NPs	Au and Ag	Alkaline extraction with TMAH	SP-ICP-MS TEM	Bioconcentration factors: 80 nm AuNPs in intestine: 46.53 L Kg^{-1} 80 nm AgNPs in intestine: 254.62 L Kg^{-1}	Method detection limit: Au: 0.5 ng L^{-1} Ag: 3.2 ng L^{-1}	[153]
	Bivalve molllusks (oysters, mussels, scallops, clams, and ark shells) samples	Ti, Cu, Zn, and Ag	Enzymatic extraction Pancreatin/lipase	SP-ICP-MS	Mean sizes: Ti: 65-71 nm Cu: 72-90 nm Zn: 98-108 nm Ag: 43-51 nm	-	[147]
	Surimi samples	TiO_2	Enzymatic extraction Pancreatin/lipase	SP-ICP-MS TEM	Mean sizes: 65±5-217±23 nm	LOD_{size} 3σ and 5σ: 31 and 37 nm LOD_{number} 5.1×10^5 NPs g^{-1}	[108]
	Milk spiked with NPs and migration to breast storage bags	Ag	Enzymatic extraction Proteinase K	SP-ICP-MS and AF4-ICP-MS TEM/DLS standards characterization	AgNPs primary size/AgNPs standard by TEM/AgNPs after enzymatic extraction: 40/41/43 nm 60/59/61 nm 80/81/79 nm	SP-ICP-MS LOD 0.5 µg L^{-1} LOQ 5.6 µg L^{-1}	[116]
	Chicken meat exposed to NPs	Ag	Enzymatic extraction Proteinase K	Interlaboratory analysis by SP-ICP-MS	Different mean sizes were obtained in each laboratory test	LOD_{size}: 20 nm	[154]
Plants	Radish exposed to NPs	TiO_2	Enzymatic extraction Macerozyme® R-10	SP-ICP-MS	30 nm TiO_2NPs exposure suspension: Roots: 3.7×10^{11} NPs L^{-1} Leaves: 3.3×10^9 NPs L^{-1}	LOD_{size}: 15 nm	[110]
	Arabidopsis plants exposed to NPs	Ag	Enzymatic extraction Macerozyme® R-10	SP-ICP-MS TEM	Most frequent size: 21 nm	LOD_{size}: 10 nm	[109]
	Mustard and lettuce plants exposed to NPs	Au	Enzymatic extraction Macerozyme® R-10	SP-ICP-MS	Mustard: 1.24×10^7 NPs L^{-1} Lettuce: 4.39×10^7 NPs L^{-1}	-	[155]

Table I.2. Continued.

	Matrix	NP type	Sample preparation	Techniques	Analytical information	LOD	Ref
	Sinapsis alba samples	Pd	Enzymatic extraction Macerozyme® R-10	SP-ICP-MS TEM	Mean size: 47 nm (leaves) 41 nm (stems) 49 nm (roots)	LOD_{size}: 20 nm	[156]
Algae	Trophic transfer from microalga *Pseudokirchneriella subcapitata* exposed to NPs to *Daphnia magna* and the omnivorous mysid *Limnomysis benedeni*	Cu	Alkaline extraction with TMAH	SP-ICP-MS Characterization CuNPs by TEM, SP-ICP-MS, DLS	Bioconcentration factors: NPs: 10^2-10^3 L Kg^{-1} d.w. Cu^{2+}: 10^3-10^4 L Kg^{-1} d.w. Mean sizes: 22-40 nm	-	[157]
	Green microalgae *Desmodesmus subspicatus* exposed to NPs	Ag	Alkaline extraction with TMAH	SP-ICP-MS	Biosorption factors of AgNPs by algal cells: AgNPs 40 nm: 45.5±3.0 % AgNPs 60 nm: 34.6±2.6 % AgNPs 75 nm: 27.0±3.0 %	LOD_{size}: 20 nm LOD_{number}: 9.7×10^5 NPs L^{-1}	[106]
Environmental	Environmental waters samples	Ag_2S	CPE	SP-ICP-MS	Mean sizes between: 94.19±2.72 and 97.25±0.22 nm	LOD_{size}: 22 nm LOD_{number}: 5×10^4 part L^{-1}	[158]
	Sewage sludge	Ag	Aqueous extraction with sodium pyrophosphate tetrabasic Overnight incubation Centrifugation (5 min, 289 g)	SP-ICP-MS TEM+EDX DLS	SP-ICP-MS reference AgNPs dispersions: 59±7 nm SP-ICP-MS after extraction: 58±6 nm TEM extracts: 62±9 nm	Ag LOD_{size}: 23 nm LOD_{number}: 3.12×10^9 part Kg^{-1}	[159]
	TiO_2NPs released from five different textiles	TiO_2	400 cm^2 of textile + 200 mL ultrapure water Ultrasound bath sonication (15 min) Shaking 24 h Ultrasound bath sonication (15 min)	SP-ICP-MS TEM	TiO_2NPs size is between 49.3±15.4 and 75.8±40.6 nm TiO_2 NPs concentration is between $1.87\times10^6\pm7.80\times10^4$ and $2.79\times10^7\pm2.94\times10^6$	LOD_{size}: 27-33 nm	[160]

- Non-specified

I.4.4.2 SC-ICP-MS

Single cell-ICP-MS (SC-ICP-MS) has opened a new research area in the analysis of inorganic NPs and dissolved metals in cells of a variety of matrices. SC-ICP-MS allows the quantification of metal concentration on an individual cell basis down to the attogram (10^{-18} g) per cell level [161]. The number of NPs per cell, the concentration of NPs and dissolved metal in the cell, the mass distribution within a cell population, and the mass of metal per cell can be determined using SC-ICP-MS [162].

SC-ICP-MS is based on the same principles as SP-ICP-MS, but in this case, a cell suspension is nebulized. Each cell enters the plasma through a specific SC-ICP-MS introduction system is ionized, and the resulting ion burst from the intrinsic metal is detected by ICP-MS [162]. Therefore, appropriate dilution of the sample, short dwell times, and a minimal sample uptake rate (10 μL min^{-1}) are needed [163].

The main challenge in SC-ICP-MS is to maintain the integrity of the cells through the introduction system before ionization. The introduction system must preserve cell integrity and have a high transport efficiency. The suitable choice of this sample introduction system can reflect on the analytical parameters such as trueness and sensitivity [164]. Although several nebulization introduction systems have been proposed for SC-ICP-MS, microflow-based nebulizers in combination with special spray chambers are commonly employed [165]. The specific spray chambers have a tangential flow with a dual make-up Ar entrance, to prevent cell collision and deposition in the chamber walls.

In SC-ICP-MS, the analyte mass in the cell (M_{cell}) can be calculated using **Equation I.6.** [164], where η_{neb} is the nebulization efficiency, Q_{sam} is the sample flow uptake, t_{dwell} is the dwell time, I_{cell} and I_{bkg} are the intensity of cell and background, respectively, and m is the slope from the calibration curve.

$$M_{cell} = \frac{\eta_{neb}\, Q_{sam}\, t_{dwell}\, (I_{cell} - I_{bkg})}{m} \quad \textbf{(Equation I. 6.)}$$

Finally, mass frequency histograms in SC-ICP-MS are obtained. These are made as a function of the mass analyte per cell versus the number of cell events.

SC-ICP-MS is a powerful emergent technique applied in different fields. Several reports have been published for the assessment of the internalization of metals and NPs in different kinds of cells. Corte-Rodríguez et al. [163] applied SC-ICP-MS for total Pt determination in cancer cells. Cao et al. [166] reported the detection of Cu in single human red blood cells. Furthermore, SC-ICP-MS have been used for Fe content measurement in bacterial single-cells [167]. On the other hand, Merrifield et al. [161] quantified the AuNPs uptake and distribution in freshwater algae *Cyptomonas ovate*. SC-ICP-MS has also been employed to study the AgNPs uptake by human THP-1 monocytes [168], and the presence of SeNPs in yeast cells [169].

USC UNIVERSIDADE DE SANTIAGO DE COMPOSTELA

I.5 BIOACCUMULATION, BIOACCESSIBILITY AND BIOAVAILABILITY STUDIES

The consumption of safe food by the world's population is necessary to ensure the health of human beings. The extensive use of NPs and NMs, and their constant release into the environment means that they are assimilated by various species, accumulated, and even enter into the food chain [170], with humans as the final acceptors [171]. Due to the existence of controversy about the toxicity of the studied NPs (AgNPs [75,76] and TiO_2NPs [99,101]) and the consumption importance of the studied species (seaweed, mussels, and turbot [1]), it is necessary to study the bioaccumulation, bioaccessibility and bioavailability of NPs from these products, to ensure the food safety.

The Organization for Economic Co-operation and Development (OECD) Test Guideline 305 (TG 305) defined *bioaccumulation* as "a process in which the chemical concentration in an organism achieves a level that exceeds the concentration in the respiratory medium (water for a fish or air for a mammal), the diet, or both" [172].

A *bioaccessible fraction* is the proportion of a component that is released from the food matrix to the digestive juice. This fraction can remain intact and be excreted, or on the contrary, it can be digested and assimilated by the gastrointestinal (GI) tract. On the other hand, the *bioavailability fraction* is the absorbed bioaccessible fraction that crosses the gastrointestinal barrier through the bloodstream.

NPs' identification and quantification during digestion in the GI tract lumen, and their absorption through the intestine epithelium are important in their risk assessment [173]. The digestion starts in the oral cavity, followed by one to two hours in the stomach, where the food is enzymatically degraded with pepsin at an acidic pH. Then the resulting chyme is released into the duodenum where it is mixed with pancreatin enzymes, bicarbonate and bile salts from the liver. The absorption takes place mainly in the large and small intestines.

Oral intake is one of the most frequent routes of NPs entry. After digestion, there are several ways by which NPs can transverse the intestine epithelium and reach the bloodstream. These mechanisms include the internalization and active transport through epithelial cells (transcytosis), transcytosis through microfold (M) cells, and paracellular transport through interepithelial tight junctions. Commonly, the inorganic NPs are undigestible and they are mainly excreted by feces, but even a small fraction that crosses the epithelial barrier can cause them to accumulate throughout an individual's lifetime [174].

Several models that closely mimic human physiology have been used to evaluate the solubility, digestion, and epithelial permeability of typical food and drugs in the buccal cavity, stomach, small intestine, and colon. These include the *in vivo* and *ex vivo* animal models, *in vitro* non-cellular fluid models, *in silico* computational models, and the *in vitro* cell culture models [173]. *In vitro* cell culture models, are the most common models used. They employ immortalized cell lines that can form a monolayer that simulates the epithelium of the GI tract. Caco-2, HT-29, and T84 cell lines are commonly used [174]. When these cell lines grow up in certain conditions, they form tight junctions, mucus from the microvilli, and exhibit characteristics of the *in vivo* intestinal epithelial cells [174]. The most common intestinal cells, Caco-2, were obtained from colorectal adenocarcinoma patients and shown to confluently form a brush border of microvilli that expresses certain small intestine hydrolases, such as sucrase-isomaltase, alkaline phosphatase, and aminopeptidase [173,174].

Cell lines can grow to confluence in a monolayer on the semi-permeable membrane of a Transwell®, which is used to assess the permeability of a compound from the donor or apical chamber (gut lumen) to the basolateral chamber (circulating blood) [173].

USC UNIVERSIDADE DE SANTIAGO DE COMPOSTELA

Thus, several reports employed the monoculture Caco-2 cells to study the effects of the NPs in the cell membrane and their absorption. Brun et al. [175] investigated the TiO_2NPs translocation through the Caco-2 monoculture by TEM and XAS when they were exposed to anatase and rutile TiO_2NPs for 24 h [175]. Taboada-López et al. [176] simulated the gastrointestinal digestion of seafood to study the AgNPs and TiO_2NPs' presence and their bioavailability employing the Caco-2 cells monoculture. The analysis of apical and basolateral fractions of the cellular transport was done by SP-ICP-MS and TEM-EDX [176]. Kose et al. [177] used the *in vitro* HCT-116 human colorectal carcinoma cells to study the physicochemical transformations of different coated AgNPs. Uncoated AgNPs reduce cell viability, increase ROS production, damage DNA and perturb the cell cycle, but they do not trigger apoptosis. Furthermore, PVP-AgNPs resulted in moderate toxicity [177]. Ferrante et al. [178] reported the DNA damage and apoptosis of colon cancer cells HCT-116 and Caco-2 when exposed to TiO_2NPs and E171. The cell viability assays showed that both Ti species reduced the cancer cell viability in a dose-dependent manner, and the results showed higher levels of cytotoxicity and genotoxicity for E171 [178].

Coculture media cell lines are also employed to obtain epithelial more realistic conditions and closer to *in vivo* models. Caco-2/HT29 coculture cell media was reported by García-Rodríguez et al. [179] to study the effects of nanorods, nanospheres, and nanowires of TiO_2NPs in the intestinal cell barrier. The different behaviour in the bio-adhesion and distribution of TiO_2NPs were detected using laser scanning confocal microscopy, and the DNA damage of the cells was detected by comet assay [179]. Saez-Tenorio et al. [180] also reported AgNPs' effects on the differentiated coculture Caco-2/HT29 cells exposed to the nanoparticles in long exposure periods. The results showed that the epithelial cell barrier is affected by AgNPs after 96 h of exposition, revealing the need for studies with longer exposure periods [180].

USC
UNIVERSIDADE DE SANTIAGO DE COMPOSTELA

REFERENCES

[1] APROMAR, Aquaculture in Spain, 2022 (2022). https://apromar.es/wp-content/uploads/2022/10/La_acuicultura_Espana_2022_v3_APROMAR.pdf (accessed February 1, 2023).
[2] Food and Agriculture Organization of the United Nations, The State of World Fisheries and Aquaculture 2020. Sustainability in action, FAO (2020). ISBN: 9789251326923. https://doi.org/10.4060/ca9229en.
[3] D. D. Mizuta, H. E. Froehlich, J. R. Wilson, The changing role and definitions of aquaculture for environmental purposes, Rev. Aquac. 15 (2023) 130–141. https://doi.org/10.1111/raq.12706.
[4] Spanish Ministry of Agriculture, Fisheries and Food, (2017), https://www.mapa.gob.es/es/pesca/temas/acuicultura/produccion-de-acuicultura/ (accessed February 21, 2023).
[5] S. K. Kim, Handbook of Marine Macroalgae: Biotechnology and Applied Phycology, John Wiley & Sons, Ltd (2011). ISB: 9781119977087. https://doi.org/10.1002/9781119977087.
[6] H. P. S. Makkar, G. Tran, V. Heuzé, S. Giger-Reverdin, M. Lessire, F. Lebas, P. Ankers, Seaweeds for livestock diets: A review, Anim. Feed Sci. Technol. 212 (2016) 1–17. https://doi.org/10.1016/j.anifeedsci.2015.09.018.
[7] C. Afonso, J. Matos, I. Guarda, A. Gomes-Bispo, R. Gomes, C. Cardoso, S. Gueifão, I. Delgado, I. Coelho, I. Castanheira, N. M. Bandarra, Bioactive and nutritional potential of *Alaria esculenta* and *Saccharina latissima*, J. Appl. Phycol. 33 (2021) 501–513. https://doi.org/10.1007/s10811-020-02298-8.
[8] P. Stévant, H. Marfaing, T. Rustad, I. Sandbakken, J. Fleurence, A. Chapman, Nutritional value of the kelps *Alaria esculenta* and *Saccharina latissima* and effects of short-term storage on biomass quality, J. Appl. Phycol. 29 (2017) 2417–2426. https://doi.org/10.1007/s10811-017-1126-2.
[9] M. Sá Monteiro, J. Sloth, S. Holdt, M. Hansen, Analysis and risk assessment of seaweed, EFSA J. 17 (2019) e170915. https://doi.org/10.2903/j.efsa.2019.e170915.
[10] E. M. Brown, P. J. Allsopp, P. J. Magee, C. I. Gill, S. Nitecki, C. R. Strain, E. M. Mcsorley, Seaweed and human health, Nutr. Rev. 72 (2014) 205–216. https://doi.org/10.1111/nure.12091.
[11] J. Cai, A. Lovatelli, J. Aguilar-Manjarrez, L. Cornish, L. Dabbadie, A. Desrochers, S. Diffey, E. Garrido Gamarro, J. Geehan, A. Hurtado, D. Lucente, G. Mair, W. Miao, P. P. C. Potin, M. Reantaso, R. Roubach, M. Tauati, X. Yuan, Seaweeds and microalgae: an overview for unlocking their potential in global aquaculture development, FAO Fisheries and Aquaculture Circular NFIA/C1229 (2021). ISBN: 9789251347102. https://doi.org/10.4060/cb5670en.
[12] Y. Matsumura, Emerging trends of nutrition: Transition and trade-offs nutrition trends in Japan, Asia Pac. J. Clin. Nutr. 10 (2001) S40–47. https://doi.org/10.1046/j.1440-6047.2001.0100s1S40.x.
[13] Scopus database, https://www.scopus.com/search/form.uri?display=basic#basic (accessed February 7, 2023).
[14] S. Kamala-Kannan, B. Prabhu Dass Batvari, K. J. Lee, N. Kannan, R. Krishnamoorthy, K. Shanthi, M. Jayaprakash, Assessment of heavy metals (Cd, Cr and Pb) in water, sediment and seaweed (*Ulva lactuca)* in the Pulicat Lake, South East India, Chemosphere 71 (2008) 1233–1240. https://doi.org/10.1016/j.chemosphere.2007.12.004.
[15] M. Filippini, A. Baldisserotto, S. Menotta, G. Fedrizzi, S. Rubini, D. Gigliotti, G. Valpiani, R. Buzzi, S. Manfredini, S. Vertuani, Heavy metals and potential risks in edible seaweed on the

USC DE COMPOSTELA

market in Italy, Chemosphere 263 (2021) 127983. https://doi.org/10.1016/j.chemosphere.2020.127983.
[16] S. Sundhar, R. J. Shakila, R. Shalini, S. Aanand, N. Jayakumar, Effect of thermal processing on toxic heavy metals in edible seaweeds of Gulf of Mannar and their health risk assessment, Reg. Stud. Mar. Sci. 60 (2023) 102827. https://doi.org/10.1016/j.rsma.2023.102827.
[17] D. García-Rodríguez, R. Cela-Torrijos, R. A. Lorenzo-Ferreira, A. M. Carro-Díaz, Analysis of pesticide residues in seaweeds using matrix solid-phase dispersion and gas chromatography–mass spectrometry detection, Food Chem. 135 (2012) 259–267. https://doi.org/10.1016/j.foodchem.2012.04.088.
[18] G. M. El Zokm, M. M. Ismail, M. A. E. Okbah, Seaweed as bioindicators of organic micropollutants polycyclic aromatic hydrocarbons (PAHs) and organochlorine pesticides (OCPs), Environ. Sci. Pollut. Res. 29 (2022) 34738–34748. https://doi.org/10.1007/s11356-022-18634-z.
[19] Q. Li, Z. Feng, T. Zhang, C. Ma, H. Shi, Microplastics in the commercial seaweed nori, J. Hazard. Mater. 388 (2020) 122060. https://doi.org/10.1016/j.jhazmat.2020.122060.
[20] A. Augusto Sfriso, M. Mistri, C. Munari, I. Moro, M. Wahsha, A. Sfriso, A. Juhmani, Hazardous effects of silver nanoparticles for primary producers in transitional water systems: The case of the seaweed *Ulva rigida* C. Agardh, Environ. Int. 131 (2019) 104942. https://doi.org/10.1016/j.envint.2019.104942.
[21] R. Smolowitz, Mollusca, 163–183, Chapter in Invertebrate histology, John Wiley & Sons, Inc. (2021). ISBN: 9781119507697. https://doi.org/10.1002/9781119507697.ch6.
[22] E. Gosling, Mussel culture, 603–674, Chapter in Marine mussels: Ecology, physiology, genetics and culture, John Wiley & Sons, Inc. (2021). ISBN: 9781119293927. https://doi.org/10.1002/9781119293927.ch10.
[23] U. Grienke, J. Silke, D. Tasdemir, Bioactive compounds from marine mussels and their effects on human health, Food Chem. 142 (2014) 48–60. https://doi.org/10.1016/j.foodchem.2013.07.027.
[24] H. Eguiraun, E. Gil-Uriarte, L. Barrenetxea, E. Lizundia, I. Zuazo, M. Soto, Comparative study of mussel shells using 3D scanning, 497-504, Chapter in Advances on mechanics, design engineering and manufacturing II, Springer International Publishing (2019). ISBN: 9783030123468. https://doi.org/10.1007/978-3-030-12346-8_48.
[25] Fisheries and aquaculture, Food and Agriculture Organizaton of the United Nations, https://www.fao.org/fishery/en/aqspecies (accessed February 24, 2023).
[26] E. Gosling, Marine Bivalve Molluscs, John Wiley & Sons, Ltd. (2015). ISBN: 9781119045212. https://doi.org/10.1002/9781119045212.
[27] S. Stankovic, M. Jovic, Health risks of heavy metals in the mediterranean mussels as seafood, Environ. Chem. Lett. 10 (2012) 119–130. https://doi.org/10.1007/s10311-011-0343-1.
[28] S. Stanković, M. Jović, R. Milanov, D. Joksimović, Trace elements concentrations (Zn, Cu, Pb, Cd, As and Hg) in the Mediterranean mussel (*Mytilus galloprovincialis*) and evaluation of mussel quality and possible human health risk from cultivated and wild sites of the southeastern Adriatic Sea, Montenegro, J. Serbian Chem. Soc. 76 (2011) 1725–1737. https://doi.org/10.2298/JSC110420095S.
[29] F. Mehouel, S. W. Fowler, Review of the toxic trace elements arsenic, cadmium , lead and mercury in seafood species from Algeria and contiguous waters in the Southwestern Mediterranean Sea, Environ. Sci. Pollut. Res. (2022) 3288–3301. https://doi.org/10.1007/s11356-021-17130-0.

[30] B. Fernández, J. A. Campillo, E. Chaves-Pozo, J. Bellas, V. M. León, M. Albentosa, Comparative role of microplastics and microalgae as vectors for chlorpyrifos bioacumulation and related physiological and immune effects in mussels, Sci. Total Environ. 807 (2022) 150983. https://doi.org/10.1016/j.scitotenv.2021.150983.
[31] A. Cuccaro, L. De Marchi, M. Oliva, G. Monni, V. Miragliotta, G. Fumagalli, R. Freitas, C. Pretti, The influence of salinity on the toxicity of chemical UV-filters to sperms of the free-spawning mussel *Mytilus galloprovincialis* (Lamark, 1819), Aquat. Toxicol. 250 (2022) 106263. https://doi.org/10.1016/j.aquatox.2022.106263.
[32] A. Jesus, E. Sousa, M. T. Cruz, H. Cidade, J. M. Sousa Lobo, I. F. Almeida, UV Filters: Challenges and Prospects, Pharmaceuticals. 15 (2022) 1-26. https://doi.org/10.3390/ph15030263.
[33] J. V. de Pinho, P. de A. Rodrigues, I. D. L. Guimarães, F. C. Monteiro, R. G. Ferrari, R. A. Hauser-Davis, C. A. Conte-Junior, The role of the ecotoxicology applied to seafood as a tool for human health risk assessments concerning polycyclic aromatic hydrocarbons, Int. J. Environ. Res. Public Health. 19 (2022) 1-25. https://doi.org/10.3390/ijerph19031211.
[34] W. Shi, X. Guan, S. Sun, Y. Han, X. Du, Y. Tang, W. Zhou, Nanoparticles decrease the byssal attachment strength of the thick shell mussel *Mytilus coruscus*, Chemosphere 257 (2020) 127200. https://doi.org/10.1016/j.chemosphere.2020.127200.
[35] Fisheries and Aquaculture, Turbot, Food and Agriculture Organizaton of the United Nations, https://www.fao.org/fishery/en/culturedspecies/psetta_maxima/en (accessed February 23, 2023).
[36] European Commision, EUMOFA, Turbot in the EU, Case Study. 47 (2018) 1-43. https://www.eumofa.eu/documents/20178/114389/Turbot+in+the+EU.
[37] J. P. L. Ruyet, Turbot (*Scophthalmus maximus*) Grow-out in Europe: Practices, Results and prospects, Turkish J. Fish. Aquat. Sci. 2 (2002) 29–39.
[38] D. Danancher, E. Garcia-Vázquez, Turbot-*Scophthalmus maximus*, 55-61, Chapter in Genimpact-Evaluation of genetic impact of aquacuture activities on native populations. A European network (EU Contract n-RICA-CT-2005-02282). Final report (2007).
[39] T. Bjørndal, V. Øiestad, Turbot - Production Technology and Markets, Fao, Globefish research programme, 103 (2011) 1-31. https://www.fao.org/in-action/globefish/publications/details-publication/zh/c/347678/ (accessed February 27, 2023).
[40] D. K. Öztürk, Element concentrations of cultured fish in the Black Sea: selenium-mercury balance and the risk assessments for consumer health, Environ. Sci. Pollut. Res. 29 (2022) 87998–88007. https://doi.org/10.1007/s11356-022-21914-3.
[41] M. Köktürk, F. B. Özgeriş, M. Atamanalp, A. Uçar, S. Özdemir, V. Parlak, H. A. Duyar, G. Alak, Microplastic-induced oxidative stress response in turbot and potential intake by humans, Drug Chem. Toxicol. (2023) 1–10. https://doi.org/DOI: 10.1080/01480545.2023.2168690.
[42] M. J. Araújo, M. L. Sousa, E. Fonseca, A. B. Felpeto, J. C. Martins, M. Vázquez, N. Mallo, L. Rodriguez-Lorenzo, M. Quarato, I. Pinheiro, M. V. Turkina, J. J. López-Mayán, E. Peña-Vázquez, M. C. Barciela-Alonso, M. Spuch-Calvar, M. Oliveira, P. Bermejo-Barrera, S. Cabaleiro, B. Espiña, V. Vasconcelos, A. Campos, Proteomics reveals multiple effects of titanium dioxide and silver nanoparticles in the metabolism of turbot, *Scophthalmus maximus*, Chemosphere 308 (2022) 136110. https://doi.org/10.1016/j.chemosphere.2022.136110.
[43] M. Nasrollahzadeh, S. M. Sajadi, M. Sajjadi, Z. Issaabadi, Chapter 1-An Introduction to nanotechnology, 1-27, https://doi.org/10.1016/B978-0-12-813586-0.00001-8, Chapter in A Introduction to green nanotechnology, Elsevier Ltd. (2019). ISBN: 9780128135860.

UNIVERSIDADE DE SANTIAGO DE COMPOSTELA

[44] D. Schaming, H. Remita, Nanotechnology: from the ancient time to nowadays, Found. Chem. 17 (2015) 187–205. https://doi.org/10.1007/s10698-015-9235-y.
[45] B. Bhushan, Introduction to nanotechnology, 1-19, Chapter in Springer handbook of nanotechnology, Springer Handbooks. (2017). ISBN: 9783662543573. https://doi.org/10.1007/978-3-662-54357-3_1.
[46] L. A. Kolahalam, I. V. Kasi Viswanath, B. S. Diwakar, B. Govindh, V. Reddy, Y. L. N. Murthy, Review on nanomaterials: Synthesis and applications, Mater. Today Proc. 18 (2019) 2182–2190. https://doi.org/10.1016/j.matpr.2019.07.371.
[47] Nanomaterial definition. United States Environmental Protection Agency, EPA. Research on nanomaterials, https://www.epa.gov/chemical-research/research-nanomaterials (accessed February 6, 2023).
[48] D. R. Boverhof, C. M. Bramante, J. H. Butala, S. F. Clancy, M. Lafranconi, J. West, S. C. Gordon, Comparative assessment of nanomaterial definitions and safety evaluation considerations, Regul. Toxicol. Pharmacol. 73 (2015) 137–150. https://doi.org/10.1016/j.yrtph.2015.06.001.
[49] European Commision, Commission Recommendation of 18 October 2011
on the definition of nanomaterial (2011/696/EU), Off. J. Eur. Union. 24 (2011) 6–6.
[50] European Commision, Commission Recommendation of 10 June 2022 on the definition of nanomaterial (2022/C 229/01), Off. J. Eur. Union. 36237 (2022) 1–5.
[51] A. López-Serrano, R. Muñoz Olivas, J. Sanz Landaluze, C. Cámara, Nanoparticles: A global vision. Characterization, separation, and quantification methods. Potential environmental and health impact, Anal. Methods 6 (2014) 38–56. https://doi.org/10.1039/c3ay40517f.
[52] F. A. Khan, Applications of nanomaterials in human health, Springer Nature Singapore Pte Ltd., (2020). ISBN: 9789811548017. https://doi.org/10.1007/978-981-15-4802-4.
[53] T. A. Saleh, Nanomaterials: Classification, properties, and environmental toxicities, Environ. Technol. Innov. 20 (2020) 101067. https://doi.org/10.1016/j.eti.2020.101067.
[54] A. B. Asha, R. Narain, Nanomaterials properties, 343-359, Chapter in Polymer science and nanotechnology, Elsevier Inc. (2020). ISBN: 9780128168066. https://doi.org/10.1016/B978-0-12-816806-6.00015-7.
[55] N. Baig, I. Kammakakam, W. Falath, Nanomaterials: A review of synthesis methods, properties, recent progress, and challenges, Mater. Adv. 2 (2021) 1821–1871. https://doi.org/10.1039/d0ma00807a.
[56] Nanomaterial products, Nanotechnology products database, https://product.statnano.com/ (accessed February 8, 2023).
[57] D. J. Barillo, D. E. Marx, Silver in medicine: A brief history BC 335 to present, Burns 40 (2014) S3–S8. https://doi.org/10.1016/j.burns.2014.09.009.
[58] K .M. F. Hasan, L. Xiaoyi, Z. Shaoqin, P. G. Horváth, M. Bak, L. Bejó, G. Sipos, T. Alpár, Functional silver nanoparticles synthesis from sustainable point of view: 2000 to 2023 – A review on game changing materials, Heliyon. 8 (2022) e12322. https://doi.org/10.1016/j.heliyon.2022.e12322.
[59] C. J. Dedman, G. C. Newson, G. L. Davies, J. A. Christie-Oleza, Mechanisms of silver nanoparticle toxicity on the marine cyanobacterium *Prochlorococcus* under environmentally-relevant conditions, Sci. Total Environ. 747 (2020) 141229. https://doi.org/10.1016/j.scitotenv.2020.141229.
[60] J. Natsuki, T Natsuki, Y. Hashimoto, A review of silver nanoparticles: Synthesis methods, properties and applications, Int. J. Mater. Sci. Appl. 4 (2015) 325-332. https://doi.org/10.11648/j.ijmsa.20150405.17.

[61] H. D. Beyene, A. A. Werkneh, H. K. Bezabh, T. G. Ambaye, Synthesis paradigm and applications of silver nanoparticles (AgNPs), a review, Sustain. Mater. Technol. 13 (2017) 18–23. https://doi.org/10.1016/j.susmat.2017.08.001.
[62] R. A. Bapat, T. V. Chaubal, C. P. Joshi, P. R. Bapat, H. Choudhury, M. Pandey, B. Gorain, P. Kesharwani, An overview of application of silver nanoparticles for biomaterials in dentistry, Mater. Sci. Eng. C. 91 (2018) 881–898. https://doi.org/10.1016/j.msec.2018.05.069.
[63] A. C. Burdușel, O. Gherasim, A. M. Grumezescu, L. Mogoantă, A. Ficai, E. Andronescu, Biomedical applications of silver nanoparticles: An up-to-date overview, Nanomaterials 8 (2018) 681. https://doi.org/10.3390/nano8090681.
[64] E. Abbasi, M. Milani, S. F. Aval, M. Kouhi, A. Akbarzadeh, H. T. Nasrabadi, P. Nikasa, S. W. Joo, Y. Hanifehpour, K. Nejati-Koshki, M. Samiei, Silver nanoparticles: Synthesis methods, bio-applications and properties, Crit. Rev. Microbiol. 42 (2016) 173–180. https://doi.org/10.3109/1040841X.2014.912200.
[65] X. F. Zhang, Z. G. Liu, W. Shen, S. Gurunathan, Silver nanoparticles: Synthesis, characterization, properties, applications, and therapeutic approaches, Int. J. Mol. Sci. 17 (2016) 1534. https://doi.org/10.3390/ijms17091534.
[66] E. Verleysen, E. Van-Doren, N. Waegeneers, P. J. De Temmerman, M. Abi Daoud-Francisco, J. Mast, TEM and SP-ICP-MS analysis of the release of silver nanoparticles from decoration of pastry, J. Agric. Food Chem. 63 (2015) 3570–3578. https://doi.org/10.1021/acs.jafc.5b00578.
[67] K. M. M. Abou El-Nour, A. Eftaiha, A. Al-Warthan, R. A. A. Ammar, Synthesis and applications of silver nanoparticles, Arab. J. Chem. 3 (2010) 135–140. https://doi.org/10.1016/j.arabjc.2010.04.008.
[68]V. V. Mody, R. Siwale, A. Singh, H. R. Mody, Introduction to metallic nanoparticles, J. Pharm. Bioallied Sci. 2 (2010) 282. https://doi.org/10.4103/0975-7406.72127.
[69] H. H. Lara, N. V. Ayala-Nuñez, L. Ixtepan-Turrent, C. Rodriguez-Padilla, Mode of antiviral action of silver nanoparticles against HIV-1, J. Nanobiotechnology. 8 (2010) 1–10. https://doi.org/10.1186/1477-3155-8-1.
[70] J. L. Elechiguerra, J. L. Burt, J. R. Morones, A. Camacho-Bragado, X. Gao, H. H. Lara, M. J. Yacaman, Interaction of silver nanoparticles with HIV-1, J. Nanobiotechnology. 3 (2005) 1–10. https://doi.org/10.1186/1477-3155-3-6.
[71] P. K. Rai, Z. Usmani, V. K. Thakur, V. K. Gupta, Y. K. Mishra, Tackling COVID-19 pandemic through nanocoatings: Confront and exactitude, Curr. Res. Green Sustain. Chem. 3 (2020) 100011. https://doi.org/10.1016/j.crgsc.2020.100011.
[72] L. Wei, J. Lu, H. Xu, A. Patel, Z. S. Chen, G. Chen, Silver nanoparticles: Synthesis, properties, and therapeutic applications, Drug Discov. Today. 20 (2015) 595–601. https://doi.org/10.1016/j.drudis.2014.11.014.
[73] T. Jaswal, J. Gupta, A review on the toxicity of silver nanoparticles on human health, Mater. Today Proc. (2021) Article in press. https://doi.org/10.1016/j.matpr.2021.04.266.
[74] N. Hadrup, H. R. Lam, Oral toxicity of silver ions, silver nanoparticles and colloidal silver-A review, Regul. Toxicol. Pharmacol. 68 (2014) 1–7. https://doi.org/10.1016/j.yrtph.2013.11.002.
[75] M. M. El Mahdy, T. A. Salah Eldin, H. Sayed Aly, F. F. Mohammed M. I. Shaalan, Evaluation of hepatotoxic and genotoxic potential of silver nanoparticles in albino rats, Exp. Toxicol. Pathol. 67 (2015) 21–29. https://doi.org/10.1016/j.etp.2014.09.005.
[76] I. Pinzaru, D. Coricovac, C. Dehelean, E. A. Moacă, M. Mioc, F. Baderca, I. Sizemore, S. Brittle, D. Marti, C. D. Calina, A. M. Tsatsakis, C. Şoica, Stable PEG-coated silver

USC UNIVERSIDADE DE SANTIAGO DE COMPOSTELA

nanoparticles – A comprehensive toxicological profile, Food Chem. Toxicol. 111 (2018) 546–556. https://doi.org/10.1016/j.fct.2017.11.051.
[77] X. F. Zhang, S. Gurunathan, J. H. Kim, Effects of silver nanoparticles on neonatal testis development in mice, Int. J. Nanomedicine 10 (2015) 6243–6256. https://doi.org/10.2147/IJN.S90733.
[78] M. Ahamed, M. Karns, M. Goodson, J. Rowe, S. M. Hussain, J. J. Schlager, Y. Hong, DNA damage response to different surface chemistry of silver nanoparticles in mammalian cells, Toxicol. Appl. Pharmacol. 233 (2008) 404–410. https://doi.org/10.1016/j.taap.2008.09.015.
[79] S. Arora, J. Jain, J. M. Rajwade, K. M. Paknikar, Interactions of silver nanoparticles with primary mouse fi broblasts and liver cells, Toxicol. Appl. Pharmacol. 236 (2009) 310–318. https://doi.org/10.1016/j.taap.2009.02.020.
[80] Y. Lan, Y. Lu, Z. Ren, Mini review on photocatalysis of titanium dioxide nanoparticles and their solar applications, Nano Energy. 2 (2013) 1031–1045. https://doi.org/10.1016/j.nanoen.2013.04.002.
[81] S. Boutillier, S. Fourmentin, B. Laperche, History of titanium dioxide regulation as a food additive: a review, Environ. Chem. Lett. 20 (2022) 1017–1033. https://doi.org/10.1007/s10311-021-01360-2.
[82] A. J. Haider, Z. N. Jameel, I. H. M. Al-Hussaini, Review on: Titanium dioxide Applications, Energy Procedia. 157 (2019) 17–29. https://doi.org/10.1016/j.egypro.2018.11.159.
[83] S. Qiu, S. J. Kalita, Synthesis, processing and characterization of nanocrystalline titanium dioxide, Mater. Sci. Eng. A. 435–436 (2006) 327–332. https://doi.org/10.1016/j.msea.2006.07.062.
[84] F. Piccinno, F. Gottschalk, S. Seeger, B. Nowack, Industrial production quantities and uses of ten engineered nanomaterials in Europe and the world, J. Nanoparticle Res. 14 (2012) 1109. https://doi.org/10.1007/s11051-012-1109-9.
[85] R. Tomar, A. A. Abdala, R. G. Chaudhary, N. B. Singh, Photocatalytic degradation of dyes by nanomaterials, Mater. Today Proc. 29 (2020) 967–973. https://doi.org/10.1016/j.matpr.2020.04.144.
[86] Ş. Sungur, Titanium dioxide nanoparticles, 1-18, Chapter in Handbook of nanomaterials and nanocomposites for energy and environmental applications, Springer Cham (2020). ISBN: 9783030362683. https://doi.org/10.1007/978-3-030-11155-7_9-1.
[87] H. G. Yang, G. Liu, G. Q. Lu, Synthetic chemistry of titanium dioxide, 281–328, Chapter in The chemistry of nanostructured materials, World Scientific Publishing Co Pte Ltd, (2011). ISBN: 9789814313056. https://doi.org/10.1142/9789814313070_0009.
[88] M. Czajka, K. Sawicki, K. Sikorska, S. Popek, M. Kruszewski, L. Kapka-Skrzypczak, Toxicity of titanium dioxide nanoparticles in central nervous system, Toxicol. Vitr. 29 (2015) 1042–1052. https://doi.org/10.1016/j.tiv.2015.04.004.
[89] S. L. Schneider, H. W. Lim, A review of inorganic UV filters zinc oxide and titanium dioxide, Photodermatol. Photoimmunol. Photomed. 35 (2019) 442–446. https://doi.org/10.1111/phpp.12439.
[90] FDA advances new proposed regulation to make sure that sunscreens are safe and effective, https://www.fda.gov/news-events/press-announcements/fda-advances-new-proposed-regulation-make-sure-sunscreens-are-safe-and-effective (accessed February 16, 2023).

USC UNIVERSIDADE DE SANTIAGO DE COMPOSTELA

[91] V. Verma, M. Al-Dossari, J. Singh, M. Rawat, M. G. M. Kordy, M. Shaban, A Review on green synthesis of TiO_2NPs: Photocatalysis and antimicrobial aplicattions, Polymers 14 (2022) 1444. https://doi.org/10.3390/polym14071444.
[92] French Government Decree, Ministère de l'Économie et des Finances, Arrêté du 17 avril 2019 portant suspension de la mise sur le marché des denrées contenant l'additif E 171 (dioxyde de titane - TiO_2), Journal Officiel de la République Française, (2019).
[93] Ministère de l'Économie et des Finances, French Government Decree - Order of 21 December 2020 suspending the placing on the market of foodstuffs containing the additive E 171 (titanium dioxide - TiO_2), Journal Officiel de la République Française, (2021).
[94] M. Younes, G. Aquilina, L. Castle, K. H. Engel, P. Fowler, M. J. Frutos Fernandez, P. Fürst, U. Gundert-Remy, R. Gürtler, T. Husøy, M. Manco, W. Mennes, P. Moldeus, S. Passamonti, R. Shah, I. Waalkens-Berendsen, D. Wölfle, E. Corsini, F. Cubadda, D. De Groot, R. Fitz Gerald, S. Gunnare, A. C. Gutleb, J. Mast, A. Mortensen, A. Oomen, A. Piersma, V. Plichta, B. Ulbrich, H. Van Loveren, D. Benford, M. Bignami, C. Bolognesi, R. Crebelli, M. Dusinska, F. Marcon, E. Nielsen, J. Schlatter, C. Vleminckx, S. Barmaz, M. Carfí, C. Civitella, A. Giarola, A. M. Rincon, R. Serafimova, C. Smeraldi, J. Tarazona, A. Tard, M. Wright, Safety assessment of titanium dioxide (E171) as a food additive, EFSA J. 19 (2021) 6585. https://doi.org/10.2903/j.efsa.2021.6585.
[95] European Commission, Commission Regulation (EU) 2022/63 of 14 January 2022 amending Annexes II and III to Regulation (EC) No 1333/2008 of European Parliament and of the Council as regards the food additive titanium dioxide (E171), Off. J. Eur. Union. 11 (2022) 1–5.
[96] TiO_2 as a food additive in Canada, https://www.canada.ca/en/health-canada/services/food-nutrition/reports-publications/titanium-dioxide-food-additive-science-report.html (accessed February 20, 2023).
[97] J. Hou, L. Wang, C. Wang, S. Zhang, H. Liu, S. Li, X. Wang, Toxicity and mechanisms of action of titanium dioxide nanoparticles in living organisms, J. Environ. Sci. 75 (2019) 40–53. https://doi.org/10.1016/j.jes.2018.06.010.
[98] I. M. Sadiq, S. Dalai, N. Chandrasekaran, A. Mukherjee, Ecotoxicity study of titania (TiO_2) NPs on two microalgae species: *Scenedesmus* sp. and *Chlorella* sp., Ecotoxicol. Environ. Saf. 74 (2011) 1180–1187. https://doi.org/10.1016/j.ecoenv.2011.03.006.
[99] M. Khan, M. S. A. Khan, K. K. Borah, Y. Goswami, K. R. Hakeem, I. Chakrabartty, The potential exposure and hazards of metal-based nanoparticles on plants and environment, with special emphasis on ZnONPs, TiO_2NPs, and AgNPs: A review, Environ. Adv. 6 (2021) 100128. https://doi.org/10.1016/j.envadv.2021.100128.
[100] M. Heinlaan, A. Ivask, I. Blinova, H. C. Dubourguier, A. Kahru, Toxicity of nanosized and bulk ZnO, CuO and TiO_2 to bacteria *Vibrio fischeri* and crustaceans *Daphnia magna* and *Thamnocephalus platyurus*, Chemosphere 71 (2008) 1308–1316. https://doi.org/10.1016/j.chemosphere.2007.11.047.
[101] T. Tang, Z. Zhang, X. Zhu, Toxic effects of TiO_2NPs on Zebrafish, Int. J. Environ. Res. Public Health. 16 (2019) 523. https://doi.org/10.3390/ijerph16040523.
[102] H. L. Karlsson, P. Cronholm, J. Gustafsson, L. Möller, Copper oxide nanoparticles are highly toxic: A comparison between metal oxide nanoparticles and carbon nanotubes, Chem. Res. Toxicol. 21 (2008) 1726–1732. https://doi.org/10.1021/tx800064j.
[103] F. Laborda, E. Bolea, G. Cepriá, M. T. Gómez, M. S. Jiménez, J. Pérez-Arantegui, J. R. Castillo, Detection, characterization and quantification of inorganic engineered nanomaterials: A review of techniques and methodological approaches for the analysis of complex samples, Anal. Chim. Acta. 904 (2016) 10–32. https://doi.org/10.1016/j.aca.2015.11.008.

USC DE COMPOSTELA

[104] M. V. Taboada-López, N. Alonso-Seijo, P. Herbello-Hermelo, P. Bermejo-Barrera, A. Moreda-Piñeiro, Determination and characterization of silver nanoparticles in bivalve molluscs by ultrasound assisted enzymatic hydrolysis and sp-ICP-MS, Microchem. J. 148 (2019) 652–660. https://doi.org/10.1016/j.microc.2019.05.023.
[105] Y. Sun, Y. Yang, F. Y. Tou, Z. S. Niu, X. P. Guo, C. Liu, J. Yan, J. Y. Wu, M. Xu, L. J. Hou, M. Liu, Extraction and quantification of metal-containing nanoparticles in marine shellfish based on single particle inductively coupled plasma-mass spectrometry technique, J. Hazard. Mater. 424 (2022) 127383. https://doi.org/10.1016/j.jhazmat.2021.127383.
[106] J. Gruszka, J. Malejko, A. Bajguz, B. Godlewska-Żyłkiewicz, Method development for speciation analysis of silver nanoparticles and silver ions in green algae and surface waters at environmentally relevant concentrations using single particle ICP-MS, J. Anal. At. Spectrom. 37 (2022) 1208–1222. https://doi.org/10.1039/d2ja00032f.
[107] K. Loeschner, J. Navratilova, C. Købler, K. Mølhave, S. Wagner, F. Von Der Kammer, E. H. Larsen, Detection and characterization of silver nanoparticles in chicken meat by asymmetric flow field flow fractionation with detection by conventional or single particle ICP-MS, Anal. Bioanal. Chem. 405 (2013) 8185–8195. https://doi.org/10.1007/s00216-013-7228-z.
[108] M. V. Taboada-López, P. Herbello-Hermelo, R. Domínguez-González, P. Bermejo-Barrera, A. Moreda-Piñeiro, Enzymatic hydrolysis as a sample pre-treatment for titanium dioxide nanoparticles assessment in surimi (crab sticks) by single particle ICP-MS, Talanta. 195 (2019) 23–32. https://doi.org/10.1016/j.talanta.2018.11.023.
[109] D. Bao, Z. G. Oh, Z. Chen, Characterization of silver nanoparticles internalized by *Arabidopsis* plants using Single Particle ICP-MS analysis, Front. Plant Sci. 7 (2016) 1–8. https://doi.org/10.3389/fpls.2016.00032.
[110] J. Wojcieszek, J. Jiménez-Lamana, L. Ruzik, M. Asztemborska, M. Jarosz, J. Szpunar, Characterization of TiO_2 NPs in Radish (*Raphanus sativus* L.) by Single-Particle ICP-QQQ-MS, Front. Environ. Sci. 8 (2020) 1–12. https://doi.org/10.3389/fenvs.2020.00100.
[111] J. J. López-Mayán, B. Cerneira-Temperán, E. Peña-Vázquez, M. C. Barciela-Alonso, M. R. Domínguez-González, P. Bermejo-Barrera, Evaluation of a cloud point extraction method for the preconcentration and quantification of silver nanoparticles in water samples by ETAAS, Int. J. Environ. Anal. Chem. 98 (2018) 1434–1447. https://doi.org/10.1080/03067319.2018.1562063.
[112] J. López-Mayan, M. C. Barciela-Alonso, M. R. Domínguez-González, E. Peña-Vázquez, P. Bermejo-Barrera, Cloud point extraction and ICP-MS for titanium speciation in water samples, Microchem. J. 152 (2020) 104264. https://doi.org/10.1016/j.microc.2019.104264.
[113] V. Nischwitz, H. Goenaga-Infante, Improved sample preparation and quality control for the characterisation of titanium dioxide nanoparticles in sunscreens using flow field flow fractionation on-line with inductively coupled plasma mass spectrometry, J. Anal. At. Spectrom. 27 (2012) 1084–1092. https://doi.org/10.1039/c2ja10387g.
[114] L. Li, K. Leopold, M. Schuster, Effective and selective extraction of noble metal nanoparticles from environmental water through a noncovalent reversible reaction on an ionic exchange resin, Chem. Commun. 48 (2012) 9165–9167. https://doi.org/10.1039/c2cc34838a.
[115] M. V. Taboada-López, D. Bartczak, S. Cuello-Núñez, H. Goenaga-Infante, P. Bermejo-Barrera, A. Moreda-Piñeiro, F4-UV-ICP-MS for detection and quantification of silver nanoparticles in seafood after enzymatic hydrolysis, Talanta 232 (2021) 122504. https://doi.org/10.1016/j.talanta.2021.122504.

USC UNIVERSIDADE DE SANTIAGO DE COMPOSTELA

[116] B. Li, S. L. Chua, D. Yu, S. H. Chan, A. Li, Detection, identification and size distribution of silver nanoparticles (AgNPs) in milk and migration study for breast milk storage bags, Molecules 27 (2022) 2539. https://doi.org/10.3390/molecules27082539.
[117] F. Geißler, M. Martínez-Cabanas, P. Lodeiro, E. P. Achterberg, Optimization of hyphenated asymmetric flow field-flow fractionation for the analysis of silver nanoparticles in aqueous solutions, Anal. Bioanal. Chem. 413 (2021) 6889–6904. https://doi.org/10.1007/s00216-021-03647-3.
[118] D. C. António, C. Cascio, Z. Jakšić, D. Jurašin, D. M. Lyons, A. J. A. Nogueira, F. Rossi, L. Calzolai, Assessing silver nanoparticles behaviour in artificial seawater by mean of AF4 and spICP-MS, Mar. Environ. Res. 111 (2015) 162–169. https://doi.org/10.1016/j.marenvres.2015.05.006.
[119] L. Naidoo, S. Kanchi, R. Drexel, F. Meier, K. Bisetty, Measurement of TiO_2 nanoscale ingredients in sunscreens by multidetector AF4, TEM, and spICP-MS supported by computational modeling, ACS Appl. Nano Mater. 4 (2021) 4665–4675. https://doi.org/10.1021/acsanm.1c00290.
[120] B. Li, S. L. Chua, D. Yu, S. H. Chan, A. Li, Separation and size characterization of highly polydisperse titanium dioxide nanoparticles (E171) in powdered beverages by using Asymmetric Flow Field-Flow Fractionation hyphenated with Multi-Angle Light Scattering and Inductively Coupled Plasma Mass Spectrometry, J. Chromatogr. A. 1643 (2021) 462059. https://doi.org/10.1016/j.chroma.2021.462059.
[121] D. Ojeda, M. V. Taboada-López, E. Bolea, J. Pérez-Arantegui, P. Bermejo-Barrera, A. Moreda-Piñeiro, F. Laborda, Size characterization and quantification of titanium dioxide nano- and microparticles-based products by Asymmetrical Flow Field-Flow Fractionation coupled to Dynamic Light Scattering and Inductively Coupled Plasma Mass Spectrometry, Anal. Chim. Acta. 1122 (2020) 20–30. https://doi.org/10.1016/j.aca.2020.04.080.
[122] L. Pitkänen, A. M. Striegel, Size-exclusion chromatography of metal nanoparticles and quantum dots, Trends Anal. Chem. 80 (2016) 311–320. https://doi.org/10.1016/j.trac.2015.06.013.
[123] M. Roman, C. Rigo, H. Castillo-Michel, I. Munivrana, V. Vindigni, I. Mičetić, F. Benetti, L. Manodori, W. R. L. Cairns, Hydrodynamic chromatography coupled to single-particle ICP-MS for the simultaneous characterization of AgNPs and determination of dissolved Ag in plasma and blood of burn patients, Anal. Bioanal. Chem. 408 (2016) 5109–5124. https://doi.org/10.1007/s00216-015-9014-6.
[124] Y. Chang, Y. Shih, C. Su, H. Ho, Comparison of three analytical methods to measure the size of silver nanoparticles in real environmental water and wastewater samples, J. Hazard. Mater. 322 (2020) 95–104. https://doi.org/10.1016/j.jhazmat.2016.03.030.
[125] X. X. Zhou, R. Liu, J. F. Liu, Rapid chromatographic separation of dissoluble Ag(I) and silver-containing nanoparticles of 1-100 Nanometer in antibacterial products and environmental waters, Environ. Sci. Technol. 48 (2014) 14516–14524. https://doi.org/10.1021/es504088e.
[126] P. C. Lin, S. Lin, P. C. Wang, R. Sridhar, Techniques for physicochemical characterization of nanomaterials, Biotechnol. Adv. 32 (2014) 711–726. https://doi.org/10.1016/j.biotechadv.2013.11.006.
[127] G. H. Matar G. Akyüz, E. Kaymazlar, M. Andac, An investigation of green synthesis of silver nanoparticles using Turkish honey against pathogenic bacterial strains, Biointerface Res. Appl. Chem. 13 (2023) 1–11. https://doi.org/10.33263/BRIAC132.195.
[128] D. K. Shekinah, A.Tabitha, E. P. Kumar, J. M. M. Aadhil, M. Saxena, P. Radha1, Sustainable biosynthesis of silver nanoparticles and their application to recover "Single Cell

USC UNIVERSIDADE DE SANTIAGO DE COMPOSTELA

Oil" from *Yarrowia lipolytica* for biodiesel synthesis, Bionanoscience. 12 (2022) 890–900. https://doi.org/10.1007/s12668-022-00985-z.
[129] N. Shyam-Sundar, S. Karthi, S. Senthil-nathan, K. Raman Narayanan, B. Santoshkumar, H. Sivanesh, K. Muthu-Pandian Chanthini, V. Stanley-Raja, R. Ramasubramanian, A. Abdel-Megeed, G. Malafaia, Eco-friendly biosynthesis of TiO_2 nanoparticles using *Desmostachya bipinnata* extract: Larvicidal and pupicidal potential against *Aedes aegypti* and *Spodoptera litura* and acute toxicity in non-target organisms, Sci. Total Environ. 858 (2023) 159512. https://doi.org/10.1016/j.scitotenv.2022.159512.
[130] B. K. Thakur, A. Kumar, D. Kumar, Green synthesis of titanium dioxide nanoparticles using *Azadirachta indica* leaf extract and evaluation of their antibacterial activity, South African J. Bot. 124 (2019) 223–227. https://doi.org/10.1016/j.sajb.2019.05.024.
[131] L. Zhang, W. X. Wang, Silver nanoparticle toxicity to the larvae of oyster *Crassostrea angulata*: Contribution of *in vivo* dissolution, Sci. Total Environ. 858 (2023) 159965. https://doi.org/10.1016/j.scitotenv.2022.159965.
[132] J. Farkas, H. Peter, P. Christian, J. A. Gallego Urrea, M. Hassellöv, J. Tuoriniemi, S. Gustafsson, E. Olsson, K. Hylland, K. V. Thomas, Characterization of the effluent from a nanosilver producing washing machine, Environ. Int. 37 (2011) 1057–1062. https://doi.org/10.1016/j.envint.2011.03.006.
[133] L. Windler, C. Lorenz, N. Von Goetz, K. Hungerbühler, M. Amberg, M. Heuberger, B. Nowack, Release of titanium dioxide from textiles during washing, Environ. Sci. Technol. 46 (2012) 8181–8188. https://doi.org/10.1021/es301633b.
[134] A. Turner, M. Filella, The role of titanium dioxide on the behaviour and fate of plastics in the aquatic environment, Sci. Total Environ. 869 (2023) 161727. https://doi.org/10.1016/j.scitotenv.2023.161727.
[135] S. Bandyopadhyay, J. R. Peralta-Videa, J. A. Hernandez-Viezcas, M. O. Montes, A. A. Keller, J. L. Gardea-Torresdey, Microscopic and spectroscopic methods applied to the measurements of nanoparticles in the environment, Appl. Spectrosc. Rev. 47 (2012) 180–206. https://doi.org/10.1080/05704928.2011.637186.
[136] J. Stetefeld, S. A. Mckenna, T. R. Patel, Dynamic light scattering: a practical guide and applications in biomedical sciences, Biophys. Rev. 8 (2016) 409–427. https://doi.org/10.1007/s12551-016-0218-6.
[137] S. Gevorgyan, R. Schubert, S. Falke, K. Lorenzen, K. Trchounian, C. Betzel, Structural characterization and antibacterial activity of silver nanoparticles synthesized using a low-molecular-weight Royal Jelly extract, Sci. Rep. 12 (2022) 14077. https://doi.org/10.1038/s41598-022-17929-y.
[138] L. M. Al Masoudi, A. S. Alqurashi, A. Abu Zaid, H. Hamdi, Characterization and biological studies of synthesized titanium dioxide nanoparticles from leaf extract of *Juniperus phoenicea* (L.) growing in Taif region, Saudi Arabia, Processes 11 (2023) 272. https://doi.org/10.3390/pr11010272.
[139] M. Mehrzad, M. Behpour, F. J. Kashi, Novel environmental method for enhanced biodegradation of contaminated wastewater via immobilizing nanoparticles on a new bacterial strain isolated industrial textile, J. Environ. Manage. 325 (2023) 116528. https://doi.org/10.1016/j.jenvman.2022.116528.
[140] D. Hernández, J. C. Vidal, F. Laborda, J. Pérez-Arantegui, A. C. Giménez-Ingalaturre, J. R. Castillo, Detection, size characterization and quantification of silver nanoparticles in consumer products by particle collision coulometry, Microchim. Acta 188 (2021) 1-10. https://doi.org/10.1007/s00604-020-04662-4.

USC UNIVERSIDADE DE SANTIAGO DE COMPOSTELA

[141] J. C. Vidal, D. Torrero, S. Menés, A. de La Fuente, J. R. Castillo, Voltammetric sensing of silver nanoparticles on electrodes modified with selective ligands by using covalent and electropolymerization procedures. Discrimination between silver(I) and metallic silver, Mikrochim. Acta 187 (2020) 1-11. https://doi.org/10.1007/s00604-020-4139-5.
[142] A. Lapresta-Fernández, A. Salinas-Castillo, S. Anderson De La Llana, J. M. Costa-Fernández, S. Domínguez-Meister, R. Cecchini, L. F. Capitán-Vallvey, M. C. Moreno-Bondi, M. P. Marco, J. C. Sánchez-López, I. S. Anderson, A general perspective of the characterization and quantification of nanoparticles: Imaging, spectroscopic, and separation techniques, Crit. Rev. Solid State Mater. Sci. 39 (2014) 423–458. https://doi.org/10.1080/10408436.2014.899890.
[143] V. S. Tiwari, T. Oleg, G. K. Darbha, W. Hardy, J. P. Singh, P. C. Ray, Non-resonance SERS effects of silver colloids with different shapes, Chem. Phys. Lett. 446 (2007) 77–82. https://doi.org/10.1016/j.cplett.2007.07.106.
[144] C. Larue, H. Castillo-Michel, S. Sobanska, L. Cécillon, S. Bureau, V. Barthès, L. Ouerdane, M. Carrière, G. Sarret, Foliar exposure of the crop *Lactuca sativa* to silver nanoparticles: Evidence for internalization and changes in Ag speciation, J. Hazard. Mater. 264 (2014) 98–106. https://doi.org/10.1016/j.jhazmat.2013.10.053.
[145] A. D. Servin, H. Castillo-Michel, J. A. Hernandez-Viezcas, B. C. Diaz, J. R. Peralta-Videa, J. L. Gardea-Torresdey, Synchrotron micro-XRF and micro-XANES confirmation of the uptake and translocation of TiO_2 nanoparticles in cucumber (*Cucumis sativus*) plants, Environ. Sci. Technol. 46 (2012) 7637–7643. https://doi.org/10.1021/es300955b.
[146] L. J. Dong, Y. J. Lai, S. J. Yu, J. F. Liu, Speciation analysis of the uptake and biodistribution of nanoparticulate and ionic silver in *Escherichia coli*, Anal. Chem. 91 (2019) 12525–12530. https://doi.org/10.1021/acs.analchem.9b03359.
[147] L. Xu, Z. Wang, J. Zhao, M. Lin, B. Xing, Accumulation of metal-based nanoparticles in marine bivalve mollusks from offshore aquaculture as detected by single particle ICP-MS, Environ. Pollut. 260 (2020) 114043. https://doi.org/10.1016/j.envpol.2020.114043.
[148] H. Y. Lu, Y. J. Wang, W. C. Hou, Bioaccumulation and depuration of TiO_2 nanoparticles by zebrafish through dietary exposure: Size- and number concentration-resolved analysis using single-particle ICP-MS, J. Hazard. Mater. 426 (2022) 127801. https://doi.org/10.1016/j.jhazmat.2021.127801.
[149] F. Laborda, E. Bolea, J. Jimenez-Lamana, Single Particle Inductively Coupled Plasma Mass Spectrometry: A powerful tool for nanoanalysis, Anal. Chem. 86 (2014) 2270–2278. https://doi.org/10.1021/ac402980q.
[150] F. Laborda, E. Bolea, J. Jiménez-Lamana, Single particle inductively coupled plasma mass spectrometry for the analysis of inorganic engineered nanoparticles in environmental samples, Trends Environ. Anal. Chem. 9 (2016) 15–23. https://doi.org/10.1016/j.teac.2016.02.001.
[151] C. Degueldre, P. Y. Favarger, Colloid analysis by single particle inductively coupled plasma-mass spectroscopy: a feasibility study, Colloids Surfaces A Physicochem. Eng. Asp. 217 (2003) 137–142. https://doi.org/10.1016/S0927-7757(02)00568-X.
[152] F. Laborda, A. C. Gimenez-Ingalaturre, E. Bolea, J. R. Castillo, About detectability and limits of detection in single particle inductively coupled plasma mass spectrometry, Spectrochim. Acta - Part B At. Spectrosc. 169 (2020) 105883. https://doi.org/10.1016/j.sab.2020.105883.
[153] H. K. Sung, E. Jo, E. Kim, S. Yoo, J. Lee, P. Kim, Y. Kim, I. C. Eom, Analysis of gold and silver nanoparticles internalized by zebrafish (*Danio rerio*) using single particle-

USC UNIVERSIDADE DE SANTIAGO DE COMPOSTELA

inductively coupled plasma-mass spectrometry, Chemosphere 209 (2018) 815–822. https://doi.org/10.1016/j.chemosphere.2018.06.149.
[154] S. Weigel, R. Peters, K. Loeschner, R. Grombe, T. P. J. Linsinger, Results of an interlaboratory method performance study for the size determination and quantification of silver nanoparticles in chicken meat by single-particle inductively coupled plasma mass spectrometry (sp-ICP-MS), Anal. Bioanal. Chem. 409 (2017) 4839–4848. https://doi.org/10.1007/s00216-017-0427-2.
[155] W. J. Wei, L. Li, Y. P. Gao, Q. Wang, Y. Y. Zhou, X. Liu, Y. Yang, Enzyme digestion combined with SP-ICP-MS analysis to characterize the bioaccumulation of gold nanoparticles by mustard and lettuce plants, Sci. Total Environ. 777 (2021) 146038. https://doi.org/10.1016/j.scitotenv.2021.146038.
[156] K. Kińska, J. Jiménez-Lamana, J. Kowalska, B. Krasnodębska-Ostręga, J. Szpunar, Study of the uptake and bioaccumulation of palladium nanoparticles by *Sinapis alba* using single particle ICP-MS, Sci. Total Environ. 615 (2018) 1078–1085. https://doi.org/10.1016/j.scitotenv.2017.09.203.
[157] Q. Yu, Z. Zhang, F. A. Monikh, J. Wu, Z. Wang, M. G. Vijver, T. Bosker, W. J. G. M. Peijnenburg, Trophic transfer of Cu nanoparticles in a simulated aquatic food chain, Ecotoxicol. Environ. Saf. 242 (2022) 113920. https://doi.org/10.1016/j.ecoenv.2022.113920.
[158] W. J. Wei, Y. Yang, X. Y. Li, P. Huang, Q. Wang, P. J. Yang, Cloud point extraction (CPE) combined with single particle -inductively coupled plasma-mass spectrometry (SP-ICP-MS) to analyze and characterize nano-silver sulfide in water environment, Talanta 239 (2022) 123117. https://doi.org/10.1016/j.talanta.2021.123117.
[159] G. Moreno-Martín, B. Gómez-Gómez, M. E. León-González, Y. Madrid, Characterization of AgNPs and AuNPs in sewage sludge by single particle inductively coupled plasma-mass spectrometry, Talanta 238 (2022) 123033. https://doi.org/10.1016/j.talanta.2021.123033.
[160] A. Mackevica, M. E. Olsson, S. F. Hansen, Quantitative characterization of TiO_2 nanoparticle release from textiles by conventional and single particle ICP-MS, J. Nanoparticle Res. 20 (2018) 1-11. https://doi.org/10.1007/s11051-017-4113-2.
[161] R. C. Merrifield, C. Stephan, J. R. Lead, Quantification of Au nanoparticle biouptake and distribution to freshwater algae using Single Cell-ICP-MS, Environ. Sci. Technol. 52 (2018) 2271–2277. https://doi.org/10.1021/acs.est.7b04968.
[162] L. Amable, C. Stephan, S. Smith, R. Merrifield, An Introduction to Single Cell ICP-MS analysis, White Paper. (2017) 1–5. Perkin Elmer. https://www.perkinelmer.com/lab-solutions/resources/docs/WHT-Introduction-to-Single-Cell-ICP-MS-012774A_01.pdf.
(accessed April 11, 2023).
[163] M. Corte Rodríguez, R. Álvarez-Fernández García, E. Blanco, J. Bettmer, M. Montes-Bayón, Quantitative evaluation of cisplatin uptake in sensitive and resistant individual cells by Single-Cell ICP-MS (SC-ICP-MS), Anal. Chem. 89 (2017) 11491–11497. https://doi.org/10.1021/acs.analchem.7b02746.
[164] A. B. S. da Silva, M. A. Z. Arruda, Single-cell ICP-MS to address the role of trace elements at a cellular level, J. Trace Elem. Med. Biol. 75 (2023) 127086. https://doi.org/10.1016/j.jtemb.2022.127086.
[165] M. Corte-Rodríguez, R. Álvarez-Fernández, P. García-Cancela, M. Montes-Bayón, J. Bettmer, Single cell ICP-MS using on line sample introduction systems: Current developments and remaining challenges, TrAC-Trends Anal. Chem. 132 (2020) 116042. https://doi.org/10.1016/j.trac.2020.116042.

USC UNIVERSIDADE DE SANTIAGO DE COMPOSTELA

[166] Y. Cao, J. Feng, L. Tang, C. Yu, G. Mo, B. Deng, A highly efficient introduction system for single cell-ICP-MS and its application to detection of copper in single human red blood cells, Talanta 206 (2020) 120174. https://doi.org/10.1016/j.talanta.2019.120174.
[167] M. Ikehata, J. Woolcock, M. E. P. Murphy, Introduction iron content measurement in individual bacterial cells using SC-ICP-MS, Application note (2018) 1-4. Perkin Elmer. http://www.perkinelmer.com/lab-solutions/resources/docs/APP_013978_01_NexION_SC-ICP-MS_Iron_in_Bacterial_Cells.pdf (accessed April 14, 2023).
[168] A. López-Serrano Oliver, S. Baumgart, W. Bremser, S. Flemig, D. Wittke, A. Grützkau, A. Luch, A. Haase, N. Jakubowski, Quantification of silver nanoparticles taken up by single cells using inductively coupled plasma mass spectrometry in the single cell measurement mode, J. Anal. At. Spectrom. 33 (2018) 1256–1263. https://doi.org/10.1039/c7ja00395a.
[169] R. Álvarez-Fernández García, M. Corte-Rodríguez, M. Macke, K. L. Leblanc, Z. Mester, M. Montes-Bayón, J. Bettmer, Addressing the presence of biogenic selenium nanoparticles in yeast cells: Analytical strategies based on ICP-TQ-MS, Analyst 145 (2020) 1457–1465. https://doi.org/10.1039/c9an01565e.
[170] S. Lekamge, A. F. Miranda, A. Abraham, A. S. Ball, R. Shukla, D. Nugegoda, The toxicity of coated silver nanoparticles to the alga *Raphidocelis subcapitata*, SN Appl. Sci. 2 (2020) 1–20. https://doi.org/10.1007/s42452-020-2430-z.
[171] Z. Wang, L. Yin, J. Zhao, B. Xing, Trophic transfer and accumulation of TiO_2 nanoparticles from clamworm (*Perinereis aibuhitensis*) to juvenile turbot (*Scophthalmus maximus*) along a marine benthic food chain, Water Res. 95 (2016) 250–259. https://doi.org/10.1016/j.watres.2016.03.027.
[172] M. Connolly, S. Martínez-Morcillo, J. Kalman, J. M. Navas, E. Bleeker, M. L. Fernández-Cruz, Considerations for bioaccumulation studies in fish with nanomaterials, Chemosphere. 312 (2023) 137299. https://doi.org/10.1016/j.chemosphere.2022.137299.
[173] D. E. Lefebvre, K. Venema, L. Gombau, L. G. Valerio, J. Raju, G. S. Bondy, H. Bouwmeester, R. P. Singh, A. J. Clippinger, E. M. Collnot, R. Mehta, V. Stone, Utility of models of the gastrointestinal tract for assessment of the digestion and absorption of engineered nanomaterials released from food matrices, Nanotoxicology 9 (2015) 523–542. https://doi.org/10.3109/17435390.2014.948091.
[174] C. McCracken, P. K. Dutta, W. J. Waldman, Critical assessment of toxicological effects of ingested nanoparticles, Environ. Sci. Nano. 3 (2016) 256–282. https://doi.org/10.1039/c5en00242g.
[175] E. Brun, M. L. Jugan, N. Herlin-Boime, D. Jaillard, B. Fayard, A. M. Flank, A. Mabondzo, M. Carrière, Investigation of TiO_2 nanoparticles translocation through a Caco-2 monolayer, J. Phys.: Conf. Ser. 304 (2011) 010248. https://doi.org/10.1088/1742-6596/304/1/012048.
[176] M. V. Taboada-López, B. H. Leal-Martínez, R. Domínguez-González, P. Bermejo-Barrera, P. Taboada-Antelo, A. Moreda-Piñeiro, Caco-2 *in vitro* model of human gastrointestinal tract for studying the absorption of titanium dioxide and silver nanoparticles from seafood, Talanta 233 (2021) 122494. https://doi.org/10.1016/j.talanta.2021.122494.
[177] O. Kose, D. Béal, S. Motellier, N. Pelissier, V. Collin-Faure, M. Blosi, R. Bengalli, A. Costa, I. Furxhi, P. Mantecca, M. Carriere, Physicochemical transformations of silver nanoparticles in the oro-gastrointestinal tract mildly affect their toxicity to intestinal cells *in vitro*: An AOP-oriented testing approach, Toxics 11 (2023) 199. https://doi.org/10.3390/toxics11030199.
[178] M. Ferrante, A. Grasso, R. Salemi, M. Libra, B. Tomasello, M. Fiore, C. Copat, DNA Damage and apoptosis as *in vitro* effect biomarkers of titanium dioxide nanoparticles (TiO_2-

NPs) and the food additive E171 toxicity in colon cancer cells: HCT-116 and Caco-2, Int. J. Environ. Res. Public Health. 20 (2023) 2002. https://doi.org/10.3390/ijerph20032002.
[179] A. García-Rodríguez, L. Vila, C. Cortés, A. Hernández, R. Marcos, Effects of differently shaped TiO_2NPs (nanospheres, nanorods and nanowires) on the *in vitro* model (Caco-2/HT29) of the intestinal barrier, Part. Fibre Toxicol. 15 (2018) 1–16. https://doi.org/10.1186/s12989-018-0269-x.
[180] M. Saez-Tenorio, J. Domenech, A. García-Rodríguez, A. Velázquez, A. Hernández, R. Marcos, C. Cortés, Assessing the relevance of exposure time in differentiated Caco-2 / HT29 cocultures. Effects of silver nanoparticles, 123 (2019) 258–267. https://doi.org/10.1016/j.fct.2018.11.009.

USC
UNIVERSIDADE DE SANTIAGO DE COMPOSTELA

II. OBJECTIVES

USC
UNIVERSIDADE
DE SANTIAGO
DE COMPOSTELA

USC
UNIVERSIDADE
DE SANTIAGO
DE COMPOSTELA

II. OBJECTIVES

The extensive use of AgNPs and TiO_2NPs, their emission into the environment and their interaction with marine organisms, make it necessary to study the bioaccumulation, distribution and effects of these nanoparticles in some of the most important aquaculture species of the Atlantic area including mussels, turbot, and red and green seaweed, as well as the bioavailability of the NPs in these food matrices.

The following objectives of this doctoral thesis are proposed:

-Development of analytical methodologies for AgNPs and TiO_2NPs extraction from the aquaculture products (seaweed), and their number content and size distribution determination by SP-ICP-MS.

-Study of the bioaccumulation of total and nanoparticle content in aquaculture products exposed to different concentrations of AgNPs and TiO_2NPs, by ICP-MS and SP-ICP-MS. Furthermore, the study of the NPs distribution in the tissues of samples by electron microscopy techniques.

-Evaluation of total Ag and Ti as well as NPs content in several samples from the Atlantic area.

-Study of the bioavailability of AgNPs and TiO_2NPs from raw and cooked aquaculture species using *in vitro* gastrointestinal digestions. Study of the cellular transport of total element content and NPs across Caco-2 cell membranes by ICP-MS and SP-ICP-MS, and the NPs internalization in Caco-2 cells by SC-ICP-MS.

USC
UNIVERSIDADE DE SANTIAGO DE COMPOSTELA

USC
UNIVERSIDADE
DE SANTIAGO
DE COMPOSTELA

III. METHODOLOGY

USC
UNIVERSIDADE
DE SANTIAGO
DE COMPOSTELA

USC
UNIVERSIDADE
DE SANTIAGO
DE COMPOSTELA

III. METHODOLOGY

The methodology applied in the eight chapters of this doctoral thesis is briefly described:

CHAPTER 1. Ultrasonication followed by enzymatic hydrolysis as a sample pre-treatment for the determination of Ag nanoparticles in edible seaweed by SP-ICP-MS.

Enzymatic extraction of AgNPs was used for maintaining the NPs integrity. Enzymatic extraction was performed using Macerozyme® R-10 as a mixture of enzymes to isolate the AgNPs from the seaweed matrix. The type, time, and amplitude of probe sonication, enzyme concentration, and extraction time were optimized. The methodology was properly validated with AgNPs efficiencies of extraction of approximately 80%. The stability of AgNPs extraction was assured by SP-ICP-MS and TEM. The optimized methodology was applied to total Ag and AgNPs determination in several seaweed samples by ICP-MS and SP-ICP-MS, respectively.

CHAPTER 2. Titanium dioxide nanoparticles assessment in seaweed by single particle inductively coupled plasma mass spectrometry.

Alkaline extraction of TiO_2NPs from seaweed was optimized without affecting the nanoparticle integrity. TMAH with ultrasound energy was employed for TiO_2NPs release from the seaweed. The extracting solution concentration, the volume of extractive solution, and the sonication extraction time were optimized. The methodology was validated and the TiO_2NPs extraction from seaweed was quantitative. The analysis of cleaned seaweed alkaline extracts verified the success of the extraction by HR-TEM-EDX. Total Ti and TiO_2NPs size and concentration were determined in several seaweed samples by ICP-MS and SP-ICP-MS, respectively.

CHAPTER 3. Study of silver nanoparticles bioaccumulation in cultured red and green seaweed.

In the bioaccumulation assays, *Palmaria palmata* and *Ulva* sp. were exposed to 0.1 and 1.0 mg L^{-1} of 15 nm PVP-AgNPs for 28 days. Microwave-assisted digestion using nitric acid, hydrogen peroxide, and ultrapure water was used as sample pre-treatment for total Ag assessment by ICP-MS. An enzymatic extraction was employed for AgNPs separation before their size characterization and number and particle concentration assessment by SP-ICP-MS. TEM was also employed to characterize AgNPs in enzymatic extracts.

CHAPTER 4. Bioaccumulation of titanium dioxide nanoparticles in green (*Ulva* sp.) and red (*Palmaria palmata*) seaweed.

In this chapter, bioaccumulation assays using *Palmaria palmata* and *Ulva* sp. exposed to 0.1 and 1.0 mg L^{-1} of 25 nm and 5 nm citrate-coated TiO_2NPs, were carried out. Microwave-assisted acid digestion sample pre-treatment was employed for total Ti determination before ICP-MS analysis. An alkaline TiO_2NPs extraction procedure was used for TiO_2NPs separation before their size characterization and number and particle concentration assessment by SP-ICP-MS. Characterization of 25 and 5 nm TiO_2NPs stock, in ultrapure water, was assessed by TEM,

DLS, and zeta potential. Nanoparticle suspensions in artificial seawater were also characterized by DLS and zeta potential. SEM, TEM, and STEM techniques were employed to examine the localization of the NPs, and EDX analysis to identify the NPs found in *Palmaria palmata* and *Ulva* sp.

CHAPTER 5. Bioaccumulation of silver nanoparticles in mussels and turbot from the Atlantic area.

The bioaccumulation assays of 15 nm PVP AgNPs were performed in *Mytilus edulis* and *Scophthalmus maximus*. Mussels were exposed to 0.1 and 1.0 mg L^{-1} of AgNPs for 28 days. Turbots were exposed to 0.25, 0.75, and 1.5 mg of PVP-AgNPs per Kg fish and day for 105 days. The whole mussels and the flesh+skin, liver, and kidney of turbots were submitted to microwave-assisted acid digestion before total Ag determination by ICP-MS. Pancreatin/lipase enzymatic extractions were employed to extract AgNPs at a neutral pH and mild temperature conditions, without AgNPs integrity changes. The size distributions and the number of AgNPs concentration in the extracts were assessed by SP-ICP-MS.

CHAPTER 6. Bioaccumulation patterns in aquaculture mussels and turbots exposed to different sizes of TiO_2NPs.

The bioaccumulation assays of 25 and 5 nm citrate-coated TiO_2NPs in *Mytilus edulis* and *Scophthalmus maximus* were carried out. Mussels were exposed to 0.1 and 1.0 mg L^{-1} of 25 or 5 nm TiO_2NPs for 28 days. Turbots were exposed to 0.25, 0.75, and 1.5 mg of 25 or 5 nm TiO_2NPs Kg^{-1} fish and day for 90 days. Microwave-assisted acid digestion and ICP-MS were employed for total Ti determination in mussels, turbot tissues (flesh+skin, liver, and kidney), and turbot feces. Pancreatin/lipase enzymatic mixtures were also employed for TiO_2NPs extraction from fish matrices, and their size characterization and concentration number were determined by SP-ICP-MS analysis.

CHAPTER 7. Presence of silver and titanium dioxide nanoparticles in marine samples from the Atlantic area.

To evaluate the environmental levels of total Ag and Ti content and the AgNPs and TiO_2NPs content in several Atlantic area species, ICP-MS and SP-ICP-MS were employed, respectively. The fin fish species studied included *Salmo*, *Dicentrarchus labrax*, and *Sparus aurata*, whose flesh+skin, liver, and kidney were analyzed separately. The seaweed studied was *Alaria esculenta*, and the mollusk was *Mytilus edulis*. The elemental content of all species was assessed by microwave-assisted acid digestion and ICP-MS analysis. The nanoparticle content was determined by enzymatic extractions with pancreatin/lipase mixtures (for fin fish and mussels), Macerozyme® R-10 (for AgNPs in seaweed), and alkaline extraction with TMAH (for TiO_2NPs in seaweed), all before SP-ICP-MS analysis.

CHAPTER 8. Bioavailability study of silver and titanium dioxide nanoparticles from seaweed and mussels using Caco-2 cells.

The bioaccessibility and bioavailability of total Ag and Ti, and AgNPs and TiO_2NPs in raw and cooked seaweed (*Palmaria palmata* and *Ulva* sp.) and cooked mussels (*Mytilus edulis*) were studied. The specimens were exposed to 1.0 mg L^{-1} of 15 nm PVP-AgNPs, 1.0 mg L^{-1} of 25 nm

citrate-TiO_2NPs or 1.0 mg L^{-1} 5 nm citrate-TiO_2NPs, in all cases for 28 days. The *in vitro* gastrointestinal simulated digestions and the cellular transport through the Caco-2 cell monolayer assays were performed to determine the bioaccessibility and bioavailability in the samples. The bioaccessible fractions, and the fractions obtained after one hour of incubation in the simulated lumen through the monoculture of Caco-2 inTranswells®, were analyzed by ICP-MS and SP-ICP-MS. SC-ICP-MS was also employed to determine the nanoparticle internalization in the Caco-2 cells.

USC
UNIVERSIDADE DE SANTIAGO DE COMPOSTELA

USC
UNIVERSIDADE
DE SANTIAGO
DE COMPOSTELA

IV. RESULTS AND DISCUSSION

USC
UNIVERSIDADE
DE SANTIAGO
DE COMPOSTELA

USC
UNIVERSIDADE
DE SANTIAGO
DE COMPOSTELA

PART A. DEVELOPMENT OF ANALYTICAL METHODOLOGIES FOR SILVER AND TITANIUM DIOXIDE NANOPARTICLES EXTRACTION

USC
UNIVERSIDADE DE SANTIAGO DE COMPOSTELA

USC
UNIVERSIDADE
DE SANTIAGO
DE COMPOSTELA

CHAPTER 1. ULTRASONICATION FOLLOWED BY ENZYMATIC HYDROLYSIS AS A SAMPLE PRE-TREATMENT FOR THE DETERMINATION OF Ag NANOPARTICLES IN EDIBLE SEAWEED BY SP-ICP-MS

USC
UNIVERSIDADE DE SANTIAGO DE COMPOSTELA

USC
UNIVERSIDADE
DE SANTIAGO
DE COMPOSTELA

CHAPTER 1. ULTRASONICATION FOLLOWED BY ENZYMATIC HYDROLYSIS AS A SAMPLE PRE-TREATMENT FOR THE DETERMINATION OF Ag NANOPARTICLES IN EDIBLE SEAWEED BY SP-ICP-MS*

*The results from this chapter have already been published as Juan José López-Mayán, Blanca Álvarez-Fernández, Elena Peña-Vázquez, María Carmen Barciela-Alonso, Antonio Moreda Piñeiro, Pilar Bermejo-Barrera, Ultrasonication followed by enzymatic hydrolysis as a sample pre-treatment for the determination of Ag nanoparticles in edible seaweed by SP-ICP-MS, Talanta 247 (2022) 123556. https://doi.org/10.1016/j.talanta.2022.123556.

Trace Element, Spectroscopy and Speciation Group (GETEE), Instituto de Materiais (iMATUS), Faculty of Chemistry, University of Santiago de Compostela, Av. das Ciencias, s/n 15782, Santiago de Compostela, Spain.

1.1 ABSTRACT

Seaweed can bioaccumulate nanomaterials that would be transferred to the trophic chain. This work describes the optimization of a method for the separation of silver nanoparticles (AgNPs) from seaweed using an ultrasound-assisted enzymatic hydrolysis method and ulterior determination by single particle inductively coupled plasma mass spectrometry (SP-ICP-MS). The following parameters affecting the isolation of AgNPs were optimized using a *Palmaria palmata* (red seaweed) sample previously exposed to AgNPs: type of sonication (bath versus ultrasonic probe), ultrasound amplitude, sonication time, sonication mode (pulsed versus continuous sonication), the concentration of the enzymes mixture (Macerozyme® R-10), and enzymatic hydrolysis time. The stability of AgNPs during extraction was tested by transmission electron microscopy (TEM) and using a standard of 15 nm of polyvinylpyrrolidone (PVP)-coated AgNPs analyzed by SP-ICP-MS. The analytical performance was evaluated with good results. For total Ti determination, the limits of detection and quantification were 2.2 and 7.7 ng g^{-1} respectively; and for the TiO_2NPs determination, the limits of detection in size and number were 14 nm and 2.4×10^6 part L^{-1} respectively. Besides, the matrix effect, the repeatability and the analytical recovery were also studied. Finally, the method was applied to the analysis of several red (*Palmaria palmata*) and green (*Ulva* sp.) seaweed samples.

1.2 INTRODUCTION

Natural nanomaterials have been present on earth since the beginning of time, mainly due to volcanic eruptions and hydrothermal processes. However, since the beginning of the 21st century, due to the expansion of Nanotechnology [1] many nanomaterials [2] found in the environment are of anthropogenic origin, either accidental or manufactured (engineered nanomaterials, ENMs). Silver nanoparticles (AgNPs) have special antibacterial, optical, electrical and thermal properties [3] that imply many applications [4] including catalysis, medical, domestic and industrial product manufacturing, health care, biosensing, electronics [5], photonics [6] food industry (food packaging, food additive E174, etc), and even in the agriculture sector [3,7]. The environmental exposure to nanoparticles can originate from their synthesis, manufacturing, distribution, the final use of the product, and end-of-life disposal [8].

AgNPs can change their properties, conformation, and chemical composition when they are present in the environment. Nanoparticles can be suspended, agglomerated or aggregated, dissolved, or even they can react with several species in the aquatic environment [8] depending on factors like pH, ionic strength, organic matter content, coating, and ligands (complexing substances) concentration.

The European population has increased the consumption of seaweed due to its high nutritional value. The presence of vitamin B-12, selenium, omega-3, dietary fibre, fatty acids, and iodine, together with changes in European lifestyles and a growing interest in a healthier, more sustainable, and environmentally friendly diet, have all contributed to this trend [9]. Seaweeds are essential marine primary producers, having a direct impact on the trophic chain as well as on the qualitative end state of many coastal environments [4]. Besides, seaweeds are commonly used for bioremediation of marine pollution [10-12] due to their capacity for biosorption and accumulation of heavy metals and trace elements [9,13]. Although there is a European recommendation (European Commission, 2018) on the monitoring of iodine and metals such as Cd, Pb, As, and Hg in seaweed [14], there is no legislation about the presence of ENMs in seaweed.

The study of the presence and bioaccumulation of nanoparticles in complex biological samples, such as seaweed, demands the use of methodologies that can offer information on the element's existence in nanoparticulated and dissolved form, as well as the concentration and size of nanoparticles at environmentally real concentrations. Single particle inductively coupled mass spectrometry (SP-ICP-MS) is the most promising technique that allows the simultaneous determination of particle concentration, size and size distribution, as well as the detection of the dissolved element. SP-ICP-MS has been used in several kinds of biological and environmental matrices. Thus, several authors have analyzed NPs in animal tissues, e.g. Au NPs in rat spleen [15], Au and AgNPs in *Daphnia Magna and Lumbriculus variegatus* [16], and AgNPs in chicken [17]. Other authors have also studied the uptake of NPs in plant tissues, such as Dan et al. [18,19] for CeO_2NPs uptake and accumulation in soybean, pumpkin, tomato, and cucumber, and AuNPs uptake by tomato plants, Jiménez-Lamana et al. [20] for PtNPs accumulation in *Sinapsis alba* and *Lepidium sativum,* and Kińska et al. [21] for PdNPs uptake by *Sinapsis alba*. Wojcieszek et al. [22] have also determined the CeO_2NPs uptake by *Raphanus sativus L,* and Bao et al. [23] the AgNPs internalization in *Arabidopsis thaliana*. Finally, Nath et al. [24] have synthesized isotopically-labeled AgNPs, CuNPs and ZnONPs to assist the traceability of the interactions between NPs and plants.

One of the biggest challenges in the characterization of NPs is their extraction from a complex matrix using mild conditions, without changing their size, conformation, and composition. Consequently, the use of strong acids should be avoided, and therefore, several authors employed basic extractions, and extractions based on enzymes. Tetramethylammonium hydroxide (TMAH) was used for alkaline solubilization of biological tissues before NPs assessment [15,16,25]. In addition, several authors have used mixtures of enzymes to isolate NPs from complex biological matrices. In the case of tissues with high content of protein and fat, a pancreatin/lipase combination has been proposed [26,27], but Macerozyme R-10® (a mixture of cellulase, hemicellulase, and pectinase) is more adequate to destroy the vegetal cell walls previously to the determination of NPs by SP-ICP-MS [20,23,24,28,29].

The aim of this work is the development of an ultrasound-assisted enzymatic methodology for the extraction of AgNPs from seaweed samples with a mixture of enzymes (Macerozyme® R-10) and the application to some red and green seaweed exposed to AgNPs. ICP-MS and SP-ICP-MS were respectively used for quantifying the total amount of Ag and for the determination of AgNPs concentration and size distributions.

USC
DE COMPOSTELA

1.3 MATERIALS AND METHODS

1.3.1 Instrumentation

Total silver determination was performed using an inductively coupled plasma mass spectrometer NexION® 2000 (Perkin Elmer, Waltham, MA, USA) equipped with an ESI Single Cell Micro DX (Perkin Elmer, Shelton, CT USA) autosampler. AgNPs data acquisition and management were performed with the help of the SP-ICP-MS Syngistix™ Nano application software (Perkin Elmer).

An Ethos Plus microwave lab station (Milestone, Bergamo, Italy) was used for sample digestion. The microwave is equipped with ten Teflon vessels (100 mL), Teflon covers, HTC adapter plate, HTC safety springs (Milestone), and pressure and temperature controller probe.

Scanning transmission electron microscopy (STEM) with a probe-corrected FEI Titan G2 80-200 kV ChemiSTEM (FEI, Hillsboro, USA), was used for the acquisition of AgNPs images present in cleaned enzymatic extracts.

A Basic20 pH meter (Crison, Barcelona, Spain) was used for buffer pH adjustments. The VibraCell™ VCX 130 V (Sonics Newtown, CT, USA) ultrasound probe was used to homogenize the seaweed samples previous to the enzymatic extraction. A VWR Ultrasonic Cleaner (Barcelona, Spain) was used to disperse the nanoparticles before their use. AgNPs isolation from seaweed was performed with a Boxcult temperature-controlled incubation chamber (Stuart Scientific, Surrey, UK) equipped with a Rotabit orbital-rocking platform shaker (J.P. Selecta, Barcelona, Spain). A Laborcentrifugen 2K15 centrifuge (Sigma, Osterode, Germany) was used for cleaning the enzymatic extracts before the STEM analysis. Other instrumentation to perform the analysis includes an analytical balance ML204 (Mettler Toledo, Barcelona, Spain), and a Reax top vortex vibrational shaker (Heidolph, Schwabach, Germany).

1.3.2 Reagents

Macerozyme® R-10 (Merck, Darmstadt, Germany) was used for AgNPs isolation from seaweed matrix. This mixture of enzymes is obtained from *Rhizopus* sp., and it is formed by cellulase (0.1 units per mg), hemicellulase (0.25 units per mg), and pectinase (0.5 units per mg). Citric acid for analysis (ACS, Panreac, Barcelona, Spain), and trisodium citrate di-hydrated for analysis (Merck) were used for buffer preparation and extracts homogenization.

Ionic silver stock solution (1000 mg L^{-1}) in 2% HNO_3 (Perkin Elmer, Shelton, CT, USA) was used to prepare the ionic silver standards; whereas, ionic Rh stock solution (1000 mg L^{-1}) in 2% HCl (Perkin Elmer) was used as an internal standard (5 µg L^{-1} in 1% nitric acid). Nitric acid 69% w/v (SUPRAPUR®, Sigma Aldrich, Darmstadt, Germany) and hydrogen peroxide 33% w/v ACS (Panreac, Barcelona, Spain) were used for the seaweed microwave-assisted acid digestion. A reference material PEG-COOH Gold Nanospheres (49.6 nm and 9.89×10^6 particles mL^{-1}) were from NanoComposix (San Diego, CA, USA), and an ionic gold stock standard (1000 mg L^{-1}) in 2 mol L^{-1} HCl (Merck) were used to calculate the transport efficiency in SP-ICP-MS. A suspension of polyvinylpyrrolidone (PVP) coated silver nanopowder of 15 nm and a concentration of 5.4×10^{14} particles mL^{-1} were from SkySpring Nanomaterials, Inc. (Houston, TX, USA), and were used for analytical performance check.

Other reagents were glycerol for analysis (Merck), absolute ethanol (PanReac, AppliChem, Barcelona, España), and NexION Setup Solution (1.0 µg L^{-1} of Be, Ce, Fe, In, Li, Mg, Pb, and U in 1% of HNO_3) from Perkin Elmer. Ultrapure water (18 MΩcm of resistivity) was obtained from a Milli-Q® purification system (Millipore Co., Bedford, MA, USA). Ar with a 99,999% of purity was from Nippon Gases (Madrid, Spain).

USC UNIVERSIDADE DE SANTIAGO DE COMPOSTELA

Other consumables were Minisart NML hydrophilic non-sterile 5.0 µm filters (Sartorius, Goettingen, Germany) for filtrating the enzymatic extracts, and regenerated cellulose Amicon Ultra- 0.5 mL centrifugal filter units (30 kDa nominal molecular weight limit, NMWL) from Merck for enzymatic extracts cleaning for STEM analysis. Plastic material (pipette tips, syringes, tubes…) was discarded after use, and all the glassware material was submitted to a decontamination procedure to avoid ultra-trace metal contamination. Glasswares were washed three times with ultrapure water and kept in nitric acid (10% v/v) for 48 hours, then washed several times with ultrapure water, dried in an oven and stored until the next use.

1.3.3 Seaweed samples harvesting and exposure trial

Seaweed samples used for the optimization of the procedure were from Indigo Rock Marine Research Center (Cork, Ireland) and they consist of five Dulse (*Palmaria palmata*) and five Sea lettuce (*Ulva* sp.) samples. Seaweeds were harvested in 40 L tanks at 16±1 ºC with periods of 12 h of white light and 12 h of darkness and exposed to AgNPs for twenty-eight days. Available fresh seaweed samples were washed in the laboratory with ultrapure water (salts and other contaminants removal) and were manually homogenized before storing in polyethylene tubes at -18 ºC.

1.3.4 Microwave-assisted acid digestion

Microwave-assisted acid digestion was performed by weighing 1.0000 g of homogenized seaweed samples and mixing them with 4.0 mL of ultrapure water, 3.0 mL of 69% (w/v) HNO_3, and 1.0 mL of 33% (w/v) H_2O_2 in Teflon vessels. The microwave digestion program lasts 34 min at 850 W. The first step consists of heating from room temperature to 90 °C (ramp of 4 min), then heating from 90 to 140 °C (ramp of 5 min), then from 140 to 200 °C (ramp of 5 min), and finally maintaining the reactors at 200ºC for 20 min. After cooling, the acid digests were made up to 25 mL with ultrapure water and stored before ICP-MS analysis. Each seaweed sample was subjected to microwave-assisted acid digestion in triplicate and two reagent blanks were prepared for each set of sample pre-treatment.

1.3.5 Enzymatic hydrolysis for AgNPs extraction

A mass of 0.0500 g of seaweed sample was introduced in a 10 mL polyethylene tube with 7 mL of 2 mM/2 mM citric acid/trisodium citrate buffer (pH= 4.5). The mixture was sonicated in an ice bath for 2.5 min with intermittent 1.0 s pulses (total time: 5 min) using the ultrasound probe operating at 20% of amplitude. Then 2.0 mL of a 25 g L^{-1} Macerozyme® R-10 solution was added. After extraction in a Boxcult temperature-controlled incubation chamber at 150 rpm and 37 ºC for 6.0 h, the extracts were filtered with 5.0 µm cellulose syringe disks and were diluted with 1.0 % (v/v) glycerol before SP-ICP-MS analysis.

1.3.6 Total Ag determination by ICP-MS

The total content of Ag in the acid digests was determined by ICP-MS under the conditions listed in **Table 1.1.(a)**. A standard addition calibration method in an Ag concentration range from 0 to 15.0 µg L^{-1} was used. Isotopes ^{107}Ag and ^{109}Ag were monitored and ^{103}Rh was used as an internal standard. The Kinetic Energy Discrimination (KED) mode was used to reduce the polyatomic interferences of silver, introducing a continuous flow of 4.5 mL min^{-1} of He in the collision cell of the instrument.

USC UNIVERSIDADE DE SANTIAGO DE COMPOSTELA

Table 1.1. Operating conditions for ICP-MS (a) and SP-ICP-MS (b) measurements.

(a) ICP-MS	
Parameter/Component	Type/Value/Mode
Nebulizer	Meinhard CT R^+
Nebulizer Chamber	5º C refrigerated glass cyclone chamber with Peltier PC^{3X}
Cone material	Nickel/aluminium
Plasma gas flow	15 L min^{-1}
Auxiliary gas flow	1.2 L min^{-1}
Nebuliser gas flow	1.15 mL min^{-1}
Power RF	1600 W
Integration time	1000 ms
Replicates per sample	3
Operation mode	KED (4.5 mL min^{-1})
Isotopes	^{107}Ag, ^{109}Ag, and ^{103}Rh (internal standard)
(b) SP-ICP-MS	
Parameter	Value
Sample flow rate	0.19-0.21 mL min^{-1}
Dwell time	50 µs
Sampling time	100 s
Number of readings	2,000,000
RPq	0.2
Operation mode	Standard
Isotope	^{107}Ag, ^{197}Au (for TE)

1.3.7 AgNPs analysis by SP-ICP-MS

Enzymatic extracts were diluted at least 100 times with 1.0% (v/v) glycerol and submitted to bath-sonication for 1.0 min previous to their analysis by SP-ICP-MS under the conditions listed in **Table 1.1.(b)**. The Syngistix™ Nano Application Software needs to perform different measurements to calculate the efficiency with which the NPs reach the nebulizer (Transport Efficiency, TE). These measurements include: (1) the calculation of the sample introduction flow rate through the peristaltic pump by aspirating a volume of ultrapure water for one minute in triplicate, (2) the analysis of the Au nanospheres (49.6 nm in size) reference material at a concentration of 9.89×10^4 particles mL^{-1}, (3) the measurement of gold ionic standards of 0, 1.0, 2.0, and 3.0 µg L^{-1}. The TE is measured in the same operational conditions as silver (**Table 1.1.(b)**) but using the m/z 197 of the gold isotope. The experimental TE was approximately 9±1 %. Once the Syngistix™ Nano Application Software obtains the TE, a silver ionic calibration

with standards of 0, 0.5, 1.0, 2.5, and 5.0 μg L^{-1} was carried out. Finally, the AgNPs concentration and size distributions in the diluted extracts were directly obtained from the software after analysis.

1.3.8 Scanning transmission electron microscopy analysis of Macerozyme® R-10 extracts

An enzymatic extract cleaning and NPs pre-concentration are necessary before STEM analysis of seaweed enzymatic extracts. The procedure consists of filtration by ultracentrifugation using Amicon® Ultra 30 KDa centrifugal filter units. Therefore, the cleaning process starts by filling the units with 0.5 mL of extract and centrifuging at 14,000 g and 4 ºC for 20 min. The process was repeated five times by refilling the units with 0.5 mL of ultrapure water. Then, a volume of 0.5 mL of absolute ethanol was added and shaken with the extract for 1.0 h to eliminate the excess of organic matter. Finally, the cleaning process using ultrapure water was repeated five more times. The clean and pre-concentrated extract (approximately 25 μL) was collected and five drops of 3.0 μL were deposited on a Ti grid for increasing the concentration of particles during microscopic analysis. These drops were successively deposited and allowed to dry at room temperature before inserting the grid in the STEM sample holder.

1.4 RESULTS AND DISCUSSION

1.4.1 Selection of ultrasound-assisted enzymatic hydrolysis conditions for AgNPs extraction

An ultrasound-assisted enzymatic hydrolysis method for silver nanoparticles analysis was properly optimized and validated. Ultrasonic energy was used to improve the extraction procedure, and parameters related to sonication, such as ultrasound amplitude, sonication time, presence versus absence of pulses during sonication, and the use of a probe versus an ultrasonic bath were evaluated. Furthermore, the effect of the concentration of Macerozyme® R-10 and the incubation (extraction) time were studied. All experiments were performed in triplicate with three blanks per condition. The experiments carried out during the optimization process were performed with portions of 0.0500 g of a pool from *Palmaria palmata* samples exposed to 1.0 mg L^{-1} of AgNPs, and an ionic silver calibration (0-5.0 μg L^{-1}) was used for AgNPs concentration determination by SP-ICP-MS.

1.4.1.1 Ultrasound amplitude

Ultrasound amplitude is correlated with the power of the ultrasonic probe. For extraction of AgNPs the amplitude cannot be very high due to the possible destruction, or ionization of the particles. Therefore, different amplitudes of the vibration movement of the probe (20, 30, and 40%) were checked. For each amplitude value, a mass of 0.0500g of red seaweed sample was mixed in a polyethylene tube with 7 mL of the sodium citrate/citric acid 0.2 mM /0.2 mM (pH=4.5) buffer and submitted to sonication for 2.5 min with intermittent 1.0 s pulses. Each tube was placed in an ice bath to prevent the sample from heating up due to the ultrasound energy. After sonication, a volume of 2.0 mL of the 25 g L^{-1} Macerozyme R-10® solution was added and then incubated in a Boxcult incubation chamber overnight at 37º C and 150 rpm. The number of AgNPs extracted from the sample was between $5.64\times10^{8}\pm5.55\times10^{7}$ part g^{-1} (mean ± standard deviation, for 20% amplitude) and $6.42\times10^{8}\pm8.97\times10^{7}$ part g^{-1} (for 30% amplitude) (**Figure 1.1.(a)**). Regarding the AgNPs size, no significant differences were

USC UNIVERSIDADE DE SANTIAGO DE COMPOSTELA

shown for the amplitudes studied, and the most frequent size was 19 nm. Then, a 20% amplitude value was selected to minimize nanoparticle degradation.

1.4.1.2 Ultrasound sonication time

Once the amplitude of sonication was set at 20%, the sonication time was the next parameter studied. Different sonication times (1.0, 2.5, and 5.0 min using intermittent 1.0 s pulses) were selected considering previous studies reported in the literature [20,21]. Results for these conditions are plotted in **Figure 1.1.(b)**. The highest AgNPs concentration in the enzymatic extracts was achieved when 2.5 min of ultrasound energy was used. Particle concentration and the most frequent size were $2.15\times10^{9}\pm1.04\times10^{7}$ Ag part g^{-1} and 18±1 nm, respectively, for 2.5 min sonication time (total time of 5.0 min). It seems that an increase in sonication time might degrade the nanoparticles and produce a rise of the temperature in the extract.

1.4.1.3 Pulsed versus continuous sonication

Once the sonication time was selected, the continuous sonication and pulsed sonication modes were compared (**Figure 1.1.(c)**). The number of nanoparticles measured in the enzymatic extracts after pulsed and continuous sonication was $1.64\times10^{9}\pm1.34\times10^{6}$ and $1.34\times10^{9}\pm1.78\times10^{8}$ part g^{-1}, respectively. The most frequent sizes were the same for both types of sonication (18±1 nm). There were no significant differences between the concentrations obtained by sonication with pulses and using continuous sonication. However, the relative standard deviation was lower for pulsed mode (0.1%) than for continuous sonication (12%). Then, the pulsed sonication mode was selected.

1.4.1.4 Type of sonication (bath versus probe)

Regarding sample preparation, sonication in an ultrasound bath would be easier than using an ultrasound probe (a sample each time). Therefore, the use of an ultrasound bath was evaluated. This experiment was performed using the enzymatic extraction with the previously optimized parameters for the probe (20% of amplitude, 2.5 min of sonication with pulses), and using an ultrasound bath for 5.0 and 10 minutes. Results for these conditions are shown in **Figure 1.1.(d)**. The concentration of nanoparticles extracted using the ultrasound probe (2.5 min) and the ultrasound bath (5 min and 10 min) were $7.49\times10^{8}\pm6.44\times10^{7}$, $1.29\times10^{9}\pm2.68\times10^{8}$, and $1.52\times10^{9}\pm4.83\times10^{8}$ part g^{-1}, respectively. Although the mean concentration of particles extracted from the sample was higher when using the ultrasonic bath, an ANOVA test (Statgraphics XVIII, Warrenton, USA) showed that there was no significant statistical differences ($P>0.05$) between the ultrasound bath and the ultrasound probe. Finally, due to the higher relative standard deviations obtained with the ultrasound bath (RSD> 22%), the decision was to continue the research with the ultrasound probe.

USC UNIVERSIDADE DE SANTIAGO DE COMPOSTELA

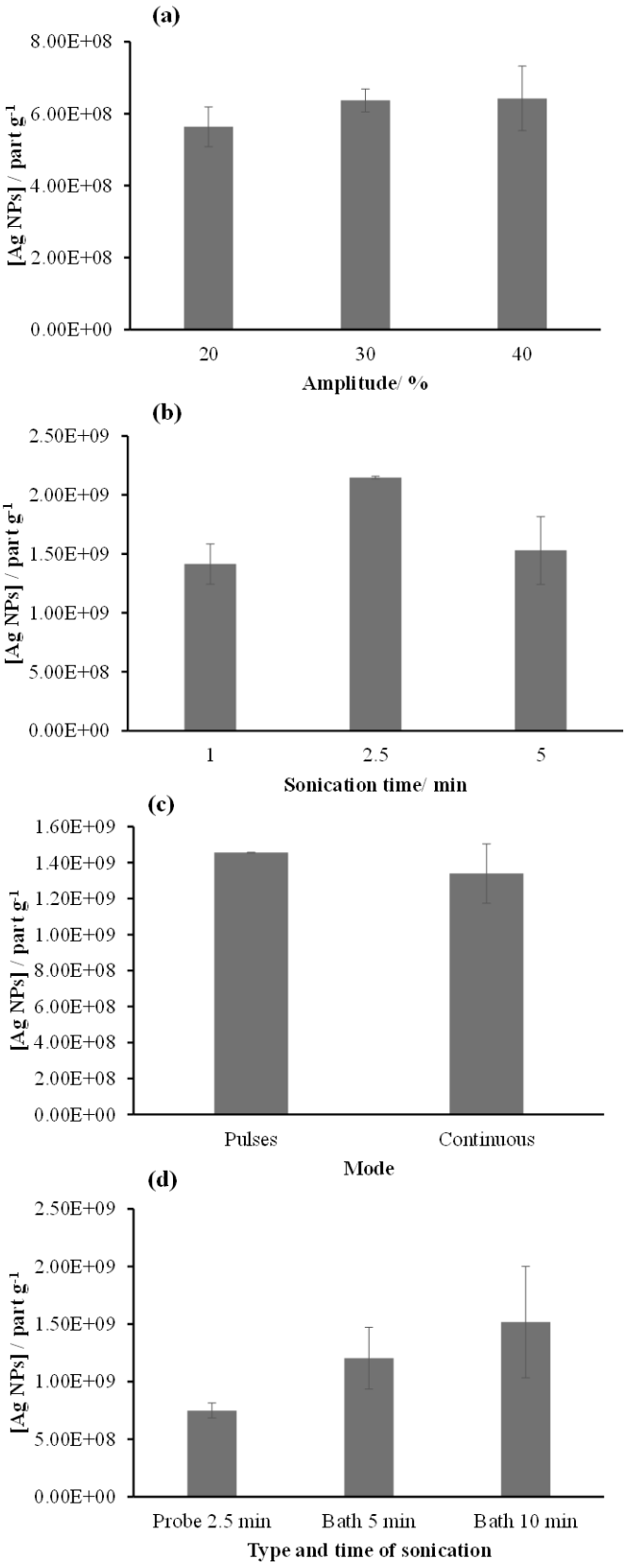

Figure 1.1. Optimization of parameters affecting sonication: (a) amplitude, (b) sonication time, (c) mode, and (d) type of sonication.

USC DE SANTIAGO DE COMPOSTELA

1.4.1.5 Macerozyme® R-10 concentration

Macerozyme® R-10 concentration was studied within the 0-37.5 g L^{-1} of enzyme range. Results for these experiments are plotted in **Figure 1.2.** The concentration of AgNPs obtained with the enzymatic extraction using 0, 12.5, 25, and 37.5 g L^{-1} of Macerozyme R-10® solution were $3.66\times10^{8}\pm7.60\times10^{7}$, $1.44\times10^{9}\pm2.86\times10^{8}$, $1.46\times10^{9}\pm1.34\times10^{6}$, and $1.33\times10^{9}\pm3.58\times10^{7}$ part g^{-1}, respectively. The most frequent sizes remained constant with the different concentrations of enzymes added (18±1 nm). Considering the extracted particle concentration, and the lower relative standard deviation (0.1%), a concentration of 25 g L^{-1} of Macerozyme® R-10 was selected as the optimum concentration for AgNPs isolation from seaweed.

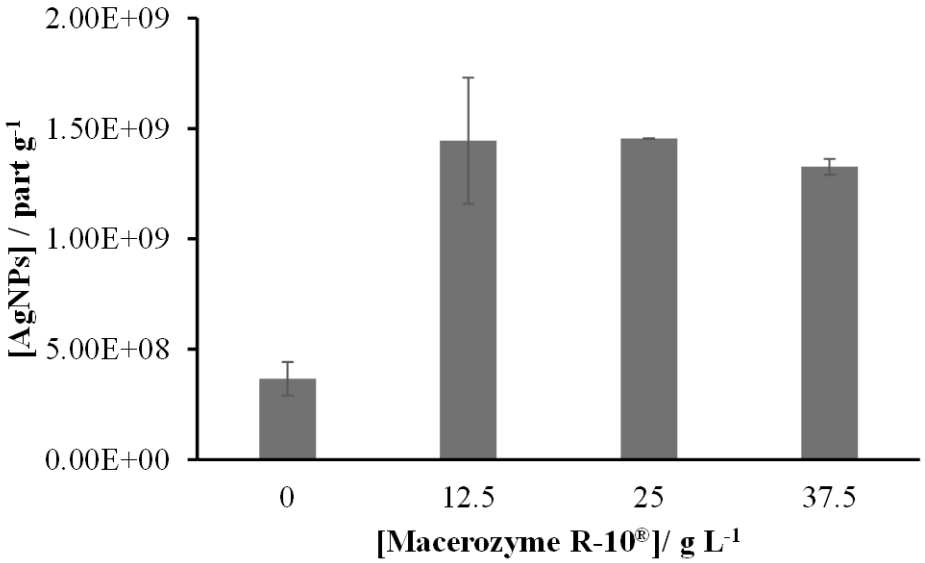

Figure 1.2. Optimization of Macerozyme R-10® concentration.

1.4.1.6 Incubation (extraction) time

Overnight extractions are highly time-consuming in terms of sample preparation. Therefore, the effect of the incubation time in the extracted AgNPs was studied. Several incubation times (6, 12, and 24 h) were evaluated. Results for this experiment are shown in **Figure 1.3.** The number of AgNPs extracted from seaweed were $6.42\times10^{9}\pm6.05\times10^{8}$, $6.33\times10^{9}\pm5.69\times10^{8}$, and $6.29\times10^{9}\pm1.87\times10^{9}$ part g^{-1} for 6, 12, and 24 h, respectively. No statistically significant differences were found for the three different incubation times. Therefore, 6.0 h was chosen due to a decrease in the sample preparation time.

USC UNIVERSIDADE DE SANTIAGO DE COMPOSTELA

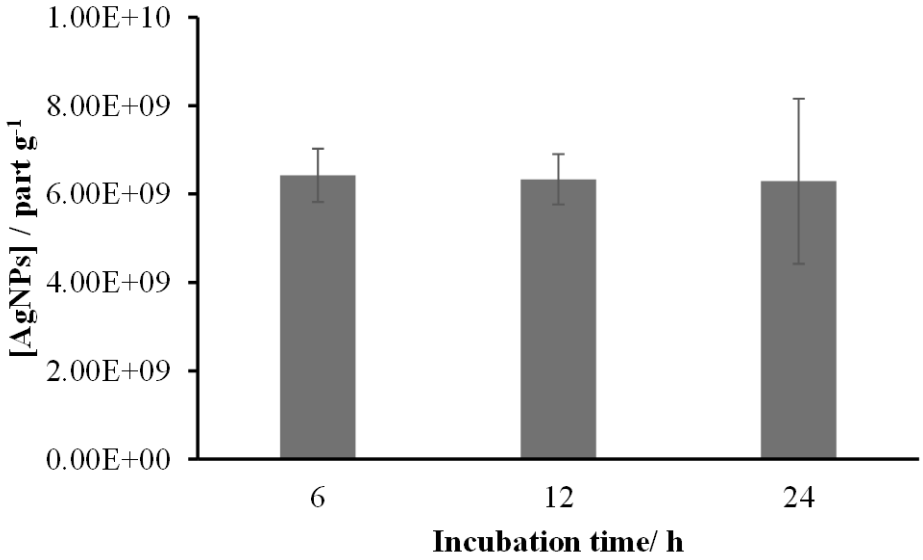

Figure 1.3. Optimization of incubation time.

1.4.2 Stability of AgNPs size under the selected extraction conditions

The stability of the nanoparticles during the extraction procedure was tested after comparing control AgNPs standards (un-treated suspensions) and the same AgNPs standards submitted to the whole procedure (sonication+enzymatic hydrolysis). A 15 nm AgNPs standard (5.4×10^{14} part mL^{-1}) was diluted with ultrapure water, subjected to the optimized enzymatic extraction and diluted with glycerol 1% (v/v) to a final theoretical concentration of 6×10^{7} part mL^{-1} before SP-ICP-MS measurements. The control AgNPs standard (without the enzymatic extraction) was diluted in the same way to the same final concentration of 6×10^{7} part mL^{-1}. This final concentration was selected to obtain a histogram with approximately one thousand single peaks, to avoid double events. Both experiments were performed in triplicate. No significant changes were observed in the most frequent sizes, taking into account that those values are close to the limit of detection in size of the technique. The sizes reported were 15±1, and 18±1 nm for the AgNPs control, and the AgNPs submitted to the enzymatic extraction, respectively. **Figure 1.4.** shows two overlapping histograms, corresponding to the AgNPs control and the AgNPs subjected to enzymatic extraction. The superimposed histograms show that enzymatic extraction does not affect the size of the AgNPs.

USC UNIVERSIDADE DE SANTIAGO DE COMPOSTELA

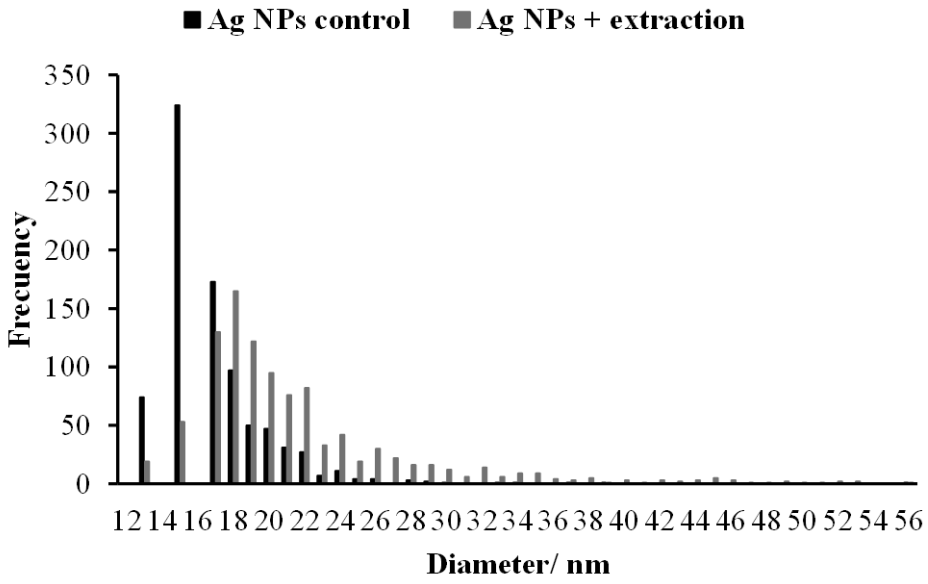

Figure 1.4. SP-ICP-MS histograms of AgNPs control and AgNPs after extraction (sonication + enzymatic hydrolysis).

1.4.3 Efficiency of AgNPs extraction

The efficiency of silver extraction was checked by comparing the Ag content in the digested samples and the total amount of Ag extracted from a seaweed sample. This study was carried out using a *Palmaria palmata* sample submitted to the microwave-assisted acid digestion method and the enzymatic extraction method in triplicate. Blanks of the sample were also prepared in duplicate by both methods. Finally, the total content of Ag, in the digested sample and the extract was analyzed by ICP-MS. The achieved average total concentration found were 0.69±0.25 µg g^{-1}, and 0.57±0.10 µg g^{-1} for the total silver in the microwave acid digest, and the enzymatic extract, respectively, providing an 80% of recovery percentage for the total silver extraction.

1.4.4 Analytical characteristics of the method

1.4.4.1 Matrix effect evaluation

For ICP-MS measurements, a silver ionic calibration prepared in HNO_3 1% (v/v) was compared to a standard addition silver calibration prepared with a pool of seaweed digested samples in the same dilution (1:25) as the samples using ultrapure water. For both calibrations, the concentrations of ionic silver were 0, 0.01, 0.05, 0.1, 1.0, 5.0, 10.0, and 15.0 µg L^{-1}. Good linearities were obtained for both calibration graphs (R^2 of 0.998 and 0.999, respectively). The slopes for the external calibration and the standard addition graphs were 8855.6 L μg^{-1} and 9848.7 L μg^{-1}, respectively. As the slopes were statistically different (t-test, 95% confidence level), the standard addition calibration method was used to measure total Ag in the digests by ICP-MS and correct the matrix effect.

For SP-ICP-MS measurements, an aqueous silver ionic calibration was compared to a silver ionic calibration matched with the enzymatic solution prepared at the same dilution (1:100) than the samples using 1.0 % (v/v) glycerol. For both calibrations, the concentrations of ionic silver were 0, 0.5, 1.0, 2.5, and 5.0 µg L^{-1}. Good linearities were obtained for both

USC UNIVERSIDADE DE SANTIAGO DE COMPOSTELA

calibration graphs (R^2 values 0.993 and 0.999, respectively). The slopes of the aqueous calibration and the matrix-matched calibration resulted in 2.01 L μg^{-1} and 1.94 L μg^{-1}, respectively. Both slopes were statistically similar (t-test, 95% confidence level), and then the matrix effect can be assumed as negligible. Therefore, the aqueous ionic silver calibration can be used in the analysis of AgNPs in enzymatic extracts from seaweed by SP-ICP-MS.

1.4.4.2 Sensitivity

The limit of detection and quantification were calculated using the 3×SD/slope and 10×SD/slope criterion (SD: standard deviation of ten measurements of a blank) and considering the treatment of the sample. For total Ag determination by ICP-MS in the digested seaweed samples, the isotope ^{107}Ag was selected due to its higher relative abundance and the lower limit of detection (LOD=2.2 ng g^{-1}) and quantification (LOQ=7.7 ng g^{-1}) achieved. Limits of detection in size (LOD_{size}) and particle concentration (LOD_{number}) for the analysis by SP-ICP-MS were calculated using the Laborda et al. [30] Microsoft Excel tool. The 5-sigma threshold is used to avoid the occurrence of false positives. Thus, the LOD_{size} was calculated using **Equation 1.1.**, where σ_B is the standard deviation of the mean baseline signal, w is the peak width at microsecond times, ρ and F_p are the density of the particle analyte (10.49 g cm^{-3} for AgNPs), and the mass fraction of the particle, respectively, and t_{dwell} is the dwell time for the analyte (μs). K_{ICPMS} is the detection efficiency, or the number of ions detected relative to the number of analyte atoms introduced into the ICP-MS, and ($K_M = AN_{av}/M_M$) is a factor dependent on the element measured (A, N_{AV}, and M_M are the atomic abundance of the selected isotope, the Avogadro's number, and the atomic mass of the selected element, respectively).

$$LOD_{size} = X_D^{size} = \left(\frac{30\ \sigma_B}{\frac{2}{w}\ \pi\ \rho\ F_p\ K_{ICPMS}\ K_M\ t_{dwell}} \right)^{1/3} \quad (\textbf{Equation 1.1.})$$

The LOD_{number} was calculated using **Equation 1.2.**, where $Y_{N,B}$, η_{neb}, Q_{sam}, and t_i are the mean number of particles counted in a blank, the nebulization efficiency of the ICP-MS, the flow rate introduction of the sample solution through the peristaltic pump, and the total acquisition time, respectively.

$$LOD_{number} = X_D^{number} = \frac{\sqrt[5]{Y_{N,B}} + 3}{\eta_{neb}\ Q_{sam}\ t_i} \quad (\textbf{Equation 1.2.})$$

The SP-ICP-MS limits of detection were calculated using a blank submitted to the whole extraction procedure and diluted 100 times in 1% (v/v) glycerol: LOD_{size}= 14 nm (5 sigma criteria; 12 nm using the less restrictive 3 sigma criteria), and LOD_{number}= 2.40×10^6 part L^{-1} (instrumental limit) or 4.34×10^7 part g^{-1} (referred to the wet seaweed sample). Bao et al. [23] characterized AgNPs in plant tissues using a Macerozyme enzymatic extraction by SP-ICP-MS and they obtained a similar LOD_{size} (10 nm), but they did not provide concentration detection limit results. In fact, to the best of our knowledge, there are no reports about ultrasound-assisted enzymatic methods to determine AgNPs from seaweed using SP-ICP-MS.

1.4.4.3 Repeatability and analytical recovery

The repeatability assay of the ultrasound-assisted enzymatic isolation method was estimated using both types of seaweed samples. A *Palmaria palmata* sample and an *Ulva* sp.

sample, both exposed to 1.0 mg L^{-1} of AgNPs, were submitted to the optimized enzymatic extraction method in quintuplicate. For five measured replicates of each specimen of seaweed, the most frequent sizes, the mean sizes, and the AgNPs concentration were obtained. The relative standard deviations are shown in **Table 1.2.** The RSD for the most frequent sizes and the mean sizes were lower than 10% in both kinds of seaweed, which confirms the good repeatability of the method. However, for the AgNPs concentration in *Palmaria palmata* and *Ulva sp.*, the RSD were 15 and 18%, respectively. These RSD values were considered adequate considering the complexity of the matrix and the overall enzymatic extraction process.

Table 1.2. Precision of the method for AgNPs determination by SP-ICP-MS. RSD (%) are included in brackets.

	Palmaria palmata	*Ulva* sp.
Most frequent size (nm)	26±1 (4%)	26±1 (4%)
Mean size (nm)	30±2 (5%)	33±3 nm (8%)
NPs concentration (part g^{-1})	$1.56\times10^{9}\pm2.45\times10^{8}$ (15%)	$2.82\times10^{8}\pm5.04\times10^{7}$ (18%)

The accuracy of the extraction method was also guaranteed with the analytical recovery assay. An SP-ICP-MS analysis was performed in triplicate using a *Palmaria palmata* sample submitted to the Macerozyme enzymatic extraction and spiked with 15 nm PVP-AgNPs with a final concentration of 6.0×10^{7} part mL^{-1}. The un-spiked Macerozyme enzymatic extract and the 15 nm PVP-AgNPs suspension of 6.0×10^{7} part mL^{-1} used for the spiking experiments were also analyzed in triplicate by SP-ICP-MS. The analytical recovery was calculated using **Equation 1.3.**, where $[Ag]_{spiked}$ is the PVP-AgNPs concentration (part mL^{-1}) in the seaweed Macerozyme enzymatic spiked extract, $[Ag]_{un\text{-}spiked}$ is PVP-AgNPs concentration (part mL^{-1}) in the seaweed Macerozyme enzymatic extract, and $[Ag]_{suspension}$ is the PVP-AgNPs concentration (part mL^{-1}) of the standard used for spiking the extract.

$$AR = \frac{[Ag]_{spiked} - [Ag]_{un-spiked}}{[Ag]_{suspension}} \times 100 \quad (\textbf{Equation 1.3.})$$

The average analytical recovery obtained by SP-ICP-MS for this experiment was close to 100% (112±12%, expressed as mean±SD), and was considered adequate.

1.4.5 Applications

The optimized and validated proposed methodology was applied to ten *Palmaria palmata* and *Ulva* sp. seaweed samples from the Atlantic area, some of them exposed to Ag NPs (sample numbers 1, 2, and 3). The samples were subjected to microwave acid digestion and the enzymatic extraction methods described in **sections 1.3.4** and **1.3.5** and then, analyzed by ICP-MS and SP-ICP-MS.

Table 1.3. shows the total concentration of Ag in the samples, the concentration of AgNPs, the mean size and the most frequent size. The total basal silver in unexposed seaweed (*Palmaria palmata* 4 and 5 and *Ulva* sp. 4 and 5) varies between 0.011±0.002 and 0.021±0.002 μg g^{-1} for *Palmaria palmata,* and between 0.010±0.001 and 0.017±0.001 μg g^{-1} for *Ulva* sp. This low basal concentration does not allow the detection of AgNPs by SP-ICP-MS. Although total Ag

USC DE COMPOSTELA

concentration in unexposed seaweed was in the same magnitude order for *Palmaria palmata* and *Ulva* sp., total Ag concentrations in exposed *Palmaria palmata* were higher (between 0.34±0.05 and 0.72±0.09 μg g^{-1}) than for exposed *Ulva* sp. (between 0.17±0.03 and 0.20±0.03 μg g^{-1}). In the same way, the AgNPs concentration was higher for exposed *Palmaria palmata* (between $8.03\times10^{8}\pm5.00\times10^{7}$ and $1.36\times10^{9}\pm1.74\times10^{8}$ AgNP g^{-1}) than for exposed *Ulva* sp. (between $6.96\times10^{8}\pm1.20\times10^{7}$ and $8.12\times10^{8}\pm7.25\times10^{7}$ AgNP g^{-1}). The most frequent sizes were very similar in both kinds of exposed seaweed, between 20±1-22±3 nm, and 20±1-22±2 nm for *Palmaria palmata* and *Ulva* sp., respectively. Similarly, mean sizes were also similar, within the 24±2-29±1 nm and 28±1-32±4 nm ranges for *Palmaria palmata* and *Ulva* sp., respectively. **Figure 1.5.** shows the histograms corresponding to *Palmaria palmata* sample 1 (**Figure 1.5(a))** and *Ulva* sp. sample 1 (**Figure 1.5.(b))**.

Table 1.3. Total Ag and AgNPs concentration and mean size (n=3) in some seaweed samples.

	[Ag]/μg g^{-1}	[AgNPs]/ part g^{-1}	Mean size/ nm	Most frequent size/ nm
Palmaria palmata 1[b]	0.34±0.05	$8.38\times10^{8}\pm7.27\times10^{7}$	29±1	22±3
Palmaria palmata 2[b]	0.72±0.09	$1.36\times10^{9}\pm1.74\times10^{8}$	26±1	22±2
Palmaria palmata 3[b]	0.51±0.06	$8.03\times10^{8}\pm5.00\times10^{7}$	24±2	20±1
Palmaria palmata 4	0.021±0.002	$<4.34\times10^{7}$	-[a]	-[a]
Palmaria palmata 5	0.011±0.002	$<4.34\times10^{7}$	-[a]	-[a]
Ulva sp. 1[b]	0.20±0.03	$6.96\times10^{8}\pm1.20\times10^{8}$	28±3	21±3
Ulva sp. 2[b]	0.20±0.03	$8.12\times10^{8}\pm7.25\times10^{7}$	32±4	22±2
Ulva sp. 3[b]	0.17±0.02	$7.44\times10^{8}\pm1.20\times10^{8}$	28±1	20±1
Ulva sp. 4	0.017±0.001	$<4.34\times10^{7}$	-[a]	-[a]
Ulva sp. 5	0.010±0.001	$<4.34\times10^{7}$	-[a]	-[a]

(a)Not evaluated (b) Seaweed exposed to 1.0 mg L^{-1} PVP-AgNPs

USC UNIVERSIDADE DE SANTIAGO DE COMPOSTELA

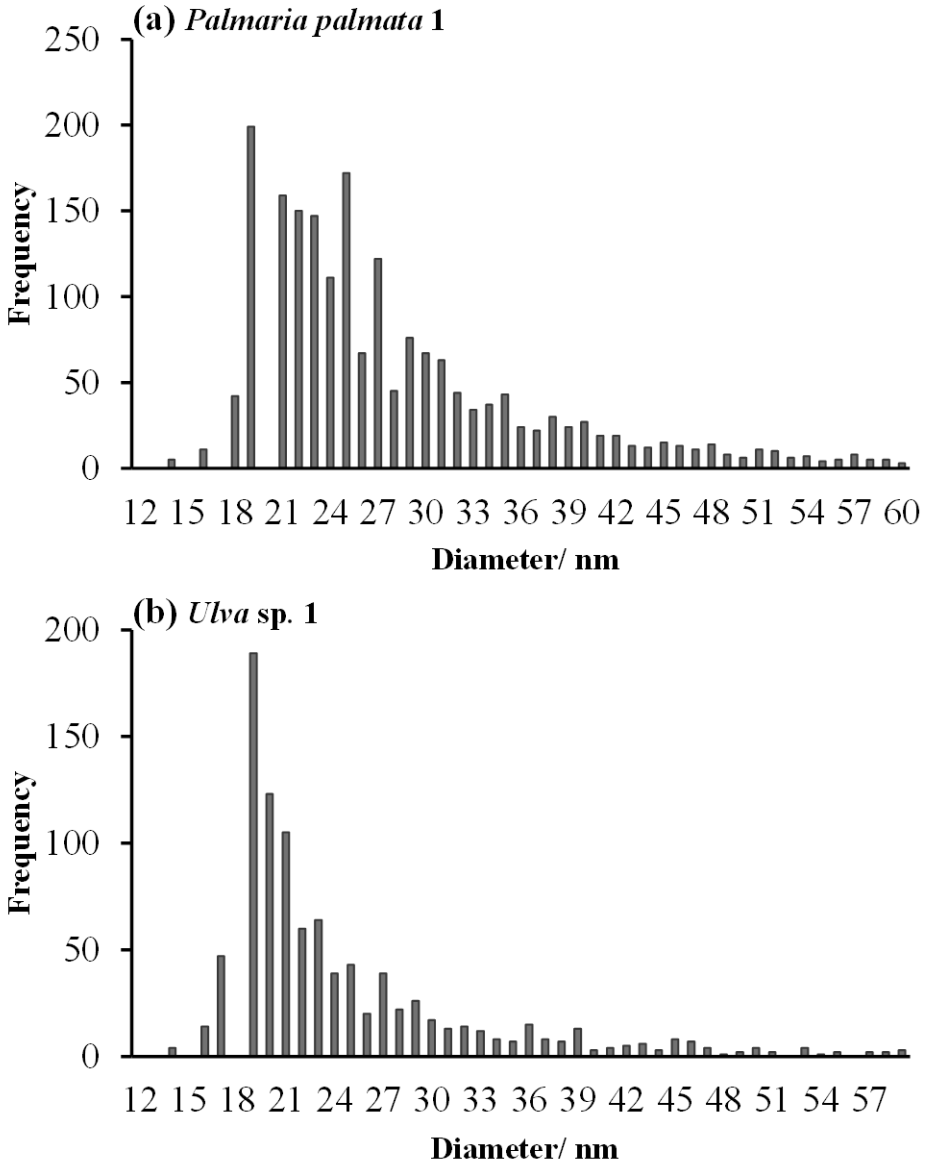

Figure 1.5. AgNPs size distribution in (a) *Palmaria palmata* (b) *Ulva* sp.

Using the procedure described in **section 1.3.8**, a Macerozyme® enzymatic extract from *Palmaria Palmata* was cleaned, pre-concentrated and deposited on a Ti grid to visualize AgNPs using STEM. **Figure 1.6.** shows the STEM images obtained working in TEM mode (**Figure 1.6.(a)**) and STEM mode (**Figure 1.6.(b)**, and **Figure 1.6. (c)**). These images confirm the presence of spherical AgNPs in the enzymatic extracts.

USC UNIVERSIDADE DE SANTIAGO DE COMPOSTELA

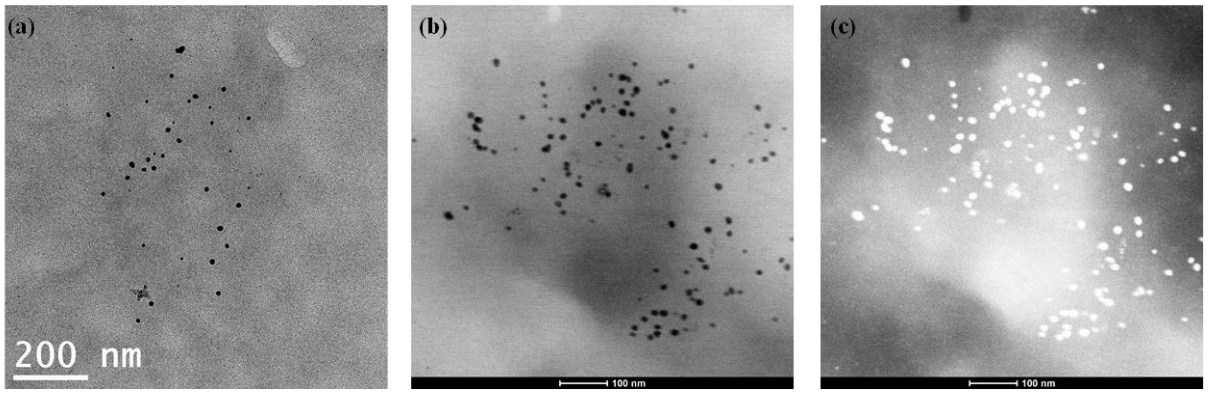

Figure 1.6. Images of AgNPs in the enzymatic extracts obtained operating in mode (a) TEM, (b) STEM bright field, and (c) STEM high angle annular dark field.

The histogram in **Figure 1.7.** shows the polydispersity sizes of 200 particles measured with Rasband, W.S., ImageJ, U. S. National Institutes of Health, Bethesda, Maryland, USA software. The mean size measured in TEM was 24 nm; this value agrees with the mean size obtained for *Palmaria palmata* by SP-ICP-MS (between 24±2 and 29±1 nm). The mean sizes observed in SP-ICP-MS and TEM were higher than the original 15 nm nanoparticles used for exposure. That could indicate that seaweed can aggregate the AgNPs inside of the organism to decrease toxicity that seems to be size-dependent [31]. This result is very similar to that obtained by Bao et al. [23] that exposed *Arabidopsis* plant cells to 10 nm silver nanoparticles and after SP-ICP-MS analysis observed average diameters of 26-27 nm. Similarly, Li et al. [29] reported an increase from 17-18 nm to 36-48.9 nm in leaves of soybean and rice plants, after foliar or root exposure. More studies about bioaccumulation are planned to be carried out in the future in our research group to deepen our knowledge about seaweed metabolism and detoxification mechanisms.

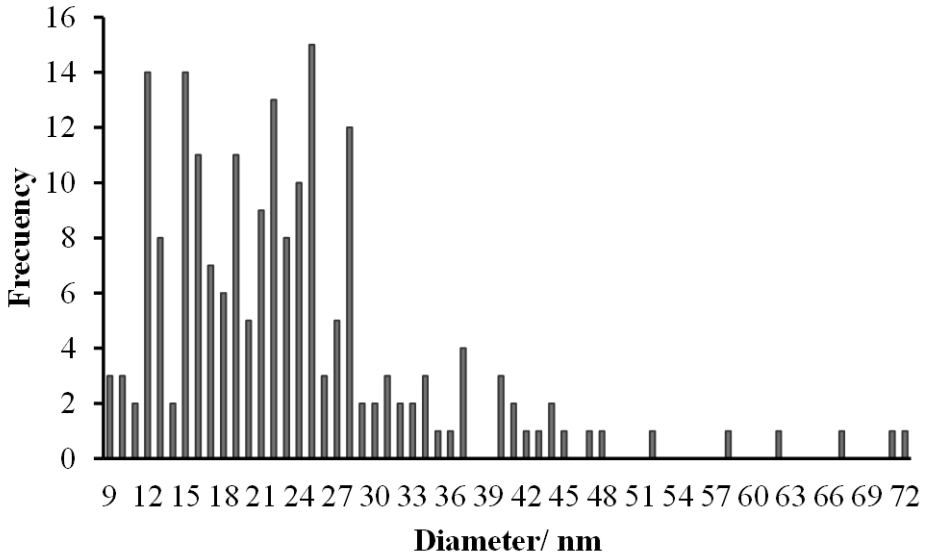

Figure 1.7. AgNPs size distribution histogram in *Palmaria palmata* (data from TEM images, n=200 nanoparticles).

USC UNIVERSIDADE DE SANTIAGO DE COMPOSTELA

1.5 CONCLUSIONS

There is a certain concern about the accumulation of nanomaterials by biota in the aquatic media. In this work, an ultrasound-assisted enzymatic extraction method was developed to analyze AgNPs by SP-ICP-MS. The extraction conditions (affecting sonication and enzymatic hydrolysis with the Macerozyme® R-10 enzyme complex) were optimized. The analytical performance was evaluated with good repeatability, sensitivity, and analytical recovery for SP-ICP-MS measurements. Then the optimized method was applied to the detection of AgNPs in red and green seaweed samples without significantly size-changing distribution of AgNPs, as it was confirmed by TEM.

USC
UNIVERSIDADE DE SANTIAGO DE COMPOSTELA

REFERENCES

[1] I. Moreno-Garrido, S. Pérez, J. Blasco, Toxicity of silver and gold nanoparticles on marine microalgae, Mar. Environ. Res. 111 (2015) 60–73. https://doi.org/10.1016/j.marenvres.2015.05.008.
[2] European Union. Commission Recommendation (EU) 2011/696 of 18 October 2011 on the definition of nanomaterial, Off. J. Eur. Union 24 (2010) 6–6. http://data.europa.eu/eli/reco/2011/696/oj.
[3] X. F. Zhang, Z. G. Liu, W. Shen, S. Gurunathan, Silver nanoparticles: Synthesis, characterization, properties, applications, and therapeutic approaches, Int. J. Mol. Sci. 17 (2016) 1534. https://doi.org/10.3390/ijms17091534.
[4] A. A. Sfriso, M. Mistri, C. Munari, I. Moro, M. Wahsha, A. Sfriso, A. Juhmani, Hazardous effects of silver nanoparticles for primary producers in transitional water systems: The case of the seaweed *Ulva rigida* C. Agardh, Environ. Int. 131 (2019) 104942. https://doi.org/10.1016/j.envint.2019.104942.
[5] S. Habouti, C. H. Solterbeck, M. Es-Souni, Synthesis of silver nano-fir-twigs and application to single molecules detection, J. Mater. Chem. 20 (2010) 5215–5219. https://doi.org/10.1039/C0JM00564A.
[6] X. Hu, C. T. Chan, Photonic crystals with silver nanowires as a near-infrared superlens, Appl. Phys. Lett. 85 (2004) 1520–1522. https://doi.org/10.1063/1.1784883.
[7] K. M. M. Abou El-Nour, A. Eftaiha, A. Al-Warthan, R. A. A. Ammar, Synthesis and applications of silver nanoparticles, Arab. J. Chem. 3 (2010) 135–140. https://doi.org/10.1016/j.arabjc.2010.04.008.
[8] E. McGillicuddy, I. Murray, S. Kavanagh, L. Morrison, A. Fogarty, M. Cormican, P. Dockery, M. Prendergast, N. Rowan, D. Morris, Silver nanoparticles in the environment: Sources, detection and ecotoxicology, Sci. Total Environ. 575 (2017) 231–246. https://doi.org/10.1016/j.scitotenv.2016.10.041.
[9] M. Sá Monteiro, J. Sloth, S. Holdt, M. Hansen, Analysis and Risk Assessment of Seaweed, EFSA J. 17 (2019) e170915. https://doi.org/10.2903/j.efsa.2019.e170915.
[10] H. Luo, Q. Wang, Z. Liu, S. Wang, A. Long, Y. Yang, Potential bioremediation effects of seaweed *Gracilaria lemaneiformis* on heavy metals in coastal sediment from a typical mariculture zone, Chemosphere 245 (2020) 125636. https://doi.org/10.1016/j.chemosphere.2019.125636.
[11] X. Sun, Z. Liu, Q. Jiang, Y. Yang, Concentrations of various elements in seaweed and seawater from Shen'ao Bay, Nan'ao Island, Guangdong coast, China: Environmental monitoring and the bioremediation potential of the seaweed, Sci. Total Environ. 659 (2019) 632–639. https://doi.org/10.1016/j.scitotenv.2018.12.364.
[12] F. Deniz, E. T. Ersanli, An ecofriendly approach for bioremediation of contaminated water environment: Potential contribution of a coastal seaweed community to environmental improvement, Int. J. Phytoremediation 20 (2018) 256–263. https://doi.org/10.1080/15226514.2017.1374335.
[13] P. Malea, A. Chatziapostolou, T. Kevrekidis, Trace element seasonality in marine macroalgae of different functional-form groups, Mar. Environ. Res. 103 (2015) 18–26.
[14] European Union. Commission Recommendation (EU) 2018/464 of 19 March 2018 on the monitoring of metals and iodine in seaweed, halophytes and products based on seaweed, Off. J. Eur. Union 78 (2018) 16–18. http://dx.doi.org/10.1016/j.marenvres.2014.11.004.
[15] K. Loeschner, M. S. J. Brabrand, J. J. Sloth, E. H. Larsen, Use of alkaline or enzymatic sample pretreatment prior to characterization of gold nanoparticles in animal tissue by single-

particle ICPMS, Anal. Bioanal. Chem. 406 (2014) 3845–3851. https://doi.org/10.1007/s00216-013-7431-y.
[16] E. P. Gray, J. G. Coleman, A. J. Bednar, A. J. Kennedy, J. F. Ranville, C. P. Higgins, Extraction and analysis of silver and gold nanoparticles from biological tissues using single particle inductively coupled plasma mass spectrometry, Environ. Sci. Technol. 47 (2013) 14315–14323. https://doi.org/10.1021/es403558c.
[17] R. J. B. Peters, Z. H. Rivera, G. Bemmel, H. J. P. Marvin, S. Weigel, H. Bouwmeester, Development and validation of single particle ICP-MS for sizing and quantitative determination of nano-silver in chicken meat, Anal. Bioanal. Chem. 406 (2014) 3875–3885. https://doi.org/10.1007/s00216-013-7571-0.
[18] Y. Dan, X. Ma, W. Zhang, K. Liu, C. Stephan, H. Shi, Single particle ICP-MS method development for the determination of plant uptake and accumulation of CeO_2 nanoparticles, Anal. Bioanal. Chem. 408 (2016) 5157–5167. https://doi.org/10.1007/s00216-016-9565-1.
[19] Y. Dan, W. Zhang, R. Xue, X. Ma, C. Stephan, H. Shi, Characterization of gold nanoparticle uptake by tomato plants using enzymatic extraction followed by single-particle inductively coupled plasma-mass spectrometry analysis, Environ. Sci. Technol. 49 (2015) 3007–3014. https://doi.org/10.1021/es506179e.
[20] J. Jiménez-Lamana, J. Wojcieszek, M. Jakubiak, M. Asztemborska, J. Szpunar, Single particle ICP-MS characterization of platinum nanoparticles uptake and bioaccumulation by: *Lepidium sativum* and *Sinapis alba* plants, J. Anal. At. Spectrom. 31 (2016) 2321–2329. https://doi.org/10.1039/C6JA00201C.
[21] K. Kińska, J. Jiménez-Lamana, J. Kowalska, B. Krasnodębska-Ostręga, J. Szpunar, Study of the uptake and bioaccumulation of palladium nanoparticles by *Sinapis alba* using single particle ICP-MS, Sci. Total Environ. 615 (2018) 1078–1085. https://doi.org/10.1016/j.scitotenv.2017.09.203.
[22] J. Wojcieszek, J. Jiménez-Lamana, K. Bierla, L. Ruizk, M. Asztemborska, M. Jarosz, J. Szpunar, Uptake, translocation, size characterization and localization of cerium oxide nanoparticles in radish (*Raphanus sativus* L.), Sci. Total Environ. 683 (2019) 284–292. https://doi.org/10.1016/j.scitotenv.2019.05.265.
[23] D. Bao, Z. G. Oh, Z. Chen, Characterization of silver nanoparticles internalized by *Arabidopsis* plants using single particle ICP-MS Analysis, Front. Plant Sci. 7 (2016) 1–8. https://doi.org/10.3389/fpls.2016.00032.
[24] J. Nath, I. Dror, P. Landa, T. Vanek, I. Kaplan-Ashiri, B. Berkowitz, Synthesis and characterization of isotopically-labeled silver, copper and zinc oxide nanoparticles for tracing studies in plants, Environ. Pollut. 242 (2018) 1827–1837. https://doi.org/10.1016/j.envpol.2018.07.084.
[25] Y. Sun, Y. Yang, F. Y. Tou, Z. S. Niu, X. P. Guo, C. Liu, J. Yan, J. Y Wu, M. Xu, L. J. Hou, M. Liu, Extraction and quantification of metal-containing nanoparticles in marine shellfish based on single particle inductively coupled plasma-mass spectrometry technique, J. Hazard. Mater. 424 (2022) 127383. https://doi.org/10.1016/j.jhazmat.2021.127383.
[26] M. V. Taboada-López, S. Iglesias-López, P. Herbello-Hermelo, P. Bermejo-Barrera, A. Moreda-Piñeiro, Ultrasound assisted enzymatic hydrolysis for isolating titanium dioxide nanoparticles from bivalve mollusk before sp-ICP-MS, Anal. Chim. Acta 1018 (2018) 16–25. https://doi.org/10.1016/j.aca.2018.02.075.
[27] M. V. Taboada-López, P. Herbello-Hermelo, R. Domínguez-González, P. Bermejo-Barrera, A. Moreda-Piñeiro, Enzymatic hydrolysis as a sample pre-treatment for titanium dioxide nanoparticles assessment in surimi (crab sticks) by single particle ICP-MS, Talanta 195 (2019) 23–32. https://doi.org/10.1016/j.talanta.2018.11.023.

USC
DE COMPOSTELA

[28] W. J. Wei, L. Li, Y. P. Gao, Q. Wang, Y. Y. Zhou, X. Liu, Y. Yang, Enzyme digestion combined with SP-ICP-MS analysis to characterize the bioaccumulation of gold nanoparticles by mustard and lettuce plants, Sci. Total Environ. 777 (2021) 146038. https://doi.org/10.1016/j.scitotenv.2021.146038.
[29] C. C. Li, F. Dang, M. Li, M. Zhu, H. Zhong, H. Hintelmann, D. M. Zhou, Effects of exposure pathways on the accumulation and phytotoxicity of silver nanoparticles in soybean and rice, Nanotoxicology 11 (2017) 699–709. http://dx.doi.org/10.1080/17435390.2017.1344740.
[30] F. Laborda, A. C. Gimenez-Ingalaturre, E. Bolea, J. R. Castillo, About detectability and limits of detection in single particle inductively coupled plasma mass spectrometry, Spectrochim. Acta-Part B At. Spectrosc. 169 (2020) 105883. https://doi.org/10.1016/j.sab.2020.105883.
[31] M. Akter, M. T. Sikder, M. M. Rahman, A. K. M. A. Ullah, K. F. B. Hossain, S. Banik, T. Hosokawa, T. Saito, M. Kurasaki, A systematic review on silver nanoparticles-induced cytotoxicity: Physicochemical properties and perspectives, J. Adv. Res. 9 (2018) 1–16. https://doi.org/10.1016/j.jare.2017.10.008

USC UNIVERSIDADE DE SANTIAGO DE COMPOSTELA

CHAPTER 2. TITANIUM DIOXIDE NANOPARTICLES ASSESSMENT IN SEAWEEDS BY SINGLE PARTICLE INDUCTIVELY COUPLED PLASMA MASS SPECTROMETRY

USC
UNIVERSIDADE DE SANTIAGO DE COMPOSTELA

USC
UNIVERSIDADE
DE SANTIAGO
DE COMPOSTELA

CHAPTER 2. TITANIUM DIOXIDE NANOPARTICLES ASSESSMENT IN SEAWEEDS BY SINGLE PARTICLE INDUCTIVELY COUPLED PLASMA MASS SPECTROMETRY*

*The results from this chapter have already been published as Juan José López-Mayán[a], Sergio del-Ángel-Monroy[a,b], Elena Peña-Vázquez[a], María Carmen Barciela-Alonso[a], Pilar Bermejo-Barrera[a], Antonio Moreda-Piñeiro[a], Titanium dioxide nanoparticles assessment in seaweeds by single particle inductively coupled plasma mass spectrometry, Talanta 236 (2022) 122856. https://doi.org/10.1016/j.talanta.2021.122856.

[a] Trace Element, Spectroscopy and Speciation Group (GETEE), Strategic Grouping in Materials (AEMAT), Department of Analytical Chemistry, Nutrition and Bromatology, Faculty of Chemistry, Universidade de Santiago de Compostela, Avenida das Ciencias, s/n, 15782, Santiago de Compostela, Spain.

[b] Facultad de Estudios Superiores Zaragoza, Universidad Nacional de México, Av. Guelatao 66, Ejército de Oriente, Iztapalapa, 09230, Ciudad de México, México.

2.1 ABSTRACT

In this study, a first attempt for isolating and determining (characterising) background levels of titanium dioxide nanoparticles (TiO_2NPs) in seaweed has been developed by using single particle inductively coupled plasma mass spectrometry (SP-ICP-MS). Seaweeds were processed using an optimized ultrasound-assisted extraction (UAE) procedure based on tetramethylammonium hydroxide (TMAH) before dilution and SP-ICP-MS analysis. The effect of the TMAH percentage in the extracting solution, as well as the volume of extracting solution and sonication (extraction) time, has been fully assessed. Additional experiments also showed that TiO_2NPs were quantitatively released from the seaweed matrix in one UAE step since the analysis of residues gave TiO_2NPs concentrations lower than the limit of quantification (LOQ) of the method. Validation of the method with 50 and 100 nm TiO_2NPs (10 μg L^{-1} as Ti) showed good analytical recovery (115% and 112% for 50 and 100 nm TiO_2NPs, respectively), and good reproducibility (2% for size and 16% for number of TiO_2NPs). Experiments regarding TiO_2NPs stability showed that the extracted NPs are stable since there were no changes in the number of TiO_2NPs and TiO_2NPs size distributions when exposing TiO_2NPs standards to the optimized extractive conditions.

2.2 INTRODUCTION

Titanium dioxide (TiO_2) is known as titania, titanium white or pigment white 6 in building paints, and E171 as a food additive. Compared to bulk TiO_2, TiO_2 nanoparticles (TiO_2NPs) present higher light scattering and opacity and they also have higher photoactivity due to the increase of their surface area to volume ratio. Therefore, TiO_2NPs are commonly used in photovoltaics and photocatalysis. In addition to several medical applications [1], TiO_2NPs can be used as UV-blockers due to their high refractive index, UV light absorption and discoloration resistance, and they have been approved as inorganic filters for sunscreen formulas [2,3]. As a food additive, E171 has been demonstrated to contain variable fractions, up to 36 %, of TiO_2 within the nanometric scale [4], and, although authorized for use in the food industry during the

USC UNIVERSIDADE DE SANTIAGO DE COMPOSTELA

last decades, it has been no longer considered safe in foodstuff by the European Union food regulators [5].

Due to the increased production and extensive use of TiO_2NPs and other nanomaterials (NMs), these species are released into the environment where they may interact with biotic and abiotic components of ecosystems, and are therefore considered as emerging contaminants [6]. The presence of NMs in the environment may cause deleterious effects in the ecosystems and they may undergo bioaccumulation, bio-magnification or biotransformation in biota [7]. Despite the several studies regarding NPs bioaccumulation, as well as biochemical and behavioural responses, in marine biota under controlled exposure to NPs, there are not many reports focused on background levels of NPs in marine biota and processed food from marine origin. Some data have been recently published regarding AgNPs and TiO_2NPs [8-10] and NPs derived from rare earth elements (Y, La, Ce, Pr, Gd) [11] in mollusks, and AgNPs and TiO_2NPs in processed seafood such as surimi (crab sticks) [12,13] and canned fish and mollusks [14,15].

Similar to other marine organisms, seaweeds have the ability to bio-concentrating dissolved pollutants from seawater. The electrostatic and complexing properties of the several anionic polysaccharides present in seaweed cell walls [16] are responsible for the retention of pollutants and the further bio-accumulation in the different seaweed tissues. However, there are not data regarding the presence of metallic NPs in seaweeds as well as the mechanisms involved in the NPs incorporation.

Inorganic NPs released from complex solid materials can be mainly achieved by using enzymatic hydrolysis procedures and also by alkaline digestion (extraction) with tetramethylammonium hydroxide (TMAH) [17-19]. Successful NPs extractions with concentrated and diluted TMAH solutions are reached since this reagent is a biological tissue solubiliser. Concentrated TMAH solutions (20 and 25%(v/v)) have been used for isolating NPs derived from rare earth elements [11], AgNPs and TiO_2NPs from canned seafood [14,15], AgNPs and AuNPs from beef and other animal tissues [20], AgNPs from rat tissues, fish tissues, cell lines of human origin, soils, and wound dressing [21-25], and TiO_2NPs from sludge [26]. However, the high ionic strength of TMAH solutions promotes NPs agglomeration and concentrated TMAH must be avoided [17,18]. Diluted TMAH solutions have been therefore used for AuNPs extraction from rat tissues [27,28] and human tissues and cells [29-31], AgNPs from human tissues [31], and TiO_2NPs from surimi [13]. Minimization of NPs agglomeration since the high ionic strength of TMAH solutions can be achieved by using bovine serum albumin (BSA) [27,28,30], Triton X-100 [14,15,23], or diluted calcium chloride solutions [22]. NPs extraction with TMAH can be performed by mechanical shaking [21-29], by assisting with ultrasounds for speeding up the process [13-15,20,24,25,27,28,31], or by allowing the alkaline digestion to progress overnight [26,30]. Bio-fluids, such as urine, blood, and serum, have been also treated with TMAH alone or combined with Triton X-100 to solubilise sample matrix components and to stabilise the extracted NPs (Ag and AuNPs [32], and PtNPs [33]).

The aim of the current research has been the optimization of a fast and reliable procedure for isolating and determining (characterizing) TiO_2NPs from seaweeds. Operating conditions of ultrasound-assisted extraction (UAE) with TMAH have been investigated, and fastness and sensitivity of single particle inductively coupled plasma mass spectrometry (SP-ICP-MS) have been used for assessing the number of TiO_2NPs as well as TiO_2NPs size distributions.

USC UNIVERSIDADE DE SANTIAGO DE COMPOSTELA

2.3 MATERIALS AND METHODS

2.3.1 Instrumentation

A NexION® 2000 ICP-MS (Perkin Elmer, Waltham, MA, USA) with dynamic reaction cell (DRC) technology was used for measurements. The instrument is equipped with Ni sampler/skimmer/hyper skimmer cones, a concentric Meinhard nebulizer and cyclonic spray chamber (Glass Expansion, Inc., Melbourne, Australia), a Single Cell Micro DX autosampler (Perkin Elmer), and the Syngistix™ Nano Application 2.5 software (Perkin Elmer). A USC 300 TH ultrasound water bath (ultrasound frequency of 45 kHz, 80 W) from VWR (Radnor, PA, USA) was used for assisting TiO_2NPs extraction. An Ethos Plus microwave oven (Milestone, Sorisole, Italy) equipped with 100 mL Teflon vessels and covers was used for acid digestion of samples. A JEM-F200CF-HR high-resolution transmission electron microscope with energy-dispersive X-ray spectroscopy (EDX) from JEOL (Tokyo, Japan) was used for comparative purposes (HRTEM-EDX images). A Laborcentrifugen 2K15 centrifuge (Sigma, Osterode, Germany) was used for pre-treating the TMAH extracts before TEM analysis. Other pieces of equipment were a vortex Reax Top (Heidolph, Schwabach, Germany), and a domestic Taurus blade grinder (Taurus, Barcelona, Spain).

2.3.2 Reagents

All solutions were prepared with ultrapure water (18 MΩ cm of resistivity) obtained from a Milli-Q IQ7003 purification device (Millipore Co., Bedford, MA, USA). Ionic Ti [$(NH_4)_2TiF_6$ 1000 mg L^{-1}], used for ICP-MS and SP-ICP-MS calibration, was from Merck (Darmstadt, Germany). TiO_2 nanoparticle stock solutions were prepared from TiO_2 nanopowder (rutile, 99.9%) of 50 and 100 nm aerodynamic particle size (APS) purchased from US Research Nanomaterials (Houston, TX, USA). A standard of AuNPs of 50 nm (49.6 nm by TEM, 12.4 ng mL^{-1}, 9.89×10^6 NPs mL^{-1}, in aqueous 1 mM citrate) from nanoComposix (San Diego, CA, USA) was used for assessing transport efficiency in SP-ICP-MS determinations. NexION Setup Solution (Be, Ce, Fe, In, Li, Mg, Pb, U), 10 µg L^{-1} (Perkin Elmer) was used for daily checking ICP-MS performance. TMAH (25 % (v/v) in water) and glycerol were from Merck; whereas, 33% (w/v) hydrogen peroxide and 69% (w/v) hyperpure nitric acid were from Panreac (Barcelona, Spain). Argon (99.999%) and ammonia (99,999%) were from Nippon Gases (Madrid, Spain). Minisart NML hydrophilic non-sterile 5.0 µm filters were from Sartorius (Goettingen, Germany), and regenerated cellulose Amicon Ultra-0.5 centrifugal filter units (30 kDa nominal molecular weight limit, NMWL) were from Merck.

Glassware and plastic ware were decontaminated by soaking in 10% (v/v) nitric acid for at least 48 h. The material was then rinsed with ultrapure water several times.

2.3.3 Seaweed samples

Samples consist of two sea lettuce (*Ulva rigida*) and two sargassum (*Sargassum bacciferum*) from the Galician coast (North-western Spain), three sea lettuce (*Ulva* sp.) and eight dulse (*Palmaria Palmata*) from the Irish coast.

Seaweeds were rinsed with tap water and ultrapure water for salt removal before homogenization by mechanical blending (approximately 100 g of fresh seaweed). The ground/homogenised samples were stored in 50 mL plastic tubes at -18 ºC until use.

2.3.4. Ultrasound-assisted TiO_2NPs lixiviation with TMAH

Approximately 1.0000 g of seaweed (in triplicate) was weighed into 10 mL plastic tubes and 7.5 mL of a 2.5% (v/v) TMAH solution was added. The tubes were placed in the ultrasound

USC DE COMPOSTELA

bath (45 kHz, 80W) for assisted extraction for 2.0 h. After that time, the extract was separated from the solid residue by filtration (5.0 µm filters) and the extract was made up to 10 mL with 2.5% (v/v) TMAH before SP-ICP-MS analysis. Two blanks were processed for each set of operating conditions and/or sample analysis.

2.3.5 Microwave-assisted acid digestion for total Ti determination

Microwave-assisted acid digestion was based on the procedure developed by García-Sartal et al. [34] with some modifications. Therefore, portions of 1.0000 g of each sample were directly weighed into the Teflon vessels, and 4 mL of ultrapure water, 3 mL of 69% (w/v) nitric acid and 1 mL of 33% (w/v) hydrogen peroxide were then added. The vessels were closed and subjected to a four stages microwave program (**Table 2.1.**). The acid digests were then made up to 25 mL with ultrapure water and stored in plastic tubes at room temperature. Each sample was submitted to the microwave-assisted acid digestion procedure in triplicate, and two blanks were prepared for each set of experiments.

Table 2.1. Microwave-assisted acid digestion program.

Step	Time (min)	Temperature (ºC)	Power (W)
1	4	Room temperature-90	800
2	5	90-140	800
3	5	140-200	800
4	20	200	800

2.3.6 Total Ti assessment by ICP-MS

The determination of total Ti from the acid digests (1:10 dilution) was performed by ICP-MS (operating conditions listed in **Table 2.2.(a)**). Dynamic reaction cell (DRC) mode with ammonia as a reaction gas (flow rate of 1.0 mL min^{-1}) was used for minimising polyatomic interferences when assessing Ti (mass shift approach by monitoring the $TiNH(NH_3)_4$ adduct at a m/z of 131). Aqueous calibrations (Ti concentrations of 0, 0.5, 1.0, 2.0, 6.0, and 12 µg L^{-1}) were used for quantification purposes. The limit of detection (LOD) and the limit of quantification (LOQ) calculated based on the 3 SD / 10 SD criterion were 1.4 and 4.8 ng g^{-1}, respectively. Within-bath precision (n=7) expressed as relative standard deviation (RSD, %) was 4, 3 and 3% for Ti concentration levels of 0.5, 2.0 and 10.0 µg L^{-1}, respectively. Analytical recovery (expressed as the mean value plus/minus the standard deviation for 7 measurements) was 109±9, 105±7, and 92±3 % for Ti concentration levels of 0.5, 2.0 and 10.0 µg L^{-1}, respectively.

USC UNIVERSIDADE DE SANTIAGO DE COMPOSTELA

Table 2.2. ICP-MS (a) and SP-ICP-MS (b) operating conditions.

(a) ICP-MS operational conditions		
RF power		1600 W
Gas flows	Nebulization	1.15–1.30 mL min^{-1}
	Auxiliary	1.2 mL min^{-1}
	Plasma	15 L min^{-1}
Analyte		$TiNH(NH_3)_4$ (m/z 131)
DRC (NH_3 flow rate)		1.0 mL min^{-1}
RPQ		0.2
(b) SP-ICP-MS operational conditions		
RF power		1600 W
Gas flows	Nebulisation	1.15–1.30 mL min^{-1}
	Auxiliary	1.2 mL min^{-1}
	Plasma	15 L min^{-1}
Analyte	Ti (quantification using mass 131, cluster $TiNH(NH_3)_4$)	
Reaction cell flow (NH_3)		1.0 mL min^{-1}
RPQ		0.2
Dwell time		100 µs
Acquisition time		60 s
Density		4.23 g cm^{-3}
Mass fraction		59.9%
Ionization efficiency		100%
Sample flow rate		0.19-0.21 mL min^{-1}

2.3.7 TiO_2NPs assessment by SP-ICP-MS

Operating SP-ICP-MS conditions (DRC mode) are listed in **Table 2.2.(b)**. Data acquisition/treatment by Syngistix™ Nano Application routine required the assessment of the sample introduction flow rate and transport efficiency (TE%): the first value was obtained by weighing after ultrapure water aspiration under selected pump conditions, and the second parameter was automatically calculated by Syngistix™ Nano Application after measuring an ionic Au calibration (concentrations within the 0-3.0 range) and a 49.6 nm Au NPs material at 124 ng L^{-1} prepared in ultrapure water). Values between 0.19 and 0.21 mL min^{-1} for the sample flow rate, and approximately 8.0% for TE were obtained throughout the work. DRC mode (ammonia as a reaction gas at a flow rate of 1.0 mL min^{-1}) was used for minimising polyatomic interferences when assessing Ti (mass shift approach by monitoring the 131 adduct).

SP-ICP-MS measurements were performed with calibration curves prepared in ultrapure water at 1.0, 2.5, 5.0 and 10.0 µg L^{-1}. Alkaline extracts were analyzed after dilution with 1% (v/v) glycerol (from 1:100 to 1:500 dilution) and the diluted extracts were exposed to ultrasounds (45 kHz) for 5.0 min before SP-ICP-MS analysis.

2.3.8 HRTEM-EDX analysis of TMAH extracts

Analysis of the alkaline extracts from seaweeds by HRTEM-EDX requires a previous cleaning/pre-concentration of the extract. Filtration by ultracentrifugation (30 kDa NMWL) was therefore applied by loading 0.5 mL of the extract and ultracentrifuging at 14,000 g and 4 ºC

USC DE SANTIAGO DE COMPOSTELA

for 20 min. The procedure continued by rinsing with 0.5 mL of ultrapure water (also ultracentrifugation at 14,000 g and 4 °C for 20 min) ten times. The clean concentrate in the filter was then recovered (25 µL) and 10 µL were dropped onto a copper grid, and allowed to air-drying at room temperature before HRTEM-EDX analysis.

2.4 RESULTS AND DISCUSSION

2.4.1 Variables affecting the TMAH extraction process

Several parameters that can affect the TiO_2NPs released from seaweeds when using TMAH as an extractant have been studied. All experiments were performed using an ultrasound water bath (45 kHz, 80 W) and 1.0000 g subsamples of the same homogenized sea lettuce seaweed. Each condition for each parameter was evaluated in triplicate, and at least two blanks were prepared for each set of conditions. Results (TiO_2NP concentrations and mean sizes) are expressed as the mean±the standard deviation).

TMAH concentration was evaluated within the 2.5-15% (v/v) range using a volume of 5.0 mL of each extracting solution under sonication for 1.0 h. As shown in **Figure 2.1.(a)**, similar TiO_2NPs concentrations have been obtained when using low TMAH concentration ($6.24\times10^5\pm5.94\times10^4$ and $5.70\times10^5\pm5.59\times10^4$ TiO_2NPs g^{-1} for 2.5 and 5.0% (v/v), respectively); whereas, the extracted concentration slightly diminishes for extracting solutions with higher TMAH percentage. These findings can be attributed to the high ionic strength of TMAH solutions which promotes NPs agglomeration and hence a low number NPs concentrations. The results agree with those obtained for TiO_2NPs size distributions (**Figure 2.1.(a)**) which shows higher mean TiO_2NPs sizes in the extracts obtained with the highest TMAH concentration (84 nm for 15% (v/v) TMAH over 73-74 nm for other TMAH extracting solutions). TiO_2NPs size distributions were not found to follow a normal distribution (selected size histograms in **Figure S.2.1.**, supplementary information), and a distribution at small sizes followed by other distributions at higher sizes were observed.

USC UNIVERSIDADE DE SANTIAGO DE COMPOSTELA

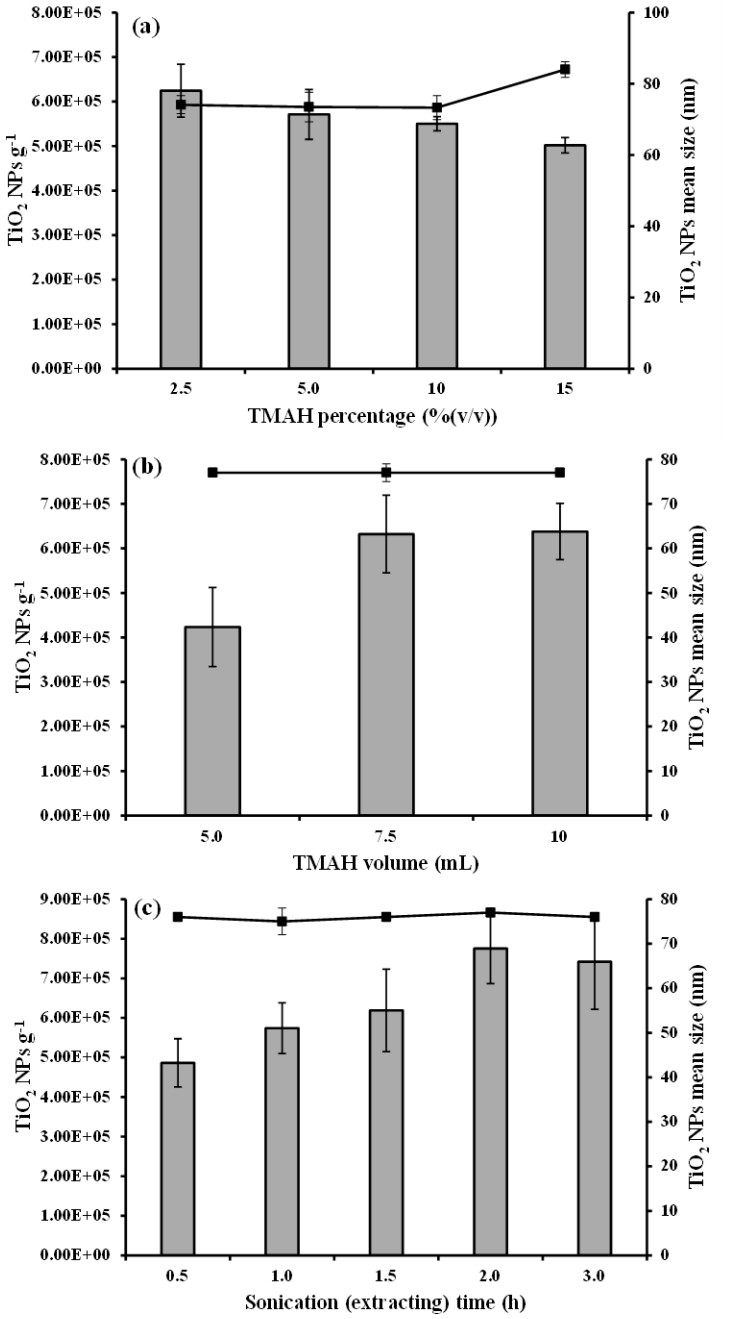

Figure 2.1. Effect of the TMAH percentage in the extracting solution (a), the volume of the TMAH extracting solution (b), and the sonication (extraction) time (c) on the number of TiO_2NPs (bars) and TiO_2NPs mean size (line).

After fixing a TMAH percentage of 2.5 % (v/v) and a sonication time of 1.0 h, the effect of the TMAH solution volume (5 mL, 7.5 mL and 10 mL) on the extraction of the NPs from TiO_2 from seaweed was evaluated. As shown in **Figure 2.1.(b)** the highest amount of NPs extracted was obtained when volumes of 7.5 mL and 10 mL were used ($6.32\times10^5\pm8.73\times10^4$ and $6.38\times10^5\pm6.32\times10^4$ TiO_2NPs g^{-1} for 7.5 and 10 mL, respectively); whereas, there are no differences on the mean sizes of the extracted TiO_2NPs (**Figure 2.1.(b)**). Therefore, a volume of 7.5 mL of a 2.5% (v/v) TMAH solution was chosen as extracting solution.

UDC UNIVERSIDADE DE SANTIAGO DE COMPOSTELA

Finally, the influence of the sonication (extracting) time was evaluated within the 0.5–3.0 h range. **Figure 2.1.(c)** shows that the extraction yield is improved moreover the sonication time is higher, and it remains constant after sonicating for 2.0 h. ANOVA (95% confidence interval) showed that there is not a statistically significant difference between the extracted TiO_2NPs concentration after 2.0 and 3.0 h ($7.75\times10^5\pm8.90\times10^4$, and $7.42\times10^5\pm1.20\times10^4$ TiO_2NPs g^{-1}, respectively). The effect of the sonication time, as well as the slight increase in the water-bath temperature when using long sonication times (temperatures within the 50–60 ºC range), does not change the TiO_2NPs size distributions, and similar TiO_2NPs mean sizes were measured after using all sonication times (**Figure 2.1.(c)**). Therefore, a sonication (extracting) time of 2.0 h was finally selected.

2.4.2 Stability of TiO_2NPs

The effect of the extractive conditions on the stability of TiO_2NPs has been tested by subjecting 50 and 100 nm TiO_2NPs aqueous suspensions (10 μg L^{-1} as Ti) to the optimized UAE conditions. Results for TiO_2NPs concentrations and mean size (experiments in triplicate, **Figure 2.2.**) show that both TiO_2NPs concentrations and mean sizes are similar for un-treated and treated (UAE) 50 and 100 nm TiO_2NPs aqueous suspensions. These findings have been verified after applying the Mann–Whitney U test at a 95.0% confidence level, which gave P-values of 0.663 and 0.0808 when comparing the median concentration of un-treated and treated 50 nm TiO_2NPs and 100 nm TiO_2NPs, respectively; and 0.0722 and 0.507 for medians comparison of un-treated and treated 50 nm and 100 nm TiO_2NPs sizes, respectively (P-values higher than 0.05). The measured TiO_2NPs mean sizes (60±1 and 58±1 nm for untreated and treated 50 nm TiO_2NPs standards, respectively; and 118±3 and 120±2 nm for untreated and treated 100 nm TiO_2NPs standards, respectively) do not match with mean size values given by the manufacturer since the reported mean sizes are 50 and 100 nm aerodynamic particle sizes. However, if we consider the measurement within ±20% of the nominal (and not certified) standard value, the sizes assessed are in good agreement with the size values given by the manufacturer.

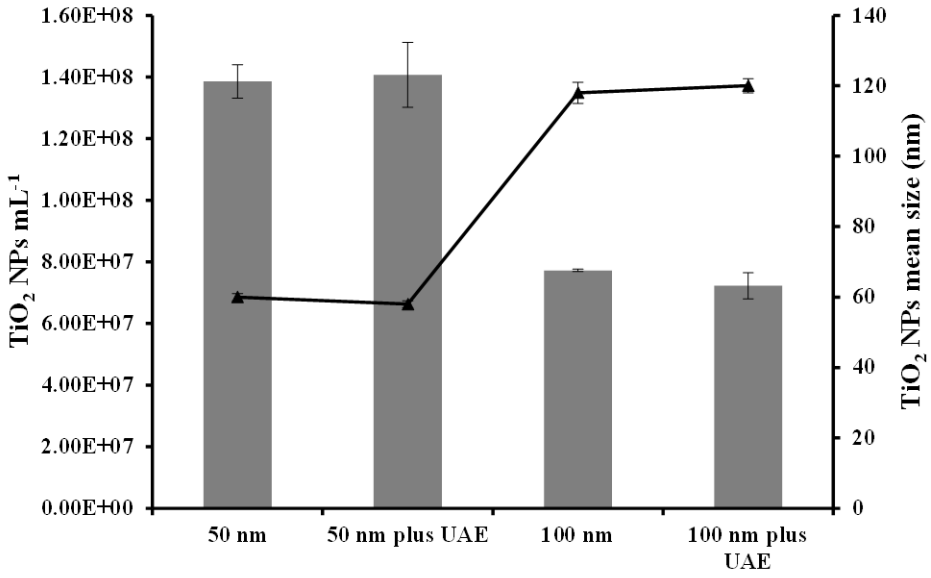

Figure 2.2. Number of TiO_2NPs (bars) and TiO_2NPs mean size (line) for untreated and treated (exposed to the UAE procedure) 50 and 100 nm TiO_2NPs standards.

USC UNIVERSIDADE DE SANTIAGO DE COMPOSTELA

2.4.3 Analytical features

Since TMAH extracts are diluted in 1% (v/v) glycerol before SP-ICP-MS analysis, a comparison has been performed by preparing ionic Ti calibrations (up to 10 µg L^{-1}) in ultrapure water and in 2.5% (v/v) TMAH/1.0% (v/v) glycerol (1:99). Slopes (mean±standard deviation) of five aqueous and matched calibration curves (0.181±0.011 for aqueous calibration, and 0.174±0.017 for calibration with TMAH) were similar, obtaining good linearity for all cases (regression coefficient higher than 0.9984 and 0.9980 for aqueous and with TMAH/glycerol matched calibration, respectively). Matrix effect can be therefore considered as negligible.

The limit of detection in size (lowest size measured by SP-ICP-MS) was obtained by using the calculation Excel tool designed by Laborda et al. [35] based on the 3σ (3×baseline standard deviation), and 5σ (5×baseline standard deviation) criterion. After measuring a 1:100 diluted reagent blank (2.5% (v/v) TMAH) in 1% (v/v) glycerol, the assessed limit of detection in size was 30.9 nm (3σ criterion) and 36.7 nm (5σ criterion). The limit of detection in size is related to the capability of distinguishing a nanoparticle from the background signal. The use of a criterion higher than 4σ virtually eliminates the occurrence of false positives when nanoparticle distributions are partially overlapped with the background [36]. Therefore, the 5σ criterion was used in this study.

The minimum number of NPs concentration was established by using the same tool by Laborda et al [35], where the $2.33\sigma_N$ criterion was applied to estimate the critical value (discrimination between the dissolved analyte and the NPs) and the $5\sigma_N+3$ criterion was used for the limit of detection in number of NPs (σ_N is the standard deviation of the number of events counted in the blank, Poisson distribution assumed). The critical value obtained was 1.25×10^6 NPs L^{-1}. This value referred to the seaweed sample was 5.00×10^4 NPs g^{-1}. Similarly, the limit of detection was 1.43×10^6 NPs L^{-1} (5.72×10^4 NPs g^{-1} referred to the seaweed sample).

The repeatability of the method was evaluated by subjecting eleven sub-samples from a seaweed sample (sea lettuce) to the proposed extractive method and measuring in triplicate each extract by SP-ICP-MS. The number of TiO_2NPs found (mean±standard deviation) was $1.76\times10^7\pm2.09\times10^6$ TiO_2NPs g^{-1} with a relative standard deviation (RSD) of 12%. Regarding TiO_2NPs size distribution, the mean size was 84 nm with and standard deviation of 2 nm and a RSD of 2%.

The accuracy of the extraction method was evaluated through the analytical recovery. A SP-ICP-MS analysis was performed after spiking TMAH extracts from a sea lettuce sample with 50 nm and 100 nm TiO_2NPs at a concentration of 10 µg L^{-1} as total Ti (experiments in triplicate). The TiO_2NPs suspensions (10 µg L^{-1} as total Ti) used for the spiking experiments, as well as un-spiked TMAH extracts, were also analyzed in triplicate by SP-ICP-MS. The analytical recovery was established by applying the **Equation 2.1.**

$$AR = \frac{[TiO_2]_{spiked} - [TiO_2]_{un-spiked}}{[TiO_2]_{suspesion}} \times 100 \quad (\textbf{Equation 2.1.})$$

where $[TiO_2]_{spiked}$ is the number of TiO_2NPs per mL in the spiked TMAH extract, $[TiO_2]_{un-spiked}$ is the number of TiO_2NPs per mL in the un-spiked TMAH extract, and $[TiO_2]_{suspension}$ is the number of TiO_2NPs per mL used for the spiking experiments.

A mean±standard deviation of 115±1% and 112±1% was obtained for 50 and 100 nm TiO_2NPs, respectively.

Finally, the extraction efficiency was evaluated by subjecting the seaweed residues obtained after the UAE to a second and a third UAE treatment. In these cases, a centrifugation stage (2,014 g, 8 ºC, 15 min) was applied for obtaining the extracts and the residues.

Experiments in triplicate (results as mean±standard deviation) for a sea lettuce sample led to a number of TiO_2NPs per gram of $6.38\times10^6\pm9.41\times10^5$ (first UAE extraction); whereas, the number of TiO_2NPs per gram obtained after treating the seaweed residues were lower than the LOD of the method (5.72×10^4 NPs g^{-1}). Therefore, TiO_2NPs determination appears to be quantitative.

2.4.4 Applications

The optimized method has been finally applied to several seaweed samples taken from the Spanish (Galician) and Irish coasts. In addition, some seaweeds (three dulse and two sea lettuce samples) previously exposed to TiO_2NPs under laboratory-controlled conditions, were also analyzed. Total Ti basal contents (unexposed seaweeds) were found to vary from 0.17 to 0.66 μg g^{-1} (**Table 2.3.**); whereas, found background TiO_2NPs concentrations (unexposed seaweeds) varied from 1.68×10^6 to 1.76×10^7 TiO_2NPs g^{-1} (**Table 2.3.**), although TiO_2NPs were undetected in several samples (TiO_2NPs concentration lower than 1.43×10^6 TiO_2NPs L^{-1}).

Table 2.3. Total Ti and TiO_2NPs concentration and mean sizes (n=3) in some seaweeds.

	[Ti] (μg g^{-1})	TiO_2NPs g^{-1}	Mean size (nm)
Sargassum 1	0.66±0.02	$3.75\times10^6\pm4.37\times10^5$	69±1
Sargassum 2	0.28±0.0083	$3.94\times10^6\pm7.99\times10^5$	71±1
Dulse 1	0.20±0.02	< 5.72×10^4	----[a]
Dulse 2	0.28±0.02	< 5.72×10^4	----[a]
Dulse 3	0.17±0.02	< 5.72×10^4	----[a]
Dulse 4	0.27±0.04	< 5.72×10^4	----[a]
Dulse 5	0.27±0.04	$1.68\times10^6\pm4.25\times10^5$	89±13
Dulse 6[b]	1.54±0.20	$4.06\times10^8\pm2.61\times10^7$	50±5
Dulse 7[b]	1.56±0.21	$3.45\times10^7\pm1.04\times10^6$	62±8
Dulse 8[b]	2.52±0.35	$8.73\times10^8\pm1.70\times10^8$	52±3
Sea lettuce 1	0.29±0.04	$6.38\times10^6\pm9.41\times10^5$	76±5
Sea lettuce 2	0.33±0.09	$9.08\times10^6\pm9.23\times10^5$	80±1
Sea lettuce 3	0.60±0.03	$1.76\times10^7\pm2.09\times10^6$ [c]	84±1
Sea lettuce 4[b]	0.69±0.02	$7.09\times10^8\pm9.37\times10^7$	55±6
Sea lettuce 5[b]	30.2±2.2	$7.35\times10^9\pm4.68\times10^8$	62±1

(a) Not assessed; (b) Seaweed exposed to TiO_2NPs; (c) n=12

The mean TiO_2NPs sizes in unexposed seaweeds were within the 69-89 nm range. Regarding exposed seaweed, total Ti contents were within the 1.54-30.2 μg g^{-1} range, and TiO_2NPs concentration were from 3.45×10^7 to 7.35×10^9 TiO_2NPs g^{-1} (**Table 2.3.**). In this case, mean sizes were within the 50-62 nm range (some size distribution as given in **Figure 2.3.** from dulse 8 (**Figure 2.3.(a)**) and sea lettuce 5 (**Figure 2.3.(b)**) samples).

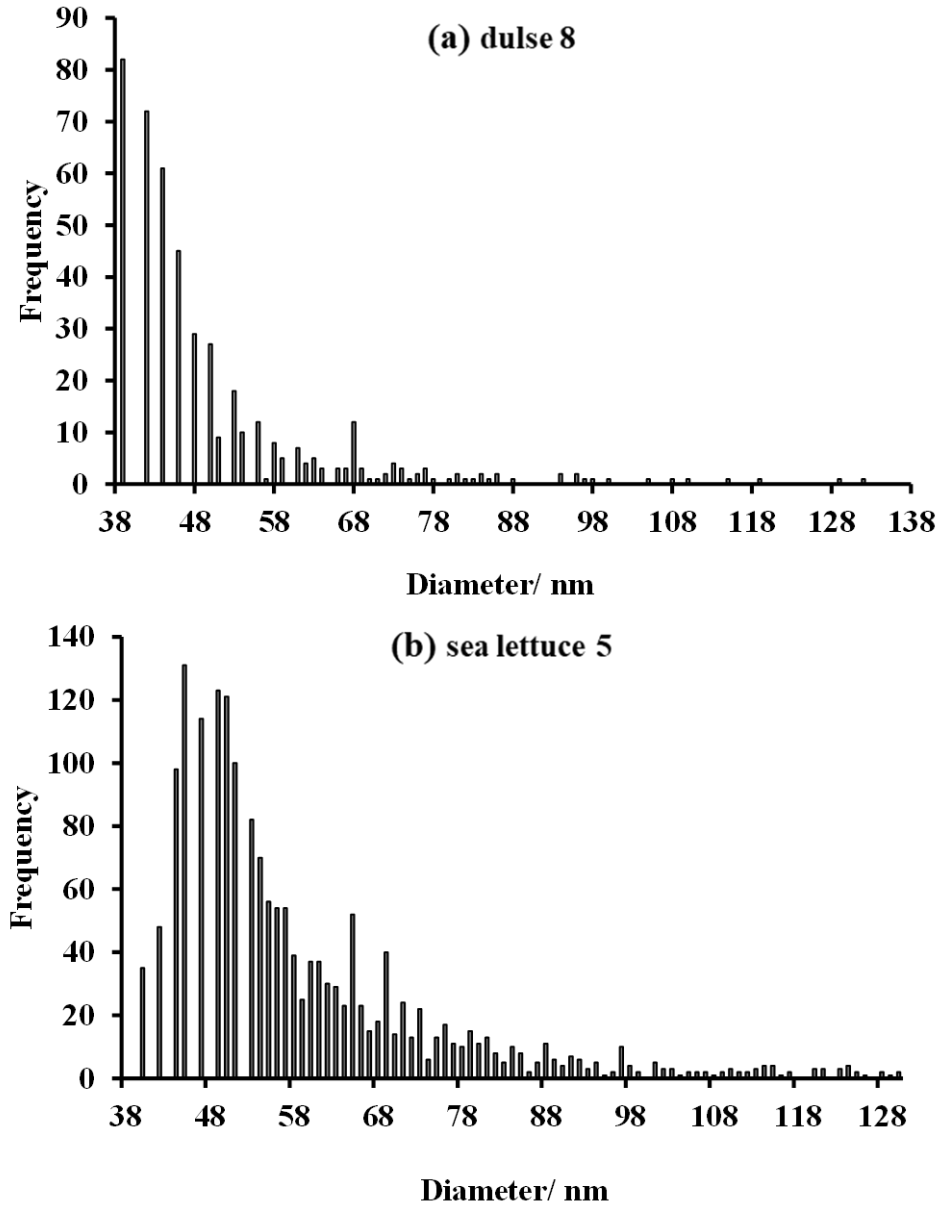

Figure 2.3. TiO_2NPs size distribution in selected seaweeds: dulse 8 (a), sea lettuce 5 (b).

Selected TMAH extracts from dulse 8 and sea lettuce 5 were also subjected to HRTEM-EDX analysis. **Figure 2.4.** and **Figure 2.5.** show the HRTEM images and EDX spectra for an extract from dulse 8 (**Figure 2.4.**) and sea lettuce 5 (**Figure 2.5.**), and several TiO_2NPs were detected at different parts of the copper grid where the clean TMAH extract was dropped before analysis. HRTEM images show a high degree of TiO_2NPs agglomeration. The presence of TiO_2NPs in the extracts by an alternative analytical tool such as HRTEM verifies the successful extraction of TiO_2NPs, which can be assessed with high sensitivity by SP-ICP-MS.

USC UNIVERSIDADE DE SANTIAGO DE COMPOSTELA

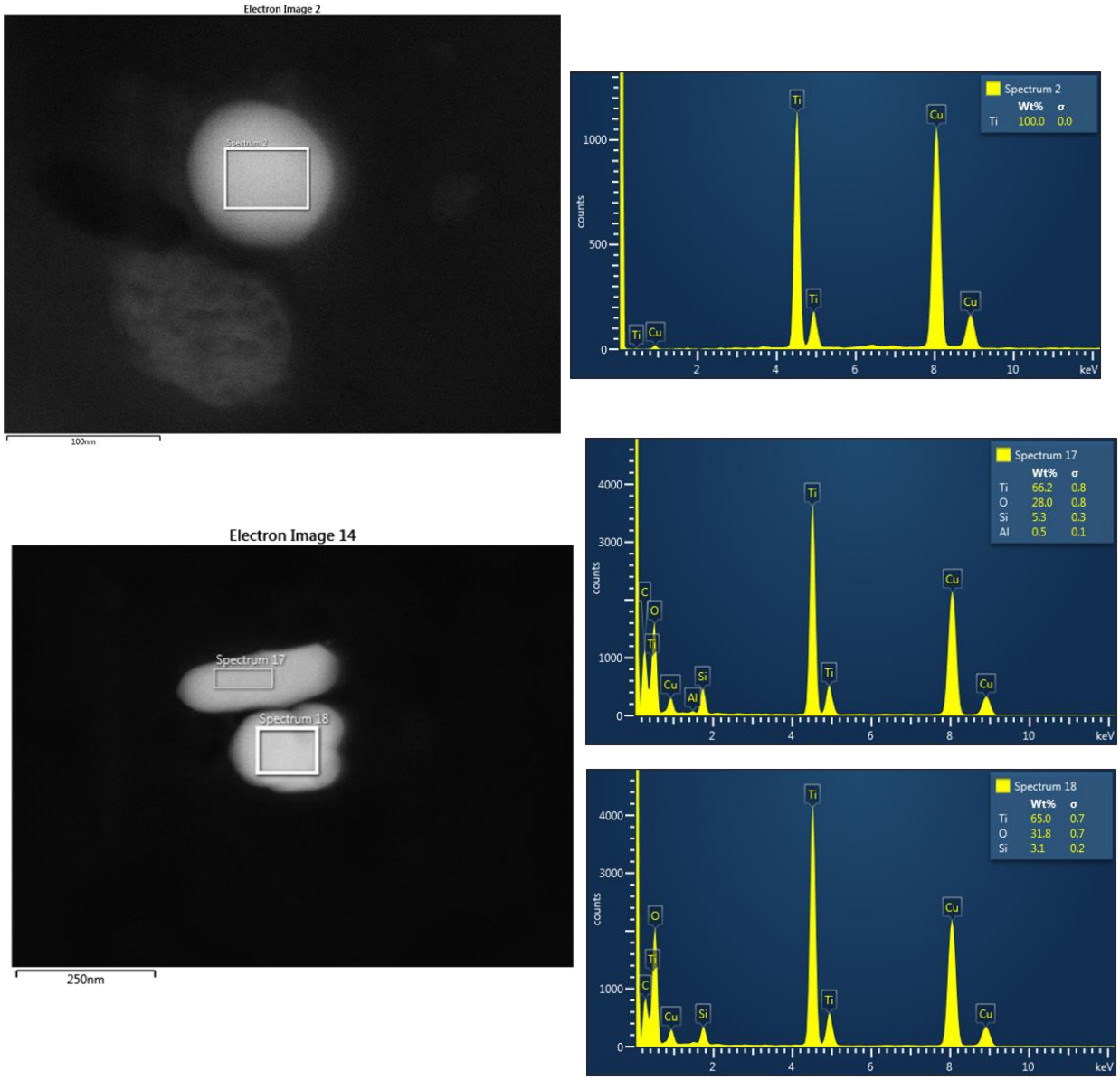

Figure 2.4. HRTEM images and EDX spectra of cleaned TMAH extracts from dulse 8.

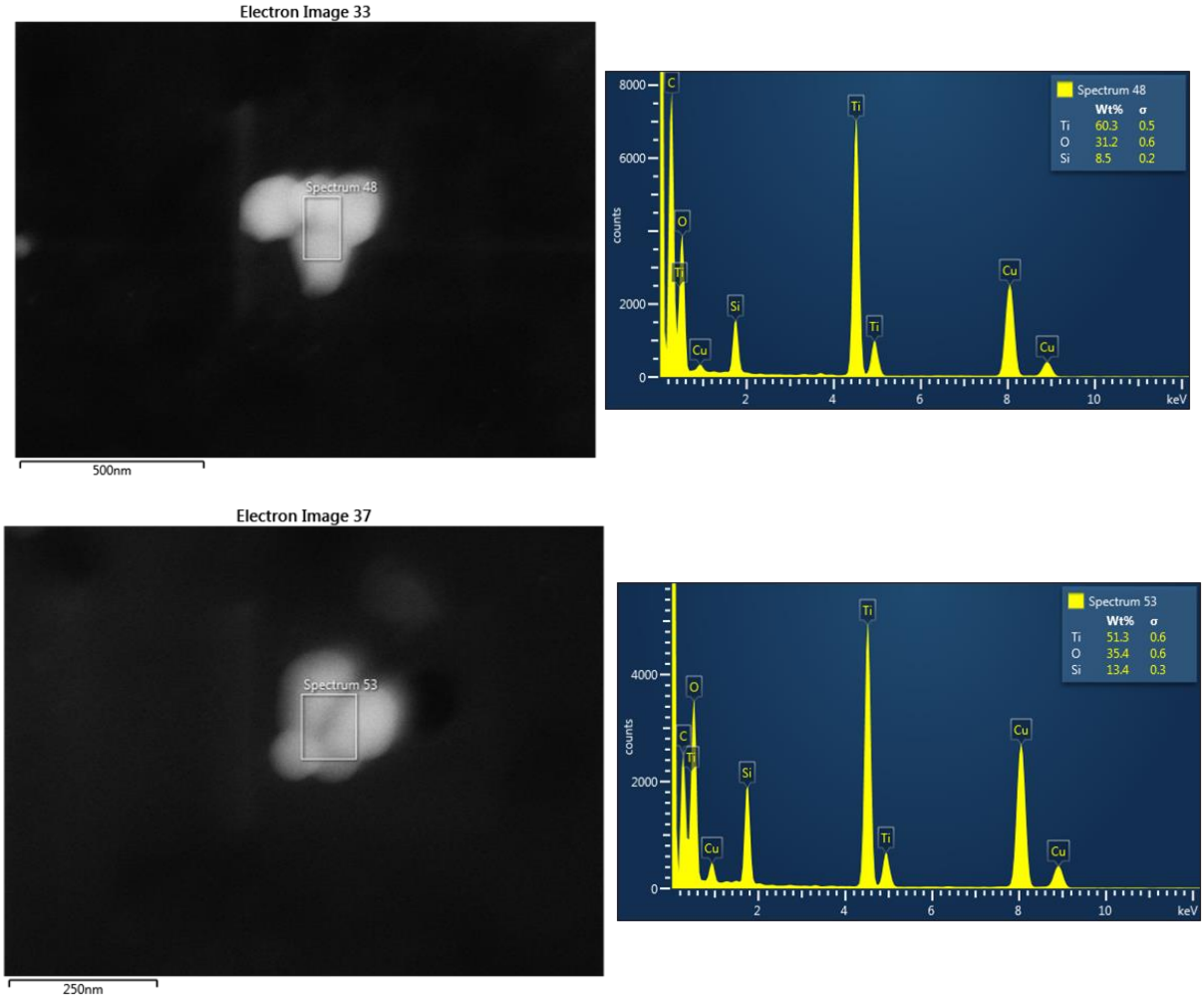

Figure 2.5. HRTEM images and EDX spectra of cleaned TMAH extracts from sea lettuce 5.

2.5 CONCLUSIONS

Results from this research demonstrated that SP-ICP-MS is a robust technique for obtaining quantitative information and particle size distribution of TiO_2NPs in complex samples such as TMAH extracts from seaweed. Good sensitivity, as well as repeatability and analytical recovery, have been obtained for SP-ICP-MS measurements. Diluted TMAH as an extracting solvent and ultrasound assistance has allowed the isolation of TiO_2NPs from seaweed without changing the particle size distribution. The robust conditions of SP-ICP-MS allowed also the direct analysis of diluted TMAH extracts with a high degree of precision and without carry-over effects. Therefore, SP-ICP-MS can be an analytical technique to be taken into account when assessing inorganic nanoparticles for screening, quantification/characterization, and comparative purposes with other instrumental tools.

USC UNIVERSIDADE DE SANTIAGO DE COMPOSTELA

SUPPLEMENTARY INFORMATION

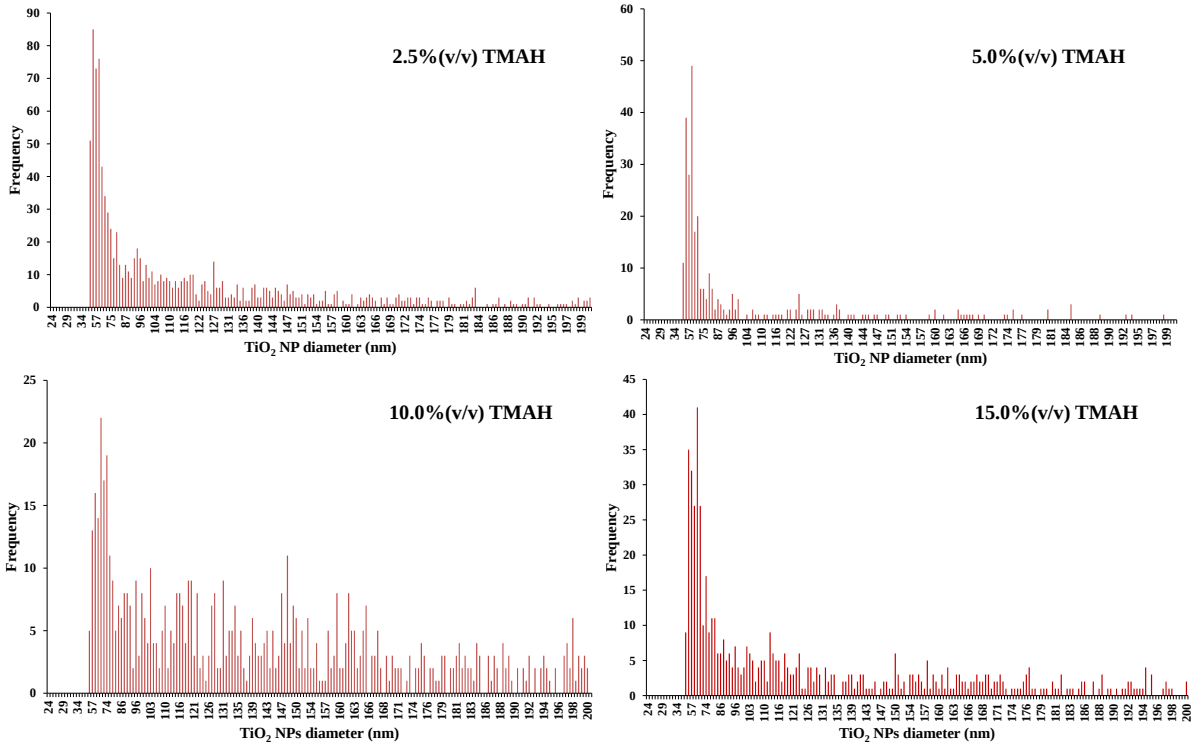

Figure S.2.1. Size distributions obtained for TiO_2NPs in alkaline extractions using 2.5, 5.0, 10.0, and 15.0% (v/v) of TMAH.

REFERENCES

[1] D. Ziental, B. Czarczynska-Goslinska, D. T. Mlynarczyk, A. Glowacka-Sobotta, B. Stanisz, T. Goslinski, L. Sobotta, Titanium dioxide nanoparticles: Prospects and applications in medicine, Nanomaterials 10 (2020) 387–418. https://doi.org/10.3390/nano10020387.
[2] B. Faure, G. Salazar-Álvarez, A. Ahniyaz, I. Villaluenga, G. Berriozabal, Y. R. De Miguel, L. Bergström, Dispersion and surface functionalization of oxide nanoparticles for transparent photocatalytic and UV-protecting coatings and sunscreens, Sci. Technol. Adv. Mater.14 (2013) 023001. https://doi.org/10.1088/1468-6996/14/2/023001.
[3] S. L. Schneider, H. W. Lim, A review of inorganic UV filters zinc oxide and titanium dioxide, Photodermatol. Photoimmunol. Photomed. 35 (2019) 442–446. https://doi.org/10.1111/phpp.12439.
[4] Y. Yang, K. Doudrick, X. Bi, K. Hristovski, P. Herckes, P. Westerhoff, R. Kaegi, Characterization of food-grade titanium dioxide: The presence of nanosized particles, Environ. Sci. Technol. 48 (2014) 6391–6400. https://doi.org/10.1021/es500436x.
[5] European Food Safety Authority, https://www.efsa.europa.eu/en/news (accessed May 29, 2021).
[6] R. Naidu, V. A. Arias Espana, Y. Liu, J. Jit, Emerging contaminants in the environment: Risk-based analysis for better management, Chemosphere 154 (2016) 350–357. https://doi.org/10.1016/j.chemosphere.2016.03.068.
[7] H. M. R. Abdel-Latif, M. A. O. Dawood, S. Menanteau-Ledouble, M. El-Matbouli, Environmental transformation of n-TiO_2 in the aquatic systems and their ecotoxicity in bivalve mollusks: A systematic review, Ecotoxicol. Environ. Saf. 200 (2020) 110776. https://doi.org/10.1016/j.ecoenv.2020.110776.
[8] M. V. Taboada-López, S. Iglesias-López, P. Herbello-Hermelo, P. Bermejo-Barrera, A. Moreda-Piñeiro, Ultrasound assisted enzymatic hydrolysis for isolating titanium dioxide nanoparticles from bivalve mollusk before sp-ICP-MS, Anal. Chim. Acta 1018 (2018) 16-25. https://doi.org/10.1016/j.aca.2018.02.075.
[9] M. V. Taboada-López, N. Alonso-Seijo, P. Herbello-Hermelo, P. Bermejo-Barrera, A. Moreda-Piñeiro, Determination and characterization of silver nanoparticles in bivalve molluscs by ultrasound assisted enzymatic hydrolysis and sp-ICP-MS, Microchem. J. 148 (2019) 652–660. https://doi.org/10.1016/j.microc.2019.05.023.
[10] M. V. Taboada-López, D. Bartczak, S. Cuello-Núñez, H. Goenaga-Infante, P. Bermejo-Barrera, A. Moreda-Piñeiro, AF4-UV-ICP-MS for detection and quantification of silver nanoparticles in seafood after enzymatic hydrolysis, Talanta 232 (2021) 122504. https://doi.org/10.1016/j.talanta.2021.122504.
[11] Q. Zhou, L. Liu, N. Liu, B. He, L. Hu, L. Wang, Determination and characterization of metal nanoparticles in clams and oysters, Ecotoxicol. Environ. Saf. 198 (2020) 110670. https://doi.org/10.1016/j.ecoenv.2020.110670.
[12] M. V. Taboada-López, P. Herbello-Hermelo, R. Domínguez-González, P. Bermejo-Barrera, A. Moreda-Piñeiro, Enzymatic hydrolysis as a sample pre-treatment for titanium dioxide nanoparticles assessment in surimi (crab sticks) by single particle ICP-MS, Talanta 195 (2019) 23–32. https://doi.org/10.1016/j.talanta.2018.11.023.
[13] D. Ojeda, M. V. Taboada-López, E. Bolea, J. Pérez-Arantegui, P. Bermejo-Barrera, A. Moreda-Piñeiro, F. Laborda, Size characterization and quantification of titanium dioxide nano- and microparticles-based products by asymmetrical flow field-flow fractionation coupled to dynamic light scattering and inductively coupled plasma mass spectrometry, Anal. Chim. Acta 1122 (2020) 20-30. https://doi.org/10.1016/j.aca.2020.04.080.

USC DE COMPOSTELA

[14] A. Grasso, M. Ferrante, G. Arena, R. Salemi, P. Zuccarello, M. Fiore, C. Copat, Chemical characterization and quantification of silver nanoparticles (Ag-NPs) and dissolved Ag in seafood by single particle ICP-MS: Assessment of Dietary Exposure, Int. J. Environ. Res. Public Health 18 (2021) 4076. https://doi.org/10.3390/ijerph18084076.
[15] A. Grasso, M. Ferrante, P. Zuccarello, T. Filippini, G. Arena, M. Fiore, A. Cristaldi, G. O. Conti, C. Copat, Chemical characterization and quantification of titanium dioxide nanoparticles (TiO_2-NPs) in seafood by single-particle ICP-MS: Assessment of Dietary Exposure, Int. J. Environ. Res. Public Health 17 (2020) 9547. https://doi.org/10.3390/ijerph17249547.
[16] L. Mišurcová, Chemical composition of seaweeds, 173-192, Chapter in Handbook of Marine macroalgae: Biotechnology and applied phycology, John Wiley & Sons (2012) ISBN:9781119977087. https://doi.org/10.1002/9781119977087.ch7.
[17] I. de la Calle, M. Menta, F. Séby, Current trends and challenges in sample preparation for metallic nanoparticles analysis in daily products and environmental samples: A review, Spectrochim. Acta Part B 125 (2016) 66–96. https://doi.org/10.1016/j.sab.2016.09.007.
[18] F. Laborda, E. Bolea, G. Cepri, M. T. Gómez, M. S. Jiménez, J. Pérez-Arantegui, J. R. Castillo, Detection, characterization and quantification of inorganic engineered nanomaterials: A review of techniques and methodological approaches for the analysis of complex samples, Anal. Chim. Acta 904 (2016) 10-32. https://doi.org/10.1016/j.aca.2015.11.008.
[19] M. Mattarozzi, M. Suman, C. Cascio, D. Calestani, S. Weigel, A. Undas, R. Peters, Analytical approaches for the characterization and quantification of nanoparticles in food and beverages, Anal. Bioanal. Chem. 409 (2017) 63–80. https://doi.org/10.1007/s00216-016-9946-5.
[20] E. P. Gray, J. G. Coleman, A. J. Bednar, A. J. Kennedy, J. F. Ranville, C. P. Higgins, Extraction and analysis of silver and gold nanoparticles from biological tissues using single particle inductively coupled plasma mass spectrometry, Environ. Sci. Technol. 47 (2013) 14315–14323. https://doi.org/10.1021/es403558c.
[21] J. Jiménez-Lamana, F. Laborda, E. Bolea, I. Abad-Álvaro, J. R. Castillo, J. Bianga, M. He, K. Bierla, S. Mounicou, L. Ouerdane, S. Gaillet, J. M. Rouanet, J. Szpunar, An insight into silver nanoparticles bioavailability in rats, Metallomics 6 (2014) 2242-2249. https://doi.org/10.1039/c4mt00200h.
[22] N. J. Clark, R. Clough, D. Boyle, R. D. Handy, Development of a suitable detection method for silver nanoparticles in fish tissue using single particle ICP-MS, Environ. Sci.: Nano 6 (2019) 3388. https://doi.org/10.1039/C9EN00547A.
[23] E. Bolea, J. Jiménez-Lamana, F. Laborda, I. Abad-Álvaro, C. Bladé, L. Arola, J. R. Castillo, Detection and characterization of silver nanoparticles and dissolved species of silver in culture medium and cells by AsFlFFF-UV-Vis-ICPMS: application to nanotoxicity tests, Analyst 139 (2014) 914–922. https://doi.org/10.1039/C3AN01443F.
[24] D. M. Schwertfeger, J. R. Velicogna, A. H. Jesmer, S. Saatcioglu, H. McShane, R. P. Scroggins, J. I. Princz, Extracting Metallic nanoparticles from soils for quantitative analysis: method development using engineered silver nanoparticles and SP-ICP-MS, Anal. Chem. 89 (2017) 2505−2513. https://doi.org/10.1021/acs.analchem.6b04668.
[25] M. Roman, C. Rigo, I. Munivrana, V. Vindigni, B. Azzena, C. Barbante, F. Fenzi, P. Guerriero, W. R. L. Cairns, Development and application of methods for the determination of silver in polymeric dressings used for the care of burns, Talanta 115 (2013) 94–103. https://doi.org/10.1016/j.talanta.2013.04.028.
[26] S. Park, Y. Kim, Feasibility study on the extraction of TiO_2 nanoparticle exposed in the activated sludge using alkaline digestion, J. Ind. Eng. Chem. 41 (2016) 62–67. https://doi.org/10.1016/j.jiec.2016.07.001.

[27] B. Schmidt, K. Loeschner, N. Hadrup, A. Mortensen, J. J. Sloth, C. B. Koch, E. H. Larsen, Quantitative characterization of gold nanoparticles by field-flow fractionation coupled online with light scattering detection and inductively coupled plasma mass spectrometry, Anal. Chem. 83 (2011) 2461–2468. https://doi.org/10.1021/ac102545e.
[28] K. Loeschner, M. Suk, J. Brabrand, J. J. Sloth, E. H. Larsen, Use of alkaline or enzymatic sample pretreatment prior to characterization of gold nanoparticles in animal tissue by single-particle ICPMS, Anal Bioanal Chem 406 (2014) 3845–3851. https://doi.org/10.1007/s00216-013-7431-y.
[29] H. Klingberg, L. B. Oddershede, K. Loeschner, E. H. Larsen, S. Loft, P. Møller, Uptake of gold nanoparticles in primary human endothelial cells, Toxicol. Res. 4 (2015) 655–666. https://doi.org/10.1039/C4TX00061G.
[30] J. Noireaux, R. Grall, M. Hullo, S. Chevillard, C. Oster, E. Brun, C. Sicard-Roselli, K. Loeschner, P. Fisicaro, Gold nanoparticle uptake in tumor cells: quantification and size distribution by sp-ICPMS, Separations 6 (2019) 3. https://doi.org/10.3390/separations6010003.
[31] J. Vidmar, T. Buerki-Thurnherr, K. Loeschner, Comparison of the suitability of alkaline or enzymatic sample pre-treatment for characterization of silver nanoparticles in human tissue by single particle ICP-MS, J. Anal. At. Spectrom. 33 (2018) 752–761. https://doi.org/10.1039/C7JA00402H.
[32] B. Bocca, B. Battistini, F. Petrucci, Silver and gold nanoparticles characterization by SP-ICP-MS and AF4-FFF-MALS-UV-ICP-MS in human samples used for biomonitoring, Talanta 220 (2020) 121404. https://doi.org/10.1016/j.talanta.2020.121404.
[33] S. Fernández-Trujillo, M. Jiménez-Moreno, Á Ríos, R. del C. Rodríguez Martín-Doimeadios, A simple analytical methodology for platinum nanoparticles control in complex clinical matrices via SP-ICP-MS, Talanta 231 (2021) 122370. https://doi.org/10.1016/j.talanta.2021.122370.
[34] C. García-Sartal, M. C. Barciela-Alonso, P. Herbello-Hermelo, P. Bermejo-Barrera, A sensitive, simple, and safe method for total arsenic determination in edible seaweed by HG-AFS, At. Spectrosc. 31 (2010) 27–33. http://dx.doi.org/10.46770/AS.2010.01.005.
[35] F. Laborda, A. C. Gimenez-Ingalaturre, E. Bolea, J. R. Castillo, About detectability and limits of detection in single particle inductively coupled plasma mass spectrometry, Spectrochim. Acta Part B 169 (2020) 105883. https://doi.org/10.1016/j.sab.2020.105883.
[36] F. Laborda, J. Jiménez-Lamana, E. Bolea, J. R. Castillo, Critical considerations for the determination of nanoparticle number concentrations, size and number size distributions by single particle ICP-MS, J. Anal. At. Spectrom. 28 (2013) 1220-1232. https://doi.org/10.1039/C3JA50100K.

USC UNIVERSIDADE DE SANTIAGO DE COMPOSTELA

USC
UNIVERSIDADE
DE SANTIAGO
DE COMPOSTELA

PART B. BIOACCUMULATION OF SILVER AND TITANIUM DIOXIDE NANOPARTICLES IN AQUACULTURE PRODUCTS

USC
UNIVERSIDADE
DE SANTIAGO
DE COMPOSTELA

USC
UNIVERSIDADE
DE SANTIAGO
DE COMPOSTELA

CHAPTER 3. STUDY OF SILVER NANOPARTICLES BIOACCUMULATION IN CULTURED RED AND GREEN SEAWEED

USC
UNIVERSIDADE DE SANTIAGO DE COMPOSTELA

USC
UNIVERSIDADE
DE SANTIAGO
DE COMPOSTELA

CHAPTER 3. STUDY OF SILVER NANOPARTICLES BIOACCUMULATION IN CULTURED RED AND GREEN SEAWEED

3.1 ABSTRACT

The increased use of nanomaterials in the industry causes them to be released into the environment where they can interact with marine organisms. In this study, the bioaccumulation of polyvinylpyrrolidone-coated silver nanoparticles (PVP-AgNPs) in red (*Palmaria palmata*) and green (*Ulva* sp.) seaweed was investigated. The bioaccumulation study lasted 28 days in which seaweeds were exposed to different concentrations of PVP-AgNPs (0.1 and 1.0 mg L^{-1}) in marine growing media containing phytoplankton. For the determination of the total Ag content, specimens were subjected to microwave energy before analysis by ICP-MS. Nanoparticles were isolated from the matrix by ultrasound-assisted enzymatic extraction before analysis by SP-ICP-MS to determine AgNPs content and size distributions.

The maximum concentrations of total Ag measured in the present study were: 0.52±0.04 µg g^{-1} w.w. (wet weight) (at day 21, exposure to 0.1 mg L^{-1} of PVP-AgNPs) and 0.79±0.06 µg g^{-1} w.w. (at day 14, 1.0 mg L^{-1}) in *Palmaria palmata*; and 0.26±0.04 µg g^{-1} w.w. (at day 28, 0.1 mg L^{-1}) and 0.46±0.15 µg g^{-1} (at day 21, 1.0 mg L^{-1}) in *Ulva* sp. These concentrations were smaller than those found in previous studies after short-term exposure (<48 h), probably due to the presence of organic matter in the growing media. The maximum concentrations of AgNPs were achieved at 14 days for *Palmaria palmata* ($1.63\times10^{9}\pm5.47\times10^{8}$ part g^{-1} w.w., 1.0 mg L^{-1}) and at 28 days for *Ulva* sp. ($3.23\times10^{9}\pm2.34\times10^{7}$ part g^{-1} w.w. , 1.0 mg L^{-1}) with most frequent sizes of approximately 20 nm. Furthermore, these size values measured by SP-ICP-MS were in agreement with those measured by TEM in the enzymatic extracts of *Palmaria palmata* and *Ulva* sp.

3.2 INTRODUCTION

In the last decades, nanotechnology has experienced exponential growth and engineered nanomaterials (ENMs) are being massively employed due to their novel properties in comparison to bulk materials. Indeed, it is expected that the worldwide production of nanomaterials will have reached a $ 55,016 million value in 2022 [1]. Silver nanoparticles (AgNPs) are one of the most widely used ENMs in the industry, mainly due to their bactericidal, antifungal and anticancer properties [2-5] which procure them in many application fields including medicine, drug delivery, odontology, health care, textiles, water and air purification, electronics, biosensing, and food production among others [6-8].

The proliferation of applications and products containing NPs inevitably results in the release of these materials into the environment, (e.g., surface/groundwater, soils/sediments, atmosphere, and marine environments) [9], where they can be considered potential emerging contaminants. Besides, AgNPs can change in size and shape, react with other species, dissolve in contact with water and can even be taken up by living organisms when there are in the environment. In marine sediments, different chemical species may be formed (Ag_2S, AgCl, and Ag^0) [9,10]. Several studies proposed that AgNPs toxicity to bacteria is produced through different mechanisms including 1) the formation of reactive oxygen species (ROS) such as O_2 [10,11], and 2) the interaction of Ag ions with thiol groups of enzymes and proteins, affecting

USC DE COMPOSTELA

cellular respiration, transport of ions through membranes, and causing cellular death [12]. Other studies demonstrated the AgNPs toxicity in plants (*Lolium multiflorum*) [13], aquatic plants (*Lemna minor*) [14], fungi and algae [15], vertebrates (zebrafish) [16], and even human cells (glioblastoma cells, lung fibroblast cells, and skin keratinocytes) [17,18]. Although the toxicity of AgNPs is partly explained by the release of Ag ions, it remains unclear if AgNPs are a direct cause of enhanced toxicity [10]. Some reports on different microalgae (*Chlamydomonas reinhardtii* [19,20], *Raphidocelis subcapitata* [21,22], *Mycrocistis auroginosa* [23], *Pseudokirchneriella subcapitata* [24], *Chlorella vulgaris* [25]), about AgNPs bioaccumulation, toxicity and trophic transfer were also found in the literature.

Seaweed is an increasingly demanded food in Europe due to changes in eating styles (towards vegetarian, vegan and sustainable diets), being a natural source of fibre, vitamin B-12, lipids, selenium, fatty acids (including Omega-3), iodine, and antioxidants (polyphenols, carotenoids and tocopherols) [26,27]. However, seaweed can accumulate metals at concentrations thousand times higher than seawater; then, they are concentrators of pollutants (organic pollutants, heavy metals, trace elements, even nanomaterials) [28-30] and they can be used as bioindicators of environmental contamination. Thus, Turner et al. [31] studied the accumulation and the toxicity of silver nanoparticles and dissolved Ag exposing the macroalga *Ulva lactuca* to AgNPs and $AgNO_3$ for 48 hours. In addition, Sfriso et al. [32] reported the toxicity of citrate-coated AgNPs and $AgNO_3$ in seawater *Ulva rigida* C. Agardh. The toxic effects (chloroplast damage, oxidative stress, lipid peroxidation) were verified by TEM microscopy after 24 h exposure to AgNPs. Siddiqui and Bielmyer-Fraser [33] compared the accumulation and effects of silver nitrate and AgNPs in a green seaweed (*Ulva lactuca*) and a red seaweed (*Agardhiella subulata*) for 24 h.

Although there are some reports on the bioaccumulation and toxicity of AgNPs in microalgae, to the best of our knowledge, there are no detailed studies about the patterns of AgNPs bioaccumulation in edible macroalgae during long exposure times (> 48 h). Therefore, this research work aims to study the bioaccumulation of PVP-coated AgNPs in two species of edible macroalgae (*Palmaria palmata* and *Ulva* sp.). Bioaccumulation experiments were performed on seaweed from the Atlantic area with different exposure doses of PVP-AgNPs for 28 days. The variation in the trend of total silver and nanoparticulate content (number and AgNPs size distribution) with exposure time was evaluated by inductively coupled plasma mass spectrometry (ICP-MS) and single-particle-ICP-MS (SP-ICP-MS), respectively.

3.3 MATERIALS AND METHODS

3.3.1 Instrumentation

An inductively coupled plasma mass spectrometer (ICP-MS) NexION® 2000 (PerkinElmer, Waltham, MA, USA) with Kinetic Energy Discrimination (KED) was used for total Ag determination. Single-particle mode (SP-ICP-MS) was used with the Syngistix™ Nano Application 2.5 software (PerkinElmer) to obtain AgNPs concentration and size distributions. An Ethos Plus microwave lab station (Milestone, Bergamo, Italy) was used for seaweed sample digestion. The microwave is equipped with ten Teflon vessels (100 mL), Teflon covers, an HTC adapter plate, HTC safety springs (Milestone), and a pressure and temperature controller probe. A Boxcult temperature-controlled incubation chamber (Stuart Scientific, Surrey, UK) equipped with a Rotabit orbital-rocking platform shaker (J.P. Selecta, Barcelona, Spain) was used for AgNPs extraction. A scanning transmission electron microscopy (STEM) with a probe-corrected FEI Titan G2 80-200 kV ChemiSTEM (FEI, Hillsboro, USA) was employed for the characterization of AgNPs in the enzymatic extracts.

USC DE COMPOSTELA

Other instruments include VibraCellTM VCX 130 V (Sonics Newtown, CT, USA), pH meter Basic20 (Crison, Barcelona, Spain), VWR Ultrasonic Cleaner (Barcelona, Spain), Reax top vortex vibrational shaker (Heidolph, Schwabach, Germany), a 2K15 centrifuge (Sigma, Osterode, Germany), and an analytical balance ML204 (Mettler Toledo, Barcelona, Spain) were used for sample preparation.

3.3.2 Reagents and materials

To perform the bioaccumulation assay and feed the seaweed, a polyvinylpyrrolidone (PVP) coated Ag nanopowder of 15 nm and a concentration of 5.4×10^{14} particles mL^{-1} from SkySpring Nanomaterials, Inc. (Houston, TX, USA) was used.

To isolate AgNPs from the seaweed matrix, a Macerozyme® R-10 enzyme mixture (Merck, Darmstadt, Germany) was used. It is formed by pectinase (0.5 units per mg), cellulase (0.1 units per mg), and hemicellulase (0.25 units per mg), and it is obtained from *Rhizopus* sp.

Trisodium citrate di-hydrated for analysis (Merck, Darmstadt, Germany) and citric acid for analysis (ACS, Panreac, Barcelona, Spain) were used for buffer preparation. 33% w/v ACS hydrogen peroxide (Panreac, Barcelona, Spain) and 69% w/v nitric acid (SUPRAPUR®, Sigma Aldrich, Darmstadt, Germany) were used for microwave-assisted acid digestion.

To prepare the ionic Ag standards, an ionic Ag stock solution (1000 mg L^{-1}) in 2% HNO_3 (Perkin Elmer, Shelton, CT, USA) was used; whereas, an ionic Rh stock solution (1000 mg L^{-1}) in 2% HCl (Perkin Elmer, Shelton, CT, USA) was diluted before use as an internal standard. 1% v/v glycerol (Merck, Darmstadt, Germany) was used for extract dilution before analysis by SP-ICP-MS.

An ionic Au stock standard (1000 mg L^{-1}) in 2 mol L^{-1} HCl (Merck), and a reference material PEG-COOH Gold Nanospheres (49.6 nm and 9.89×10^{6} particles mL^{-1}) from NanoComposix (San Diego, CA, USA), were used for transport efficiency calculations in SP-ICP-MS.

Regenerated cellulose Amicon Ultra-0.5 mL centrifugal filter units of 30 kDa nominal molecular weight limit (Merck, Darmstadt) were employed to clean the seaweed enzymatic extracts before AgNPs characterization by STEM.

Other reagents were used to perform the analysis by ICP-MS. They included NexION Setup Solution (1.0 µg L^{-1} of Be, Ce, Fe, In, Li, Mg, Pb, and U in 1% of HNO_3) from Perkin Elmer; He, and Ar both with a 99.999% of purity were from Nippon Gases (Madrid, Spain). Other materials included plasticware (e.g. tubes, pipette tips, and syringes) and Minisart NML hydrophilic non-sterile 5.0 µm filters (Sartorius, Goettingen, Germany). Ultrapure water (18 MΩ cm of resistivity) was obtained from a Milli-Q® IQ7003 (Millipore Co., Bedford, MA, USA) purification system.

3.3.3 Seaweed culture and exposure to AgNPs

Palmaria palmata (red seaweed) and *Ulva* sp. (green seaweed) were cultured at Indigo Rock Marine Research Centre (Cork, Ireland). Both seaweed species were exposed to 15 nm PVP-AgNPs at two different nominal doses (0.1 and 1.0 mg L^{-1}) for 28 days.

Seaweeds were cultivated in 40 L tanks at 15±1 ºC with periods of 12 hours of white light and 12 hours of darkness. Parameters like pH, temperature, dissolved O_2, and salinity were measured every day. However, conductivity, ammonium, and nitrites were tested twice a week. The seaweed were fed using cell-Hi F2P growth medium (a soluble nutrient blend commonly used in the production of marine microalgae). Each tank received 30 mL of the F2P medium (0.1 g mL^{-1}) three times a week following the total and partial water changes. A total water change was conducted on the day of the trial, after all algal samples were extracted and

processed, and before the addition of the nanoparticles. Fifty per cent of the water was replaced twice per week, two days before and two days after the addition of nanoparticles. The nanoparticles were resuspended using an ultrasonic bath and added once per week with the F2P medium by micro pipetting and manual shaking to obtain the final concentration in the low and high dose tanks (i.e. 0.1 and 1.0 mg L^{-1} respectively). Three control tanks (A-C: seaweed in growing medium without nanoparticles), three solvent control tanks (D-F: seaweed exposed to polyvinylpyrrolidone coating, without nanoparticles), three low-dose tanks (G-I: seaweed exposed to 0.1 mg L^{-1} of PVP-AgNPs), and three high dose tanks (J-L: seaweed exposed to 1.0 mg L^{-1} of PVP-AgNPs) were employed. Three replicate samples were taken from each tank every 7 days, resulting in 180 samples per trial managed.

Each seaweed was washed with ultrapure water to remove salts and contaminants from seawater. The manually homogenized algae were subjected to acid digestion with microwave energy for total Ag determination by ICP-MS, and to an enzymatic extraction for AgNPs content determination by SP-ICP-MS.

3.3.4 Total Ag determination by ICP-MS after microwave-assisted acid digestion

Microwave-assisted acid digestion was used for sample preparation before total Ag determination by ICP-MS. A mass of 1.0000 g of crushed and homogenized sample was introduced in the Teflon vessels of the microwave lab station described in **section 3.3.1**. The samples were mixed with 3 mL of 69% HNO_3 (w/v), 1 mL of 33% H_2O_2 (w/v) and 4 mL of ultrapure water. The MW program consisted of four steps at 800W of MW energy:

1) From room temperature to 90º C in 4 min.
2) From 90 to 140ºC in 5 min.
3) From 140 to 200ºC in 5 min.
4) Hold at 200ºC for 20 min.

Three seaweed replicates were taken from each tank and digested in triplicate, together with two blanks per set of digestions. Finally, the digests were diluted at 25 mL with ultrapure water before ICP-MS analysis.

The digested samples were analyzed by ICP-MS using the instrument described in **section 3.3.1** and the operational conditions listed in **Table 3.1.(a)**. Kinetic Energy Discrimination (KED) was used to avoid the polyatomic interferences in ICP-MS introducing 4.5 mL min^{-1} of He flow in the collision cell. Furthermore, due to the matrix effect, standard addition calibrations were performed between 0 and 15.0 µg L^{-1} of Ag and using 5.0 µg L^{-1} of ^{103}Rh as an internal standard.

USC UNIVERSIDADE DE SANTIAGO DE COMPOSTELA

Table 3.1. Operational conditions for ICP-MS (a) and SP-ICP-MS (b).

(a) Operational conditions for ICP-MS	
Parameter/component	**Type/mode/value**
Nebulizer	Meinhard CR R^+
Nebulizer chamber	5 ºC refrigerated glass cyclone chamber with Peltier PC^{3X}
Cone material	Nickel/aluminum
Radiofrequency power	1600 W
Ar gas flow	15 L min^{-1} (Plasma) 1.15 L min^{-1} (Nebulizer) 1.2 L min^{-1}(Auxiliary)
Analyte	Ag
Operation mode	KED
He gas flow	4.5 mL min^{-1}
Integration time	1000 ms
m/z	^{107}Ag (^{103}Rh as internal standard)
Replicates per sample	3
RPQ	0.2
(b) Operational conditions for SP-ICP-MS	
Operation mode	Standard
Sample flow rate	0.182-0.199 mL min^{-1}
Acquisition time	100 s
Dwell time	50 µs
Number of readings	2,000,000
Transport efficiency	8.8-11.5%

3.3.5 AgNPs analysis by SP-ICP-MS after ultrasound-assisted enzymatic extraction

An ultrasound-assisted extraction with an enzymatic mixture (Macerozyme® R-10) was selected to separate PVP-AgNPs from the seaweed matrix, without primary size and AgNPs concentration changes. The methodology was previously developed and validated by López-Mayán et al. [34]. For the extraction, 0.0500 g of homogenized wet seaweed was weighed and mixed with a buffer of citric acid/sodium citrate (7 mL of 2/2 mM buffer, pH 4.5). The mixture was submitted to 2.5 min of 20% amplitude ultrasonication with an ultrasound probe working in pulse mode (1/1 s on/off). Then 25 g L^{-1} of the enzyme mixture from *Rhizopus* sp. (hemicellulose, pectinase, and cellulase) was added. The enzymatic extracts were incubated for 6 hours in a Boxcult temperature-controlled incubation chamber at 37 ºC and 150 rpm. The enzymatic extracts with solid remains of seaweed were filtered with 5 µm cellulose syringe filters. Two blanks were prepared for each set of operational conditions or day of analysis. Finally, the extracts were diluted with 1% (v/v) glycerol before SP-ICP-MS analysis.

The diluted extracts were analyzed by ICP-MS working in Single-Particle (SP-ICP-MS) mode. The operational conditions of SP-ICP-MS are listed in **Table 3.1.(b)**. Syngistix™ Nano Application software requires the measurements of the sample flow rate and the transport efficiency (TE%) before sample analysis. The sample flow rate was calculated by aspirating ultrapure water through the peristaltic pump for 1 minute (in triplicate) and measuring the mass. The transport efficiency was calculated by the software after measuring the signals for an ionic

Au calibration (0-3.0 µg L^{-1}) and the Au nanospheres reference material of 49.6 nm in size at a concentration of 9.89×10^4 particles mL^{-1}. For individualized nanoparticle detection, it was necessary to reduce the acquisition time to the order of µs-ms and a large dilution of the samples (100-350 times). The large dilution of the samples avoids the matrix effect; then, the SP-ICP-MS measurements were performed using an external Ag ionic calibration between 0 and 5.0 µg L^{-1} prepared in ultrapure water. Finally, the AgNPs concentration and size distributions in the diluted extracts were directly obtained from the software after analysis, and they were used to calculate the concentrations in the seaweed samples.

3.3.6 Analysis of AgNPs in the enzymatic extracts by electron microscopy

The nanoparticles present in seaweed enzymatic extracts of *Palmaria palmata* and *Ulva* sp., both exposed to 1.0 mg L^{-1} of AgNPs, were characterized by transmission electron microscopy (TEM) and scanning transmission electron microscopy (STEM). For this purpose, the extracts were previously subjected to a cleaning and purification process to remove organic matter. The cleaning procedure consisted of filtration by ultracentrifugation using Amicon® Ultra 30 KDa centrifugal filter units. The filters were filled up with 0.5 mL of the extracts and centrifugated to 14,000 g at 4 ºC for 20 min. The process was repeated five times adding 0.5 mL of ultrapure water. Finally, 0.5 mL of absolute ethanol was added to the extract and shaken to remove the organic matter excess. The preconcentrated and cleaned seaweed extracts (25 µL) were collected and 5 drops of 3 µL were added dropwise to the microscopy Ti grid, dried at room temperature and inserted in the STEM holder.

The image processing software ImageJ (developed by W. Rasband, National Institutes of Health and the Laboratory for Optical and Computational Instrumentation, Bethesda, Maryland, USA) was used to measure the AgNPs sizes by TEM.

3.3.7 Statistical analysis

Statgraphics XVIII was used for the statistical analysis in this research work. One-way ANOVA tests were performed to compare if there are significant differences between the total Ag and AgNPs concentrations with time in control, solvent, 0.1 mg L^{-1} and 1.0 mg L^{-1} of PVP-AgNPs exposure tanks.

3.4 RESULTS AND DISCUSSION

3.4.1 Total Ag determination in seaweed exposed to AgNPs by ICP-MS

Total Ag contents (ionic Ag and Ag as AgNPs) in *Palmaria palmata* and *Ulva* sp. were determined by ICP-MS following the methodology described in **section 3.3.4**. The digested samples were diluted 25 and 50 times before ICP-MS analysis. The analytical performance of the methodology for the total Ag determination was also assessed. The Limit of Detection (LOD) and Limit of Quantification (LOQ) were calculated using the 3σ/slope and 10σ/slope criteria, respectively (where σ is the standard deviation of the blank, that was divided by the slope of the standard addition calibration). The isotope ^{107}Ag was selected due to its higher relative abundance and the lower limit of detection; the LOD and LOQ obtained were 2.2 and 7.7 ng g^{-1}, respectively. The accuracy was evaluated through the analytical recovery due to a lack of reference materials. The analytical recovery percentages were 103±4, 97±3, 97±2, and 103±5% for 0.05, 0.1, 1.0, and 10.0 µg L^{-1} of spiked Ag to the sample. Furthermore, the precision was evaluated through repeatability (n=5) with correlation coefficients lower than 5%.

USC UNIVERSIDADE DE SANTIAGO DE COMPOSTELA

3.4.1.1 Variation of total Ag content in *Palmaria palmata*

The concentration of total Ag was determined in red algae (*Palmaria palmata*) exposed to different concentrations (0.1 and 1.0 mg L^{-1}) of PVP-AgNPs. **Figure 3.1.(a)** shows the concentration of total Ag in *Palmaria palmata* grown in control and solvent tanks for 28 days (concentration as mean±standard deviation of the values measured for each group of tanks). The seaweed cultured in control tanks (A-C) and tanks exposed to the nanoparticle coating of PVP (D-F) did not present bioaccumulation of total Ag. These basal Ag concentrations were lower than 0.02 µg g^{-1} w.w. (wet weight). The one-way ANOVA test performed using the software Statgraphics XVIII (Warrenton, USA) showed for control and solvent tanks P-values greater than 0.05; then, this confirms no statistically significant differences between the averages at the different sampling days at a 95 % of significance level. **Figure 3.1.(b)** shows the total concentration of Ag in *Palmaria palmata* in control, solvent, low (G-I), and high (J-L) exposure dose tanks for 28 days. *Palmaria palmata* exposed to 0.1 mg L^{-1} of PVP-AgNPs showed bioaccumulation of total Ag with exposure time until 21 days when the highest concentration of 0.52±0.04 µg g^{-1} w.w. was reached. The one-way ANOVA showed P-values lower than 0.05; then, significant differences were found in the Ag total concentration with exposure time at a 95% of confidence level. The multiple range test showed a linear increase until 21 days and then the concentration remains practically constant. In the case of red algae exposed to 1.0 mg L^{-1} PVP-AgNPs, bioaccumulation is not proportional to the exposure dose when compared to seaweed exposed to 0.1 mg L^{-1}. The highest concentration of total Ag reached 0.79±0.06 µg g^{-1} w.w. at 14 days after exposure. Significant differences were found between the mean intervals for the different exposure days, with the one-way ANOVA test providing P-values lower than 0.05. The multiple range test also showed the linear increase of total Ag concentration until reaching a maximum at 14 days after exposure, followed by a concentration decrease; however, no significant differences were found between the concentrations measured at days 7, 21 and 28.

Table S.3.1. (supplementary information) summarizes the concentrations of total Ag measured at days 0 and 28 after exposure in *Palmaria palmata* for the control, solvent, low, and high exposure dose (0.1 mg L^{-1} and 1.0 mg L^{-1} of PVP-AgNPs, respectively) tanks, and **Figure S.3.1.** (supplementary information) shows the total Ag concentration in *Palmaria palmata* taken from all the different control tanks (tanks A-C, **Figure S.3.1.(a)**), the tanks exposed to the nanoparticle coating (tanks D-F, **Figure S.3.1.(b)**), the tanks exposed to 0.1 mg L^{-1} of PVP-AgNPs (tanks G-I, **Figure S.3.1.(c)**), and the tanks exposed to 1.0 mg L^{-1} of PVP-AgNPs (tanks J-L, **Figure S.3.1.(d)**).

USC UNIVERSIDADE DE SANTIAGO DE COMPOSTELA

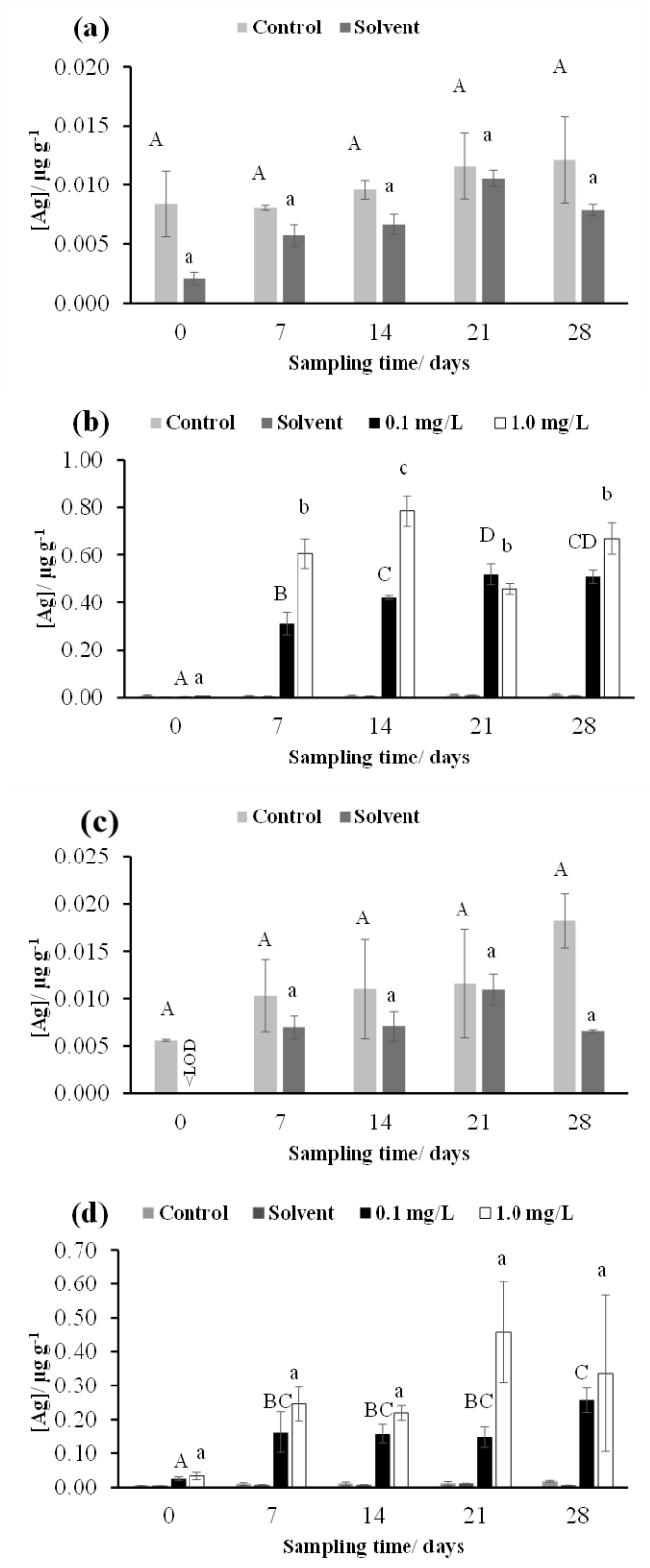

Figure 3.1. Total Ag bioaccumulation: (a) control and solvent in *Palmaria palmata*; (b) control, solvent, 0.1, and 1.0 mg L^{-1} in *Palmaria palmata*; (c) control and solvent in *Ulva* sp.; and (d) control, solvent, 0.1, and 1.0 mg L^{-1} in *Ulva* sp. for 28 days. Error bars represent the standard deviation of the values measured for each group of tanks. Different letters indicate significant differences (one-way ANOVA, P-value<0.05) between sampling times for each exposure dose (uppercase for control and 0.1 mg L^{-1} tanks, and lowercase for solvent and 1.0 mg L^{-1} tanks).

USC DE SANTIAGO DE COMPOSTELA

3.4.1.2 Variation of total Ag content in *Ulva* sp.

The concentration of total Ag was also determined in green seaweed (*Ulva* sp.) exposed to different concentrations (0.1 and 1.0 mg L^{-1}) of PVP-AgNPs. **Figure 3.1.(c)** shows the concentration of total Ag in *Ulva* sp. from control and solvent tanks during the 28 days (concentration as mean±standard deviation of the values measured for each group of tanks). As in *Palmaria palmata*, the control tanks and the tanks exposed to PVP did not show bioaccumulation, with basal Ag concentrations lower than 0.03 µg g^{-1} w.w. Besides, no significant differences were found for Ag concentration in the control and solvent tanks as a function of exposure time at a 95% of significance level in the one-way ANOVA tests. **Figure 3.1.(d)** shows the bioaccumulation trend in *Ulva* sp. exposed to 0.1 and 1.0 mg L^{-1} of PVP-AgNPs for 28 days. The *Ulva* sp. specimens exposed to 0.1 mg L^{-1} of PVP-AgNPs showed lower bioaccumulation than *Palmaria palmata*. The highest mean concentration measured was 0.26±0.04 µg g^{-1} w.w., reached 28 days after exposure. The P-value for the one-way ANOVA test in the study performed for *Ulva* sp. exposed to 0.1 mg L^{-1} of PVP-AgNPs was lower than 0.05, which indicates significant differences between the total Ag concentrations as a function of exposure days at a 95% confidence level. The multiple range test showed an increase of bioaccumulation until 7 days; after that the concentrations remained practically constant with the exposure time, reaching the highest mean concentration at 28 exposure days. In the case of the green seaweed exposed to 1.0 mg L^{-1}, the bioaccumulation was a bit higher than for 0.1 mg L^{-1}, reaching the maximum concentration of 0.46±0.15 µg g^{-1} w.w. at day 21 of exposure. However, the one-way ANOVA test showed a P-value higher than 0.05, and then no statistically significant differences were found between total Ag concentrations as a function of the exposure day. This finding could be due to the high variability of the concentrations observed for seaweed taken from the different tanks on days 21 and 28 after exposure. **Table S.3.1.** also summarizes the concentrations of total Ag in *Ulva* sp. from the control, solvent, low and high exposure dose (0.1 mg L^{-1} and 1.0 mg L^{-1} of PVP-AgNPs) tanks at days 0 and 28 of exposure. **Figure S.3.2.** shows the concentration of total Ag in *Ulva* sp. samples extracted from the different control tanks (tanks A-C, **Figure S.3.2.(a)**), the tanks exposed to the PVP nanoparticle coating (tanks D-F, **Figure S.3.2.(b)**), the tanks exposed to 0.1 mg L^{-1} of PVP-AgNPs (tanks G-I, **Figure S.3.2.(c)**), and the tanks exposed to 1.0 mg L^{-1} of PVP-AgNPs (tanks J-L, **Figure S.3.2.(d)**).

3.4.2 AgNPs determination in seaweed exposed to AgNPs by SP-ICP-MS

The AgNPs content in *Palmaria palmata* and *Ulva* sp. was determined by ICP-MS working in SP-ICP-MS mode following the methodology described in **section 3.3.5**. A solution of 1% (v/v) glycerol was used to dilute the seaweed extracts from 100 to 350 times. The experimental flow rates and transport efficiencies were between 0.182-0.199 mL min^{-1} and 8.8-11.5%, respectively. The analytical performance was also studied for SP-ICP-MS. The sensitivity was evaluated through the limit of detection in size (LOD_{size}) and particle number (LOD_{number}) using Laborda et al. [35] criteria. A blank submitted to the whole extraction procedure and diluted 100 times in 1% (v/v) glycerol was used to calculate the limits of detection. The LOD_{size} resulted in 14 and 12 nm using the 5σ and 3σ criteria, respectively (the 5σ criteria was selected to avoid false positives). Moreover, the LOD_{number} resulted in 2.40×10^{6} part L^{-1} (instrumental limit) and 4.34×10^{7} part g^{-1} (referred to the wet seaweed sample). The precision of the methodology was evaluated through the study of the repeatability in the analysis of *Palmaria palmata* and *Ulva* sp. extracts submitted to the enzymatic extraction; the measurements (n=5) of the most frequent sizes, mean sizes and AgNPs concentration reported variation coefficients lower than 18%. Furthermore, the accuracy of the extraction method was guaranteed, with mean analytical

USC DE COMPOSTELA

recoveries of 112±12% (n=3) at a concentration level of 6.0×10^7 part mL^{-1}. The stability of the AgNPs during the extraction procedure from exposed *Palmaria palmata* and *Ulva* sp. was tested in a previous study of the research group by SP-ICP-MS and transmission electron microscopy [34].

3.4.2.1 AgNPs content and size distribution in *Palmaria palmata*

The AgNPs content and their size distributions were studied in *Palmaria palmata* after ultrasound-assisted enzymatic extraction. Since the total Ag content in the control tanks corresponded to the basal content, only the algae samples exposed to 0.1 and 1.0 mg L^{-1} PVP-AgNPs were studied by SP-ICP-MS.

Figure 3.2.(a) and **Figure 3.2.(b)** show the average intertank concentrations of *Palmaria palmata* exposed to 0.1 mg L^{-1} (average of Tanks G, H, and I) and 1.0 mg L^{-1} (average of tanks J, K, L) of PVP-AgNPs for 28 exposure days, respectively. The one-way ANOVA test was performed to study the variation of AgNPs' mean concentrations with time. The P-value was lower than 0.05 for *Palmaria palmata* exposed to 0.1 mg L^{-1}, and then statistical differences were found in the AgNPs concentrations with exposure time at a 95% of confidence level. The AgNPs concentration increased with the exposure time until $7.14\times10^8\pm2.38\times10^8$ part g^{-1} w.w. at 28 days. The multiple range test also showed the statistical differences between concentrations between 7 and 28 days, and between 14 and 28 days. Furthermore, **Figure 3.2.(c)** shows the most frequent and mean sizes in the case of *Palmaria palmata* exposed to 0.1 mg L^{-1} of PVP-AgNPs for 28 days. The most frequent and mean sizes were between 18±2 nm (7 days) and 19±1 nm (28 days), and between 22±2 nm (7 days) and 23±1 nm (28 days), respectively. Moreover, as expected, in the case of red seaweed exposed to 1.0 mg L^{-1}, the AgNPs content increased more than for the same seaweed exposed to 0.1 mg L^{-1}. The P-value in the case of *Palmaria palmata* exposed to the high dose was lower than 0.05, and then there were statistical differences between the concentrations measured on different days, and the concentration increased until $1.63\times10^9\pm5.47\times10^8$ part g^{-1} w.w. at day 14, and after that, the mean concentration decreased. The multiple range test only showed statistical differences between 0 and 14 days, and between 0 and 28 days. **Figure 3.2.(d)** shows the most frequent and mean sizes in the case of *Palmaria palmata* exposed to 1.0 mg L^{-1} of PVP-AgNPs for 28 days. The most frequent and mean sizes were between 21±1 nm (7 days) and 19±4 nm (28 days), and between 30±3 nm (7 days) and 24±1 nm (28 days), respectively.

Finally, **Figure 3.3.(a)** and **Figure 3.3.(b)** show two examples of the size distribution histograms obtained for the enzymatic extracts of *Palmaria palmata* exposed to 0.1 and 1.0 mg L^{-1} of PVP-AgNPs, respectively.

USC UNIVERSIDADE DE SANTIAGO DE COMPOSTELA

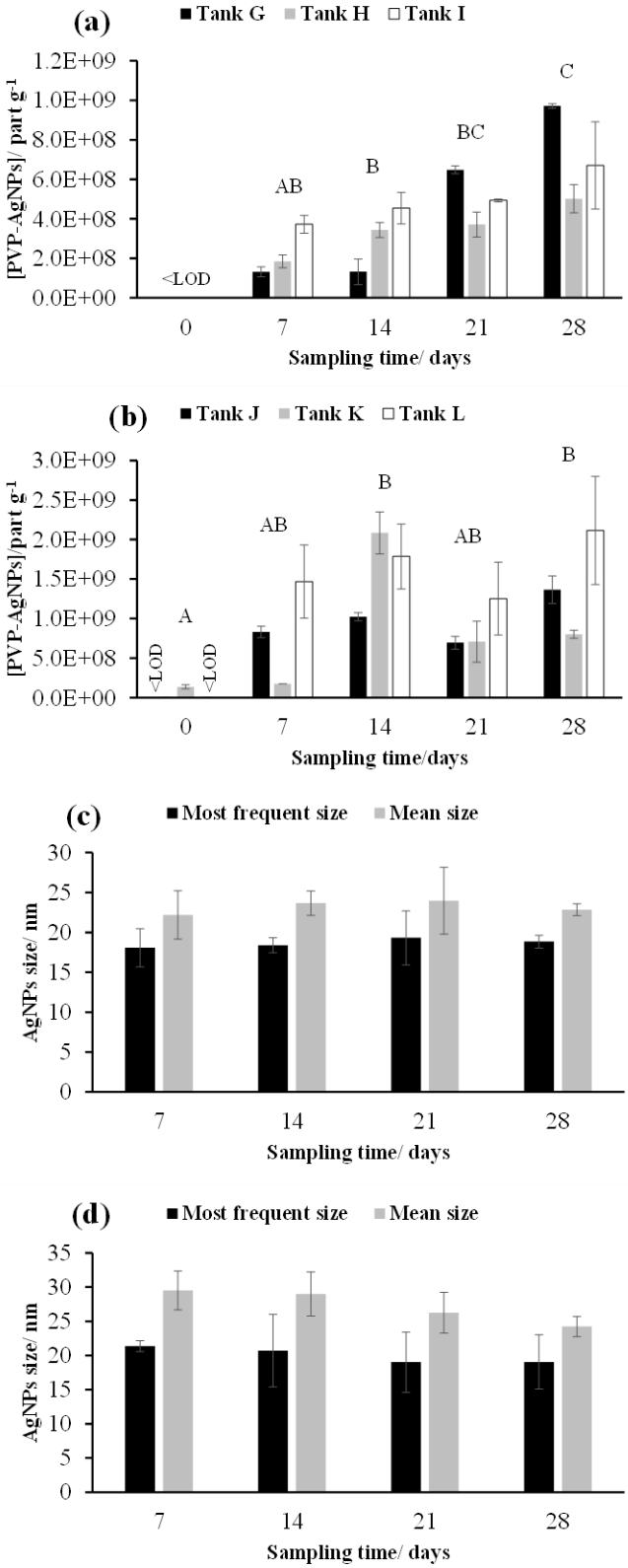

Figure 3.2. AgNPs content in *Palmaria palmata* exposed to (a) 0.1 mg L^{-1} and (b) 1.0 mg L^{-1} of PVP-AgNPs, and most frequent and mean sizes exposed to (c) 0.1 mg L^{-1} and (d) 1.0 mg L^{-1}. Error bars represent the standard deviation of the values measured for each seaweed sample (n=3) (a and b), and the standard deviation of the values measured for each group of tanks (c and d). Different letters indicate significant differences (one-way ANOVA, P-value<0.05) between tank means at different sampling times for each exposure dose.

USC UNIVERSIDADE DE SANTIAGO DE COMPOSTELA

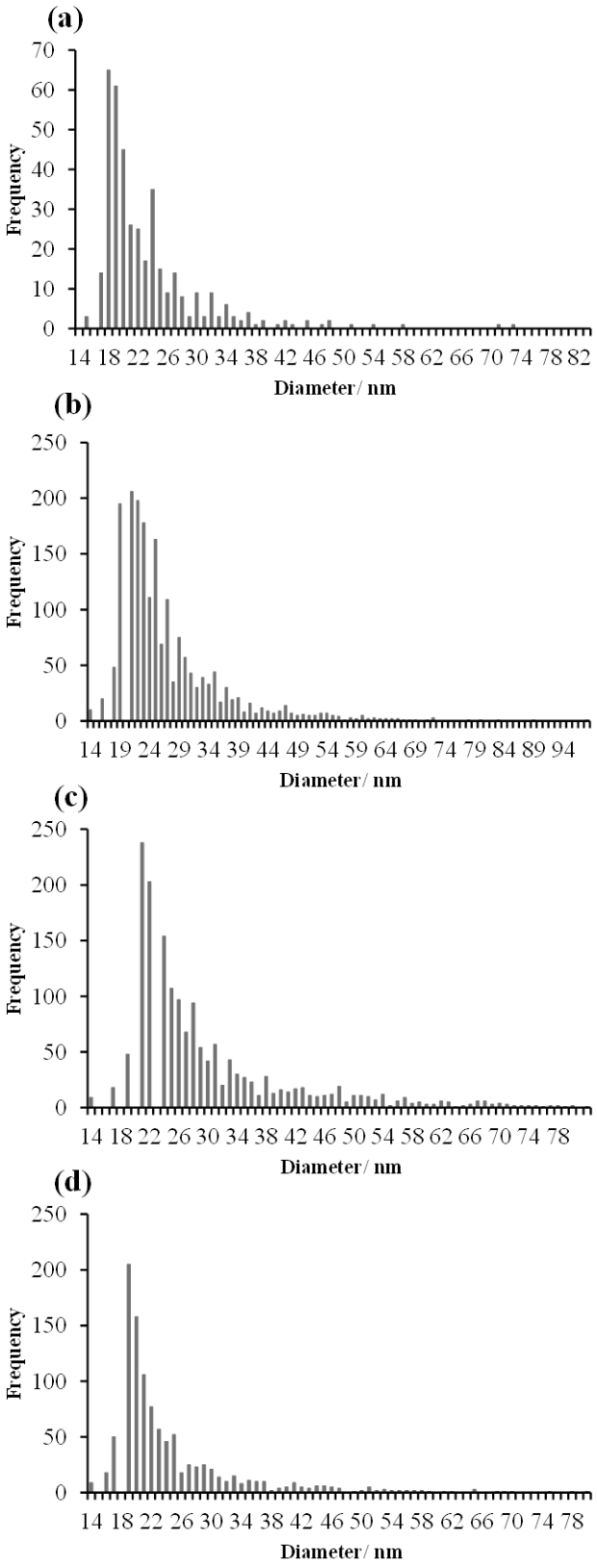

Figure 3.3. Size distribution histograms of PVP-AgNPs corresponding to extracts of *Palmaria palmata* exposed to (a) 0.1 mg L^{-1} and (b) 1.0 mg L^{-1}, and *Ulva sp*. exposed to (c) 0.1 mg L^{-1} and (d)1.0 mg L^{-1} of PVP-AgNPs.

USC DE SANTIAGO DE COMPOSTELA

3.4.2.2 AgNPs content and size distribution in *Ulva* sp.

The AgNPs content and their size distributions were studied in *Ulva* sp. after ultrasound-assisted enzymatic extraction. Since the total Ag content in the control tanks corresponded to the basal content, only the algae samples exposed to 0.1 and 1.0 mg L^{-1} PVP-AgNPs were studied by SP-ICP-MS.

Figure 3.4.(a), and **Figure 3.4.(b)** show the average intertank nanoparticle content in *Ulva* sp. seaweed from tanks exposed to 0.1 mg L^{-1}, and 1.0 mg L^{-1} of PVP-AgNPs, respectively, and the most frequent and mean sizes of those nanoparticles in specimens exposed to 0.1 mg L^{-1} (**Figure 3.4.(c)**), and 1.0 mg L^{-1} of PVP-AgNPs (**Figure 3.4.(d)**).

The one-way ANOVA tests were performed again to compare the variation of mean concentrations of AgNPs with exposure time. The P-value for *Ulva* sp. exposed to 0.1 mg L^{-1} was lower than 0.05, and then statistical differences were found between the AgNPs concentrations for *Ulva* sp. exposed to 0.1 mg L^{-1} on different days. The AgNPs content increased with the exposure time until $1.19\times10^{9}\pm2.81\times10^{8}$ part g^{-1} w.w. at day 28. The multiple range test showed the concentration overlapping only between 7 and 14 days, 14 and 21 days, and 21 and 28 days. Furthermore, **Figure 3.4.(c)** shows the most frequent sizes and mean sizes for *Ulva* sp. exposed to 0.1 mg L^{-1} of AgNPs for 28 days. The most frequent and mean sizes were between 21±1 nm (7 days) and 21±1 nm (28 days), and between 32±2 nm (7 days) and 31±1 nm (28 days), respectively. Moreover, as expected the *Ulva* sp. exposed to 1.0 mg L^{-1} reached higher AgNPs concentrations than *Ulva* sp. exposed to 0.1 mg L^{-1}. The AgNPs concentration increased with the exposure time until $3.23\times10^{9}\pm2.34\times10^{7}$ part g^{-1} w.w. at 28 exposure days. The one-way ANOVA test showed again in this case a P-value lower than 0.05, and then statistical differences between the AgNPs concentration of seaweed exposed to 1.0 mg L^{-1} at different times were found, with a 95% of confidence level. The multiple range test also showed the overlapping in the concentrations except in the case of 0 days with 21 and 28 days.

Figure 3.4.(d) shows the most frequent sizes and mean sizes for *Ulva* sp. exposed to 1.0 mg L^{-1} of AgNPs for 28 days. The most frequent sizes and mean sizes were between 22±1 nm (7 days) and 20±2 nm (28 days), and between 28±4 nm (7 days) and 26±4 nm (28 days), respectively.

USC UNIVERSIDADE DE SANTIAGO DE COMPOSTELA

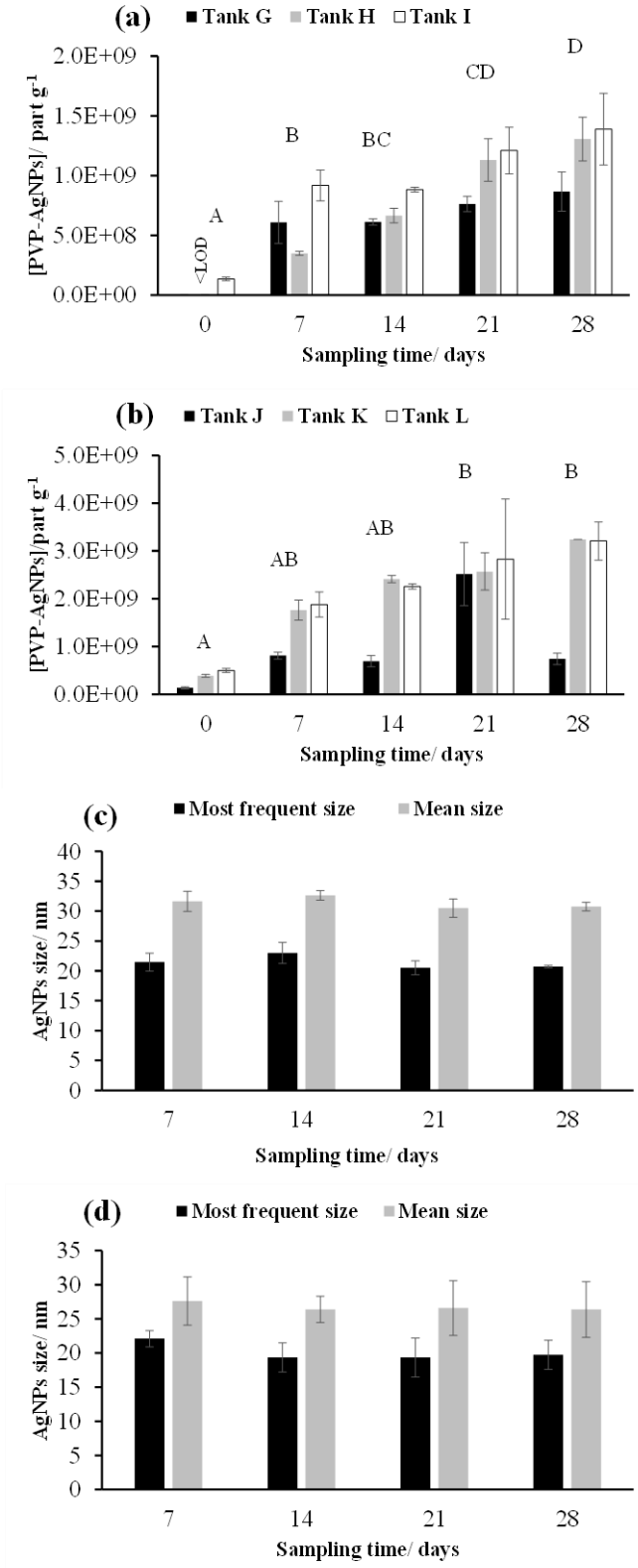

Figure 3.4. AgNPs content in *Ulva sp.* exposed to (a) 0.1 mg L^{-1} and (b) 1.0 mg L^{-1} of PVP-AgNPs, and most frequent and mean sizes exposed to (c) 0.1 mg L^{-1} and (d) 1.0 mg L^{-1}. Error bars represent the standard deviation of the values measured for each seaweed sample (n=3) (a and b), and the standard deviation of the values measured for each group of tanks (c and d). Different letters indicate significant differences (one-way ANOVA, P-value<0.05) between tank means at different sampling times for each exposure dose.

Finally, **Figure 3.3.(c)** and **Figure 3.3.(d)** show two examples of size distribution histograms obtained for the enzymatic extracts of *Ulva* sp. seaweeds exposed to 0.1 and 1.0 mg L^{-1} of PVP-AgNPs, respectively.

The presence of Ag in the environment deserves to be studied because of its elevated toxicity to marine organisms including seaweed. Lee et al. [36] developed a semi-automated toxicity test based on the measurement of the inhibition of reproduction of *Ulva pertusa* by different compounds (Ag, As, phenol, herbicides, volatile organic compounds, antifouling agents) after 96 h of exposure. The half maximal effective concentration (EC50) for Ag was 0.132 mg L^{-1}, a value between those obtained for the most toxic compounds (the antifouling agent Irgarol with an EC50 = 0.048 mg L^{-1}, and As with an EC50 = 0.172 mg L^{-1}). In a previous study, Siddiqui and Bielmyer-Fraser [33] compared the accumulation of $AgNO_3$ and AgNPs in two seaweed species (*Ulva lactuca* and *Agardhiella subulata*), finding that the accumulation was species-dependant. The green algae *Ulva lactuca* showed more accumulation at 24 h after exposure to 100 and 1000 µg L^{-1} $AgNO_3$ and 1000 µg L^{-1} AgNPs, followed by a decrease in the concentration of Ag in the tissue at 48 h. However, the concentration of Ag in red algae *A. subulata* increased at 48 h after exposure to $AgNO_3$. The authors concluded that: 1) *U. lactuca* regulated Ag tissue concentration better than *A. subulata*; 2) the accumulation of AgNPs (40-70 nm in size) were better regulated or they were less available than ionic Ag. *U. lactuca* exposed to 10–1000 µg L^{-1} of $AgNO_3$ or AgNPs, accumulated approximately 7–150 µg g^{-1} d.w. and 5–100 µg g^{-1} d.w., respectively. Those concentrations were similar to those measured by Turner et al. [31] of approximately 30–110 µg g^{-1} and 5–30 µg g^{-1} d.w., after the exposure of *U. lactuca* to nominal concentrations ranging from 0 to 100 µg L^{-1} of $AgNO_3$ or AgNPs (58±27 nm), respectively, for 48 h. These authors reported a dose-response for AgNPs similar to that observed for ionic Ag at much lower concentrations, suggesting that the toxicity of AgNPs is related to their dissolution rate in aquatic media. Sfriso et al. [32] studied the effects of short-time exposure of *Ulva rigida* C. Agardh seaweed to citrate-coated AgNPs (35±9 nm in size) and $AgNO_3$ in artificial seawater for 24 h. The accumulation of Ag followed a Langmuir isotherm with a saturation point of 11.3 µg Ag g^{-1} w.w. from a 5 mg L^{-1} solution of AgNPs. The uptake of the element was very fast, with Ag reaching concentrations in the seaweed of 8.50 µg g^{-1} w.w. after exposure to 1 mg L^{-1} of AgNPs for 24 hours. These authors suggest that the toxicity of Ag on seaweed should be reduced by the presence of inorganic and organic ligands concentrations in real marine transitional environments. The differences in accumulation can be explained according to the diverse behaviour of species, different sizes and coatings of the nanoparticles tested in the experiments. Zhang et al. [25] reported that the type of coating and surface charge of AgNPs influences the bioaccumulation dynamics in freshwater algae (*Chlorella vulgaris*). The algae surface cells are a negatively charged plasma membrane, with negatively charged groups. Therefore, polyethylene-coated AgNPs (positively charged) and citrate-coated AgNPs (negatively charged) experienced electrostatic attraction and repulsion with the algal membrane, respectively. The sizes of the nanoparticles used in the present study were smaller than those used in previous studies with seaweed, and therefore, they are expected to have more industrial applications as bactericides. It has been demonstrated that the antibacterial effect increases with lowering particle size and could be explained due to the increased number concentration of particles [37]. The maximum concentrations of total Ag measured in the present study were: 0.52±0.04 µg g^{-1} w.w. (at day 21, exposure to 0.1 mg L^{-1} of PVP-AgNPs) and 0.79±0.06 µg g^{-1} w.w. (at day 14, 1.0 mg L^{-1}) in *Palmaria palmata,* and 0.26±0.04 µg g^{-1} w.w. (at day 28, 0.1 mg L^{-1}) and 0.46±0.15 µg g^{-1} (at day 21, 1.0 mg L^{-1}) in *Ulva* sp. Therefore, *Palmaria palmata* reached the maximum concentration faster than *Ulva* sp. Concentration in seaweed does not rise in equal proportion to the concentration of exposure;

USC DE COMPOSTELA

thus, it can be observed that increasing ten times the exposure concentration implies an increase of 1.5 and 1.8 times the content of Ag in *Palmaria palmata* and *Ulva* sp., respectively. Hypothesis F-tests and t-tests were performed to compare the variances and means of the maximum concentrations reached for the two types of seaweed. For *Palmaria palmata* and *Ulva* sp. exposed to 0.1 and 1.0 mg L^{-1}, no significant differences were found (in both cases) in the variance and the mean concentrations with a 95% of confidence level. The percentage of humidity of *Palmaria* and *Ulva* is approximately 90%. Therefore, the concentrations of Ag determined in the present work were smaller than those found in previous studies, probably because seaweeds were exposed to nanoparticles mixed with growing media and the phytoplankton that was used for feeding. It was expected that the accumulation of Ag would be reduced in the presence of organic matter in marine media. Thus, Xiang et al. [23] reported the toxicity of AgNPs in freshwater green algae (*Microcystis aeruginosa*), where the AgNPs adhesion, penetration and changes in the cell membranes decreased with the organic matter present, due to the dissolved Ag ratio decrease.

The maximum concentrations of AgNPs were achieved at 14 days for *Palmaria palmata* ($1.63\times10^{9}\pm5.47\times10^{8}$ part g^{-1} w.w., 1.0 mg L^{-1}) and at 28 days for *Ulva* sp. ($3.23\times10^{9}\pm2.34\times10^{7}$ part g^{-1} w.w., 1.0 mg L^{-1}) with most frequent sizes of approximately 20 nm. A hypothesis F-test and a t-test were also performed to compare the variances and means of the maximum AgNPs concentration reached for the two types of seaweed exposed to 1.0 mg L^{-1}, where the variance and the means were statistically different from *Palmaria palmata* and *Ulva* sp. at a 95% of confidence level. The maximum concentration of AgNPs measured in *Ulva* sp. was higher than in *Palmaria palmata*, even when the total concentration of the element was smaller. This finding confirms again the different accumulation patterns observed for both species, representative of green and red seaweed. Then, this study contributes to increasing the knowledge about AgNPs in marine organisms after a longer-term exposure (28 days) to relatively small-size nanoparticles (15 nm) in a real marine growing media.

3.4.3 Characterization of AgNPs in seaweed enzymatic extracts by electron microscopy

The enzymatic extracts of *Palmaria palmata* and *Ulva* sp. exposed to 1.0 mg L^{-1} of PVP-AgNPs were submitted to the preconcentration and cleaning process described in **section 3.3.6**, before their deposition in the Ti grid to visualize AgNPs using STEM. **Figure 3.5.** shows the STEM micrographs for *Palmaria palmata* extracts working in TEM (**Figure 3.5.(a)**) and STEM mode (**Figure 3.5.(b)** and **Figure 3.5.(c)**), and for *Ulva* sp. extracts working in TEM (**Figure 3.5.(d)**) and STEM mode (**Figure 3.5.(e)** and **Figure 3.5.(f)**).

USC UNIVERSIDADE DE SANTIAGO DE COMPOSTELA

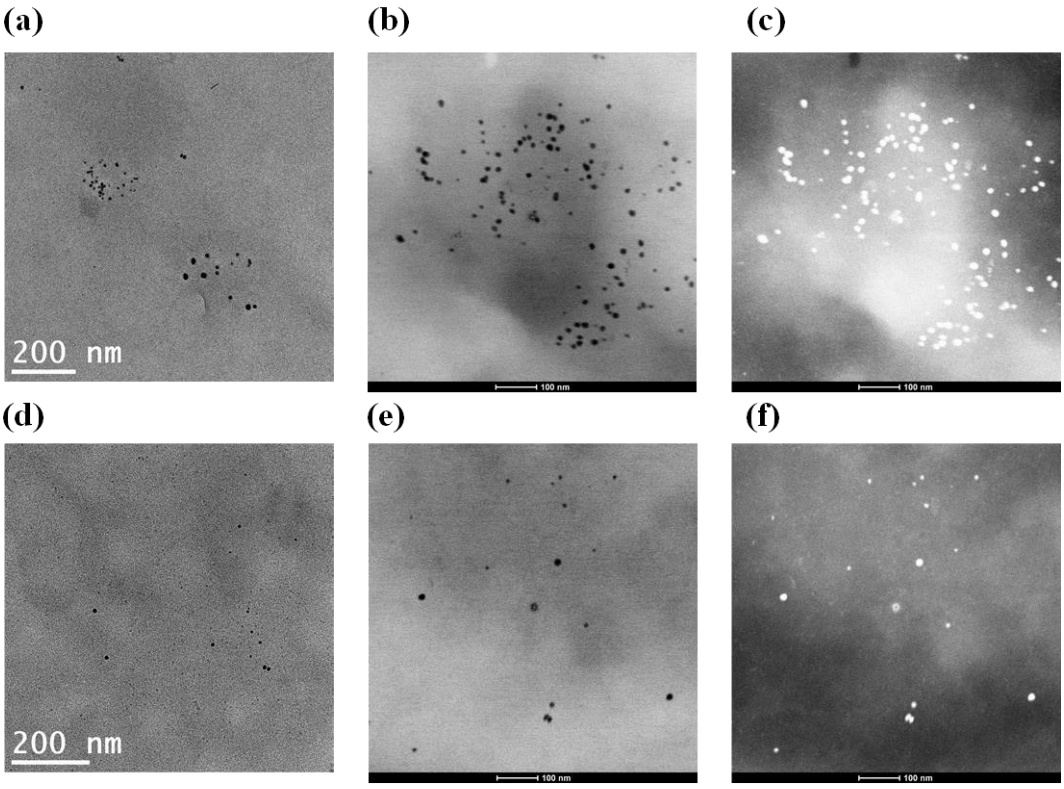

Figure 3.5. Micrographs obtained by: (a) TEM, (b) STEM bright field, and (c) STEM High Angle Annular Dark Field of enzymatic extracts *Palmaria palmata* exposed to 1.0 mg L^{-1} of PVP-AgNPs; (d) TEM, (e) STEM bright field, and (f) STEM high angle annular dark field enzymatic extracts of *Ulva* sp. exposed to 1.0 mg L^{-1} of PVP-AgNPs.

In both types of seaweed extracts, the TEM and STEM micrographs confirm the presence of spherical AgNPs. The mean sizes measured (n=200) were 24 and 20 nm for *Palmaria palmata* and *Ulva* sp., respectively. The sizes found in the TEM micrographs agreed with the most frequent sizes obtained by SP-ICP-MS for *Palmaria palmata* (between 21±1-19±4 nm) and *Ulva* sp. (between 22±1 and 20±2 nm). Furthermore, in a previous study [38], the size of the PVP-AgNPs in ultrapure water was characterized by TEM, resulting in a particle size of 24 nm. This higher size than the theoretical 15 nm of PVP-AgNPs was also in agreement with the sizes found in the enzymatic extracts by SP-ICP-MS and TEM.

3.5 CONCLUSIONS

Seaweeds are known for their ability to bioaccumulate heavy metals and trace elements. However, little is known about the ability of marine macroalgae to bioaccumulate nanomaterials and nanoparticles. We demonstrated that *Palmaria palmata* and *Ulva* sp. were bio-accumulators of AgNPs when they were subjected to the exposure experiment. Both seaweed bioaccumulated AgNPs at different rates, and the increase of total Ag and AgNPs was not proportional to the exposure concentration. Furthermore, to the best of our knowledge, there are no reports about the determination of the bioaccumulation of AgNPs in cultured seaweed (*Palmaria palmata* and *Ulva sp.*) after 28 days of exposure to 15 nm AgNPs in marine growing media. There are no regulations on maximum permitted levels of nanoparticle content in foods such as algae, so further studies about bioaccumulation and toxicity are needed to elucidate the extent to which algae may be safe for human consumption.

USC DE SANTIAGO DE COMPOSTELA

SUPPLEMENTARY INFORMATION

Table S.3.1. Total Ag content in *Palmaria palmata* and *Ulva* sp. at 0 and 28 exposure days.

		[Ag] in *Palmaria palmata* (µg g^{-1} w.w.)		[Ag] in *Ulva* sp. (µg g^{-1} w.w.)	
Tanks/ Exposure time		0 days	28 days	0 days	28 days
Control	Tank A	0.007±0.003	0.034±0.007	0.006	0.020±0.003
	Tank B	0.012±0.006	0.015±0.004	-	0.016±0.002
	Tank C	0.006±0.003	0.010±0.002	0.005	0.009±0.001
Solvent	Tank D	0.003±0.001	0.010±0.001	-	0.006±0.001
	Tank E	-	0.008±0.001	-	0.007±0.001
	Tank F	0.008±0.001	0.008±0.001	-	0.027±0.003
0.1 mg L^{-1}	Tank G	0.004±0.001	0.422±0.022	0.023±0.002	0.233±0.084
	Tank H	0.004±0.001	0.529±0.114	0.023±0.006	0.240±0.025
	Tank I	0.006±0.002	0.490±0.038	0.032±0.001	0.298±0.118
1.0 mg L^{-1}	Tank J	0.017±0.009	0.717±0.090	0.041±0.010	0.173±0.016
	Tank K	0.017±0.009	0.622±0.104	0.026±0.002	0.499±0.116
	Tank L	0.007±0.001	0.511±0.065	0.022±0.001	*

- Not detected * No data available

USC UNIVERSIDADE DE SANTIAGO DE COMPOSTELA

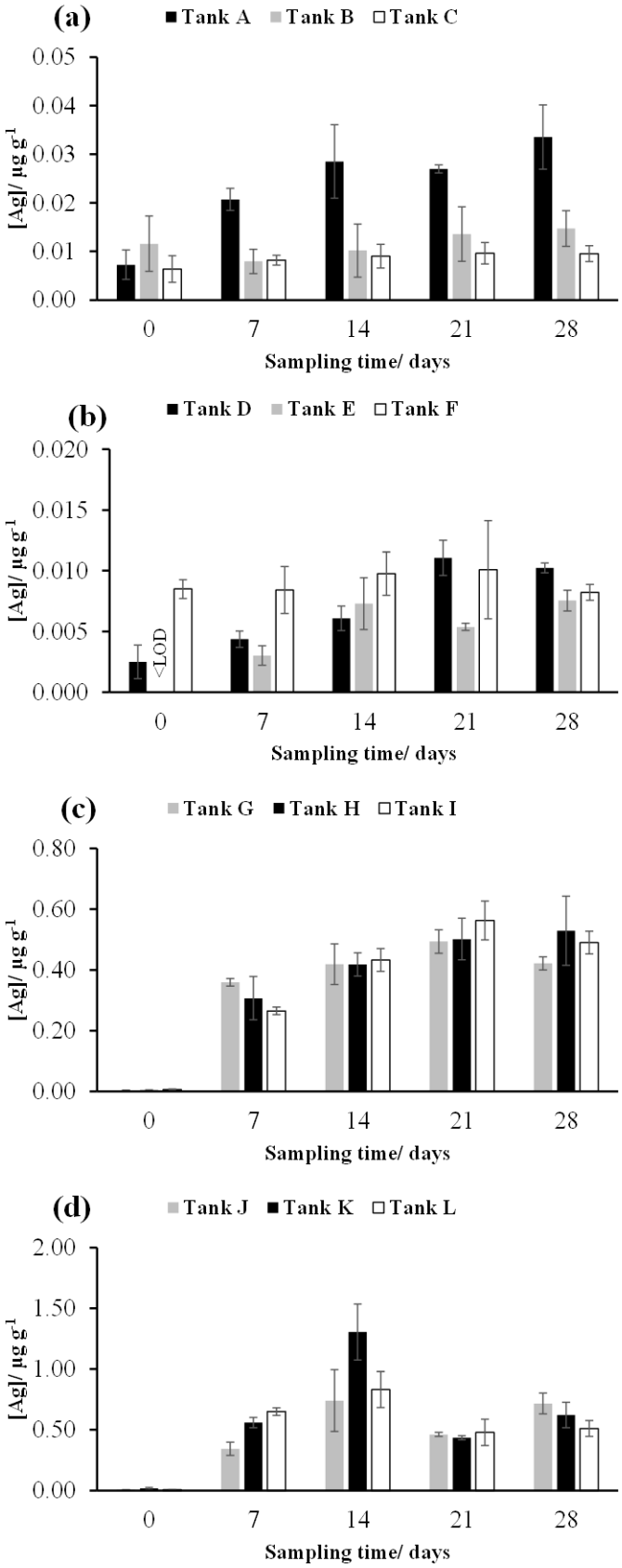

Figure S.3.1. *Palmaria palmata* total Ag bioaccumulation in control tanks (a), solvent tanks (b), 0.1 mg L^{-1} of PVP-AgNPs exposure tanks (c), and 1.0 mg L^{-1} of PVP-AgNPs exposure tanks(d).

USC UNIVERSIDADE DE SANTIAGO DE COMPOSTELA

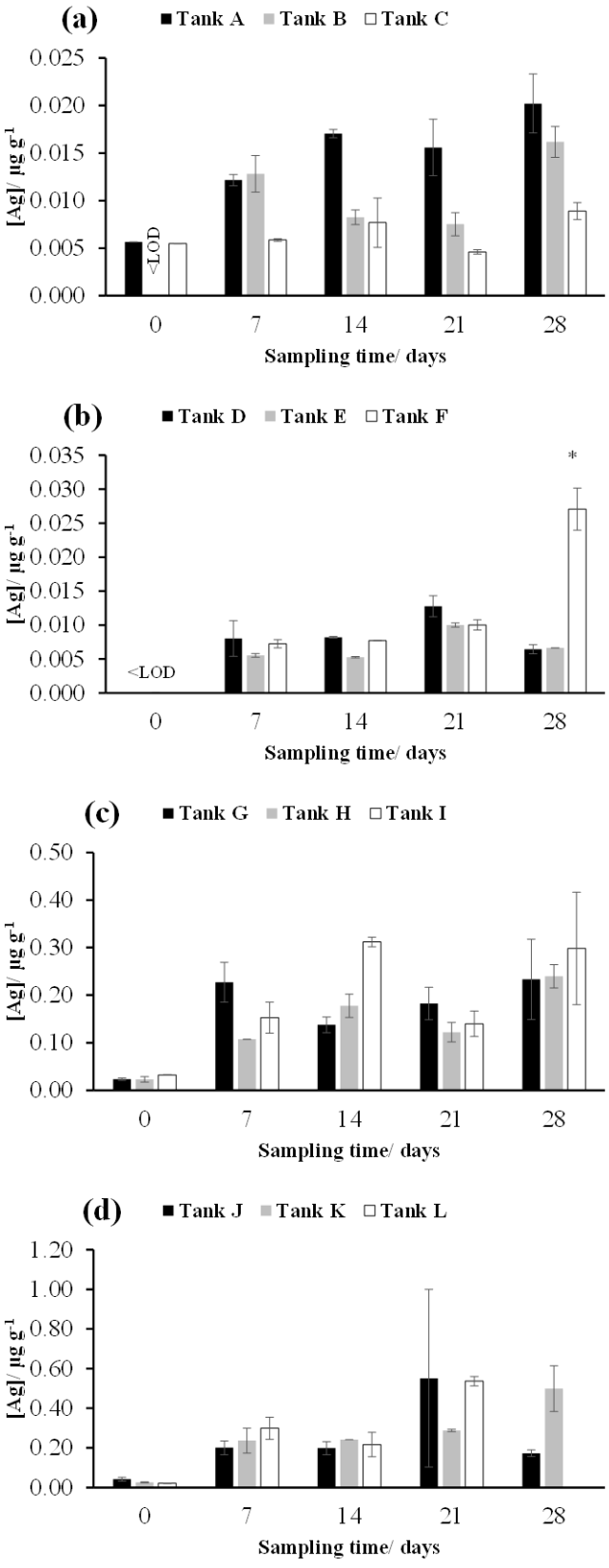

Figure S.3.2. ***Ulva*** **sp. total Ag bioaccumulation in control tanks (a), solvent tanks (b), 0.1 mg L^{-1} of PVP-AgNPs exposure tanks (c), and 1.0 mg L^{-1} of PVP-AgNPs exposure tanks(d).**
*** Not taken into account for the calculation of mean concentration.**

USC UNIVERSIDADE DE SANTIAGO DE COMPOSTELA

REFERENCES

[1] A. N. Banu, N. Kudesia, A. M. Raut, I. Pakrudheen, J. Wahengbam, Toxicity, bioaccumulation, and transformation of silver nanoparticles in aqua biota: a review, Environ. Chem. Lett. 19 (2021), 4275–4296. https://doi.org/10.1007/s10311-021-01304-w.
[2] L. Wei, J. Lu, H. Xu, A. Patel, Z. S. Chen, G. Chen, Silver nanoparticles: synthesis, properties, and therapeutic applications, Drug Discov. Today 20 (2015) 595–601. http://dx.doi.org/10.1016/j.drudis.2014.11.014.
[3] J. Pulit-Prociak, K. Stokłosa, M. Banach, Nanosilver products and toxicity, Environ. Chem. Lett. 13 (2015) 59–68. https://doi.org/10.1007/s10311-014-0490-2.
[4] G. V. Vimbela, S. M. Ngo, C. Fraze, L. Yang, D. A. Stout, Antibacterial properties and toxicity from metallic nanomaterials, Int. J. Nanomedicine 12 (2017) 3941–3965. https://doi.org/10.2147/IJN.S134526.
[5] A. Banerjee, A. Roychoudhury, Chapter 7-Nanoparticle-induced ecotoxicological risks in aquatic environments: Concepts and controversies, 129-141, Chapter in Nanomaterials in plants, algae and microorganisms. Concepts and Controversies, Elsevier Inc. All (2018). ISBN:9780128114889. https://doi.org/10.1016/B978-0-12-811488-9.00007-X.
[6] G. R. Tortella, O. Rubilar, N. Durán, M. C. Diez, M. Martínez, J. Parada, A. B. Seabra, Silver nanoparticles: Toxicity in model organisms as an overview of its hazard for human health and the environment, J. Hazard. Mater. 390 (2020) 121974. https://doi.org/10.1016/j.jhazmat.2019.121974.
[7] Q. H. Tran, V. Q. Nguyen, A. Le, Corrigendum: Silver nanoparticles: synthesis, properties, toxicology, applications and perspectives, Adv. Nat. Sci: Nanosci. Nanotechnol. 4 (2018) 033001. https://doi.org/10.1088/2043-6254/aad12b.
[8] S. Chernousova, M. Epple, Silver as antibacterial agent: ion, nanoparticle, and metal, Angew. Chem. Int. Ed. 52 (2013) 1636–1653. https://doi.org/10.1002/anie.201205923.
[9] H. Wang, K. T. Ho, K. G. Scheckel, F. Wu, M. G. Cantwell, D. R. Katz, D. B. Horowitz, W. S. Boothman, R. M. Burgess, Toxicity, bioaccumulation, and biotransformation of silver nanoparticles in marine organisms, Environ. Sci. Technol. 48 (2014) 13711-13717. https://doi.org/10.1021/es502976y.
[10] C. Levard, E. M. Hotze, G. V. Lowry, G. E. Brown, Environmental transformations of silver nanoparticles: Impact on stability and toxicity, Environ. Sci. Technol. 46 (2012) 6900–6914. https://doi.org/10.1021/es2037405.
[11] O. Choi, Z. Hu, Size dependent and reactive oxygen species related nanosilver toxicity to nitrifying bacteria, Environ. Sci. Technol. 42 (2008) 4583–4588. https://doi.org/10.1021/es703238h.
[12] E. T. Hwang, J. H. Lee, Y. J. Chae, Y. S. Kim, B. C. Kim, B. I. Sang, M. B. Gu, Analysis of the toxic mode of action of silver nanoparticles using stress-specific bioluminescent bacteria, Small 4 (2008) 746–750. https://doi.org/10.1002/smll.200700954.
[13] L. Yin, Y. Cheng, B. Espinasse, B. P. Colman, M. Auffan, M. Wiesner, J. Rose, J. Liu, E. S. Bernhardt, More than the ions: The effects of silver nanoparticles on *Lolium multiflorum*, Environ. Sci. Technol. 45 (2011) 2360–2367. https://doi.org/10.1021/es103995x.
[14] E. J. Gubbins, L. C. Batty, J. R. Lead, Phytotoxicity of silver nanoparticles to *Lemna minor* L, Environ. Pollut. 159 (2011) 1551–1559. https://doi.org/10.1016/j.envpol.2011.03.002.
[15] E. Navarro, A. Baun, R. Behra, N. B. Hartmann, J. Filser, A. J. Miao, A. Quigg, P. H. Santschi, L. Sigg, Environmental behavior and ecotoxicity of engineered nanoparticles to algae, plants, and fungi, Ecotoxicology 17 (2008) 372–386. https://doi.org/10.1007/s10646-008-0214-0.

[16] P. V. Asharani, Y. Lian Wu, Z. Gong, S. Valiyaveettil, Toxicity of silver nanoparticles in zebrafish models, Nanotechnology 19 (2008) 255102. DOI 10.1088/0957-4484/19/25/255102.
[17] P. V. AshaRani, G. L. K. Mun, M. P. Hande, S. Valiyaveettil, Cytotoxicity and genotoxicity of silver nanoparticles in human cells, Nanomaterials 3 (2009) 279–290. https://doi.org/10.1021/nn800596w.
[18] W. Lu, D. Senapati, S. Wang, O. Tovmachenko, A. K. Singh, H. Yu, P. C. Ray, Effect of surface coating on the toxicity of silver nanomaterials on human skin keratinocytes, Chem. Phys. Lett. 487 (2010) 92–96. https://doi.org/10.1016/j.cplett.2010.01.027.
[19] Y. Chae, Y. J. An, Toxicity and transfer of polyvinylpyrrolidone-coated silver nanowires in an aquatic food chain consisting of algae, water fleas, and zebrafish, Aquat. Toxicol. 173 (2016) 94–104. https://doi.org/10.1016/j.aquatox.2016.01.011.
[20] J. McTeer, A. P. Dean, K. N. White, J. K. Pittman, Bioaccumulation of silver nanoparticles into *Daphnia magna* from a freshwater algal diet and the impact of phosphate availability, Nanotoxicology 8 (2014) 305–316. https://doi.org/10.3109/17435390.2013.778346.
[21] S. Lekamge, A. F. Miranda, A. Abraham, A. S. Ball, R. Shukla, D. Nugegoda, The toxicity of coated silver nanoparticles to *Daphnia carinata* and trophic transfer from alga *Raphidocelis subcapitata*, Appl. Sci. 2 (2020) 1–20. https://doi.org/10.1371/journal.pone.0214398.
[22] F. Ribeiro, J. A. Gallego-Urrea, R. M. Goodhead, C. A. M. Van Gestel, J. Moger, A. M. V. M. Soares, S. Loureiro, Uptake and elimination kinetics of silver nanoparticles and silver nitrate by *Raphidocelis subcapitata*: The influence of silver behaviour in solution, Nanotoxicology 9 (2015) 686–695. https://doi.org/10.3109/17435390.2014.963724.
[23] L. Xiang, J. Fang, H. Cheng, Toxicity of silver nanoparticles to green algae *M. aeruginosa* and alleviation by organic matter, Environ. Monit. Assess. 190 (2018) 683. https://doi.org/10.1007/s10661-018-7022-7.
[24] M. Książyk, M. Asztemborska, R. Stęborowski, G. Bystrzejewska-Piotrowska, Toxic effect of silver and platinum nanoparticles toward the freshwater microalga *Pseudokirchneriella subcapitata*, Bull. Environ. Contam. Toxicol. 94 (2015) 554–558. https://doi.org/10.1007/s00128-015-1505-9.
[25] J. Zhang, Q. Xiang, L. Shen, J. Ling, C. Zhou, J. Hu, L. Chen, Surface charge-dependent bioaccumulation dynamics of silver nanoparticles in freshwater algae, Chemosphere 247 (2020) 125936. https://doi.org/10.1016/j.chemosphere.2020.125936.
[26] E. Gómez-Ordóñez, A. Jiménez-Escrig, P. Rupérez, Dietary fibre and physicochemical properties of several edible seaweeds from the northwestern Spanish coast, Food Res. Int. 43 (2010) 2289–2294. https://doi.org/10.1016/j.foodres.2010.08.005.
[27] S. Cofrades, I. López-Lopez, L. Bravo, C. Ruiz-Capillas, S. Bastida, M. T. Larrea, F. Jiménez-Colmenero, Nutritional and antioxidant properties of different brown and red spanish edible seaweeds, Food Sci. Technol. Int. 16 (2010) 361–370. https://doi.org/10.1177/1082013210367049.
[28] A. Y. A. Ali, A. M. Idris, M. A. H. Eltayeb, A. A. El-Zahhar, I. M. Ashraf, Bioaccumulation and health risk assessment of toxic metals in red algae in Sudanese Red Sea coast, Toxin Rev. 40 (2021) 1327–1337. https://doi.org/10.1080/15569543.2019.1697886.
[29] G. Bonanno, M. Orlando-Bonaca, Trace elements in Mediterranean seagrasses and macroalgae. A review, Sci. Total Environ. 618 (2018) 1152–1159. https://doi.org/10.1016/j.scitotenv.2017.09.192.
[30] M. Sinaei, M. Loghmani, M. Bolouki, Application of biomarkers in brown algae (*Cystoseria indica*) to assess heavy metals (Cd, Cu, Zn, Pb, Hg, Ni, Cr) pollution in the northern coasts of the Gulf of Oman, Ecotoxicol. Environ. Saf. 164 (2018) 675–680. https://doi.org/10.1016/j.ecoenv.2018.08.074.

[31] A. Turner, D. Brice, M. T. Brown, Interactions of silver nanoparticles with the marine macroalga, *Ulva lactuca*, Ecotoxicology 21 (2012) 148–154. https://doi.org/10.1007/s10646-011-0774-2.
[32] A. A. Sfriso, M. Mistri, C. Munari, I. Moro, M. Wahsha, A. Sfriso, A. S. Juhmani, Hazardous effects of silver nanoparticles for primary producers in transitional water systems: The case of the seaweed *Ulva rigida* C. Agardh, Environ. Int. 131 (2019) 104942. https://doi.org/10.1016/j.envint.2019.104942.
[33] S. Siddiqui, G. Bielmyer-Fraser, Accumulation and effects of dissolved and nanoparticle silver and copper in two marine seaweed species, Georg. J. Sci. 77 (2019) 1.
[34] J. J. López-Mayán, B. Álvarez-Fernández, E. Peña-Vázquez, M. C. Barciela-Alonso, A. Moreda-Piñeiro, P. Bermejo-Barrera, Ultrasonication followed by enzymatic hydrolysis as a sample pre-treatment for the determination of Ag nanoparticles in edible seaweed by SP-ICP-MS, Talanta 247 (2022) 123556. https://doi.org/10.1016/j.talanta.2022.123556.
[35] F. Laborda, A. C. Gimenez-Ingalaturre, E. Bolea, J. R. Castillo, About detectability and limits of detection in single particle inductively coupled plasma mass spectrometry, Spectrochim. Acta-Part B At. Spectrosc. 169 (2020) 105883. https://doi-org.ezbusc.usc.gal/10.1016/j.sab.2020.105883.
[36] H. Lee, J. Park, K. Shin, S. Depuydt, S. Choi, J. De Saeger, T. Han, Application of a programmed semi-automated *Ulva pertusa* bioassay for testing single toxicants and stream water quality, Aquat. Toxicol. 221 (2020) 105426. https://doi.org/10.1016/j.aquatox.2020.105426.
[37] S. Agnihotri, S. Mukherji, S. Mukherji, Size-controlled silver nanoparticles synthesized over the range 5–100 nm using the same protocol and their antibacterial efficacy, RSC Adv. 4 (2014) 3974–3983. https://doi.org/10.1039/C3RA44507K.
[38] M. J. Araújo, M. L. Sousa, E. Fonseca, A. Barreiro-Felpeto, J. C. Martins, M. Vázquez, N. Mallo, L. Rodriguez-Lorenzo, M. Quarato, I. Pinheiro, M. V. Turkina, J. J. López-Mayán, E. Peña-Vázquez, M. C. Barciela-Alonso, M. Spuch-Calvar, M. Oliveira, P. Bermejo-Barrera, S. Cabaleiro, B. Espiña, V. Vasconcelos, A. Campos, Proteomics reveals multiple effects of titanium dioxide and silver nanoparticles in the metabolism of turbot, *Scophthalmus maximus*, Chemosphere 308 (2022) 136110. https://doi.org/10.1016/j.chemosphere.2022.136110.

USC UNIVERSIDADE DE SANTIAGO DE COMPOSTELA

USC
UNIVERSIDADE
DE SANTIAGO
DE COMPOSTELA

CHAPTER 4. BIOACCUMULATION OF TITANIUM DIOXIDE NANOPARTICLES IN GREEN (*Ulva* sp.) AND RED (*Palmaria palmata*) SEAWEED

USC
UNIVERSIDADE DE SANTIAGO DE COMPOSTELA

USC
UNIVERSIDADE
DE SANTIAGO
DE COMPOSTELA

CHAPTER 4. BIOACCUMULATION OF TITANIUM DIOXIDE NANOPARTICLES IN GREEN (*Ulva* sp.) AND RED (*Palmaria palmata*) SEAWEED*

*The results from this chapter have already been accepted for publication as Juan José López-Mayán[1], Blanca Álvarez-Fernández[1], Elena Peña-Vázquez[1], María Carmen Barciela-Alonso[1], Antonio Moreda Piñeiro[1], Julie Maguire[2], Mick Mackey[2], Monica Quarato[3], Ivone Pinheiro[3], Begoña Espiña[3], Laura Rodríguez-Lorenzo[3], Pilar Bermejo-Barrera[1], Bioaccumulation of titanium dioxide nanoparticles in green (*Ulva* sp.) and red (*Palmaria palmata*) seaweed, Microchim Acta 190 (2023) 287. https://doi.org/10.1007/s00604-023-05849-1.

[1] Trace Element, Spectroscopy and Speciation Group (GETEE), Instituto de Materiais (iMATUS), Faculty of Chemistry, University of Santiago de Compostela, Av. das Ciencias, s/n 15782, Santiago de Compostela, Spain. [2] Indigo Rock Marine Research, Gearhies, Bantry, Co. Cork, P75 AX07, Ireland. [3] International Iberian Nanotechnology Laboratory, Av. Mestre José Veiga, s/n, 4715-330, Braga, Portugal.

4.1 ABSTRACT

A bioaccumulation study in red (*Palmaria palmata*) and green (*Ulva* sp.) seaweed has been carried out after exposure to different concentrations of citrate-coated titanium dioxide nanoparticles (5 and 25 nm) for 28 days. The concentration of total Ti and the number and size of accumulated nanoparticles in the seaweeds has been determined throughout the study by inductively coupled plasma mass spectrometry (ICP-MS) and single particle-ICP-MS (SP-ICP-MS), respectively. Ammonia was used as reaction gas to minimize the effect of the interferences in the ^{48}Ti determination by ICP-MS. Ti concentrations measured in *Ulva* sp. were higher than those found in *Palmaria palmata* for the same exposure conditions. The maximum concentration of Ti (61.96±15.49 μg g^{-1}) was found in *Ulva* sp. after 28 days of exposure to 1.0 mg L^{-1} of 5 nm TiO_2NPs. The concentration and sizes of TiO_2NPs determined by SP-ICP-MS in alkaline seaweed extracts were similar for both seaweeds exposed to 5 and 25 nm TiO_2NPs, which indicates that probably the element is accumulated in *Ulva* sp. mainly as ionic Ti or nanoparticles smaller than the limit of detection in size (27 nm). The internalization of TiO_2NPs in *Ulva* sp. was confirmed by electron microscopy (TEM/STEM) in combination with Energy Dispersive X-Ray analysis (EDX).

4.2 INTRODUCTION

Titanium dioxide (TiO_2), known as titanium white or titania, is a metallic oxide widely used in the industry as a pigment due to its high refractive index, brightness, and resistance to discoloration [1,2]. Despite the widespread use of TiO_2, the European Food Safety Authority (EFSA) concluded that it cannot be considered safe for human health [3], and the European Union has implemented a regulation to ban the use of food additive E171 since February 2022 [4]. TiO_2 had been also classified as possibly carcinogenic to humans by the International Agency for Research on Cancer (IARC) [5].

There is consensus in scientific studies that indicate that the rise in the use and production of nanomaterial (NMs) increases their release into the environment (through air, soil, and water)

[1]. Then, titanium dioxide nanoparticles (TiO_2NPs) can enter the marine systems and interact [6] and endanger the biota [7]. There are a couple of published review papers with information about the nanotoxicity of TiO_2NPs in marine organisms [8,9], and several recent studies have evaluated the interaction and toxic effects of TiO_2NPs in marine microalgae *Dunaliella tertiolecta* [10], *Dunaliella salina* and *Chlorella* sp. [11]. Bhuvaneshwari et al. [12] also studied the trophic transfer of 25 nm TiO_2NPs from *Dunaliella salina* to crustacean *Artemia salina* in terms of toxicity and accumulation. However, information is still lacking about the accumulation and effects of NPs in marine macroalgae (seaweed).

Seaweed are bioconcentrator organisms, and their use is increasing in the food industry not only as gelling agents or food supplements but also as a potential source of fiber, nutrients, and trace elements [13,14]. Therefore, they can act as a vector of NPs through the food chain and can be transferred to humans. Some authors studied the presence and the bioaccumulation of heavy metals in seaweed [15]. Ryan et al. [16] studied the distribution of Pb, Zn, As, Cd, Co, Cr, Cu, Mn, and Ni in *Polysiphonia lanosa*, *Ascophyllum nodosum*, *Fucus vesiculosus,* and *Ulva* sp. from the south of Ireland. Jarvis et al. [17] reported the accumulation of Cu, Ni, Pb, Cd, and Zn in *Ulva lactuca* and *Agardhiella subulate* exposed to the metals individually and in mixtures (100 and 1000 μg L^{-1}) for 48 h. The distribution of metals in both seaweed species changed with increasing metal exposure concentrations. *U. lactuca* exposed to single metals showed higher concentrations as compared to exposure to metal mixtures, with Cu and Zn generally accumulating to the highest magnitudes. Carvalho et al. [18] studied the presence of heavy metals including Ti in different parts (base, stipe, reproductive organs, and growing tips) of *Fucus vesiculosis* by energy-dispersive X-ray fluorescence. Misher et al. evaluated the metal uptake (including Ti) of *Caulerpa racemosa* [19], *Ulva lactuca* [20], *Gelidium abbottiorum* [21], and *Plocamium corallorhirza* [22] from the coast of South Africa. Desideri et al. [23] measured 21 elements (including Ti) in 14 edible seaweed bought in Italy, and Corrias et al. [24] reported the environmental evaluation of heavy metals and metalloids (Al, As, B, Ba, Be, Cd, Co, Cr, Cu, Fe, Hg, Mn, Mo, Ni, Pb, Sb, Se, Sn, Sr, Te, Ti, V, and Zn) in seaweeds (*Padina pavonica*, and *Cystoseria mediterranea*) from the Mediterranean Sea, where Ti was found in all seaweed specimen from all sampling zones (n=3). There are also a few studies about the interactions and uptake of AgNPs by *Ulva lactuca* [25], and CuONPs by *Ulva lactuca* and *Agardhiella subulate* [26], and *Ulva rigida* [27] after short term exposure (less than 72 hours).

However, to the best of our knowledge, there are no reports available in the scientific literature about bioaccumulation assays in edible macroalgae exposed to TiO_2NPs. This research work aims to study the bioaccumulation of TiO_2NPs in two red and green edible seaweeds (*Palmaria palmata* and *Ulva* sp.) exposed to different sizes (25 and 5 nm in diameter) and concentrations of citrate coated-TiO_2NPs for 28 days. The variation in the trend of total Ti and nanoparticulate content (number and TiO_2NPs size) with exposure time was evaluated by inductively coupled plasma mass spectrometry (ICP-MS) and single particle-ICP-MS (SP-ICP-MS), respectively. TEM/SEM combined with EDX were used to find the localization of TiO_2NPs in some of the specimens studied.

4.3 MATERIALS AND METHODS

4.3.1 Instrumentation

For total Ti quantification, an inductively coupled plasma mass spectrometer (ICP-MS) NexION® 2000 (Perkin Elmer, Waltham, MA, USA) equipped with dynamic reaction cell (DRC) technology, was used. The Syngistix™ Nano Application 2.5 software (PerkinElmer) allows working in the single-particle mode (SP-ICP-MS) to obtain TiO_2NPs concentration and

size distributions. An Ethos Plus microwave lab station (Milestone, Bergamo, Italy) was used for sample acid digestion. An USC 300 TH ultrasound water bath (ultrasound frequency of 45 kHz, 80 W) from VWR (Radnor, PA, USA) was used for TiO_2NPs isolation.

The analysis of the size and shape of the TiO_2NPs stocks was performed using JEOL 2100 Transmission Electron Microscopy (TEM) operating at 200 kV (Izasa Scientific, Carnaxide, Portugal) for 25 nm TiO_2NPs and FEI Titan Cubed Themis 60-300 kV operating at 200 kV (Thermo Fisher Scientific, Portugal) for 5 nm TiO_2NPs. The colloidal stability was characterized by dynamic light scattering and zeta potential using the SZ-100 device (Horiba, ABX SAS, Amadora, Portugal). The nano crystallite size of 5 nm TiO_2NPs was estimated by XRD pattern using the Scherrer equation. XRD pattern was collected on a X'Pert PRO diffractometer (PANalytical) set at 45 kV and 40 mA, using Cu Kα radiation (λ = 1.541874 Å) and a PIXcel detector.

Scanning electron microscopy (SEM) images for the 5 nm TiO_2NPs localization and identification on seaweed surface were obtained with a FEI Quanta 650 FEG SEM in combination with Energy Dispersive X-Ray analysis (EDX), with an Everhart-Thornley secondary electron (ETD) operating at high vacuum, at an acceleration voltage of 10 kV and spot size of 3.0 (FEI Europe B.V.). SEM images for 25 nm TiO_2NPs were acquired using a Helios G2 NanoLab 450S dual-beam focused ion beam SEM in combination with EDX, with an Everhart-Thornley secondary electron (ETD) operating at high vacuum, at an acceleration voltage of 10 kV (FEI Europe B.V). The obtained data from EDX were treated using Origin 9.0. The SEM samples were coated with conductive carbon using an EM ACE600 coating system (Leica microsystems).

The analysis of the internalization of NPs and their identification was carried out by high-resolution TEM (HRTEM) and HR scanning TEM (HRSTEM) coupled with EDX using a Probe-Corrected FEI Titan G2 ChemiSTEM TEM operating at an acceleration voltage of 80 kV for 25 nm TiO_2NPs exposed samples and FEI Titan (G3) Cubed Themis 60-300 kV, operating at 60 kV for 5 nm TiO_2NPs exposed samples. The TEM samples were prepared using an EM TP Tissue processor (Leica microsystems) and the ultrathin sections (70 – 80 nm thick) were prepared using a PowerTome PC ultramicrotome (RMC Boeckeler, USA).

4.3.2 Reagents

Commercially available 25 nm TiO_2NPs and 5 nm TiO_2NPs powders were supplied by Sigma-Aldrich (Merk Life science, product code: 718467; 99.5% purity, with a mixture of rutile and anatase) and Nanostructured & Amorphous Materials, Inc. (Katy, TX, USA; anatase, 5 nm size, 99%) respectively, and used without any further purification. The citrate NPs stock dispersions were prepared in ultrapure water (see supplementary information).

Ultrapure water (18 MΩ cm of resistivity), obtained from a Milli-Q® IQ7003 (Millipore Co., Bedford, MA, USA) purification system, was used as the main solvent to prepare solutions. A Ti ionic standard of 1000 mg L^{-1} H_2O/0.24% F^- (Perkin Elmer, Shelton, USA) was employed to prepare the calibration standards for ICP-MS and SP-ICP-MS measurements. For microwave-assisted acid digestion, 69% (w/v) nitric acid (SUPRAPUR®, Sigma Aldrich, Darmstadt, Germany) and 33% (w/v) hydrogen peroxide (ACS, ISO, AppliChem Panreac, Barcelona, Spain) were used. Tetramethylammonium hydroxide (TMAH) 25% (v/v) solution in water (Merck, Darmstadt Germany) was used for the basic ultrasound-assisted extraction. Glycerol for analysis (ACS, EMSURE®, Merck, Darmstadt, Germany) was used for dilution of the TMAH extracts before SP-ICP-MS analysis. Gold ionic standard of 1000 mg L^{-1} in 2 mol L^{-1} HCl (Merck, Darmstadt, Germany), and a suspension of Gold Nanospheres of 50 nm (49.6 nm by TEM) and 9.89×10^6 NPs mL^{-1} (NanoComposix, San Diego, California, USA) in aqueous

1 mM citrate, were used to calculate the transport efficiency in SP-ICP-MS. Argon and ammonia (both with 99.999% of purity) from Nippon Gases (Madrid, Spain), were required for ICP-MS operation.

To prepare the samples for TEM analysis, paraformaldehyde, sodium cacodylate trihydrate (Sigma-Aldrich, Merck Life Science, Algés, Portugal); glutaraldehyde (25% in water, specially purified for use as an electron microscopy fixative; Agar Scientific, Dias de Sousa S.A, Alcochete, Portugal); propylene oxide (ReagentPlus® ≥ 99%; Sigma-Aldrich, Merck Life Science, Algés, Portugal); osmium tetroxide (2% and 4% aqueous solution), epoxy resin (EMBed-812 kit) (Science Services, Munich, Germany); and ethanol were used for the fixation, dehydration and resin embedding of the tissue.

4.3.3 Seaweed sample cultivation and exposure to TiO_2NPs

The Ti dioxide nanoparticles bioaccumulation assays were performed in two kinds of edible seaweed species, *Palmaria palmata* (Dulse), and *Ulva* sp. (Sea lettuce). Besides, two sizes of TiO_2NPs (25 and 5 nm TiO_2NPs, both citrate-coated), and two different exposure doses (nominal concentrations of 0.1 and 1.0 mg L^{-1} TiO_2NPs) were evaluated in the study. In total, four trials were carried out at different times. These bioaccumulation trials consisted of (1) *Palmaria palmata* exposed to 25 nm TiO_2NPs, (2) *Palmaria palmata* exposed to 5 nm TiO_2NPs, (3) *Ulva* sp. exposed to 25 nm TiO_2NPs, and (4) *Ulva* sp. exposed to 5 nm TiO_2NPs.

Details about seaweed sample cultivation and exposure to TiO_2NPs are included in the supplementary information. Three seaweed sample replicates were collected from each tank on days 0, 7, 14, 21, and 28 for analysis by ICP-MS, TEM, and SEM.

Seaweed sample preparation for SEM and TEM analysis was carried out after 28 days of exposure to TiO_2NPs. Two seaweed samples of each specie from each treatment group were used to collect 0.7 cm square fragments of seaweed leaf. The fragments were fixated overnight at 4 ºC in Karnovsky fixative solution, which involves a mixture of 2% paraformaldehyde and 2.5% glutaraldehyde in 0.1 M sodium cacodylate buffer. These fragments were stored at 4 ºC under shaking for later use. The bigger fragments of the seaweed (around 2 cm squares) were fixated in 10% neutral buffered formalin for 48 h (replacing the formalin solution every 24) and subsequently stored in 70% ethanol at room temperature until further use. The SEM and TEM fragments were stored until their processing routine for electron microscopy (EM) analysis.

4.3.4 Microwave-assisted acid digestion

A microwave-assisted acid digestion method is necessary to destroy the seaweed matrix for total Ti determination by ICP-MS. Seaweed samples were digested with a mixture of nitric acid and hydrogen peroxide following the method described in previous work [28]. The digested samples were diluted with ultrapure water (dilutions 1:10 to 1:100) until 25 mL before their analysis by ICP-MS. This procedure was applied in triplicate to each sample, and two blanks were prepared for each set of experiments.

4.3.5 TMAH ultrasound-assisted TiO_2NPs extraction

A basic extraction with 2.5 % tetramethylammonium hydroxide (TMAH) was selected to isolate TiO_2NPs from the seaweed matrix without changing the primary size, and concentration of the metal particles. This procedure was developed in a previous study carried out in our laboratory [28], and it was applied in triplicate to each sample; two blanks were prepared for each set of operational conditions or day of analysis. Finally, the extracts were diluted with 1% (v/v) glycerol before SP-ICP-MS analysis (dilutions from 1:100 to 1:6000).

USC UNIVERSIDADE DE SANTIAGO DE COMPOSTELA

4.3.6 Total Ti determination by ICP-MS and TiO_2NPs analysis by SP-ICP-MS

Total Ti concentration in the digested samples was determined by the ICP-MS, using the conditions listed in **Table S.4.1.(a)** (supplementary information). The Dynamic Reaction Cell (DRC), with ammonia as reaction gas (flow rate 1.0 mL min^{-1}), was used to minimize interferences in the determination of Ti. The purpose of ammonia is to form the Ti-NH_3 cluster [$^{48}Ti^{14}N^{1}H(^{14}N^{1}H_3)_4^+$] of *m/z* 131 [29]. Standard addition calibration with ionic Ti concentrations between 0 and 50.0 µg L^{-1}, was used to correct the matrix effect.

The TiO_2NPs content was measured in the alkaline extracts using the operational conditions of SP-ICP-MS (DRC mode) that are listed in **Table S.4.1.(b)**. Transport efficiency (TE (%)) was automatically calculated by the software Syngistix™ Nano after the introduction of an ionic gold calibration from 0 to 3.0 µg L^{-1}, and Au nanospheres (49.6 nm in size) at a concentration of 9.89×10^4 particles mL^{-1}. SP-ICP-MS measurements were performed using a Ti external calibration prepared in ultrapure water in a concentration range between 0 to 10.0 µg L^{-1}. TMAH extracts were diluted with 1 % (v/v) glycerol before SP-ICP-MS analysis. Finally, the TiO_2NPs concentration and size distributions in the diluted extracts were directly obtained from the software after analysis and used to calculate the concentrations in the seaweed samples.

4.3.7 Localization and identification of TiO_2NPs on/in seaweed tissue by electron microscopy techniques.

SEM coupled with EDX analysis of both fixated TiO_2NPs exposed *Palmaria palmata* and *Ulva* sp. fragments were performed to study the interaction/association of both TiO_2NPs, 5 and 25 nm, with the seaweed' surface as well as their identification by EDX. The fixated fragments were cut into smaller pieces of < 10 mm square, placed on pin stubs (Standard 12.7 mm, 8 mm pin length, Ted Pella) and subsequently coated with conductive carbon using an EM ACE600 coating system (Leica microsystems). The samples were analyzed using the SEM-EDX system described in **section 4.3.1**.

The internalization and localization of both TiO_2NPs as well as their identification were investigated via 28 days of exposure to both seaweeds by STEM-EDX. The fixated fragments were subjected to a TEM processing routine. Osmium tetroxide solution at 1% was used for the post-fixation step. The fragments were dehydrated by sequential washings in increasing solutions in ethanol until 100% and finally with propylene oxide. This was also used for gradual impregnation with the epoxy resin. The fragments were placed in silicone moulds with resin and left for three days to cure at 60°C. Ultrathin sections (≈80 nm thick) were made in an ultramicrotome (**section 4.3.1**), with a diamond knife (Diato), and placed on formavar/carbon 200 mesh grids. TEM and STEM micrographs of the sections and the EDX mapping were acquired with the electron microscopes described in **section 4.3.1**.

4.4 RESULTS AND DISCUSSION

4.4.1 TiO_2NPs characterization

The initial stock dispersions of citrate-25 nm TiO_2NPs and citrate-5 nm TiO_2NPs were characterized by TEM, DLS, and zeta potential. **Figure S.4.1.** (supplementary section) shows representative TEM images of both NPs dispersed in ultrapure water at a concentration of 50 mg L^{-1}. TEM images show that both NPs tend to form aggregates. The size of primary particles of the citrate-25 nm TiO_2NPs can be estimated as 29±10 nm; however, this estimation for citrate-5 nm TiO_2NPs was not possible despite having used an aberration-corrected HRTEM because the NPs overlap each other in the aggregate. The nano crystallite size of this 5 nm TiO_2NPs was calculated by X-Ray diffraction (XRD) pattern using the Scherrer equation [30],

obtaining a size of 8.6 nm (**Figure S.4.2.**). The sonication of TiO_2NPs standards was necessary to avoid the common phenomena of TiO_2NPs aggregation.

Table S.4.2. shows the characterization of both NPs before exposure to ultrapure water and artificial seawater at 50 mg L^{-1} of concentration, by DLS and zeta potential. The TiO_2 NPs in extracts of exposed seaweed were analyzed by SP-ICP-MS, previous dilution with glycerol 1% (v/v) and sonication. The NPs sizes obtained were bigger than their primary size, and smaller sizes were obtained in seaweed extracts (128 nm versus 52 nm for citrate-25 nm TiO_2NPs, and 65 nm versus 48 nm for citrate-5 nm TiO_2NPs). This could be attributed to the variation of the aggregation degree produced by the addition of the nanoparticles prepared in F2P growing media and mixed with phytoplankton, to the possible interaction of the algae' polysaccharides or other components such as polyphenols [31], and subsequently the TMAH extraction and sonication previous to analysis.

The colloidal stability was also analyzed in artificial seawater since the bioaccumulation assays were performed with marine algae cultured in a medium based on seawater. Both TiO_2NPs aggregated immediately after their dispersion in artificial seawater as shown in the DLS analysis (**Table S.4.2.**). The Z-potential values were almost zero in this medium for both NPs, which supports the NPs' destabilization due to the very high ionic strength of the seawater (i.e. high concentration of salts) [32].

4.4.2 Total Ti determination in seaweed samples exposed to TiO_2NPs

The total Ti concentration was determined following the procedure described in **section 4.3.6**. Average concentrations were calculated using the nine replicates of seaweed taken from the three tanks with the same exposure dose (3 replicates per tank and sampling day). The limit of detection (LOD) and the limit of quantification (LOQ) were 1.5 and 4.8 ng g^{-1}, respectively. The repeatability (n=5) in the measurements resulted in a relative standard deviation (RSD) <6% and the analytical recovery percentages were 91±5% and 113±5%, respectively for 0.5 and 10.0 µg L^{-1} of Ti added (n=5).

4.4.2.1 Variation of total Ti content in *Palmaria palmata* (red seaweed)

Ti was determined in *Palmaria palmata* exposed to different concentrations of TiO_2NPs of two different sizes (25 and 5 nm) for 28 days by ICP-MS. **Figure 4.1.** shows the mean concentrations and standard deviations of Ti in *Palmaria palmata* exposed to these NPs. **Table S.4.3.** shows the ranges of total Ti content (0-28 days) in *Palmaria palmata* for control, solvent, low exposure dose (0.1 mg L^{-1} of 25 nm TiO_2NPs or 5 nm TiO_2NPs), and high exposure dose (1.0 mg L^{-1} of 25 nm TiO_2NPs or 5 nm TiO_2NPs) tanks.

USC UNIVERSIDADE DE SANTIAGO DE COMPOSTELA

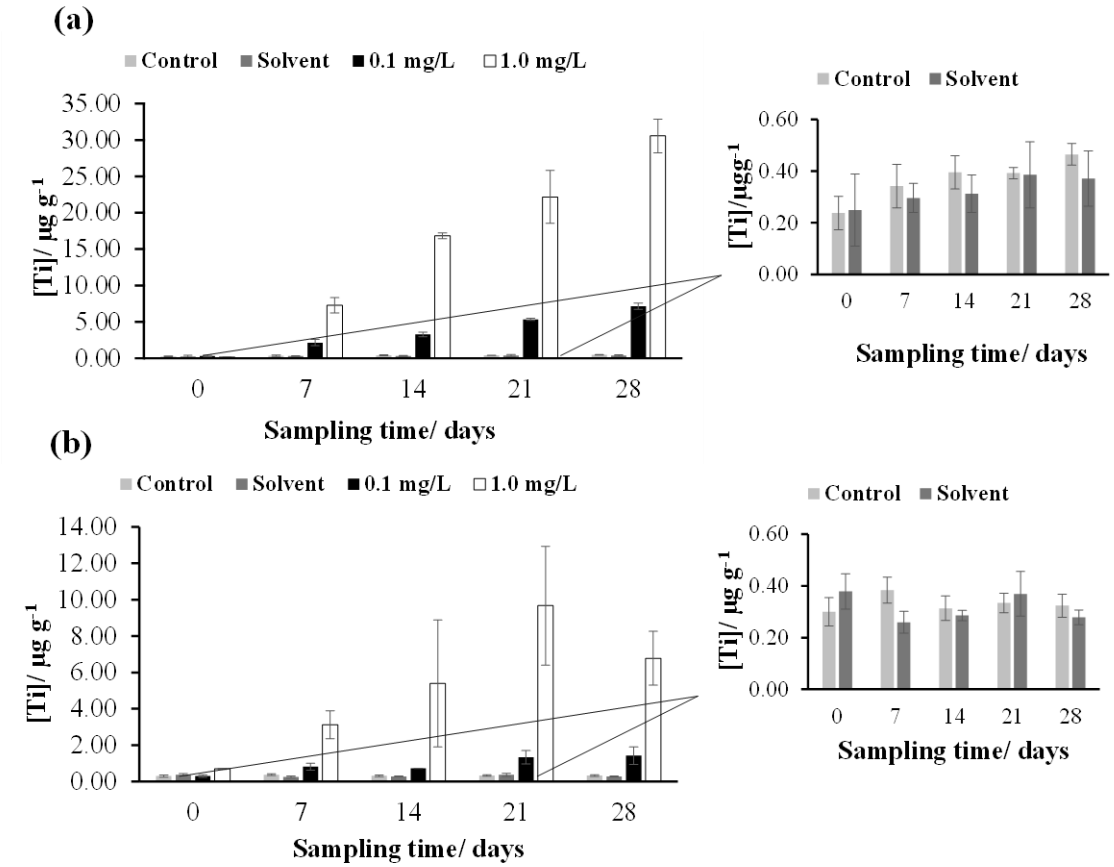

Figure 4.1. Total Ti bioaccumulation in *Palmaria palmata* exposed to: (a) 25 nm TiO_2NPs and (b) 5 nm TiO_2NPs for 28 days.

These results showed that Ti bioaccumulation in *Palmaria palmata* exposed to 25 nm TiO_2NPs, at a high exposure dose, increased with time until 28 days. Lower bioaccumulation was observed for *Palmaria palmata* exposed to 5 nm TiO_2NPs, and the results showed greater variability. As can be observed, Ti concentration increased with the sampling time until 21 days, for seaweeds exposed to 1.0 mg L^{-1} of these NPs, and then decreased.

Figure S.4.3. shows in detail the total Ti concentrations measured in seaweed grown in control (**Figure S.4.3.(a)**), solvent (**Figure S.4.3.(b)**), 0.1 mg L^{-1} 25 nm TiO_2NPs (**Figure S.4.3.(c)**), and 1.0 mg L^{-1} 25 nm TiO_2NPs (**Figure S.4.3.(d)**) media for 28 days. As can be observed in the figure, Ti concentration in control tanks and in citrate-containing tanks remained approximately constant with exposure time (from 0 to 28 days). In both cases, the P-values obtained after the application of a one-way ANOVA test were greater than 0.05 (software Statgraphics XVIII, Warrenton, USA); then, no statistically significant differences were observed between the averages from the different sampling days at a 95 % of the significance level. The concentrations of Ti in seaweed grown in tanks exposed to 0.1 mg L^{-1} and 1.0 mg L^{-1} 25 nm TiO_2NPs increased with the exposure time up to 7.15±0.43 µg g^{-1}, and 30.55±2.31 µg g^{-1} (both at day 28; values mean of three tanks), respectively. The accumulation was dose-dependent, and the concentration measured was 4.3 higher after exposure to 1.0 mg L^{-1} 25 nm TiO_2NPs. There were significant variations in the average concentrations of Ti (P-value <0.05). The multiple range test confirmed a linear increase in the concentration of Ti with time in seaweed exposed to 0.1 mg L^{-1}, but in the case of seaweed exposed to 1.0 mg L^{-1}, there was

USC UNIVERSIDADE DE SANTIAGO DE COMPOSTELA

an increase in the concentration till day 14, and no significant differences between the concentrations were determined in days 14 and 21.

Figure S.4.4. shows in detail the total Ti concentration measured in seaweed grown in control (**Figure S.4.4.(a)**), solvent (**Figure S.4.4.(b)**), 0.1 mg L^{-1} of 5 nm TiO_2NPs (**Figure S.4.4.(c)**), and 1.0 mg L^{-1} of 5 nm TiO_2NPs (**Figure S.4.4.(d)**) media for 28 days. Ti concentration in control and solvent tanks remained constant with exposure time and no significant differences were found between the average concentrations at the sampling days (in both cases P-value was higher than 0.05). Ti concentrations in seaweed exposed to 0.1 mg L^{-1} and 1.0 mg L^{-1} of 5 nm TiO_2NPs increased with the exposure time up to 1.42±0.48 µg g^{-1} and 6.78±1.48 µg g^{-1} (both at day 28), respectively. The ANOVA tests showed significant differences in concentrations between the sampling days (P-value<0.05) for *Palmaria palmata* exposed to 0.1 and 1.0 mg L^{-1}. However, the multiple range test did not show significative differences between 7, 14, 21, and 28 days, and between 14, 21, and 28 days for *Palmaria palmata* exposed to 0.1 and 1.0 mg L^{-1} of 5 nm TiO_2NPs, respectively.

4.4.2.2 Variation of total Ti content in *Ulva* sp. (green seaweed)

Ti was determined in *Ulva* sp. exposed to different concentrations of the element present as TiO_2NPs nanoparticles of two different sizes (25 and 5 nm) by ICP-MS. **Figure 4.2.** shows the mean concentration of Ti measured in the tanks and the total Ti bioaccumulation pattern in *Ulva* sp. exposed to 25 nm (**Figure 4.2.(a)**) and 5 nm TiO_2NPs (**Figure 4.2.(b)**). Total Ti concentration ranges (0-28 days) in *Ulva* sp. for control, solvent, low exposure dose (0.1 mg L^{-1} of 25 nm TiO_2NPs or 5nm TiO_2NPs) and high exposure dose (1.0 mg L^{-1} of 25 nm TiO_2NPs or 5 nm TiO_2NPs) tanks are shown in **Table S.4.3.**

Figure S.4.5. also shows the total Ti concentration in seaweed grown in control (**Figure S.4.5.(a)**), solvent (**Figure S.4.5.(b)**), 0.1 mg L^{-1} of 25 nm TiO_2NPs (**Figure S.4.5.(c)**), and 1.0 mg L^{-1} of 25 nm TiO_2NPs (**Figure S.4.5.(d)**) media.

USC UNIVERSIDADE DE SANTIAGO DE COMPOSTELA

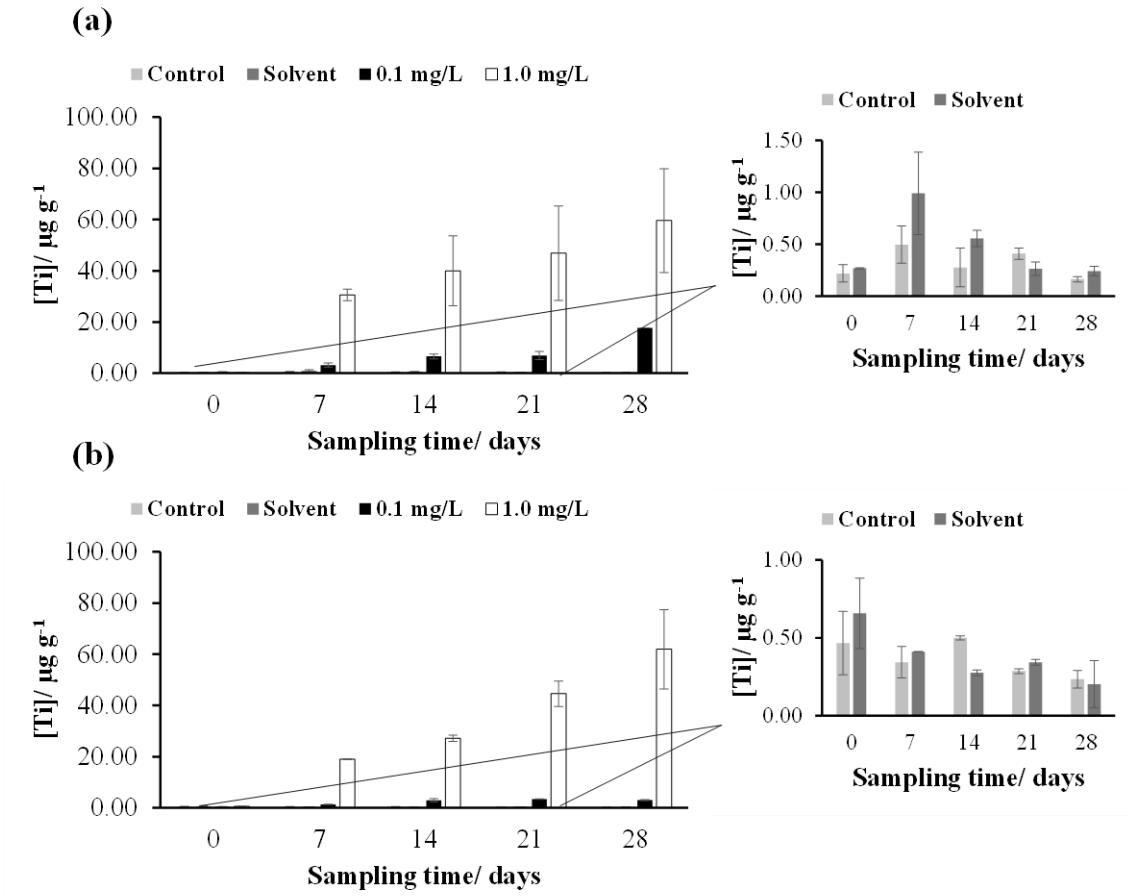

Figure 4.2. Total Ti bioaccumulation in *Ulva* sp. exposed to (a) 25 nm TiO_2NPs and (b) 5 nm TiO_2NPs for 28 days.

In the case of *Ulva* sp., the control tanks and the solvent tanks had greater variability than for *Palmaria palmata* where the concentrations remained practically constant. The total Ti bioaccumulation in *Ulva* sp. at a high exposure dose increased with the exposure time until 28 days in both experiments.

For *Ulva* sp. exposed to 25 nm TiO_2NPs, the basal Ti concentration remained constant with exposure time from 0 to 28 days. The ANOVA test showed no significant difference in concentrations with time (P-value>0.05). The concentration in tanks exposed to citrate coating also remained constant with exposure time, but there was an increase in concentration on day 7 in the three tanks, after which the concentration decreased. The concentration on the 7th day was statistically different from the other average concentrations at different sampling days, as observed after applying an ANOVA test (P-value<0.05) and the multiple range test, but no statistical differences were found between 0, 14, 21, and 28 days (multiple range test). The concentrations in seaweed from tanks exposed to 0.1 mg L^{-1} 25 nm TiO_2NPs were not statistically significative different from the 7-28 days exposure period (P-value>0.05). The concentrations in tanks exposed to 1.0 mg L^{-1} of 25 nm TiO_2NPs showed a linear increasing trend with the exposure time up to 59.63±20.3 µg g^{-1} (at day 28, mean of the three tanks J-L). This concentration was approximately nine times higher than that measured after exposure at 0.1 mg L^{-1} of 25 nm TiO_2NPs. The ANOVA test showed that there is a significant difference in concentration with exposure time (P-value<0.05). Furthermore, the multiple range test

USC UNIVERSIDADE DE SANTIAGO DE COMPOSTELA

showed the overlapping in concentration intervals at 7, 14, 21, and 28 days, with differences between days 0 and 7, 14, 21, and 28 days, and differences between 7 and 28 exposure days.

Figure S.4.6. shows the total Ti concentration in seaweed grown in control (**Figure S.4.6.(a)**), solvent (**Figure S.4.6. (b)**), 0.1 mg L^{-1} of 5 nm TiO_2NPs (**Figure S.4.6.(c)**), and 1.0 mg L^{-1} of 5 nm TiO_2NPs (**Figure S.4.6.(d)**) tanks. For *Ulva* sp. exposed to 5 nm TiO_2NPs, the Ti concentration in control and solvent tanks remained constant with exposure time. The concentration measured was slightly higher at day 0 in the tanks. But in both cases, the ANOVA test and the multiple range tests showed no significant difference ($P>0.05$) among the tanks from day 7 to day 28. The concentrations in seaweed from tanks exposed to 0.1 mg L^{-1} of 5 nm TiO_2NPs increased with the exposure time until 14 days, and stabilized after that, reaching a concentration of 3.06±0.18 μg g^{-1} on the 28th day. The ANOVA test for *Ulva* sp. exposed to 0.1 mg L^{-1} showed a statistical difference ($P<0.05$) among the average concentrations as a function of the sampling time, and the multiple range test showed an overlapping in the concentrations after 14 days. The total Ti concentrations in seaweed from tanks exposed to 1.0 mg L^{-1} of 5 nm TiO_2NPs had a linear increasing trend with exposure time until 61.96±15.49 μg g^{-1} at day 28 (mean of the three tanks J-L; concentration 20 times higher than after exposure to 0.1 mg L^{-1} of 5 nm TiO_2NPs). The ANOVA test for *Ulva* sp. exposed to 1.0 mg L^{-1} showed a statistical difference ($P<0.05$) among the average concentrations as a function of the sampling time. The multiple range test confirmed the overlapping of Ti concentrations at 14, and 21 days, and afterwards an increase at day 28.

In summary, the bioaccumulation of total Ti in *Palmaria palmata* exposed to 25 nm TiO_2NPs was lower than for *Ulva* sp. exposed to 25 nm TiO_2NPs. *Palmaria palmata* reached 30.55±2.31 μg g^{-1} and *Ulva* sp. reached 59.63±20.3 μg g^{-1} of total Ti. However, the bioaccumulation in *Palmaria palmata* was more gradual and the reproducibility was better than for *Ulva* sp. (which already exhibited a sharp increase in Ti concentration on day 7). The bioaccumulation in *Palmaria palmata* exposed to 5 nm TiO_2NPs was also lower than for *Ulva* sp. exposed to 5 nm TiO_2NPs. *Ulva* sp. reached a concentration of Ti of 61.96±15.49 μg g^{-1} whereas the maximum *Palmaria palmata* concentration was 8.08±2.50 μg g^{-1} (on the 21st day). This different behavior between species is normal, and it can be attributed to the various chemical composition of seaweed, e.g. to the different polysaccharides present in cell walls [33]. The different assimilation of TiO_2NPs in different tanks containing the same seaweed could be due to small differences between the tanks (e.g., differences in light, water flow, feed, etc.).

This study corroborates the use of *Ulva* sp. as one of the most important macroalgae species used for monitoring seawater pollution, with a big surface area and elevated capacity to bioaccumulate metals, and also applied to evaluate the presence of Ti on the coast of South Africa during the different seasons [20]. Desideri et al. [23] measured concentrations in edible seaweed purchased in Italian supermarkets. The concentration of Ti ranged from 1.7±0.1 (*Ulva enteromorpha*) to 156±10.9 (*Ulva lactuca*) mg kg^{-1} d.w. in *Ulva* sp., while the concentration of *Palmaria palmata* was 5.3±0.4 mg kg^{-1}. The highest concentration of Ti was found by this research group in *Lithothamnium calcareum* (1364±95.5 mg Kg^{-1}) [23].

4.4.3 Analysis of TiO_2NPs in seaweed

The TiO_2NPs g^{-1} content and the size distribution of the nanoparticles in seaweed were determined by SP-ICP-MS following the procedure described in **section 4.3.6**. The experimental TE (%) of the instrument was approximately 9±1% for flow rates between 0.189-0.210 mL min^{-1}. The LOD and LOQ were calculated using the Laborda et al. criteria [34]. The LOD_{number} were 2.82×10^6 TiO_2NPs L^{-1} (instrumental LOD) and 2.82×10^6 TiO_2NPs g^{-1} (referred

to sample, for 1:100 dilution). The LOD_{size} were 27 and 23 nm for 5σ and 3σ criteria, respectively. The 5σ criteria was used to avoid the presence of false positives. Averages were taken for the nine replicates of seaweed for each dose of exposure on each sampling day. The size analysis by DLS and TEM (described in **section 4.4.1**) confirmed that both kinds of particles (25 nm TiO_2NPs and 5 nm TiO_2NPs) formed aggregates that were larger than LOD_{size} (>27 nm) both before and after nanoparticle exposure. This typical aggregation in TiO_2NPs allowed performing the characterization of NPs by SP-ICP-MS.

As total Ti analysis confirmed the absence of bioaccumulation of 25 nm TiO_2NPs and 5 nm TiO_2NPs in the control and solvent tanks, the alkaline TMAH extractions were performed only in the tanks with seaweed exposed to low and high exposure doses for both sizes of particles.

Figure 4.3. shows the mean concentrations of nanoparticles measured in the extracts after exposure of 25 nm TiO_2NPs (at 0.1 and 1.0 mg L^{-1} exposure doses) and 5 nm TiO_2NPs (at 1.0 mg L^{-1} exposure dose) for *Palmaria palmata* and *Ulva* sp. **Table S.4.4.** shows the concentration of 25 nm TiO_2NPs and 5 nm TiO_2NPs, the most frequent sizes, and mean sizes range (0-28 days), at high and low exposure doses in the extracts of samples. As it can be observed, in the case of 5 nm TiO_2NPs, the tanks with seaweed exposed to a dose of 0.1 mg L^{-1} resulted in nanoparticle concentrations lower than LOD_{number} (<2.82×10^6 TiO_2NPs g^{-1}).

USC UNIVERSIDADE DE SANTIAGO DE COMPOSTELA

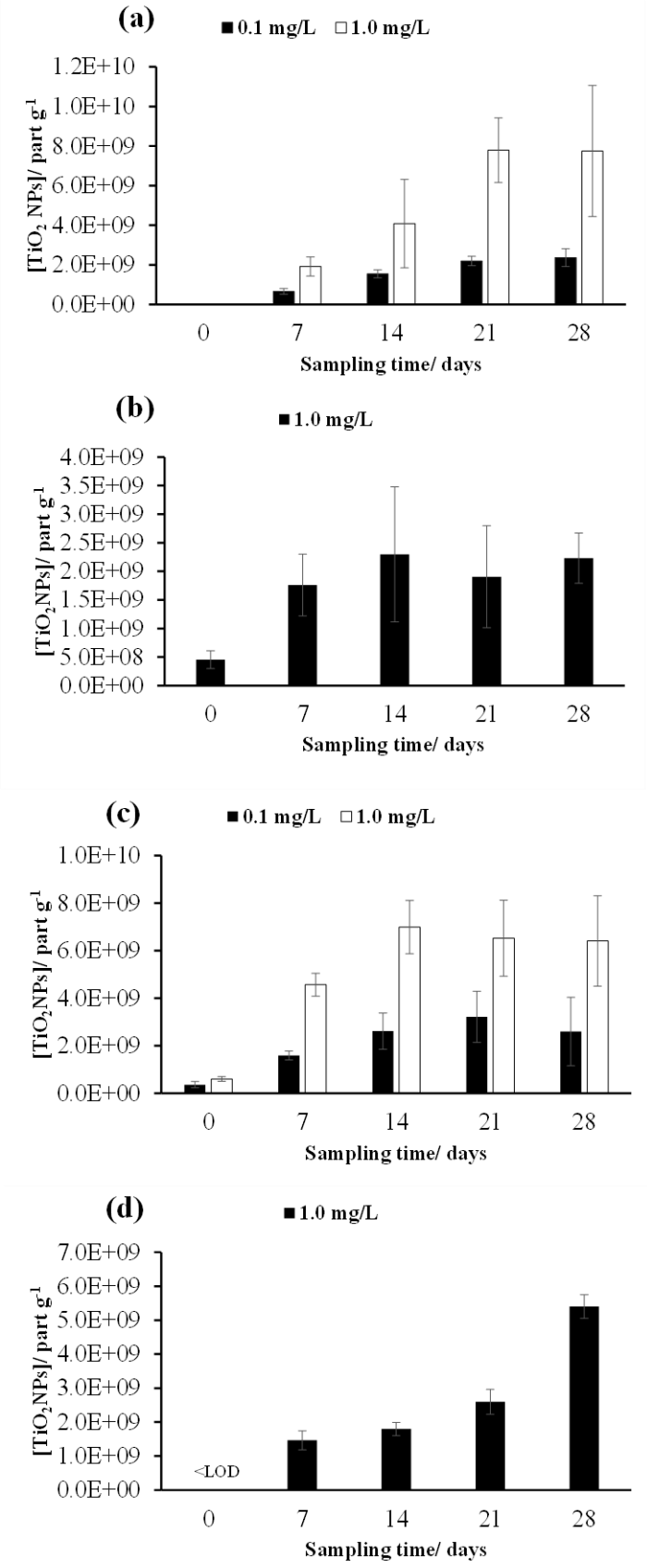

Figure 4.3. TiO_2NPs bioaccumulation in *Palmaria palmata* exposed to (a) 25 nm TiO_2NPs, (b) 5 nm TiO_2NPs, and in *Ulva* sp. exposed to (c) 25 nm TiO_2NPs, and (d) 5 nm TiO_2NPs.

4.4.3.1 Size distribution and TiO_2NPs content in *Palmaria palmata*

Nanoparticle content and size distributions were studied in samples of alkaline extracts of *Palmaria palmata* exposed to 25 and 5 nm TiO_2NPs. Nanoparticle size distribution histograms of *Palmaria palmata* exposed to 0.1 mg L^{-1} of 25 nm TiO_2NPs or 1.0 mg L^{-1} of 5 nm TiO_2NPs are shown in **Figure 4.4.(a)** and **Figure 4.4.(b)**, respectively.

Figure S.4.7. shows *Palmaria palmata* nanoparticle content in seaweed from tanks exposed to 0.1 mg L^{-1} (**Figure S.4.7.(a)**), 1.0 mg L^{-1} of 25 nm TiO_2NPs (**Figure S.4.7.(b)**), and 1.0 mg L^{-1} of 5 nm TiO_2NPs (**Figure S.4.7(c)**).

Figure S.4.8. shows the most frequent and mean sizes of *Palmaria palmata* exposed to 0.1 mg L^{-1}(**Figure S.4.8.(a)**), 1.0 mg L^{-1} of 25 nm TiO_2NPs (**Figure S.4.8(b)**), and 1.0 mg L^{-1} of 5 nm TiO_2NPs (**Figure S.4.8.(c)**).

For *Palmaria palmata* exposed to 25 nm TiO_2NPs, the TiO_2NPs content in tanks exposed to 0.1 mg L^{-1} of NPs increased linearly with the exposure time until $2.37\times10^9\pm4.49\times10^8$ NPs g^{-1} (day 28). The TiO_2NPs content in tanks exposed to 1.0 mg L^{-1} showed bioaccumulation with exposure time until $7.75\times10^9\pm3.31\times10^9$ NP g^{-1} (day 28; concentration 3.3 times higher than after exposure to 0.1 mg L^{-1}). For *Palmaria palmata* exposed to 0.1 mg L^{-1} 25 nm TiO_2NPs, the most frequent sizes (mean of three tanks) were between 40±2 nm (at day seven) and 41±1 nm (at day 28), and the mean sizes were between 52±2 nm (day 7) and 54±2 nm (day 28). However, for *Palmaria palmata* exposed to 1.0 mg L^{-1} 25 nm TiO_2NPs, the most frequent sizes were between 49±6 nm (day 7) and 47±3 nm (day 28), and the mean sizes were 70±9 nm (days 7) and 64±6 nm (day 28). It seems that TiO_2NPs tend to aggregate with increasing concentration, but the sizes remained constant at the same doses with exposure time.

USC UNIVERSIDADE DE SANTIAGO DE COMPOSTELA

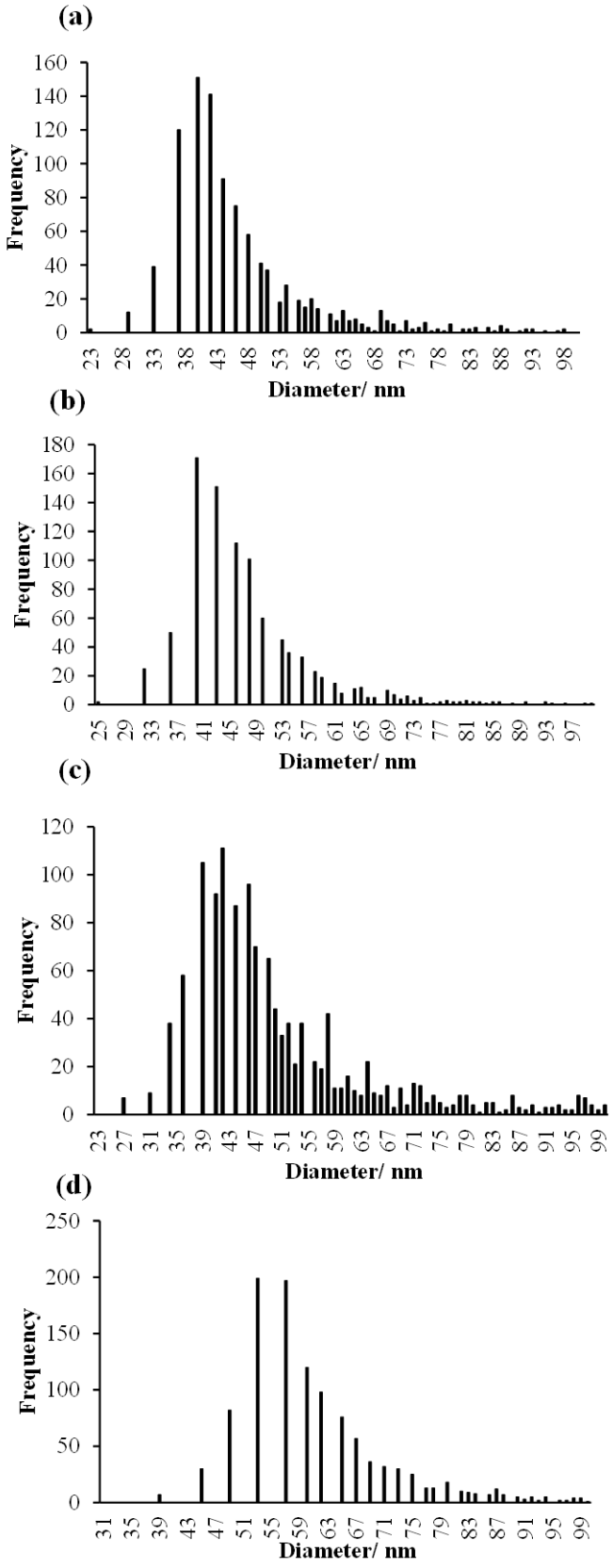

Figure 4.4. Size distribution histograms of TiO_2NPs corresponding to extracts of: *Palmaria palmata* exposed to (a) 0.1 mg L^{-1} 25 nm TiO_2NPs, (b) 1.0 mg L^{-1} 5 nm TiO_2NPs; and *Ulva* sp. exposed to (c) 0.1 mg L^{-1} 25 nm TiO_2NPs, and (d) 1.0 mg L^{-1} 5 nm TiO_2NPs.

USC UNIVERSIDADE DE SANTIAGO DE COMPOSTELA

For *Palmaria palmata* exposed to 5 nm TiO_2NPs, the TiO_2NPs content in tanks exposed to 0.1 mg L^{-1} of NPs was under the LOD_{number} (<2.82×10^6 NPs g^{-1}). In the case of high-dose exposed tanks, the NPs content reached $2.23\times10^9\pm4.39\times10^8$ NPs g^{-1} (day 28). The most frequent sizes varied from 33±1 nm (day 0) to 41±1 nm (day 28), and the mean sizes varied from 38±1 nm (day 0) to 50 ±1 nm (day 28).

SEM, TEM, and STEM techniques were employed to examine the localization of the NPs and EDX analysis to identify the NPs found. **Figure 4.5.(a)** and **Figure 4.5.(b)** show SEM images of *Palmaria palmata* exposed for 28 days to 1.0 mg L^{-1} of both NPs sizes, respectively. Aggregates with a size bigger than 1 µm were found and they were identified as TiO_2 in the sample exposed to 25 nm TiO_2NPs. However, none of the aggregates could be identified as TiO_2 in the case of samples exposed to 5nm TiO_2NPs. In both cases, no NP was observed/localized into the tissues by TEM or STEM micrographs (data not shown) after 28 exposure days, and therefore, the internalization could not be confirmed by electron microscopy. The bioaccumulation of 5 nm TiO_2NPs in *Palmaria palmata* measured as total Ti content was lower than for 25 nm TiO_2NPs; this could explain why it was not possible to localize the aggregated NPs using SEM or TEM. However, more information could be extracted from electron microscopy analysis for citrate-25 nm TiO_2NPs. It seems that aggregates bigger than 1 µm were associated with the seaweed surface most likely by adsorption as reported previously. The adsorption capacity of TiO_2NPs by algae was in the range of 59 to 5701 µg g^{-1} d.w. (dry weight) in 72 h [35]. The initial concentration and the colloidal stability of the NPs affect the adsorption kinetic. In this case, the NPs dispersed in the medium formed bigger aggregates than in ultrapure water as demonstrated by DLS analysis (**Table S.4.2.**). Therefore, it is expected that the aggregates would adsorb on the surface instead of being internalized due to their size. It should be highlighted that the size of the aggregates is different in SEM analysis when compared to the one obtained by SP-ICP-MS. This could be attributed to a stabilization effect of phytoplankton during seaweed exposure, or in the extraction procedure due to the presence of polysaccharides and polyphenols from the seaweed, which could coat the NPs forming smaller aggregates.

USC UNIVERSIDADE DE SANTIAGO DE COMPOSTELA

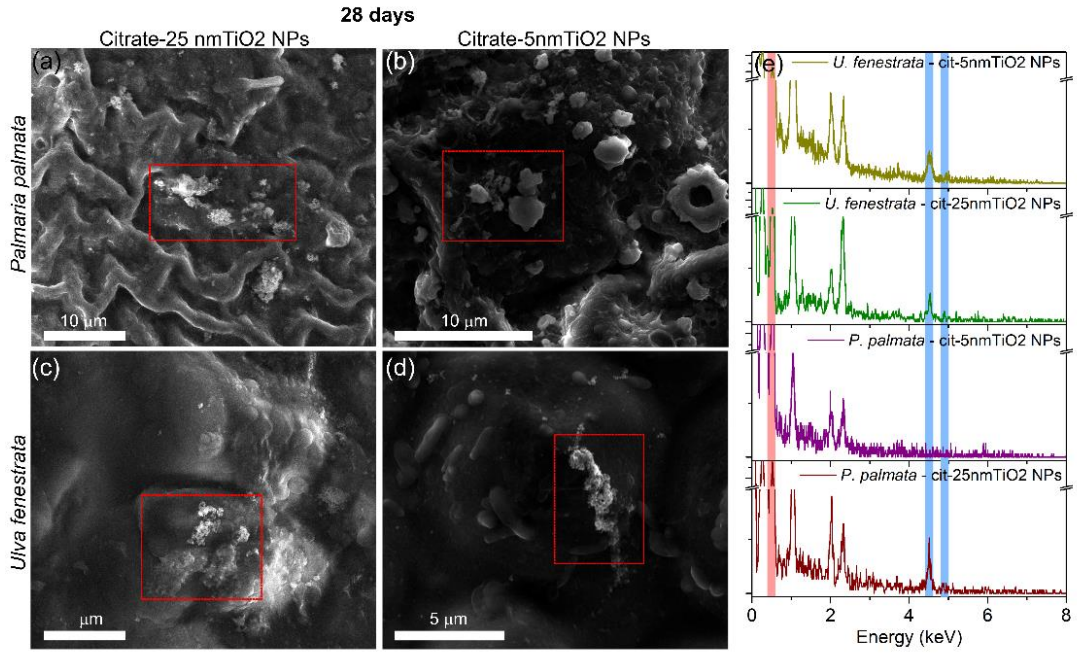

Figure 4.5. Representative SEM images of (a, b) *Palmaria palmata* and (c, d) *Ulva* sp. exposed for 28 days to 1.0 mg L^{-1} of (a, c) 25 nm TiO_2NPs and (b, d) 5 nm TiO_2NPs. (e) It shows the corresponding EDX spectra acquired in the limited area indicated by a dashed red square. The shadowed areas indicate the peaks corresponding to oxygen (pink) and titanium (blue) elements.

4.4.3.2 Size distribution and TiO_2NPs content in *Ulva* sp.

Nanoparticle content and size distributions were studied in alkaline extracts from *Ulva* sp. exposed to 25 and 5 nm TiO_2NPs. Nanoparticle size distribution histograms of *Ulva* sp. exposed to 0.1 mg L^{-1} of 25 nm TiO_2NPs or 1.0 mg L^{-1} of 5 nm TiO_2NPs are shown in **Figure 4.4.(c)** and **Figure 4.4.(d)**, respectively.

Figure S.4.9. shows the *Ulva* sp. nanoparticles content in tanks with seaweed exposed to 0.1 mg L^{-1} (**Figure S.4.9.(a)**), 1.0 mg L^{-1} of 25 nm TiO_2NPs (**Figure S.4.9(b)**), and 1.0 mg L^{-1} of 5 nm TiO_2NPs (**Figure S.4.9.(c)**).

Figure S.4.10. shows the most frequent and mean sizes of *Ulva* sp. exposed to 0.1 mg L^{-1} (**Figure S.4.10.(a)**), 1.0 mg L^{-1} of 25 nm TiO_2NPs (**Figure S.4.10.(b)**), and 1.0 mg L^{-1} of 5 nm TiO_2NPs (**Figure S.4.10.(c)**).

For *Ulva* sp. exposed to 25 nm TiO_2NPs, the TiO_2NPs content in tanks exposed to 0.1 mg L^{-1} of NPs increased with exposure time until $2.60\times10^9\pm1.44\times10^9$ NPs g^{-1} (day 28). The TiO_2NPs content in tanks exposed to 1.0 mg L^{-1} showed a stabilized bioaccumulation until $6.41\times10^9\pm1.90\times10^9$ NPs g^{-1} (day 28; concentration 2.5 times higher than after exposure to 0.1 mg L^{-1}). For *Ulva* sp. exposed to 0.1 mg L^{-1} 25 nm TiO_2NPs, the most frequent sizes were between 36±2 nm (day 0) and 43±6 nm (day 28), and the mean sizes were between 52±2 nm (day 0) and 54±5 nm (day 28). However, for *Ulva* sp. exposed to 1.0 mg L^{-1} of 25 nm TiO_2NPs, the most frequent sizes varied from 44±7 nm (day 0) to 52±14 nm (day 28), and the mean sizes from 53±9 nm (day 0) to 66±15 nm (day 28). Like in *Palmaria palmata*, TiO_2NPs tend to aggregate with increasing concentration, but the sizes remained constant at the same doses with the exposure time. This could explain the increase in size measured in SP-ICP-MS. Other authors have observed the increase in the size of nanoparticles measured in plant extracts after exposure in comparison to the primary particles, e.g. in the case of AgNPs [36]. However, Deng et al. [37] did not find significant differences between the most frequent and the mean sizes of

TiO_2NPs or bulk particles measured by SP-ICP-MS in nanoparticle controls and after the enzymatic or acid extraction of TiO_2NPs from rice.

For *Ulva* sp. exposed to 5 nm TiO_2NPs the content of nanoparticles in tanks exposed to 0.1 mg L^{-1} of NPs was under the LOD_{number} (<2.82×10^6 TiO_2NPs g^{-1}). However, for 1.0 mg L^{-1} of exposure dose, the bioaccumulation in seaweed increased linearly with the exposure time until $5.41\times10^9\pm3.47\times10^8$ NPs g^{-1} at 28 days. Besides, the most frequent sizes were 48±3 nm (day 0) and 52±3 nm (day 28), and the mean sizes were between 76±4 nm (day 0) and 64±1 nm (day 28). The most frequent and mean sizes remained approximately constant with the exposure time.

Although the total concentration of Ti bioaccumulated for 25 nm TiO_2NPs was higher in *Ulva* sp. than in *Palmaria palmata* (**section 4.4.2**), there were no significant differences in the concentrations of TiO_2NPs bioaccumulated in both kinds of seaweed at low and high exposure 25 nm TiO_2NPs doses. Thus, *Ulva* sp. seems to have accumulated a higher proportion of ionic Ti or contains TiO_2NPs smaller than the LOD in size (27 nm for 5σ criteria). Besides, no differences were found in the most frequent and mean sizes in *Palmaria palmata* and *Ulva* sp. exposed to 25 nm TiO_2NPs. In the case of 5 nm TiO_2NPs, the total Ti bioaccumulation was also higher for *Ulva* sp. than for *Palmaria palmata*. Nevertheless, no significant differences in the TiO_2NPs content were found in both kinds of seaweed.

The set of electron microscopy techniques and EDX analysis described in **section 4.3.1** were also employed to examine the localization and identification of the NPs in *Ulva* sp. SEM images (**Figure 4.5.(c)** and **Figure 4.5.(d)**) clearly show the presence of TiO_2 aggregates (size > 1 μm) confirmed by EDX (**Figure 4.5.(e)**) on their surface after 28 days of exposure to both sizes of NPs studied here. In addition, the internalization could be visualized by TEM/STEM and the identity of NPs was confirmed as TiO_2 by EDX analysis (**Figure 4.6.**). Interestingly, the size of the internalized aggregates was smaller than the aggregates localized on the surface. The aggregates of 25 nm TiO_2NPs presented high polydispersity (i.e. high variability in the size distribution), while fewer aggregates of 5 nm TiO_2NPs were localized and the size was smaller than in the case of 25 nm NPs. This supports the hypothesis that big aggregates were adsorbed firstly on the seaweed's surface via interaction with the glycoproteins and polysaccharides present in the cell wall [35]. These aggregates were "broken" during the internalization forming smaller aggregates embedded in the cell wall. Thus, the interaction of the NPs with some seaweed components together with the effect of ultrasonication used during the extraction process could explain the smaller size obtained by SP-ICP-MS, as it has been reported that the use of ultrasound could improve the dispersion of TiO_2NPs [38].

USC UNIVERSIDADE DE SANTIAGO DE COMPOSTELA

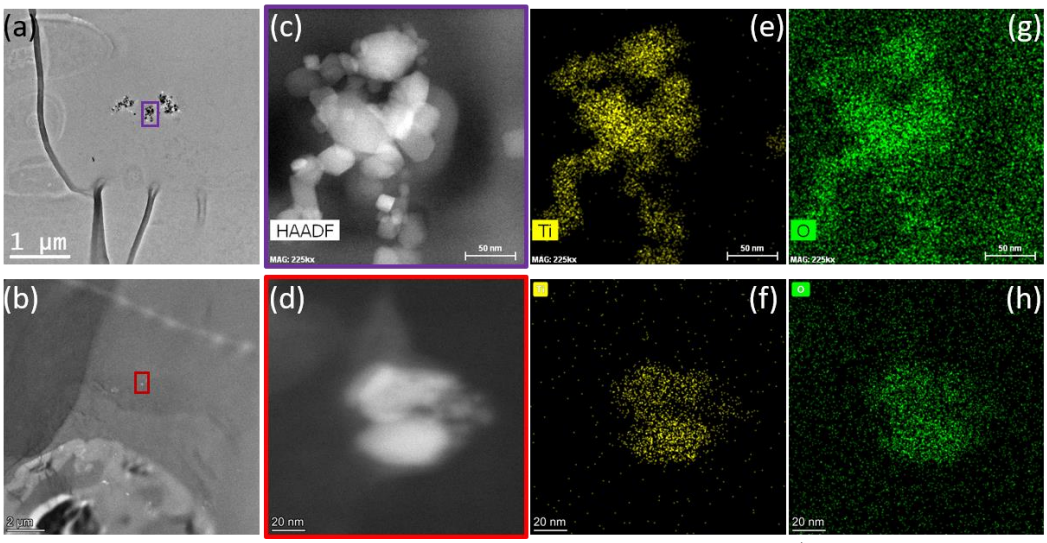

Figure 4.6. TEM micrograph of *Ulva* sp. after 28 days exposure to 1.0 mg L^{-1} of 25 nm TiO_2NPs (a) and STEM micrograph of *Ulva* sp. after 28 exposure days to 1.0 mg L^{-1} of 5 nm TiO_2NPs (b). In both cases, inorganic nanoparticles were localized. STEM-EDX maps, with the HAADF-STEM image of 25 nm TiO_2NPs(c) and 5 nm TiO_2NPs (d) and EDX elemental maps of Ti(e, f) and O (g, h) confirmed that the NPs localized were TiO_2.

4.5 CONCLUSIONS

The present research provides information about the bioaccumulation of TiO_2NPs in marine macroalgae after exposure periods longer than those usually employed in other studies. The analysis of total Ti, the TiO_2NPs content, and TiO_2NPs size has been carried out by ICP-MS and SP-ICP-MS while the NPs localization in the tissues was investigated by SEM and TEM. Ti concentrations measured in *Ulva* sp. were higher than those found in *Palmaria palmata* for the same conditions of exposure, and internalization was only verified in the former. Finally, the ability to bioaccumulate TiO_2NPs of different sizes has been demonstrated in the seaweed species, resulting in more ionic Ti or small-size nanoparticulate TiO_2 bioaccumulation in green rather than red seaweed. Due to the lack of cut-off values in the regulatory landscape, further research is needed to ensure a good level of quality and safety in alimentary products.

USC UNIVERSIDADE DE SANTIAGO DE COMPOSTELA

SUPPLEMENTARY INFORMATION

Preparation of citrate NPs dispersions

Citrate-5 nm TiO_2NPs and citrate-25 nm TiO_2NPs dispersions were prepared by dispersing a mixture of trisodium citrate dihydrate (Sigma-Aldrich) and TiO_2 powder at a weight ratio of TiO_2: citrate 1:1.5 wt/wt for 5 nm and 1:0.8 wt/wt for 25 nm using an ultrasonic probe (Branson Disintegrator Ultrasonic Mod. 450) for 30 min (30 s pulse on /5 s pulse off, and 50 % amplitude). The final concentration of both citrate-TiO_2NPs was 15.5 g L^{-1}. The TiO_2NPs stocks were diluted in 0.1 g mL^{-1} Cell-Hi F2P growing medium (Varicon Aqua, Hallow, Worcester, UK) to reach 0.1 and 1.0 mg L^{-1} for bioaccumulation assays with seaweeds.

Seaweed sample cultivation

The seaweed's growth and feeding with the Cell-Hi F2P medium (a soluble nutrient blend commonly used in the production of marine microalgae) were taken care of for 28 days. Seaweeds were cultivated in 40 L tanks at 16±1 ºC with periods of 12 hours of white light and 12 hours of darkness. Parameters like pH, temperature, dissolved O_2, and salinity were measured every day. However, conductivity, ammonium, and nitrites were tested twice a week. For each of the four trials, there were three control tanks (A-C: seaweed in growing medium without nanoparticles), three solvent control tanks (D-F: seaweed exposed to citrate, without nanoparticles), three low dose tanks (G-I: seaweed exposed to 0.1 mg L^{-1} of citrate-coated TiO_2NPs), and three high dose tanks (J-L: seaweed exposed to 1.0 mg L^{-1} of citrate-coated TiO_2NPs). 30 mL (0.1g mL^{-1}) of the F2P growing medium containing the phytoplankton was added three times per week. Fifty percent of the water was replaced twice per week, two days before and two days after the addition of nanoparticles. The particles were added only once per week to the F2P medium by micro pipetting and manual shaking to obtain the final concentration (0.1 and 1.0 mg L^{-1}) in the forty-liter tanks. Indigo Rock's staff collected three seaweed samples replicates from each tank on days 0, 7, 14, 21, and 28 for analysis by ICP-MS, TEM, and SEM. Three replicate samples from each tank and each trial for ICP-MS and SP-ICP-MS analysis of Ti and TiO_2NPs were collected respectively, resulting in 180 samples per trial. The seaweed samples were washed with ultrapure water to remove salts and contaminants from the seawater. Wet seaweed samples were manually crushed, homogenized, and stored in polyethylene tubes at -18.0 ºC until microwave acid digestion and basic extraction of TiO_2NPs were performed.

USC UNIVERSIDADE DE SANTIAGO DE COMPOSTELA

Table S.4.1. Operational conditions for ICP-MS (a) and SP-ICP-MS (b).

(a) ICP-MS operational conditions	
Parameter/component	**Type/mode/value**
Nebulizer	Meinhard CR R^+
Nebulizer Chamber	5 ºC refrigerated glass cyclone chamber with Peltier PC^{3X}
Cone material	Nickel/aluminum
Radiofrequency power	1600 W
Ar gas flow	15 L min^{-1} (Plasma) 1.15 L min^{-1} (Nebulizer) 1.2 L min^{-1} (Auxiliary)
Analyte	Ti
Operation mode	DRC (dynamic reaction cell)
Ammonia flow rate	1.0 mL min^{-1}
Integration time	1000 ms
m/z	131, cluster $[^{48}Ti^{14}N^1H(^{14}N^1H_3)_4{}^+]$
Replicates per sample	3
RPQ	0.2
(b) SP-ICP-MS operational conditions	
Sample flow rate	0.189-0.210 mL min^{-1}
Acquisition time	60 s
Dwell time	50 µs
Number of readings	1,200,000

USC UNIVERSIDADE DE SANTIAGO DE COMPOSTELA

UPC UNIVERSITAT POLITÈCNICA DE CATALUNYA

Table S.4.2. Physicochemical characterization of selected TiO_2NPs before exposure by DLS (n=10) and zeta potential (n=5), and after exposure and alkaline extraction by SP-ICP-MS (n=5).

Type of particle	Initial NPs dispersion in water		Initial NPs dispersion in artificial seawater		NPs Dispersion after exposure and extraction	
	Hydrodynamic diameter/ nm	Zeta potential/mV	Hydrodynamic diameter/ nm	Zeta potential/mV	Most frequent size/ nm	Mean size/ nm
Citrate-25 nmTiO_2NPs	128±2.9	-79±2	3168±1089	-1.4±2.4	37±1	52±1
Citrate-5 nm TiO_2NPs	65±14	-31±1	3320±1248	-1.4±2.8	44±7	48±6

[1] Mean hydrodynamic diameter obtained by DLS at a scattering angle of 173° and 25 °C. Ten DLS measurements were acquired: mean±standard deviation (SD).

[2] Zeta potentials were measured in 5 runs (mean±SD).

Table S.4.3. Total Ti content in *Palmaria palmata* and *Ulva* sp. exposed to TiO_2NPs.

		Palmaria palmata				*Ulva* sp.			
		Total content/ μg g^{-1}				Total content/ μg g^{-1}			
NPs size/ nm		25		5		25		5	
Tanks/ Exposure time		0 days	28 days	0 days	28 days	0 days	28 days	0 days	28 days
Control	A	0.30±0.08	0.43±0.01	0.28±0.03	0.27±0.05	0.28±0.08	0.15±0.04	1.38±0.62	0.28±0.16
	B	0.17±0.07	0.45±0.01	0.26±0.05	0.35±0.02	0.43±0.08	0.40±0.17	1.08±0.27	0.19
	C	0.24±0.05	0.51±0.01	0.36±0.01	0.34±0.01	0.16±0.07	0.18±0.02	0.25±0.05	0.40±0.10*
Solvent	D	0.21±0.03	0.31±0.06	0.40±0.10	0.31±0.02	0.26±0.03	0.21±0.01	0.82±0.31	0.36±0.02
	E	0.13±0.02	0.31±0.06	0.43±0.12	0.54±0.08	0.27±0.10	0.38±0.14	1.85±0.05	0.31±0.05
	F	0.40±0.02	0.49±0.06	0.30±0.01	0.26±0.02	0.71±0.10	0.28±0.05	0.50±0.12	0.10±0.01
0.1 mg L^{-1}	G	0.31±0.04	7.32±0.60	0.35±0.02	1.97±0.01	0.46±0.01	6.41±0.24	0.34±0.05	4.15±2.18
	H	0.23±0.01	7.47±0.40	0.69±0.01	1.17±0.14	0.58±0.05	2.78±0.17	0.63±0.09	3.25±0.82
	I	0.40±0.21	6.66±0.10	0.25±0.02	1.13±0.08	0.20±0.01	17.71±0.01	0.42±0.09	4.44±0.82
1.0 mg L^{-1}	J	0.30±0.02	31.21±1.10	0.68±0.15	7.33±0.89	0.16±0.01	50.58±2.47	0.33±0.05	52.84±21.69
	K	0.15±0.03	32.47±5.88	0.73±0.18	5.10±0.47	0.67±0.02	45.44±2.05	0.53±0.20	79.85±9.95
	L	0.18±0.02	27.98±1.63	0.26±0.05	7.91±1.38	0.16±0.04	82.89±1.35	0.57±0.30	53.19±5.99

* 21 days of exposure

Table S.4.4. TiO_2NPs content, most frequent and mean size in *Palmaria palmata* and *Ulva* sp.

Palmaria palmata

		NPs content/ NPs g^{-1}				Most frequent size/ nm		Mean size/ nm		Most frequent size/ nm		Mean size/ nm	
NPs size/ nm		25		5		25				5			
Exposure time/ days		0	28	0	28	7	28	7	28	0	28	0	28
0.1 mg L^{-1}	Tank G	-	$2.12\times10^{9}\pm9.27\times10^{7}$	-	-	42±6	41±1	54±7	52±2	-	-	-	-
	Tank H	$4.54\times10^{6}\pm4.01\times10^{5}$	$2.10\times10^{9}\pm1.58\times10^{8}$	-	-	38±2	42±5	50±5	56±9	-	-	-	-
	Tank I	-	$2.89\times10^{9}\pm1.71\times10^{8}$	-	-	39±6	41±2	52±2	54±2	-	-	-	-
1.0 mg L^{-1}	Tank J	-	$1.11\times10^{10}\pm5.17\times10^{8}$	-	$1.83\times10^{9}\pm1.02\times10^{8}$	54±1	49±3	76±6	64±2	53±4	42±1	82±16	49±5
	Tank K	-	$7.57\times10^{9}\pm1.36\times10^{9}$	$5.66\times10^{8}\pm2.38\times10^{8}$	$2.17\times10^{9}\pm4.16\times10^{8}$	42±3	44±2	59±5	58±2	32±1	42±3	38±4	50±2
	Tank L	-	$4.52\times10^{9}\pm5.71\times10^{8}$	$3.44\times10^{8}\pm1.07\times10^{8}$	$2.70\times10^{9}\pm4.36\times10^{8}$	51±2	48±5	75±4	70±6	33±1	40±3	39±4	49±3

Ulva sp.

		NPs content/ NPs g^{-1}				Most frequent size/ nm		Mean size/ nm		Most frequent size/ nm		Mean size/ nm	
NPs size/ nm		25		5		25				5			
Exposure time/ days		0	28	0	28	0	28	0	28	0	28	0	28
0.1 mg L^{-1}	Tank G	$2.74\times10^{8}\pm1.55\times10^{8}$	$1.64\times10^{9}\pm2.26\times10^{8}$	-	-	34±2	47±3	51±5	58±6	-	-	-	-
	Tank H	-	$1.90\times10^{9}\pm4.97\times10^{8}$	-	-	38±9	36±1	50±6	48±1	-	-	-	-
	Tank I	$4.53\times10^{8}\pm2.49\times10^{7}$	$4.25\times10^{9}\pm5.57\times10^{8}$	-	-	36±3	45±4	54±2	55±4	-	-	-	-
1.0 mg L^{-1}	Tank J	-	$8.59\times10^{9}\pm1.28\times10^{9}$	-	$5.59\times10^{9}\pm3.28\times10^{8}$	42±2	36±6	53±13	49±9	51±8	55±2	71±18	65±3
	Tank K	$5.31\times10^{8}\pm9.47\times10^{7}$	$5.56\times10^{9}\pm5.19\times10^{8}$	-	$5.01\times10^{9}\pm8.32\times10^{7}$	38±2	62±5	44±3	77±8	46±4	51±1	80±11	64±2
	Tank L	$6.47\times10^{8}\pm1.78\times10^{7}$	$5.07\times10^{9}\pm2.53\times10^{8}$	-	$5.62\times10^{9}\pm1.53\times10^{9}$	51±1	57±8	61±1	72±6	41±4	49±5	77±4	63±6

- Indicates "<LOD"

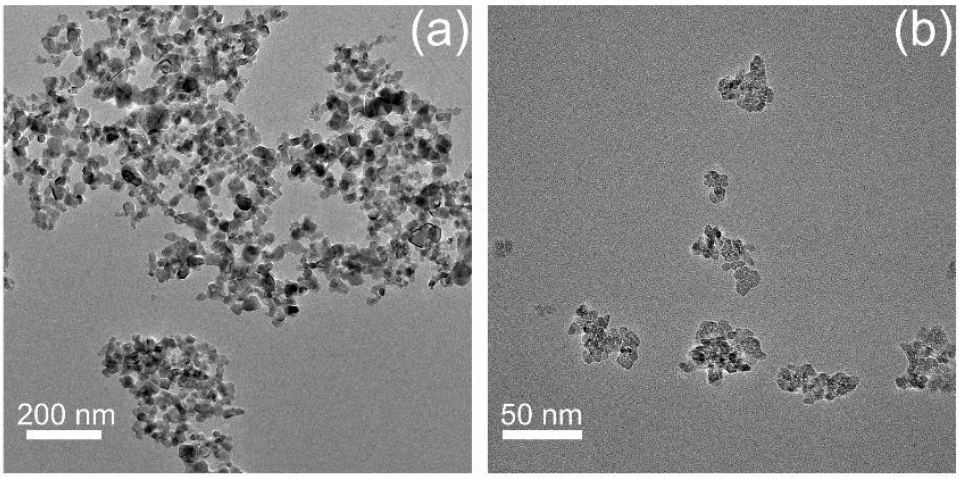

Figure S.4.1. Representative TEM images of (a) citrate-25 nm TiO_2NPs and (b) citrate-5 nm TiO_2NPs.

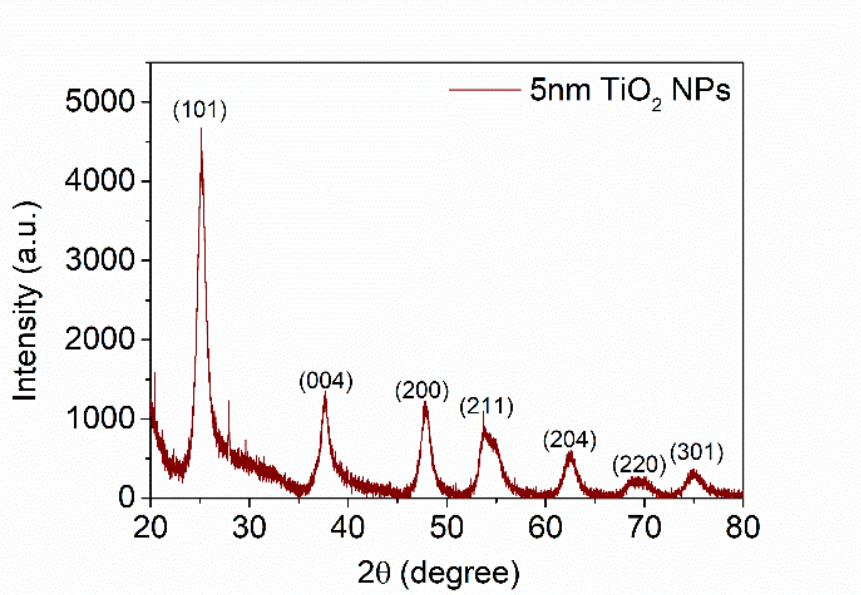

Figure S.4.2. X-ray diffraction pattern of anatase 5 nm TiO_2NPs. The nano crystalline size was calculated using Scherrer equation $L=K\lambda/\beta\cos\theta$ (L= nano crystallite size; λ *(nm)*= XRD radiation of wavelength; B= full width at half maximum of peaks; θ= peak centered at 2θ in the pattern). The crystalline nanosize obtained was 8.6 nm.

USC
UNIVERSIDADE DE SANTIAGO DE COMPOSTELA

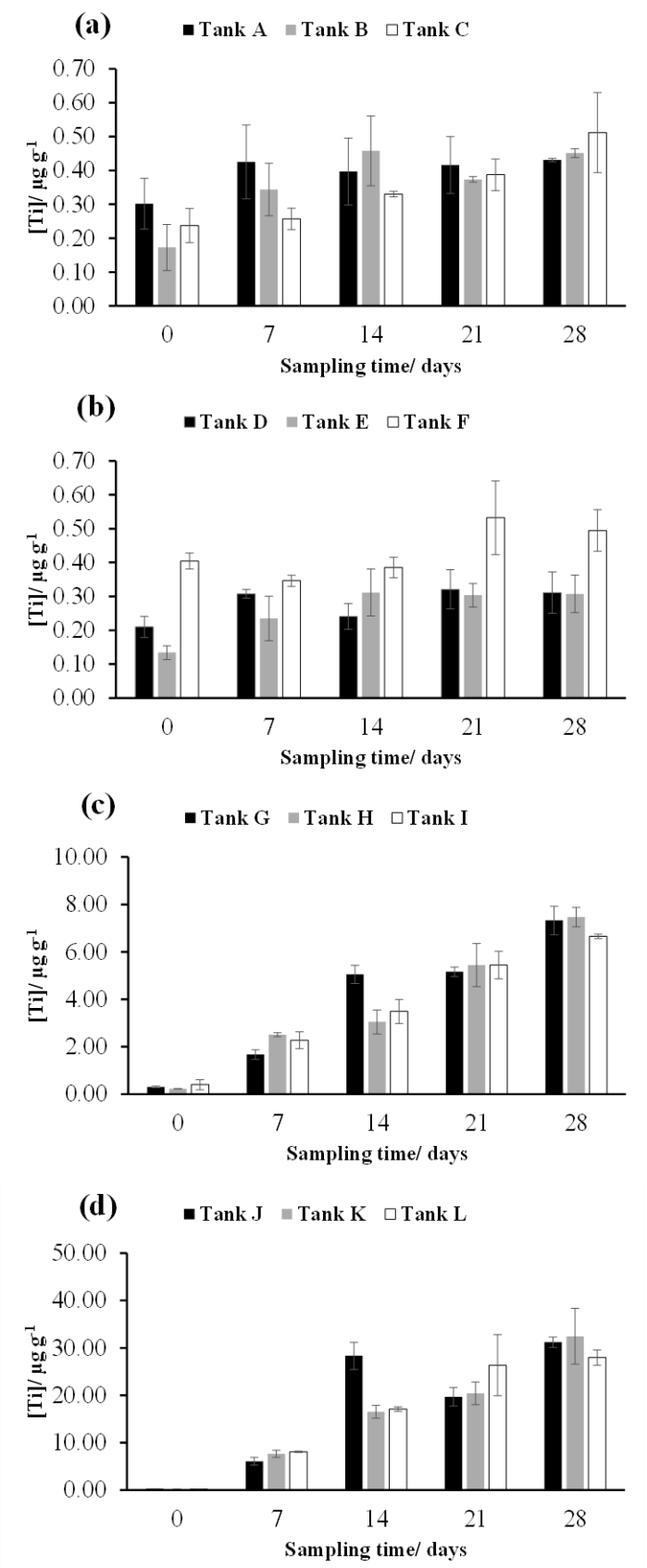

Figure S.4.3. Total content of Ti in *Palmaria palmata* grown in: (a) control tanks, (b) solvent tanks, (c) tanks with 0.1 mg L^{-1} of 25 nm TiO_2NPs, and (d) tanks with 1.0 mg L^{-1} of 25 nm TiO_2NPs.

USC UNIVERSIDADE DE SANTIAGO DE COMPOSTELA

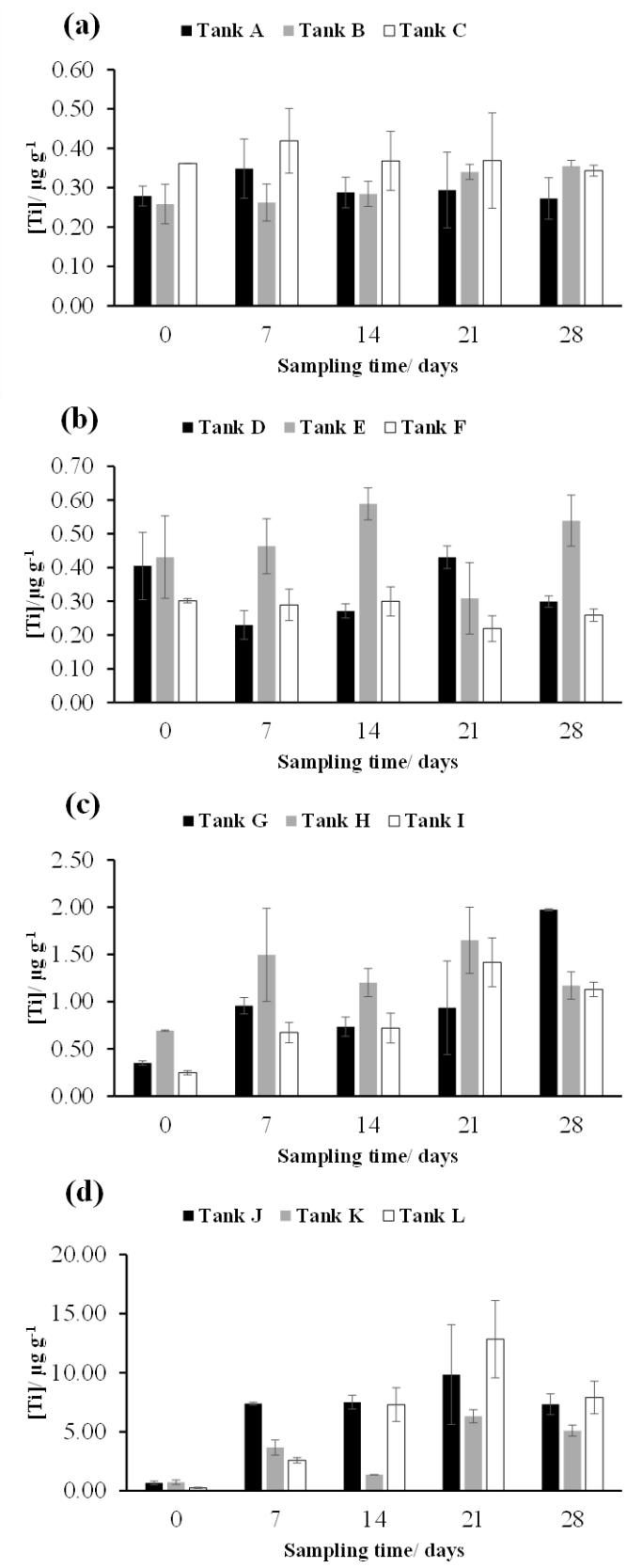

Figure S.4.4. Total content of Ti in *Palmaria palmata* grown in: (a) control tanks, (b) solvent tanks, (c) tanks with 0.1 mg L^{-1} of 5 nm TiO_2NPs, and (d) tanks with 1.0 mg L^{-1} of 5 nm TiO_2NPs.

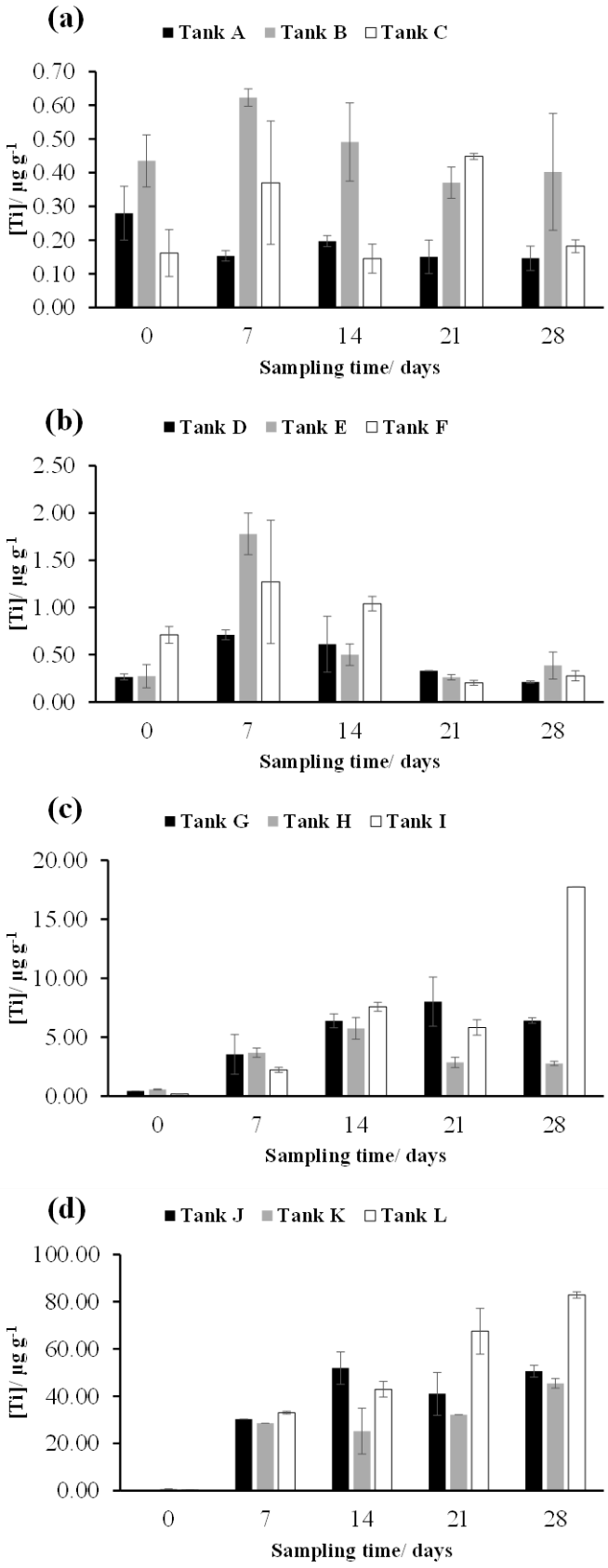

Figure S.4.5. Total content of Ti in *Ulva* sp. grown in: (a) control tanks, (b) solvent tanks, (c) tanks with 0.1 mg L^{-1} of 25 nm TiO_2NPs, and (d) tanks with 1.0 mg L^{-1} of 25 nm TiO_2NPs.

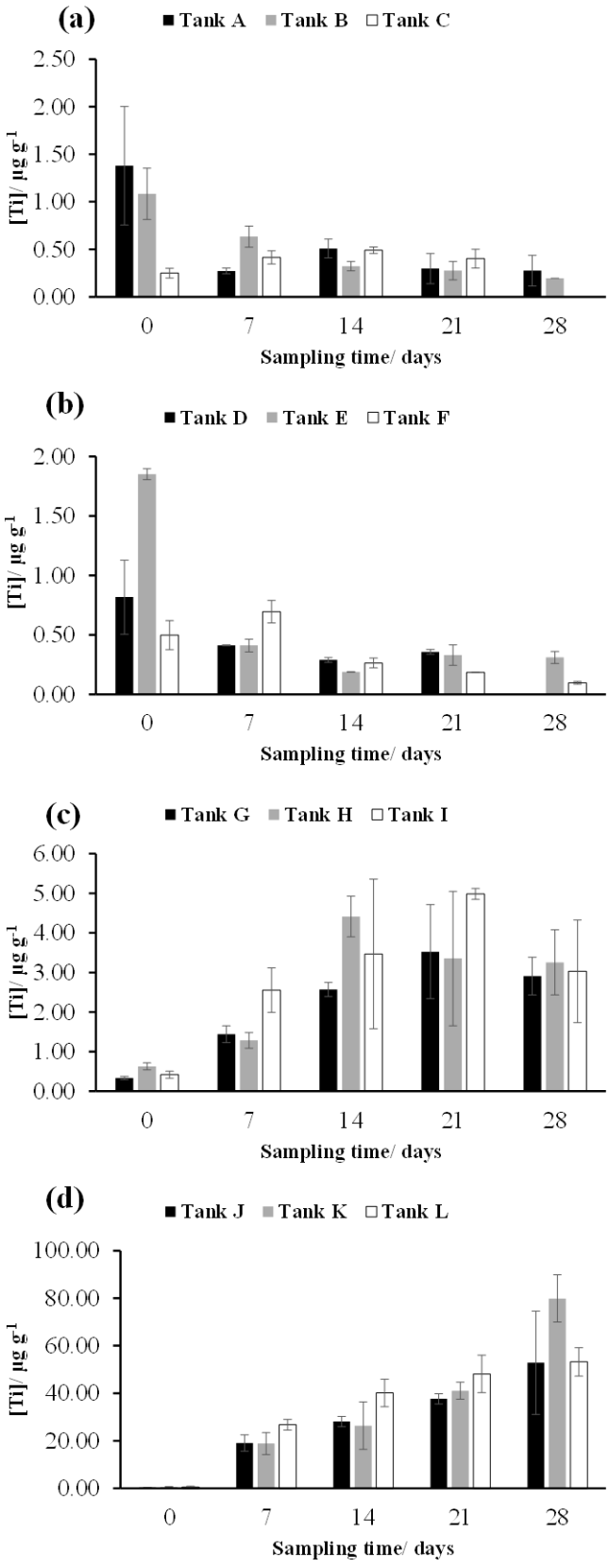

Figure S.4.6. Total content of Ti in *Ulva* sp. grown in: (a) control tanks, (b) solvent tanks, (c) tanks with 0.1 mg L^{-1} of 5 nm TiO_2NPs, and (d) tanks with 1.0 mg L^{-1} of 5 nm TiO_2NPs.

USC DE SANTIAGO DE COMPOSTELA

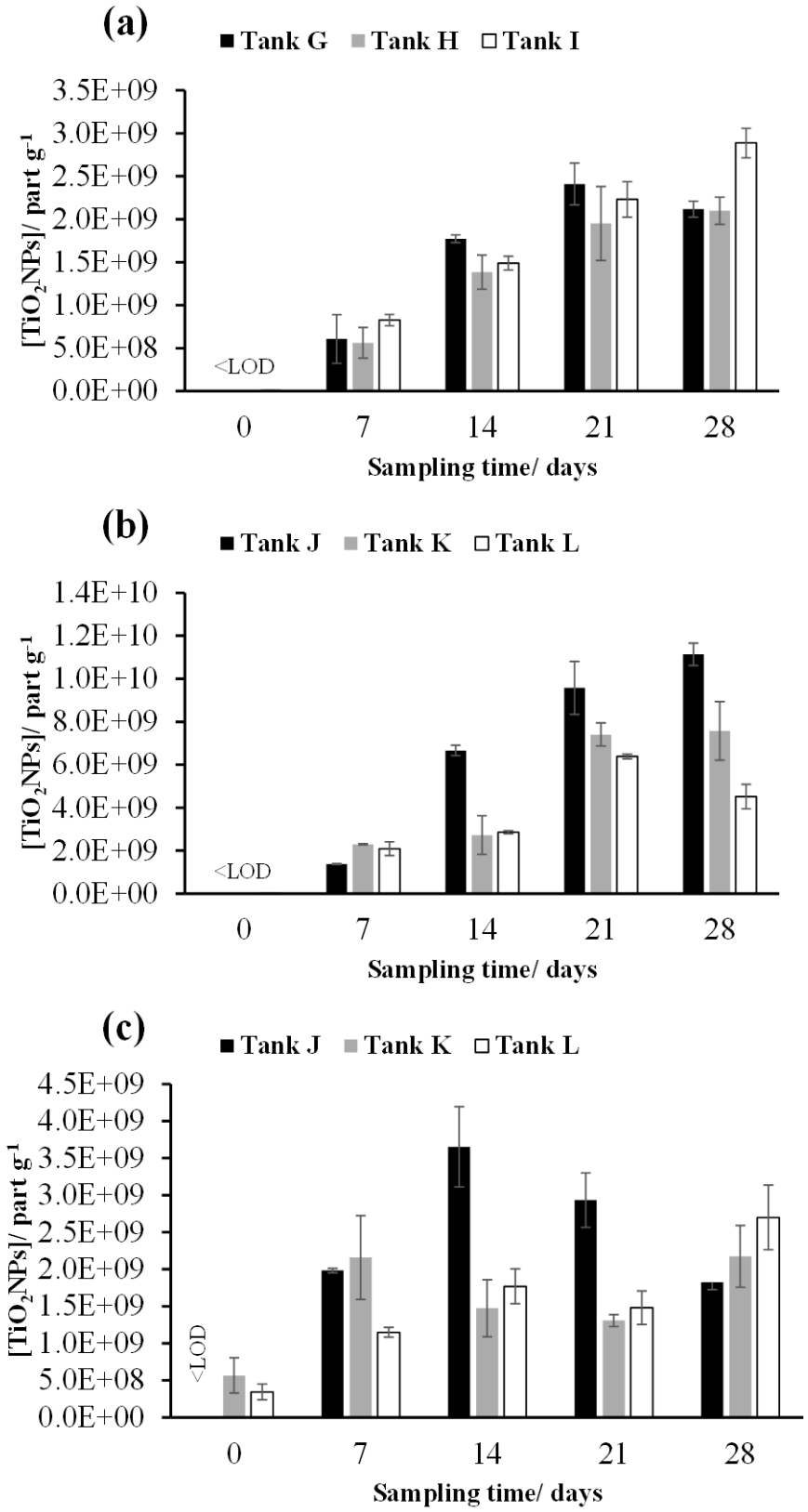

Figure S.4.7. Content of TiO_2NPs g^{-1} in *Palmaria palmata* exposed to: (a) 0.1 mg L^{-1} of 25 nm TiO_2NPs, (b) 1.0 mg L^{-1} of 25 nm TiO_2NP, and (c) 1.0 mg L^{-1} of 5 nm TiO_2NPs.

USC UNIVERSIDADE DE SANTIAGO DE COMPOSTELA

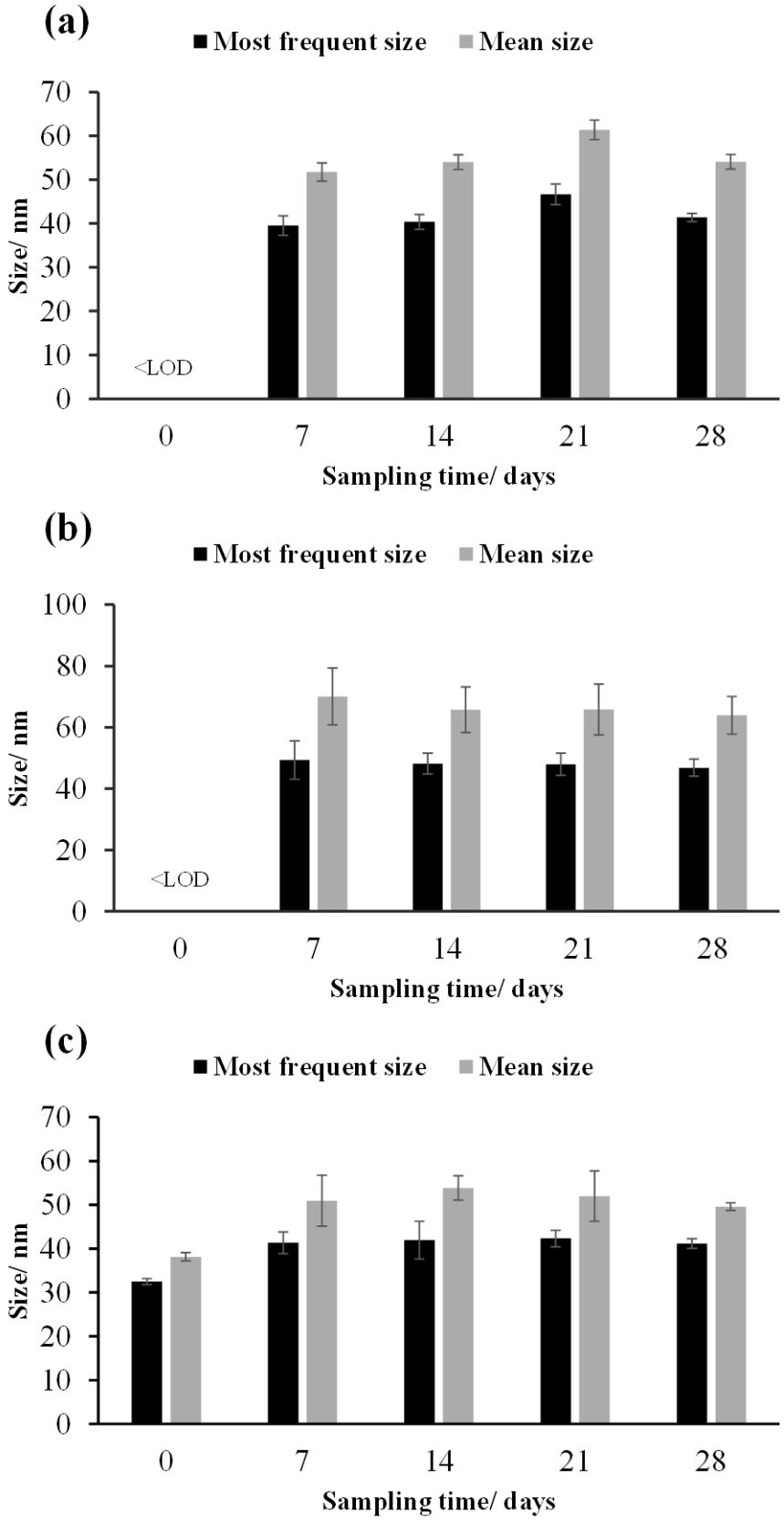

Figure S.4.8. Most frequent and mean sizes of nanoparticles in *Palmaria palmata* exposed to: (a) 0.1 mg L^{-1}, (b) 1.0 mg L^{-1} of 25 nm TiO_2NPs, and (c) 1.0 mg L^{-1} of 5 nm TiO_2NPs.

USC UNIVERSIDADE DE SANTIAGO DE COMPOSTELA

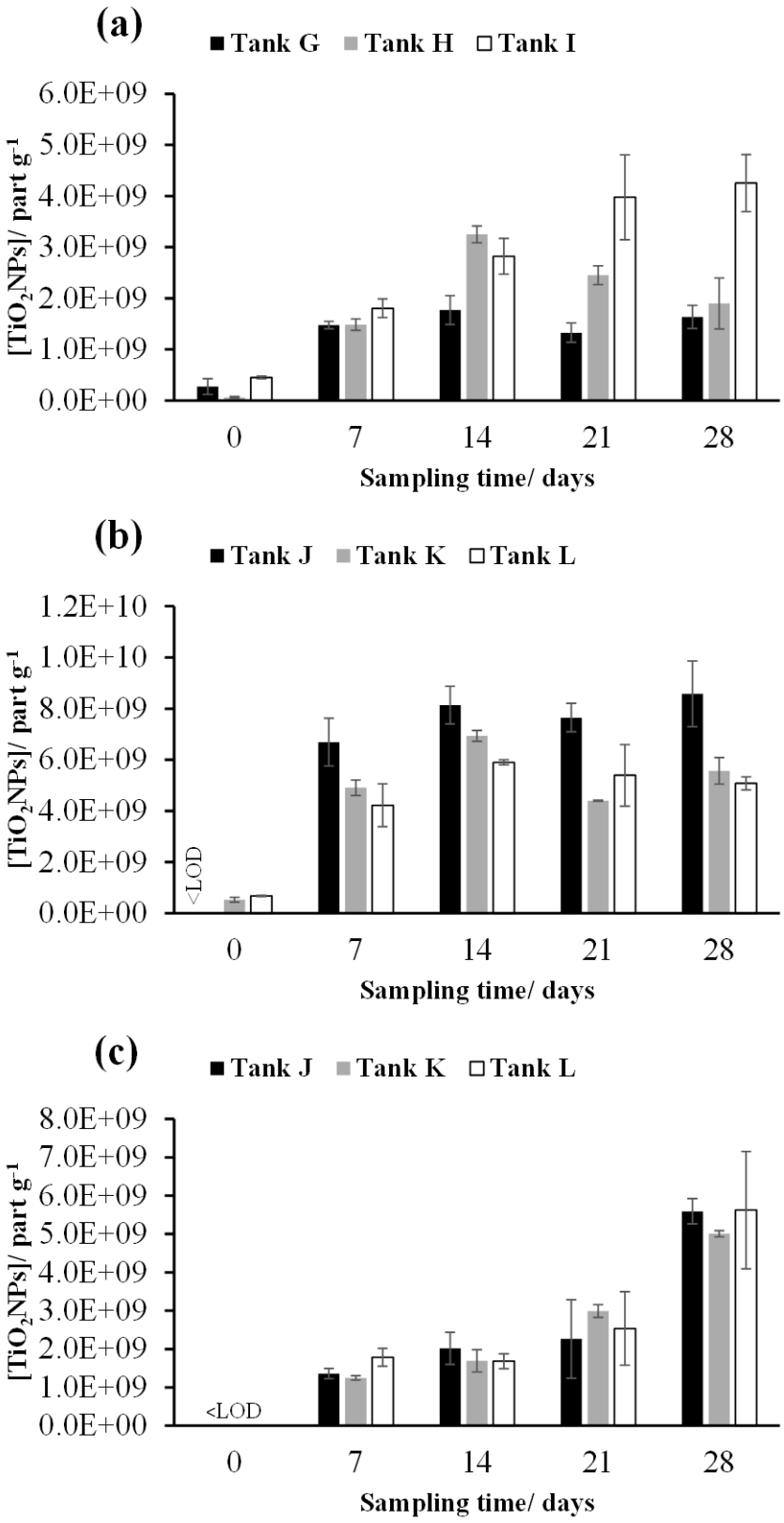

Figure S.4.9. Content of TiO_2NPs g^{-1} in *Ulva* sp. exposed to: (a) 0.1 mg L^{-1}, (b) 1.0 mg L^{-1} of 25 nm TiO_2NPs, and (c) 1.0 mg L^{-1} of 5 nm TiO_2NPs.

USC UNIVERSIDADE DE SANTIAGO DE COMPOSTELA

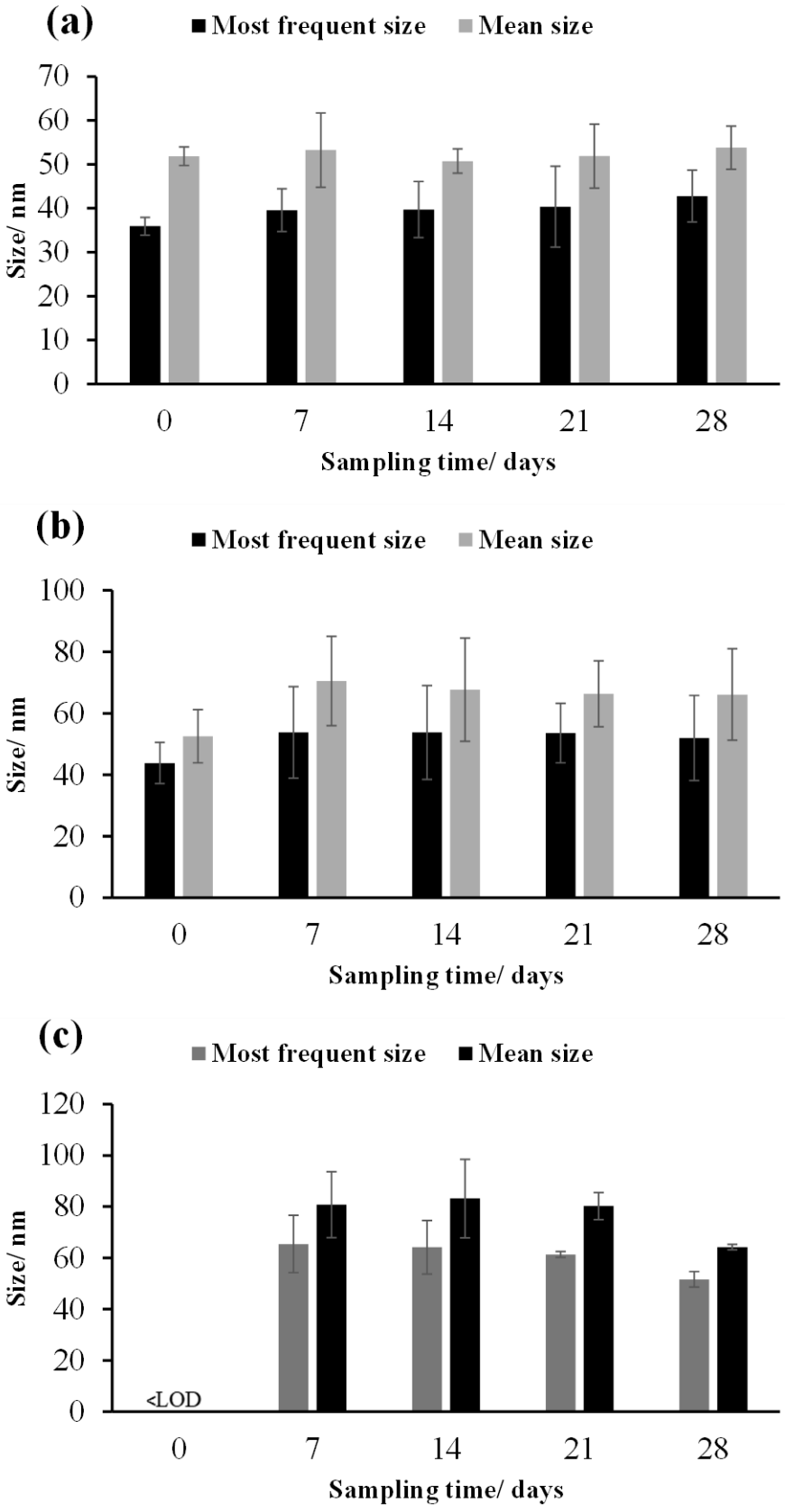

Figure S.4.10. Most frequent and mean sizes of nanoparticles in *Ulva* sp. exposed to: (a) 0.1 mg L^{-1}, (b) 1.0 mg L^{-1} of 25 nm TiO_2NPs, and (c) 1.0 mg L^{-1} of 5 nm TiO_2NPs.

REFERENCES

[1] A. Weir, P. Westerhoff, L. Fabricius, K. Hristovski, N. Von Goetz, Titanium dioxide nanoparticles in food and personal care products, Environ. Sci. Technol. 46 (2012) 2242–2250. https://doi.org/10.1021/es204168d.
[2] H. Shi, R. Magaye, V. Castranova, J. Zhao, Titanium dioxide nanoparticles: a review of current toxicological data, Part. and Fibre Toxicol. 10 (2013) 15. https://doi.org/10.1186/1743-8977-10-15.
[3] M. Younes, G. Aquilina, L. Castle, K. H. Engel, P. Fowler, M. J. Frutos Fernandez, P. Fürst, U. Gundert-Remy, R. Gürtler, T. Husøy, M. Manco, W. Mennes, P. Moldeus, S. Passamonti, R. Shah, I. Waalkens-Berendsen, D. Wölfle, E. Corsini, F. Cubadda, D. De Groot, R. Fitz Gerald, S. Gunnare, A. C. Gutleb, J. Mast, A. Mortensen, A. Oomen, A. Piersma, V. Plichta, B. Ulbrich, H. Van Loveren, D. Benford, M. Bignami, C. Bolognesi, R. Crebelli, M. Dusinska, F. Marcon, E. Nielsen, J. Schlatter, C. Vleminckx, S. Barmaz, M. Carfì, C. Civitella, A. Giarola, A. M. Rincon, R. Serafimova, C. Smeraldi, J. Tarazona, A. Tard, M. Wright, Safety assessment of titanium dioxide (E171) as a food additive, EFSA J. 19 (2021) 6585. https://doi.org/10.2903/j.efsa.2021.6585.
[4] European Commission, Commission Regulation (EU) 2022/63 of 14 January 2022 amending Annexes II and III to Regulation (EC) No 1333/2008 of European Parliament and of the Council as regards the food additive titanium dioxide (E171), Off. J. Eur. Union. 11 (2022) 1–5.
[5] IARC, IARC monographs on the evaluation of carcinogenic risks to humans, Monogr. Eval. Carcinog Risks to Humans 93 (2010) 9–38.https://doi.org/10.1136/jcp.48.7.691-a.
[6] L. Canesi, C. Ciacci, D. Vallotto, G. Gallo, A. Marcomini, G. Pojana, *In vitro* effects of suspensions of selected nanoparticles (C60 fullerene, TiO_2, SiO_2) on *Mytilus* hemocytes, Aquat Toxicol. 96 (2010) 151–158.https://doi.org/10.1016/j.aquatox.2009.10.017.
[7] X. Zhu, J. Zhou, Z. Cai, The toxicity and oxidative stress of TiO_2 nanoparticles in marine abalone (*Haliotis diversicolor supertexta*), Mar Pollut Bull 63 (2011) 334–338. https://doi.org/10.1016/j.marpolbul.2011.03.006.
[8] D. Minetto, G. Libralato, A. Volpi Ghirardini, Ecotoxicity of engineered TiO_2 nanoparticles to saltwater organisms: An overview, Environ Int 66 (2014) 18–27. https://doi.org/10.1016/j.envint.2014.01.012.
[9] A. Menard, D. Drobne, A. Jemec, Ecotoxicity of nanosized TiO_2. Review of in vivo data, Environ. Pollut. 159 (2011) 677–684. https://doi.org/10.1016/j.envpol.2010.11.027.
[10] S. Manzo, S. Buono, G. Rametta, M. Miglietta, S. Schiavo, G. Di Francia, The diverse toxic effect of SiO_2 and TiO_2 nanoparticles toward the marine microalgae *Dunaliella tertiolecta*, Environ Sci Pollut Res 22 (2015) 15941–15951. https://doi.org/10.1007/s11356-015-4790-2.
[11] V. Thiagarajan, M. Pavani, S. Archanaa, R. Seenivasan, N. Chandrasekaran, G. K. Suraishkumar, A. Mukherjee, Diminishing bioavailability and toxicity of P25 TiO_2 NPs during continuous exposure to marine algae *Chlorella* sp., Chemosphere 233 (2019) 363–372. https://doi.org/10.1016/j.chemosphere.2019.05.270.
[12] M. Bhuvaneshwari, V. Thiagarajan, P. Nemade, N. Chandrasekaran, A. Mukherjee, Toxicity and trophic transfer of P25 TiO_2 NPs from *Dunaliella salina* to *Artemia salina*: Effect of dietary and waterborne exposure, Environ. Res. 160 (2018) 39–46. https://doi.org/10.1016/j.envres.2017.09.022.

USC UNIVERSIDADE DE SANTIAGO DE COMPOSTELA

[13] H. Yaich, H. Garna, S. Besbes, M. Paquot, C. Blecker, H. Attia, Chemical composition and functional properties of *Ulva lactuca* seaweed collected in Tunisia, Food Chem. 128 (2011) 895–890. https://doi.org/10.1016/j.foodchem.2011.03.114.
[14] H. P. S. Abdul Khalil, T. K. Lai, Y. Y. Tye, S. Rizal, E. W. N. Chong, S. W. Yap, A. A. Hamzah, M. R. Nurul Fazita, M. T. Paridahe, A review of extractions of seaweed hydrocolloids: Properties and applications, Express Polym. Lett. 12 (2018) 296–317. https://doi.org/10.3144/expresspolymlett.2018.27.
[15] A. Moreda-Piñeiro, E. Peña-Vázquez, P. Bermejo-Barrera, Significance of the presence of trace and ultratrace elements in seaweeds, 116–170, Chapter in Handbook of marine macroalgae, Biotechnol. Appl. Phycol, John Wiley & Sons, Ltd (2011). ISBN:9781119977087. https://doi.org/10.1002/9781119977087.ch6.
[16] S. Ryan, P. McLoughlin, O. 'Donovan, A comprehensive study of metal distribution in three main classes of seaweed, Environ. Pollut. 167 (2012) 171–177. https://doi.org/10.1016/j.envpol.2012.04.006.
[17] T. A. Jarvis, G. K. Bielmyer-Fraser, Accumulation and effects of metal mixtures in two seaweed species. Comp. Biochem. Physiol. Part-C Toxicol. Pharmacol. 171 (2015) 28–33. https://doi.org/10.1016/j.cbpc.2015.03.005.
[18] M. L. Carvalho, J. G. Ferreira, P. Amorim, M. I. M. Marques, M. T. Ramos, Study of heavy metals and other elements in macrophyte algae using energy-dispersive X-ray fluorescence, Environ. Toxicol. Chem. 16 (1997) 807–812. https://doi.org/10.1002/etc.5620160427.
[19] N. Misheer, A. Kindness, S. B. Jonnalagadda, Seaweeds along KwaZulu-Natal coast of South Africa-4: Elemental uptake by edible seaweed *Caulerpa racemosa* (Sea grapes) and the arsenic speciation, J. Environ. Sci. Health-Part A Toxic/Hazardous Subst. Environ. Eng. 41 (2006) 1217–1233. https://doi.org/10.1080/10934520600656489.
[20] N. Misheer, A. Kindness, S. Jonnalagadda, Seaweeds along KwaZulu-Natal coast of South Africa-3: Elemental uptake by *Ulva lactuca* (Sea lettuce), J. Environ. Sci. Health-Part A Toxic/Hazardous Subst. Environ. Eng. 41 (2006) 1249–1259. https://doi.org/10.1080/10934520600623158.
[21] N. Misheer, A. Kindness, S. Jonnalagadda, Elemental distribution in seaweed, Gelidium abbottiorum along the KwaZulu-Natal coastline, South Africa, J. Environ. Sci. Health-Part A Toxic/Hazardous Subst. Environ. Eng. 41 (2006) 1639–1653. https://doi.org/10.1080/10934520600754441.
[22] N. Misheer, A. Kindness, S. B. Jonnalagadda, Elemental uptake by seaweed, *Plocamium corallorhirza* along the KwaZulu-Natal Coast of Indian Ocean, South Africa, J. Environ. Sci. Health.-Part B Pestic. Food Contam. Agric. Wastes 41 (2006) 1037–1048. http://dx.doi.org/10.1080/03601230600808893.
[23] D. Desideri, C. Cantaluppi, F. Ceccotto, M. A. Meli, C. Roselli, L. Feduzi, Essential and toxic elements in seaweeds for human consumption, J. Toxicol. Environ. Health-Part A Curr. Issues 79 (2016) 112–122. https://doi.org/10.1080/15287394.2015.1113598.
[24] F. Corrias, A. Atzei, P. Addis, M. Secci, M. Russo, A. Angioni, Integrated environmental evaluation of heavy metals and metalloids bioaccumulation in invertebrates and seaweeds from different marine coastal areas of Sardinia, Mediterranean Sea, Environ. Pollut. 266 (2020) 115048. https://doi.org/10.1016/j.envpol.2020.115048.
[25] A. Turner, D. Brice, M. T. Brown, Interactions of silver nanoparticles with the marine macroalga, *Ulva lactuca*, Ecotoxicology 21 (2012) 148–154. https://doi.org/10.1007/s10646-011-0774-2.

USC UNIVERSIDADE DE SANTIAGO DE COMPOSTELA

[26] S. Siddiqui, G. Bielmyer-Fraser, Accumulation and effects of dissolved and nanoparticle silver and copper in two marine seaweed species, Georg. J. Sci. 77 (2019) 1-17.
[27] P. Malea, A. Emmanouilidis, D. P. Kevrekidis, M. Moustakas, Copper uptake kinetics and toxicological effects of ionic Cu and CuO nanoparticles on the seaweed *Ulva rigida*, Environ. Sci. Pollut. Res. 29 (2022) 57523-57542. https://doi.org/10.1007/s11356-022-19571-7.
[28]. J. J. López-Mayán, S. del A. Monroy, E. Peña-Vázquez, M. C. Barciela-Alonso, P. Bermejo-Barrera, A. Moreda-Piñeiro, Titanium dioxide nanoparticles assessment in seaweeds by single particle inductively coupled plasma–mass spectrometry, Talanta 236 (2022) 122856. https://doi.org/10.1016/j.talanta.2021.122856.
[29] C. Stephan, K. Neubauer, E. Pruszkowski, New frontiers in biomonitoring : Total and single particle analysis of titanium in serum, Application Note (2018) 1–4. Perkin Elmer. https://resources.perkinelmer.com/lab-solutions/resources/docs/app_014338_01_nexion_sp-icp-ms_ti_nps_in_serum.pdf.
[30] Y. Canchanya-Huaman, A. F. Mayta-Armas, J. Pomalaya-Velasco, Y. Bendezú-Roca, J. A. Guerra, J. A. Ramos-Guivar, Strain and grain size determination of CeO_2 and TiO_2 nanoparticles: Comparing integral breadth methods versus Rietveld, μ-raman, and TEM. Nanomaterials 11 (2021) 2311. https://doi.org/10.3390/nano11092311.
[31] K. Ponnuchamy, J. A. Jacob, Metal nanoparticles from marine seaweeds-A review. Nanotechnol. Rev. 5 (2016) 589–600. https://doi.org/10.1515/ntrev-2016-0010.
[32] T. L. Moore, L. Rodriguez-Lorenzo, V. Hirsch, S. Balog, D. Urban, C. Jud, B. Rothen-Rutishauser, M. Lattuada, A. Petri-Fink, Nanoparticle colloidal stability in cell culture media and impact on cellular interactions, Chem. Soc. Rev. 44 (2015) 6287–6305. https://doi.org/10.1039/C4CS00487F.
[33] Handbook of Marine Macroalgae, Appl Phycol, John Wiley & Sons, Ltd. (2011). ISBN:9781119977087. https://doi.org/10.1002/9781119977087.
[34] F. Laborda, A. C. Giménez-Ingalaturre, E. Bolea, J. R. Castillo, About detectability and limits of detection in single particle inductively coupled plasma mass spectrometry, Spectrochim. Acta-Part B At. Spectrosc. 169 (2020) 105883. https://doi.org/10.1016/j.sab.2020.105883.
[35] F. Wang, W. Guan, L. Xu, Z. Ding, H. Ma, A. Ma, N. Terry, Effects of nanoparticles on algae: Adsorption, distribution, ecotoxicity and fate, Appl. Sci. 9 (2019) 1534. https://doi.org/10.3390/app9081534.
[36] C. C. Li, F. Dang, M. Li, M. Zhu, H. Zhong, H. Hintelmann, D. Zhou, Effects of exposure pathways on the accumulation and phytotoxicity of silver nanoparticles in soybean and rice, Nanotoxicology 11 (2017) 699–709. https://doi.org/10.1080/17435390.2017.1344740.
[37] Y. Deng, E. J. Petersen, K. E. Challis, S. A. Rabb, R. D. Holbrook, J. F. Ranville, B. C. Nelson, B. Xing, Multiple method analysis of TiO_2 nanoparticle uptake in rice (*Oryza sativa L.*) Plants, Environ. Sci. Technol. 51 (2017) 10615–10623. https://doi.org/10.1021/acs.est.7b01364.
[38.] M. Hasan-Nia, M. Rezaei-Tavirani, A. R. Nikoofar, H. Masoumi, R. Nasr, H. Hasanzadeh, M. Jadidi, M. Shadnush, Stabilizing and dispersing methods of TiO_2 nanoparticles in biological studies, J. Paramed. Sci. Spring 6 (2015) 96-105. https://doi.org/10.22037/jps.v6i2.8686.

USC UNIVERSIDADE DE SANTIAGO DE COMPOSTELA

USC
UNIVERSIDADE
DE SANTIAGO
DE COMPOSTELA

CHAPTER 5. BIOACCUMULATION OF SILVER NANOPARTICLES IN MUSSELS AND TURBOT FROM THE ATLANTIC AREA

USC
UNIVERSIDADE DE SANTIAGO DE COMPOSTELA

USC
UNIVERSIDADE
DE SANTIAGO
DE COMPOSTELA

CHAPTER 5. BIOACCUMULATION OF SILVER NANOPARTICLES IN MUSSELS AND TURBOT FROM THE ATLANTIC AREA

5.1 ABSTRACT

Silver nanoparticles (AgNPs) are widely used in the industry due to their properties, and they could interact with and damage marine organisms. To maintain the safety and food quality of significant aquaculture species in the Atlantic area, such as *Mytilus edulis* (mussels) and *Scophthalmus maximus* (turbot), bioaccumulation studies of Ag nanoparticles are required. In this research work, mussels and turbot were exposed to 15 nm PVP-AgNPs for a long time. For mussels, the bioaccumulation assay lasted 28 days and they were exposed to 0.1 and 1.0 mg L^{-1} of PVP-AgNPs. For turbot, the bioaccumulation assay lasted 105 days, and specimens were exposed to 0, 0.25, 0.75, and 1.5 mg PVP-AgNPs kg^{-1} fish and day. The entire mussel was examined in the bioaccumulation assay, whereas in the case of turbot, flesh+skin, liver, and kidney were analyzed separately. Total Ag concentration and AgNPs concentration and size distributions in both species were determined by inductively coupled plasma mass spectrometry (ICP-MS) and single-particle-ICP-MS (SP-ICP-MS), respectively.

The highest Ag concentration measured in mussels was 1.40±0.25 µg g^{-1} w.w. (wet weight) at the low exposure dose on the 28th day, and the highest AgNPs concentration was $2.14\times10^{8}\pm4.49\times10^{7}$ part g^{-1} w.w. at the high exposure dose on the 28th day. The presence in the tanks of a discharged surface scum containing Ag and AgNPs agrees with the absence of bioaccumulation at the high exposure dose in comparison to the low exposure dose. Furthermore, in the turbot bioaccumulation assay, the highest Ag concentrations were found in the liver (non-edible part) reaching 6.47±2.46 µg g^{-1} w.w., but no particles were detected. The results confirm the safety of turbot consumption and highlight the need for a proper depuration process in mussels.

5.2 INTRODUCTION

Nanotechnology is at constant growth due to the novel properties of nanomaterials (NMs). In fact, according to the Scopus database, the use of the term nanoparticle increased from appearing in 35 papers in 1990 to 72,421 papers in 2021[1]. Besides, the Nanotechnology Products Database [2] contains 10,373 nanomaterials products manufactured by 3,399 companies in 65 different countries. Of all these nanomaterials, 1,210 products contain Ag nanoparticles (AgNPs) and are applied in 15 different sectors, with medicine, textile, cosmetics, home appliance, environment and construction dominating the scene [2]. They are one of the most common inorganic NPs used due to their novel properties, which include mainly antimicrobial, antifungal, and antibacterial characteristics among others [3,4]. Due to the different application sectors of AgNPs, it is expected that the AgNPs' presence will increase in the environment mostly in marine ecosystems, where they could interact with some important aquatic species like *Mytilus* sp., and *Scophthalmus maximus*.

Although China is the main aquaculture producer in the world, Spain is the main aquaculture producer in tons in the European Union (EU) [5]. The main species produced in the EU is *Mytilus* sp., and turbot ranked 10th. Besides, according to the Spanish Ministry of Agriculture, Fisheries and Food, mussels were the main aquaculture mollusk produced in Spain

USC DE COMPOSTELA

in 2021 with 255,283 tons, where more than 95% of the production was from Galicia [6]. In contrast, turbot ranked third in 2021 in terms of fish aquaculture output (behind sea bass and sea bream) with 7,630 tons. In this scenario, Galicia is the sole source of turbot farming.

Mollusks are traditionally considered indicators of environmental pollution because they are filter feeders and accumulate contaminants in seawater [4]. Mussels are stationary benthic bivalves that filter large amounts of seawater to obtain phytoplankton (their main food) [7]. Then, their tissues can process and accumulate microalgae, sediments, bacteria, toxins, trace elements, heavy metals, and even nanomaterials (NMs) including AgNPs from the aquatic media [8,9]. Furthermore, mussels could be an essential vector for the trophic transfer of metals from microalgae and sediment to economically important species [10]. In contrast, turbot is an economically important flatfish around the world [11], and it is very highly appreciated due to its nutritional value. It is a benthic carnivorous fish [12], and could ingest contaminated benthic organisms present in the biota (e.g. bivalve mollusks like clams), enhancing the bioaccumulation through trophic transfer. Thus, the bioaccumulation and toxic effects of AgNPs in benthic organisms and their possible predators must be elucidated, due to their commercial importance.

Some reports showed the importance of studying the bioaccumulation of AgNPs in different benthic organisms. Sun et al. [13] employed tetramethylammonium hydroxide (TMAH) with the addition of bovine serum albumin (BSA) for the extraction of Ag, Au and Ti-containing NPs from mussels, and analysis by SP-ICP-MS [13]. Taboada-López et al. [8] developed a methodology to study AgNPs in mollusks samples (clams, cockles, mussels, razor clams, oysters and variegated scallops) using ultrasound-assisted enzymatic extractions with a pancreatin/lipase mixture, and analysis of samples by SP-ICP-MS. Xu et al. [14] studied the bioconcentration factors (BCFs) of AgNPs in oysters, mussels, scallops, clams, and ark shells from offshore aquaculture farms using pancreatin/lipase extractions and SP-ICP-MS analysis. The lowest BCFs were found in clams, and the largest amount of particles were found in the gills and digestive glands of the five species [14].

Besides, some reports showed the toxicity of Ag nanomaterials in different shellfish. Mohamed et al. [15] studied the toxicity of Ag nanocomposites in a freshwater clam, *Caelatura aegyptiaca* that exhibited histological alterations in labial palp, gills, and foot tissues [15]. Buffet et al. [16] studied bioaccumulation and the toxic effects in *Scrobicularia plana* exposed to AgNPs and $AgNO_3$ in a marine mesocosm for 21 days. The results showed that AgNPs induced oxidative stress and DNA damage. Buffet et al. [10] also studied the biochemical and behavioural responses of *Scrobicularia plana* exposed to 10 µg L^{-1} of AgNPs for 14 days directly in seawater and through a microalgae diet. Ag bioaccumulation was higher after waterborne than dietary exposure but the response to different stress biomarkers was more important after dietary exposure to Ag (ionic or as NPs) [10]. Liu et al. [17] also studied the toxicity effects of AgNPs in freshwater bivalves in *Corbicula fluminea*. The results revealed that the bioaccumulation of Ag resulted in oxidative damage and inhibition of physiological metabolism in the shellfish [17]. Gomes et al. [18] studied the effect of 15 days of exposure to 10 µg L^{-1} AgNPs in *Mytilus galloprovincialis*. Biomarkers of oxidative stress and metal accumulation were determined. Results showed an accumulation of Ag^+ and AgNPs in gills and digestive glands. However, it was not clear if the oxidative stress process is due to the nanoparticulate form or the dissolved ions [18]. Duroudier et al. [19] also studied the cell and tissue responses of *Mytilus galloprovincialis* exposed to PEI/PVP-AgNPs in two different seasons. The results showed a significative accumulation of Ag after 21 exposure days to 10 µg AgNPs L^{-1} in autumn and spring. The higher Ag levels were found in autumn compared to

USC UNIVERSIDADE DE SANTIAGO DE COMPOSTELA

spring. DNA strand breaks increased significantly in hemocytes at both exposure doses during the 21 days in spring [19].

On the other hand, some reports were found about AgNPs in different kinds of fish. Scown et al. [20] studied the effects of AgNPs in rainbow trout exposed to AgNPs (10 and 35 nm), bulk Ag particles (600-1600 nm), or $AgNO_3$ for 10 days. The uptake into gills, liver, and kidney was quantified by inductively coupled plasma optical emission spectrometry (ICP-OES). Lacave et al. [21] studied the presence and effects of maltose-AgNPs and ionic Ag in adult zebrafish exposed for 21 days, and the damage 6 months afterwards. Ag concentrations were determined in the whole fish tissue by ICP-OES. However, the use of autometallographical staining was used to examine metal accumulation in specific organs, with metallic buildup occurring in the liver and intestine of fish treated with the two Ag forms, particularly in the intestine of fish exposed to Ag NPs. X-ray microanalysis was more sensitive to detecting Ag in the gills. The hepatic transcriptome showed a bigger effect for AgNPs than ionic Ag after 21 days of exposure [21]. The bioaccumulation kinetics and tissue distribution of AgNPs in zebrafish were also described by Xiao et al. [22]. The BCFs in the zebrafish body were lowered by the natural organic matter (NOM) presence, which also accelerated the rate of depuration. The ICP-MS showed the presence of Ag in the whole fish, but mainly in the liver, intestine and gills [22]. Sung et al. [23] also reported the BCFs in target tissues (liver, intestine, and gill) of zebrafish exposed to 30 and 80 nm PVP-AgNPs for 7 days. The alkaline extraction and SP-ICP-MS analysis showed lower BCFs for the smaller particles. The highest bioaccumulation factor was found for the 80 nm PVP-AgNPs in the intestine whereas smaller NPs were filtered and attached to the gill lamella [23].

Jang et al. [24] studied the toxicokinetics of Ag in common carp exposed to AgNPs for 7 days followed by two weeks depuration period. In the depuration period, there were indications of partial removal of Ag from tissues and a delayed removal of citrate-coated AgNPs from liver tissues. Clark et al. [25] also measured Ag concentration in rainbow trout after 28 exposure days to $AgNO_3$, AgNPs, or Ag_2SNPs, and after 14 days of depuration process. The highest concentration of Ag was found in the liver, and only minor reductions in organ concentrations were observed after the depuration time.

However, only a few reports are found about bioaccumulation in turbot. Farkas et al. [26] studied the exposure of juvenile turbots to PVP-AgNPs, ionic Ag, and 17α-ethinylestradiol (EE2) (in mixtures and individually) for 14 days by high resolution (HR)-ICP-MS. The highest ionic Ag and AgNPs concentrations were determined in the liver and gills, respectively.

To the best of our knowledge, although some publications are evaluating the bioaccumulation of Ag and the biomarker responses of AgNPs in mussels and turbot, no reports were found that studied the bioaccumulation pattern of 15 nm PVP-AgNPs over a long period nor determined the total content and AgNPs content and size distributions using ICP-MS and SP-ICP-MS, respectively. Thus, the main goal of this work is to study AgNPs bioaccumulation in mussels and different organs of turbots (muscle+skin, liver, and kidney) after chronic exposure to different doses of 15 nm PVP-AgNPs using enzymatic extractions and SP-ICP-MS analysis.

5.3 MATERIALS AND METHODS

5.3.1 Instrumentation

A quadrupole-based inductively coupled plasma-mass spectrometer NexION® 2000 from Perkin Elmer, (Waltham, MA, USA) with a Kinetic Energy Discrimination (KED) module was employed for total Ag determination. The ICP-MS instrument was equipped with a quartz torch

USC DE COMPOSTELA

and a quartz injector (2.5 mm i.d.), and a triple nickel cone system (sampler, skimmer, and hyperskimmer). The single-particle mode of ICP-MS (SP-ICP-MS) controlled by the Syngistix™ Nano Application 2.5 software (Perkin Elmer) was employed for the determination of AgNPs concentration and size distribution. An Ethos Plus microwave lab station from Milestone (Bergamo, Italy) was used for fish and mussel tissue digestion. A Boxcult temperature-controlled incubation chamber from Stuart Scientific (Surrey, UK) equipped with a Rotabit orbital-rocking platform shaker from J.P. Selecta (Barcelona, Spain) was used for AgNPs extraction. A VWR Ultrasonic Cleaner (Barcelona, Spain) and a Basic20 pH meter from Crison (Barcelona, Spain) were employed for NPs dispersion and buffer pH adjustments, respectively. Other instrumentation employed to perform the analysis included a Reax top vortex vibrational shaker from Heidolph (Schwabach, Germany), and an analytical balance ML204 from Mettler Toledo (Barcelona, Spain).

5.3.2 Reagents, standards, and materials

The AgNPs employed in the bioaccumulation assays in turbot and mussel assays were a polyvinylpyrrolidone (PVP) coated Ag nanopowder of 15 nm and a concentration of 5.4×10^{14} particles mL^{-1} from SkySpring Nanomaterials, Inc. (Houston, TX, USA). Ultrapure water (18 MΩ cm of resistivity), obtained from a Milli-Q® IQ7003 from Millipore Co. (Bedford, MA, USA) purification system was used to prepare most of the work solutions. For acid digestions, 69% (w/v) hyperpure nitric acid from Sigma Aldrich (Darmstadt, Germany) and 33% (w/v) hydrogen peroxide from Panreac (Barcelona, Spain), were used. To carry out AgNPs extractions, porcine pancreatin and lipase from *Candida rugose* both from Sigma Aldrich, (Osterode, Germany) were diluted in a buffer (pH=7.4) prepared from $NaH_2PO_4{\cdot}H_2O$ and NaOH, both from Merck (Darmstadt, Germany). To perform the calibrations an ionic Ag stock solution (1000 mg L^{-1}) in 2% HNO_3 from Perkin Elmer (Shelton, CT, USA) was used. An Rh stock solution (1000 mg L^{-1}) in 2% HCl from Perkin Elmer was diluted to be used as an internal standard. Reference material of PEG-COOH Gold Nanospheres (49.6 nm and 9.89×10^{6} particles mL^{-1}) from NanoComposix (San Diego, CA, USA), and ionic Au stock standard (1000 mg L^{-1}) in 2 mol L^{-1} HCl from Merck (Darmstadt, Germany) were used for transport efficiency calculations in SP-ICP-MS.

Other used reagents were 1% (v/v) glycerol from Merck for AgNPs extracts dilutions before SP-ICP-MS analysis, a NexION Setup Solution (1.0 µg L^{-1} of Be, Ce, Fe, In, Li, Mg, Pb, and U in 1% HNO_3) from Perkin Elmer for ICP-MS adjustments, and He and Ar both with a 99,999% of purity from Nippon Gases (Madrid, Spain) for ICP-MS performance. Some used plastic materials include Minisart NML hydrophilic non-sterile 5.0 µm filters from Sartorius (Goettingen, Germany), tubes, pipette tips, and syringes. Finally, all the glassware materials were submitted to an ultra-trace decontamination protocol with 10% (v/v) nitric acid.

5.3.3 Mussel and turbot cultivation

The aquaculture species of this research work were cultured in the Atlantic area. *Mytilus edulis* (mussels) were from the Indigo Rock Marine Research Center (Cork, Ireland) and *Scophthalmus maximus* (turbots) were from the Technological Center of Aquaculture of Galicia (Galicia, Spain). Both aquaculture species were fed with PVP-AgNPs of 15 nm. The mussel bioaccumulation assay lasted 28 days and mussels were exposed to 0, 0.1, and 1.0 mg L^{-1} of PVP-AgNPs. However, due to turbot's slower growth, their bioaccumulation assay lasted 3 months and they were exposed to 0, 0.25, 0.75, and 1.5 mg kg^{-1} fish and a day of PVP-AgNPs.

Indigo Rock's facilities included the forty-liter tanks where the mussels were grown and fed. The bioaccumulation experiment consisted of twelve tanks: three control tanks (A, B, and

C) without NPs exposure, three solvent control tanks (D, E, and F) exposed to NPs coating (PVP), three low-exposure dose tanks (G, H, and I) of 0.1 mg L^{-1} of PVP-AgNPs, and three high-exposure tanks (J, K, and L) of 1.0 mg L^{-1} of PVP-AgNPs. Mussels were exposed to periods of 12 hours of white light and 12 hours of darkness at 16±1 ºC. Common parameters were monitored every day (pH, temperature, dissolved O_2, and salinity), and other parameters like conductivity, ammonium, and nitrites were tested twice a week. Mussels were fed with zooplankton made by capepods and rotifers, every Monday, Tuesday, Thursday, and Friday. The addition of particles occurred on Wednesday with a 30 mL solution containing 3 mL of phytoplankton, and the corresponding AgNPs concentration depending on the tank or the coating (in the case of solvent control tanks). Three mussel replicates were sampled from each tank every 7 days, resulting in 180 mussels samples. The mussels were washed with ultrapure water to remove salts and contaminants, and frozen at -18 ºC before their analysis.

The Technological Center of Aquaculture of Galicia (CETGA´s) facilities included the five hundred-liter tanks where the juvenile turbots (initial weight around 70 g) were grown and fed, at 14±1 ºC. The bioaccumulation experiment consisted of twelve tanks: three control tanks without PVP-AgNPs exposure (0 mg PVP-AgNPs kg^{-1} fish and day), three tanks exposed to 0.25 mg PVP-AgNPs kg^{-1} fish and day, three tanks exposed to 0.75 mg PVP-AgNPs kg^{-1} fish and day, and three tanks exposed to 1.5 mg PVP-AgNPs kg^{-1} fish and day. The feed was mixed with the NPs to obtain the final concentrations required. To prepare the feed with the PVP-AgNPs was necessary to take into account the different average turbot weights (n=50 turbots per tank) at different sampling times.

Two tanks of each type (0, 0.25, 0.75 and 1.5 mg PVP-AgNPs kg^{-1} fish and day) were sampled randomly (1 specimen was taken from every tank and sample day and dissected) every 15 days, resulting in 102 finally dissected samples. The liver, kidney, and tissue+skin samples were frozen at -18 ºC before their analysis.

5.3.4 Microwave-assisted acid digestion and total Ag determination

Microwave-assisted acid digestion was employed to treat the aquaculture samples before total Ag determination by ICP-MS. Mussels and different turbot samples were crushed and homogenized and introduced in the Teflon vessels of the microwave oven described in **section 5.3.1**. The wet samples were mixed with 1 mL of 33% (w/v) H_2O_2, 3 mL of 69% (w/v) HNO_3, and 4 mL of ultrapure water. **Table S.5.1.** (supplementary information) shows the microwave program to which the samples were subjected. When the amount of sample was sufficient, 3 replicates and 2 blanks per set of digests, were processed. For total Ag determinations, the digests diluted with ultrapure water were analyzed by ICP-MS as described in **section 5.3.1**. To ensure the quality of ICP-MS measurements, daily adjustment of the equipment must be guaranteed (torch alignment, nebulization flow, voltage adjustments, check of setup solution analytes intensities, and background control). The standard addition calibration procedure was used between 0 and 15 µg L^{-1} for Ag determination in mussel and turbot. The signals corresponding to ^{107}Ag and ^{109}Ag isotopes, and a solution of 5 µg L^{-1} of ^{103}Rh (internal standard) were registered. The operational conditions of ICP-MS are shown in **Table S.5.2.(a)**. The Kinetic Energy Discrimination (KED) measurement mode with 4.5 mL min^{-1} of He as collision gas was used to avoid polyatomic interferences.

5.3.5 Enzymatic extraction and AgNPs analysis

Enzymatic extractions were used to perform the isolation of PVP-AgNPs from fish and mussel samples. The extraction has to guarantee the integrity and size of the particles; thus, enzymatic extractions with mild conditions were chosen. The pancreatin/lipase combination

USC DE COMPOSTELA

was selected due to its ability to solubilize the fats present in fish tissues during the procedure. The methodology was properly optimized and validated in our investigation group [8]. Approximately 1.000 g of homogenized mussel or turbot samples (in triplicate if the sample is available) were mixed with 7.5 mL of a suspension containing 3.0 g L^{-1} of pancreatin and 3.0 g L^{-1} of lipase prepared in a buffer of 0.2M NaH_2PO_4/0.2M NaOH at physiological pH (7.4). The mixtures were submitted to overnight incubation in the chamber described in **section 5.3.1** at 150 rpm and 37 ºC. Finally, the enzymatic extracts were filtered with 5 µm filter disks and diluted with 1% (v/v) glycerol before SP-ICP-MS analysis.

The diluted extracts were properly analyzed by ICP-MS working in Single-Particle mode (SP-ICP-MS). The operational conditions of SP-ICP-MS are listed in **Table S.5.2.(b)**. Analytical measurements and calculations were performed with the help of the Syngistix™ ICP-MS 2.5 software, after obtaining the flow rate and transport efficiency (TE%) values. To measure the flow rate, ultrapure water was aspirated through the peristaltic pump for one minute (n=3) in triplicate, and the mass difference corresponded to the flow rate. The SP-ICP-MS provided the TE% after the analysis of a Au ionic calibration (0-3.0 µg L^{-1}) and the certified reference NPs material of 49.6 nm Au nanospheres with a concentration of 9.89×10^4 particles mL^{-1}. The experimental TE% values were between 8.8-11.5%. The high dilution used in SP-ICP-MS and the short dwell times in the order of µs allowed the discrimination of the transitory signals of NPs from the continuous signal of the dissolved metal. Besides, the high dilution of the extracts avoids the matrix effect and then Ag ionic calibrations (0-5.0 µg L^{-1}) can be performed in ultrapure water. The NPs suspensions were stirred in an ultrasound bath to avoid agglomeration. Finally, the concentrations and size distributions of AgNPs were obtained directly from the software, and used to calculate the concentrations referred to the wet weight of aquaculture samples.

5.4 RESULTS AND DISCUSSION

5.4.1 Mussel bioaccumulation assay

5.4.1.1 Total Ag content in mussel samples exposed to PVP-AgNPs

Total Ag content in mussels was assessed using the methodology described in **section 5.3.4**. The digested samples were diluted with ultrapure water 10 times before ICP-MS analysis. The analytical performance was also guaranteed. The LOD and LOQ were calculated with the 3σ/m and 10σ/m criteria (where σ is the standard deviation of ten measurements of a blank, and m is the slope of the standard addition calibration graph). The LOD and LOQ resulted in 0.45 and 1.49 ng g^{-1} w.w., respectively. The precision of the methodology was validated through the repeatability of the measurements (n=5) with RSD<2%. Due to the lack of certified reference materials for AgNPs, the accuracy was evaluated through the analytical recovery, and it resulted in 106±9 % for a concentration of 0.5 µg L^{-1} of added Ag.

Ag was determined in control mussels, solvent control mussels exposed to PVP, mussels exposed to 0.1 mg L^{-1} of PVP-AgNPs, and exposed to 1.0 mg L^{-1} of PVP-AgNPs for 28 exposure days.

Figure 5.1.(a) shows the intertank average basal Ag concentration in control tanks (average of tanks A, B, and C) and tanks exposed to the PVP coating of the particles (average of tanks D, E, and F). One-way ANOVA tests were performed using the statistical software Statgraphics XVIII (Warrenton, USA) to compare the concentrations of Ag in control and solvent tanks at different exposure times. The P-value in the case of mussels in control tanks was higher than 0.05. Then, no statistical differences were found among Ag concentrations at

different times at a 95% of confidence level. However, the P-value in the case of mussels exposed to the PVP-coating was lower than 0.05, and then statistical differences were found between Ag concentrations at different exposure times. The multiple range test showed differences between 0 and 14, 21, and 28 days; between 7 and 14 days; and between 14 and 21 days. Despite this, in all cases, total Ag concentrations were lower than 0.05 μg g^{-1} w.w. and very close to the values measured in control tanks, and then no bioaccumulation was considered.

Figure 5.1.(b) also shows the bioaccumulation of Ag in tanks exposed to 0.1 and 1.0 mg L^{-1}. Ag concentration in mussels exposed to the low PVP-AgNPs concentration increased linearly with the exposure time until 28 days reaching 1.40±0.25 μg g^{-1} w.w. of Ag (intertank average concentration). The one-way ANOVA test showed in this case a P-value lower than 0.05, and then statistical differences between Ag concentrations were observed at the sampling times studied. The multiple range test in this case showed an overlap in concentrations between 7 days and 14 days, between 14 days and 21 days, and between 21 days and 28 days. In the case of mussels exposed to the high PVP-AgNPs concentration, Ag bioaccumulation increased until 28 days reaching 1.20±0.07 μg g^{-1} w.w. The one-way ANOVA test showed, in this case, a P-value again lower than 0.05, and then statistical differences among Ag concentrations as a function of sampling times. The multiple range test in this case showed an overlap in concentrations between 7 days with 14 and 21 days. Statistical analysis was also performed to compare the Ag concentrations between the different exposure concentrations (0.1 and 1.0 mg L^{-1}) on the same exposure days. No statistical differences at a 95% confidence level in the one-way ANOVA test were found between concentrations in mussels exposed to 0.1 and mussels exposed to 1.0 mg L^{-1} of PVP-AgNPs at 0, 14, 21 and 28 days. This could mean that maximum bioaccumulation was already reached after exposure to 0.1 mg L^{-1} of PVP-AgNPs.

USC
UNIVERSIDADE DE SANTIAGO DE COMPOSTELA

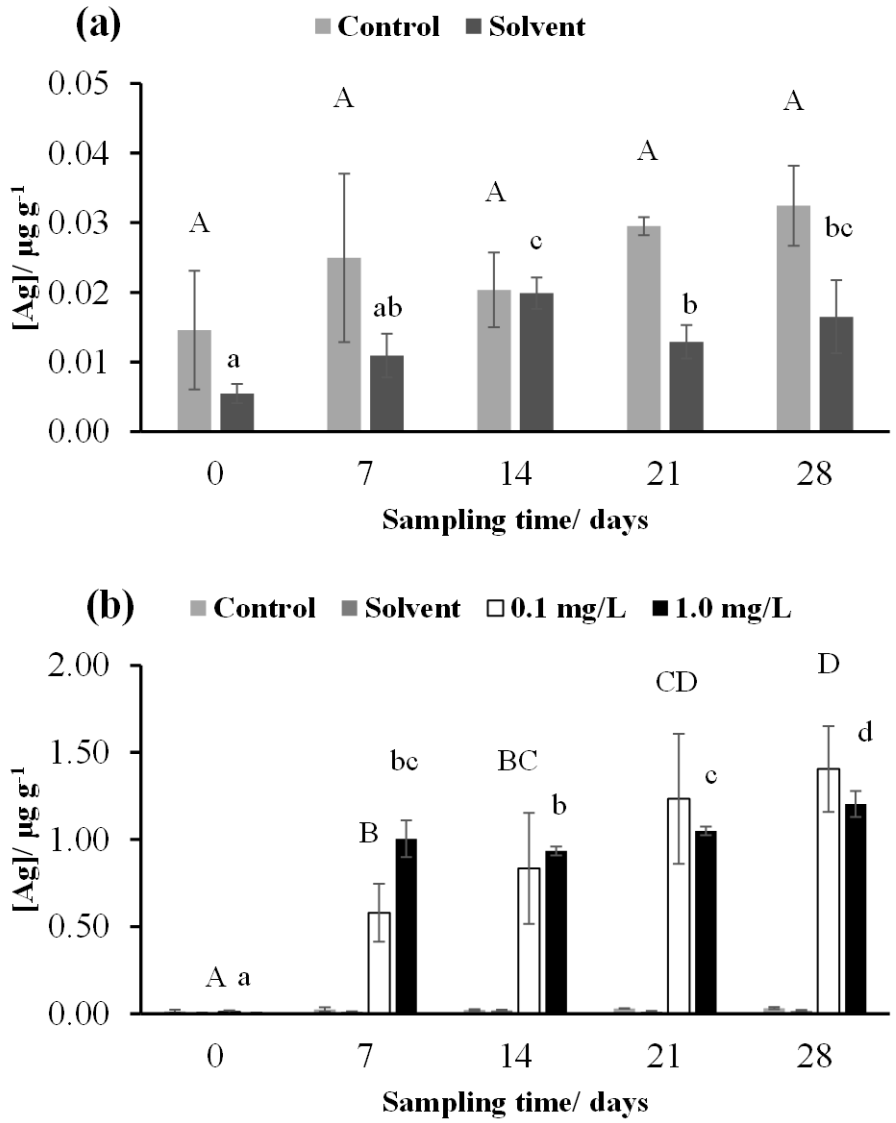

Figure 5.1. Intertank total Ag bioaccumulation in mussels exposed to PVP-AgNPs for 28 days: (a) control and PVP solvent control tanks; (b) control, PVP solvent control, 0.1 and 1.0 mg L^{-1} of PVP-AgNPs. Different letters indicate significative differences (one-way ANOVA, P-value<0.05) between the exposure time for each exposure dose (uppercase for control and 0.1 mg L^{-1} tanks and lowercase for solvent and 1.0 mg L^{-1} tanks).

Figure S.5.1. (supplementary information) shows total Ag bioaccumulation data corresponding to all the tanks of the experiment.

Besides, it was observed that after 23 days of exposure to 1.0 mg L^{-1} of PVP-AgNPs, a surface scum (shown in **Figure S.5.2.**) appeared in the tanks, probably due to the increase of dead cells from mussels in the presence of the current of the water movement of the tank.

Figure 5.2. shows the total Ag concentration measured in the surface scum from tanks J, K and L during the bioaccumulation trial and afterwards. The concentration of total Ag in the scum was measured at 23, 26 and 30 days. The highest Ag content was 1.14±0.02 µg L^{-1} w.w. in tank K at 26 days of PVP-AgNPs exposure. Total Ag content remained constant in the three tanks at 23 and 26 days but decreased on day 30 due to the cessation of NPs administration after 28 days (end of the experiment). This could explain why the bioaccumulation of Ag in mussels exposed to 1.0 mg L^{-1} did not increase in comparison to mussels exposed to 0.1 mg L^{-1}.

However, the fact that the surface scum with Ag continues appearing 3 days after the end of the experiment highlights the need for further purification of these mollusks.

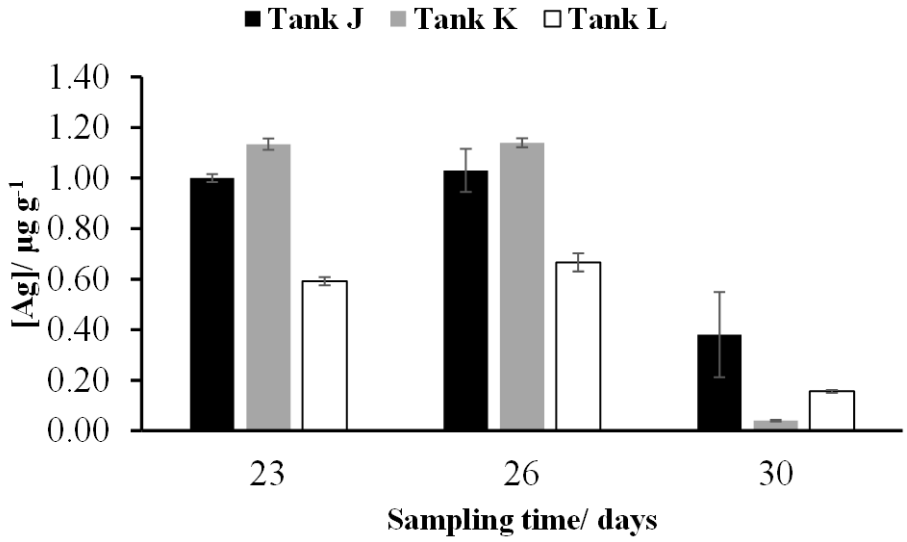

Figure 5.2. Total Ag content in surface scum from mussels tanks exposed to PVP-AgNPs for 28 days.

Taboada-López et al. [8] reported a basal Ag concentration in a mussel sample lower than 0.025 µg g^{-1}, which is in agreement with the basal Ag concentrations found in control and solvent tanks (<0.05 µg g^{-1}). However, Xu et al [14] reported a total basal Ag concentration in aquaculture mussels samples of 1.45±0.83 µg g^{-1}, which is in the same order as that found in the mussels samples exposed to 0.1 and 1.0 mg L^{-1} of PVP-AgNPs in this work.

5.4.1.2 AgNPs content in mussel samples after exposure

AgNPs content and size distribution in mussels were determined using the methodology described in **section 5.3.5**. The enzymatic extracts of mussels were diluted with 1% (v/v) glycerol 500 times before SP-ICP-MS measurements. The experimental transport efficiencies (TE%) for SP-ICP-MS were between 8.8-11.5%, and the flow rates were between 0.182-0.199 mL min^{-1}. The LODs were calculated using Laborda et al. [27] criteria. The instrumental LOD_{number} achieved was 1.71×10^6 AgNPs L^{-1} w.w. and the LOD_{number} referred to the sample was 6.42×10^6 AgNPs g^{-1} w.w. (calculated taking into account the dilution of 500 times). The LOD_{size} 3σ was 19 nm and the more restrictive LOD_{size} 5 σ was 23 nm. The precision of SP-ICP-MS was also validated through the repeatability in enzymatic extraction measurements, with RSD<15% (n=7).

Since total Ag in mussels from control tanks and tanks containing the PVP coating of the particles showed low basal Ag concentration, the pancreatin/lipase extractions were only performed in mussels exposed to the low and high PVP-AgNPs doses.

Figure 5.3.(a) shows the intertank average AgNPs concentration in the case of mussels exposed to 0.1 mg L^{-1} (average of tanks G, H, and I) and 1.0 mg L^{-1} of PVP-AgNPs (average of tanks J, K, and L). AgNPs concentrations were between $1.04\times10^7\pm1.90\times10^6$ part g^{-1} w.w. (day 0) and $1.22\times10^8\pm1.01\times10^8$ part g^{-1} w.w. (day 28) for 0.1 mg L^{-1} of PVP-AgNPs, and between $2.29\times10^7\pm5.90\times10^6$ part g^{-1} w.w. (day 0) and $2.14\times10^8\pm4.49\times10^7$ part g^{-1} w.w. (day 28) for 1.0 mg L^{-1} of PVP-AgNPs.

USC UNIVERSIDADE DE SANTIAGO DE COMPOSTELA

One-way ANOVA tests were performed to compare AgNPs mean concentrations at the different exposure days. The P-value was higher than 0.05 for mussels exposed to 0.1 mg L^{-1} of PVP-AgNPs; then no statistical differences were found between the AgNPs concentrations at a 95% of confidence level, probably due to the great variability of the data. However, in the case of mussels exposed to 1.0 mg L^{-1} of PVP-AgNPs, statistical differences between the AgNPs concentrations as a function of exposure time were found (P-value<0.05). In this case, the multiple range test showed differences in the concentrations between 0 and 21-28 exposure days. Bioaccumulation of PVP-AgNPs was observed for both exposure doses in comparison to day 0. **Figure S.5.3.** shows the AgNPs content in mussels from all the tanks of the experiment. Statistical analysis was also performed to compare AgNPs concentrations between the different exposure concentrations (0.1 and 1.0 mg L^{-1}) on the same exposure days. No statistical differences at a 95% confidence level in the one-way ANOVA test were found between mussels exposed to 0.1 and mussels exposed to 1.0 mg L^{-1} of PVP-AgNPs at 7, 14, 21 and 28 days. These results were in agreement with total Ag results, where the maximum bioaccumulation was already achieved at 0.1 mg L^{-1} PVP-AgNPs doses.

Figure 5.3.(b) and **Figure 5.3.(c)** show the most frequent and mean sizes of AgNPs in extracts from mussels exposed to 0.1 and 1.0 mg L^{-1} of PVP-AgNPs, respectively. The most frequent sizes were between 27±1 nm (0 days) and 30±7 nm (28 days), and between 23±3 nm (0 days) and 40±1 nm (28 days) for mussels exposed to 0.1 and 1.0 mg L^{-1} of PVP-AgNPs, respectively. On other hand, the mean sizes were between 34±1 nm (0 days) and 39±3 nm (28 days), and between 30±4 nm (0 days) and 49±3 nm (28 days) for mussels exposed to 0.1 and 1.0 mg L^{-1} of PVP-AgNPs, respectively.

These results showed higher sizes than the initial PVP-AgNPs measured by SP-ICP-MS in a previous work [28], where the most frequent size for the dissolved PVP-AgNPs standard was 15±1 nm. Besides, these results show an agglomeration of the nanoparticles that affected the most frequent and mean sizes measured at high exposure doses and exposure times. This agglomeration could be due to the interaction of the PVP-AgNPs with the mussels.

USC UNIVERSIDADE DE SANTIAGO DE COMPOSTELA

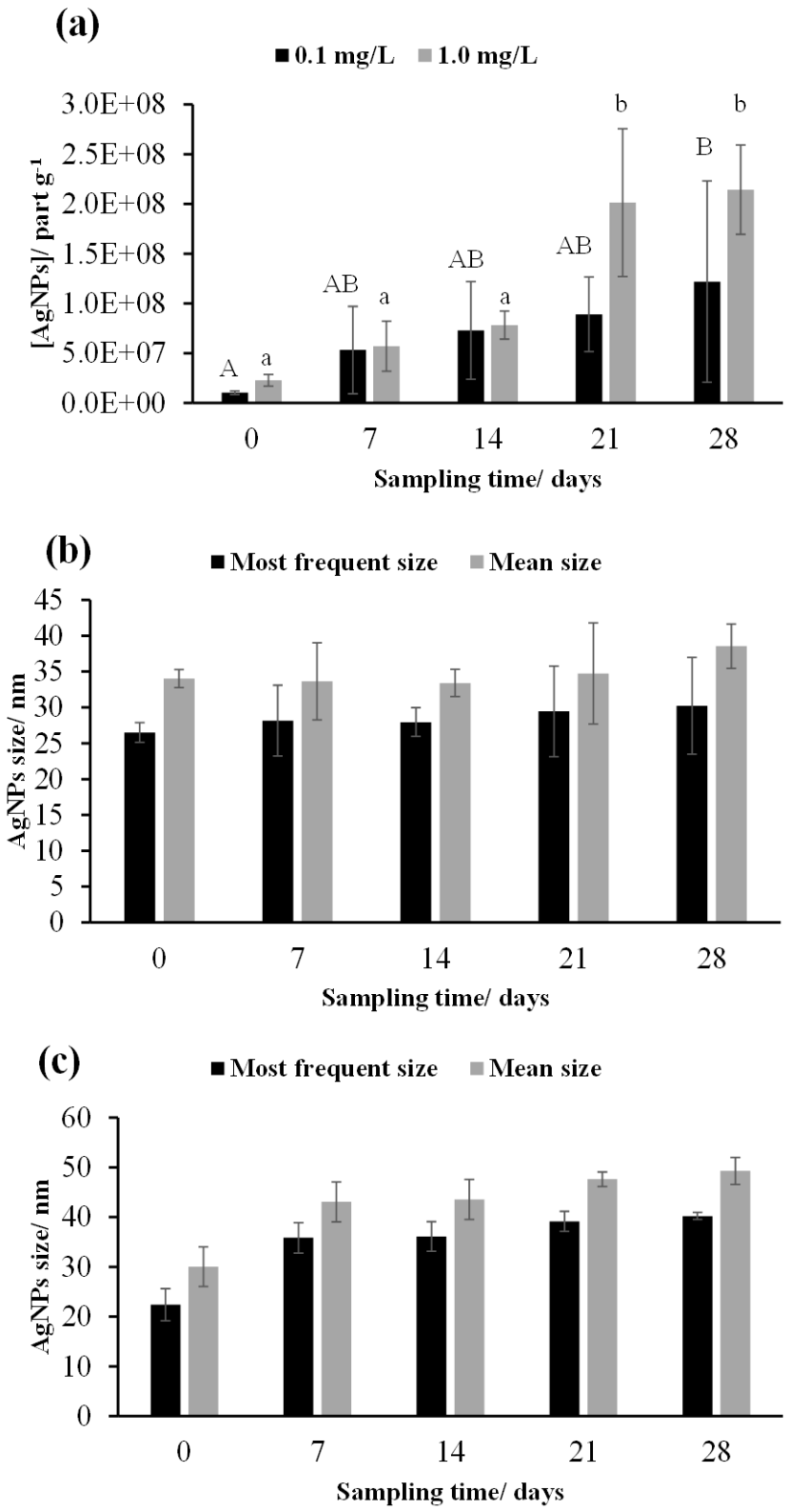

Figure 5.3. Intertank AgNPs bioaccumulation in cultured mussels exposed to PVP-AgNPs for 28 days: (a) AgNPs content, (b) most frequent and mean sizes in extracts from mussels exposed to 0.1 mg L^{-1} of PVP-AgNPs, and (c) 1.0 mg L^{-1} of PVP-AgNPs. Different letters indicate significative differences (one-way ANOVA, P-value<0.05) between the exposure time for each exposure dose (uppercase for 0.1 mg L^{-1} tanks and lowercase for 1.0 mg L^{-1} tanks).

USC UNIVERSIDADE DE SANTIAGO DE COMPOSTELA

Figure S.5.4.(a) and **Figure S.5.4.(b)** show example histograms achieved by SP-ICP-MS for enzymatic extracts from mussels exposed to 0.1 and 1.0 mg L^{-1} of PVP-AgNPs, both for 7 exposure days, respectively.

As for total Ag determination, AgNPs were also studied in the surface scum present in the mussels tanks after 23 days of exposure to 1.0 mg L^{-1} of PVP-AgNPs.

Figure 5.4.(a) shows the concentration of AgNPs in the surface scum of J, K, and L tanks after 23, 26, and 30 days. Unlike the total content, the AgNPs concentration increased with sampling time, even after the end of the experiment.

The most frequent and mean sizes were also determined in the NPs present in the surface scum. **Figure 5.4.(b)** shows the most frequent and mean sizes (average from tanks J, K, and L) at 23 and 26 days, and after the end of the experiment (day 30). The most frequent and mean sizes were between 41±5 nm (day 23) and 23±1 nm (day 30), and between 51±7 nm (day 23) and 27±2 nm (day 30), respectively. It can be observed that even when the number of NPs increased at day 30 in two of the tanks (J and L), their size decreased almost by half. It seems that mussels excreted death cells with AgNPs that produce this surface scum.

Although Xu et al. [14] reported higher total Ag in mussel samples than the basal Ag concentration achieved in this work, the concentration of AgNPs in their mussels samples was $2.94\times10^{7}\pm0.37\times10^{7}$ part g^{-1}, values smaller than the highest AgNPs achieved in this research work ($2.14\times10^{8}\pm4.49\times10^{7}$ part g^{-1}) after the exposure to 1.0 mg L^{-1} of PVP-AgNPs for 28 days.

USC UNIVERSIDADE DE SANTIAGO DE COMPOSTELA

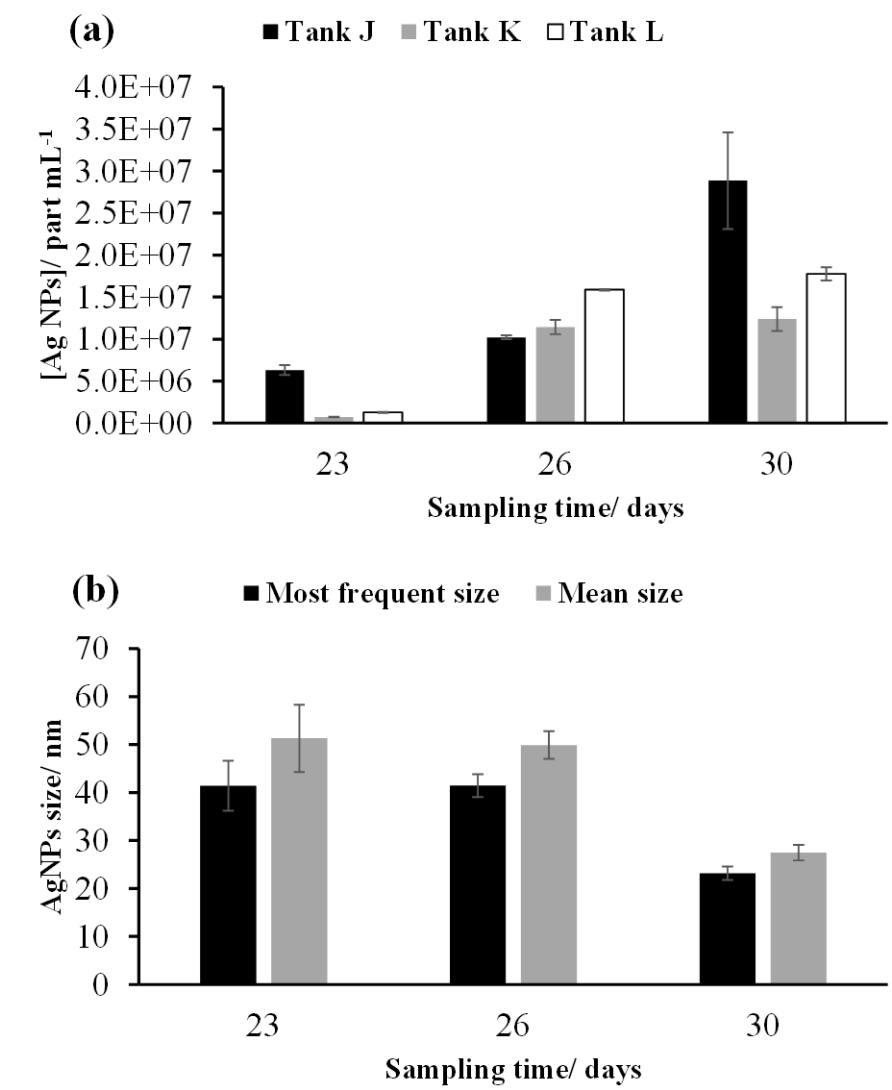

Figure 5.4. AgNPs content in surface scum from mussels exposed to PVP-AgNPs (a), and most frequent and mean sizes of AgNPs (b) (average of tanks J, K, and L at days 23, 26 and 30).

5.4.2 Turbot bioaccumulation assay

5.4.2.1 Total Ag content in turbot samples exposed to PVP-AgNPs

Total Ag content in the turbot was determined using the methodology described in **section 5.3.4**. The dissected turbot (flesh+skin, liver, and kidney) was submitted to microwave-assisted acid digestion. Whenever a sufficient amount of sample was available, the digestion was performed in triplicate. The digested samples were diluted 10 times with ultrapure water before ICP-MS analysis. The analytical performance of the methodology was also validated. The linearity was guaranteed through the standard addition calibration method. The LOD and LOQ, calculated as in **section 5.4.1.1**, resulted in 1.36 and 4.54 ng g^{-1}, respectively. The accuracy calculated through the analytical recovery resulted in an average of 98±10% for added concentrations of 0.05 to 15.0 µg L^{-1} of Ag, and the precision through the repeatability resulted in RSD<2% (n=7).

Total Ag content in flesh+skin samples was lower than the LOD (<1.36 ng g^{-1}) in all sampling days and for the different PVP-AgNPs exposure doses (0, 0.25, 0.75, and 1.5 mg Kg^{-1}

fish and day). Thus, non-bioaccumulation of Ag was found in the edible part of the turbot. **Figure 5.5.(a)** and **Figure 5.5.(b)** show the bioaccumulation of total Ag in the liver and kidney, respectively. The high variability (RSD bars) in some of the experiments can be explained by the natural variability of these living organisms, the heterogeneity of the matrix, and the small amount of sample that did not allow for preparing enough replicates of digestion. The results show that liver bioaccumulates higher amount of Ag than kidney. The highest Ag concentration reached in the liver was 6.47±2.46 μg g^{-1} w.w. after 75 exposure days to the high NPs dose. The concentration remained constant until 90 days and decreased at the end of the experiment. The statistical analysis using the one-way ANOVA tests was performed to compare Ag concentration with the exposure time at the same NPs doses. Only in the liver of turbot exposed to 0.25 mg PVP-AgNPs kg^{-1} were found statistical differences between the exposure days (P-value<0.05). The multiple range test for this exposure dose showed overlapping concentrations between 15 and 75 exposure days, and between 90 and 105 days.

In the case of kidney, the concentrations were stable after 75 days of exposure to the high NPs dose, reaching a maximum concentration of 0.27±0.07 μg g^{-1} w.w. at the end of the experiment (105 days). Statistical differences between concentrations at different exposure days were only found in the kidneys of turbots exposed to 1.5 mg PVP-AgNPs kg^{-1} (P-value<0.05). The multiple range test for this exposure dose showed overlapping concentrations between 75, 90 and 105 exposure days.

Farkas et al. [26] reported the total Ag concentration of turbot exposed to 200 μg L^{-1} of 15 nm PVP-AgNPs for 14 days. Like in this study, authors found higher Ag concentrations in the liver than in the kidney. The liver, kidney, and muscle concentrations reported were 0.39±0.34, 0.23±0.21, and 0.012±0.005 μg g^{-1}, respectively. However, in the present research work the highest total Ag concentration in the liver, kidney, and muscle were 6.47±2.46, 0.27±0.07, and <0.0014 μg g^{-1}, respectively. Thus, the total Ag for the liver exposed to 1.5 mg Kg^{-1} of PVP-AgNPs for 75 days was higher than the AgNPs concentrations of turbot exposed to 200 μg L^{-1} of AgNPs for 14 days reported by Farkas et al. [26].

USC
UNIVERSIDADE DE SANTIAGO DE COMPOSTELA

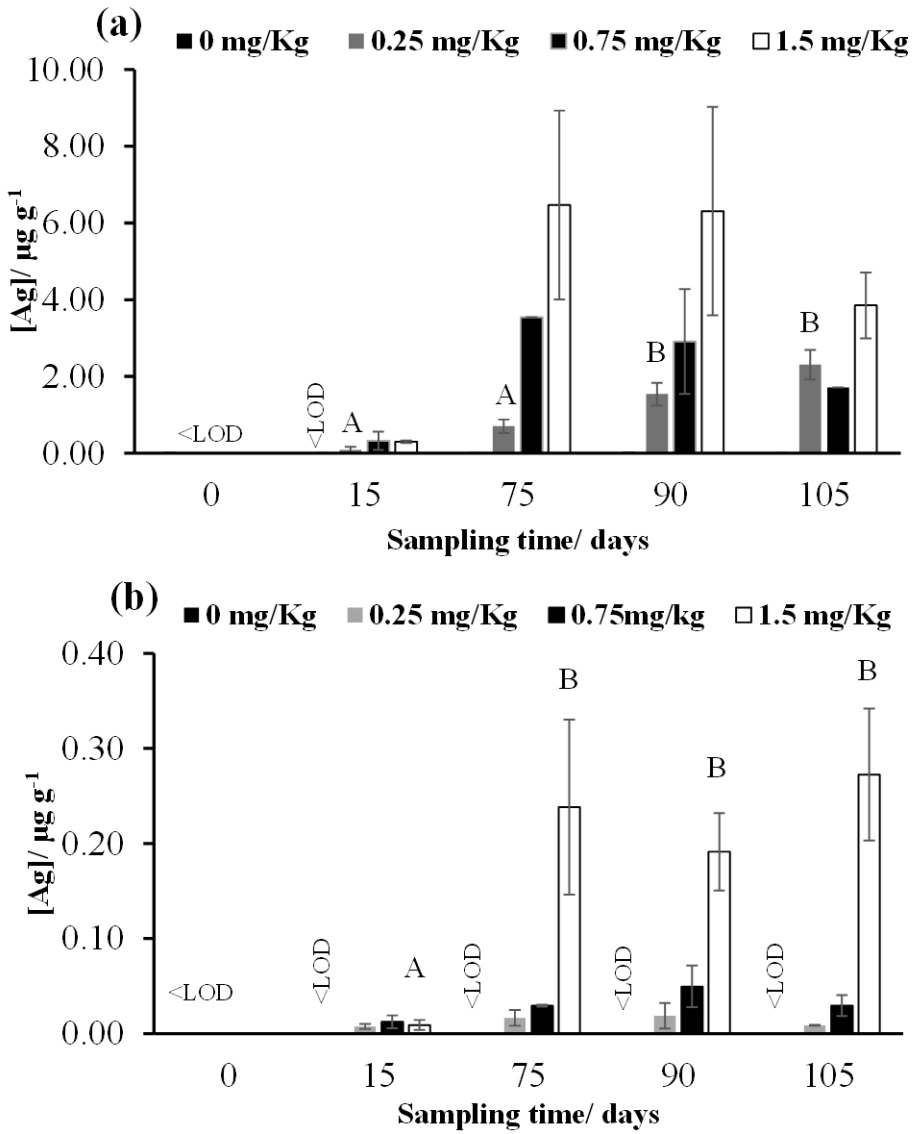

Figure 5.5. Total Ag bioaccumulation in the (a) liver and (b) kidney of turbots exposed to 0, 0.25, 0.75, and 1.5 mg of PVP-AgNPs kg^{-1} fish and day for 105 days. Different letters indicate significative differences (one-way ANOVA, P-value<0.05) between the exposure time for each exposure dose.

5.4.2.2 AgNPs content in turbot samples after exposure

Enzymatic extraction of AgNPs using pancreatin/lipase mixture was used before AgNPs analysis by SP-ICP-MS for determining their content and size distribution using the methodology described in **section 5.3.5**. Enzymatic extracts were diluted with 1% (v/v) glycerol 500 times before the SP-ICP-MS measurements. The LOD_{size} 3σ was 17 nm and the more restrictive LOD_{size} 5σ was 21 nm. The instrumental LOD_{number} was 2.21×10^6 AgNPs L^{-1} of extract, and the LOD_{number} referred to the 500 times diluted sample was 8.29×10^6 AgNPs g^{-1} w.w.

Since Ag concentration in turbot flesh+skin was lower than the LOD, enzymatic extraction was only carried out in turbot liver. The AgNPs concentrations measured in turbot liver extracts were lower than the LOD_{number} (<8.29×10^6 AgNPs g^{-1}) for all sampling days and exposure concentrations. In the case of the kidney, this organ was very difficult to dissect due to its viscous consistency and very small size. In fact, the average weight of the juvenile specimens at the beginning of the experiment was 70.93±0.32 g, and at the end of the

experiment was 222.03±3.63 g. Thus, there was not enough kidney sample available to perform the AgNPs determination experiment.

In previous studies, Araujo et al. [29] studied histological alterations in the liver and kidney of turbot exposed to PVP-AgNPs for 14 days. Although no AgNPs were found in turbot tissues by TEM, TEM micrographs showed a lower diameter of lipid droplets of hepatocytes than in control livers. On the other hand, differentially expressed proteins (DEPs) were found in the liver and kidney of turbot. Thus, AgNPs also affected protein synthesis and nucleic acid transcription [29].

5.5 CONCLUSIONS

The bioaccumulation assays in mussels and different parts of turbot (flesh+skin, liver, and kidney) were accomplished using microwave-assisted acid digestions and enzymatic extractions with pancreatin/lipase mixtures before analysis by ICP-MS and SP-ICP-MS, respectively. The results showed the capacity of mussels to bioaccumulate Ag and AgNPs as a function of the dose and exposure time. In the bioaccumulation study, the excretion of a surface scum containing Ag and AgNPs was observed in the tanks of mussels exposed to high doses of nanoparticles after 23 days of exposure, probably to regulate the concentration of this element in the organism. This elimination was in agreement with the absence of Ag bioaccumulation at the high exposure dose in comparison to the low exposure dose. Furthermore, this fact highlights the need for purification stages in mussel cultivation and more investigation into this field. The turbot bioaccumulation assay showed only the presence of total Ag in the kidney and mostly in the liver, but these are considered unedible parts. Therefore, the food safety of this highly appreciated flat fish is guaranteed.

USC
UNIVERSIDADE DE SANTIAGO DE COMPOSTELA

SUPPLEMENTARY INFORMATION

Table S.5.1. Microwave program for sample digestion.

Step	Initial T/ ºC	Final T/ ºC	Time/ min	Power/ W
1	25	90	4	800
2	90	140	5	800
3	140	200	5	800
4	200	200	20	800
5	200	25	120	0

Table S.5.2. Operational conditions for (a) ICP-MS and (b) SP-ICP-MS.

(a) ICP-MS operational conditions	
Parameter/component	**Type/mode/value**
Nebulizer	Meinhard CR R^+
Nebulizer chamber	5 ºC refrigerated glass cyclone chamber with Peltier PC^{3X}
Cone material	Nickel/aluminium
Radiofrequency power	1600 W
Ar gas flow	15 L min^{-1} (Plasma) 1.15 L min^{-1} (Nebulizer) 1.2 L min^{-1} (Auxiliary)
Analyte	Ag
Operation mode	KED
He gas flow	4.5 mL min^{-1}
Integration time	1000 ms
m/z	^{107}Ag (^{103}Rh as Internal Standard)
Replicates per sample	3
RPQ	0.2
(b) SP-ICP-MS operational conditions	
Operation mode	Standard
Sample flow rate	0.182-0.199 mL min^{-1}
Acquisition time	100 s
Dwell time	50 µs
Number of readings	2.000.000
Transport efficiencies	8.8-11.5%

USC UNIVERSIDADE DE SANTIAGO DE COMPOSTELA

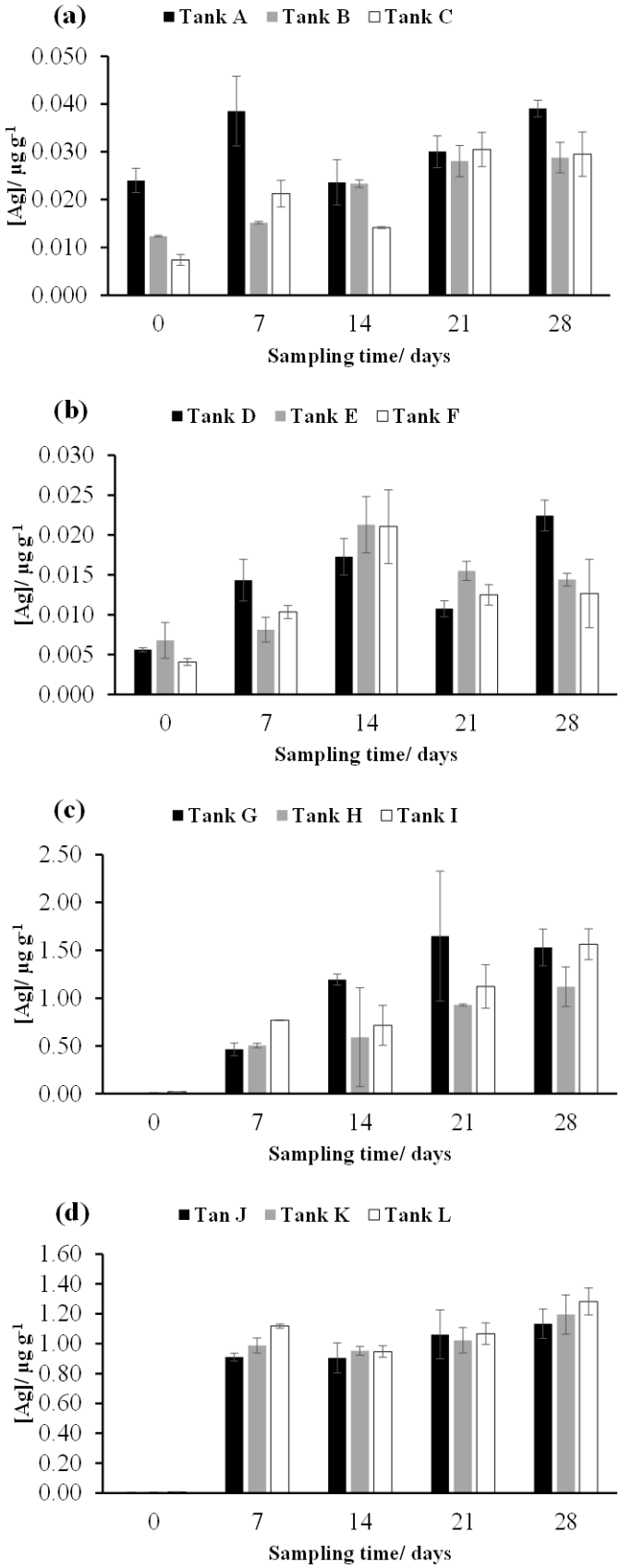

Figure S.5.1. Total Ag content in cultured mussels exposed to PVP-AgNPs for 28 days: (a) control, (b) control solvent with PVP, (c) 0.1 mg L^{-1} of PVP-AgNPs, and (d) 1.0 mg L^{-1} of PVP-AgNPs.

Figure S.5.2. Surface scum in tanks with mussels exposed to 1.0 mg L^{-1} after 23 days.

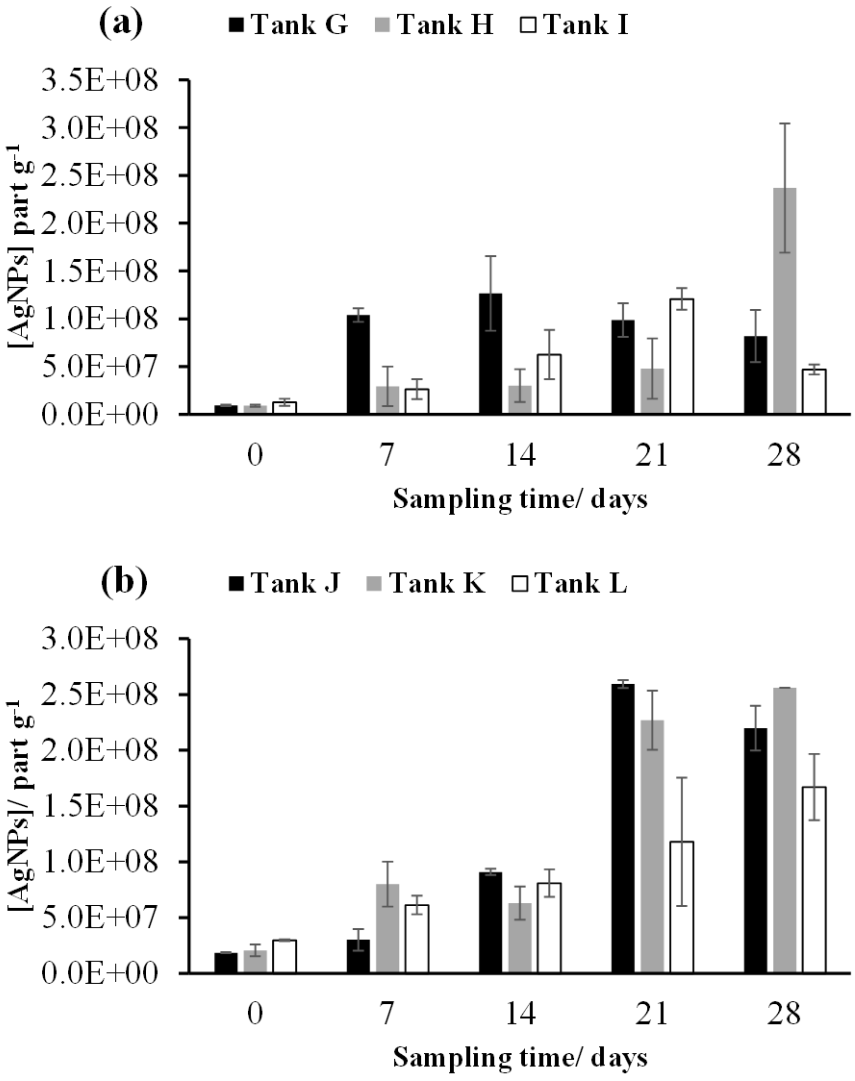

Figure S.5.3. AgNPs content in cultured mussels exposed to PVP-AgNPs for 28 days: (a) 0.1 mg L^{-1} of PVP-AgNPs; (b) 1.0 mg L^{-1} of PVP-AgNPs tanks.

USC UNIVERSIDADE DE SANTIAGO DE COMPOSTELA

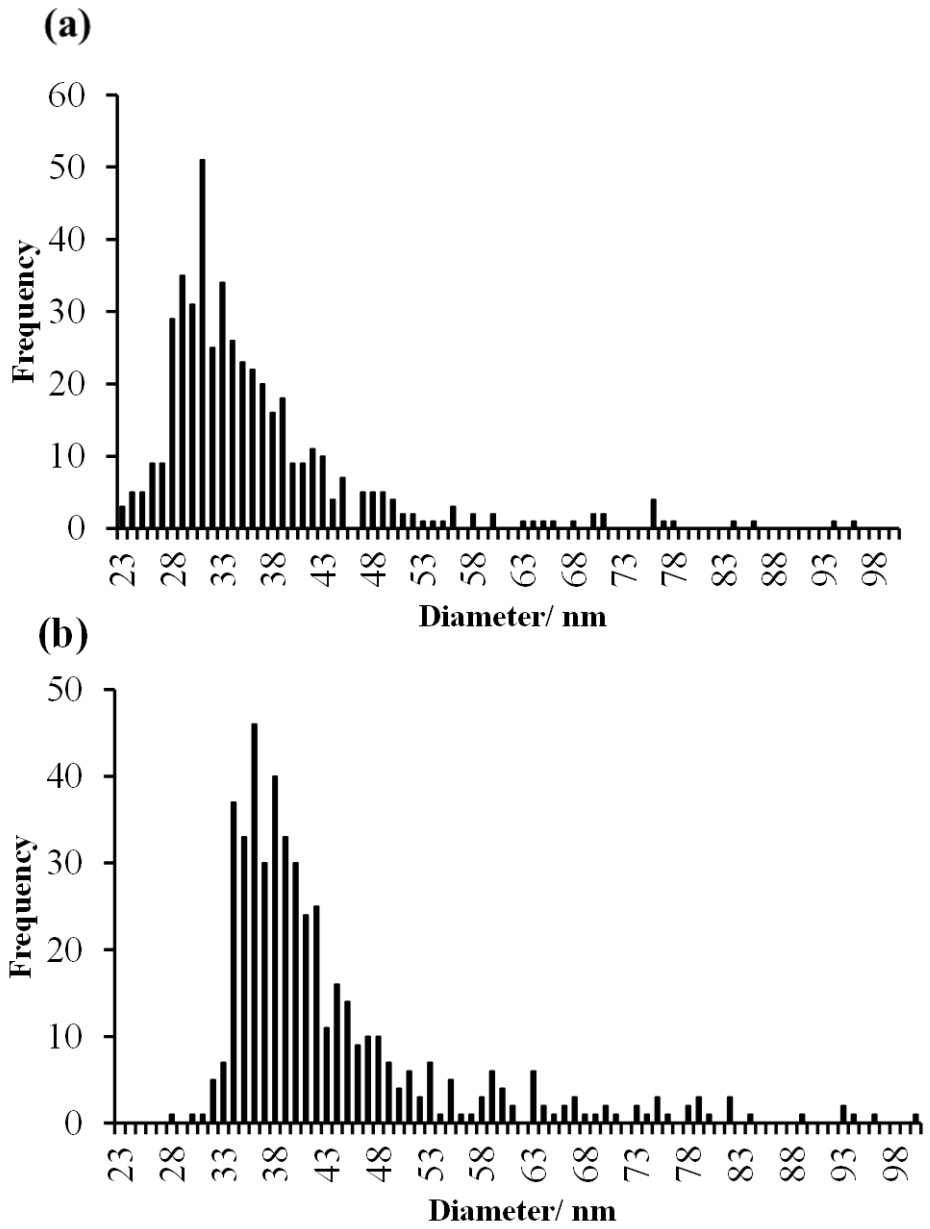

Figure S.5.4. SP-ICP-MS histograms of enzymatic extracts from mussels exposed to: (a) 0.1 and (b) 1.0 mg L^{-1} of PVP-AgNPs, both for 7 exposure days.

USC UNIVERSIDADE DE SANTIAGO DE COMPOSTELA

REFERENCES

[1] Scopus Database, https://www.scopus.com/search/form.uri?display=basic#basic (accessed December 23, 2022).
[2] Nanotechnology Products Database, https://product.statnano.com/ (accessed December 23, 2022).
[3] A. Calisi, C. Lorusso, J. A. Gallego-Urrea, M. Hassellöv, F. Dondero, Ecotoxicological effects of silver nanoparticles in marine mussels, Sci. Total Environ. 851 (2022) 158113. https://doi.org/10.1016/j.scitotenv.2022.158113.
[4] M. V. Taboada-López, D. Bartczak, S. Cuello-Núñez, H. Goenaga-Infante, P. Bermejo-Barrera, A. Moreda-Piñeiro, AF4-UV-ICP-MS for detection and quantification of silver nanoparticles in seafood after enzymatic hydrolysis, Talanta. 232 (2021) 122504. https://doi.org/10.1016/j.talanta.2021.122504.
[5] APROMAR, APROMAR OPP30. La acuicultura en España, Informe 2021, (2021). https://apromar.es/wp-content/uploads/2021/12/La-Acuicultura-en-Espana-2021.pdf (accessed December 20, 2022).
[6] Spanish Ministry of Agriculture, Fisheries and Food, https://www.mapa.gob.es/es/pesca/temas/acuicultura/produccion-de-acuicultura/produccion-nacional/ (accessed December 23, 2022).
[7] J. R. Conway, S. K. Hanna, H. S. Lenihan, A. A. Keller, Effects and implications of trophic transfer and accumulation of CeO_2 nanoparticles in a marine mussel, Environ. Sci. Technol. 48 (2014) 1517-1524. https://doi.org/10.1021/es404549u.
[8] M. V. Taboada-López, N. Alonso-Seijo, P. Herbello-Hermelo, P. Bermejo-Barrera, A. Moreda-Piñeiro, Determination and characterization of silver nanoparticles in bivalve molluscs by ultrasound assisted enzymatic hydrolysis and sp-ICP-MS, Microchem. J. 148 (2019) 652–660. https://doi.org/10.1016/j.microc.2019.05.023.
[9] L. Canesi, C. Ciacci, R. Fabbri, A. Marcomini, G. Pojana, G. Gallo, Bivalve molluscs as a unique target group for nanoparticle toxicity, Mar. Environ. Res. 76 (2012) 16–21. https://doi.org/10.1016/j.marenvres.2011.06.005.
[10] P. E. Buffet, J. F. Pan, L. Poirier, C. Amiard-Triquet, J. C. Amiard, P. Gaudin, C. R. de Faverney, M. Guibbolini, D. Gilliland, E. Valsami-Jones, C. Mouneyrac, Biochemical and behavioural responses of the endobenthic bivalve *Scrobicularia plana* to silver nanoparticles in seawater and microalgal food, Ecotoxicol. Environ. Saf. 89 (2013) 117–124. https://doi.org/10.1016/j.ecoenv.2012.11.019.
[11] X. Xu, W. Zheng, Z. Meng, W. Xu, Y. Liu, S. Chen, Identification of stress-related genes by co-expression network analysis based on the improved turbot genome, Sci. Data. 9 (2022) 1–10. https://doi.org/10.1038/s41597-022-01458-4.
[12] Z. Wang, L. Yin, J. Zhao, B. Xing, Trophic transfer and accumulation of TiO_2 nanoparticles from clamworm (*Perinereis aibuhitensis*) to juvenile turbot (*Scophthalmus maximus*) along a marine benthic food chain, Water Res. 95 (2016) 250–259. https://doi.org/10.1016/j.watres.2016.03.027.
[13] Y. Sun, Y. Yang, F. Y. Tou, Z. S. Niu, X. P. Guo, C. Liu, J. Yan, J. Y. Wu, M. Xu, L. J. Hou, M. Liu, Extraction and quantification of metal-containing nanoparticles in marine shellfish based on single particle inductively coupled plasma-mass spectrometry technique, J. Hazard. Mater. 424 (2022) 127383. https://doi.org/10.1016/j.jhazmat.2021.127383.
[14] L. Xu, Z. Wang, J. Zhao, M. Lin, B. Xing, Accumulation of metal-based nanoparticles in marine bivalve mollusks from offshore aquaculture as detected by single particle ICP-MS, Environ. Pollut. 260 (2020) 114043. https://doi.org/10.1016/j.envpol.2020.114043.

USC DE COMPOSTELA

[15] A. S. Mohamed, S. Bin Dajem, M. Al-Kahtani, S. B. Ali, M. Alshehri, A. Shati, K. Morsy, S. R. Fahmy, Freshwater clam as a potential bioindicator for silver/saponin nanocomposites toxicity, Bull. Environ. Contam. Toxicol. 105 (2020) 827–834. https://doi.org/10.1007/s00128-020-03038-x.
[16] P. E. Buffet, A. Zalouk-Vergnoux, A. Châtel, B. Berthet, I. Métais, H. Perrein-Ettajani, L. Poirier, A. Luna-Acosta, H. Thomas-Guyon, C. Risso-de Faverney, M. Guibbolini, D. Gilliland, E. Valsami-Jones, C. Mouneyrac, A marine mesocosm study on the environmental fate of silver nanoparticles and toxicity effects on two endobenthic species: The ragworm *Hediste diversicolor* and the bivalve mollusc *Scrobicularia plana*, Sci. Total Environ. 470–471 (2014) 1151–1159. https://doi.org/10.1016/j.scitotenv.2013.10.114.
[17] W. Liu, Z. Zeng, A. Chen, G. Zeng, R. Xiao, Z. Guo, F. Yi, Z. Huang, K. He, L. Hu, Toxicity effects of silver nanoparticles on the freshwater bivalve *Corbicula fluminea*, J. Environ. Chem. Eng. 6 (2018) 4236–4244. https://doi.org/10.1016/j.jece.2018.06.032.
[18] T. Gomes, C. G. Pereira, C. Cardoso, V. S. Sousa, M. R. Teixeira, J. P. Pinheiro, M. J. Bebianno, Effects of silver nanoparticles exposure in the mussel *Mytilus galloprovincialis*, Mar. Environ. Res. 101 (2014) 208–214. https://doi.org/10.1016/j.marenvres.2014.07.004.
[19] N. Duroudier, A. Katsumiti, M. Mikolaczyk, J. Schäfer, E. Bilbao, M. P. Cajaraville, Cell and tissue level responses in mussels *Mytilus galloprovincialis* dietarily exposed to PVP/PEI coated Ag nanoparticles at two seasons, Sci. Total Environ. 750 (2021) 141303. https://doi.org/10.1016/j.scitotenv.2020.141303.
[20] T. M. Scown, E. M. Santos, B. D. Johnston, B. Gaiser, M. Baalousha, S. Mitov, J. R. Lead, V. Stone, T. F. Fernandes, M. Jepson, R. Van Aerle, C. R. Tyler, Effects of aqueous exposure to silver nanoparticles of different sizes in rainbow trout, Toxicol. Sci. 115 (2010) 521–534. https://doi.org/10.1093/toxsci/kfq076.
[21] J. M. Lacave, U. Vicario-Parés, E. Bilbao, D. Gilliland, F. Mura, L. Dini, M. P. Cajaraville, A. Orbea, Waterborne exposure of adult zebrafish to silver nanoparticles and to ionic silver results in differential silver accumulation and effects at cellular and molecular levels, Sci. Total Environ. 642 (2018) 1209–1220. https://doi.org/10.1016/j.scitotenv.2018.06.128.
[22] B. Xiao, X. Wang, J. Yang, K. Wang, Y. Zhang, B. Sun, T. Zhang, L. Zhu, Bioaccumulation kinetics and tissue distribution of silver nanoparticles in zebrafish: The mechanisms and influence of natural organic matter, Ecotoxicol. Environ. Saf. 194 (2020) 110454. https://doi.org/10.1016/j.ecoenv.2020.110454.
[23] H. K. Sung, E. Jo, E. Kim, S. Kyoung Yoo, J. Lee, P. Kim, Y. Kim, I. C. Eom, Analysis of gold and silver nanoparticles internalized by zebrafish (*Danio rerio*) using single particle-inductively coupled plasma-mass spectrometry, Chemosphere 209 (2018) 815–822. https://doi.org/10.1016/j.chemosphere.2018.06.149.
[24] M. H. Jang, W. K. Kim, S. K. Lee, T. B. Henry, J. W. Park, Uptake, tissue distribution, and depuration of total silver in common carp (*Cyprinus carpio*) after aqueous exposure to silver nanoparticles, Environ. Sci. Technol. 48 (2014) 11568–11574. https://doi.org/10.1021/es5022813.
[25] N. J. Clark, D. Boyle, B. P. Eynon, R. D. Handy, Dietary exposure to silver nitrate compared to two forms of silver nanoparticles in rainbow trout: bioaccumulation potential with minimal physiological effects, Environ. Sci.: Nano 6 (2019) 1393–1405. https://doi.org/10.1039/c9en00261h.
[26] J. Farkas, I. Salaberria, B. Styrishave, R. Staňková, T. M. Ciesielski, A. J. Olsen, W. Posch, T. P. Flaten, Å. Krøkje, W. Salvenmoser, B. M. Jenssen, Exposure of juvenile turbot (*Scophthalmus maximus*) to silver nanoparticles and 17α-ethinylestradiol mixtures:

USC UNIVERSIDADE DE SANTIAGO DE COMPOSTELA

Implications for contaminant uptake and plasma steroid hormone levels, Environ. Pollut. 220 (2017) 328–336. https://doi.org/10.1016/j.envpol.2016.09.067.
[27] F. Laborda, A. C. Gimenez-Ingalaturre, E. Bolea, J. R. Castillo, About detectability and limits of detection in single particle inductively coupled plasma mass spectrometry, Spectrochim. Acta Part B: At. Spectrosc. 169 (2020) 105883. https://doi.org/10.1016/j.sab.2020.105883.
[28] J. J. López-Mayán, B. Álvarez-Fernández, E. Peña-Vázquez, M. C. Barciela-Alonso, A. Moreda-Piñeiro, P. Bermejo-Barrera, Ultrasonication followed by enzymatic hydrolysis as a sample pre-treatment for the determination of Ag nanoparticles in edible seaweed by SP-ICP-MS, Talanta 247 (2022) 123556. https://doi.org/10.1016/j.talanta.2022.123556.
[29] M. J. Araújo, M. L. Sousa, E. Fonseca, A. B. Felpeto, J. C. Martins, M. Vázquez, N. Mallo, L. Rodriguez-Lorenzo, M. Quarato, I. Pinheiro, M. V. Turkina, J. J. López-Mayán, E. Peña-Vázquez, M. C. Barciela-Alonso, M. Spuch-Calvar, M. Oliveira, P. Bermejo-Barrera, S. Cabaleiro, B. Espiña, V. Vasconcelos, A. Campos, Proteomics reveals multiple effects of titanium dioxide and silver nanoparticles in the metabolism of turbot, *Scophthalmus maximus*, Chemosphere 308 (2022) 136110. https://doi.org/10.1016/j.chemosphere.2022.136110.

USC
UNIVERSIDADE DE SANTIAGO DE COMPOSTELA

USC
UNIVERSIDADE
DE SANTIAGO
DE COMPOSTELA

CHAPTER 6. BIOACCUMULATION PATTERNS IN AQUACULTURE MUSSELS AND TURBOTS EXPOSED TO DIFFERENT SIZES OF TIO_2NP

USC
UNIVERSIDADE DE SANTIAGO DE COMPOSTELA

USC
UNIVERSIDADE
DE SANTIAGO
DE COMPOSTELA

CHAPTER 6. BIOACCUMULATION PATTERNS IN AQUACULTURE MUSSELS AND TURBOTS EXPOSED TO DIFFERENT SIZES OF TIO_2NPS

6.1 ABSTRACT

Titanium dioxide nanoparticles (TiO_2NPs) are extensively used in the industry due to their properties, and as a result, they are ending up in the marine environment where they may interact and damage the biota. In this study, two predominant aquaculture species in Spain are being examined to determine TiO_2NPs' impact and bioaccumulation. A benthic filtering bivalve (*Mytilus edulis*) and a benthic predator (*Scophthalmus maximus*) were selected for the bioaccumulation assays. The exposure study lasted 28 days in mussels and 90 days in turbot, and specimens were exposed to different concentrations of citrate-coated TiO_2NPs of 25 and 5 nm. Inductively coupled plasma mass spectrometry (ICP-MS) and single-particle-ICP-MS (SP-ICP-MS) were used for Ti determination, and TiO_2NPs content and size distribution determination, respectively. Ti and TiO_2NPs concentrations reached 5.19±3.19 μg g^{-1} w.w. (wet weight) and $2.28\times10^8\pm5.84\times10^7$ NPs g^{-1} w.w. after exposure to 1.0 mg L^{-1} of 25 nm TiO_2NPs for 28 days, and 4.26±0.85 μg g^{-1} w.w. and $4.79\times10^8\pm2.36\times10^8$ NPs g^{-1} w.w. for 1.0 mg L^{-1} of 5 nm TiO_2NPs for 14 and 21 exposure days, respectively. Bioaccumulation was also observed in shells of mussels exposed to the high dose of 5 nm TiO_2NPs, which were more fragile and appeared broken in the tanks. In shells, the highest Ti concentration reached was 12.43±3.45 μg g^{-1} d.w. (dried weight).

Regarding turbot bioaccumulation assay, the highest Ti concentration was found in the liver (non-edible part), reaching 1.62±0.44 μg g^{-1} w.w. at 90 exposure days and a dose of 1.5 mg Kg^{-1} fish and day of 5 nm TiO_2NPs. Furthermore, the feces from turbots were also studied, and the result showed expelled Ti, reaching a concentration of 40.99±6.62 μg g^{-1} w.w. in the feces of turbot fed with 1.5 mg kg^{-1} fish and day of 5 nm TiO_2NPs. The results of this investigation show the safety of turbot consumption and highlight the need for a correct depuration process of mussels before commercialization.

6.2 INTRODUCTION

Titanium dioxide nanoparticles (TiO_2NPs) are one of the most employed metallic oxide NPs due to their stability, anticorrosion, antibacterial, and catalytic properties. TiO_2NPs are commonly found in papers, plastics, paints, medicines, pharmaceuticals and personal care products like sunscreens, toothpaste or even soaps [1]. Besides, TiO_2NPs have innovative applications in solar cells, photocatalytic water purification systems, and photodynamic tumour therapy [2,3]. Until February 2022, TiO_2 was commonly used in the EU as a food additive (coded as E171) for color and consistency. However, EFSA has concluded that it can no longer be considered safe and the European Commission has implemented a regulation to ban its use [4,5].

Due to the wide use and dissemination of TiO_2NPs around the world, they can enter marine systems and interact with biota, these being potential sinks for NPs [1]. The study of the interaction and behaviour of TiO_2NPs with living beings is still a challenge because little is known about NP bioavailability, mode of uptake, ingestion rates, and actual internal exposure concentrations [6]. To understand the bioaccumulation, biomagnification, trophic transfer to

USC UNIVERSIDADE DE COMPOSTELA

the food chain and potential toxicity of TiO_2 in marine species, several aspects must be considered. The kind of organism tested, the size and the coating of the particle, the matrix of dispersion (natural water, sea water or even brackish water), the presence of organic matter, or the route of NPs exposure (NPs in water suspension or mixed and homogenized in food) are variables to take into account.

According to the APROMAR report on aquaculture in Spain, Europe and the World in 2019 [7], *Mytilus* sp. is the most important benthic bivalve mollusk species in Europe and it is harvested mainly in the Atlantic area. Mussels are considered targets for monitoring aquatic pollutants due to their capacity to filter high amounts of seawater, processing microalgae, bacteria, sediments, particulates, and natural nanoparticles [6,8]. *Scophthalmus maximus* is a benthic carnivore flat fish [9], highly prized in Spain [7], and that was produced in tenth place by tons in Europe in 2019.

To test bioaccumulation in fish, the Organization for Economic Co-operation and Development (OECD) Test Guideline 305 (TG 305) is the current main standard. It takes into account both water exposure and food exposure [1,10,11]; however, there is still a lack of studies in the bibliography that use the dietary exposure route to NPs instead of the aqueous route [11]. Some reports were found regarding TiO_2NPs bioaccumulation in fish. The most used species were the freshwater zebrafish (*Danio rerio*) [12-16], rainbow trout (*Oncorhynchus mykiss*) [17-19], and carp (*Cyprinus carpio*) [20]. However, fewer reports were found for marine and brackish water. Turbot (*Scophthalmus maximus)* bioaccumulation assays were performed to evaluate aqueous, dietary exposure, and trophic transfer [11]. Thus, Wang et al. [9] studied the trophic transfer from the benthic marine clamworm (*Perinereis aibuhitensis*) exposed to 10, 50, and 100 mg L^{-1} TiO_2NPs to juvenile turbots and the waterborne exposure of turbot to 100 mg L^{-1} TiO_2NPs. Uptake and depuration periods were 20 and 7 days, respectively, and total Ti was determined by ICP-MS. No biomagnification of Ti was observed through the food chain, and the bioaccumulation was higher in the gill, intestine and stomach of juvenile turbots, followed by skin, liver, and muscle.

On the other hand, some reports were found regarding the effects of TiO_2NPs in different species of mussels including *M. Coruscus*, *M. edulis* and *M. galloprovincialis*, usually after exposures of several days [21,22]. These effects were assessed in terms of modifications to their physiology and ability to reproduce as well as their immunotoxicity, genotoxicity, cytotoxicity, metabolic reactions, and production of oxidative stress [23-25].

Besides, Larios et al. [8] studied the exposure of TiO_2NPs to *Dreissena polymorpha* (zebra mussel) by inductively coupled plasma optical emission spectrometry (ICP-OES). The zebra mussel was fed with *Chlorella* mixed with 0.35, 0.7, and 3.5 mg L^{-1} of TiO_2NPs for 3 days. The results showed Ti accumulation with the exposure time (till 36 h); it was observed slightly more accumulation of Ti when it was mixed with the fed microalgae, and the amount of Ti in the sediments was higher in the presence of mussels due to their filtration activity [8]. Gallocchio et al. [1] reported the bioaccumulation of Ti in *Mytilus galloprovincialis* after 4 exposure days to 0.25 and 2.5 mg L^{-1} of TiO_2NPs or 1.6 mg L^{-1} of ionic Ti. SP-ICP-MS results showed the presence of TiO_2NPs in the treated mussels, but they had the ability to eliminate more than 70% of the particles after 3 days of depuration [1].

To the best of our knowledge, no reports were found about the study of citrate-coated TiO_2NPs bioaccumulation in *Mytilus edulis* (mussel) and *Scophthalmus maximus* (turbot) through the diet during long exposure periods (28 and 90 days, respectively), and using single particle inductively coupled plasma mass spectrometry (SP-ICP-MS) for TiO_2NPs concentration and size distribution determination. Thus, the main goal of this research work is to study the bioaccumulation of different sizes (5 and 25 nm) of citrate-coated TiO_2NPs in two

of the most important aquaculture species farmed in the Atlantic area. Total Ti and TiO_2NPs concentration and size distributions in *Mytilus edulis* and *Scophthalmus maximus* were determined by inductively coupled plasma mass spectrometry (ICP-MS) and single-particle-ICP-MS (SP-ICP-MS), respectively.

6.3 MATERIALS AND METHODS

6.3.1 Instrumentation

The main instrumentation of this research work includes a quadrupole-based inductively coupled plasma-mass spectrometer (ICP-MS) NexION® 2000 from Perkin Elmer (Waltham, MA, USA) equipped with a dynamic reaction cell (DRC). The ICP-MS is also equipped with a Single Cell Micro DX autosampler from Perkin Elmer. To obtain the TiO_2NPs concentration and size distributions an ICP-MS working in single-particle mode (SP-ICP-MS) was used. The Syngistix™ and the Syngistix™ Nano Application 2.5 software (Perkin Elmer) were used to obtain the total Ti and TiO_2NPs results, respectively. An Ethos Plus microwave lab station from Milestone (Bergamo, Italy), equipped with a temperature and pressure control probe, and 100 mL Teflon vessels, was used for sample digestion. To obtain the enzymatic extracts from the aquaculture samples, a Boxcult temperature-controlled incubation chamber from Stuart Scientific (Surrey, UK), equipped with a Rotabit orbital-rocking platform shaker from J.P. Selecta (Barcelona, Spain) was used. Other small laboratory instrumentation includes a pH meter from Crison (Barcelona, Spain) for buffer pH adjustments, an ultrasound bath from VWR (Barcelona, Spain) for obtaining NPs dispersions, a Reax top vortex vibrational shaker from Heidolph (Schwabach, Germany) to homogenize solutions, an analytical balance ML204 from Mettler Toledo (Barcelona, Spain), a laboratory oven from J.P. Selecta (Barcelona, Spain) for sample drying, and a zirconium ball mill from Retsch (Haan, Germany) for mussel shell grinding.

6.3.2 Reagents and materials

The TiO_2NPs used for the bioaccumulation tests were commercially available and used without any further purification. The 25 nm TiO_2NPs and 5 nm TiO_2NPs powders were from Sigma Aldrich (citrate P-25 TiO_2NPs, Darmstadt, Germany; a mixture of rutile and anatase), and Nanostructured & Amorphous Materials, Inc. (Katy, TX, USA; anatase, 5 nm size, 99%), respectively. The NPs stock dispersions were prepared in ultrapure water. To create citrate-5 nm TiO_2NPs and citrate-25 nm TiO_2NPs, trisodium citrate dihydrate from Sigma-Aldrich was mixed with TiO_2 powder at weight ratios of 1:1.5 for 5 nm and 1:0.8 for 25 nm, respectively. An ultrasonic probe (Branson Disintegrator Ultrasonic Mod. 450) was used for 30 min (30 s pulse on /5 s pulse off) to disperse NPs in citrate. Both sizes of citrate-TiO_2NPs suspensions had a final concentration of 15.5 g L^{-1}.

To perform the microwave-assisted acid digestion, 33% (w/v) hydrogen peroxide from ACS, ISO, AppliChem Panreac (Barcelona, Spain), 69% (w/v) nitric acid SUPRAPUR® from Sigma Aldrich, and ultrapure water (18 MΩ cm of resistivity) obtained from a Milli-Q® IQ7003 from Millipore Co. (Bedford, MA, USA) were needed. To perform TiO_2NPs enzymatic extraction, porcine pancreatin and lipase from *Candida rugose* (both from Sigma Aldrich) were diluted in a buffer (pH=7.4) prepared from $NaH_2PO_4 \cdot H_2O$ and NaOH from Merck (Darmstadt, Germany). Glycerol 1% (v/v) from Merck (Darmstadt, Germany) was used to dilute the extracts before SP-ICP-MS.

The ICP-MS equipment uses Ar and NH_3 as nebulization and reaction gases, respectively; both with 99.999% purity from Nippon Gases (Madrid, Spain). To perform the initial check of

USC DE COMPOSTELA

the ICP-MS, a NexION Setup Solution containing 1.0 µg L^{-1} of Be, Ce, Fe, In, Li, Mg, Pb, and U in 1% of HNO_3 from Perkin Elmer (Shelton, USA) is needed. To obtain the transport efficiency (TE%) required in the SP-ICP-MS mode, an ionic Au-stock standard of 1000 mg L^{-1} in 2 mol L^{-1} HCl from Merck (Darmstadt, Germany), and a suspension of reference material PEG-COOH Au Nanospheres of 50 nm (49.6 nm by TEM) and 9.89×10^6 particles mL^{-1} from NanoComposix (San Diego, California, USA) in aqueous 1 mM citrate, are needed. Ti ionic standard of 1000 mg L^{-1} H_2O/0.24% F^- from Perkin Elmer (Shelton, USA) was employed for ICP-MS and SP-ICP-MS measurements.

Other materials used included plastic tubes, pipette tips, syringes, and Minisart NML hydrophilic non-sterile 5.0 µm filters from Sartorius (Goettingen, Germany). All glassware used was submitted to an acid ultra-trace decontamination procedure before its use.

6.3.3 Bioaccumulation study design

Mytilus edulis and *Scophthalmus maximus* were the species selected for the bioaccumulation test. The cultivation of these aquaculture species took place in the Atlantic area. Mussels were cultivated in the Indigo Rock Marine Research Center (Cork, Ireland) and turbots were cultivated in the Technological Center of Aquaculture of Galicia (Galicia, Spain). Citrate-coated TiO_2NPs of primary sizes of 25 and 5 nm diameters were supplied to both species at different trials. The mussel trials (25 and 5 nm TiO_2NPs) lasted 28 days and they were exposed to 0, 0.1, and 1.0 mg L^{-1} of 25 or 5 nm TiO_2NPs. NPs were dispersed in mussels feed (*Tisochrysis lutea*, T-iso), before feeding them, once per week. On the other hand, turbot trials (25 and 5 nm TiO_2NPs) lasted 90 days and they were exposed to 0, 0.25, 0.75, and 1.5 mg of 25 or 5 nm TiO_2NPs kg^{-1} fish and day. All fish were fed with commercial pellets (Biomar Iberia S.A.) four times per day at a 1-2% feeding rate. NPs were mixed with micronized calcium carbonate (C.T.S. España, S.L.) to favour the dispersion into the pellets (except for the control group).

The facilities at Indigo Rock included the 40-liter tanks where the mussels were raised and fed. Twelve tanks made up each trial of the bioaccumulation experiments: three control tanks (A, B, and C) without any exposure to nanoparticles; three solvent control tanks (D, E, and F) with the addition of citrate; three low-exposure dose tanks (G, H, and I), each containing 0.1 mg L^{-1} of TiO_2NPs; and three high exposure tanks (J, K, and L), each containing 1.0 mg L^{-1} of TiO_2NPs. Mussels were sampled every seven days (n=5 times) from each tank in triplicate, resulting in 180 samples of mussels by trial (25 or 5 nm TiO_2NPs). Mussels were exposed to periods of 12 hours of white light and 12 hours of darkness at 16±1 ºC. Common parameters were monitored every day (pH, temperature, dissolved O_2, and salinity), and other parameters like conductivity, ammonium, and nitrites were tested twice a week. Mussels were fed with zooplankton made by capepods and rotifers, every Monday, Tuesday, Thursday, and Friday. The addition of particles occurred on Wednesday with a 30 mL solution containing 3 mL of phytoplankton, and the corresponding TiO_2NPs concentration or citrate coating (in the case of solvent tanks).

The facilities at CETGA included the open flow 500-liter tanks where the juvenile turbots (average body weight of 45 and 73 g for 25 and 5 nm TiO_2NPs trials, respectively) were raised and fed at 14±2 ºC. Each bioaccumulation trial (25 and 5 nm TiO_2NPs) consisted of twelve tanks: three control tanks without TiO_2NPs exposure (0 mg TiO_2NP kg^{-1} fish and day); three tanks exposed to 0.25 mg TiO_2NPs kg^{-1} fish and day; three tanks exposed to 0.75 mg TiO_2NPs kg^{-1} fish and day; and three tanks exposed to 1.5 mg TiO_2NPs kg^{-1} fish and day. The feed was mixed with the nanoparticles to obtain the above mention concentrations. To prepare the feed with the TiO_2NPs was necessary to take into account the different average turbot weights at

different sampling times. The daily feed rates were between 1 and 2.5%. Every 15 days, samples were taken (randomly) from at least two of the three tanks for each exposure level, resulting in 150 samples per trial (25 and 5 nm TiO_2NPs). Finally, the turbot samples were then delivered to the laboratory after being euthanased, dissected into liver, kidney, and flesh+skin, and frozen at -18 ºC until their analysis.

6.3.4 Microwave-assisted acid digestion and total Ti determination by ICP-MS

Microwave-assisted acid digestion was employed to process the aquaculture samples before total Ti determination by ICP-MS. Wet mussel and turbot samples were ground and mixed with nitric acid and hydrogen peroxide and submitted to the microwave-assisted acid digestion protocol described previously by López-Mayán et al. [26]. When the sample amount was enough, three replicate digestions per sample were done, accompanied by two digestion blanks. The digested samples were diluted with ultrapure water before total Ti determination by the ICP-MS described in **section 6.3.1** using the conditions listed in **Table S.6.1.(a)** (supplementary information). To perform the ICP-MS analysis, an initial performance check of the equipment using the NexION Setup solution is needed. The torch alignment, nebulization flow, voltage adjustments, check of Setup solution analytes intensities, and background signal, were parameters to take into account and optimize before the analysis. Calibration using the standard addition in a concentration range from 0 and 15.0 µg L^{-1} of Ti, was used to avoid the matrix effect. To minimize interferences in the determination of Ti, the Dynamic Reaction Cell (DRC) with ammonia as reaction gas (flow rate 1.0 mL min^{-1}), was used. The purpose of ammonia gas is to form the Ti-NH_3 cluster [$^{48}Ti^{14}N^1H(^{14}N^1H_3)_4^+$] of *m/z* 131 to avoid the main interference present in aquaculture species (^{48}Ca) during the determination of the analyte [27].

6.3.5 Enzymatic extractions and determination of TiO_2NPs by SP-ICP-MS

Enzymatic extractions were employed for TiO_2NPs extraction to extract the 25 and 5 nm TiO_2NPs from the aquaculture matrix before analysis by SP-ICP-MS. The enzymatic extraction procedure was selected due to its mild conditions and to avoid the size and shape change of TiO_2NPs during extraction [28]. The pancreatin/lipase mixture was selected to extract the particles due to their ability to solubilize fats from fish samples. The methodology used was previously developed by Taboada-López et al. [28], where a volume of 7.5 mL of 8.0 g L^{-1} of each enzyme solution in a buffer of 0.2M NaH_2PO_4/0.2M NaOH (pH=7.4) was added to 1.0000 g samples for extraction. Three replicate extractions per sample along with two blanks were performed when the amount of sample was enough. The mixtures were submitted to overnight incubation in a chamber at 37 ºC and 200 rpm. Finally, the extracts were filtered with 5 µm filter disks, diluted with 1% (v/v) glycerol, and analyzed by SP-ICP-MS. **Table S.6.1.(b)** shows the specific operational conditions for SP-ICP-MS. TiO_2NPs concentrations and size distributions were determined by the Syngistix™ Nano software 2.5. The transport efficiency (TE %) of SP-ICP-MS was calculated by the software after measuring the sample flow rate, the analysis of an ionic gold calibration between 0 and 3.0 µg L^{-1}, and the certified reference NPs material of 49.6 nm Au nanospheres with 9.89×10^4 particles mL^{-1}. The experimental TE % was between 8-12 %. The ionic Ti calibrations between 0 and 5.0 µg L^{-1} were prepared in ultrapure water due to the high dilution of sample extracts. Finally, the software obtained TiO_2NPs concentrations and size distributions in the diluted extracts samples.

USC UNIVERSIDADE DE SANTIAGO DE COMPOSTELA

6.4 RESULTS AND DISCUSSION

6.4.1 Mussel bioaccumulation tests

6.4.1.1 Total Ti in mussels

Total Ti concentration was determined in digested mussels using the methodology described in **section 6.3.4**. The samples were diluted with ultrapure water from 10 to 25 times. The analytical features of the methodology were guaranteed. The ratio between the slopes of the external calibration graph and the standard addition calibration graph was greater than 60%; thus, there was a matrix effect and the standard addition calibration graph (with correlation coefficients of 0.999) was used. The LOD and LOQ resulted in 2.50 and 8.33 ng g^{-1} w.w. (wet weight), respectively, and they were calculated as 3σ/m and 10σ/m (where σ is the standard deviation of ten measurements of a blank of digestion, and m is the slope of the standard addition calibration graph). The accuracy of the method was evaluated through the analytical recovery, which resulted in 117±5, 109±3, and 118±4 % for 0.5, 5.0, and 10.0 μg L^{-1} of Ti added (n=5). The precision was also evaluated through the repeatability of ICP-MS measurements of Ti in the diluted digested samples, with RSD <4% (n=10).

Total Ti was determined in mussels exposed to 25 nm TiO_2NPs (Trial 1) and mussels exposed to 5 nm TiO_2NPs (Trial 2).

Figure 6.1.(a), corresponding to Trial 1, shows the intertank average Ti concentrations in control tanks (average of A, B, and C), tanks exposed to the nanoparticle citrate coating (average of D, E, and F), and tanks exposed to 0.1 mg L^{-1} of 25 nm TiO_2NPs (average of G, H, and I) for 28 days. No bioaccumulation was found in control tanks within the exposure days, reaching the highest average basal Ti concentration for control tanks at 21 exposure days, being 0.06±0.02 μg g^{-1} w.w. A statistical test was performed to check if there were significant differences between the control tanks at different exposure times. The one-way ANOVA test was performed using the statistical software Statgraphics Centurion XVIII (Warrenton, USA). The P-value in control tanks was higher than 0.05; then, no statistical differences were found between the concentrations in control tanks at different exposure days at a 95 % of confidence level. In the same way, no bioaccumulation was found in solvent citrate tanks, reaching the highest average Ti concentration at 21 exposure days, being 0.05±0.01 μg g^{-1} w.w. However, the one-way ANOVA test showed statistical differences between Ti concentrations in the solvent tanks (P-value<0.05). The multiple range test showed statistical differences between Ti concentrations on some of the studied days, e.g. between day 0 and days 7 and 14. However, no statistical differences were observed between the concentrations at day 0 and days 21 and 28; therefore, no bioaccumulation was observed, and these small changes were attributed to the natural variability among the different specimens at such small concentrations of the element.

The intertank average Ti concentrations, in tanks exposed to 0.1 mg L^{-1} of 25 nm TiO_2NPs, increased with the exposure time until 0.22±0.04 μg g^{-1} w.w. at 28 days. The one-way ANOVA test showed statistical differences (P-value<0.05) between the concentration in mussels exposed to these NPs at different exposure days. The multiple range test showed statistical differences between concentrations at days 0 with 14 and 28, 7 with 28 days, 14 with 28 days, and 21 with 28 days.

Figure 6.1.(b), corresponding to Trial 1, also shows the intertank average Ti concentrations in tanks exposed to 1.0 mg L^{-1} of 25 nm TiO_2NPs (average of concentrations in mussels from tanks J, K, and L) for 28 days. The figure shows total Ti bioaccumulation with exposure time, reaching 5.19±3.19 μg g^{-1} w.w. of total Ti content at day 28 of exposure. The one-way ANOVA test showed again statistical differences among the concentration of mussels

exposed to 1.0 mg L^{-1} as a function of time (P-value<0.05). The multiple range test showed the differences between 0, 7, and 14 days with 28 days.

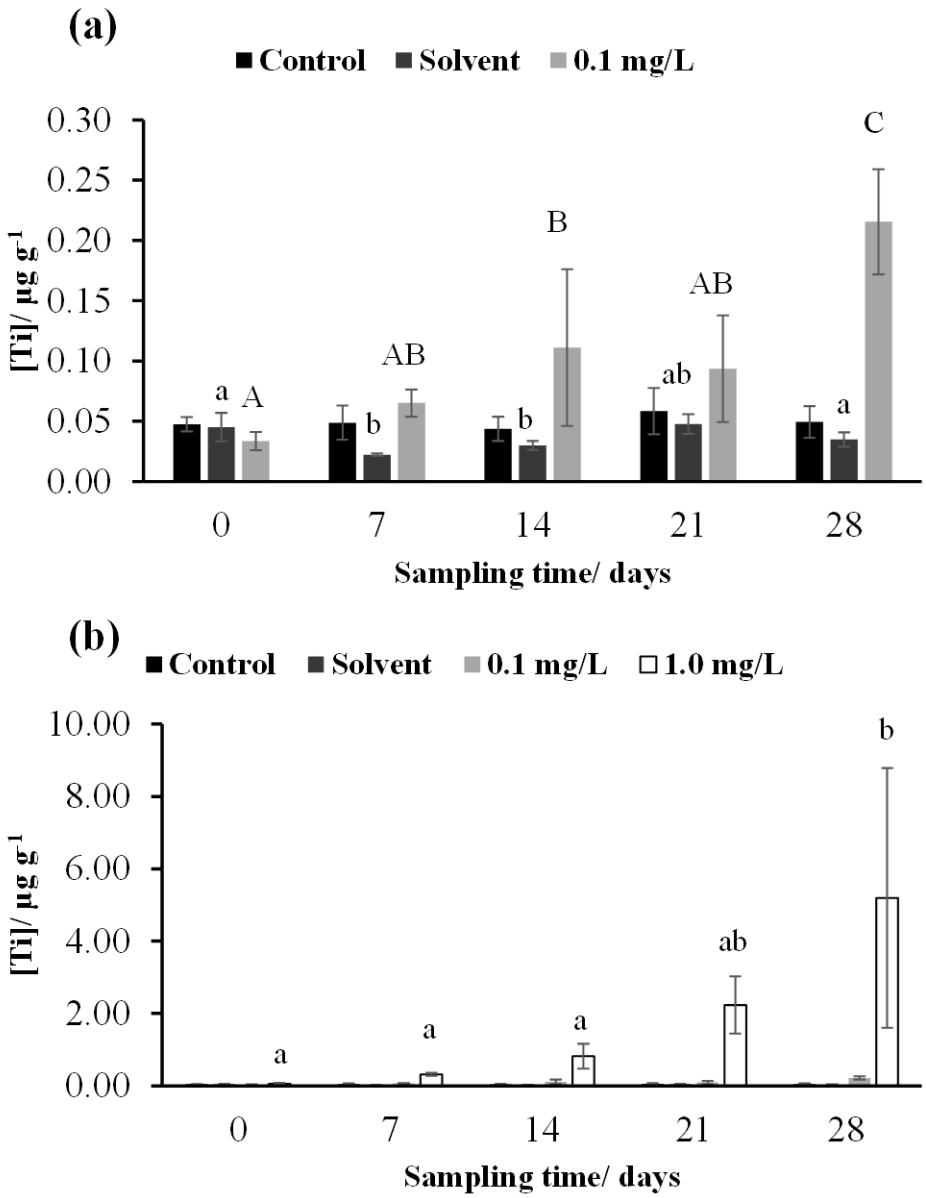

Figure 6.1. Bioaccumulation of Ti in mussels exposed to 25 nm TiO_2NPs for 28 days. Intertank Ti concentration in specimens from: (a) control, solvent with citrate, and 0.1 mg L^{-1} of 25 nm TiO_2NPs tanks, and (b) control, solvent with citrate, 0.1 mg L^{-1}, and 1.0 mg L^{-1} of 25 nm TiO_2NPs tanks. Different letters indicate significative differences (one-way ANOVA, P-value<0.05) between the exposure time for each exposure dose (uppercase for 0.1 mg L^{-1} tanks and lowercase for solvent and 1.0 mg L^{-1} tanks).

Figure 6.2.(a), corresponding to Trial 2, shows the intertank average Ti concentrations in mussels from control tanks (average of A, B, and C), tanks exposed to the nanoparticle citrate coating (average of D, E, and F), and tanks exposed to 0.1 mg L^{-1} of 5 nm TiO_2NPs (average of G, H, and I) for 28 days. No bioaccumulation was found in control and solvent tanks with the exposure days. The basal Ti concentration in control and solvent tanks reached 0.39±0.15 and 0.26±0.04 µg g^{-1} w.w., both at 28 days, respectively. The one-way ANOVA test showed no statistical differences between Ti concentrations in control and solvent tanks as a function

of exposure time (P-value>0.05). Total Ti concentration in mussels exposed to 0.1 mg L^{-1} of 5 nm TiO_2NPs reached a maximum mean value of 1.51±0.53 µg g^{-1} w.w. of Ti after 28 days of exposure. However, the one-way ANOVA test showed that no statistical differences were found among the concentrations (P-value>0.05), probably due to the great variability of the concentrations in the specimens.

Figure 6.2.(b), corresponding to Trial 2, also shows the intertank average Ti concentration in mussels from tanks exposed to 1.0 mg L^{-1} of 5 nm TiO_2NPs (average of J, K, and L) for 28 days. The concentration of the element increased with exposure time until 21 days, reaching 4.76±0.86 µg g^{-1} w.w. of Ti. The ANOVA test confirmed the statistical differences between the concentrations of mussels exposed to 1.0 mg L^{-1} as a function of time (P-value<0.05). The multiple range test showed the differences between concentrations at days 0 and 7, between 0 and 14, 21, and 28 days, and between 7 and 14, 21, and 28 days of exposure. The concentration remained approximately constant at 14, 21, and 28 days. **Figure S.6.1.** and **Figure S.6.2.** (supplementary information) show total titanium concentrations found in all the control, solvent, 0.1 mg L^{-1} and 1.0 mg L^{-1} tanks exposed to 25 and 5 nm TiO_2NPs, respectively.

USC
UNIVERSIDADE DE SANTIAGO DE COMPOSTELA

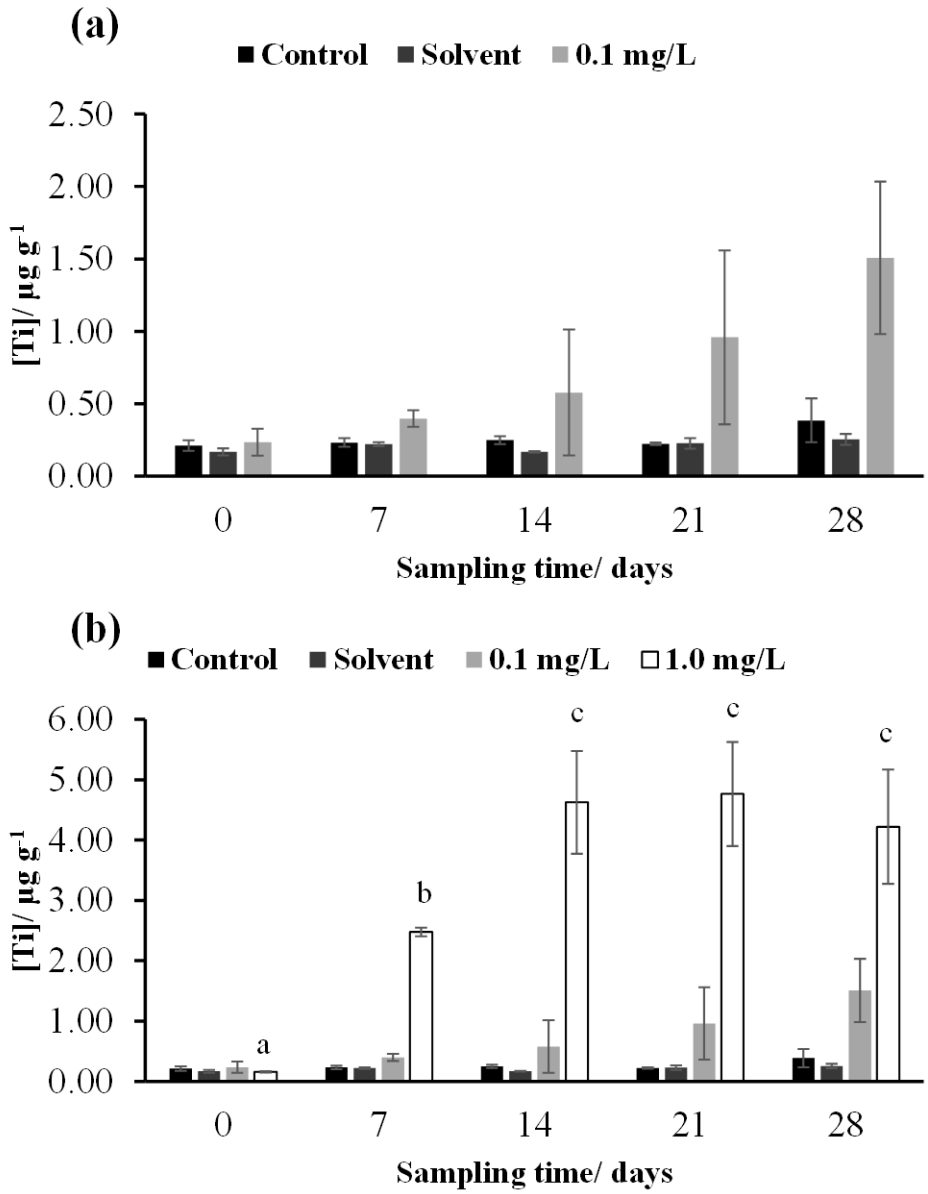

Figure 6.2. Bioaccumulation of Ti in mussels exposed to 5 nm TiO_2NPs for 28 days. Intertank Ti concentration in specimens from: (a) control, solvent with citrate, and 0.1 mg L^{-1} of 5 nm TiO_2NPs tanks and (b) control, solvent with citrate, 0.1 mg L^{-1}, and 1.0 mg L^{-1} of 5 nm TiO_2NPs tanks. Different letters indicate significative differences (one-way ANOVA, P-value<0.05) between the exposure time for each exposure dose.

In summary, the results showed that mussels bioaccumulate Ti when they are exposed to 25 and 5 nm TiO_2NPs. The results also showed that the concentration of bioaccumulated Ti increased with the exposure dose. Total Ti concentrations were higher in mussels exposed to 1.0 mg L^{-1} than in mussels exposed to 0.1 mg L^{-1} for both sizes. The one-way ANOVA statistical test was also used to compare whether there were significant differences between Ti concentrations found in mussels exposed to 0.1 and 1.0 mg L^{-1}. For mussels exposed to 25 nm TiO_2NPs, ANOVA tests showed statistical differences on days 7, 14, and 21 days between the exposure doses. On the other hand, for mussels exposed to 5 nm TiO_2NPs, the ANOVA tests showed statistical differences on days 7, 14, and 28 days between the exposure doses. Although at the end of the bioaccumulation assays the total Ti concentration reached in both trials was of

the same order of magnitude, the bioaccumulation in mussels exposed to 5 nm TiO_2NPs occurred earlier, with a stabilization of the concentration at 14 days after exposure at a dose of 1.0 mg L^{-1}.

In a previous study, Gallocchio et al. [1] evaluated the accumulation of TiO_2NPs in *Mytillus galloprovincialis* grown in artificial seawater and exposed to ionic Ti (concentration in the tank of 1.6 mg L^{-1}) or TiO_2NPs (0.25 or 2.5 mg L^{-1}) for 4 days. The authors observed that the concentration of Ti (209-1119 µg kg^{-1}) in exposed mussels was proportional to the dose and independent of the form (ionic or nanoparticulate). The concentrations found in that study were of the same order as those obtained in the present work.

The estimated daily intake (EDI) of Ti can be calculated according to the following **Equation 6.1.** [29]:

$$\text{EDI} = \frac{\text{Concentration of metal} \times \text{Average daily ingestion rate}}{\text{Body weight}} \quad (\textbf{Equation 6.1.})$$

The value of EDI was calculated for the maximum average concentration of Ti determined (5.19 µg g^{-1} w.w.), an average ingestion rate of 0.33 g mussel per day in Spain for adults between 18-74 years old [30], and a body weight of 70 kg. The value obtained was 0.0245 µg of Ti per day and Kg of body weight, lower than the EDI (0.84-1.34) calculated by Xu et al. [29] for mollusk consumption, and much lower than the adverse effect level of the element proposed by Lim et al. [31] (6.25×10^4 µg per kg BW and day). However, depuration is still important to minimize the possible effect of the nanoparticles that can also act as vectors for the introduction of other pollutants in living beings.

6.4.1.2 Total Ti in mussel shells

Weakening and fractures were observed in some mussel shells exposed to NPs in Trial 2 (bioaccumulation of mussels exposed to 5 nm TiO_2NPs). Shi et al. [32] had observed that the presence of TiO_2NPs decreased the byssal attachment strength of *Mytilus coruscus* after 10 days of exposure to a concentration of Ti as low as 100 µg L^{-1}. Due to the unknown possible interactions of Ti with mussels, the decision was made to investigate also the potential presence of Ti in the shells.

Shells from one control tank (tank A), one solvent tank (tank D), one of 0.1 mg L^{-1} of 5 nm TiO_2NPs tank (tank G), and one of 1.0 mg L^{-1} of 5 nm TiO_2NPs tank (tank J), were sampled at 7, 14, 21, and 28 days. The shells were washed with ultrapure water, dried in a laboratory stove, and pulverized in a zirconia ball mill. The pulverized samples were submitted, to microwave-assisted acid digestion, in triplicate, and analyzed by ICP-MS following the process described in **section 6.3.4**.

Figure 6.3. shows the total Ti concentration in the mussel shells from control, solvent, 0.1 and 1.0 mg L^{-1} of 5 nm TiO_2NPs tanks at different exposure times. The highest Ti concentration was found at 1.0 mg L^{-1} of exposure dose after 21 days, reaching 12.43±3.45 µg g^{-1} d.w. One-way ANOVA tests were performed to study the variation of Ti concentration in the shells from different tanks with exposure time. ANOVA did not show significant differences between Ti concentration in shells from control tanks, solvent tanks, and tanks exposed to 0.1 and 1.0 mg L^{-1} with the exposure days (P-values>0.05). The one-way ANOVA test was also performed to compare the effect of the different exposure doses on the same day. Ti concentrations of mussels from control, solvent, low, and high exposure doses tanks presented significative statistical differences on the same exposure day at a 95% of confidence level (P-values<0.05). The multiple range tests showed that the concentrations of Ti in shells of mussels

exposed to 1.0 mg L^{-1} were higher than those found in mussels from the other tanks. Thus, it can be concluded that the shells of mussels bioaccumulated Ti after exposure to the high dose of TiO_2NPs, and it could be the reason for the weakening and breakage of those shells.

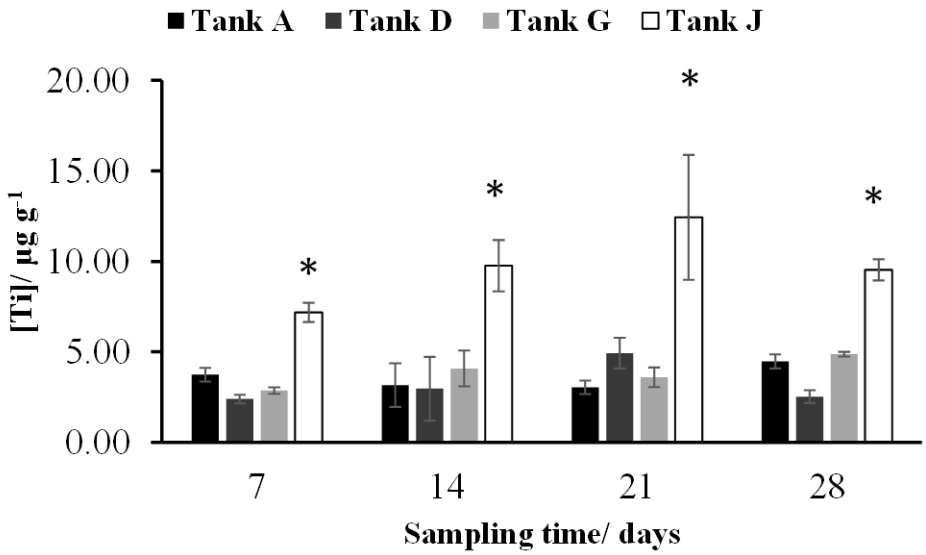

Figure 6.3. Bioaccumulation of Ti in shells of mussels collected from different tanks: control (tank A), solvent (tank D), 0.1 mg L^{-1} 5 nm TiO_2NPs (tank G), and 1.0 mg L^{-1} 5 nm TiO_2NPs (tank J). * Indicate significative differences (one-way ANOVA, P-value<0.05) between the high exposure dose and the control, solvent, and low exposure dose at the same exposure day.

6.4.1.3 TiO_2NPs in mussels

TiO_2NPs content and size distribution in mussels exposed to 25 nm TiO_2NPs (Trial 1) and 5 nm TiO_2NPs (Trial 2) were determined using the methodology described in **section 6.3.5**. The enzymatic extracts were diluted with 1% (v/v) glycerol 500 times before SP-ICP-MS analysis. The experimental flow rates and transport efficiencies were between 0.185 and 0.223 mL min^{-1}, and between 7.3 and 10.72 %, respectively. Laborda et al. [33] criteria were used to calculate the limits of detection in single-particle mode. The LOD_{number} resulted in 1.99×10^6 TiO_2NPs L^{-1} in the extract and 7.46×10^7 TiO_2NPs g^{-1} in the sample. The LOD_{size} using the 3σ and the more restrictive 5σ criteria resulted in 24 and 28 nm, respectively.

Pancreatin/lipase extractions were performed only in mussels from tanks exposed to 0.1 and 1.0 mg L^{-1} of TiO_2NPs (NPs of both sizes).

Figure 6.4.(a) shows the average intertank TiO_2NPs concentrations in mussels exposed to 0.1 and 1.0 mg L^{-1} of 25 nm TiO_2NPs for 28 exposure days. The highest NPs concentrations found were $1.15\times10^8\pm2.84\times10^7$ and $2.28\times10^8\pm5.84\times10^7$ TiO_2NPs g^{-1} for 0.1 and 1.0 mg L^{-1} of TiO_2NPs, respectively, both at the 28^{th} day.

One-way ANOVA tests were also performed in the case of nanoparticles to evaluate if there were significant differences between TiO_2NPs concentrations at different exposure times. The ANOVA test for mussels exposed to 0.1 mg L^{-1} resulted in a P-value>0.05; thus no statistical differences were found between TiO_2NPs concentrations at different exposure days with a 95% of confidence level. However, significant differences (P-value<0.05) were obtained for mussels exposed to 1.0 mg L^{-1}. The multiple range test showed significant differences between concentrations at day 0 and days 21 and 28, at day 7 and days 21 and 28, at day 14 and day 28, and between concentrations at days 21 and 28. Therefore, the concentrations of TiO_2NPs in the samples increased with time, especially at the high exposure dose.

USC

Figure 6.4.(b) and **Figure 6.4.(c)** show the most frequent and the mean sizes of nanoparticles detected in mussels exposed to 0.1 and 1.0 mg L^{-1} 25 nm TiO_2NPs for 28 days, respectively. For mussels exposed to 0.1 mg L^{-1} of 25 nm TiO_2NPs, the most frequent and mean sizes ranged between 60±1 nm (0 days) and 62±4 nm (28 days), and from 81±2 nm (0 days) to 85±10 nm (28 days), respectively. On the other hand, in mussels exposed to 1.0 mg L^{-1} of 25 nm TiO_2NPs, the most frequent and mean sizes ranged between 55±4 nm (0 days) and 57±2 nm (28 days), and from 70±5 nm (0 days) to 74±1 nm (28 days), respectively.

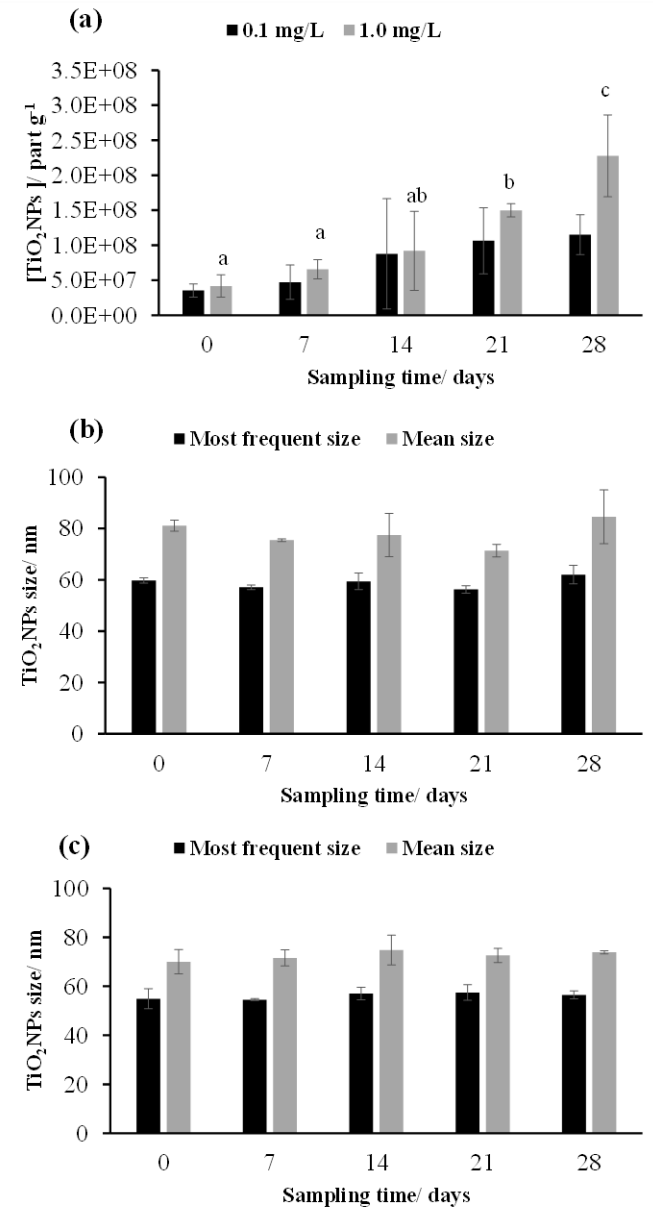

Figure 6.4. TiO_2NPs bioaccumulation in mussels exposed to 0.1 and 1.0 mg L^{-1} of 25 nm TiO_2NPs. Intertank average: (a) NP concentrations, (b) most frequent and mean sizes of NPs in mussels exposed to 0.1 mg L^{-1} of 25 nm TiO_2NPs, (c) and 1.0 mg L^{-1} of 25 nm TiO_2NPs. Different letters indicate significative differences (one-way ANOVA, P-value<0.05) between the exposure time for each exposure dose.

Figure 6.5.(a) shows the average intertank TiO_2NPs concentrations in mussels exposed to 1.0 mg L^{-1} 5 nm TiO_2NPs for 28 exposure days. In Trial 2 the enzymatic extractions in mussels exposed to 0.1 mg L^{-1} TiO_2NPs resulted in values lower than LOD_{number} (<7.46×10^7

TiO_2NPs g^{-1}). TiO_2NPs content in mussels exposed to the high dose increased with the exposure time, reaching $4.79\times10^8\pm2.63\times10^8$ TiO_2NPs g^{-1} at 21 exposure days. The ANOVA test for mussels exposed to 1.0 mg L^{-1} resulted in a P-value>0.05; thus no statistical differences were found between TiO_2NPs concentrations at different exposure days with a 95% of confidence level. **Figure 6.5.(b)** shows the most frequent and the mean sizes of nanoparticles detected in these samples. The most frequent and mean sizes were between 59±7 nm (0 days) and 45±1 nm (28 days), and between 96±4 nm (0 days) and 60±1 nm (28 days), respectively.

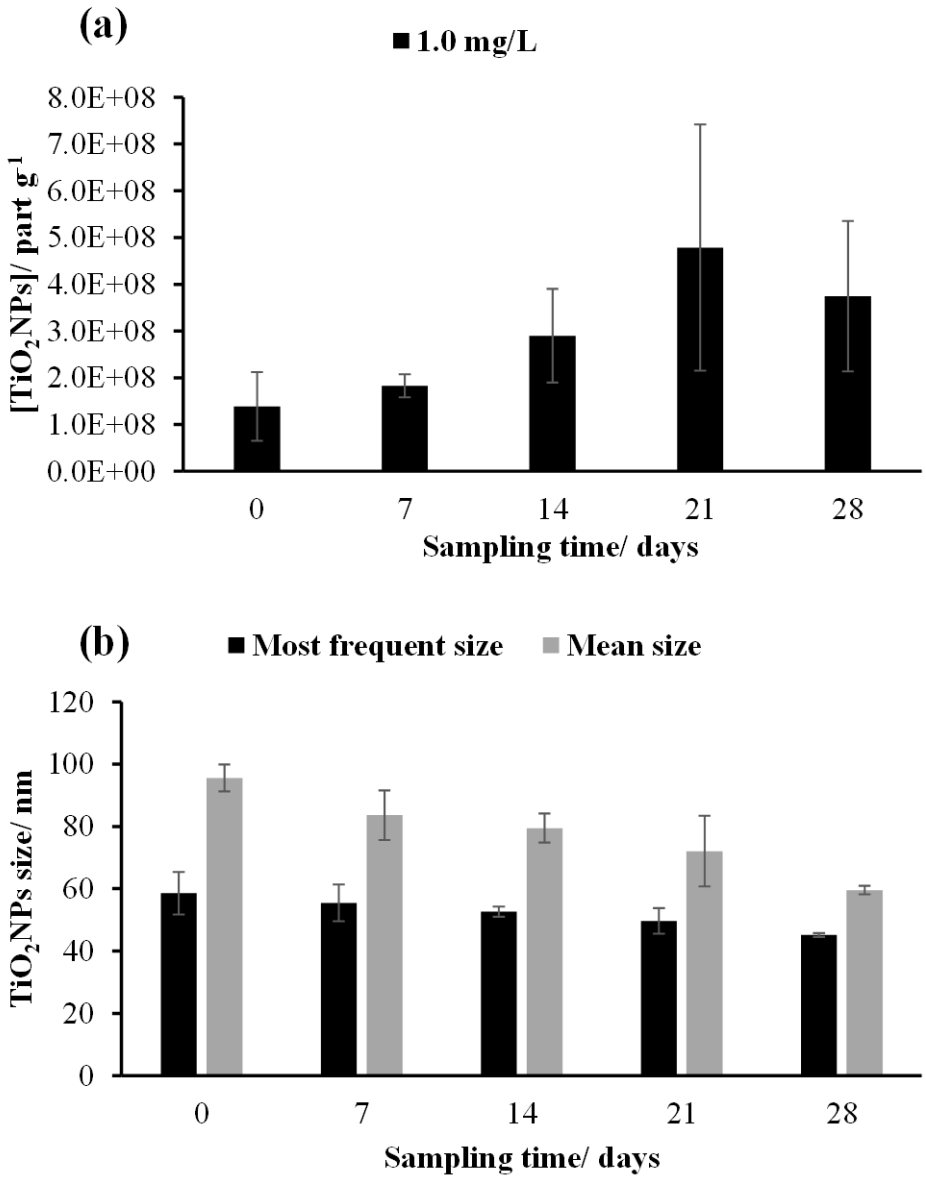

Fig. 6.5. TiO_2NPs bioaccumulation in mussels exposed to 1.0 mg L^{-1} of 5 nm TiO_2NPs. Intertank average: (a) NP concentrations, (b) most frequent and mean sizes of NPs.

The sizes for both trials were different from the theoretical primary size of 25 and 5 nm TiO_2NPs; it was mainly due to the common aggregation phenomenon of TiO_2NPs. The citrate-coated TiO_2NPs aggregation was previously tested by Dynamic Light Scattering and SP-ICP-MS. The TiO_2NPs of 25 and 5 nm presented aggregation in contact with ultrapure

USC UNIVERSIDADE DE SANTIAGO DE COMPOSTELA

water, and even more in the presence of seawater, where the TiO_2NPs formed large micrometer aggregates (128±2.9/65±14 nm for 25/5nm TiO_2NPs in ultrapure water, and 3168±1089/3320±1248 nm for 25/5 nm TiO_2NPs in artificial seawater). Once the particles were internalized in the fish matrix, the size (determined by SP-ICP-MS) changed again, maybe due to a stabilization effect during the enzymatic extraction forming small TiO_2NPs aggregates with mean sizes between 70-75 nm and between 60-100 nm for TiO_2NPs of 25 and 5 nm. **Figure S.6.3.** shows an SP-ICP-MS histogram corresponding to mussels exposed to a dose of 1.0 mg L^{-1} of 25 nm TiO_2NPs for 21 days.

In their study about *Mytillus galloprovincialis*, Gallochio et al. [1] observed by SP-ICP-MS that the specimens accumulated NPs with average sizes of 93-111 nm (the same size as the NPs in the suspensions used). However, in the case of mussels exposed to ionic Ti, they also observed aggregation with NPs of an average size of 55 nm. In the case of offshore aquaculture mussels, Xu et al. [29] determined that the mean size of TiO_2NPs in the muscle of the specimens studied was 70.6±12.7 nm.

6.4.2 Turbot bioaccumulation tests

6.4.2.1 Total Ti in turbot

Total Ti determination in turbot was performed using the methodology described in **section 6.3.4**. The liver, kidney, and flesh of the animal were submitted to microwave-assisted acid digestion. The digests were performed in triplicate when the amount of sample was enough. The digested samples were diluted with ultrapure water at least 10 times before the ICP-MS analysis. The standard addition calibration method was employed, and the analytical performance was also evaluated for total Ti in turbot. Limits of detection were calculated as in **section 6.4.1.1**. The LOD and LOQ were 1.36 and 4.54 ng g^{-1}, respectively. The average analytical recovery was 98±3 % (n=5), and the repeatability of the measurements achieved RSD<2% (n=5).

Total Ti concentrations were determined in the liver, kidney, and muscle+skin in Trial 1 (juvenile turbots fed with 25 nm TiO_2NPs), and Trial 2 (juvenile turbots fed with 5 nm TiO_2NPs). Ti concentrations were lower than LOQ (<4.54 ng g^{-1}) in the case of the kidney, for all exposure doses and days. In both trials, only Ti bioaccumulation was observed in the liver. In the case of flesh+skin, the amount of Ti found in the samples was approximately the basal Ti concentration present in fish.

Figure 6.6.(a) and **Figure 6.6.(b)** show total Ti concentrations in muscle+skin of turbots exposed to 0, 0.25, 0.75, and 1.5 mg TiO_2NPs Kg^{-1} fish and day of 25 nm for 90 days, and 5 nm for 75 days, respectively. One-way ANOVA tests were performed to study the variation of Ti concentration with exposure time at the same exposure dose, and of Ti concentrations with exposure dose at the same exposure time. In the case of turbot exposed to 25 nm TiO_2NPs, the P-values were always higher than 0.05; thus, no statistical differences were found among Ti concentrations as a function of exposure time, and among Ti concentrations as a function of exposure dose. In the case of turbot exposed to 5 nm TiO_2NPs, similar results were obtained. In summary, no bioaccumulation was observed in turbot muscle (Trials 1 and 2), with most Ti concentrations being lower than basal Ti in turbot muscle (at day 0).

USC UNIVERSIDADE DE SANTIAGO DE COMPOSTELA

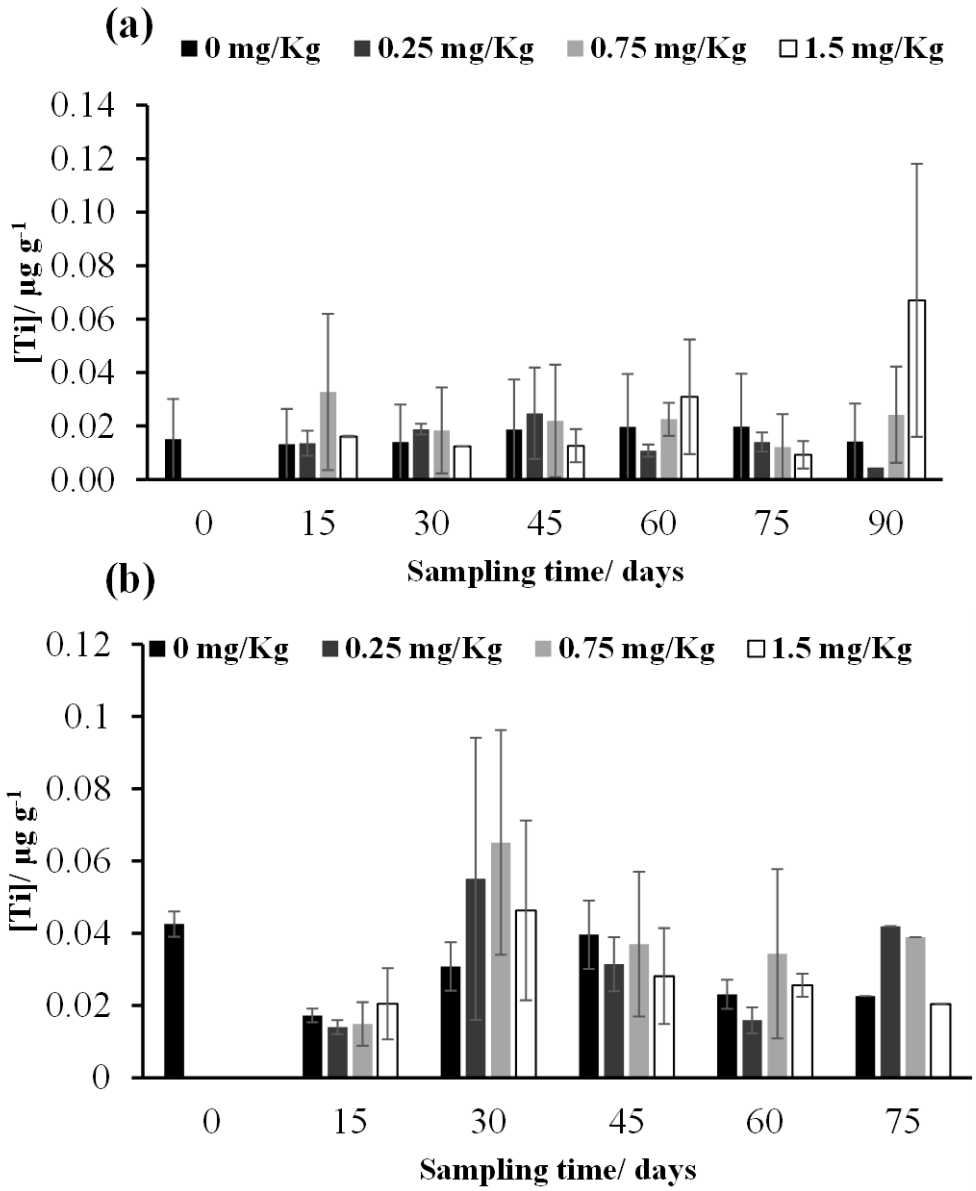

Figure 6.6. Flesh+skin Ti bioaccumulation in turbots exposed to (a) 0, 0.25, 0.75, and 1.5 mg of 25 nm TiO_2NPs Kg^{-1} fish and day, and to (b) 0, 0.25, 0.75, and 1.5 mg of 5 nmTiO_2NPs Kg^{-1} fish and day.

Figure 6.7.(a) and **Figure 6.7.(b)** show total Ti concentration in turbot liver exposed to 0, 0.25, 0.75, and 1.5 mg TiO_2NPs Kg^{-1} fish and days of 25 nm and 5 nm for 90 days, respectively. The highest Ti concentrations reached in the liver of turbot exposed to 25 and 5 nm of TiO_2NPs were 0.28±0.18 and 1.62±0.44 µg g^{-1} w.w., respectively, both measured after 90 days of exposure to the highest dose. ANOVA tests were performed to compare Ti concentrations in turbot liver at different exposure times at different exposure doses. In the case of turbot fed with 25 nm TiO_2NPs, all the ANOVA tests (for 0, 0.25, 0.75, and 1.5 mg Kg^{-1}) showed P-values>0.05; thus, no statistical differences were found between Ti concentrations. However, in the case of turbot fed with 5 nm TiO_2NPs, statistical differences were found at different exposure times in the liver from turbots exposed to 0.75 mg Kg^{-1} of TiO_2NPs (P-value<0.05). The multiple range test provided significant differences between 15 days and 75 and 90 days, and between 30 days and 60, 75, and 90 days. Therefore, it seems that there is a

slight increase in the concentration of Ti in the liver from turbots exposed to nanoparticles of 5 nm, and that is difficult to observe due to the variability of the samples.

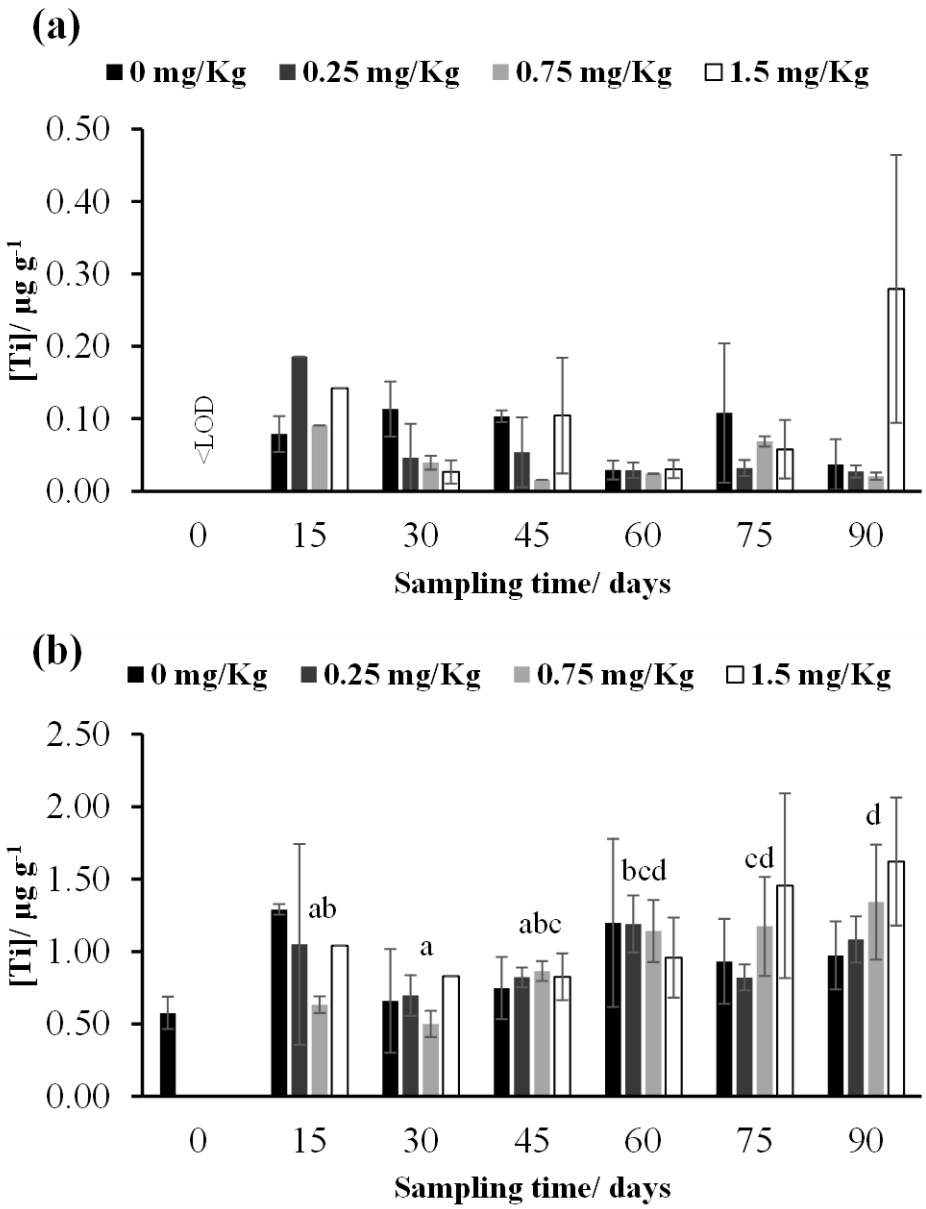

Figure 6.7. Liver Ti bioaccumulation in turbots exposed to (a) 0, 0.25, 0.75, and 1.5 mg of 25 nm TiO_2NPs Kg^{-1} fish and day, and (b) 0, 0.25, 0.75, and 1.5 mg of 5 nmTiO_2NPs Kg^{-1} fish and day. Different letters indicate significative differences (one-way ANOVA, P-value<0.05) between the exposure time for 0.75 mg Kg^{-1} exposure dose.

6.4.2.2 Total Ti in turbot feces

The presence of Ti in feces collected from aquaculture tanks was also studied. The samples were dried in a laboratory stove, homogenized, and digested as in the case of turbot (previously described). By the end of the experiment, the feces were collected in both Trials in tanks of different exposure TiO_2NPs doses.

Figure 6.8.(a) and **Figure 6.8.(b)** show the linear increase of Ti in feces with the increasing dose of 25 and 5 nm TiO_2NPs nanoparticles, respectively. The highest Ti

concentrations measured were 11.88±1.71 and 40.99±6.62 µg g^{-1} w.w. for an equivalent dose of 1.5 mg Kg^{-1} TiO_2NPs fish and day of 25 and 5 nm, respectively. One-way ANOVA tests were performed in Trials 1 and 2 to compare if there were statistical differences between Ti concentrations as a function of the administrated dose. In both cases, P-values were lower than 0.05, indicating statistical differences between Ti content in feces. The multiple range test showed an overlapping in the Ti concentration of feces from turbots exposed to 0 and 0.25 mg Kg^{-1} of 25 nm TiO_2NPs, but no overlapping in concentration was found in feces of turbot exposed to 5 nm TiO_2NPs, and the concentration increased with time.

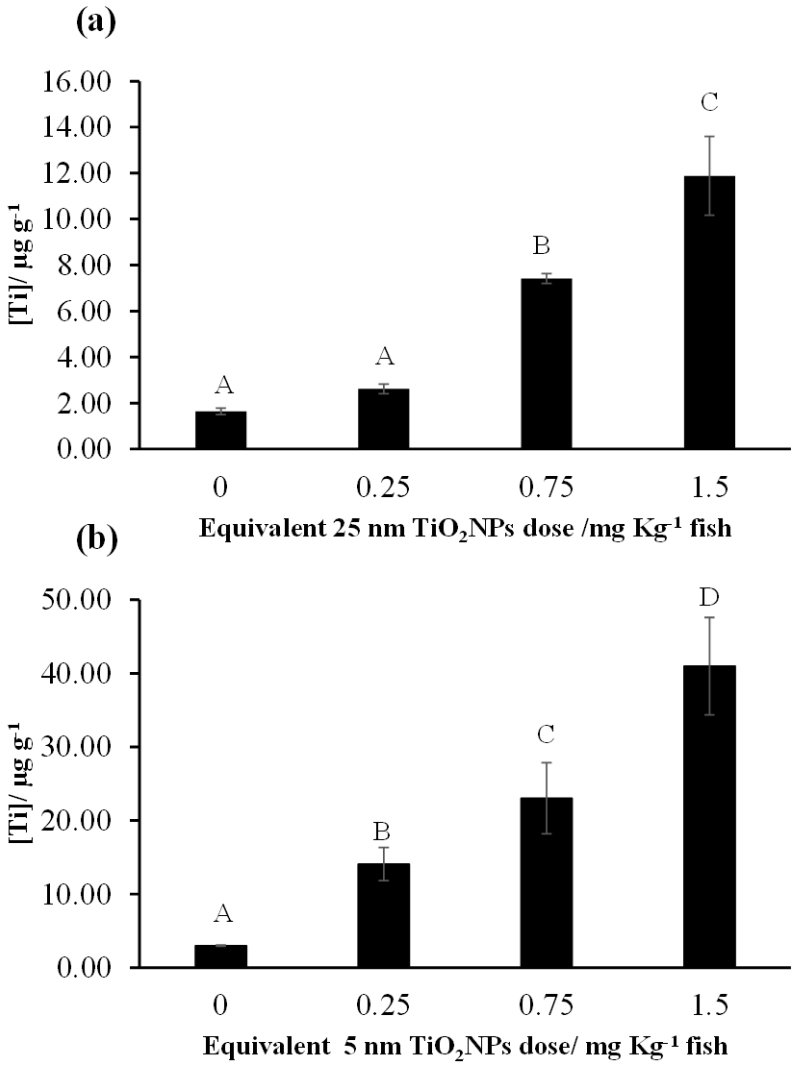

Figure 6.8. Ti concentration in feces of turbots exposed to 0, 0.25, 0.75, and 1.5 mg TiO_2NPs Kg^{-1} fish and day: (a) NPs of 25 nm, (b) NPs of 5 nm. Different letters indicate significative differences (one-way ANOVA, P-value<0.05) between the exposure time for each exposure dose.

The highest concentrations of Ti were found in Trial 2, which is in agreement with the results obtained for turbot liver, with a bigger accumulation and subsequent excretion of Ti observed for 5 nm nanoparticles, probably due to the higher Ti ingestion rate. The results indicate that most of Ti is excreted through the feces and only a small portion is accumulated in the turbot liver.

USC UNIVERSIDADE DE SANTIAGO DE COMPOSTELA

6.4.2.3 TiO_2NPs in turbot

TiO_2NPs content and size distributions were determined in turbot specimens from both Trials. The enzymatic extractions in turbot samples were carried out in the same way as mussels, following the methodology described in **section 6.3.5**. Since total Ti in the kidney was lower than the LOQ, and total Ti in muscle was present at the basal Ti concentration, the enzymatic extractions were performed only in the liver of turbot specimens exposed to 25 and 5 nm TiO_2NPs. The enzymatic extracts were diluted 500 times with 1% (v/v) glycerol before SP-ICP-MS analysis. The LOD_{number} achieved was 1.19×10^6 NPs L^{-1} and 4.46×10^6 NPs g^{-1} (referred to the 500 times diluted sample), and the LOD_{size} were 42 and 36 nm for the 5σ and 3σ criteria, respectively. No peaks corresponding to NPs were detected in SP-ICP-MS monitoring in any liver extract sample; thus all the concentrations in the samples were lower than 4.46×10^6 NPs g^{-1}. This indicates that the accumulation in the liver is only related to ionic Ti, metabolizing NPs into ionic Ti or TiO_2NPs lower in size than 42 nm.

Even when the concentration of Ti or nanoparticles did not increase with time in turbot, other effects of the exposure were observed. Thus, the weight of the specimens of turbot decreased with the dose of exposure to nanoparticles of 25 nm. The multiple range test showed some significant differences between non-exposed turbots and turbots exposed to the different doses of nanoparticles. When turbots were exposed to 1.5 mg Kg^{-1} of fish and day, significant differences were found between concentrations in non-exposed turbots and turbots exposed for 15, 45, 60, 75 and 90 days.

Exposure to NPs through the diet decreases the dispersibility problems of the nanomaterials and facilitates the control of the exposure doses [11]. As an example, Wang et al. [9] observed a fast aggregation and sedimentation of TiO_2 NPs in seawater used for feeding juvenile turbots. However, a similar pattern of accumulation of Ti was found for both types of exposure (aqueous or through the diet of treated clamworms), with specimens showing a higher concentration of the element in gills, intestines and stomach, followed by skin, liver and muscle. After 20 days, histological analysis by microscopy showed pathological changes in the tissue of the liver and spleen. Histological alterations in the liver were also observed by our research group in juvenile turbots after 14 days of exposure to citrate-coated 25 nm TiO_2NPs [34]. The number of lipid droplets in hepatocytes decreased but their diameters increased, and proteomic analysis revealed lipid and energy metabolism modifications. Then, the active contribution of the fish liver for detoxification was confirmed, whereas the analysis of whole mussels seems more helpful as a sentinel organism for TiO_2NPs in environmental research.

USC
UNIVERSIDADE DE SANTIAGO DE COMPOSTELA

6.5 CONCLUSIONS

This research work studied the bioaccumulation of TiO_2NPs in an aquaculture benthic bivalve (*Mytilus edulis*) and a benthic predator (*Scophthalmus maximus*). The bioaccumulation assays using different sizes of nanoparticles (25 nm and 5 nm) and different exposure concentrations were carried out during long exposure times (till 90 days in the case of fish). Mussels bioaccumulated Ti and TiO_2NPs of 25 and 5 nm, with the concentrations increasing with the dose and exposure time. The total Ti content in fractured and weakened shells of mussels exposed to 5 nm TiO_2NPs was also determined, resulting in a higher amount of the element in tanks of mussels exposed to high doses in comparison to the control tanks. The bioaccumulation of Ti in mussels highlights the need for purification periods of these filtering organisms to ensure the food quality of this highly consumed product around the world. Ti was also determined in the muscle+skin, kidney and liver of turbot, and the highest Ti concentrations were measured in the liver, an un-edible part of this appreciated flat fish. Finally, the fact that the muscle tissue does not accumulate Ti and that the element is excreted through the feces, shows that turbot can be considered safe for human consumption.

USC
UNIVERSIDADE DE SANTIAGO DE COMPOSTELA

SUPPLEMENTARY INFORMATION

Table S.6.1. Operational conditions for (a) ICP-MS and (b) SP-ICP-MS.

(a) ICP-MS operational conditions	
Parameter/component	**Type/mode/value**
Nebulizer	Meinhard CR R^+
Nebulizer Chamber	5 ºC refrigerated glass cyclone chamber with Peltier PC^{3X}
Cone material	Nickel/aluminum
Radiofrequency power	1600 W
Ar gas flow	15 L min^{-1} (Plasma) 1.15 L min^{-1} (Nebulizer) 1.2 L min^{-1} (Auxiliary)
Analyte	Ti
Operation mode	DRC (dynamic reaction cell)
Ammonia flow rate	1.0 mL min^{-1}
Integration time	1000 ms
m/z	131, cluster $[^{48}Ti^{14}N^1H(^{14}N^1H_3)_4^+]$
Replicates per sample	3
RPQ	0.2
(b) SP-ICP-MS operational conditions	
Sample flow rate	0.189-0.223 mL min^{-1}
Acquisition time	60 s
Dwell time	100 µs
Number of readings	600,000

USC UNIVERSIDADE DE SANTIAGO DE COMPOSTELA

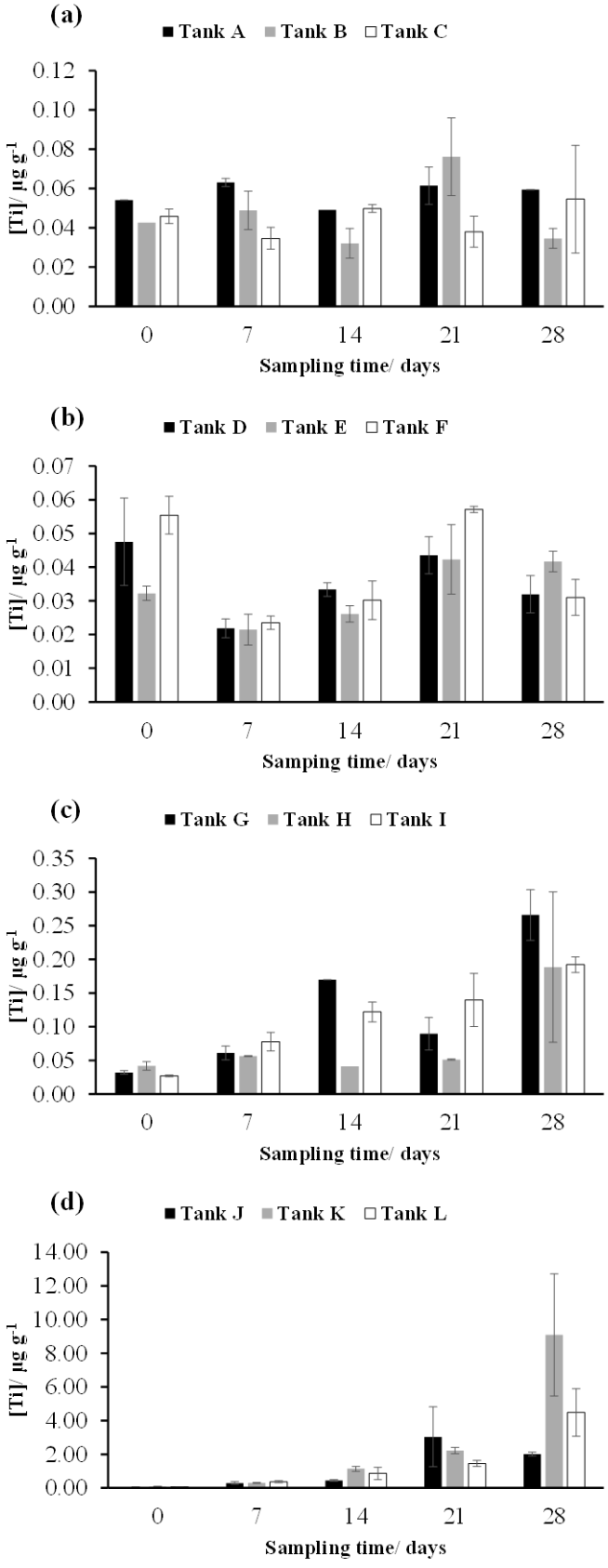

Figure S.6.1. Total Ti bioaccumulation in mussels from (a) control, (b) solvent, (c) 0.1 mg L^{-1}, and (d) 1.0 mg L^{-1} of 25 nm TiO_2NPs tanks.

USC UNIVERSIDADE DE SANTIAGO DE COMPOSTELA

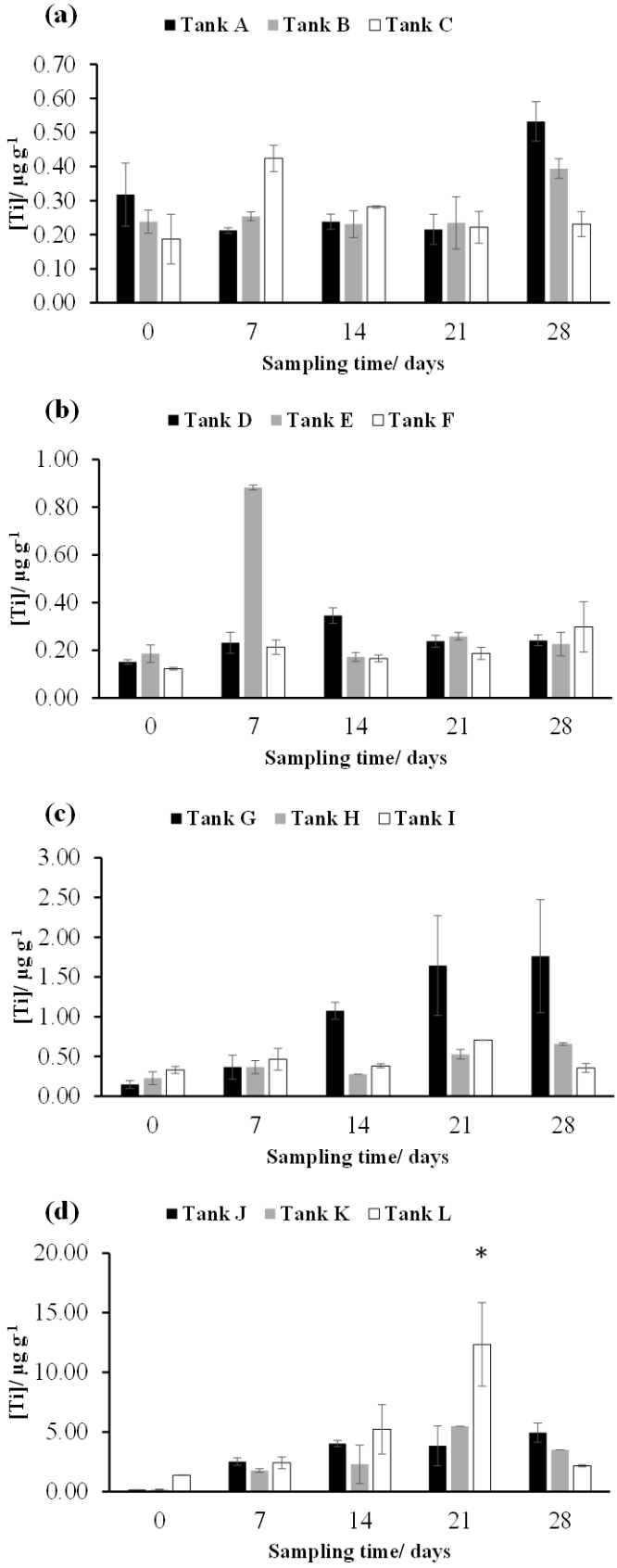

Figure S.6.2. Total Ti bioaccumulation in mussels from (a) control, (b) solvent, (c) 0.1 mg L^{-1}, and (d) 1.0 mg L^{-1} of 5 nm TiO_2NPs tanks. *Not used for average calculations.

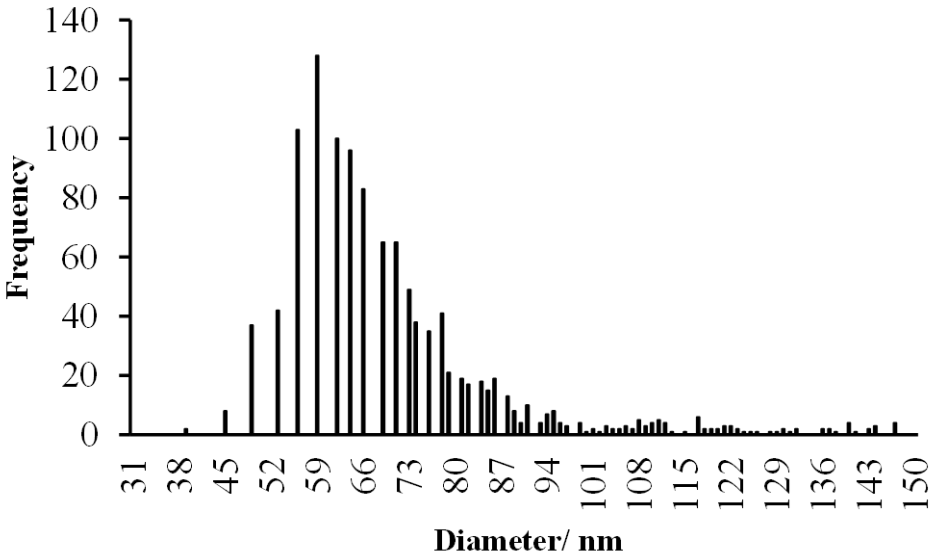

Figure S.6.3. SP-ICP-MS example histogram corresponding to mussels exposed to 1.0 mg L^{-1} of 25 nn TiO_2NPs for 21 exposure days.

USC
UNIVERSIDADE DE SANTIAGO DE COMPOSTELA

REFERENCES

[1] F. Gallocchio, G. Biancotto, A. Moressa, F. Pascoli, T. Pretto, A. Toffan, G. Arcangeli, F. Montesi, R. Peters, A. Ricci, Bioaccumulation and *in vivo* formation of titanium dioxide nanoparticles in edible mussels, Food Chem. 323 (2020) 126841. https://doi.org/10.1016/j.foodchem.2020.126841.
[2] M. Abd El-Atti, M. M. A. Desouky, A. Mohamadien, R. M. Said, Effects of titanium dioxide nanoparticles on red swamp crayfish, *Procambarus clarkii*: Bioaccumulation, oxidative stress and histopathological biomarkers, Egypt. J. Aquat. Res. 45 (2019) 11–18. https://doi.org/10.1016/j.ejar.2019.01.001.
[3] R. Gornati, A. Longo, F. Rossi, M. Maisano, G. Sabatino, A. Mauceri, G. Bernardini, S. Fasulo, Effects of titanium dioxide nanoparticle exposure in *Mytilus galloprovincialis* gills and digestive gland, Nanotoxicology 10 (2016) 807-817. https://doi.org/10.3109/17435390.2015.1132348.
[4] M. Younes, G. Aquilina, L. Castle, K. H. Engel, P. Fowler, M. J. Frutos Fernandez, P. Fürst, U. Gundert-Remy, R. Gürtler, T. Husøy, M. Manco, W. Mennes, P. Moldeus, S. Passamonti, R. Shah, I. Waalkens-Berendsen, D. Wölfle, E. Corsini, F. Cubadda, D. De Groot, R. Fitz Gerald, S. Gunnare, A. C. Gutleb, J. Mast, A. Mortensen, A. Oomen, A. Piersma, V. Plichta, B. Ulbrich, H. Van Loveren, D. Benford, M. Bignami, C. Bolognesi, R. Crebelli, M. Dusinska, F. Marcon, E. Nielsen, J. Schlatter, C. Vleminckx, S. Barmaz, M. Carfí, C. Civitella, A. Giarola, A. M. Rincon, R. Serafimova, C. Smeraldi, J. Tarazona, A. Tard, M. Wright, Safety assessment of titanium dioxide (E171) as a food additive, EFSA J. 19 (2021) 6585. https://doi.org/10.2903/j.efsa.2021.6585.
[5] European Commission, Commission Regulation (EU) 2022/63 of 14 January 2022 amending Annexes II and III to Regulation (EC) No 1333/2008 of European Parliament and of the Council as regards the food additive titanium dioxide (E171), Off. J. Eur. Union. 11 (2022) 1–5.
[6] L. Canesi, C. Ciacci, R. Fabbri, A. Marcomini, G. Pojana, G. Gallo, Bivalve molluscs as a unique target group for nanoparticle toxicity, Mar. Environ. Res. 76 (2012) 16–21. https://doi.org/10.1016/j.marenvres.2011.06.005.
[7] APROMAR OPP30. La acuicultura en España, Informe 2021, (2021). https://apromar.es/wp-content/uploads/2021/12/La-Acuicultura-en-Espana-2021.pdf (accessed January 21, 2023).
[8] A. D. Larios, R. Pulicharla, S. K. Brar, M. Cledón, Filter feeders increase sedimentation of titanium dioxide: The case of zebra mussels, Sci. Total Environ. 618 (2018) 746–752. https://doi.org/10.1016/j.scitotenv.2017.08.150.
[9] Z. Wang, L. Yin, J. Zhao, B. Xing, Trophic transfer and accumulation of TiO_2 nanoparticles from clamworm (*Perinereis aibuhitensis*) to juvenile turbot (*Scophthalmus maximus*) along a marine benthic food chain, Water Res. 95 (2016) 250–259. https://doi.org/10.1016/j.watres.2016.03.027.
[10] OECD, Test No. 316: Phototransformation of chemicals in water–direct photolysis, Test No 305 bioaccumulation fish aqueous diet. Expo. Section 3 (2008) 1–72.
[11] M. Conolly, S. Martínez-Morcillo, J. Kalman, J. M. Navas, E. Bleeker, M. L. Fernández-Cruz, Considerations for bioaccumulation studies in fish with nanomaterials, Chemosphere 312 (2023) 137229. https://doi.org/10.1016/j.chemosphere.2022.137299.
[12] X. Zhu, J. Wang, X. Zhang, Y. Chang, Y. Chen, Trophic transfer of TiO_2 nanoparticles from daphnia to zebrafish in a simplified freshwater food chain, Chemosphere 79 (2010) 928–933. https://doi.org/10.1016/j.chemosphere.2010.03.022.

[13] X. Ren, X. Zhao, X. Duan, Z. Fang, Enhanced bio-concentration of tris(1,3-dichloro-2-propyl) phosphate in the presence of nano-TiO_2 can lead to adverse reproductive outcomes in zebrafish, Environ. Pollut. 233 (2018) 612–622. https://doi.org/10.1016/j.envpol.2017.10.101.
[14] Q. Fang, Q. Shi, Y. Guo, J. Hua, X. Wang, B. Zhou, Enhanced bioconcentration of bisphenol A in the presence of nano-TiO_2 can lead to adverse reproductive outcomes in zebrafish, Environ. Sci. Technol. 50 (2016) 1005–1013. https://doi.org/10.1021/acs.est.5b05024.
[15] M. Asztemborska, M. Jakubiak, R. Stęborowski, E. Chajduk, G. Bystrzejewska-Piotrowska, Titanium dioxide nanoparticle circulation in an aquatic ecosystem, Water. Air. Soil Pollut. 229 (2018) 1-9. https://doi.org/10.1007/s11270-018-3852-8.
[16] H. Y. Lu, Y. J. Wang, W. C. Hou, Bioaccumulation and depuration of TiO_2 nanoparticles by zebrafish through dietary exposure: Size- and number concentration-resolved analysis using single-particle ICP-MS, J. Hazard. Mater. 426 (2022) 127801. https://doi.org/10.1016/j.jhazmat.2021.127801.
[17] M. Connolly, D. Hernández-Moreno, E. Conde, A. Garnica, J. M. Navas, F. Torrent, I. Rucandio, M. L. Fernandez-Cruz, Influence of citrate and PEG coatings on the bioaccumulation of TiO_2 and CeO_2 nanoparticles following dietary exposure in rainbow trout, Environ. Sci. Eur. 34 (2022) 1–17. https://doi.org/10.1186/s12302-021-00581-0.
[18] G. Federici, B. J. Shaw, R. D. Handy, Toxicity of titanium dioxide nanoparticles to rainbow trout (*Oncorhynchus mykiss*): Gill injury, oxidative stress, and other physiological effects, Aquat. Toxicol. 84 (2007) 415–430. https://doi.org/10.1016/j.aquatox.2007.07.009.
[19] B. D. Johnston, T. M. Scown, J. Moger, S. A. Cumberland, M. Baalousha, K. Linge, R. van Aerle, K. Jarvis, J. R. Lead, C. R. Tyler, Bioavailability of nanoscale metal oxides TiO_2, CeO_2, and ZnO to fish, Environ. Sci. Technol. 44 (2010) 1144–1151. https://doi.org/10.1021/es901971a.
[20] X. Zhang, H. Sun, Z. Zhang, Q. Niu, Y. Chen, J. C. Crittenden, Enhanced bioaccumulation of cadmium in carp in the presence of titanium dioxide nanoparticles, Chemosphere 67 (2007) 160–166. https://doi.org/10.1016/j.chemosphere.2006.09.003.
[21] J. Roma, A. R. Matos, C. Vinagre, B. Duarte, Engineered metal nanoparticles in the marine environment: A review of the effects on marine fauna, Mar. Environ. Res. 161 (2020) 105110. https://doi.org/10.1016/j.marenvres.2020.105110.
[22] T. L. Rocha, T. Gomes, V. S. Sousa, N. C. Mestre, M. J. Bebianno, Ecotoxicological impact of engineered nanomaterials in bivalve molluscs: An overview, Mar. Environ. Res. 111 (2015) 74–88. https://doi.org/10.1016/j.marenvres.2015.06.013.
[23] D. Minetto, G. Libralato, A. Volpi Ghirardini, Ecotoxicity of engineered TiO_2 nanoparticles to saltwater organisms: An overview, Environ. Int. 66 (2014) 18–27. https://doi.org/10.1016/j.envint.2014.01.012.
[24] L. Canesi, R. Fabbri, G. Gallo, D. Vallotto, A. Marcomini, G. Pojana, Biomarkers in *Mytilus galloprovincialis* exposed to suspensions of selected nanoparticles (nano carbon black, C60 fullerene, nano-TiO_2, nano-SiO_2), Aquat. Toxicol. 100 (2010) 168–177. https://doi.org/10.1016/j.aquatox.2010.04.009.
[25] L. Canesi, C. Ciacci, D. Vallotto, G. Gallo, A. Marcomini, G. Pojana, *In vitro* effects of suspensions of selected nanoparticles (C60 fullerene, TiO_2, SiO_2) on *Mytilus* hemocytes, Aquat. Toxicol. 96 (2010) 151–158. https://doi.org/10.1016/j.aquatox.2009.10.017.
[26] J. J. López-Mayán, B. Álvarez-Fernández, E. Peña-Vázquez, M. C. Barciela-Alonso, A. Moreda-Piñeiro, P. Bermejo-Barrera, Ultrasonication followed by enzymatic hydrolysis as a sample pre-treatment for the determination of Ag nanoparticles in edible seaweed by SP-ICP-MS, Talanta 247 (2022) 123556. https://doi.org/10.1016/j.talanta.2022.123556.

USC DE COMPOSTELA

[27] C. Stephan, K. Neubauer, E. Pruszkowski, New Frontiers in Biomonitoring: Total and single particle analysis of titanium in serum, Application Note (2018) 1–4. Perkin Elmer. https://resources.perkinelmer.com/lab-solutions/resources/docs/app_014338_01_nexion_sp-icp-ms_ti_nps_in_serum.pdf. (accessed February 3, 2023).
[28] M. V. Taboada-López, P. Herbello-Hermelo, R. Domínguez-González, P. Bermejo-Barrera, A. Moreda-Piñeiro, Enzymatic hydrolysis as a sample pre-treatment for titanium dioxide nanoparticles assessment in surimi (crab sticks) by single particle ICP-MS, Talanta 195 (2019) 23–32. https://doi.org/10.1016/j.talanta.2018.11.023.
[29] L. Xu, Z. Wang, J. Zhao, M. Lin, B. Xing, Accumulation of metal-based nanoparticles in marine bivalve mollusks from offshore aquaculture as detected by single particle ICP-MS, Environ. Pollut. 260 (2020) 114043. https://doi.org/10.1016/j.envpol.2020.114043.
[30] ENALIA 2 Survey. National Food Survey on adults, the elderly and pregnant women, https://www.aesan.gob.es/en/AECOSAN/web/seguridad_alimentaria/subdetalle/enalia_2.htm. (accessed February 11, 2023).
[31] D. S. Lim, T. H. Roh, M. K. Kim, Y. C. Kwon, S. M. Choi, S. J. Kwack, K. B. Kim, S. Yoon, H. S. Kim, B. M. Lee, Non-cancer, cancer, and dermal sensitization risk assessment of heavy metals in cosmetics, J. Toxicol. Environ. Health-Part A Curr. Issues. 81 (2018) 432–452. https://doi.org/10.1080/15287394.2018.1451191.
[32] W. Shi, X. Guan, S. Sun, Y. Han, X. Du, Y. Tang, W. Zhou, G. Liu, Nanoparticles decrease the byssal attachment strength of the thick shell mussel *Mytilus coruscus*, Chemosphere 257 (2020) 127200. https://doi.org/10.1016/j.chemosphere.2020.127200.
[33] F. Laborda, A. C. Gimenez-Ingalaturre, E. Bolea, J. R. Castillo, About detectability and limits of detection in single particle inductively coupled plasma mass spectrometry, Spectrochim. Acta Part B At. Spectrosc. 169 (2020) 105883. https://doi.org/10.1016/j.sab.2020.105883.
[34] M. J. Araújo, M. L. Sousa, E. Fonseca, A. B. Felpeto, J. C. Martins, M. Vázquez, N. Mallo, L. Rodriguez-Lorenzo, M. Quarato, I. Pinheiro, M. V. Turkina, J. J. López-Mayán, E. Peña-Vázquez, M. C. Barciela-Alonso, M. Spuch-Calvar, M. Oliveira, P. Bermejo-Barrera, S. Cabaleiro, B. Espiña, V. Vasconcelos, A. Campos, Proteomics reveals multiple effects of titanium dioxide and silver nanoparticles in the metabolism of turbot, *Scophthalmus maximus*, Chemosphere 308 (2022) 136110. https://doi.org/10.1016/j.chemosphere.2022.136110.

USC
UNIVERSIDADE DE SANTIAGO DE COMPOSTELA

CHAPTER 7. PRESENCE OF SILVER AND TITANIUM DIOXIDE NANOPARTICLES IN MARINE SAMPLES FROM THE ATLANTIC AREA

USC
UNIVERSIDADE DE SANTIAGO DE COMPOSTELA

USC
UNIVERSIDADE
DE SANTIAGO
DE COMPOSTELA

CHAPTER 7. PRESENCE OF SILVER AND TITANIUM DIOXIDE NANOPARTICLES IN MARINE SAMPLES FROM THE ATLANTIC AREA

7.1 ABSTRACT

The extensive use of silver nanoparticles (AgNPs) and titanium dioxide nanoparticles (TiO_2NPs), their possible toxicity in the environment and biota, and their advance through the trophic chain make it necessary to shed light on their presence in several aquatic organisms widely consumed in the Atlantic region to preserve food safety. This research work reports the concentrations of AgNPs and TiO_2NPs in photosynthetic organisms such as edible seaweed (*Alaria esculenta*), bivalve mollusks as mussels (*Mytilus edulis*), and predatory fishes (*Salmo*, *Dicentrarchus labrax*, and *Sparus aurata*). Seaweed, mussels, and dissected fishes were submitted to microwave-assisted acid digestions before inductively coupled plasma mass spectrometry (ICP-MS) to determine the total content of Ag and Ti; whereas, AgNPs and TiO_2NPs content and size distributions were determined after enzymatic and alkaline extractions, by SP-ICP-MS analysis. Pancreatin and lipase were used to extract the NPs from fish and mussels, while Macerozyme® R-10 and tetramethyl ammonium hydroxide were employed for the respective extraction of AgNPs and TiO_2NPs from seaweed.

The highest Ag concentrations were found in salmon livers, reaching levels of 0.73±0.07 μg g^{-1} w.w. (wet weight) of Ag, and $2.74\times10^{8}\pm7.78\times10^{7}$ AgNPs g^{-1} w.w. However, the highest Ti concentration was found in seaweed. The total Ti concentration reached 8.48±1.69 μg g^{-1} w.w., and the highest concentration of TiO_2NPs achieved was $1.35\times10^{8}\pm8.06\times10^{7}$ TiO_2NPs g^{-1}. The results confirmed the highest accumulation of Ag and Ti in unedible parts of the fishes, but the concentrations found in the analyzed mussels, and especially in seaweed, highlight the need for proper depuration before their consumption.

7.2 INTRODUCTION

According to the Nanotechnology Product Database (StatNano) silver nanoparticles (AgNPs) and titanium dioxide nanoparticles (TiO_2NPs) are two of the most commonly used inorganic nanoparticles due to their properties [1]. The widespread usage of both kinds of particles causes them to be emitted into the environment, particularly into the ocean. There, nanoparticles can change in shape and size as well as in their degree of dissolution and aggregation, that may be aided by the presence of other environmental pollutants, pH fluctuations, and organic matter [2,3], increasing or reducing their toxicity [4]. Additionally, their size, shape, specific surface area, and potential coating have an impact on all these modifications [5].

Although it is well known that NPs have variable concentrations in different parts of the earth, a low concentration in water (up to μg L^{-1}) is the prevailing pattern [6]. Thus, NPs present in the environment can interact with marine life, be ingested, and preconcentrated through the trophic chain [7,8]. Primary producers are vulnerable to water-borne exposure while higher organisms are affected by both water-borne and diet-borne exposure [9]; then, studies are necessary to elucidate the possible accumulation and toxic effects in marine organisms.

Some reports were found about the presence, bioaccumulation, and possible effects of TiO_2NPs in different fish species. Most of the studies found were about TiO_2NPs in zebrafish (*Danio rerio*) as a highly representative freshwater species. López-Serrano et al. [10] reported

USC DE COMPOSTELA

bioconcentration factors (BCFs) lower than 100, classifying ionic Ti and TiO_2NPs as non-bioaccumulative substances for zebrafish eleutheroembryos after 48 or 72 h of exposure to 0.1 and 1.0 mg L^{-1} of ionic Ti and 2.0 and 10.0 mg L^{-1} of TiO_2NPs. Lu et al. [11] studied the bioaccumulation of TiO_2NPs in zebrafish through dietary exposure for 16 days and a depuration phase of 28 days. SP-ICP-MS results showed TiO_2NPs bioaccumulation until the end of the exposure reaching $3.00\times10^{11}\pm0.36\times10^{11}$ TiO_2NPs Kg^{-1} w.w., and Ti levels decreased until control levels after four days of depuration. De Silva et al. [12] also reported the genotoxicity and histological lesions in Nile tilapia (*Oreochromis niloticus*) induced by TiO_2NPs. The comet assay revealed that TiO_2NPs induced DNA damage, and produced histological alterations in the liver and intestine. The influence of the TiO_2NPs coating was also evaluated. Connolly et al. [13] studied the influence of citrate and PEG coating in the bioaccumulation of TiO_2NPs dietary exposure in rainbow trout (*Oncorhynchus mykiss*). The exposure to 100 mg TiO_2NPs Kg^{-1} (un-coated, citrate-coated, and PEG-coated) for 10 days induced higher uptake of TiO_2NPs in the liver, gills, stomach, intestine, and carcass of the coated-NPs. Ramsden et al. [14] assessed Ti levels above natural background levels in the gill, gut, liver, brain, and spleen of rainbow trout after 8 weeks of exposure to TiO_2NPs (uncoated, 25 nm, 10 and 100 mg TiO_2 NPs kg^{-1} feed) and 2 weeks of depuration. TiO_2NPs did not affect the growth, the nutritional yield, and the hematocrit, but Ti was accumulated in the gills, intestine, liver, spleen, and brain. Furthermore, the element was not removed from the brain after exposure and suffered biochemical disturbances [14]. Although most of the species examined are freshwater fish, studies on saltwater fish are beginning to be carried out. Wang et al. [15] reported the trophic transfer and accumulation of TiO_2NPs from clamworm (*Perinereis aibuhitensis*) to juvenile turbot (*Scophthalmus maximus*). Juvenile turbot's gill, intestine, and stomach showed the highest levels of TiO_2NPs, followed by skin, liver, and muscle, for both dietary and waterborne exposure.

Regarding Ti presence in mollusks, some reports studied the effects and toxicity of TiO_2NPs in mussels (*Mytilus galloprovincialis*) [16,17] and clams (*Ruditapes philippinarum*) [18]. Taboada-López et al. [19] determined total Ti and TiO_2NPs by ICP-MS and SP-ICP-MS, respectively in clams, cockles, mussels, razor clams, and variegated scallops with TiO_2NPs concentrations between 2.36×10^{7}-1.25×10^{8} NPs g^{-1}. Moreover, Siddique et al. [20] studied heavy metals and metalloids in six different seaweed from Bangladesh. The highest Ti concentration, found in the ICP-MS analysis, was 736.62 mg kg^{-1} in sea lettuce (*Ulva intestinalis*). Besides, Corrias et al. [21] also studied heavy metals and metalloids including Ti in seaweed (*Padina pavonica*, and *Cystoseira mediterranea*) from the Sardinia coastal zones using ICP-OES, reporting Ti concentrations in the seaweed of 4.41 µg g^{-1}. López-Mayán et al. [22] studied TiO_2NPs background in different seaweed (*Ulva rigida*, *Sargassum bacciferum*, and *Palmaria palmata*) from the Galician (Northwest of Spain) and Irish coasts using SP-ICP-MS. The background TiO_2NPs levels found in seaweed were between 1.68×10^{6}-1.76×10^{7} NPs g^{-1}.

Regarding AgNPs determination in fish matrices, some reports were found. Bioaccumulation studies of AgNPs were found in freshwater fish (zebrafish) [23,24]. Xiao et al. [23] assessed the BCF factors in zebrafish exposed to PVP-AgNPs for 7 days, and they reported a decrease in the BCF factors in the presence of humic and fulvic acids. AgNPs trophic transfer was also evaluated by some authors [25,26]. Lekamge et al. [9] studied the toxicity and trophic transfer of different coated AgNPs from *Raphidocelis subcapitata* to *Daphnia carinata*. Daphnid feeding rates were significantly reduced by NP-contaminated algae, and the bioaccumulation in algae and daphnids depended on the AgNPs coating. Zhao and Wang [27] also demonstrated that AgNPs were more difficult to depurate when they were ingested through

dietary intake than after water-borne exposure in daphnids. AgNPs effects were also evaluated in seawater fish. Araújo et al. [28] studied the multiple effects of AgNPs in the metabolism of turbot (*Scophthalmus maximus*), where they induced histological and proteomic alterations in liver. Furthermore, some reports were found about the presence, genotoxicity, and sublethal effects of AgNPs in mussels [29,30]. Taboada-López et al. [31] reported the AgNPs concentrations found in different kinds of mollusks using SP-ICP-MS, where the highest AgNPs concentration were found in variegated scallops. Finally, AgNPs' hazardous effects were also evaluated in primary producers like seaweed. Sfriso et al. [32] reported biochemical and physiological biomarkers in *Ulva rigida*, where lipid peroxidation was found in seaweed exposed to AgNPs. Silver bioaccumulation, altered chloroplast, inhibition of primary production and lipid peroxidation were assessed in the seaweed after 24 h of exposure [32].

To the best of our knowledge, although some reports exist about bioaccumulation, distribution, and possible toxicity and effects of TiO_2NPs and AgNPs in different aquatic specimens, no reports were found in the case of studying the presence of both particles in samples from the Atlantic area. Thus, the main goal of this research work is to study the presence of TiO_2NPs and AgNPs in different aquatic species from this region. The selected species include mussels as benthic seawater-filter organisms, and seaweed as an aquatic plant, due to their ability to preconcentrate possible toxic substances and be an important link in the food chain. Furthermore, common fishes consumed around the Atlantic area were also studied; one euryhaline and two stenohaline species were selected. Then, this research tries to elucidate and shed light on the total Ag and Ti presence and AgNPs and TiO_2NPs content. To perform the analysis, inductively coupled plasma mass spectrometry (ICP-MS) and single-particle-ICP-MS (SP-ICP-MS) were used as the main determination techniques in this research work.

7.3 MATERIALS AND METHODS

7.3.1 Instrumentation

The main equipment for Ag and Ti determination is a quadrupole-ICP-MS spectrometer NexION® 2000 from Perkin Elmer (Waltham, MA, USA). The spectrometer is equipped with a collision cell (KED) to reduce the polyatomic interferences using He, and with a reaction cell (DRC) to create stable adducts introducing ammonia as a reaction gas. The Syngistix™ Nano Application 2.5 software (Perkin Elmer) allows working in single-particle-ICP-MS (SP-ICP-MS) mode, for determining Ag and Ti dioxide nanoparticles content, and size distributions. An Ethos Plus microwave oven from Milestone (Bergamo, Italy) was used to digest the aquaculture samples. The microwave is equipped with ten Teflon vessels of 100 mL and a pressure and temperature control system. An ultrasound bath from VWR (Barcelona, Spain), a Boxcult incubation temperature-controlled incubation chamber from Stuart Scientific (Surrey, UK), equipped with a Rotabit orbital-rocking platform shaker from J.P. Selecta (Barcelona, Spain), and an ultrasound probe VibraCell VCX 130 from Sonics (Newtown, CT, USA) were needed to perform the alkaline and enzymatic extractions. Other small instrumentation used in this work includes a pH meter from VWR (Barcelona, Spain), a vortex vibrational shaker from Heidolph (Schwabach, Germany), and an analytical balance ML204 from Mettler Toledo (Barcelona, Spain).

7.3.2 Reagents, standards, and materials

The reagents employed in microwave-assisted acid digestion include 69% (w/v) nitric acid Suprapur® from Sigma Aldrich, (Darmstadt, Germany), 33% (w/v) hydrogen peroxide from ACS, ISO, AppliChem Panreac (Barcelona, Spain), and ultrapure water (18 MΩ cm of

USC UNIVERSIDADE DE COMPOSTELA

resistivity), obtained from a Milli-Q® IQ7003 from Millipore Co. (Bedford, MA, USA). The alkaline extractions were performed with a 25% (v/v) tetramethylammonium hydroxide (TMAH) solution in water from Merck (Darmstadt Germany). The enzymatic extractions were carried out with lipase (from Candida rugose) and porcine pancreatin solution, both from Sigma Aldrich. The enzymatic solution was prepared in a physiological pH buffer of NaOH and $NaH_2PO_4 \cdot H_2O$ both from Merck (Darmstadt, Germany). A solution of 1% (v/v) glycerol from Merck was employed for the dilution of NPs extractions.

The ICP-MS spectrometer uses Ar, He, and NH_3 as nebulization, collision and reaction gases, respectively. All gases have a purity of 99,999% and they were from Nippon Gases (Madrid, Spain). A NexION Setup Solution of 1.0 µg L^{-1} of Be, Ce, Fe, In, Li, Mg, Pb, and U in 1% of HNO_3 from PerkinElmer (Norwalk, CT, USA) is needed for the initial check of ICP-MS. A reference material of PEG-COOH Gold Nanospheres suspension of 49.6 nm of 9.89×10^6 particles mL^{-1} from NanoComposix (San Diego, CA, USA) in aqueous 1 mM citrate, and Au ionic standard of 1000 mg L^{-1} in 2 mol L^{-1} HCl from Merck (Darmstadt, Germany) are needed to obtain the transport efficiency (TE) in SP-ICP-MS. A Ti ionic standard of 1000 mg L^{-1} H_2O/0.24% F^- and ionic Ag stock solution of 1000 mg L^{-1} in 2% HNO_3 both from Perkin Elmer (Shelton, CT, USA), were employed to perform the ionic Ti and Ag calibrations. A Rh stock solution of 1000 mg L^{-1} in 2% HCl from Perkin Elmer (Shelton, CT, USA) was also employed as an internal standard.

Ceramic precision blades and Teflon boards were used for the dissection of the aquaculture samples. Other materials employed include Minisart NML hydrophilic non-sterile 5.0 µm filter disks of regenerated cellulose from Sartorius (Goettingen, Germany), and some disposable plastic materials like syringes, tubes, and micropipette tips.

7.3.3 Sampling and sample pretreatment

To study the background levels of AgNPs and TiO_2NPs in the Atlantic region, a sampling of species that are widely consumed by the European population and possible targets of this type of contamination was carried out. For this investigation, three different kinds of samples were selected from different countries; three different fish species, one mollusk species, and one seaweed species. Every single sample was taken in the Atlantic region, normally close to industrial areas. All the samples collected are wild species.

The fish species included salmon (*Salmo*), sea bass (*Dicentrarchus labrax*), and sea bream (*Sparus aurata*). These were sampled in the Northwest of France, close to the English Channel. Three specimens of sea bass and sea bream were collected, as well as three female and three male salmon. The mollusks selected were mussels (*Mytilus edulis*), and they were from Northern Ireland in the United Kingdom. Mussels were collected from four different estuaries in the Irish Sea (A, B, C, and D), and five samples from each sampling zone were collected at different points (1-5). The seaweed sampled was badderlocks (*Alaria esculenta*) a traditional food along the coasts of the far north Atlantic Ocean in countries like Ireland, Scotland, Iceland, and Greenland. They were taken from Southern Ireland in three different estuaries (E, F, and G), and five samples of each sampling zone were collected at different points (1-5).

Once sampled, fish were euthanized using iced water; the scales were removed and the fish specimens were dissected into liver, kidney, and flesh with skin. In the case of salmons, the female gonads were also separated, but the kidneys were impossible to dissect due to their liquid consistency. After removing the shells, the mussels were cleaned with ultrapure water. In the case of the sampled seaweed, they were cleaned with ultrapure water. Finally, all the wet samples were triturated and homogenized manually with ceramic precision blades and stored at -18 ºC until use.

USC DE COMPOSTELA

7.3.4 Total Ag and Ti determination

Before the ICP-MS analysis to determine the total Ag and Ti content, microwave-assisted acid digestion was employed to digest the samples using the microwave oven described in **section 7.3.1**. A mass of 1.0000 g of wet and homogenized sample was mixed with nitric acid, hydrogen peroxide, and ultrapure water to digest the samples, applying the microwave program previously described by López-Mayán et al. [33]. Two blanks for the digestion set and three replicates per sample were digested when the amount of sample was enough. The digested samples were diluted 10 to 25 times with ultrapure water before ICP-MS analysis. The standard addition calibration method was used for both analytes to avoid matrix effects. Ag calibrations were between 0 and 10.0 µg L^{-1} using 5.0 µg L^{-1} of ^{103}Rh as an internal standard, and the KED mode (4,5 mL min^{-1} of He) to avoid polyatomic interferences. On the other hand, Ti calibrations were between 0 and 15.0 µg L^{-1} using the dynamic reaction cell (DRC) mode (1.0 mL min^{-1} of NH_3) forming the Ti-NH_3 cluster [$^{48}Ti^{14}N^{1}H(^{14}N^{1}H_3)_4^+$] of *m/z* 131 to reduce the main interference (^{48}Ca) present in aquaculture samples. **Table S.7.1.(a)** (supplementary information) shows the operational conditions of ICP-MS.

7.3.5. Determination of AgNPs and TiO_2NPs

TiO_2NPs and AgNPs determination in the samples was carried out by single-particle-ICP-MS (SP-ICP-MS). Mild conditions for nanoparticle extractions without dissolving, and modifying the nanoparticle size were necessary before SP-ICP-MS determination. Suitable NPs extractions were selected based on the fish matrix and the type of nanoparticle to be determined. Enzymatic extractions were selected in the case of fish (salmon, sea bass, and sea bream) and mussels. The enzymes selected were the pancreatin/lipase mixture, to solubilize these kinds of matrix. The enzymatic extraction methodologies were previously optimized and validated by our research group. Taboada-López et al. [31,34] optimized AgNPs and TiO_2NPs extraction using pancreatin/lipase mixtures. For these treatments, a mass of 1.0000 g of homogenized fish and mollusk samples was added to 7.5 mL of 8.0: 8.0 g L^{-1} or 3.0: 3.0 g L^{-1} of pancreatin/lipase solution prepared in 0.2M NaH_2PO_4/0.2M NaOH (pH=7.4) buffer, for TiO_2NPs or AgNPs separation, respectively. The samples were incubated overnight at 37º C and 200 or 150 rpm for TiO_2NPs or AgNPs extraction, respectively. Finally, the extracts were filtered with filter disks (5 µm), diluted several times with 1% (v/v) of glycerol, and analyzed by SP-ICP-MS.

In the case of seaweed, due to its different composition, AgNPs extractions were performed using a mixture of enzymes capable of breaking down the cell wall. On the other hand, the TiO_2NPs extractions from seaweed were performed using alkaline media. Both methodologies were validated and optimized previously in our research group. López-Mayán et al. [22,33] developed the TiO_2NPs alkaline extraction procedure using tetramethylammonium hydroxide (TMAH) and developed the AgNPs enzymatic extraction procedure using a mixture of cellulase, hemicellulose, and pectinase (Macerozyme® R-10 solution). For alkaline extractions, a mass of 1.0000 g of homogenized and crushed seaweed was mixed with 7.5 mL of 2.5% (v/v) of TMAH and submitted to sonication in an ultrasonic bath for 2 hours. Then, the extracts were filtered with the filter disk, diluted several times with 1% (v/v) of glycerol, and analyzed by SP-ICP-MS. For the enzymatic extraction from seaweed, 0.0500 g of seaweed was mixed with 7 mL of 2 mM citric acid/ 2 mM trisodium citrate buffer (pH=4.5). The mixture was sonicated with an ultrasound probe for 2.5 min using 20% of amplitude and pulses (1 s on and 1 s off). Then, the mixture was mixed with 2 mL of 25 g L^{-1} of Macerozyme® R-10 solution and incubated for 6 hours in an agitating chamber at 37º C and 150 rpm. The obtained extracts were filtered with 5 µm filter disks, diluted several times with 1% (v/v) of glycerol, and analyzed by

USC DE COMPOSTELA

SP-ICP-MS. Three extraction replicates and two blanks per set of extraction day were performed.

Finally, the NPs content and size distribution were determined by SP-ICP-MS, using the conditions listed in **Table S.7.1.(b)**. The transport efficiency of SP-ICP-MS (varying between 8 and 12%) is determined by the software measuring the ionic Au external calibrations between 0 and 3.0 μg L^{-1} and the reference material of AuNPs with a concentration of 9.89×10^4 particles mL^{-1} when the flow rate is between 0.18-0.22 mL min^{-1}. External calibrations were carried out in SP-ICP-MS due to the absence of matrix effects for the high dilution of enzymatic and basic extracts (from 500 to 2000 times). Ag and Ti calibrations were performed between 0 and 5.0 μg L^{-1}, and between 0 and 10.0 μg L^{-1}, respectively.

7.4 RESULTS AND DISCUSSION

7.4.1 Analytical features of the methodologies

The analytical features of the methodologies were evaluated for total Ag and Ti determination in all the studied species. The standard addition calibration was used to avoid the matrix effects of the fish matrices guaranteeing linearity with correlation coefficients of 0.999. For total Ag and Ti determination, the LOD and LOQs were calculated using the 3σ/m and 10σ/m criteria (where σ is the standard deviation of ten blank measurements, and m is the slope of the standard addition calibration), respectively. **Table S.7.2.** shows the LOD and LOQs for Ag and Ti in fish and seaweed referred to 1.0000 g of sample and 0.7500 g of mussel sample. Due to the lack of reference materials in fish matrices, the accuracy was evaluated through the analytical recovery. **Table S.7.3.** shows the analytical recovery percentages for all the matrices at a low level and a medium-high level of Ag and Ti. The analytical recoveries were in the range of 100±20% for all the methodologies. The precision was also validated through the repeatability in the ICP-MS measurements for all the kinds of matrices and both analytes, obtaining coefficient variations lower than 8% (n=5). In SP-ICP-MS, the instrumental and referred to sample limits of detection were calculated using Laborda et al. [35] criteria. **Table S.7.4.** shows the LOD_{number} and LOD_{sizes} for the specimens studied.

7.4.2 Applications

7.4.2.1 Total Ag determination

Total Ag concentrations were determined in all the samples using the methodology described in **section 7.3.4.**

Figure 7.1. shows the Ag concentrations measured in the different fish matrices analyzed (salmon, sea bass, and sea bream). **Figure 7.1.(a)** shows total Ag concentrations in flesh+skin and gonads of the dissected salmons. Silver was detected in the flesh+skin of all the specimens, reaching a maximum concentration of 0.015±0.0005 μg g^{-1} w.w. (wet weight). The highest Ag concentration found in the female salmons gonads was 0.005±0.001 μg g^{-1} w.w. To compare Ag concentrations present in the flesh of salmon and the gonads of female salmons the statistic software Statgraphics Centurion XVIII was employed. One-way ANOVA tests were used to compare the Ag concentration of the flesh and the gonads in the different specimens. In the case of the gonads, the P-value was higher than 0.05, and then the Ag concentration in the three gonads was statistically equal at a 95% of confidence level. However, in the case of flesh, statistical differences were found between the Ag concentration in the different flesh salmon specimens (P-value<0.05). **Figure 7.1.(b)** also shows the total Ag content of dissected salmons of **Figure 7.1.(a)** but includes the total Ag concentration in the

USC DE COMPOSTELA

salmon liver. The highest Ag concentrations in salmons were found in the liver, reaching 0.73±0.07 μg g^{-1} w.w. The one-way ANOVA test in the case of the liver showed P-values higher than 0.05, and then the liver concentrations in different specimens were statistically equal at a 95% of confidence level.

Regarding sea bass and sea bream, total Ag in flesh+skin, and kidney were in both species lower than LOD. **Figure 7.1.(c)** and **Figure 7.1.(d)** show total Ag concentration in sea bass and sea bream livers, respectively. Ag was found only in the livers, reaching a concentration of 0.37±0.01 and 0.16±0.09 μg g^{-1} w.w. for sea bass and sea bream, respectively. Ag concentrations in the different sea bass and sea bream specimens were statistically equal (P-values>0.05). **Table S.7.5.** shows the average Ag concentration in the tissues of the three fish species tested.

USC
UNIVERSIDADE DE SANTIAGO DE COMPOSTELA

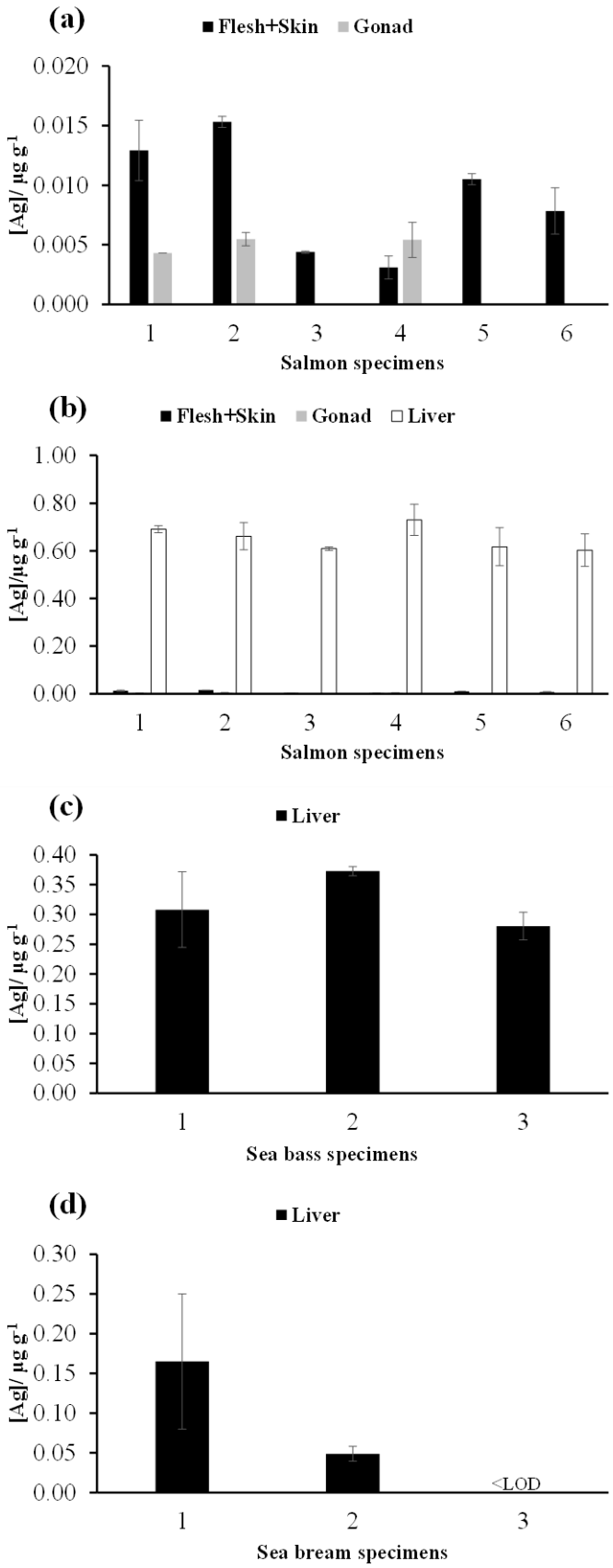

Figure 7.1. Total Ag concentration in (a) salmon flesh+skin and gonads, (b) flesh+skin, gonads, and liver, (c) sea bass liver, (d) sea bream liver.

USC UNIVERSIDADE DE SANTIAGO DE COMPOSTELA

Silver concentrations were also determined in mussel samples. **Figure 7.2.(a)** shows the total Ag concentrations in four different sampling zone codes A, B, C, and D, where for each sampling zone, five specimens were sampled. Although Ag was quantified in all the mussels, the average concentrations (three replicates by sample) in each sampling zone were lower than 0.05 μg g^{-1} w.w. of Ag. **Figure 7.2.(b)** shows the summary average Ag concentrations for each specimen from each sampling zone. The highest average Ag concentration was found in zone A, with a value of 0.03±0.01 μg g^{-1} w.w. of Ag, but between 0.01±0.003 and 0.02±0.01 μg g^{-1} w.w in zones B, C, and D. The one-way ANOVA showed P-values>0.05, and then no statistical differences were found between the Ag concentration of mussels from different estuarine zones.

Finally, the Ag concentrations were determined in *Alaria esculenta* from three estuaries (coded E, F, and G). From each sampling zone, Ag concentration was determined by triplicate in the five specimens (except for the E zone, only 4 specimens). **Figure 7.2.(c)** shows Ag concentration in the specimens of *Alaria esculenta* from each sampling zone. Ag was only detected in 3 of 4 seaweed samples in zone E. The highest Ag concentration found in E was 0.08±0.01 μg g^{-1} w.w. The Ag concentration in zone F was detected in all the seaweed specimens reaching 0.09±0.01 μg g^{-1} w.w. However, for zone G, the Ag concentration was under the LOD. **Table S.7.6.** shows the average total Ag concentrations in mussels and seaweed from each sampling zone.

USC
UNIVERSIDADE DE SANTIAGO DE COMPOSTELA

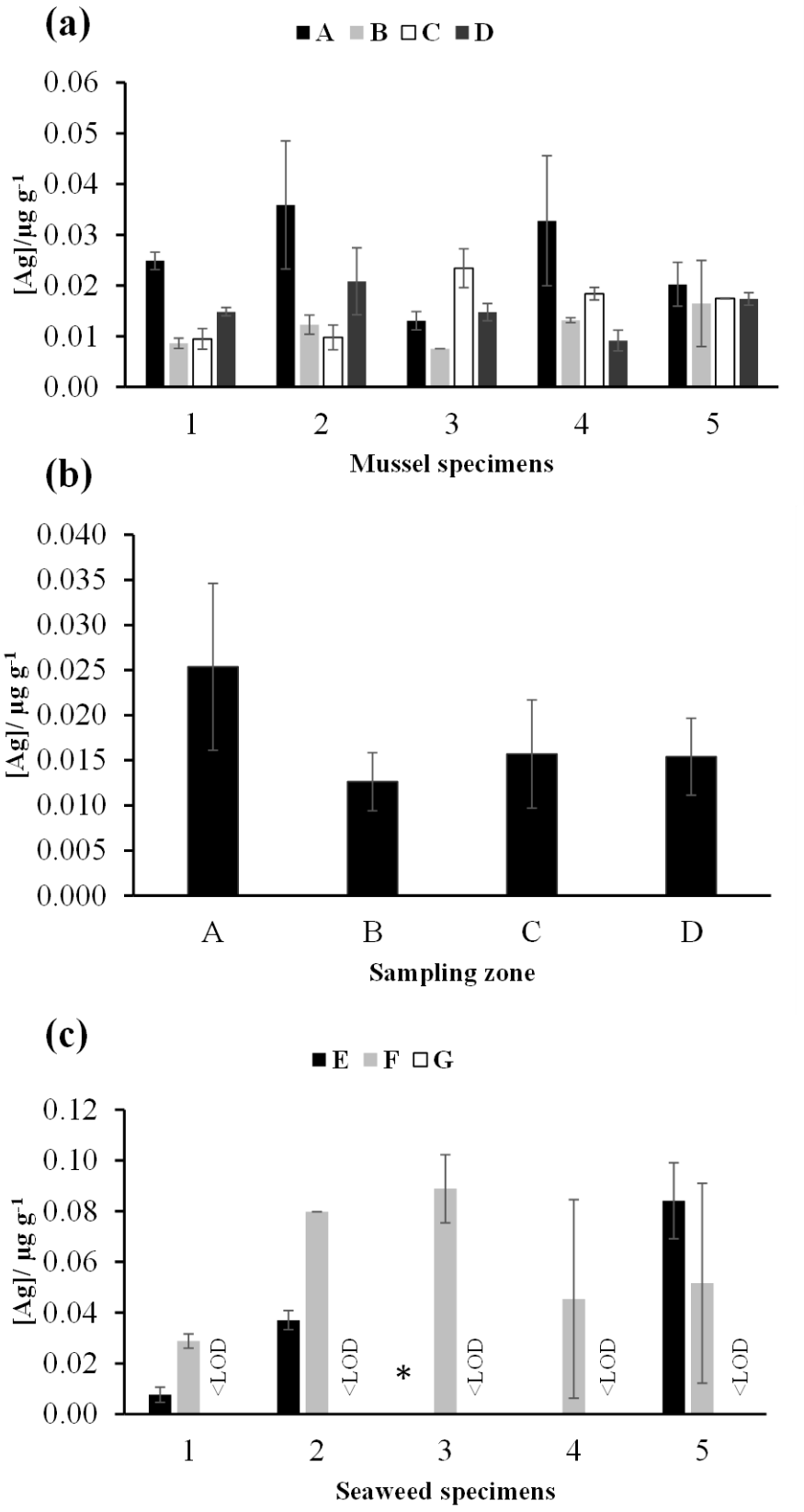

Figure 7. 2. Total Ag concentration in (a) five mussels' specimens of A, B, C, and D sampling zones, (b), mussels in A, B, C, and D sampling zones, (c) five seaweed's specimens in E, F, and G sampling zones. * Indicates "not sampled".

7.4.2.2 Total Ti determination

The total Ti concentrations were also determined in all the samples using the methodology described in **section 7.3.4**.

Figure 7.3. shows Ti concentrations measured in the fish samples (salmon, sea bass, and sea bream). **Figure 7.3.(a)** shows total Ti concentrations in the flesh+skin of the six salmons and the gonads of the three female salmons. The total concentration of Ti in the flesh+skin was low; it was detected in five of six samples, and the concentration varied between 0.02±0.01 and 0.08±0.03 μg g^{-1} w.w. A one-way ANOVA test was applied to compare the Ti concentrations measured in the flesh+skin of different specimens. It showed no statistical differences between Ti concentration (P-value>0.05). In the case of gonads, Ti concentration remained constant in the three specimens with a concentration lower than 0.09 μg g^{-1} w.w. (P-value>0.05). In addition, **Figure 7.3.(b)** shows the information of **Figure 7.3.(a)** plus total Ti in the liver of salmons. The concentration of Ti in the liver was higher than in flesh+skin and gonads, and concentrations were between 0.21±0.01 and 0.34±0.09 μg g^{-1} w.w. The one-way ANOVA test, comparing Ti concentrations reached in the liver of different specimens, showed statistical differences (P-value<0.05).

Furthermore, **Figure 7.3.(c)** and **Figure 7.3.(d)** show the total Ti concentration measured in the flesh+skin, the liver, and the kidney of the three specimens of sea bass and sea bream, respectively. Due to the small size of the sea bass and sea bream specimens, the amount of the kidney sample available in each specimen was very low, then only one digestion replicate could be made in the case of the kidney. The highest Ti concentrations for sea bass flesh+skin, liver, and kidney were 0.56±0.18, 0.64±0.30, and 0.96 μg g^{-1} w.w. of Ti, respectively. On the other hand, the highest Ti concentrations for sea bream flesh, liver, and kidney were 0.34±0.07, 0.46±0.02, and 0.77 μg g^{-1} w.w. of Ti, respectively. Regarding sea bass for the flesh+skin and the liver, no statistical differences were found between the Ti concentration in both tissues of the different specimens (P-value>0.05). Regarding the sea bream the one-way ANOVA tests to compare Ti concentrations in flesh+skin and liver tissues of the specimens were performed. No significant statistical differences were found in the Ti concentration for flesh+skin in the three specimens (P-value>0.05), but statical differences were found for the liver of sea bream (P-value<0.05). **Table S.7.7.** shows the total Ti concentrations measured in the parts of dissected fishes.

USC UNIVERSIDADE DE SANTIAGO DE COMPOSTELA

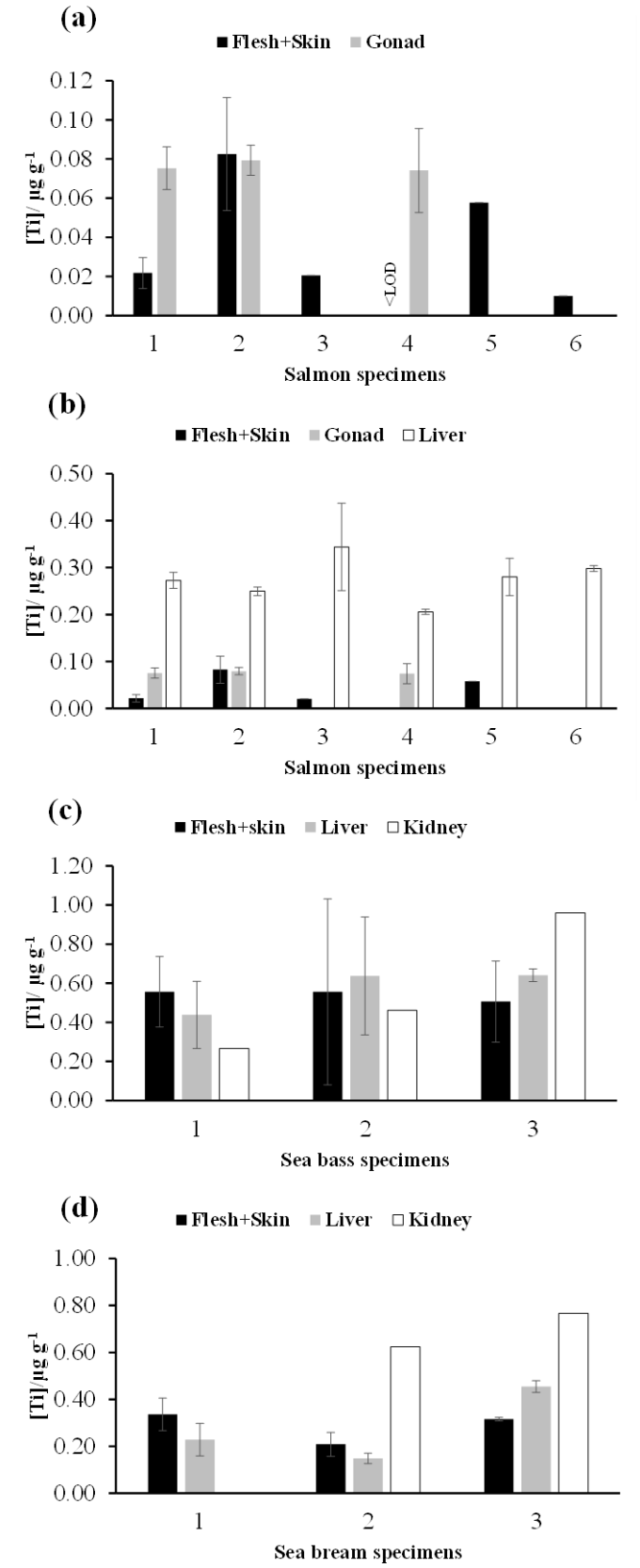

Fig. 7.3. Total Ti concentration in (a) salmon flesh+skin and gonads, (b) salmon flesh+skin, gonads, and liver, (c) sea bass flesh+skin, liver, and kidney, (d) sea bream flesh+skin, liver, and kidney.

USC UNIVERSIDADE DE SANTIAGO DE COMPOSTELA

The total Ti concentrations were also determined in the mussels. **Figure 7.4.(a)** shows the total Ti presence in the five mussels of the sampling zones A, B, C, and D. Only one mussel sample in sampling zone C was below the LOD. Furthermore, **Figure 7.4.(b)** shows the average concentration in five mussels samples of each sampling zone. The highest concentrations were achieved in sampling zone A, reaching 1.73±0.50 μg g^{-1} w.w. of Ti. No statistical differences were found between the total Ti content in mussels from different estuaries (ANOVA P-value>0.05).

Total Ti concentration was determined in seaweed samples. **Figure 7.4.(c)** shows the total Ti in the seaweed sampled in the E, F, and G sampling zones. Five different seaweed were sampled in zone F and G but only four seaweed were sampled in zone E. **Figure 7.4.(d)** shows the average concentrations of seaweed in each sampling zone. The highest Ti concentration was found in seaweed, reaching 8.48±1.69 μg g^{-1} w.w. of Ti. No statistical differences were found between the total Ti content in *Alaria esculenta* from different estuaries (ANOVA P-value>0.05). **Table S.7.8.** shows total Ti concentrations obtained in each mussel and seaweed specimen from the different estuarine zones.

USC UNIVERSIDADE DE SANTIAGO DE COMPOSTELA

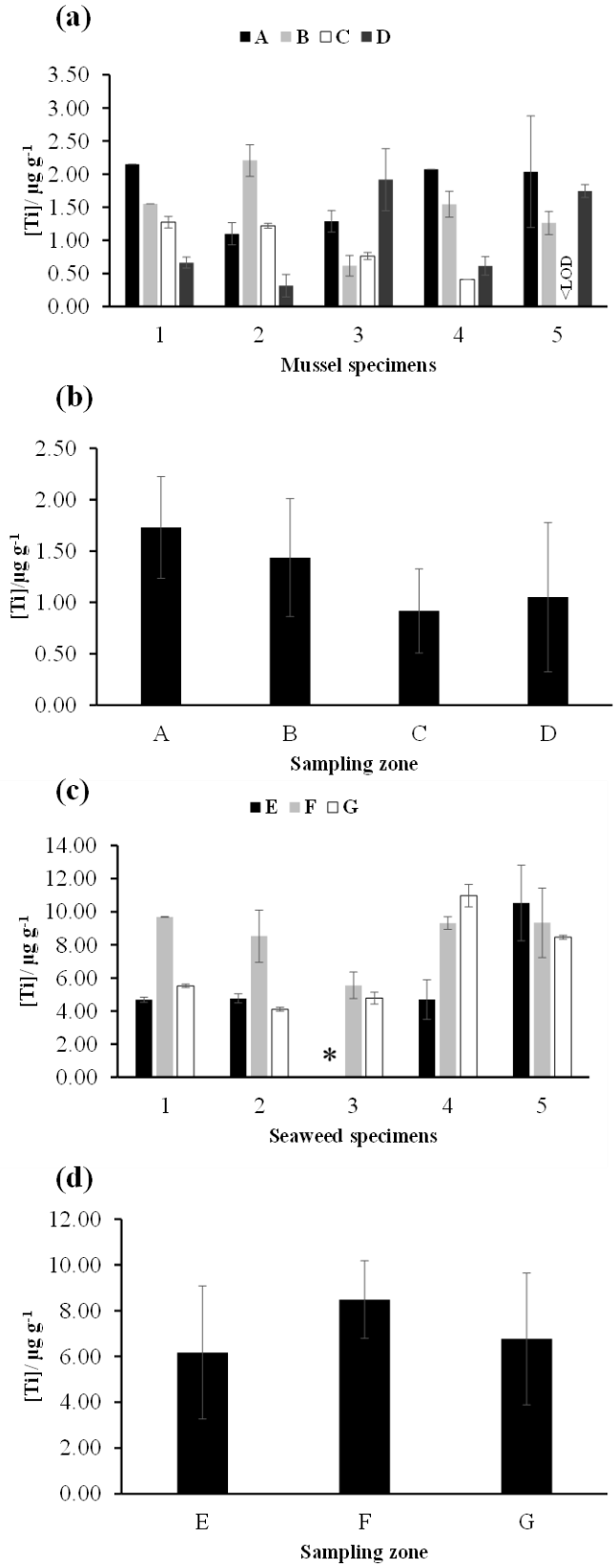

Figure 7.4. Total Ti concentration in (a) five mussels' specimens of A, B, C, and D sampling zones, (b) mussels from A, B, C, and D sampling zone (average concentration), (c) five seaweed's specimens of E, F, and G sampling zones, (d) seaweed of E, F, and G sampling zones (average concentration). * Indicates "not sampled".

USC DE COMPOSTELA

7.4.2.3 AgNPs determination

AgNPs determination was performed using the methodologies described in **section 7.3.5.** AgNPs enzymatic extractions using pancreatin/lipase were employed for the fish tissues. Since the total Ag content was very low in the case of flesh+skin and gonad from salmons, the SP-ICP-MS measurements provided concentrations values lower than the LOD_{number} ($<4.58\times10^{7}$ NPs g^{-1}). However, in the case of salmon liver, AgNPs were determined in five of six samples. **Figure 7.5.(a)** shows the AgNPs content in the liver of salmon samples. These concentrations were between $9.43\times10^{7}\pm1.12\times10^{6}$ AgNPs g^{-1} w.w. and $2.74\times10^{8}\pm7.78\times10^{7}$ AgNPs g^{-1} w.w. Besides, **Figure 7.5.(b)** shows the most frequent and mean sizes for AgNPs in salmon liver; they were between 18±1 nm and 22±2 nm, and between 18±1 nm and 25±2 nm, respectively. **Figure 7.5.(c)** shows a histogram example obtained from one of liver salmon enzymatic extracts. Due to the total Ag being lower than LOD in the case of flesh+skin and kidney of sea bass and sea bream, the enzymatic extractions were only carried out in the liver. However, in all the sea bass and sea bream liver, AgNPs concentrations were below the LOD_{number} ($<6.77\times10^{7}$ NPs g^{-1}).

In the case of mussels, the total Ag content measured was very low (lower than 0.05 μg g^{-1} w.w.), and the pancreatin/lipase extractions were below the LOD ($<6.42\times10^{6}$ NPs g^{-1}). AgNPs determination was carried out using the Macerozyme R-10® mixture to extract nanoparticles from *Alaria esculenta*. The enzymatic extractions were only performed in the sampling zones E and F (where total Ag was detected), but in both cases, the AgNPs concentrations were lower than LOD_{number} ($<4.32\times10^{7}$ NPs g^{-1}).

USC UNIVERSIDADE DE SANTIAGO DE COMPOSTELA

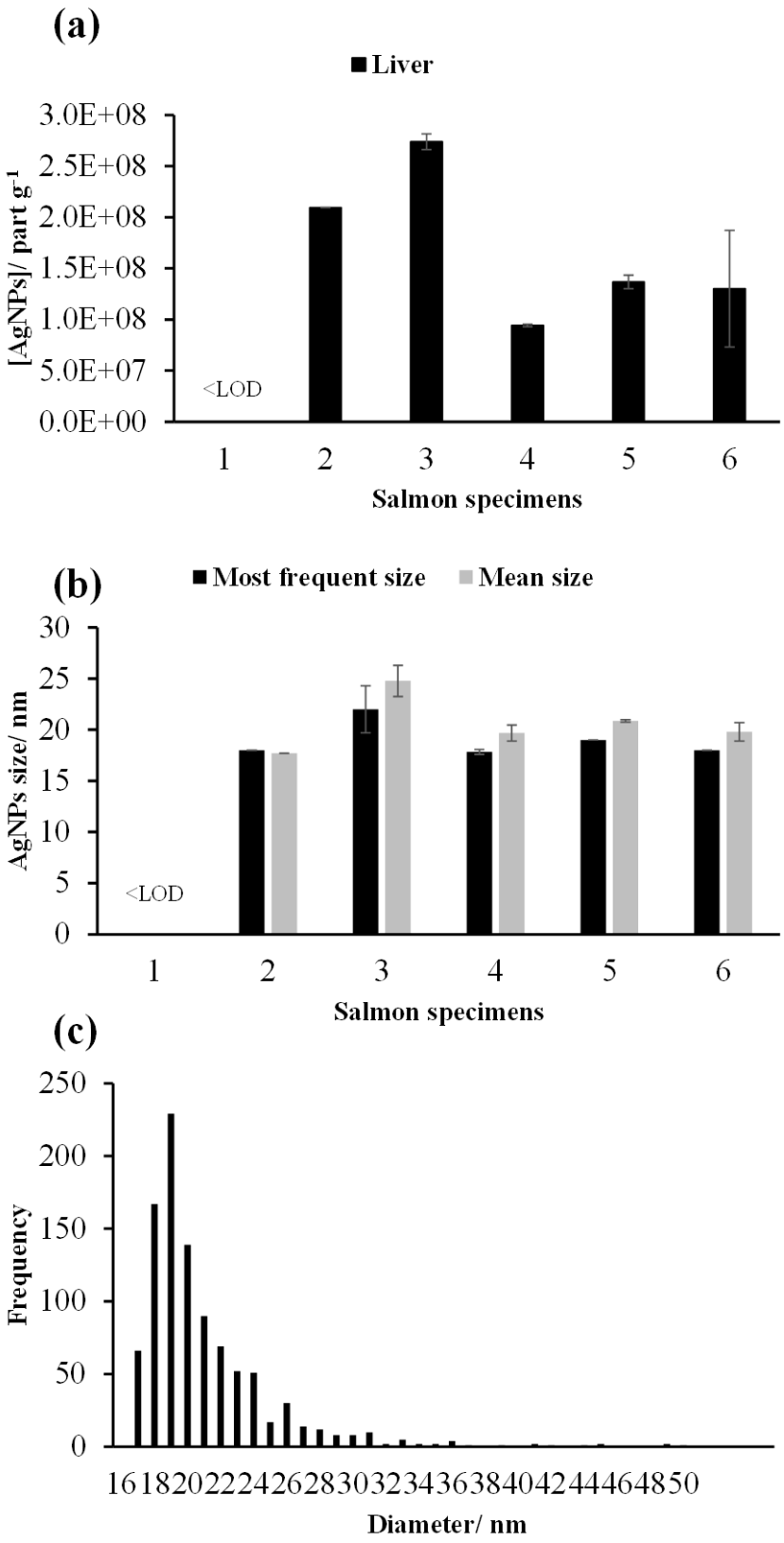

USC UNIVERSIDADE DE SANTIAGO DE COMPOSTELA

Figure 7.5. (a) AgNPs content in six salmon liver samples, (b) most frequent and mean size of AgNPs found in the six salmon liver samples, and (c) AgNPs histogram from a salmon liver.

7.4.2.4 TiO_2NPs determination

TiO_2NPs determination was also performed using the methodologies described in **section 7.3.5.** depending on the type of matrix. The enzymatic extractions using pancreatin/lipase were performed in the case of salmons (flesh+skin, liver, and gonads), sea bass and sea bream (in flesh+skin and liver), and mussels. On the other hand, alkaline extractions were used in the case of seaweed.

In the case of fish, TiO_2NPs were detected only in salmon liver and gonads, being lower than LOD in the case of salmon flesh+skin. **Figure 7.6.** shows TiO_2NPs concentration in the liver (**Figure 7.6.(a)**), in the gonads (**Figure 7.6.(b)**), and the most frequent and mean sizes in the liver (**Figure 7.6.(c)**), and gonads (**Figure 7.6.(d)**). TiO_2NPs concentrations in the liver were between $2.79\times10^7\pm7.50\times10^6$ TiO_2NPs g^{-1} w.w. and $1.98\times10^8\pm1.22\times10^7$ TiO_2NPs g^{-1} w.w. The most frequent and the mean sizes were between 41±6 nm and 79±4 nm, and between 66±15 nm and 122±5 nm, respectively. In the case of gonads, the TiO_2NPs content and the sizes were lower than those for the liver. TiO_2NPs content was between $2.34\times10^7\pm6.23\times10^5$ TiO_2NPs g^{-1} w.w. and $5.11\times10^7\pm5.84\times10^6$ TiO_2NPs g^{-1} w.w. The most frequent and mean sizes were between 35±3 nm and 43±5 nm, and between 60±9 nm and 76±25 nm, respectively.

In the case of sea bass and sea bream, the signals measured corresponded to TiO_2NPs that were below the LOD_{size} (<32 nm) for the flesh+skin and liver (the small amount of kidney had already been used up for digestion). Then, the Ti detected in the sea bass and sea bream is in the ionic form or as TiO_2NPs smaller than 32 nm. Furthermore, in the case of mussels, signals also corresponded to TiO_2NPs below LOD_{size} (<28 nm).

USC UNIVERSIDADE DE SANTIAGO DE COMPOSTELA

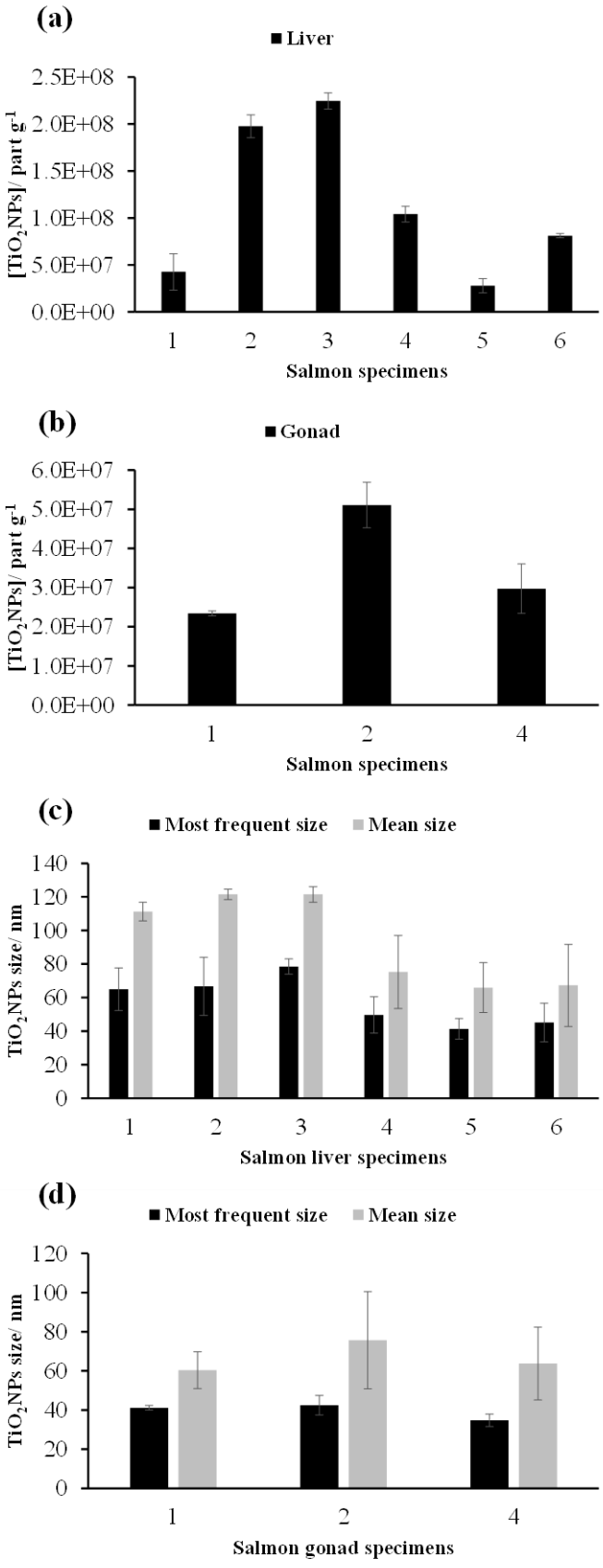

Figure 7.6. TiO_2NPs concentration in (a) salmon livers and (b) salmon gonads; most frequent and mean sizes of TiO_2NPs in (c) salmon livers, and (d) salmon gonads.

Finally, the alkaline extractions using TMAH were used in the case of *Alaria esculenta* in each seaweed sample of the sampling zones E, F, and G. **Figure 7.7.(a)** shows the TiO_2NPs content in sampling zone E, F, and G. In sampling zone E, the TiO_2NPs content was determined in three of four seaweed samples, but in sampling zone F, and G, the TiO_2NPs were detected in all five seaweed samples. The TiO_2NPs content was between $4.64\times10^7\pm1.90\times10^7$ and $7.31\times10^7\pm3.83\times10^7$ TiO_2NPs g^{-1} w.w. for sampling zone E, between $3.75\times10^7\pm2.90\times10^6$ and $9.00\times10^7\pm6.06\times10^7$ TiO_2NPs g^{-1} w.w. for sampling zone F, and between 3.35×10^7 and $1.35\times10^8\pm8.06\times10^7$ TiO_2NPs g^{-1} w.w. for sampling zone G. **Figure 7.7.(b)**, **Figure 7.7.(c)**, and **Figure 7.7.(d)** show the most frequent and mean sizes for the seaweed in sampling zones E, F, and G, respectively. The most frequent and mean sizes were between 63±8 nm and 79±6 nm, and between 121±18 nm and 133±11nm, respectively for sampling zone E. In sampling zone F, the most frequent and mean sizes were between 62±1 nm and 112±25 nm, and between 104±10 and 165±25 nm, respectively. For sampling zone G, the most frequent sizes and mean sizes were between 60±1 nm, and 85±29 nm and between 105±9 and 132±40 nm, respectively.

USC
UNIVERSIDADE DE SANTIAGO DE COMPOSTELA

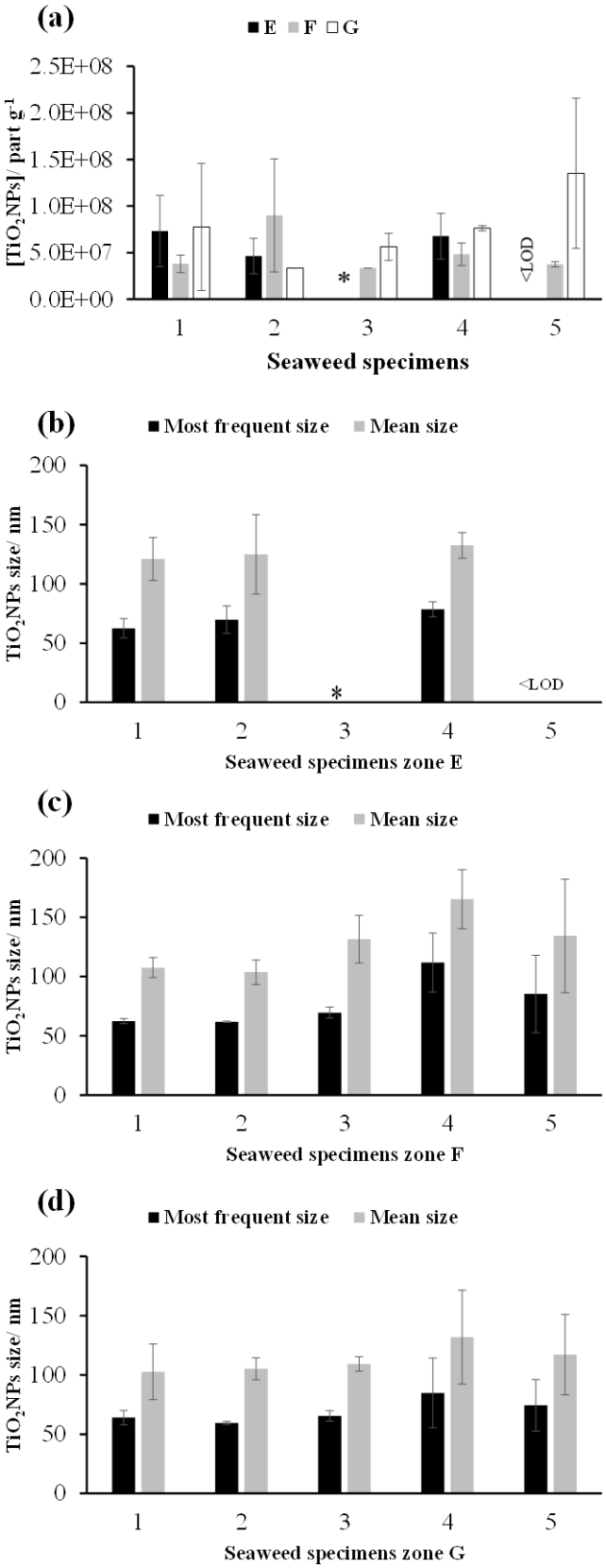

Figure 7.7. TiO_2NPs concentration in (a) seaweed from sampling zones E, F, and G, and most frequent and mean sizes of seaweed from: (b) sampling zone E, (c) sampling zone F and (d) sampling zone G.

USC DE SANTIAGO DE COMPOSTELA

A literature search of basal levels of Ag and Ti as well as AgNPs and TiO_2NPs in different specimens of fish, mussels, and seaweed has been carried out to compare the levels with those obtained in this study. **Table 7.1.** shows the different range of concentrations for Ag, Ti, AgNPs and TiO_2NPs obtained in this study in comparison with the results found in the literature. No studies were found showing basal levels of Ag and Ti in salmon. Grasso et al. [36] studied the levels of Ti in different fishes. Although tuna is similar in size to salmon, they reported higher tissue Ti values than those found in salmon tissue in this study. However, the concentration of TiO_2NPs in salmon and tuna tissue was in the same range. Furthermore, Grasso et al. [36] found higher Ti concentrations in canned Mackerel than reported by our study in the case of sea bass and sea bream flesh. Alasalvar et al. [37] studied the total levels of Ag and Ti in the case of cultured and wild sea bass. The total Ag content in sea bass in the present study was less than 0.05 μg g^{-1}, which is in agreement with the values obtained for wild and cultured sea bass reported by Alasalvar et al. [37] (0.09±0.02 and 0.07±0.01 for cultured and wild sea bass). On the other hand, Alasalvar et al. [37] reported higher Ti concentrations in the flesh+skin of cultured and wild sea bass (2.01±0.08 and 1.59±0.09 μg g^{-1}, respectively) in comparison with the obtained in sea bass flesh in this study (0.56±0.18 μg g^{-1}). However, they reported the concentration in dried weight.

Concerning *Mytilus edulis*, the Ag concentrations measured in this work were very low, ranging from (0.01±0.003 to 0.03±0.01 μg g^{-1}); this result agrees with the content found in *Mytilus galloprovincialis* by Taboada-López et al. [39] which was lower than 0.025 μg g^{-1}. Although Xu et al. [38] reported an Ag concentration in *Mytilus edulis* higher (1.45±0.83 μg g^{-1}) than in this study, the Ti concentration found (1.51±0.21 μg g^{-1}) agreed with the range of concentrations from this study (0.92±0.04 to 1.73±0.50 μg g^{-1}). Furthermore, Taboada-López et al. [19] found a Ti concentration in *Mytilus galloprovincialis* (0.27±0.04 μg g^{-1}) from Galicia (Northwest of Spain) lower than in this study. Despite this, contrary to our study, they detected the TiO_2NPs content ($12.5\times10^7\pm10.6\times10^6$ NPs g^{-1}).

The Ti concentration in seaweed is commonly high. In the case of *Alaria Esculenta* Ti concentration was in the range of 6.77±2.88 to 8.48±1.69 μg g^{-1}. The few research works found in the literature showed higher Ti concentrations in the studied seaweeds. Siddique et al. [20] and Desideri et al. [39] reported wide ranges of variability from 66.45±1.62 to 736.62±4.54 μg g^{-1}, and from 1.7 to 1364 μg g^{-1}, respectively for different kinds of seaweed.

USC UNIVERSIDADE DE SANTIAGO DE COMPOSTELA

Table 7.1. Concentration of total Ag, Ti, AgNPs, and TiO_2NPs in this study in comparison to several studies from the literature.

	Specimen	Total Ag/µg g^{-1}	AgNPs/ part g^{-1}	Total Ti/ µg g^{-1}	TiO_2NPs/ part g^{-1}	Ref
Present study	**Salmon**	**Liver:** 0.60±0.07-0.73±0.07	**Liver:** $9.43\times10^{7}\pm1.12\times10^{6}$- $2.74\times10^{8}\pm7.78\times10^{7}$	**Flesh:** 0.02±0.01-0.08±0.03 **Liver:** 0.21±0.01-0.34±0.09 **Gonad:** 0.07±0.02-0.08±0.01	**Liver:** $2.79\times10^{7}\pm 7.50\times10^{6}$ - $1.98\times10^{8}\pm1.22\times10^{7}$ **Gonad:** $2.34\times10^{7}\pm6.23\times10^{5}$- $5.11\times10^{7}\pm5.84\times10^{6}$	
Grasso et al.	**Canned Tuna**	-	-	1.02±0.12	$9.77\times10^{7}\pm6.27\times10^{7}$	[36]
Grasso et al.	**Canned Mackerel**	-	-	1.15±0.11	$1.47\times10^{7}\pm 7.17\times10^{6}$	[36]
Present study	**Sea bream**	**Liver:** 0.05±0.01-0.16±0.09	<LOD	**Flesh:** 0.34±0.07 **Liver:** 0.46±0.02 **Kidney:**0.77	<LOD	
Present study	**Sea bass**	**Liver:** 0.28±0.02-0.37±0.01	<LOD	**Flesh:** 0.56±0.18 **Liver:** 0.64±0.30 **Kidney:** 0.96	<LOD	
Alasalvar et al.	**Sea bass cultured**	0.09± 0.02*	-	2.01±0.08*	-	[37]
Alasalvar et al.	**Sea bass wild**	0.07± 0.01*	-	1.59±0.09*	-	[37]
Present study	***Mytilus edulis***	0.01±0.0.003-0.03±0.01	-	0.92±0.041-1.73±0.50	<LOD	
Taboada-López et al.	***Mytilus galloprovincialis***			0.27±0.04	$12.5\times10^{7}\pm10.6\times10^{6}$	[19]
Taboada-López et al.	***Mytilus galloprovincialis***	<0.025	-			[31]

USC UNIVERSIDADE DE SANTIAGO DE COMPOSTELA

Table 7.1. Continued

	Specimen	Total Ag/μg g^{-1}	AgNPs/ part g^{-1}	Total Ti/ μg g^{-1}	TiO_2NPs/ part g^{-1}	Ref
Xu et al.	***Mytilus edulis***	1.45±0.83	$2.94\times10^{7}\pm 0.32\times10^{7}$	1.51±0.21	$2.36\times10^{7}\pm0.57\times10^{7}$	[38]
Present study	***Alaria esculenta***	0.008±0.003-0.09±0.01	<LOD	6.77±2.88-8.48±1.69	$3.79\times10^{7}\pm9.29\times10^{6}$-$1.35\times10^{8}\pm8.06\times10^{7}$	
Siddique et al.	**Different kinds of seaweed**	-	-	66.45±1.62-736.62±4.54	-	[20]
Desideri et al.	**Different kinds of seaweed**	-	-	1.7-1364	-	[39]

- Indicates “not determined” * Indicates “dried weight”

7.5 CONCLUSIONS

This research work sheds light on the current status of Ag and Ti, and nanoparticulate content in fish samples in the Atlantic area. Total Ag content in salmon flesh+skin and gonads were lower than LOD. In the case of salmon liver, the total Ag concentration reached 0.73±0.07 μg g^{-1} w.w. and the AgNPs content reached $2.74\times10^{8}\pm7.78\times10^{7}$ AgNPs g^{-1} w.w. Total Ag in sea bass and sea bream flesh+skin and kidney was lower than LOD, but the sea bass and sea bream liver reached 0.37±0.01 and 0.16±0.09 μg g^{-1} w.w. of Ag, respectively. The concentrations of AgNPs in the liver were lower than LOD. In the case of mussels and seaweed, total Ag concentrations were in all cases lower than 0.05 μg g^{-1} and 0.10 μg g^{-1}, respectively. These results showed that fish consumption is safe because the highest concentrations of Ag were found in unedible parts and the Ag concentrations found in mussels and seaweed were low.

The total Ti concentration in salmon flesh+skin was also very low, and nanoparticle content was not detected. In the case of the salmon gonad and liver, the total Ti concentrations reached were lower than 0.09 and 0.34±0.09 μg g^{-1} w.w., respectively. The enzymatic extractions reported concentrations of $5.11\times10^{7}\pm5.84\times10^{6}$ TiO_2NPs g^{-1} w.w. and $1.98\times10^{8}\pm1.22\times10^{7}$ TiO_2NPs g^{-1} w.w. for salmon gonads and livers, respectively. Although total Ti was found in sea bass and sea bream, the nanoparticle content was lower than LOD. Total Ti in mussels reached 1.73±0.50 μg g^{-1} w.w. of Ti, but nanoparticles were not detected. Finally, the highest Ti concentrations were reported in the case of seaweed reaching 8.48±1.69 μg g^{-1} w.w. and $1.35\times10^{8}\pm8.06\times10^{7}$ TiO_2NPs g^{-1} w.w. These results suggest the need for a purification process in seaweed and mussels to ensure food quality.

.

USC UNIVERSIDADE DE SANTIAGO DE COMPOSTELA

SUPPLEMENTARY INFORMATION

Table S.7.1. Operational conditions for (a) ICP-MS and (b) SP-ICP-MS.

(a) **Operational conditions ICP-MS**	
Parameter/component	**Type/mode/value**
Nebulizer	Meinhard CR R^+
Nebulizer Chamber	5 ºC refrigerated glass cyclone chamber with Peltier PC^{3X}
Cone material	Nickel/aluminum
Radiofrequency power	1600 W
Ar gas flow	15 L min^{-1} (Plasma) 1.15 L min^{-1} (Nebulizer) 1.2 L min^{-1} (Auxiliary)
Analytes	Ti and Ag
Operation mode	DRC (for Ti) and KED (for Ag)
Ammonia flow rate	1.0 mL min^{-1}
Helium flow rate	4.5 mL min^{-1}
Integration time	1000 ms
m/z	^{131} [$^{48}Ti^{14}N^1H(^{14}N^1H_3)_4^+$] ^{107}Ag
Replicates per sample	3
RPQ	0.2
(b) **Specific operational conditions for SP-ICP-MS**	
Sample flow rate	0.189-0.223 mL min^{-1}
Acquisition time Ti/Ag	60 s/ 100s
Dwell time Ti/Ag	100 µs/ 50 µs
Number of readings Ti/Ag	600,000/2,000,000

Table S.7.2. Limits of detection and quantification for total Ag and Ti in all the species analyzed.

		Salmon	Sea bass and sea bream	Seaweed	Mussel
Ag	LOD/ ng g^{-1}	0.98	5.06	1.48	2.09
	LOQ/ ng g^{-1}	3.25	16.87	4.92	6.96
Ti	LOD/ ng g^{-1}	6.70	18.97	6.09	1.82
	LOQ/ ng g^{-1}	22.34	63.25	20.29	6.08

USC UNIVERSIDADE DE SANTIAGO DE COMPOSTELA

Table S.7.3. Analytical recoveries in % for total Ag and Ti.

	Concentration added/ μg L^{-1}	Salmon	Sea bass and sea bream	Seaweed	Mussel
Ag	0.05	105±3	100±33	112±22	102±1
	5	98±1	91±3	93±5	105±1
Ti	0.5	111±3	87±10	107±5	119±21
	5	124±5	113±11	109±3	119±6

Table S.7.4. Limits of detection of SP-ICP-MS in salmon, sea bass and sea bream, seaweed, and mussel.

		Salmon	Sea bass and sea bream	Seaweed	Mussel
AgNPs	LOD_{number}/ Part L^{-1}	4.07×10^{6}	6.02×10^{6}	2.40×10^{6}	1.71×10^{6}
	LOD_{number}/ Part g^{-1}	4.58×10^{7}	6.77×10^{7}	4.32×10^{7}	6.42×10^{6}
	LOD_{size} 5σ/ nm	16	20	14	23
	LOD_{size} 3σ/ nm	14	17	12	19
TiO_2NPs	LOD_{number}/ Part L^{-1}	2.61×10^{6}	4.51×10^{6}	1.45×10^{6}	6.01×10^{6}
	LOD_{number}/ Part g^{-1}	9.77×10^{6}	1.69×10^{7}	2.90×10^{7}	6.76×10^{7}
	LOD_{size} 5σ/ nm	26	32	26	28
	LOD_{size} 3σ/ nm	22	28	24	24

Table S.7.5. Average total Ag concentrations in salmon, sea bass and sea bream dissected tissues.

	Salmon			Sea bass			Sea bream		
	Muscle/ μg g^{-1}	Gonad/ μg g^{-1}	Liver/ μg g^{-1}	Muscle/ μg g^{-1}	Kidney/ μg g^{-1}	Liver/ μg g^{-1}	Muscle/ μg g^{-1}	Kidney/ μg g^{-1}	Liver/ μg g^{-1}
1*	0.013±0.003	0.004±0.0001	0.69±0.02	-	-	0.31±0.06	-	-	0.16±0.09
2*	0.015±0.0005	0.005±0.001	0.66±0.06	-	-	0.37±0.01	-	-	0.05±0.01
3	0.004±0.0001		0.61±0.01	-	-	0.28±0.02	-	-	-
4*	0.003±0.001	0.005±0.0004	0.73±0.07						
5	0.011±0.0005		0.62±0.08						
6	0.008±0.002		0.60±0.07						

- Indicates <LOD *Indicates "female salmon"

USC UNIVERSIDADE DE SANTIAGO DE COMPOSTELA

Table S.7.6. Average total Ag concentrations in mussels and seaweed from different sampling zones.

	Sampling zone	A	B	C	D
	1	0.025±0.002	0.009±0.001	0.009±0.002	0.015±0.001
	2	0.036±0.013	0.012±0.002	0.010±0.002	0.021±0.007
[Ag mussels]/ µg g^{-1}	3	0.013±0.002	0.008	0.027±0.004	0.015±0.002
	4	0.033±0.013	0.013±0.0005	0.018±0.001	0.009±0.002
	5	0.020±0.004	0.016±0.008	0.017±0.0001	0.017±0.001
	Sampling zone	**E**	**F**	**G**	
	1	0.008±0.003	0.029±0.003	-	
	2	0.037±0.004	0.080	-	
[Ag seaweed]/ µg g^{-1}	3		0.089±0.013	-	
	4	-	0.045±0.039	-	
	5	0.084±0.015	0.052±0.039	-	

- Indicates "<LOD"

Table S7. Average total Ti concentrations in salmon, sea bass and sea bream dissected tissues.

	Salmon			Sea bass			Sea bream		
	Muscle/ µg g^{-1}	Gonad/ µg g^{-1}	Liver/ µg g^{-1}	Muscle/ µg g^{-1}	Kidney/ µg g^{-1}	Liver/ µg g^{-1}	Muscle/ µg g^{-1}	Kidney/ µg g^{-1}	Liver/ µg g^{-1}
1*	0.02±0.01	0.08±0.01	0.27±0.02	0.56±0.18	0.27	0.44±0.17	0.34±0.07	-	0.23±0.07
2*	0.08±0.03	0.08±0.01	0.25±0.01	0.56±0.48	0.46	0.64±0.30	0.21±0.05	0.62	0.15±0.02
3	0.02		0.34±0.09	0.51±0.21	0.96	0.64±0.03	0.32±0.01	0.77	0.46±0.02
4*	-	0.07±0.02	0.21±0.01						
5	0.06		0.28±0.04						
6	0.01		0.30±0.01						

- Indicates "<LOD" * Indicates "female salmon"

USC UNIVERSIDADE DE SANTIAGO DE COMPOSTELA

Table S.7.8. Average total Ti concentrations in mussels and seaweed from different sampling zones.

	Sampling zone	A	B	C	D
	1	2.15	1.55	1.28±0.08	0.66±0.08
	2	1.10±0.17	2.21±0.24	1.22±0.04	0.32±0.17
[Ti]mussels/ µg g^{-1}	3	1.29±0.16	0.62±0.15	0.76±0.05	1.91±0.47
	4	2.07	1.55±0.20	0.41	0.61±0.14
	5	2.04±0.84	1.26±0.17	-	1.74±0.10
	Sampling zone	E	**F**	**G**	
	1	4.69±0.16	9.69±0.02	5.52±0.10	
	2	4.76±0.28	8.53±1.57	4.11±0.11	
[Ti] seaweed/ µg g^{-1}	3		5.55±0.80	4.78±0.36	
	4	4.70±1.20	9.32±0.38	10.97±0.68	
	5	10.53±2.28	9.34±2.10	8.46±0.12	

- Indicates "<LOD"

USC UNIVERSIDADE DE SANTIAGO DE COMPOSTELA

REFERENCES

[1] Nanomaterial products, Nanotechnology products database, https://product.statnano.com/ (accessed February 8, 2023).
[2] J. Gao, K. Powers, Y. Wang, H. Zhou, S. M. Roberts, B. M. Moudgil, B. Koopman, D. S. Barber, Influence of Suwannee River humic acid on particle properties and toxicity of silver nanoparticles, Chemosphere 89 (2012) 96–101. https://doi.org/10.1016/j.chemosphere.2012.04.024.
[3] W. Younas, F. U. Khan, M. Zaman, D. Lin, A. Zuberi, Y. Wang, Toxicity of synthesized silver nanoparticles in a widespread fish: A comparison between green and chemical, Sci. Total Environ. 845 (2022) 157366. https://doi.org/10.1016/j.scitotenv.2022.157366.
[4] I. X. Yin, J. Zhang, I. S. Zhao, M. L. Mei, Q. Li, C. H. Chu, The antibacterial mechanism of silver nanoparticles and its application in dentistry, Int. J. Nanomedicine. 15 (2020) 2555–2562. https://doi.org/10.2147/IJN.S246764.
[5] J. Fabrega, S. R. Fawcett, J. C. Renshaw, J. R. Lead, Silver nanoparticle impact on bacterial growth: Effect of pH, concentration, and organic matter, Environ. Sci. Technol. 43 (2009) 7285–7290. https://doi.org/10.1021/es803259g.
[6] H. Guo, Y. Kuang, K. Ouyang, C. Zhang, H. Yang, S. Chen, R. Tang, X. Zhang, D. Li, L. Li, Ammonia in the presence of nano titanium dioxide (nano-TiO_2) induces greater oxidative damage in the gill and liver of female zebrafish, Ecotoxicol. Environ. Saf. 236 (2022) 113458. https://doi.org/10.1016/j.ecoenv.2022.113458.
[7] M. Asztemborska, M. Jakubiak, R. Stęborowski, E. Chajduk, G. Bystrzejewska-Piotrowska, Titanium dioxide nanoparticle circulation in an aquatic ecosystem, Water. Air. Soil Pollut. 229 (2018) 1-9. https://doi.org/10.1007/s11270-018-3852-8.
[8] F. Dang, Y. Huang, Y. Wang, D. Zhou, B. Xing, Transfer and toxicity of silver nanoparticles in the food chain, Environ. Sci. Nano. 8 (2021) 1519–1535. https://doi.org/10.1039/d0en01190h.
[9] S. Lekamge, A. F. Miranda, A. Abraham, A. S. Ball, R. Shukla, D. Nugegoda, The toxicity of coated silver nanoparticles to the alga *Raphidocelis subcapitata*, SN Appl. Sci. 2 (2020) 1–20. https://doi.org/10.1007/s42452-020-2430-z.
[10] A. López-Serrano Oliver, R. Muñoz-Olivas, J. Sanz Landaluze, S. Rainieri, C. Cámara, Bioaccumulation of ionic titanium and titanium dioxide nanoparticles in zebrafish eleutheroembryos, Nanotoxicology 9 (2015) 835–842. https://doi.org/10.3109/17435390.2014.980758.
[11] H. Y. Lu, Y. J. Wang, W. C. Hou, Bioaccumulation and depuration of TiO_2 nanoparticles by zebrafish through dietary exposure: Size- and number concentration-resolved analysis using single-particle ICP-MS, J. Hazard. Mater. 426 (2022) 127801. https://doi.org/10.1016/j.jhazmat.2021.127801.
[12] W. A. P. M. De Silva, A. Pathiratne, Nano-titanium dioxide induced genotoxicity and histological lesions in a tropical fish model, Nile tilapia (*Oreochromis niloticus*), Environ. Toxicol. Pharmacol. 98 (2023) 104043. https://doi.org/10.1016/j.etap.2022.104043.
[13] M. Connolly, D. Hernández-Moreno, E. Conde, A. Garnica, J. M. Navas, F. Torrent, I. Rucandio, M. L. Fernandez-Cruz, Influence of citrate and PEG coatings on the bioaccumulation of TiO_2 and CeO_2 nanoparticles following dietary exposure in rainbow trout, Environ. Sci. Eur. 34 (2022) 1–17. https://doi.org/10.1186/s12302-021-00581-0.
[14] C. S. Ramsden, T. J. Smith, B. J. Shaw, R. D. Handy, Dietary exposure to titanium dioxide nanoparticles in rainbow trout, (*Oncorhynchus mykiss*): No effect on growth, but subtle

USC UNIVERSIDADE DE SANTIAGO DE COMPOSTELA

biochemical disturbances in the brain, Ecotoxicology 18 (2009) 939–951. https://doi.org/10.1007/s10646-009-0357-7.
[15] Z. Wang, L. Yin, J. Zhao, B. Xing, Trophic transfer and accumulation of TiO_2 nanoparticles from clamworm (*Perinereis aibuhitensis*) to juvenile turbot (*Scophthalmus maximus*) along a marine benthic food chain, Water Res. 95 (2016) 250–259. https://doi.org/10.1016/j.watres.2016.03.027.
[16] C. Barmo, C. Ciacci, B. Canonico, R. Fabbri, K. Cortese, T. Balbi, A. Marcomini, G. Pojana, G. Gallo, L. Canesi, *In vivo* effects of n-TiO_2 on digestive gland and immune function of the marine bivalve *Mytilus galloprovincialis*, Aquat. Toxicol. 132–133 (2013) 9–18. https://doi.org/10.1016/j.aquatox.2013.01.014.
[17] G. Libralato, D. Minetto, S. Totaro, I. Mičetić, A. Pigozzo, E. Sabbioni, A. Marcomini, A. Volpi Ghirardini, Embryotoxicity of TiO_2 nanoparticles to *Mytilus galloprovincialis* (Lmk), Mar. Environ. Res. 92 (2013) 71–78. https://doi.org/10.1016/j.marenvres.2013.08.015.
[18] I. Marisa, M. G. Marin, F. Caicci, E. Franceschinis, A. Martucci, V. Matozzo, *In vitro* exposure of haemocytes of the clam *Ruditapes philippinarum* to titanium dioxide (TiO_2) nanoparticles: Nanoparticle characterisation, effects on phagocytic activity and internalisation of nanoparticles into haemocytes, Mar. Environ. Res. 103 (2015) 11–17. https://doi.org/10.1016/j.marenvres.2014.11.002.
[19] M. V. Taboada-López, S. Iglesias-López, P. Herbello-Hermelo, P. Bermejo-Barrera, A. Moreda-Piñeiro, Ultrasound assisted enzymatic hydrolysis for isolating titanium dioxide nanoparticles from bivalve mollusk before sp-ICP-MS, Anal. Chim. Acta 1018 (2018) 16–25. https://doi.org/10.1016/j.aca.2018.02.075.
[20] M. A. M. Siddique, M. S. Hossain, M. M. Islam, M. Rahman, G. Kibria, Heavy metals and metalloids in edible seaweeds of Saint Martin's Island, Bay of Bengal, and their potential health risks, Mar. Pollut. Bull. 181 (2022) 113866. https://doi.org/10.1016/j.marpolbul.2022.113866.
[21] F. Corrias, A. Atzei, P. Addis, M. Secci, M. Russo, A. Angioni, Integrated environmental evaluation of heavy metals and metalloids bioaccumulation in invertebrates and seaweeds from different marine coastal areas of sardinia, Mediterranean Sea, Environ. Pollut. 266 (2020) 115048. https://doi.org/10.1016/j.envpol.2020.115048.
[22] J. J. López-Mayán, S. del-Ángel-Monroy, E. Peña-Vázquez, M. C. Barciela-Alonso, P. Bermejo-Barrera, A. Moreda-Piñeiro, Titanium dioxide nanoparticles assessment in seaweeds by single particle inductively coupled plasma–Mass spectrometry, Talanta 236 (2022) 122856. https://doi.org/10.1016/j.talanta.2021.122856.
[23] B. Xiao, X. Wang, J. Yang, K. Wang, Y. Zhang, B. Sun, T. Zhang, L. Zhu, Bioaccumulation kinetics and tissue distribution of silver nanoparticles in zebrafish: The mechanisms and influence of natural organic matter, Ecotoxicol. Environ. Saf. 194 (2020) 110454. https://doi.org/10.1016/j.ecoenv.2020.110454.
[24] H. K. Sung, E. Jo, E. Kim, S. Kyoung Yoo, J. Lee, P. Kim, Y. Kim, I. C. Eom, Analysis of gold and silver nanoparticles internalized by zebrafish (*Danio rerio*) using single particle-inductively coupled plasma-mass spectrometry, Chemosphere 209 (2018) 815–822. https://doi.org/10.1016/j.chemosphere.2018.06.149.
[25] Y. Chae, Y. J. An, Toxicity and transfer of polyvinylpyrrolidone-coated silver nanowires in an aquatic food chain consisting of algae, water fleas, and zebrafish, Aquat. Toxicol. 173 (2016) 94–104. https://doi.org/10.1016/j.aquatox.2016.01.011.
[26] J. McTeer, A. P. Dean, K. N. White, J. K. Pittman, Bioaccumulation of silver nanoparticles into *Daphnia magna* from a freshwater algal diet and the impact of phosphate availability, Nanotoxicology 8 (2014) 305–316. https://doi.org/10.3109/17435390.2013.778346.

USC UNIVERSIDADE DE SANTIAGO DE COMPOSTELA

[27] C. M. Zhao, W. X. Wang, Biokinetic uptake and efflux of silver nanoparticles in *Daphnia magna*, Environ. Sci. Technol. 44 (2010) 7699–7704. https://doi.org/10.1021/es101484s.
[28] M. J. Araújo, M. L. Sousa, E. Fonseca, A. B. Felpeto, J. C. Martins, M. Vázquez, N. Mallo, L. Rodriguez-Lorenzo, M. Quarato, I. Pinheiro, M. V. Turkina, J. J. López-Mayán, E. Peña-Vázquez, M. C. Barciela-Alonso, M. Spuch-Calvar, M. Oliveira, P. Bermejo-Barrera, S. Cabaleiro, B. Espiña, V. Vasconcelos, A. Campos, Proteomics reveals multiple effects of titanium dioxide and silver nanoparticles in the metabolism of turbot, *Scophthalmus maximus*, Chemosphere 308 (2022) 136110. https://doi.org/10.1016/j.chemosphere.2022.136110.
[29] T. Gomes, O. Araújo, R. Pereira, A. C. Almeida, A. Cravo, M. J. Bebianno, Genotoxicity of copper oxide and silver nanoparticles in the mussel *Mytilus galloprovincialis*, Mar. Environ. Res. 84 (2013) 51–59. https://doi.org/10.1016/j.marenvres.2012.11.009.
[30] F. Gagné, J. Auclair, P. Turcotte, C. Gagnon, Sublethal effects of silver nanoparticles and dissolved silver in freshwater mussels, J. Toxicol. Environ. Health-Part A Curr. Issues 76 (2013) 479–490. https://doi.org/10.1080/15287394.2013.779561.
[31] M. V. Taboada-López, N. Alonso-Seijo, P. Herbello-Hermelo, P. Bermejo-Barrera, A. Moreda-Piñeiro, Determination and characterization of silver nanoparticles in bivalve molluscs by ultrasound assisted enzymatic hydrolysis and sp-ICP-MS, Microchem. J. 148 (2019) 652–660. https://doi.org/10.1016/j.microc.2019.05.023.
[32] A. A. Sfriso, M. Mistri, C. Munari, I. Moro, M. Wahsha, A. Sfriso, A. S. Juhmani, Hazardous effects of silver nanoparticles for primary producers in transitional water systems: The case of the seaweed *Ulva rigida* C. Agardh, Environ. Int. 131 (2019) 104942. https://doi.org/10.1016/j.envint.2019.104942.
[33] J. J. López-Mayán, B. Álvarez-Fernández, E. Peña-Vázquez, M. C. Barciela-Alonso, A. Moreda-Piñeiro, P. Bermejo-Barrera, Ultrasonication followed by enzymatic hydrolysis as a sample pre-treatment for the determination of Ag nanoparticles in edible seaweed by SP-ICP-MS, Talanta 247 (2022) 123556. https://doi.org/10.1016/j.talanta.2022.123556.
[34] M. V. Taboada-López, P. Herbello-Hermelo, R. Domínguez-González, P. Bermejo-Barrera, A. Moreda-Piñeiro, Enzymatic hydrolysis as a sample pre-treatment for titanium dioxide nanoparticles assessment in surimi (crab sticks) by single particle ICP-MS, Talanta 195 (2019) 23–32. https://doi.org/10.1016/j.talanta.2018.11.023.
[35] F. Laborda, A. C. Gimenez-Ingalaturre, E. Bolea, J. R. Castillo, About detectability and limits of detection in single particle inductively coupled plasma mass spectrometry, Spectrochim. Acta-Part B At. Spectrosc. 169 (2020) 105883. https://doi.org/10.1016/j.sab.2020.105883.
[36] A. Grasso, M. Ferrante, P. Zuccarello, T. Filippini, G. Arena, M. Fiore, A. Cristaldi, G. O. Conti, C. Copat, Chemical characterization and quantification of titanium dioxide nanoparticles (TiO_2-NPs) in seafood by single-particle ICP-MS: Assessment of dietary exposure, Int. J. Environ. Res. Public Health. 17 (2020) 1–15. https://doi.org/10.3390/ijerph17249547.
[37] C. Alasalvar, K. D. A. Taylor, E. Zubcov, F. Shahidi, M. Alexis, Differentiation of cultured and wild sea bass (*Dicentrarchus labrax*): Total lipid content, fatty acid and trace mineral composition, Food Chem. 79 (2002) 145–150. https://doi.org/10.1016/S0308-8146(02)00122-X.
[38] L. Xu, Z. Wang, J. Zhao, M. Lin, B. Xing, Accumulation of metal-based nanoparticles in marine bivalve mollusks from offshore aquaculture as detected by single particle ICP-MS, Environ. Pollut. 260 (2020) 114043. https://doi.org/10.1016/j.envpol.2020.114043.
[39] D. Desideri, C. Cantaluppi, F. Ceccotto, M. A. Meli, C. Roselli, L. Feduzi, Essential and toxic elements in seaweeds for human consumption, J. Toxicol. Environ. Health-Part A Curr. Issues 79 (2016) 112–122. https://doi.org/10.1080/15287394.2015.1113598.

USC DE COMPOSTELA

USC
UNIVERSIDADE
DE SANTIAGO
DE COMPOSTELA

PART C. BIOAVAILABILITY OF SILVER AND TITANIUM DIOXIDE NANOPARTICLES IN AQUACULTURE PRODUCTS

USC
UNIVERSIDADE
DE SANTIAGO
DE COMPOSTELA

USC
UNIVERSIDADE
DE SANTIAGO
DE COMPOSTELA

CHAPTER 8. BIOAVAILABILITY STUDY OF SILVER AND TITANIUM DIOXIDE NANOPARTICLES FROM SEAWEED AND MUSSELS USING CACO-2 CELLS

USC
UNIVERSIDADE DE SANTIAGO DE COMPOSTELA

USC
UNIVERSIDADE
DE SANTIAGO
DE COMPOSTELA

CHAPTER 8. BIOAVAILABILITY STUDY OF SILVER AND TITANIUM DIOXIDE NANOPARTICLES FROM SEAWEED AND MUSSELS USING CACO-2 CELLS

8.1 ABSTRACT

Seaweed and mussels are preconcentrating organisms that can bioaccumulate pollutants, among them AgNPs and TiO_2NPs from the surrounding medium. Thus, bioavailability studies are needed to ensure food safety.

The bioaccessibility and the bioavailability of total Ag and Ti, AgNPs and TiO_2NPs from raw and cooked seaweed (*Palmaria palmata* and *Ulva* sp.), and cooked mussels (*Mytilus edulis*) exposed to 1.0 mg L^{-1} of 15 nm PVP-AgNPs, to 1.0 mg L^{-1} of 25 nm citrate-TiO_2NPs, or 1.0 mg L^{-1} 5 nm citrate-TiO_2NPs, for 28 days, were evaluated in this study. The samples were submitted to an *in vitro* process simulating the human gastrointestinal digestion in the stomach and the small and large intestine to determine total Ag, total Ti, AgNPs and TiO_2NPs bioaccessibility. The cellular transports for the bioavailability assay through the lumen to the bloodstream were simulated using Caco-2 cell cultures.

Total Ag and Ti in the digest samples, the bioaccessible fractions, and the apical, and basolateral fractions were determined by ICP-MS. AgNPs and TiO_2NPs in the sample extracts, bioaccessible fractions, apical, and basolateral fractions were determined by single particle-ICP-MS (SP-ICP-MS). Finally, the content of AgNPs and TiO_2NPs internalized in the Caco-2 cells was verified by single-cell-ICP-MS (SC-ICP-MS).

8.2 INTRODUCTION

According to the Nanotechnology Products Database, silver nanoparticles (AgNPs) and titanium dioxide nanoparticles (TiO_2NPs) are one of the most commonly used nanoparticles in the industry due to their novel properties in comparison to their bulk materials [1]. The antiviral activity, antibacterial, antifungal and anticancer properties of AgNPs [2,3] make them widely used, mainly in medicine, textile, cosmetics, home appliances, environment applications, construction, and food industry [1]. The photocatalytic activity of TiO_2NPs is useful for applications in cosmetics, construction, textile and renewable energy industries [1,4]. TiO_2 was also commonly used as a food additive E-171 but the European Food Safety Authority (EFSA) [5] has concluded that it can no longer be considered safe and has banned its use from February 2022 [6].

The dispersed and extensive use of AgNPs and TiO_2NPs causes them to be emitted into the environment, where marine organisms are often the final acceptors, which can interact with and even bioaccumulate these NMs [7]. Edible seaweed and mollusks like mussels are considered bioindicators of pollution. They can preconcentrate and bioaccumulate heavy metals, organic compounds, and other emergent contaminants like nanomaterials. The health of the marine environment can be monitored by bivalve mollusks, which are valuable and well-recognized sensitive bioindicators for biomonitoring the possible impacts of anthropogenic pollutants on the health of the aquatic environment. As suspension filter feeders, bivalve mollusks can tolerate and collect potentially hazardous substances in their tissues [8]. Furthermore, seaweeds are used in bioremediation to remove heavy metals from water due to their ability to pre-concentrate heavy metals and emergent contaminants like NPs at concentrations a thousand

USC DE COMPOSTELA

times higher than seawater, and this may be a problem due to their use for human consumption and food additives [9].

The major route of entry of NPs into the body was found to be oral uptake due to the high levels of NPs in food, the large absorption area, and the relatively high translocation rate [10]. The ingested nanoparticles can cross the epithelium of the small and large intestines, reach the circulatory system and consequently be distributed through several organs, while the non-absorbed nanoparticles are excreted by the feces [8,11,12].

Due to the growing number of modified NPs that can not all be tested in animal trials, *in vitro* models have drawn a lot of attention to study the bioaccessible and bioavailable fractions of compounds potentially toxic to an organism [10]. Several studies were found in the case of *in vitro* gastrointestinal digestion and transcellular transport assays using the Caco-2 cells (human epithelial colorectal adenocarcinoma) for several AgNPs [13-18] and TiO_2NPs standards [19-23].

Regarding AgNPs, Kämpfer et al. [18] studied the $AgNO_3$ and AgNPs response in a simulated healthy and inflamed intestine with co-culture of Caco-2/THP-1 cells. The AgNPs and $AgNO_3$ responses were affected more by the inflamed simulated intestine than the healthy one, and then, the intestinal health status in the safety assessment of nanomaterials needs to be considered [18]. Salman et al. [24] reported that AgNPs decreased the viability of Caco-2 cells in a dose and time-dependent manner, and they are capable to induce Caco-2 cellular apoptosis [24]. Xu et al. [25] used cell line models (Caco-2 and HIEC-6) to study the effects of common dietary NPs on the molecular, biochemical, and cellular levels to determine whether exposure could cause disruption of junction complex in epithelial cells, which might then increase allergic response to food allergens. Authors concluded that polyethyleneimine-AgNPs-induced toxicity followed the entire hypothesized pathway, causing disruption of the cell junction complex, and reducing the intestinal barrier function [25].

On the other hand, regarding TiO_2NPs, Tada-Oikawa et al. [26] studied the effects of different TiO_2NPs crystal structures on Caco-2 cells. Results showed that anatase TiO_2NPs induced an inflammatory response, and the high concentrations of anatase, rutile, and P25 TiO_2NPs reduced the cellular viability in Caco-2 cells [26]. Gerloff et al. [27] studied the cytotoxicity, oxidative stress, and DNA damage of five different TiO_2NPs compositions, where the anatase/rutile showed mild DNA damage in comparison to the pure anatase powders [27]. Krüger et al. [28] also reported the activation of inflammatory pathways in Caco-2 cells exposed to 5-10 nm TiO_2NPs [28]. Furthermore, Vila et al. [29] reported a non-toxic effect in the range of 1-200 mg L^{-1} of TiO_2NPs in the biomarkers analyzed. The TiO_2NPs uptake and translocation through the Caco-2 cells did not modify the integrity of the monolayer [29].

Although Taboada-López et al. [8] studied the presence of AgNPs and TiO_2NPs and their bioaccessibility and bioavailability through the Caco-2 cells monolayer in real mollusk samples, to the best of our knowledge no reports were found in marine samples preexposed to bioaccumulation assays of PVP-AgNPs and citrated-TiO_2NPs. Thus, the main objectives of this study are the evaluation of total Ag, total Ti, AgNPs and TiO_2NPs bioaccessibility and bioavailability with cellular transport through the Caco-2 cell monolayer in raw and cooked seaweed (*Palmaria palmata* and *Ulva* sp.), and in cooked mussels (*Mytilus edulis*). All the seaweed and mussel samples were previously exposed to 1.0 mg L^{-1} of AgNPs (15 nm PVP-AgNPs) or 1.0 mg L^{-1} of TiO_2NPs (25 nm citrated-TiO_2NPs or 5 nm citrated-TiO_2NPs), for 28 exposure days. Total Ag and Ti, and AgNPs and TiO_2NPs were determined by ICP-MS, and SP-ICP-MS in the digest samples, in the *in vitro* gastrointestinal fractions and in the apical and basolateral fractions after the cellular transport. Finally, the AgNPs and TiO_2NPs content in the Caco-2 monolayer was analyzed by SC-ICP-MS.

USC DE COMPOSTELA

8.3 MATERIALS AND METHODS

8.3.1 Instrumentation

A NexION® 2000 inductively coupled plasma mass spectrometer from Perkin Elmer (Waltham, MA, USA) was used for Ag and Ti determination using the Syngistix™ 2.5 software from Perkin Elmer. The ICP-MS working in single-particle mode (SP-ICP-MS) with the Syngistix™ Nano Application 2.5 software, from Perkin Elmer, was used for the determination of AgNPs and TiO_2NPs content and size distribution. The single-cell Micro DX autosampler from PerkinElmer (Waltham, MA, USA) with the Asperon™ spray chamber allows to work in single-cell mode (SC-ICP-MS), with the Syngistix™ Single Cell Application Software, for determination of AgNPs and TiO_2NPs internalised in cells. The Ethos Plus microwave lab station from Milestone (Bergamo, Italy) was used for sample acid digestion previous to the total determination of the total content of the elements.

The ultrasound probe VibraCell™ VCX 130 V from Sonics (Newtown, CT, USA) and the ultrasound bath from VWR (Barcelona, Spain) were used for enzymatic and alkaline extractions, respectively. The Boxcult temperature-controlled incubation chamber from Stuart Scientific (Surrey, UK), equipped with a Rotabit orbital-rocking platform shaker from J.P. Selecta (Barcelona, Spain) was employed for enzymatic extractions and *in vitro* digestions. The pH meter from Crison (Barcelona, Spain) was also used for sample preparation.

The UV-Vis spectrometer 689 from Bio-Rad (Hercules, CA, USA) with microplate absorbance reads at 450 nm, was used for the cell viability assessment. The Semi-Micro Osmometer K-7400S form KNAUER (Berlin, Germany) was used for osmolarity adjustments of bioaccessible fractions. The SMH-100 laminar flow cupboard from Telstar (Tarrasa, Spain) was employed to perform the cellular transport experiment. The icoMed incubator from Memmert, (Schwabach, Germany) with a controlled atmosphere was employed for cell culturing. The Electrical Resistance System millicell ERS-2 from Millipore Co. (Massachusetts, USA) and the fluorimeter FLUOstar Omega with a microplate reader from BMG Labtech (Leicester, UK) were used for transepithelial electrical resistance (TEER) and Lucifer Yellow (LY) measurements, respectively. Other instrumentations employed were a Reax top vortex vibrational shaker from Heidolph (Schwabach, Germany), and a heating bath from J.P. Selecta (Barcelona, Spain).

8.3.2 Standards, reagents, and materials

Ultrapure water (18 MΩ cm of resistivity), obtained from a Milli-Q® IQ7003 from Millipore Co. (Bedford, MA, USA), 69% (w/v) SUPRAPUR® nitric acid from Sigma Aldrich, (Darmstadt, Germany), and 33% (w/v) hydrogen peroxide from ACS, ISO, AppliChem Panreac (Barcelona, Spain) were used for microwave-assisted acid performance,

Pancreatin from porcine pancreas and lipase from Candida rugose, both from Sigma Aldrich, a physiological buffer of $NaH_2PO_4 \cdot H_2O$ and NaOH both from Merck (Darmstadt, Germany), a mixture of enzymes obtained from *Rhizopus* sp. (Macerozyme® R-10) from Merck (Darmstadt, Germany), a buffer of citric acid for analysis ACS, from Panreac (Barcelona, Spain), and trisodium citrate di-hydrated from Merck were used for enzymatic nanoparticle extractions. For the alkaline nanoparticle extractions, 25 % (v/v) tetramethylammonium hydroxide (TMAH) from Merck was employed.

For *in vitro* digestions, P-7000 pepsin from porcine gastric mucosa, P-1750 pancreatin from porcine pancreas, and bile salts (50% sodium cholate, 50% deoxycholate) –all from Sigma Aldrich, 96% sodium taurocholate hydrated from Alfa Aesar (Kandel, Germany), 37%

USC UNIVERSIDADE DE SANTIAGO DE COMPOSTELA

hydrochloric acid from Merck, sodium hydrogen carbonate from Panreac, D(+)-glucose and sodium chloride both from Merck, were used.

For cellular transport, Lucifer yellow (LY) from Sigma Aldrich, Caco-2 cells cultured at standard conditions (5% CO_2 at 37 ºC) in Dulbecco's Modified Eagle Medium (DMEM), supplemented with 10% (v/v) fetal bovine serum (FBS) and 1% (v/v) penicillin/streptomycin, 1 mM sodium pyruvate, and 0,1 mM nonessential amino acids (NEAAs), and Transwell® permeable supports of 24 mm insert, 6 well plates and 0.4 µm polyester membrane, from Corning (Kennebunk, ME, USA) were used. A CCK-8 cytotoxicity kit was employed for the cell viability assay. Trypsin-EDTA solution from Sigma Aldrich, Fetal bovine serum from Sigma Aldrich, and Cryopres dimethyl sulfoxide from MP Biomedicals, LLC, were employed to lift the cells from the transwell and freeze them.

Other reagents, standards, and materials include an ionic Ag stock solution of 1000 mg L^{-1} in 2% HNO_3 and Ti 1000 mg L^{-1} H_2O/0.24% F^- both from Perkin Elmer, PEG-COOH Gold Nanospheres in aqueous 1 mM citrate suspension of 49.6 nm of 9.89×10^6 particles mL^{-1} from NanoComposix (San Diego, CA, USA), Citrate Silver Nanospheres, NanoXact™ standards of 20, 40, and 60 nm from nanoComposix (San Diego, CA, USA), TiO_2NPs suspension (mixture of rutile and anatase, 99.5%, <150 nm, 40wt. % in water) from Sigma-Aldrich, Rh stock solution of 1000 mg L^{-1} in 2% HCl from Perkin Elmer, NexION Setup Solution of 1.0 µg L^{-1} of Be, Ce, Fe, In, Li, Mg, Pb, and U in 1% of HNO_3 from Perkin Elmer, 99,999% of Ar, He, and NH_3 all from Nippon Gases (Madrid, Spain), 1% (v/v) glycerol ACS, EMSURE®, from Merck, 1% (v/v) phosphate-buffered saline (PBS) from Thermo Fisher (Dublin, Ireland), and Minisart NML hydrophilic non-sterile 5.0 µm filter disks, from Sartorius (Goettingen, Germany) were also employed.

8.3.3 Seaweed and mussels samples

The seaweed (*Palmaria palmata* and *Ulva* sp.) and mussels (*Mytilus edulis*) used for bioaccessibility and cellular transport experiments were cultured at Indigo Rock Marine Research Center (Cork, Ireland). The study was carried out with specimen samples exposed to 1.0 mg L^{-1} of 15 nm PVP-AgNPs or 1.0 mg L^{-1} citrate-coated TiO_2NPs (25 nm or 5 nm), for 28 days with three replicate tanks per type of particle. Seaweed and mussels were sampled from the three different tanks and mixed and homogenized to obtain enough amount of sample for the experiments (pool of samples). Due to the different forms of consumption of seaweed around the world, *in vitro* digestions were carried out with raw and cooked seaweed. As mussels are commonly eaten cooked, gastrointestinal digestion was performed only in cooked mussels. The study was carried out with fifteen samples that were studied: three raw *Palmaria palmata* samples (one exposed to AgNPs, one exposed to 25 nm TiO_2NPs and one exposed to 5 nm TiO_2NPs), three cooked *Palmaria palmata* samples, three raw *Ulva* sp. samples, three cooked *Ulva* sp. samples, and three cooked *Mytilus edulis* samples. The cooking procedure consisted of boiling approximately 10 g of samples in 600 mL of ultrapure water for 5 minutes. Finally, the cooking water was removed by gravity filtration and the samples were collected and stored in polypropylene tubes at -18 ºC until use.

8.3.4 Sample digestion and extraction procedures

For total Ag and Ti determination in seaweed and mussels samples, microwave-assited acid digestion was employed before the ICP-MS analysis. The microwave employed is described in **section 8.3.1**, and the program used was previously reported by López-Mayán et al. [30], using a volume of 3 mL of 69% HNO_3, 1 mL of 33% H_2O_2, and 4 mL of ultrapure water to digest the 1.0000 g of wet samples. The acid digestions were performed in triplicate with two blanks per

digestion batch. The digest samples were diluted with ultrapure water up to 25 mL and stored in plastic tubes until ICP-MS analysis.

For AgNPs and TiO_2NPs determination in samples, different types of extraction procedures were selected depending on the matrix and the type of nanoparticle to extract, trying to guarantee the stability of the particles. The enzymatic extraction procedures using pancreatin/lipase mixtures were optimized in our laboratory to extract AgNPs [31] and TiO_2NPs [32] from mollusk samples. The enzymatic extraction for AgNPs from seaweed was also previously developed in our research group [30]. Macerozyme® R-10 was employed as a mixture of enzymes to extract AgNPs from seaweed, due to their ability to break the vegetal cell wall. The alkaline extraction using TMAH to extract TiO_2NPs from the seaweed matrix was also previously developed in our research group [33]. **Table S.8.1.** (supplementary information) shows the main conditions used for nanoparticle extractions in the procedure above mentioned.

8.3.5 *In vitro* digestion procedures

Each raw and cooked seaweed sample, and each cooked mussel sample exposed to each type of particle (15 nm AgNPs, 25 nm TiO_2NPs, or 5 nm TiO_2NPs), were submitted in triplicate to the *in vitro* digestion and the cellular transport through the Caco-2 cell barrier.

8.3.5.1 Bioaccesibility assay

The human gastrointestinal *in vitro* digestion was carried out in laboratory conditions in two successive steps simulating the gastric and intestinal conditions. To perform the gastric step, 0.500 g of triturated and homogenized samples (raw and cooked) were mixed with 10 mL of ultrapure water. After waiting a few minutes for pH stabilizations (pH= 2 with 0.1M HCl), and adding the gastric solution (160 g L^{-1} of pepsin in 0.1M HCl), the Erlermeyer flasks were covered with Parafilm® and incubated in the Boxcult chamber at 37 ºC and 150 rpm, for 2 hours. The gastric extracts were then introduced in an ice bath to stop the enzymatic activity. The intestinal step begins adjusting the gastric fraction to pH 7 (0.1M NaOH), and the addition of the intestinal simulating solution (4 g L^{-1} of pancreatin and 2.58 g L^{-1} of sodium taurocholate hydrated in 0.1M of $NaHCO_3$). The Erlenmeyer flasks were covered again and submitted to incubation at 37 ºC and 150 rpm, for 2 hours. The intestinal extracts were cooled in an ice bath to stop the enzymatic activity. Finally, the intestinal extracts were filtered with 5.0 µm filter disks, and the bioaccessible fractions were stored in plastic tubes at -18 ºC until use. Three replicates of samples and two blanks were performed for each *in vitro* digestion batch.

8.3.5.2 Cellular transport assay

The bioaccessible fractions (around 10 mL) obtained after the *in vitro* digestion, described in **section 8.3.5.1**, were heated at 90º C for 5 min to decompose the residual gastrointestinal enzymes. Afterwards, the fractions were divided into two tubes containing 5 mL of the bioaccessible fraction, and 50 µL of 100 g L^{-1} of D(+)-glucose solution was added. The osmolarity of each fraction was adjusted with the addition of 5M NaCl solution dropwise to obtain an osmolarity between 290±10 mOsm kg^{-1}, required for cell viability. Finally, 100 µL of 5 mM of Lucifer yellow (LY) was added to each bioaccessible fraction as a fluorescent marker, and maintained at 37 ºC in a heating bath before their deposition in the Transwells® containing the Caco-2 monolayer.

The Caco-2 cells line was maintained in Dulbecco´s Modified Eagle Medium (DMEM) supplemented with 10% (v/v) fetal bovine serum (FBS), 1 mM sodium pyruvate, 1 mM non-essential amino acids (NEAAs), and 1% (v/v) penicillin/streptomycin. The cells were

USC UNIVERSIDADE DE SANTIAGO DE COMPOSTELA

incubated at standard conditions at 37 ºC with 95% of relative humidity, with a 5% of CO_2 flow. Every two or three days the medium was replaced, reaching 80% of confluence. Then, the cells were detached with 0.5 g L^{-1} trypsin and resuspended in DMEM. Finally, the cells were seeded in the polyester membranes of the 6-well Transwells® with an initial cell concentration of 5×10^4 cells cm^{-2}. The Transwells® are divided into the apical compartment (upper) which simulates the intestinal lumen, and the basolateral compartment (lower) which simulates the serous cavity. Both parts are separated by the polyester membrane where the monolayer of Caco-2 cells grows. Cells were deposited apically (1.5 mL) and the nutrient medium was deposited basolaterally (2 mL of DEMEN). The transwells containing the cells were incubated in the chamber at 37 ºC with 95% of humidity and 5% of CO_2 flow. The basal DEMEN was replaced every three days. The monolayer was allowed to grow until TEER values around 150 mΩ cm^2 were obtained, and no holes were observed in the monolayer under the microscope.

Once the monolayer was formed the transport assays were performed adding 1.5 mL of the bioaccessible fraction into the apical compartment and 2 mL of HBSS in the basolateral chamber. The Transwell® containing the bioaccessible fractions were incubated in the same conditions as the Caco-2 cells for one hour. After this time of incubation, the integrity of the monolayer was determined by monitoring the transepithelial electric resistance (TEER) and by assessing the permeability of the monolayer to Lucifer Yellow (LY). The LY assays measure the fluorescence differences between the basal fraction and the initial bioaccessible fraction with the LY, where <2% of transport of LY through the membrane is necessary to ensure membrane integrity. After the incubation, the TEER measurements must be the initial value TEER±25% to ensure also the cell membrane integrity. The apical and basolateral fractions were collected and stored until their analysis by SP-ICP-MS. The cells adhering to the membrane must be lifted without breaking them, to perform the SC-ICP-MS analysis of the nanoparticles. For that, 1.0 mL of PBS was added to the apical compartment to clean the membrane, and then, the addition of trypsin and incubation for 4 min at 37 ºC, 95% relative humidity, and 5% CO_2 flow was carried out to separate the cells. Finally, the cells were frozen at -18 ºC keeping their integrity using Cryiopres dimethyl sulfoxide, until their analysis by SC-ICP-MS. Each bioaccessible fraction was submitted in triplicate to the cellular transport across the Caco-2 cell membrane.

8.3.6 Cell viability

The viability assay using the CCK-8 cytotoxicity kit was assessed to study the viability of the Caco-2 cells membrane after 24 h of the addition of bioaccessible fractions containing different salts from the *in vitro* intestinal digestion (bile salts or sodium taurocholate). The use of bile salts might result in the cell monolayer rupture, and then a viability experiment using a purer reagent was assessed.

For the *in vitro* toxicity assay Caco-2 cells were seeded into 96-well plates at 1×10^4 cells/well. To allow complete cell attachment, cells were incubated for 24 h at 37ºC and 5% CO_2 in 100 µL growth medium. The cells in the culture medium were used as the negative control. After 24 h of incubation, 100 µL of a sample with bile salts, a sample with sodium taurocholate and two blanks (one with bile salts and the other with sodium taurocholate) were added into the wells and incubated for 2h, 3h, 4h, and 24h. After incubation, the culture medium was discarded, and the cells were washed with 10 mM PBS, (pH=7.4) three times. Then, 100 µL of culture medium containing 10 µL of CCK-8 reagent was added to each well and left for incubation for 1 h. The cell viability was quantified via UV-Vis absorption measurements at 450 nm using a microplate absorbance reader. Cell viability was calculated using **Equation 8.1.**

$$\text{Cell viability (\%)} = \frac{\text{Abs}_{\text{sample}}}{\text{Abs}_{\text{control}}} \text{ x } 100 \text{ (}\mathbf{\text{Equation 8.1.}}\text{)}$$

Where Abs_{sample} is the absorbance at 450 nm for cells incubated with the solutions, and $Abs_{control}$ is the absorbance for control (only cells). Experiments were performed in quadruplicate

8.3.7 Ag and Ti determination by ICP-MS

Total Ag and Ti concentrations were determined in raw and cooked seaweed and cooked mussels samples' acid digests, in the bioaccessible fractions, and in the basolateral solutions from the Caco-2 *in vitro* assays, by ICP-MS. **Table S.8.2.(a)** shows the operational conditions of ICP-MS. Total Ag determination was performed using the standard addition calibration (0-10.0 µg L^{-1}) to avoid the matrix effects, using ^{103}Rh as an internal standard, and Kinetic Electronic Discrimination (KED) mode with He to avoid polyatomic interferences. Total Ti determination was also performed using the standard addition calibration (0-15.0 µg L^{-1}) and using the Dynamic Reaction Cell (DRC) with 1.0 mL min^{-1} of ammonia to generate the Ti-ammonia cluster of m/z 131, avoiding the potential ^{48}Ca interference.

The limits of detection (LOD) and quantification (LOQ) were calculated using the 3σ/m and 10σ/m criteria where σ is the standard deviation of ten measurements of a blank, and m is the slope of the standard addition calibration graph. **Table S.8.3.** shows the LOD and LOQ for Ag and Ti in the seaweed and the mussel digestions, in the bioaccessible fractions, and the basolateral fractions after the Caco-2 cellular transport.

8.3.8 AgNPs and TiO_2NPs nanoparticles determination by SP-ICP-MS and SC-ICP-MS

The AgNPs and TiO_2NPs content and size distribution were determined in the raw and cooked seaweed and the cooked mussel by SP-ICP-MS. The AgNPs and TiO_2NPs extractions were performed in the pool of samples used for the bioaccessibility and cellular transport assays. The AgNPs and TiO_2NPs were also determined directly in the bioaccessible fractions and the apical and basolateral fractions from the cellular transport through the Caco-2 cell membrane. **Table S.8.2.(b)** shows the specific instrumental conditions for SP-ICP-MS. The transport efficiency in SP-ICP-MS is automatically assessed by the software after measuring the flow rate, an ionic gold calibration (0-3.0 µg L^{-1}), and using the gold nanosphere reference material. Due to the high dilution of the samples (500 to 1000 times) in SP-ICP-MS, external calibrations were performed for Ag (0-5.0 µg L^{-1}) and Ti (0-10.0 µg L^{-1}). The Syngistix™ Nano Application software also allows working in DRC mode in the case of TiO_2NPs determination. The enzymatic and alkaline extractions of the samples, the bioaccessible, and the apical and basolateral fractions were diluted with 1% (v/v) of glycerol before SP-ICP-MS analysis. Laborda et al. [34] criteria were used for the LOD determination in SP-ICP-MS mode. **Table S.8.4.** shows the LOD_{number} and the LOD_{size} of Ag and TiO_2NPs obtained in the enzymatic and alkaline extractions, and the bioaccessible and the apical and basolateral fractions.

SC-ICP-MS was employed to determine the AgNPs and TiO_2NPs internalized in the Caco-2 cells. The appropriate dilution of the sample, short dwell times, and a minimal sample uptake rate (10 µL min^{-1}) are needed. **Table S.8.2.(c)** shows the specific operational conditions for SC-ICP-MS. External ionic calibrations (0-3.0 µg L^{-1} and 0-10.0 µg L^{-1} for Ag and Ti), and standards containing AgNPs (20, 40, and 60 nm, 1.0 µg L^{-1}) and TiO_2NPs (150 nm, 8 µg L^{-1})

were employed. The LODs have been automatically assessed with the Syngistix™ ICP-MS software and 5.0±1.4 and 95±11 attograms per cell for Ag and Ti were obtained, respectively.

8.4 RESULTS AND DISCUSSION

The results obtained from this research work will be described in terms of the bioaccessibility of total Ag, and total Ti, AgNPs, and TiO_2NPs in seaweed and mussel, and in terms of the bioavailability of total Ag, and total Ti, AgNPs, and TiO_2NPs in seaweed and mussel through the cellular transport using the Caco-2 cells. The bioaccessible fraction is considered the soluble fraction of a compound in the gastrointestinal medium available for absorption in the intestinal wall, whereas bioavailability (transported percentage ratio) refers to the fraction of a total dose of a substance ingested that arrives at the circulatory system of an organism [8]. The bioaccessibility ratio (in percentage) was calculated as the relation between the concentration in the bioaccessible fraction and the initial concentration in the sample. The transported percentage was calculated as the ratio between the concentration of an analyte in the basolateral compartment divided by the concentration in the apical fraction.

8.4.1 Viability assay

The viability assay of the Caco-2 cellular monolayer was performed using the methodology described in **section 8.3.5.1**. The CCK-8 cytotoxicity kit was assessed to study the viability of the Caco-2 cells membrane after 24 h of the addition of bioaccessible fractions containing bile salts or sodium taurocholate in the *in vitro* intestinal digestion.

The solutions containing the different tested samples and blanks were evaluated at 2, 3, 4, and 24 h. All results were expressed as mean values with standard deviations. Statistical data evaluations were performed with Prism 9 software (GraphPad, Software, LLC). After 2 h, the samples containing sodium taurocholate, bile salts, and the blanks with taurocholate reported viability percentages higher than 80%, being higher than the viability of the blank with bile salts. A reduction was shown in the viability for all samples after 3 h, being these solutions toxic at 24 h. In summary, these solutions with sodium taurocholate are biocompatible within the first two hours, which is the maximum duration time of the experiments.

8.4.2 Total Ag and AgNPs bioaccessibility

Table 8.1. shows the results regarding the bioaccessible assays of total Ag and AgNPs in the raw and cooked *Palmaria palmata*, and *Ulva* sp., and in the cooked *Mytilus edulis* studied specimens.

Total Ag was determined in the digested pool samples, and in the bioaccessible fractions after the gastrointestinal digestions of raw and cooked *Palmaria palmata*, *Ulva* sp., and cooked *Mytilus edulis*. The content of Ag in the digested samples was between 1.48±0.23 and 3.66±0.01 μg g^{-1} w.w. (wet weight) of Ag for cooked *Palmaria palmata*, and raw *Ulva* sp., respectively. The total content Ag in the bioaccessible fractions was between 0.29±0.05 and 1.35±0.08 μg g^{-1} w.w. of Ag for cooked *Palmaria palmata* and raw *Ulva* sp., respectively. Hypothesis tests to compare the means and variances of samples were performed. F-test and t-test from Statgraphics Centurion XVIII were used to compare the total Ag concentrations in the digests of raw and cooked *Palmaria palmata* and in the digests of raw and cooked *Ulva* sp. P-values in both cases were higher than 0.05, and therefore, no statistical differences were found between the mean Ag concentrations in raw and cooked seaweed. However, in both kinds of seaweed (even in cooked and raw), a decrease in total Ag concentration was found between the digested samples and the bioaccessible fractions, resulting in bioaccessible ratios between 20 and 42% for raw *Palmaria palmata* and cooked *Ulva* sp., respectively.

USC DE COMPOSTELA

In the case of *Mytilus edulis*, total Ag concentration remained constant after the gastrointestinal digestion in comparison to total Ag measured after the microwave-assisted acid digestion, resulting in bioaccessibility percentages of 100%.

USC
UNIVERSIDADE DE SANTIAGO DE COMPOSTELA

Table 8.1. Total Ag and AgNPs bioaccessibility ratios for seaweed and mussels.

	Ag			AgNPs						
	Digests	Bioaccessible	B. ratio (%)	Extracts		Bioaccessible		Extracts	Bioaccessible	B. ratio (%)
	[Ag]/ μg g^{-1}	[Ag]/ μg g^{-1}		[AgNPs]/ part g^{-1}	Size/ nm	[AgNPs]/ part g^{-1}	Size/ nm	[Ag] as NPs/ μg g^{-1}	[Ag] as NPs/ μg g^{-1}	
Raw *Palmaria*	1.48±0.23	0.29±0.05	20	$1.52\times10^{9}\pm2.18\times10^{8}$	23±1	$3.51\times10^{8}\pm8.04\times10^{7}$	27±2	0.09±0.02	0.04±0.01	41
Cooked *Palmaria*	1.50±0.33	0.36±0.01	24	$1.33\times10^{9}\pm2.33\times10^{8}$	22±2	$2.06\times10^{8}\pm4.81\times10^{6}$	34±8	0.08±0.01	0.02±0.01	22
Raw *Ulva*	3.66±0.01	1.35±0.08	37	$1.04\times10^{9}\pm3.35\times10^{8}$	29±2	$2.76\times10^{8}\pm4.81\times10^{6}$	34±8	0.13±0.02	0.08±0.01	63
Cooked *Ulva*	2.56±0.96	1.09±0.13	42	$2.46\times10^{8}\pm1.14\times10^{8}$	31±1	$2.55\times10^{8}\pm9.06\times10^{7}$	30±1	0.04±0.01	0.04±0.01	98
Cooked *Mytilus edulis*	1.60±0.50	1.65±0.19	100	$3.80\times10^{8}\pm1.31\times10^{7}$	39±1	$7.68\times10^{7}\pm1.36\times10^{7}$	37±2	0.12±0.01	0.02±0.01	30

B. indicates “Bioaccessibility”

AgNPs concentration was determined in the enzymatic extracts of raw and cooked *Palmaria palmata*, *Ulva* sp., and the cooked *Mytilus edulis*. AgNPs were also determined directly in the bioaccessible fractions after gastrointestinal digestion. The mean sizes for the seaweed extracts were between 22±2 nm and 31±1 nm, and the mean sizes of AgNPs for seaweed bioaccessible fractions were between 27±2 nm and 34±8 nm. Nevertheless, in the case of mussels, the sizes of AgNPs in the enzymatic extracts and the bioaccessible fractions were similar at 39±1 nm and 37±2 nm, respectively. Mass concentrations were calculated, taking into account: the mean size, the AgNPs concentration (part g^{-1}), and assuming that AgNPs are spheric. Results in mass concentration (μg g^{-1} of Ag as NPs) were between 0.04±0.01 and 0.13±0.02 μg of Ag as NPs g^{-1} w.w. in cooked and raw *Ulva* sp., respectively. The bioaccessible fractions were between 0.02±0.01 and 0.08±0.01 μg of Ag as NPs g^{-1} w.w. for cooked *Palmaria palmata* and raw *Ulva* sp., respectively. The comparison of the results using a t-test showed that in all cases P-values> 0.05 for means; therefore, no statistical differences were found between the cooked and raw seaweeds.

The bioaccessibility percentage ratios of Ag as NPs in seaweed ranged from 22 to 98% in the case of cooked *Palmaria palmata* and *Ulva* sp. In cooked *Ulva* sp., 42% of the total Ag content was bioaccessible, while 98% of AgNPs were bioaccessible. However, in the case of cooked *Mytilus edulis*, although 100% of the Ag was bioaccessible, only 30% of the AgNPs in the sample were bioaccessible.

8.4.3 Total Ti and TiO_2NPs bioaccessibility

The results obtained for the bioaccessibility assays of total Ti and TiO_2NPs in raw and cooked *Palmaria palmata*, and *Ulva* sp., and in cooked *Mytilus edulis* are shown in **Table 8.2.** Total Ti was determined in the digest pool samples, and in the bioaccessible fractions after the gastrointestinal digestions of raw and cooked *Palmaria palmata*, *Ulva* sp., and cooked *Mytilus edulis*.

Total Ti concentrations in seaweed digest samples were between 1.78±0.13 and 49.18±3.87 μg g^{-1} w.w. of Ti for cooked *Palmaria palmata* exposed to 5 nm TiO_2NPs and for raw *Ulva* sp. exposed to 25 nm TiO_2NPs, respectively. Total Ti concentrations in the digest after the cooking procedure in the case of *Palmaria palmata* exposed to 25 nm TiO_2NPs and in the case of *Palmaria* exposed to 5 nm TiO_2NPs were compared. In both cases, the hypothesis tests achieved P-values<0.05 for Ti means concentrations, confirming the difference between cooked and raw *Palmaria* at a 95% of confidence level. A higher Ti concentration was found in *Palmaria palmata* exposed to 25 nm than to 5 nm TiO_2NPs. Total Ti was also determined in the bioaccessible fractions of cooked and raw *Palmaria* exposed to these NPs. Bioaccessibility percentages between 15% (for raw *Palmaria* exposed to 5 nm TiO_2NPs) and 32% (for cooked *Palmaria* exposed to 25 nm TiO_2NPs) were obtained. In the case of *Ulva* sp. digests, a decrease in total Ti concentrations was also found after the cooking procedure (hypothesis test with P-values<0.05). Ti concentration also decreased in the case of the bioaccessible fractions concerning the digests in all kinds of seaweed. Then, the bioaccessibility ratios were between 34 and 78% for raw and cooked *Ulva* sp. exposed to 5 nm TiO_2NPs, respectively.

USC UNIVERSIDADE DE SANTIAGO DE COMPOSTELA

Table 8.2. Total Ti and TiO_2NPs bioaccessibility ratios for seaweed and mussels.

	Ti			TiO_2NPs						
	Digests	Bioaccessible	B ratio (%)	Extracts		Bioaccessible		Extracts	Bioaccessible	B. ratio (%)
	[Ti]/ µg g^{-1}	[Ti] / µg g^{-1}		[TiO_2NPs]/ part g^{-1}	Size/ nm	[TiO_2NPs]/ part g^{-1}	Size/ nm	[Ti] as NPs/ µg g^{-1}	[Ti] as NPs/ µg g^{-1}	
Raw *Palmaria* (25 nm)	34.05±3.59	9.94±2.28	29	$2.36\times10^{9}\pm1.12\times10^{8}$	86±2	$4.12\times10^{9}\pm1.44\times10^{9}$	67±2	2.07±0.32	1.52±0.66	73
Cooked *Palmaria* (25 nm)	14.20±1.91	4.61±1.02	32	$2.72\times10^{9}\pm6.72\times10^{7}$	86±2	$7.16\times10^{8}\pm3.36\times10^{8}$	77±9	2.43±0.03	0.40±0.06	17
Raw *Palmaria* (5 nm)	5.73±0.57	0.84±0.01	15	$7.47\times10^{8}\pm2.06\times10^{8}$	67±5	-	-	0.28±0.01	-	
Cooked *Palmaria* (5 nm)	1.78±0.13	0.47±0.05	26	-	-	-	-	-	-	
Raw *Ulva* (25 nm)	49.18±3.87	28.06±0.01	57	$3.79\times10^{9}\pm5.00\times10^{8}$	80±1	$6.01\times10^{9}\pm1.44\times10^{9}$	65±2	2.50±0.17	2.02±0.92	81
Cooked *Ulva* (25 nm)	19.03±1.01	9.54±0.73	50	3.39×10^{9}	87±1	$1.57\times10^{9}\pm1.23\times10^{8}$	81±2	2.97±0.09	1.10±0.16	37
Raw *Ulva* (5 nm)	47.50±3.78	16.28±0.65	34	$4.69\times10^{9}\pm5.12\times10^{8}$	74±7	$3.09\times10^{9}\pm8.25\times10^{8}$	64±2	2.50±0.36	1.06±0.23	42
Cooked *Ulva* (5 nm)	16.08±1.62	12.48±4.87	78	$5.20\times10^{9}\pm3.58\times10^{8}$	62±5	$3.58\times10^{9}\pm1.08\times10^{9}$	57±9	1.65±0.51	0.82±0.14	50
Cooked *Mytilus* (25 nm)	1.48±0.22	1.52±0.49	102	$8.45\times10^{7}\pm7.19\times10^{6}$	96±27	$1.77\times10^{8}\pm1.41\times10^{7}$	67±11	0.09±0.01	0.10±0.02	103
Cooked *Mytilus* (5nm)	1.33±0.02	1.89±1.06	100	$1.03\times10^{8}\pm1.44\times10^{7}$	78±13	$1.67\times10^{8}\pm1.01\times10^{7}$	76±19	0.06±0.02	0.05±0.02	76

B. indicates “Bioaccessibility” – Indicates “<LOD”

Total Ti concentrations in the digested and bioaccessible fractions of cooked *Mytilus edulis* were also determined. Total Ti contents in cooked mussels exposed to 25 and 5 nm TiO_2NPs were statistically similar (P-value>0.05). Moreover, total Ti in the bioaccessible fractions of cooked mussels exposed to 25 and 5 nm, was equal to the digest concentrations, and then the bioaccessible ratios resulted in both cases of 100%.

TiO_2NPs were determined by SP-ICP-MS in the alkaline extracts of raw and cooked *Palmaria palmata* and *Ulva* sp., and in the enzymatic extracts of cooked *Mytilus edulis* exposed to these NPs (25 and 5 nm TiO_2NPs) as well as in the bioaccessible fractions after gastrointestinal digestion.

The mean sizes found in raw and cooked seaweed were between 62±5 nm and 87±1 nm and between 57±9 nm and 81±2 nm, for the alkaline extractions and the bioaccessible fractions, respectively. In the case of cooked mussels, the mean sizes were between 78±13 nm and 96±27 nm and between 67±1 nm and 76±19 nm for the enzymatic extracts and the bioaccessible fractions, respectively. The mean sizes obtained were higher than the nominal size of NPs used to expose the samples (5 and 25 nm), due to the common aggregation phenomenon of TiO_2NPs. Due to the different mean sizes reported, the TiO_2NPs (part g^{-1}) concentration was also transformed into the mass of Ti (µg of Ti as NPs). The concentration of Ti as NPs in alkaline extracts in *Palmaria palmata* were between 0.28±0.01 and 2.43±0.03 µg of Ti as NPs g^{-1} w.w. for raw *Palmaria* exposed to 5 nm TiO_2NPs and cooked *Palmaria* exposed to 25 nm TiO_2NPs, respectively. The content of Ti as NPs in the cooked *Palmaria palmata* exposed to 5 nm was lower than LOD. Therefore, no statistical differences between *Palmaria Palmata* before and after the cooked procedure were found. The mass of Ti as NPs in the bioaccessible fraction was detected only in cooked and raw *Palmaria* exposed to 25 nm TiO_2NPs. The bioaccessibility percentages were 17% and 73% for cooked and raw *Palmaria* exposed to 25 nm TiO_2NPs, respectively. On the other hand, Ti as NPs was detected in all the alkaline extracts and bioaccessible fractions of *Ulva* sp., with contents between 1.65±0.51 and 2.97±0.09 µg of Ti as NPs g^{-1} w.w. for cooked *Ulva* sp. exposed to 5 nm TiO_2NPs and cooked *Ulva* sp. exposed to 25 nm TiO_2NPs, respectively.

A decrease in total Ti concentrations was observed after the cooking procedure but the concentration of TiO_2NPs remained practically constant after this procedure (P-values>0.05). The concentration of Ti as NPs in the bioaccessible fraction of *Ulva* sp. decreased providing bioaccessibility percentages between 37% and 81% for cooked and raw *Ulva* sp., both exposed to 25 nm TiO_2NPs. Regarding *Mytilus edulis*, Ti as NPs was determined in the enzymatic extracts and the bioaccessible fractions. The mass of Ti as NPs was between 0.06±0.02 and 0.09±0.01 µg of Ti as NPs g^{-1} w.w. of cooked mussels exposed to 5 and 25 nm, respectively (P-value>0.05), and then, no differences between cooked mussels were found. Bioaccessibility ratios of 76 to 100% were obtained for cooked mussels exposed to 5 and 25 nm TiO_2NPs, respectively. These high bioaccessibility ratios were in agreement with the bioaccessibility ratios of total Ti found in mussels. The results indicate that all the Ti (ionic and nanoparticulate form) in the mussel is bioaccessible after gastrointestinal digestion.

8.4.4 Total Ag and AgNPs cellular transport

The bioavailability of total Ag and AgNPs was studied in raw and cooked seaweed samples and the cooked mussels exposed to AgNPs, using an intestinal epithelium model and studying the transport of Ag and AgNPs through the Caco-2 cells monolayer. The seaweed and mussel samples were incubated following the protocol described in **section 8.3.5.2**. The apical and basolateral fractions were analyzed by ICP-MS and SP-ICP-MS.

USC DE COMPOSTELA

Table 8.3. shows the results for total Ag and AgNPs cellular transport during one hour through the Caco-2 cell membrane. The total Ag concentrations in the basolateral fractions were lower than the LOD (0.05 μg g^{-1}), therefore the total Ag transport was 0% for all the samples analyzed.

These results were in agreement with those obtained by Abdelkhaliq et al. [35] that reported the impact of *in vitro* digestion on gastrointestinal fate and uptake of AgNPs with different surface modifications through the coculture medium Caco-2/HT29-MTX (human epithelial colorectal adenocarcinoma/ human colon adenocarcinoma mucus-secreting cells), and used ICP-MS and SP-ICP-MS for total Ag and AgNPs determinations in the apical and basolateral layers. They reported cellular transport lowers than 0.1% for total Ag and AgNPs [35].

USC UNIVERSIDADE DE SANTIAGO DE COMPOSTELA

Table 8.3. Total Ag and AgNPs cellular transport ratios.

	Total Ag			AgNPs						
	[Ag] Apical/ µg g^{-1}	[Ag] Basal/ µg g^{-1}	Transport %	[AgNPs] Apical/ part g^{-1}	Apical size/ nm	[AgNPs] Basal/ part g^{-1}	Basal size/ nm	[Ag] as NPs Apical/ µg g^{-1}	[Ag] as NPs Basal/ µg g^{-1}	Transport %
Raw *Palmaria*	0.21	-	0	$4.39\times10^{8}\pm6.24\times10^{7}$	31±1	$5.38\times10^{5}\pm8.90\times10^{4}$	29±2	0.08±0.01	$5.35\times10^{-5}\pm1.97\times10^{-5}$	0.1
Cooked *Palmaria*	0.38	-	0	$7.09\times10^{7}\pm6.14\times10^{6}$	40±1	5.16×10^{5}	26±1	0.02±0.01	5.16×10^{-5}	0.2
Raw *Ulva*	1.73	-	0	$3.11\times10^{8}\pm3.38\times10^{7}$	38±1	$6.49\times10^{5}\pm2.43\times10^{5}$	27±2	0.10±0.01	$7.01\times10^{-5}\pm6.83\times10^{-6}$	0.1
Cooked *Ulva*	1.69	-	0	$1.16\times10^{8}\pm1.25\times10^{6}$	46±2	3.08×10^{6}	22±1	0.06±0.01	1.75×10^{-4}	0.3
Cooked *Mytilus edulis*	4.79	-	0	$8.62\times10^{7}\pm2.31\times10^{7}$	45±1	$1.19\times10^{6}\pm6.90\times10^{5}$	21±2	0.04±0.01	$6.07\times10^{-5}\pm2.34\times10^{-5}$	0.1

- Indicates "<LOD"

8.4.5 Total Ti and TiO_2NPs cellular transport

The bioavailabilities of total Ti and TiO_2NPs were also determined in the cooked and raw seaweed samples and the cooked mussels exposed to 25 or 5 nm TiO_2NPs, using an intestinal epithelium model and studying the transport of Ti and TiO_2NPs through the Caco-2 cells monolayer. The seaweed and mussel samples were incubated following the protocol described in **section 8.3.5.2**, and, the apical and basolateral fractions were then analyzed by ICP-MS and SP-ICP-MS.

Table 8.4. shows the results for total Ti and Ti as NPs cellular transport through the Caco-2 cell membrane. Since the Ti concentration as NPs in the alkaline extracts and bioaccessible fractions of cooked and raw *Palmaria palmata* exposed to 5 nm TiO_2NPs were <LOD, the cellular transport was studied only in the cooked and raw *Palmaria palmata* exposed to 25 nm TiO_2NPs. No cellular transport was observed for total Ti in raw *Palmaria palmata* (cellular transport close to 0%), but the cooked *Palmaria palmata* achieved a Caco-2 cellular transport ratio of 3.1 %. However, no cellular transport was observed for Ti as NPs.

In the case of raw and cooked *Ulva* sp. exposed to 25 nm TiO_2NPs, the total cellular transport ratios were between 0.9 and 2.7 %, respectively, and in the case of raw and cooked *Ulva* sp. exposed to 5 nm TiO_2NPs total Ti cellular transport ratios for Ti as NPs were between 1.1 and 1.6 %, respectively. However, the cellular transport ratios for Ti as NPs were 0.4 % in both cases.

The highest total Ti cellular transport ratio was found in the cooked *Mytilus edulis* exposed to 25 nm TiO_2NPs, reaching a cellular transport ratio of 7.4 %. On the other hand, the total content of Ti in the basolateral chamber for *Mytilus edulis* exposed to 5 nm TiO_2NPs was lower than LOD; then, the total Ti cellular transport ratio was not calculated.

The results obtained in this study indicate that although the bioaccessibility ratios for total Ti and Ti as NPs from seaweed and mussels were very high (even 100% in the case of mussels), total Ti and Ti as NPs transport ratios were in all cases lower than 10%. Then, less than 7.4% of total Ti can cross the epithelium and reach the bloodstream.

USC UNIVERSIDADE DE SANTIAGO DE COMPOSTELA

USC UNIVERSIDADE DE SANTIAGO DE COMPOSTELA

Table 8.4. Total Ti and TiO_2NPs cellular transport ratios.

	Total Ti			TiO_2NPs						
	[Ti] Apical/ µg g^{-1}	[Ti] Basal/ µg g^{-1}	Transport %	[TiO_2NPs] Apical/ part g^{-1}	Apical size/ nm	[TiO_2NPs] Basal/ part g^{-1}	Basal size/ nm	[Ti] as NPs Apical/ µg g^{-1}	[Ti] as NPs Basal/ µg g^{-1}	Transport %
Raw *Palmaria* 25	6.54	-	0	$1.19\times10^{9}\pm1.43\times10^{8}$	115±5	$6.54\times10^{5}\pm1.10\times10^{5}$	111±7	2.40±0.13	0.001±0.0002	0
Cooked *Palmaria* 25	2.79	0.09±0.06	3.1	$1.31\times10^{9}\pm3.36\times10^{7}$	120±14	6.60×10^{6}	51±1	3.02±0.92	0.001±0.0003	0
Raw *Palmaria* 5	-	-		-	-	-	-	-	-	
Cooked *Palmaria* 5	-	-		-	-	-	-	-	-	
Raw *Ulva* 25	9.46	0.09	0.9	$1.68\times10^{9}\pm3.36\times10^{7}$	105±1	$2.53\times10^{6}\pm4.54\times10^{6}$	143±31	2.61±0.05	0.011±0.007	0.4
Cooked *Ulva* 25	4.32	0.12±0.02	2.7	$1.55\times10^{9}\pm4.79\times10^{7}$	106±1	4.57×10^{6}	60±1	2.46±0.03	-	
Hydrated *Ulva* 5	6.46	0.07	1.1	$1.84\times10^{9}\pm3.96\times10^{7}$	89±3	$9.38\times10^{5}\pm2.51\times10^{5}$	114±18	1.72±0.17	0.002±0.001	0.1
Cooked *Ulva* 5	4.19	0.07	1.6	$4.76\times10^{8}\pm4.08\times10^{6}$	134±1	-	-	1.51±0.01	-	
Cooked *Mytilus edulis* 25	0.72	0.05	7.4	$8.12\times10^{8}\pm1.82\times10^{7}$	75±1	-	-	0.45±0.01	-	
Cooked *Mytilus edulis* 5	1.48	-		$2.36\times10^{8}\pm1.15\times10^{7}$	116±2	-	-	0.55±0.05	-	

- Indicates "<LOD"

8.4.6 AgNPs and TiO_2NPs in the Caco-2 cell monolayer

Since Ag and Ti are not highly transported from the apical to the basolateral chamber in one hour of incubation, the presence of these NPs in the cell membrane was studied using SC-ICP-MS.

Raw and cooked *Palmaria* exposed to AgNPs, and raw and cooked *Ulva* exposed to 25 nm TiO_2NPs were used for the *in vitro* digestion and cellular transport. In this experiment, the Caco-2 cell monolayers were analyzed by SC-ICP-MS to verify the presence of AgNPs and TiO_2NPs. The bioaccessible, apical, and basal fractions and the supernatant obtained from the centrifugated cells were analyzed by SP-ICP-MS to carry out a mass balance. The SP-ICP-MS and SC-ICP-MS results were transformed as the mass of the element. **Figure 8.1.(a)** show the mass balance for raw and cooked *Palmaria palmata* exposed to AgNPs, and **Figure 8.1.(b)** show the mass balance for raw and cooked *Ulva* sp. exposed to 25 nm TiO_2NPs. The results for the mass balance are also shown in **Table S.8.5.** The results show that most of the mass of particles remained in the apical fraction, but part of the mass of the nanoparticles was internalized in the cells and the supernatant of cells. The Ag mass balance for nanoparticles in raw and cooked seaweed showed a loss of 21% and 54% of AgNPs mass during the process, respectively. The mass balance for Ti showed a loss of 1% and 23% in raw and cooked seaweed of the mass of Ti as NPs during the process, respectively. This loss of nanoparticle mass in the SP-ICP-MS analysis can be attributed to the dissolution of part of the nanoparticles with sizes smaller than the LOD.

The mass percentages of Ag as NPs in the Caco-2 cell monolayer (cells+supernatant) were 11 and 8 % of the bioaccessible fraction in the raw and cooked *Palmaria palmata*, respectively (where the 9% and 7% of Ag mass correspond to the NPs internalized in the cells). On the other hand, the mass percentages of Ti as NPs in the Caco-2 cell monolayer were 22 and 7% for raw and cooked *Ulva* sp., respectively (where the 20% and 6% of Ti as NPs correspond to the NPs internalized in the cells).

USC UNIVERSIDADE DE SANTIAGO DE COMPOSTELA

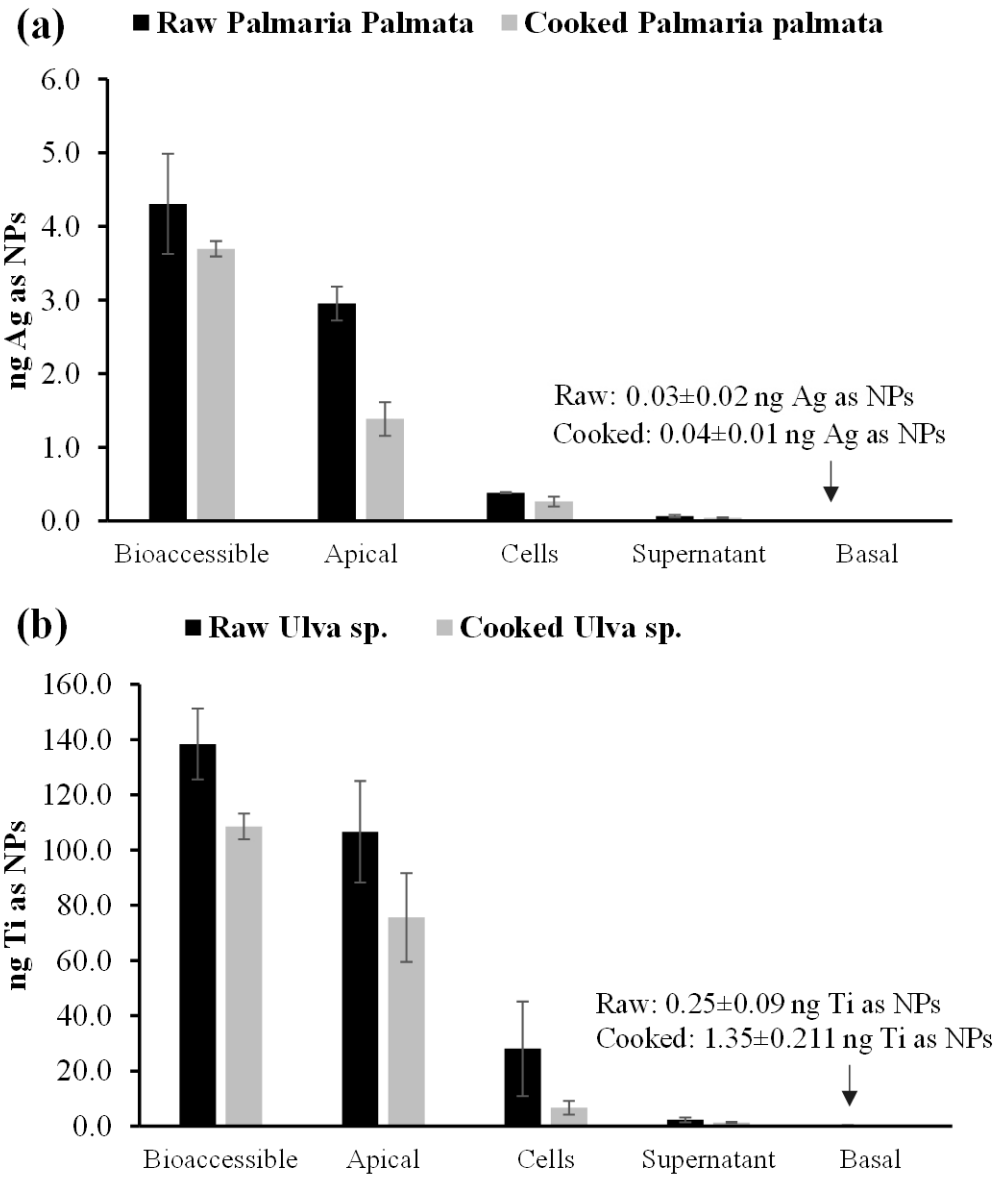

Figure 8.1. Mass balance in the cellular transport of (a) Ag as NPs in exposed raw and cooked *Palmaria palmata*, (b) Ti as nanoparticles in exposed raw and cooked *Ulva* sp.

This current research work showed the bioaccessibility and bioavailability results obtained from raw and cooked seaweed and cooked mussels exposed to 1.0 mg L^{-1} of AgNPs (15 nm) or TiO_2NPs (25 or 5 nm) for long exposure times (28 days) and submitted to the *in vitro* digestion process and cellular transport through Caco-2 cells monolayers. Although no research works were found in the literature that studied the bioavailability of seaweed and mussels samples exposed to NPs, Taboada-López et al. [8] studied the bioaccessibility and bioavailability of unexposed raw mussels samples. The bioaccessibility results for cooked mussels exposed to PVP-AgNPs differ from those previously reported by Taboada-López et al. [8], where no total Ag and AgNPs had been detected in their bioaccessible fractions from raw unexposed mussel samples, maybe due to the low amount of Ag in the unexposed mussels. However, they reported bioaccessibility ratios of 28±7 and 21±3% for total Ti and Ti as NPs, respectively. These

USC DE COMPOSTELA

percentages differ from the bioaccessibility ratios obtained in this research that resulted in 100% for total Ti and Ti as NPs for cooked mussels exposed to 25 nm TiO_2NPs, and 100 and 76% for total Ti and Ti as NPs for cooked mussels exposed to 5 mm TiO_2NPs, respectively. On the other hand, the cellular transport achieved in the Taboada-López et al. [8] research showed a 40% of cellular transport for the total Ti in raw mussels, value higher than the 7.4% cellular transport achieved in the present study for total Ti in cooked mussels exposed to 25 nm TiO_2NPs. Song et al. [19] achieved insignificant cellular transports for native TiO_2NPs through the Caco-2 monolayer. However, Koeneman et al. [23] observed a cellular transport of TiO_2NPs of 14.4% after exposure to 100 μg mL^{-1} of TiO_2NPs. On the other hand, Imai et al. [14] observed that the cellular transport through the Caco-2 cell monolayer in apical fractions treated with AgNPs depends on the size of the particles and the time of exposure of AgNPs to the cellular medium. They saw that the smallest AgNPs pass through the cell membrane more than large ones, and cellular transport increases with the incubation time [14].

These contradictory results come from the use of the different culture conditions, the study of different matrices exposed or not to NPs, and the study of AgNPs and TiO_2NPs with different sizes and surface properties [19]. Therefore more studies are needed to elucidate the AgNPs and TiO_2NPs bioavailability patterns as a function of the sizes, coating, types of species exposed, and culture conditions.

USC
UNIVERSIDADE DE SANTIAGO DE COMPOSTELA

8.5 CONCLUSIONS

The raw and cooked seaweed and the cooked mussels exposed to 15 nm PVP-AgNPs, 25 nm or 5 nm citrate TiO_2NPs were submitted to *in vitro* gastrointestinal digestions for bioaccessibility determinations. Caco-2 cells simulating the epithelial intestine were selected to perform the bioavailability experiments. The bioaccessibility and bioavailability were determined for total Ag and Ti, and AgNPs and TiO_2NPs using the ICP-MS and SP-ICP-MS, respectively. The bioaccessibility and cellular transport ratios were calculated for the samples, and the AgNPs and TiO_2NPs internalized in the Caco-2 cells were also determined by SC-ICP-MS.

Total Ag and AgNPs bioaccessibility ratios in seaweed were between 20-42% and between 22-98%, respectively. Total Ag and AgNPs bioaccessibility ratios in mussels were 100% and 30%, respectively. The decrease in the percentage ratio in mussels in the case of AgNPs indicated that the small AgNPs fraction is less accessible than the ionic Ag. On the other hand, total Ti and TiO_2NPs bioaccessibility fractions for seaweed were between 15-78% and between 17-81%, respectively. In the case of mussels, total Ti and TiO_2NPs bioaccessibility fractions were 100% and between 76-100%, respectively. Regarding the transport assays in seaweed, total Ag and AgNPs transport percentages were close to 0%. Total Ti and TiO_2NPs cellular transport percentages, in seaweed, were between 0.9-3.1% and between 0.1-0.4%, respectively. However, in the case of mussels, total Ti and TiO_2NPs cellular transport percentages were 7.4% and 0% respectively. The internalization percentage of Ag as NPs and Ti as NPs mass in raw and cooked seaweed were 9 and 7%, and 20 and 6 %, respectively.

The results showed a very small total Ag, Ti, AgNPs and TiO_2NPs transport through the Caco-2 cells for 1h incubation, and these results confirm that AgNPs and TiO_2NPs are not able to reach the bloodstream, under the experimental conditions exposed. However, the results refer to a single *in vitro* digestion; so even if the percentage of transport is very low, the continued consumption of AgNPs and TiO_2NPs may increase widely the risk throughout an individual's lifetime.

USC UNIVERSIDADE DE SANTIAGO DE COMPOSTELA

SUPPLEMENTARY INFORMATION

Table S.8.1. Nanoparticle extraction conditions for Ag and TiO_2NPs hydrolysis from mussel and seaweed.

Mussels' enzymatic extraction		
Parameter	Ag	Ti
Mass of sample	1.0000 g	1.0000 g
Pancreatin/lipase concentration	3.0 g L^{-1}	8.0 g L^{-1}
Volume of enzymatic solution	7.5 mL	7.5 mL
Chamber time of incubation	12 h	12 h
Temperature of incubation	37 ºC	37 ºC
Incubation chamber speed	150 rpm	200 rpm
Seaweed's enzymatic extraction		
Parameter	**Ag**	
Mass of sample	0.0500 g	
Macerozyme R-10® concentration	25 g L^{-1}	
Volumen of enzymatic solution	9 mL	
Probe sonication time	2.5 min (pulses: 1s on, 1s off)	
Chamber time of incubation	6 h	
Temperature of incubation	37 ºC	
Incubation chamber speed	150 rpm	
Seaweed's alkaline extraction		
Parameter	**Ti**	
Mass of sample	1.0000 g	
Final volume of 2.5 % (v/v) TMAH	10 mL	
Ultrasound sonication time	2 h (continuous)	

USC UNIVERSIDADE DE SANTIAGO DE COMPOSTELA

Table S.8.2. Operational conditions for (a) ICP-MS, (b) SP-ICP-MS, and (c) SC-ICP-MS.

***(a)* Operational conditions ICP-MS**	
Parameter/component	**Type/mode/value**
Nebulizer	Meinhard CR R^+
Nebulizer Chamber	5 ºC refrigerated glass cyclone chamber with Peltier PC^{3X}
Cone material	Nickel/aluminum
Radiofrequency power	1600 W
Ar gas flow	15 L min^{-1} (Plasma) 1.15 L min^{-1} (Nebulizer) 1.2 L min^{-1} (Auxiliary)
Sample loop	1 mL
Analytes	Ti and Ag
Operation mode	KED for Ag and DRC for Ti
Helium flow rate	4.5 mL min^{-1}
Ammonia flow rate	1.0 mL min^{-1}
Integration time	1000 ms
m/z	^{107}Ag ^{131} $[^{48}Ti^{14}N^1H(^{14}N^1H_3)_4{}^+]$
Replicates per sample	3
Rejection parameter q	0.2

(b) Specific operational conditions for SP-ICP-MS	
Sample flow rate	0.19-0.23 mL min^{-1}
Operation mode	Standard for Ag and DRC for Ti
Acquisition time Ag / Ti	100s / 60 s
Dwell time Ag / Ti	50 µs / 100 µs
Number of readings	2,000,000/600,000
Transport efficiency	11.03-12.70%

(c) Specific operational conditions for SP-ICP-MS		
Ar gas flow	Nebulizer	0.35 L min^{-1}
	Makeup	0.70 L min^{-1}
Sample flow rate		10 µL min^{-1}
Loop		100 µL
Operation mode		Standard for Ag and DRC for Ti
Acquisition time		100s
Dwell time Ag / Ti		50 µs / 100 µs
Transport efficiency		40-60%

USC UNIVERSIDADE DE SANTIAGO DE COMPOSTELA

Table S.8.3. Limits of detection and quantification of total Ag and Ti in the sample digests, bioaccessible, and basolateral fractions after the cellular transport.

Microwave-assisted acid digestions				
	Seaweed		Mussels	
	Ag	Ti	Ag	Ti
LOD/ μg g^{-1}	0.01	0.06	0.01	0.05
LOQ/ μg g^{-1}	0.03	0.21	0.03	0.17
Bioaccessible fractions				
	Seaweed and mussels			
	Ag	Ti		
LOD/ μg g^{-1}	0.09	0.28		
LOQ/ μg g^{-1}	0.29	0.94		
Basolateral fractions after the Caco-2 cell transport				
	Seaweed and mussels			
	Ag	Ti		
LOD/ μg g^{-1}	0.05	0.02		
LOQ/ μg g^{-1}	0.10	0.06		

Table S.8.4. Limits of detection of AgNPs and TiO_2NPs in sample extracts, bioaccessible, and basolateral fractions.

Enzymatic extracts from the pool seaweed and mussel samples		
	AgNPs	TiO_2NPs
LOD_{number}/ NPs L^{-1}	5.60×10^{5}	1.17×10^{6}
LOD_{number}/ NPs g^{-1}	1.01×10^{8}	7.17×10^{7}
LOD_{size} 5σ/ nm	18	29
Bioaccessible fractions		
	AgNPs	TiO_2NPs
LOD_{number}/ NPs L^{-1}	1.41×10^{6}	3.27×10^{6}
LOD_{number}/ NPs g^{-1}	3.67×10^{7}	9.69×10^{7}
LOD_{size} 5σ/ nm	19	28
Basolateral fractions after Caco-2 cellular transport		
	AgNPs	TiO_2NPs
LOD_{number}/ NPs L^{-1}	1.75×10^{6}	4.17×10^{5}
LOD_{number}/ NPs g^{-1}	4.17×10^{7}	4.86×10^{7}
LOD_{size} 5σ/ nm	19	29

USC UNIVERSIDADE DE SANTIAGO DE COMPOSTELA

Table S.8.5. Mass balance in the cellular transport of Ag as NPs in exposed raw and cooked *Palmaria palmata*, and Ti as nanoparticles in exposed raw and cooked *Ulva* sp.

	ng Ag as NPs in *Palmaria Palmata*	ng Ti as NPs in *Ulva* sp.
Raw seaweed		
Bioaccessible	4.31±0.68	138.39±12.78
Apical	2.95±0.93	106.60±18.36
Cells	0.39±0.01	28.03±17.12
Supernatant	0.07±0.02	2.29±0.83
Basolateral	0.003±0.002	0.25±0.09
Cooked seaweed		
Bioaccessible	3.70±0.10	108.57±4.66
Apical	1.39±0.23	75.60±16.06
Cells	0.27±0.07	6.73±2.48
Supernatant	0.04±0.01	1.35±0.21
Basolateral	0.002±0.001	0.23±0.01

USC UNIVERSIDADE DE SANTIAGO DE COMPOSTELA

REFERENCES

[1] Nanotechnology Products Database, https://product.statnano.com/. (accessed January 30, 2023).
[2] L. Wei, J. Lu, H. Xu, A. Patel, Z. S. Chen, G. Chen, Silver nanoparticles: Synthesis, properties, and therapeutic applications, Drug Discov. Today 20 (2015) 595–601. https://doi.org/10.1016/j.drudis.2014.11.014.
[3] M. Rybka, Ł. Mazurek, M. Konop, Beneficial effect of wound dressings containing silver and silver nanoparticles in wound healing—From experimental studies to clinical practice, Life. 13 (2023) 69. https://doi.org/10.3390/life13010069.
[4] M. S. Waghmode, A. B. Gunjal, J. A. Mulla, N. N. Patil, N. N. Nawani, Studies on the titanium dioxide nanoparticles: biosynthesis, applications and remediation, Appl. Sci. 1 (2019) 1–9. https://doi.org/10.1007/s42452-019-0337-3.
[5] M. Younes, G. Aquilina, L. Castle, K. H. Engel, P. Fowler, M. J. Frutos Fernandez, P. Fürst, U. Gundert-Remy, R. Gürtler, T. Husøy, M. Manco, W. Mennes, P. Moldeus, S. Passamonti, R. Shah, I. Waalkens-Berendsen, D. Wölfle, E. Corsini, F. Cubadda, D. De Groot, R. Fitz Gerald, S. Gunnare, A. C. Gutleb, J. Mast, A. Mortensen, A. Oomen, A. Piersma, V. Plichta, B. Ulbrich, H. Van Loveren, D. Benford, M. Bignami, C. Bolognesi, R. Crebelli, M. Dusinska, F. Marcon, E. Nielsen, J. Schlatter, C. Vleminckx, S. Barmaz, M. Carfí, C. Civitella, A. Giarola, A. M. Rincon, R. Serafimova, C. Smeraldi, J. Tarazona, A. Tard, M. Wright, Safety assessment of titanium dioxide (E171) as a food additive, EFSA J. 19 (2021) 6585. https://doi.org/10.2903/j.efsa.2021.6585.
[6] European Commission, Commission Regulation (EU) 2022/63 of 14 January 2022 amending Annexes II and III to Regulation (EC) No 1333/2008 of European Parliament and of the Council as regards the food additive titanium dioxide (E171), Off. J. Eur. Union. 11 (2022) 1–5.
[7] S. Jahan, I. Bin Yusoff, Y. B. Alias, A. F. B. A. Bakar, Reviews of the toxicity behavior of five potential engineered nanomaterials (ENMs) into the aquatic ecosystem, Toxicol. Reports 4 (2017) 211–220. https://doi.org/10.1016/j.toxrep.2017.04.001.
[8] M. V. Taboada-López, B. H. Leal-Martínez, R. Domínguez-González, P. Bermejo-Barrera, P. Taboada-Antelo, A. Moreda-Piñeiro, Caco-2 *in vitro* model of human gastrointestinal tract for studying the absorption of titanium dioxide and silver nanoparticles from seafood, Talanta. 233 (2021). https://doi.org/10.1016/j.talanta.2021.122494.
[9] Z. Peng, Z. Guo, Z. Wang, R. Zhang, Q. Wu, H. Gao, Y. Wang, Z. Shen, S. Lek, J. Xiao, Species-specific bioaccumulation and health risk assessment of heavy metal in seaweeds in tropic coasts of South China Sea, Sci. Total Environ. 832 (2022) 155031. https://doi.org/10.1016/j.scitotenv.2022.155031.
[10] E. Fröhlich, E. Roblegg, Oral uptake of nanoparticles: human relevance and the role of in vitro systems, Arch. Toxicol. 90 (2016) 2297–2314. https://doi.org/10.1007/s00204-016-1765-0.
[11] C. McCracken, P. K. Dutta, W. J. Waldman, Critical assessment of toxicological effects of ingested nanoparticles, Environ. Sci. Nano. 3 (2016) 256–282. https://doi.org/10.1039/c5en00242g.
[12] M. J. Rein, M. Renouf, C. Cruz-Hernandez, L. Actis-Goretta, S. K. Thakkar, M. da Silva Pinto, Bioavailability of bioactive food compounds: A challenging journey to bioefficacy, Br. J. Clin. Pharmacol. 75 (2013) 588–602. https://doi.org/10.1111/j.1365-2125.2012.04425.x.

USC UNIVERSIDADE DE SANTIAGO DE COMPOSTELA

[13] L. Vila, A. García-Rodríguez, C. Cortés, R. Marcos, A. Hernández, Assessing the effects of silver nanoparticles on monolayers of differentiated Caco-2 cells, as a model of intestinal barrier, Food Chem. Toxicol. 116 (2018) 1–10. https://doi.org/10.1016/j.fct.2018.04.008.
[14] S. Imai, Y. Morishita, T. Hata, M. Kondoh, K. Yagi, J. Q. Gao, K. Nagano, K. Higashisaka, Y. Yoshioka, Y. Tsutsumi, Cellular internalization, transcellular transport, and cellular effects of silver nanoparticles in polarized Caco-2 cells following apical or basolateral exposure, Biochem. Biophys. Res. Commun. 484 (2017) 543–549. https://doi.org/10.1016/j.bbrc.2017.01.114.
[15] S. C. Sahu, J. Zheng, L. Graham, L. Chen, J. Ihrie, J. J. Yourick, R. L. Sprando, Comparative cytotoxicity of nanosilver in human liver HepG2 and colon Caco2 cells in culture, J. Appl. Toxicol. 34 (2014) 1155–1166. https://doi.org/10.1002/jat.2994.
[16] M. Polet, L. Laloux, S. Cambier, J. Ziebel, A. C. Gutleb, Y. J. Schneider, Soluble silver ions from silver nanoparticles induce a polarised secretion of interleukin-8 in differentiated Caco-2 cells, Toxicol. Lett. 325 (2020) 14–24. https://doi.org/10.1016/j.toxlet.2020.02.004.
[17] N. Chen, Z. M. Song, H. Tang, W. S. Xi, A. Cao, Y. Liu, H. Wang, Toxicological effects of Caco-2 cells following short-term and long-term exposure to Ag nanoparticles, Int. J. Mol. Sci. 17 (2016) 974. https://doi.org/10.3390/ijms17060974.
[18] A. A. M. Kämpfer, P. Urbán, R. La Spina, I. O. Jiménez, N. Kanase, V. Stone, A. Kinsner-Ovaskainen, Ongoing inflammation enhances the toxicity of engineered nanomaterials: Application of an *in vitro* co-culture model of the healthy and inflamed intestine, Toxicol. Vitr. 63 (2020) 104738. https://doi.org/10.1016/j.tiv.2019.104738.
[19] Z. M. Song, N. Chen, J. H. Liu, H. Tang, X. Deng, W. S. Xi, K. Han, A. Cao, Y. Liu, H. Wang, Biological effect of food additive titanium dioxide nanoparticles on intestine: An *in vitro* study, J. Appl. Toxicol. 35 (2015) 1169–1178. https://doi.org/10.1002/jat.3171.
[20] C. Gitrowski, A. R. Al-Jubory, R. D. Handy, Uptake of different crystal structures of TiO_2 nanoparticles by Caco-2 intestinal cells, Toxicol. Lett. 226 (2014) 264–276. https://doi.org/10.1016/j.toxlet.2014.02.014.
[21] P. Pedata, G. Ricci, L. Malorni, A. Venezia, M. Cammarota, M. G. Volpe, N. Iannaccone, V. Guida, C. Schiraldi, M. Romano, G. Iacomino, *In vitro* intestinal epithelium responses to titanium dioxide nanoparticles, Food Res. Int. 119 (2019) 634–642. https://doi.org/10.1016/j.foodres.2018.10.041.
[22] M. Dorier, C. Tisseyre, F. Dussert, D. Béal, M. E. Arnal, T. Douki, V. Valdiglesias, B. Laffon, S. Fraga, F. Brandão, N. Herlin-Boime, F. Barreau, T. Rabilloud, M. Carriere, Toxicological impact of acute exposure to E171 food additive and TiO_2 nanoparticles on a co-culture of Caco-2 and HT29-MTX intestinal cells, Mutat. Res-Genet. Toxicol. Environ. Mutagen. 845 (2019) 402980. https://doi.org/10.1016/j.mrgentox.2018.11.004.
[23] B. A. Koeneman, Y. Zhang, P. Westerhoff, Y. Chen, J. C. Crittenden, D. G. Capco, Toxicity and cellular responses of intestinal cells exposed to titanium dioxide, Cell Biol. Toxicol. 26 (2010) 225–238. https://doi.org/10.1007/s10565-009-9132-z.
[24] A. Salman, C. Soukkarieh, S. Alzeer, Cytotoxic effect of silver nanoparticles on colorectal adenocarcinoma cell line, Bulletin of Pharmaceutical Sciences, 44 (2021) 587–597. DOI:10.21608/bfsa.2021.207188
[25] K. Xu, N. Basu, S. George, Dietary nanoparticles compromise epithelial integrity and enhance translocation and antigenicity of milk proteins: An *in vitro* investigation, NanoImpact. 24 (2021) 100369. https://doi.org/10.1016/j.impact.2021.100369.
[26] S. Tada-Oikawa, G. Ichihara, H. Fukatsu, Y. Shimanuki, N. Tanaka, E. Watanabe, Y. Suzuki, M. Murakami, K. Izuoka, J. Chang, W. Wu, Y. Yamada, S. Ichihara, Titanium dioxide

USC UNIVERSIDADE DE SANTIAGO DE COMPOSTELA

particle type and concentration influence the inflammatory response in Caco-2 cells, Int. J. Mol. Sci. 17 (2016) 576. https://doi.org/10.3390/ijms17040576.
[27] K. Gerloff, I. Fenoglio, E. Carella, J. Kolling, C. Albrecht, A. W. Boots, I. Förster, R. P. F. Schins, Distinctive toxicity of TiO_2 rutile/anatase mixed phase nanoparticles on Caco-2 cells, Chem. Res. Toxicol. 25 (2012) 646–655. https://doi.org/10.1021/tx200334k.
[28] K. Krüger, F. Cossais, H. Neve, M. Klempt, Titanium dioxide nanoparticles activate IL8-related inflammatory pathways in human colonic epithelial Caco-2 cells, J. Nanoparticle Res. 16 (2014) 2402. https://doi.org/10.1007/s11051-014-2402-6.
[29] L. Vila, A. García-Rodríguez, R. Marcos, A. Hernández, Titanium dioxide nanoparticles translocate through differentiated Caco-2 cell monolayers, without disrupting the barrier functionality or inducing genotoxic damage, J. Appl. Toxicol. 38 (2018) 1195–1205. https://doi.org/10.1002/jat.3630.
[30] J. J. López-Mayán, B. Álvarez-Fernández, E. Peña-Vázquez, M. C. Barciela-Alonso, A. Moreda-Piñeiro, P. Bermejo-Barrera, Ultrasonication followed by enzymatic hydrolysis as a sample pre-treatment for the determination of Ag nanoparticles in edible seaweed by SP-ICP-MS, Talanta 247 (2022) 123556. https://doi.org/10.1016/j.talanta.2022.123556.
[31] M. V. Taboada-López, N. Alonso-Seijo, P. Herbello-Hermelo, P. Bermejo-Barrera, A. Moreda-Piñeiro, Determination and characterization of silver nanoparticles in bivalve molluscs by ultrasound assisted enzymatic hydrolysis and sp-ICP-MS, Microchem. J. 148 (2019) 652–660. https://doi.org/10.1016/j.microc.2019.05.023.
[32] M. V. Taboada-López, S. Iglesias-López, P. Herbello-Hermelo, P. Bermejo-Barrera, A. Moreda-Piñeiro, Ultrasound assisted enzymatic hydrolysis for isolating titanium dioxide nanoparticles from bivalve mollusk before sp-ICP-MS, Anal. Chim. Acta. 1018 (2018) 16–25. https://doi.org/10.1016/j.aca.2018.02.075.
[33] J. J. López-Mayán, S. del-Ángel-Monroy, E. Peña-Vázquez, M. C. Barciela-Alonso, P. Bermejo-Barrera, A. Moreda-Piñeiro, Titanium dioxide nanoparticles assessment in seaweeds by single particle inductively coupled plasma–Mass spectrometry, Talanta 236 (2022) 122856. https://doi.org/10.1016/j.talanta.2021.122856.
[34] F. Laborda, A. C. Gimenez-Ingalaturre, E. Bolea, J. R. Castillo, About detectability and limits of detection in single particle inductively coupled plasma mass spectrometry, Spectrochim. Acta-Part B At. Spectrosc. 169 (2020) 105883. https://doi.org/10.1016/j.sab.2020.105883.
[35] A. Abdelkhaliq, M. van der Zande, A. K. Undas, R. J. B. Peters, H. Bouwmeester, Impact of *in vitro* digestion on gastrointestinal fate and uptake of silver nanoparticles with different surface modifications, Nanotoxicology 14 (2020) 111–126. https://doi.org/10.1080/17435390.2019.1675794.

USC UNIVERSIDADE DE SANTIAGO DE COMPOSTELA

V. CONCLUSIONS

USC
UNIVERSIDADE
DE SANTIAGO
DE COMPOSTELA

USC
UNIVERSIDADE
DE SANTIAGO
DE COMPOSTELA

V. CONCLUSIONS

The main conclusions of this doctoral thesis are briefly summarized below:

- The methodologies for AgNPs and TiO_2NPs separation from seaweed employing enzymatic and alkaline extractions, respectively, were optimized, validated, and applied. The stability of the nanoparticles during extraction was confirmed by SP-ICP-MS and TEM analysis.

- The study showed the safety of the consumption of *Scophthalmus maximus* due to the bioaccumulation of AgNPs and TiO_2NPs in the not edible parts (liver and kidney). Furthermore, turbots excreted Ti through the feces.

- Mussels (*Mytilus edulis*) and seaweed (*Palmaria palmata* and *Ulva* sp.) bioaccumulated the highest concentrations of AgNPs and TiO_2NPs. The bioaccumulation patterns in seaweed were species-dependent, and TEM/STEM and EDX confirmed the internalization of TiO_2NPs by *Ulva* sp.

- Some alterations were found in mussels during the bioaccumulation tests (segregation of a surface scum in the AgNPs assay or the weakening of shells of mussels exposed to 5 nm TiO_2NPs).

- The analysis of different specimens collected in the Atlantic area confirmed the highest accumulation of Ag and Ti in the unedible parts of the fishes (*Salmo salar*, *Dicentrachus labrax*, and *Sparus aurata*). The concentrations found in the analyzed mussels and especially in seaweed highlighted again the need for proper depuration before their consumption.

- The bioavailability experiments with raw and cooked *Ulva sp*. and *Palmaria palmata* and cooked *Mytilus edulis* showed transport percentages that were in all cases lower than 10% (most of them close to 0). Internalization of nanoparticles in Caco-2 cells was also observed by SC-ICP-MS.

-The continued consumption of seaweed and mussels containing AgNPs and TiO_2NPs would probably increase the concentration of these elements in the circulatory system and the internalization in the intestinal epithelial cells.

USC UNIVERSIDADE DE SANTIAGO DE COMPOSTELA

USC
UNIVERSIDADE
DE SANTIAGO
DE COMPOSTELA

ANNEX I. LIST OF PUBLICATIONS AND CONTRIBUTION

USC
UNIVERSIDADE
DE SANTIAGO
DE COMPOSTELA

USC
UNIVERSIDADE
DE SANTIAGO
DE COMPOSTELA

ANNEX I. LIST OF PUBLICATIONS AND CONTRIBUTION

***Juan José López-Mayán**, Blanca Álvarez-Fernández, Elena Peña-Vázquez, María Carmen Barciela-Alonso, Antonio Moreda Piñeiro, Pilar Bermejo-Barrera, Ultrasonication followed by enzymatic hydrolysis as a sample pre-treatment for the determination of Ag nanoparticles in edible seaweed by SP-ICP-MS, Talanta 247 (2022) 123556. https://doi.org/10.1016/j.talanta.2022.123556.

Juan José López-Mayán contribution: Methodology, Formal analysis, Investigation, Validation, Visualization, Writing -original draft preparation

- Impact factor (2022):6.1.
- Rank by Journal Impact Factor (2022) Analytical Chemistry, 9/86 (Q1).
- Citations: 3.

***Juan José López-Mayán**, Sergio del-Ángel-Monroy, Elena Peña-Vázquez, María Carmen Barciela-Alonso, Pilar Bermejo-Barrera, Antonio Moreda-Piñeiro, Titanium dioxide nanoparticles assessment in seaweeds by single particle inductively coupled plasma–Mass spectrometry, Talanta 236 (2022) 122856. https://doi.org/10.1016/j.talanta.2021.122856.

Juan José López-Mayán contribution: Formal analysis, Investigation, Validation, Visualization, Writing- original draft preparation.

- Impact factor (2021):6.1.
- Rank by Journal Impact Factor (2021) Analytical Chemistry, 9/86 (Q1).
- Citations: 7.

***Juan José López-Mayán**, Blanca Álvarez-Fernández, Elena Peña-Vázquez, María Carmen Barciela-Alonso, Antonio Moreda Piñeiro, Julie Maguire, Mick Mackey, Monica Quarato, Ivone Pinheiro, Begoña Espiña, Laura Rodríguez-Lorenzo, Pilar Bermejo-Barrera, Bioaccumulation of titanium dioxide nanoparticles in green (*Ulva* sp.) and red (*Palmaria palmata*) seaweed, Microchim Acta. Accepted, publication pending. https://doi.org/10.1007/s00604-023-05849-1.

Juan José López-Mayán contribution: Formal analysis, Investigation, Validation, Visualization, Writing- original draft preparation.

- Impact factor (2022):5.7.
- Rank by Journal Impact Factor (2022) Analytical Chemistry, 12/86 (Q1).
- Citations: 0.

Data obtained from Web of Science (Clarivate Analytics) on July 04th, 2023.

USC UNIVERSIDADE DE SANTIAGO DE COMPOSTELA

USC
UNIVERSIDADE
DE SANTIAGO
DE COMPOSTELA

ANNEX II. PERMISSIONS

USC
UNIVERSIDADE
DE SANTIAGO
DE COMPOSTELA

USC
UNIVERSIDADE
DE SANTIAGO
DE COMPOSTELA

ANNEX II. PERMISSIONS

The supervisors Elena María Peña Vázquez and María Carmen Barciela Alonso and the author Juan José López Mayán declare that all the information mentioned in all the chapters will not be used totally or partially in another doctoral thesis by another student.

FIGURES: All the figures included in the thesis are of Juan José López-Mayán authorship.

CHAPTER 1. (IV RESULTS AND DISCUSSION)

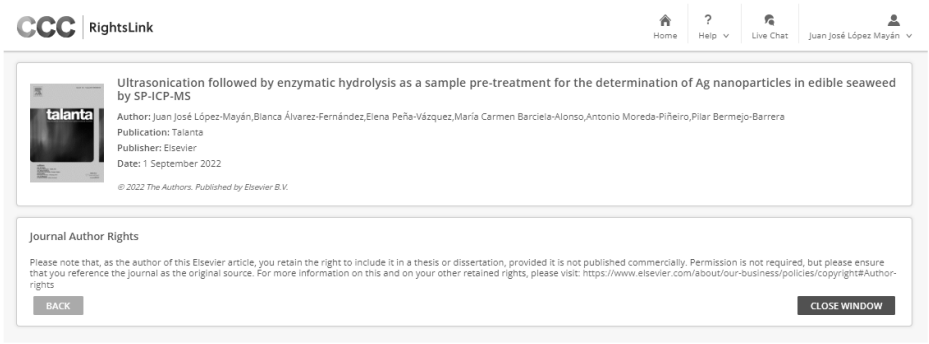

CHAPTER 2. (IV RESULTS AND DISCUSSION)

CHAPTER 4. (IV RESULTS AND DISCUSSION)

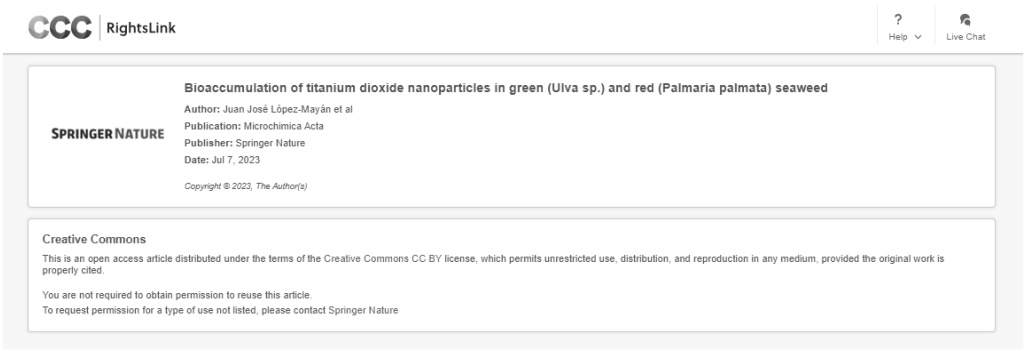

USC UNIVERSIDADE DE SANTIAGO DE COMPOSTELA

USC
UNIVERSIDADE
DE SANTIAGO
DE COMPOSTELA

Silver and titanium dioxide nanoparticles are considered emergent pollutants that can interact with different organisms. This doctoral thesis focuses on the bioaccumulation and bioavailability studies of these materials in some of the most important aquaculture species of the Atlantic area, including seaweed, mussels, and turbot.

Different methodologies for nanoparticle extraction from the aquaculture matrices were used and developed. They were also applied to the analysis of marine samples from Ireland, France and UK. Furthermore, the potential release of nanoparticles from the food matrix to the systemic circulation and the intestinal epithelial cells was assessed after simulated *in vitro* gastrointestinal digestions and transport through Caco-2 cells by SP-ICP-MS and SC-ICP-MS.